Transactions of the ASME

Technical Editor, L. B. FREUND

Division of Engineering
Brown University
Providence, R.I. 02912

APPLIED MECHANICS DIVISION

Chairman, J. R. RICE
Secretary, THOMAS L. GEERS
Associate Editors,
D. B. BOGY
R. M. CHRISTENSEN
R. J. CLIFTON
THOMAS J. R. HUGHES
W. D. IWAN
W. G. KNAUSS
F. A. LECKIE
J. T. C. LIU
FRANCIS C. MOON
J. W. NUNZIATO
R. H. PLAUT
J. G. SIMMONDS
K. R. SREENIVASAN
Z. WARHAFT
L. T. WHEELER
S. E. WIDNALL

BOARD ON COMMUNICATIONS
Chairman and Vice-President
K. N. REID, JR.

Members-at-Large
W. BEGELL
J. T. COKONIS
M. FRANKE
W. G. GOTTENBERG
M. KUTZ
F. LANDIS
J. R. LLOYD
T. C. MIN
R. E. NICKELL
R. E. REDER
F. W. SCHMIDT

President, N. D. FITZROY
Exec. Dir.
PAUL ALLMENDINGER
Treasurer, ROBERT A. BENNETT

PUBLISHING STAFF
Mng. Dir., Pub., J. J. FREY
Dep. Mng. Dir., Pub.
JOS. SANSONE
Managing Editor,
CORNELIA MONAHAN
Production Editor, REMO SALTA
Prod. Asst., MARISOL ANDINO

Transactions of the ASME, Journal of Applied Mechanics (ISSN 0021-8936) is published quarterly (Mar., June, Sept., Dec.) for $105 per year by The American Society of Mechanical Engineers, 345 East 47th Street, New York, NY 10017. Second class postage paid at New York, NY and additional mailing offices. POSTMASTER: Send address changes to The Journal of Applied Mechanics, c/o THE AMERICAN SOCIETY OF MECHANICAL ENGINEERS, 22 Law Drive, Box 2300, Fairfield, NJ 07007-2300. CHANGES OF ADDRESS must be received at Society headquarters seven weeks before they are to be effective. Please send old label and new address.

PRICES: To members, $24.00, annually; to nonmembers, $105.00. Add $6.00 for postage to countries outside the United States and Canada.

STATEMENT from By-Laws. The Society shall not be responsible for statements or opinions advanced in papers or . . . printed in its publications (B7.1, Par. 3).

COPYRIGHT © 1987 by the American Society of Mechanical Engineers. Reprints from this publication may be made on condition that full credit be given the TRANSACTIONS OF THE ASME, JOURNAL OF APPLIED MECHANICS, and the author, and date of publication be stated.

INDEXED by the Engineering Information

Journal of Applied Mechanics

Published Quarterly by The American Society of Mechanical Engineers

VOLUME 54 • NUMBER 2 • JUNE 1987

TECHNICAL PAPERS

255 **Optimal Beam and Plate Foundations for Minimum Compliance** (87-APM-24)
R. H. Plaut

258 **Nonlinear Beam Kinematics by Decomposition of the Rotation Tensor** (87-APM-17)
D. A. Danielson and D. H. Hodges

263 **Design of Material Properties That Yield a Prescribed Global Buckling Response**
S. S. Antman and C. L. Adler

269 **General Solutions for the Inelastic Behavior of Pressurized Membranes**
K. W. Neale and E. Chater

275 **A Sixth-Order Plate Theory – Derivation and Error Estimates**
Z. Rychter

280 **On Boundary Layers in a Pressurized Mooney Cylinder** (87-APM-27)
L. A. Taber

287 **Large-Strain Axisymmetric Deformation of Cylindrical Shells** (87-APM-35)
G. W. Brodland and H. Cohen

292 **Imperfection-Sensitivity of Long Antisymmetric Cross-Ply Cylindrical Panels Under Shear Loads** (87-APM-28)
David Hui and I. H. Y. Du

299 **Natural Frequencies of a Railroad Track** (87-APM-32)
S. P. Patil

305 **Effects of Nonconstant Spin Rate on the Vibration of a Rotating Beam**
D. C. Kammer and A. L. Schlack, Jr.

311 **Bending Vibrations of a Class of Rotating Beams with Hypergeometric Solutions** (87-APM-21)
D. Storti and Y. Aboelnaga

315 **Large Amplitude Oscillations of Thin Circular Rings**
S. P. Maganty and W. B. Bickford

323 **An Evaluation of Recent Developments in Hardening and Flow Rules for Rate-Independent, Nonproportional Cyclic Plasticity** (87-APM-37)
D. L. McDowell

335 **A Boundary Element Analysis of Metal Extrusion Processes**
A. Chandra and S. Mukherjee

341 **A Complementary Work Bounding Principle for Forward Integration Along the Path of Loading for Elasto-Plastic Bodies**
J. B. Martin

346 **On Using Stress Relaxation Tests to Characterize Material Behavior** (87-APM-25)
J. L. Ding and W. N. Findley

351 **Elastic Moduli of Lungs**
B. Budiansky and E. Kimmel

359 **The Normal Impact on an Elastic Half Space of an Elastic Rod-Mass System** (87-APM-19)
H. A. Downey, Jr. and D. B. Bogy

367 **The Normal Impact of an Elastic Rod-Mass System on a Viscoelastic Half Space** (87-APM-26)
H. A. Downey, Jr. and D. B. Bogy

373 **Impact on Ceramic Targets**
M. Mayseless, W. Goldsmith, S. P. Virostek, and S. A. Finnegan

379 **Plastic Stress Intensity Factors in Steady Crack Growth**
P. Ponte Castañeda

388 **Energy Release Rates and Related Balance Laws in Linear Elastic Defect Mechanics** (87-APM-33)
J. W. Eischen and G. Herrmann

393 **Subsurface Cracks Under Conditions of Slip, Stick, and Separation Caused by a Moving Compressive Load** (87-APM-29)
S. D. Sheppard, J. R. Barber, and M. Comninou

399 **Energy Release Rates in a Fiber-Reinforced Strip** (87-APM-20)
L. F. Mannion

403 **Static Loads in Layered Halfspaces**
E. Kausel and S. H. Seale

409 **An Approach to Calculating Random Vibration Integrals** (87-APM-18)
P-T. D. Spanos

414 **Exact Stationary-Response Solution for Second Order Nonlinear Systems Under Parametric and External White-Noise Excitations** (87-APM-30)
Y. Yong and Y. K. Lin

419 **Response Bounds for Linear Underdamped Systems** (87-APM-34)
K. H. Yae and D. J. Inman

(Contents continued on Inside Back Cover)

Downloaded 04 May 2010 to 171.66.16.49. Redistribution subject to ASME license or copyright; see http://www.asme.org/terms/Terms_Use.cfm

CONTENTS (CONTINUED)

424 **Kane's Equations With Undetermined Multipliers – Application to Constrained Multibody Systems** (87-APM-36)
J. T. Wang and R. L. Huston

430 **Response Bounds for Nonclassically Damped Mechanical Systems Under Transient Loads** (87-APM-31)
D. W. Nicholson

434 **Nonstationary Response Analysis of a Duffing Oscillator by the Wiener-Hermite Expansion Method** (87-APM-22)
I. I. Orabi and G. Ahmadi

441 **Constituent Diffusion in a Deformable Thermoelastic Solid** (87-APM-16)
S. P. Girrens and F. W. Smith

447 **Discharge From a Vessel Through an Axisymmetric Control Valve** (87-APM-23)
W. L. Chow, Alice A. L. Ting, and P. H. Tsai

BRIEF NOTES

The Strain-Energy Density of Compressible, Rubber-Like Axishells — **J. G. Simmonds** — 453

An Approximation for Deep Crack-Front Perturbation — **L. R. F. Rose** — 454

On the Mechanical Properties of Electro-Rheological Fluids — **N. G. Stevens, J. L. Sproston, and R. Stanway** — 456

A Path-Independent Integral for Plates — **K. B. Broberg** — 458

A Simple Analysis for the Blowup Phenomenon of Inelastic Members in Compression — **P. Vielsack** — 459

Sudden Loading of an Orthotropic Plate Containing a Central Crack — **M. K. Kassir and J. Xu** — 460

The Effect of Pore Fluid Flow on Extrusion — **E. P. Fahrenthold and J. B. Cheatham, Jr.** — 462

464 Surface Waves Perturbed by Rotation — **T. Wren and J. S. Burdess**

466 A Differential Effective Medium Theory With a Composite Sphere Embedding — **Y. Benveniste**

468 Transient Waves in a Beam Excited by Sinusoidal Edge Shear Force — **W. L. Hallauer, Jr.**

470 *Interface Stress Singularities at a Notch Tip in Antiplane Shear* — **D. Durban and E. Ore**

472 On the Singular Nature of Linearization of Certain Constrained Theories of Shells — **M. B. Rubin**

474 *The Shrink Fit With Nonlinearly Hardening Elastic-Plastic Hub* — **Udo Gamer**

476 Forced Flexural Motions of Plates — **P. B. Beaudan and H. Reismann**

DISCUSSION

479 **Discussion on a previously published paper by E. Suhir**

479 **Discussion on a previously published paper by S. S. Wang, E. S.-M. Chim, and H. Suemasu**

BOOK REVIEWS

481 ***Introduction to Continuum Damage Mechanics by*** **L. M. Kachanov** . . . Reviewed by **D. Krajcinovic**

481 ***Photoelasticity, Proceedings of the International Symposium on Photoelasticity, Tokyo, 1986, edited by*** **M. Nishida and K. Kawata** . . . Reviewed by **A. S. Kobayashi**

482 ***Engineering Rheology by*** **R. I. Tanner** . . . Reviewed by **R. S. Rivlin**

482 ***Finite Difference Methods in Dynamics of Continuous Media by*** **J. L. Davis** . . . Reviewed by **G. Ravichandran**

483 ***Numerical Methods in Engineering and Science by*** **G. de Vahl Davis** . . . Reviewed by **P. D. Richardson**

483 Books Received by the Office of the Technical Editor

440, 484, 485 Worldwide Mechanics Meeting List

262 IUTAM Symposium on Structural Optimization

268 17th International Congress of Theoretical and Applied Mechanics

279 Proposals to Host a IUTAM Symposium

286 IUTAM Symposium on Elastic Wave Propagation

291 Symposium on Three-Dimensional Fracture Processes

480 Change of Address Form

486 Postdoctoral Research Awards

298, 310, 314, 322, 358 378, 387, 402, 408, 413 Applied Mechanics Symposium Proceedings

Downloaded 04 May 2010 to 171.66.16.49. Redistribution subject to ASME license or copyright; see http://www.asme.org/terms/Terms_Use.cfm

Optimal Beam and Plate Foundations for Minimum Compliance

R. H. Plaut
Professor,
Department of Civil Engineering,
Virginia Polytechnic Institute
and State University,
Blacksburg, VA 24061
Mem. ASME

Uniform beams and circular plates on nonuniform elastic foundations are considered. They are subjected to a uniformly distributed load and have various boundary conditions. For a specified total stiffness of the foundation, the distribution of foundation stiffness is determined which minimizes the compliance (i.e., the work done by the applied load). The optimal solutions for the beams consist of either a single elastic support or a region of uniform foundation bounded by elastic supports (except at free ends). For the plates, there is a central, circular region with a uniform foundation, bounded by a circular elastic support. In comparison to a uniform foundation, the decrease in compliance may be substantial.

Introduction

Beams and circular plates attached to an elastic foundation of the Winkler type are considered. The beams and plates are uniform and elastic, and are subjected to a uniformly distributed load. The foundation has a specified total stiffness, but its stiffness distribution is variable. The objective is to determine the foundation stiffness distribution which will minimize the compliance (i.e., the work done by the load).

Optimization of elastic foundations was treated previously in three papers. A pinned-pinned beam was considered by Szelag and Mróz (1979). For specified fundamental frequency of free vibrations, the total foundation stiffness was minimized. In (Taylor and Bendsøe, 1984), a beam resting on a nonuniform foundation was displaced downward at its ends, and the foundation stiffness distribution was chosen to minimize the maximum foundation pressure. The present paper is a continuation of the work presented in Dems et al. (to appear), where the compliance or another deflection measure was minimized for given total foundation stiffness. Results were obtained there for beams attached to foundations of piecewise constant stiffness.

Both beams and plates are considered here. The following sets of boundary conditions are treated for the beams: pinned-pinned, clamped-clamped, clamped-pinned, and clamped-free. For the plates, the circular edge is either simply supported or clamped. The optimal solutions involve regions of uniform foundation stiffness and regions of no foundation, separated by elastic supports.

Contributed by the Applied Mechanics Division for presentation at the 1987 Applied Mechanics, Biomechanics, and Fluids Engineering Conference, Cincinnati, OH, June 14–17, 1987, of the American Society of Mechanical Engineers.

Discussion of this paper should be addressed to the Editorial Department, ASME, United Engineering Center, 345 East 47th Street, New York, N.Y. 10017, and will be accepted until two months after final publication of the paper itself in the JOURNAL OF APPLIED MECHANICS. Manuscript received by ASME Applied Mechanics Division, August 5, 1986.

Paper No. 87-APM-24.

Optimal Foundations for Beams

Consider a uniform elastic beam with length L and bending stiffness EI, subjected to a downward, uniformly distributed load q. The beam is attached to an elastic foundation with stiffness (per unit length) $K(X) \geq 0$, $0 \leq X \leq L$, and also possibly to elastic supports (i.e., concentrated springs) with stiffnesses $C_i \geq 0$ at $X = L_i$, $i = 1, \ldots, n$. It is assumed that $K(X)$ is continuous except possibly at the elastic supports. The downward deflection of the beam is denoted $W(X)$.

Define the nondimensional quantities

$$x = X/L, \quad a_i = L_i/L, \quad w = (EI/qL^4)W, \tag{1}$$
$$k = (L^4/EI)K, \quad c_i = (L^3/EI)C_i.$$

The equilibrium equation is given by

$$w''''(x) + k(x)w(x) = 1, \tag{2}$$

and at $x = a_i$ the functions w, w', and w'' are continuous, while

$$w'''(a_i^-) - w'''(a_i^+) = c_i w(a_i). \tag{3}$$

The (nondimensional) total foundation stiffness K_T is specified, i.e.,

$$\int_0^1 k(x)dx + \sum_{i=1}^{n} c_i = K_T, \tag{4}$$

and the compliance G, given by

$$G = \int_0^1 w(x)dx, \tag{5}$$

is to be minimized. The design variables are $k(x)$, c_i, and a_i.

With the use of the calculus of variations, the following optimality conditions are obtained (Dems et al., to appear):

$$w^2(x) = \mu \text{ if } k(x) > 0; \tag{6}$$

$$w^2(a_i) = \mu \text{ if } c_i > 0; \tag{7}$$

and

$$2c_i w(a_i) w'(a_i) + [k(a_i^-) - k(a_i^+)][w^2(a_i) - \mu] = 0, \tag{8}$$

Copyright © 1987 by ASME
Downloaded 03 May 2010 to 171.66.16.27. Redistribution subject to ASME license or copyright; see http://www.asme.org/terms/Terms_Use.cfm

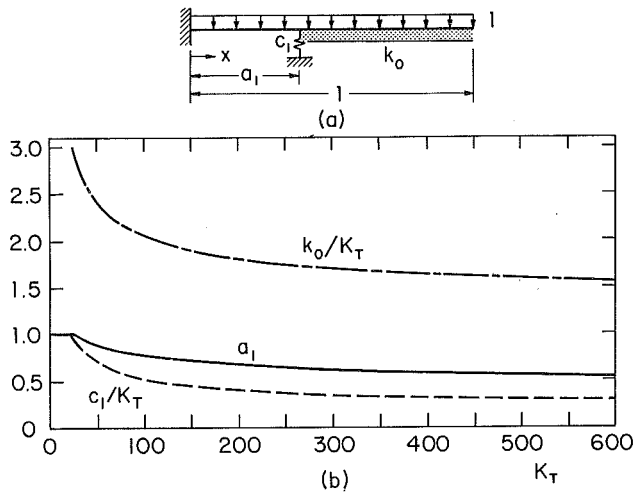


Fig. 1 Cantilever

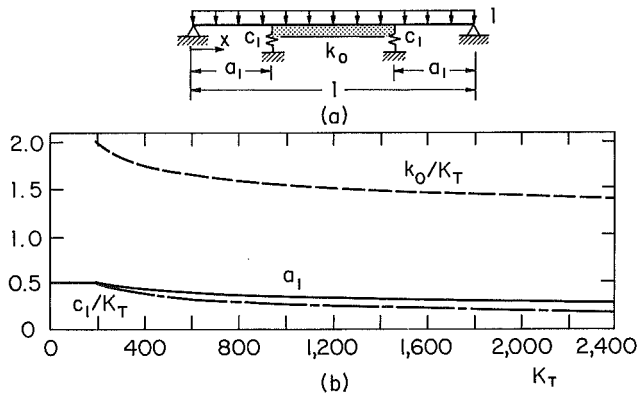


Fig. 2 Pinned-pinned beam

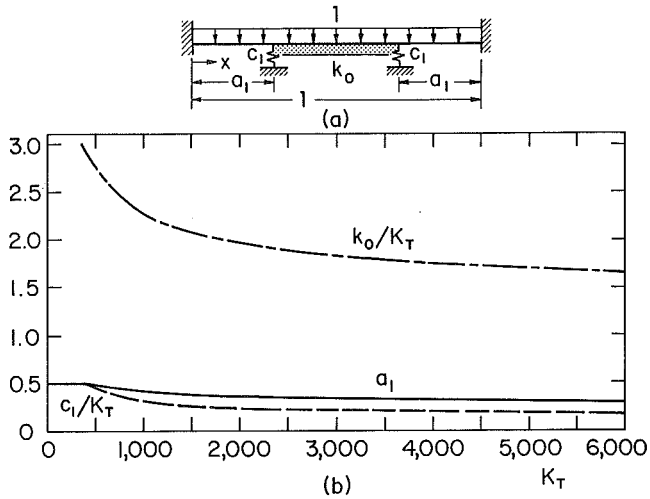


Fig. 3 Clamped-clamped beam

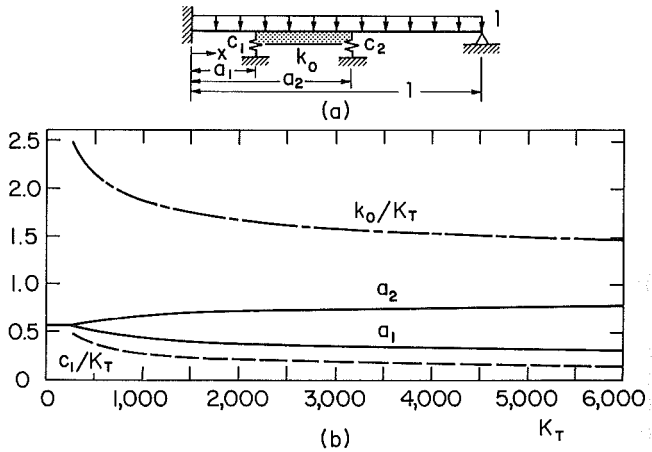


Fig. 4 Clamped-pinned beam

where μ is a constant. Since $k(x)$ is continuous except at elastic supports, equation (8) reduces to $w(a_i)w'(a_i)=0$. Also, it follows from equations (2) and (6) that $k=1/\sqrt{\mu}$ if $k\neq 0$.

For the first example, consider a cantilever which is clamped at $x=0$ and free at $x=1$. In the optimal solution, $k(x)=0$ for $0<x<a_1$ and $k(x)=k_o$, a constant, for $a_1<x<1$, as shown in Fig. 1(*a*). A similar type of optimal support was obtained in an example of Mróz and Rozvany (1975). One can show here that the optimal values of a_1, c_1, and k_o satisfy the equations

$$K_T a_1^4 + 48a_1 = 72, \quad c_1 = 24/a_1^3, \quad k_o = 72/a_1^4 \tag{9}$$

if $K_T > 24$. If $K_T \leq 24$, the optimal solution only consists of an elastic support with stiffness $c_1 = K_T$ at $x=1$. The results are plotted in Fig. 1(*b*). When $K_T = 24$, the optimal compliance is 35 percent of that for the reference case of a uniform foundation ($k_o = K_T$). This percentage increases as K_T increases. As $K_T \to \infty$, one finds that $a_1 \to 0$ and the optimal foundation approaches a uniform one along the entire beam.

The optimal foundation for a pinned-pinned beam consists of elastic supports with stiffness c_1 at $x=a_1$ and $x=1-a_1$, and a uniform foundation with $k(x)=k_o$ in the section $a_1<x<1-a_1$, if $K_T>192$, as depicted in Fig. 2(*a*). Optimal values of a_1, c_1, and k_o are obtained from the equations

$$K_T a_1^4 + 24a_1 = 24, \quad c_1 = 12/a_1^3, \quad k_o = 24/a_1^4. \tag{10}$$

If $K_T \leq 192$, there is only a single spring at $x=1/2$. Results are presented in Fig. 2(*b*). When $K_T = 192$, the optimal compliance is 65 percent of that for a uniform foundation. This percentage increases as K_T increases. As $K_T \to \infty$, one again finds that $a_1 \to 0$, $c_1 \to 0$, and $k_o \to K_T$.

For a clamped-clamped beam, the optimal foundation is similar in form to that for a pinned-pinned beam and is shown in Fig. 3(*a*). If $K_T > 384$, the optimal values of a_1, c_1, and k_o are determined from the equations

$$K_T a_1^4 + 96a_1 = 72, \quad c_1 = 24/a_1^3, \quad k_o = 72/a_1^4. \tag{11}$$

If $K_T \leq 384$, there is a single spring at $x=1/2$. The results are plotted in Fig. 3(*b*). As before, $a_1 \to 0$ as $K_T \to \infty$.

Finally, consider a beam that is clamped at $x=0$ and pinned at $x=1$, as shown in Fig. 4(*a*). If $K_T \leq 279.9$, the optimal solution consists of a single spring at a position which varies from $x=0.578$ for $K_T=0$ to $x=0.568$ for $K_T=279.9$. If $K_T > 279.9$, there are elastic supports with stiffnesses c_1 and c_2 at $x=a_1$ and $x=a_2$, respectively, and a uniform foundation of stiffness k_o between them, as shown in Fig. 4(*a*). Optimal values are determined from the equations

$$K_T a_1^4 + 75.35a_1 = 72, \quad a_2 = 1 - 0.76a_1, \quad c_1 = 24/a_1^3,$$
$$c_2 = 1.14\, c_1, \quad k_o = 72/a_1^4. \tag{12}$$

The quantities a_1, a_2, c_1/K_T, and k_o/K_T are plotted versus K_T in Fig. 4(*b*). As K_T is increased from 279.9 to ∞, one finds that k_o/K_T decreases from 2.47 to 1, c_1/K_T decreases from 0.47 to 0, $a_1 \to 0$, and $a_2 \to 1$. Compared to a uniform foundation, the decrease in the compliance varies up to 17 percent.

Optimal Foundations for Circular Plates

Consider a uniform, elastic, circular plate with radius R_o and flexural rigidity D, subjected to a downward, uniformly distributed load Q. The plate is attached to an axisymmetric elastic foundation with stiffness (per unit area) $K(R) \geq 0$,

Downloaded 03 May 2010 to 171.66.16.27. Redistribution subject to ASME license or copyright; see http://www.asme.org/terms/Terms_Use.cfm

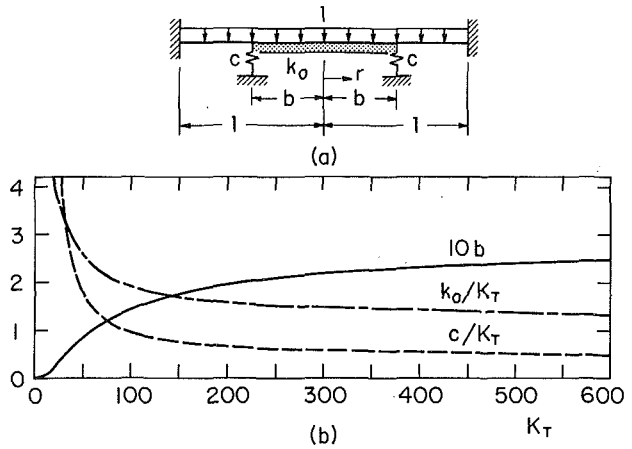


Fig. 5 Clamped circular plate

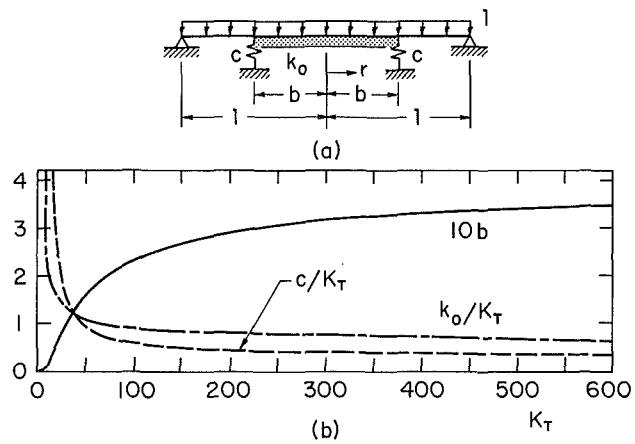


Fig. 6 Simply supported circular plate ($\nu = 0.3$)

$0 \le R < R_o$, and also possibly to a circular elastic support with stiffness (per unit length) $C \ge 0$ at $R = B$. It is assumed that $K(R)$ is continuous except possibly at $R = B$. The axisymmetric downward deflection of the plate is denoted $W(R)$.

Define the nondimensional quantities

$$r = R/R_o, \quad b = B/R_o, \quad w = (D/QR_o^4)W,$$
$$k = (R_o^4/D)K, \quad c = (R_o^4/D)C. \tag{13}$$

The equilibrium equation is given by

$$\nabla^2 \nabla^2 w(r) + k(r) w(r) = 1,$$

where
$$\nabla^2 = \frac{d^2}{dr^2} + \frac{1}{r}\frac{d}{dr}. \tag{14}$$

At $r = b$, the functions w, w', and w'' are continuous, while

$$V_r(b^-) - V_r(b^+) = -cw(b) \tag{15}$$

where

$$V_r = -[w'' + (1/r)w']'. \tag{16}$$

The total foundation stiffness K_T is specified, i.e.,

$$2\pi \int_0^1 k(r) r dr + 2\pi bc = K_T, \tag{17}$$

and the compliance G, given by

$$G = 2\pi \int_0^1 w(r) r dr, \tag{18}$$

is to be minimized. The design variables are $k(r)$, c, and b.

For these plates, the optimality conditions again include the condition

$$w^2(r) = \mu \text{ if } k(r) > 0. \tag{19}$$

From equations (14) and (19), it then follows that $k = 1/\sqrt{\mu}$ if $k \neq 0$. The optimal foundations for circular plates which are either clamped or simply supported at the edge $r = 1$ consist of a uniform foundation with $k(r) = k_o$ in a central region $0 \le r < b$, a circular elastic support with stiffness c at $r = b$, and no foundation for $b < r < 1$, as shown in Figs. 5(*a*) and 6(*a*). Optimal values of b, c, and k_o are determined from the following equations:

$$\{1 - b^2 - 4b^4 \ell nb - 64g[1 - b^2 + (1 + b^2)\ell nb]\} K_T = 32\pi g, \tag{20}$$
$$c = (g + 2b^2)K_T/(2\pi g), \quad k_o = -2K_T/(\pi g),$$

where

$$g = (1 - b^2)^2/(1 - b^2 + 2\ell nb) \tag{21}$$

for clamped plates and

$$g = [3 + \nu - 2(1 + \nu)b^2 - (1 - \nu)b^4]/[(1 - \nu)(b^2 - 1) + 2(1 + \nu)\ell nb] \tag{22}$$

for simply supported plates, with ν denoting Poisson's ratio.

Results are presented in Fig. 5(*b*) for clamped plates and in Fig. 6(*b*) for simply supported plates with $\nu = 0.3$. The region $0 \le r < b$ increases in size as K_T increases. For clamped plates, as $K_T \to \infty$, one obtains $b \to 0.28$, $c \to 0.41K_T$, and $k_o \to 1.23K_T$. For simply supported plates with $\nu = 0.3$, one finds that $b \to 0.38$, $c \to 0.29K_T$, and $k_o \to 0.68K_T$ as $K_T \to \infty$.

Concluding Remarks

Optimal distributions of foundation stiffness have been determined for some problems involving beams and circular plates. In order to simplify the analysis, the applied loading was chosen to be uniformly distributed over the structure and the objective function was chosen to be the compliance (which is then proportional to the displaced area or volume of the structure). This caused the adjoint problem to be identical to the original problem (Dems et al., to appear), and hence the governing equations, including the optimality conditions, did not involve additional adjoint variables (i.e., Lagrange multipliers). It also led to optimal foundations which were uniform over a portion of the structure. The deflections in those regions were constant, and elastic supports were located at the edges of those regions to allow the deflections outside the regions to vary and satisfy the equilibrium equation and boundary conditions.

The optimal solutions for the beams and plates have some similar characteristics. However, two differences are worth noting. As the total foundation stiffness K_T is decreased, the foundation region disappears at a positive value of K_T for the beam examples. For the plates, the foundation is present for all positive values of K_T and only disappears as $K_T \to 0$. A second difference occurs as $K_T \to \infty$. For the beams, the foundation spreads out to cover the entire beam length. For the plates, there is a limit to the foundation region, which covers a maximum of 7.8 percent of the plate area when the edge is clamped and 14.4 percent when the edge is simply supported (corresponding to nondimensional radii of $b = 0.28$ and $b = 0.38$, respectively).

References

Dems, K., Plaut, R. H., Banach, A. S., and Johnson, L. W., "Optimization of Elastic Foundation for Minimum Beam Deflection," *International Journal of Solids and Structures*, to appear.

Mróz, Z., and Rozvany, G. I. N., 1975, "Optimal Design of Structures with Variable Support Conditions," *Journal of Optimization Theory and Applications*, Vol. 15, pp. 85-101.

Szelag, D., and Mróz, Z., 1979, "Optimal Design of Vibrating Beams with Unspecified Support Reactions," *Computer Methods in Applied Mechanics and Engineering*, Vol. 19, pp. 333-349.

Taylor, J. E., and Bendsøe, M. P., 1984, "An Interpretation for Min-max Structural Design Problems Including a Method for Relaxing Constraints," *International Journal of Solids and Structures*, Vol. 20, pp. 301-314.

Downloaded 03 May 2010 to 171.66.16.27. Redistribution subject to ASME license or copyright; see http://www.asme.org/terms/Terms_Use.cfm

Nonlinear Beam Kinematics by Decomposition of the Rotation Tensor

D. A. Danielson
Associate Professor,
Department of Mathematics,
Naval Postgraduate School,
Monterey, CA 93943
Mem. ASME

D. H. Hodges[1]
Research Scientist and
Theoretical Group Leader,
Rotorcraft Dynamics Division,
Aeroflightdynamics Directorate,
US Army Aviation Research & Technology
Activity (AVSCOM),
Ames Research Center,
Moffett Field, CA 94035

A simple matrix expression is obtained for the strain components of a beam in which the displacements and rotations are large. The only restrictions are on the magnitudes of the strain and of the local rotation, a newly-identified kinematical quantity. The local rotation is defined as the change of orientation of material elements relative to the change of orientation of the beam reference triad. The vectors and tensors in the theory are resolved along orthogonal triads of base vectors centered along the undeformed and deformed beam reference axes, so Cartesian tensor notation is used. Although a curvilinear coordinate system is natural to the beam problem, the complications usually associated with its use are circumvented. Local rotations appear explicitly in the resulting strain expressions, facilitating the treatment of beams with both open and closed cross sections in applications of the theory. The theory is used to obtain the kinematical relations for coupled bending, torsion, extension, shear deformation, and warping of an initially curved and twisted beam.

1 Introduction

Beam theory has a long history (see Timoshenko, 1983). An understanding of fundamental aspects of beam theory may be obtained from the book by Wempner (1981). A summary of recent literature concerned chiefly with nonlinear beam theory is given by Hodges (1987b). In this paper our purpose is to obtain, by means of the polar decomposition theorem, an accurate but simple expression for the strain in a beam or rod undergoing large deflections. By this theorem, the change of configuration for any material element in the beam is decomposed into a pure strain and a pure rotation. A similar decomposition was obtained for thin shells by Simmonds and Danielson (1970, 1972).

The concept of decomposition was applied to beams in unpublished work by the second author in which the novel idea of separating the rotation into two parts was introduced—an arbitrarily large *global* rotation associated with the beam reference triad, and a moderately small *local* rotation associated with warp, shear, and other deformations. The physically reasonable assumptions of small strain and moderate *local* rotation led to a rather simple kinematical expression that was valid for arbitrarily large deflections and rotations of the reference triad. The original analysis was carried out entirely in terms of matrices, however, and consequently it was rather tedious, imprecise, and difficult to understand.

Interaction between the authors led to introduction of dyads into the analysis and attendant simplifications and improvements. The present paper presents a development of the theory based on Cartesian tensors, together with a comprehensive example. Hodges (1987b) embodies a rectified matrix derivation in order to accommodate engineers who are unfamiliar with tensor notation. The present derivation, however, offers far greater insight into the nature of the kinematical assumptions. It is believed that decomposition of the rotation tensor is new to beam literature and that the simplified kinematical relations obtained go beyond others in rigor and generality.

2 Beam Geometry and the Global Rotation Tensor

Let x_1 denote length along a reference line r within an undeformed beam. Let x_α denote lengths along lines orthogonal to the reference line r. (Here and throughout the paper Greek indices assume values 2 and 3 while Latin indices assume values 1, 2, and 3.) A particle of the beam is located from a fixed point in space by the position vector $\mathbf{r}(x_1, x_2, x_3)$. The covariant base vectors $\mathbf{g}_i$ are tangent to the coordinate curves:

$$\mathbf{g}_i(x_1,x_2,x_3)=\frac{\partial \mathbf{r}}{\partial x_i} \tag{1}$$

Contravariant base vectors can be obtained by standard means (see Budiansky, 1983, or Simmonds, 1982):

$$\mathbf{g}^i(x_1,x_2,x_3)=\frac{1}{2\sqrt{g}}\, e_{ijk}\mathbf{g}_j\times\mathbf{g}_k \tag{2}$$

[1]Presently Professor, School of Aerospace Engineering, Georgia Institute of Technology, Atlanta, GA 30332.

Contributed by the Applied Mechanics Division for presentation at the 1987 Applied Mechanics, Biomechanics, and Fluids Engineering Conference, Cincinnati, OH, June 14–17, 1987, of the American Society of Mechanical Engineers.

Discussion of this paper should be addressed to the Editorial Department, ASME, United Engineering Center, 345 East 47th Street, New York, N.Y. 10017, and will be accepted until two months after final publication of the paper itself in the JOURNAL OF APPLIED MECHANICS. Manuscript received by ASME Applied Mechanics Division, May 3, 1986; final revision, September 2, 1986.

Paper No. 87-APM-17.

Copyright © 1987 by ASME
Downloaded 03 May 2010 to 171.66.16.27. Redistribution subject to ASME license or copyright; see http://www.asme.org/terms/Terms_Use.cfm

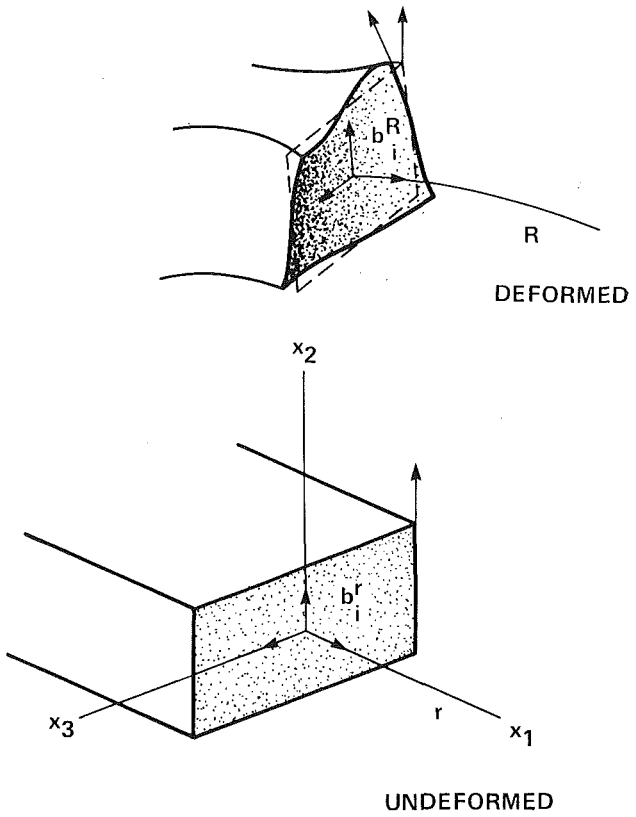


Fig. 1 Beam of thin rectangular cross section

Here

$$g = \det(\mathbf{g}_i \cdot \mathbf{g}_j) \tag{3}$$

and e_{ijk} are the components of the permutation tensor in a Cartesian coordinate system. (Repeated indices are always summed over their range.) The reference cross section at the point x_1^* is the surface whose position vector is $\mathbf{r}(x_1^*, x_2, x_3)$.

In a similar manner, consider the deformed state configuration. The locus of material points along $\mathbf{r}$ has now assumed a different curved line denoted by R. The particle which had position vector $\mathbf{r}(x_1, x_2, x_3)$ in the undeformed beam now has position vector $\mathbf{R}(x_1, x_2, x_3)$, relative to the same fixed point. The covariant base vectors $\mathbf{G}_i$ are tangent to the coordinate curves of the deformed beam:

$$\mathbf{G}_i(x_1, x_2, x_3) = \frac{\partial \mathbf{R}}{\partial x_i} \tag{4}$$

We will eventually resolve the position vectors along triads of unit base vectors on the undeformed and deformed reference lines. At each point along r define an orthogonal reference triad $\mathbf{b}_i^r(x_1)$ tangent to the coordinate curves at r with $\mathbf{b}_1^r$ tangent to r (see Fig. 1). At each point along R introduce an orthogonal reference triad $\mathbf{b}_i^R(x_1)$ such that $\mathbf{b}_\alpha^R(x_1^*) = \mathbf{G}_\alpha^*$, where $\mathbf{G}_\alpha^*$ denotes the part of $\mathbf{G}_\alpha(x_1^*, 0, 0)$ arising from the rigid body rotation of the cross section at x_1^*. Note that $\mathbf{b}_1^R = \mathbf{b}_2^R \times \mathbf{b}_3^R$ is not necessarily tangent to R unless the Euler-Bernoulli hypothesis (that the reference cross section remains normal to R when the beam is deformed) is adopted.

Rotation from $\mathbf{b}_i^r$ to $\mathbf{b}_i^R$ is accomplished by pre-dot multiplication with an orthogonal tensor which we call the global rotation tensor $\mathbf{C}^{Rr}$.

$$\mathbf{b}_i^R = \mathbf{C}^{Rr} \cdot \mathbf{b}_i^r = C_{ij}^{Rr} \mathbf{b}_j^r \tag{5}$$

The global rotation tensor can be represented as a linear combination of the dyads formed from the base vectors:

$$\mathbf{C}^{Rr} = \mathbf{b}_i^R \mathbf{b}_i^r \tag{6}$$

Rotation from $\mathbf{b}_i^R$ to $\mathbf{b}_i^r$ is accomplished by pre-dot multiplication with the rotation tensor $\mathbf{C}^{rR}$.

$$\mathbf{b}_i^r = \mathbf{C}^{rR} \cdot \mathbf{b}_i^R \tag{7}$$

The components C_{ij}^{Rr} are the direction cosines

$$C_{ij}^{Rr} = \mathbf{b}_i^R \cdot \mathbf{b}_j^r \tag{8}$$

The tensors $\mathbf{C}^{Rr}$ and $\mathbf{C}^{rR}$ are the transpose and inverse of each other, so that

$$\mathbf{C}^{Rr} \cdot \mathbf{C}^{rR} = \mathbf{I} \tag{9}$$

where $\mathbf{I}$ is the identity tensor. Note that $\mathbf{I}$ can be represented by a dyadic $\mathbf{b}_i \mathbf{b}_i$ in which $\mathbf{b}_i$ is any orthonormal base vector.

3 Strain and the Local Rotation Tensor

Consider the deformation gradient tensor $\mathbf{A}$ defined by

$$\mathbf{A} = \mathbf{G}_i \mathbf{g}^i \tag{10}$$

The polar decomposition theorem states that $\mathbf{A}$ can be uniquely decomposed into an orthogonal rotation tensor $\mathbf{C}$ dotted into a symmetric right stretch tensor $\mathbf{U}$ (see Ogden, 1984):

$$\mathbf{A} = \mathbf{C} \cdot \mathbf{U} \tag{11}$$

Note that

$$\mathbf{A} \cdot \mathbf{g}_i = \mathbf{C} \cdot \mathbf{U} \cdot \mathbf{g}_i = \mathbf{G}_i \tag{12}$$

This implies that $\mathbf{g}_i$ is transformed by first undergoing a pure strain to an intermediate state $\mathbf{U} \cdot \mathbf{g}_i$ and then undergoing a rotation to coincide with $\mathbf{G}_i$. The rotation may be decomposed into two parts: a large rotation equal to the *global* rotation $\mathbf{C}^{Rr}$ and an additional rotation which we call *local* rotation. Note that the local rotation may not vanish at the reference line.[2]

For the purpose of eventually allowing only small local rotation, we use the following representation for the local rotation tensor (see Sedov, 1966):

$$\exp(\tilde{\phi}) = \mathbf{I} + \tilde{\phi} + \frac{\tilde{\phi}^2}{2} + \frac{\tilde{\phi}^3}{6} + \ldots \tag{13}$$

(Here and hereafter a tilde over a tensor or matrix denotes that it is skew-symmetric) The antisymmetric tensor $\tilde{\phi}$ is related to the local rotation vector $\boldsymbol{\phi}$ by

$$\tilde{\phi} = \boldsymbol{\phi} \times \mathbf{I} \tag{14}$$

The direction of $\boldsymbol{\phi}$ is along the axis of local rotation and the amplitude of $\boldsymbol{\phi}$ is the angle of local rotation. Various other finite rotation vectors have been used in the literature, all differing from $\boldsymbol{\phi}$ in amplitude only (for example, see Simmonds and Danielson, 1970, 1972; Reissner, 1973; or Kane et al., 1983).

We thus have the decomposition of the total rotation into local rotation and global rotation:

$$\mathbf{C} = \exp(\tilde{\phi}) \cdot \mathbf{C}^{Rr} \tag{15}$$

A physical feeling for this may be gained by studying Fig. 1 and by experimenting with a rectangular rubber eraser. We picture an initially straight beam of thin rectangular cross section with an arrow embedded in its side. The beam is then bent, twisted, and stretched. The final orientation of the arrow may be obtained by two rotations. First the cross section, with arrow attached, undergoes a large rigid body rotation to bring the base vectors $\mathbf{b}_i^r$ into coincidence with $\mathbf{b}_i^R$. Then the cross section, with the arrow remaining embedded in its side, undergoes a small warping to bring it into its final orientation.

The Jaumann-Biot-Cauchy strain tensor $\boldsymbol{\Gamma}$ is defined by

[2] It is possible to formulate the theory so that the local rotation always vanishes at the reference line. We could choose $\mathbf{b}_i^R = \mathbf{C}(x_1, 0, 0) \cdot \mathbf{b}_i^r$. Hodges (1987b) defines the global rotation at the reference axis to be equal to the total rotation there. The present analysis results in the simplest algebra.

Downloaded 03 May 2010 to 171.66.16.27. Redistribution subject to ASME license or copyright; see http://www.asme.org/terms/Terms_Use.cfm

$$\boldsymbol{\Gamma} = \mathbf{U} - \mathbf{I} \tag{16}$$

Other strain tensors based on $\mathbf{U}$ could be chosen. With this definition when the strains are small, as in subsequent sections, the components of $\boldsymbol{\Gamma}$ are simply the relative elongations and shears of material elements lying along the coordinate curves. Use of equations (9), (11), (15), and the above leads us to

$$\mathbf{C}^{Rr} \cdot \boldsymbol{\Gamma} \cdot \mathbf{C}^{rR} = \exp(-\tilde{\boldsymbol{\phi}}) \cdot \mathbf{A} \cdot \mathbf{C}^{rR} - \mathbf{I} \tag{17}$$

The ensuing formulas will look simpler if we now write the tensors in component form. Since $\boldsymbol{\Gamma}$ is a Lagrangean strain tensor, it is appropriate to resolve it along the *undeformed* beam reference triad $\mathbf{b}_i^r$ yielding

$$\boldsymbol{\Gamma} = \mathbf{b}_i^r \gamma_{ij} \mathbf{b}_j^r \tag{18}$$

Since the left side of equation (17) then becomes $\mathbf{b}_i^R \gamma_{ij} \mathbf{b}_j^R$, it is appropriate to resolve the tensor $\tilde{\boldsymbol{\phi}}$ along the *deformed* beam triad $\mathbf{b}_i^R$ yielding

$$\tilde{\boldsymbol{\phi}} = \mathbf{b}_i^R \tilde{\phi}_{ij} \mathbf{b}_j^R \tag{19}$$

Comparison of equations (14) and the above leads to resolution of the local rotation vector $\boldsymbol{\phi}$ along the triad $\mathbf{b}_i^R$ yielding

$$\boldsymbol{\phi} = \phi_i \mathbf{b}_i^R = -\frac{1}{2} e_{ijk} \tilde{\phi}_{jk} \mathbf{b}_i^R \tag{20}$$

It follows from equation (17) that the deformation gradient tensor is resolved along the *mixed* bases

$$\mathbf{A} = \mathbf{b}_i^R A_{ij} \mathbf{b}_j^r \tag{21}$$

Our formula (17) thus becomes in matrix form

$$\gamma = \exp(-\tilde{\phi}) A - I \tag{22}$$

4 Simplifications for Small Strain and Local Rotation

Our expression (22) for the strain is exact but very complex. Let ϵ and ϕ denote the maximum absolute values of the components of the matrices γ and $\tilde{\phi}$, respectively:

$$\begin{aligned} &\max |\gamma_{ij}(x_1, x_2, x_3)| = \epsilon << 1 \\ &\max |\tilde{\phi}_{ij}(x_1, x_2, x_3)| = \phi < 1 \end{aligned} \tag{23}$$

We will retain only terms of the lowest order in ϵ and ϕ. The Taylor expansion of $\exp(-\tilde{\phi})$ is easily obtained from equation (13):

$$\exp(-\tilde{\phi}) = I - \tilde{\phi} + \frac{\tilde{\phi}^2}{2} - \frac{\tilde{\phi}^3}{6} + O(\phi^4) \tag{24}$$

To expand A we first break it up into symmetric and antisymmetric components:

$$A = I + E + \tilde{A} \tag{25}$$

Here we have defined

$$\begin{aligned} E &= \frac{A + A^T}{2} - I \\ \tilde{A} &= \frac{A - A^T}{2} \end{aligned} \tag{26}$$

where A^T denotes the transpose of A. Substituting the above into equation (22) and solving for E, we obtain

$$E = \exp(\tilde{\phi})(I + \gamma) - I - \tilde{A} \tag{27}$$

Noting that the left side of equation (27) is symmetric, we can obtain an equation for $\tilde{A}$ by equating the right side of equation (27) with its transpose:

$$\tilde{A} = \frac{1}{2}[\exp(\tilde{\phi})(I + \gamma) - (I + \gamma)\exp(-\tilde{\phi})] \tag{28}$$

Using equation (24), we now expand the above in powers of $\tilde{\phi}$:

$$\tilde{A} = \tilde{\phi} + \frac{\tilde{\phi}^3}{6} + \frac{1}{2}(\gamma\tilde{\phi} + \tilde{\phi}\gamma) + O(\phi^4, \phi^2\epsilon) \tag{29}$$

Substituting equations (29) and (24) into (27), we obtain

$$E = \gamma + \frac{\tilde{\phi}^2}{2} + \frac{1}{2}(\tilde{\phi}\gamma - \gamma\tilde{\phi}) + O(\phi^4, \phi^2\epsilon) \tag{30}$$

Finally, we solve equation (30) for the strain

$$\gamma = E - \frac{\tilde{\phi}^2}{2} + \frac{1}{2}(E\tilde{\phi} - \tilde{\phi}E) + O(\phi^4, \phi^2\epsilon) \tag{31}$$

The question now is when can the higher order terms be neglected? We assume that ϵ can be neglected in comparison with unity. We also assume that $\phi = O(\epsilon^r)$. Two cases are of interest:

(1) *Small local rotation*: $r \geq 1$. A theory based on this assumption would be suitable for solid beams without thin cross sections or thick-walled beams with open or closed cross sections, where effects of local rotations would be expected to be negligible. The strain for this case reduces to

$$\gamma = E \tag{32}$$

(2) *Moderate local rotation*: $1/2 \leq r < 1$. A theory based on this assumption would be suitable for thin cross sections such as thin-walled open cross sections, thin strips, rotor blades, etc., where local rotations could be appreciable. This case yields the rotation from equation (29) and strain from equation (31) as

$$\begin{aligned} \tilde{\phi} &= \tilde{A} \\ \gamma &= E - \frac{\tilde{\phi}^2}{2} + \frac{1}{2}(E\tilde{\phi} - \tilde{\phi}E) \end{aligned} \tag{33}$$

The matrices E and $\tilde{A}$ are related to A by the definitions (26). The components of A follow from equations (10) and (21):

$$A_{ij} = (\mathbf{b}_i^R \cdot \mathbf{G}_k)(\mathbf{g}^k \cdot \mathbf{b}_j^r) \tag{34}$$

These components are rather easily obtained because in a beam theory it is convenient to resolve the base vectors of the undeformed state in the directions of the $\mathbf{b}_i^r$, and to resolve the base vectors of the deformed state in the directions of the $\mathbf{b}_i^R$. This will be illustrated by a comprehensive example in the next section.

5 Application to an Initially Curved and Twisted Beam

The position vector to points in any undeformed beam may be written as

$$\mathbf{r}(x_1, x_2, x_3) = \bar{\mathbf{r}}(x_1) + x_\alpha \mathbf{b}_\alpha^r \tag{35}$$

where $\bar{\mathbf{r}}(x_1) = \mathbf{r}(x_1, 0, 0)$ is the position vector to points on the reference line r. With this choice of coordinates the reference cross section is planar. The covariant base vectors are obtained from equation (1) by differentiation of equation (35). This may be accomplished using the formulas

$$\begin{aligned} \bar{\mathbf{r}}' &= \mathbf{b}_1^r \\ (\mathbf{b}_i^r)' &= \mathbf{k} \times \mathbf{b}_i^r = \tilde{\mathbf{k}} \cdot \mathbf{b}_i^r \end{aligned} \tag{36}$$

where primes denote differentiation with respect to x_1. Here $\mathbf{k} = k_i \mathbf{b}_i^r$ is the curvature vector of the undeformed beam (k_1 is the pretwist of the beam while k_α are components of the curvature of the reference line (see Love, 1944)) and $\tilde{\mathbf{k}}$ is the curvature tensor of the undeformed beam defined by

$$\tilde{\mathbf{k}} = \mathbf{k} \times \mathbf{I} = \mathbf{b}_i^r \tilde{k}_{ij} \mathbf{b}_j^r = -\mathbf{b}_i^r e_{ijl} k_l \mathbf{b}_j^r \tag{37}$$

The contravariant base vectors are obtained from equation (2). The final result is

Downloaded 03 May 2010 to 171.66.16.27. Redistribution subject to ASME license or copyright; see http://www.asme.org/terms/Terms_Use.cfm

$$\mathbf{g}^1 = \frac{\mathbf{b}_1^r}{\sqrt{g}}$$

$$\mathbf{g}^2 = \frac{x_3 k_1 \mathbf{b}_1^r}{\sqrt{g}} + \mathbf{b}_2^r \tag{38}$$

$$\mathbf{g}^3 = \frac{-x_2 k_1 \mathbf{b}_1^r}{\sqrt{g}} + \mathbf{b}_3^r$$

where we have obtained from equation (3) the relation

$$\sqrt{g} = 1 - x_2 k_3 + x_3 k_2 \tag{39}$$

We assume that the reference cross section does not distort in its plane.[3] Thus, the position vector to points in the deformed beam can be represented by

$$\mathbf{R}(x_1, x_2, x_3) = \bar{\mathbf{r}} + \mathbf{u} + x_\alpha \mathbf{b}_\alpha^R + \lambda\psi \mathbf{b}_1^R \tag{40}$$

Here $\mathbf{u} = u_i \mathbf{b}_i^r$ is the displacement vector of points on the reference line $\mathbf{r}$, $\lambda(x_2, x_3)$ is the Saint-Venant warping function for the local cross section, and $\psi(x_1)$ is the warp amplitude. The $\mathbf{b}_\alpha^R$ are chosen tangent to the x_α coordinate curves at R. The reference axis is chosen so that $\lambda(0, 0) = \lambda_\alpha(0, 0) = 0$ where $\lambda_\alpha = \partial\lambda/\partial x_\alpha$. The covariant base vectors of the deformed beam are obtained from equation (4) by differentiation of equation (40). This is accomplished using formulas analogous to equations (36):

$$\begin{aligned} \bar{\mathbf{R}}' &= (1 + \bar{\gamma}_{11})\mathbf{b}_1^R + 2\bar{\gamma}_{1\alpha}\mathbf{b}_\alpha^R \\ (\mathbf{b}_i^R)' &= \mathbf{K} \times \mathbf{b}_i^R = \tilde{\mathbf{K}} \cdot \mathbf{b}_i^R \end{aligned} \tag{41}$$

Here $\mathbf{K} = K_i \mathbf{b}_i^R$ is the curvature vector of the deformed beam (the components of $\mathbf{K}$ are $(1 + \bar{\gamma}_{11})$ times the twist and curvatures of the deformed beam), and the components $\tilde{K}_{ij} = -e_{ijl}K_l$ of the curvature tensor $\tilde{\mathbf{K}}$ of the deformed beam are in matrix form

$$\tilde{K} = -(C^{Rr})' C^{rR} + C^{Rr} \tilde{k} C^{rR} \tag{42}$$

The strains $\bar{\gamma}_{1i}(x_1) = \gamma_{1i}(x_1, 0, 0)$ at the reference line are obtained by evaluation of equations (33)–(34) at the reference line

$$\begin{aligned} \bar{\gamma}_{11} &= C_{11}^{Rr} - 1 + C_{1i}^{Rr}(u_i' + \tilde{k}_{ij} u_j) \\ 2\bar{\gamma}_{1\alpha} &= C_{\alpha 1}^{Rr} + C_{\alpha i}^{Rr}(u_i' + \tilde{k}_{ij} u_j) \end{aligned} \tag{43}$$

We thus have

$$\begin{aligned} \mathbf{G}_1 &= (1 + \bar{\gamma}_{11} - x_2 K_3 + x_3 K_2 + \lambda\psi')\mathbf{b}_1^R \\ &\quad + (2\bar{\gamma}_{12} - x_3 K_1 + \lambda\psi K_3)\mathbf{b}_2^R \\ &\quad + (2\bar{\gamma}_{13} + x_2 K_1 - \lambda\psi K_2)\mathbf{b}_3^R \\ \mathbf{G}_\alpha &= \mathbf{b}_\alpha^R + \lambda_\alpha \psi \mathbf{b}_1^R \end{aligned} \tag{44}$$

The components A_{ij} of the deformation gradient matrix may now be calculated from equations (34), (38), and (44). The result is

$$\begin{aligned} A_{11} &= \frac{1 + \bar{\gamma}_{11} + x_3 K_2 - x_2 K_3 + \lambda\psi' + \psi k_1 (x_3 \lambda_2 - x_2 \lambda_3)}{\sqrt{g}} \\ A_{21} &= \frac{2\bar{\gamma}_{12} - x_3(K_1 - k_1) + \lambda\psi K_3}{\sqrt{g}} \\ A_{31} &= \frac{2\bar{\gamma}_{13} + x_2(K_1 - k_1) - \lambda\psi K_2}{\sqrt{g}} \\ A_{12} &= \lambda_2 \psi \quad A_{13} = \lambda_3 \psi \\ A_{22} &= A_{33} = 1 \quad A_{23} = A_{32} = 0 \end{aligned} \tag{45}$$

Now let

$$\kappa_i = K_i - k_i \tag{46}$$

Components of the symmetric matrix E are obtained from equations (26) and (45):

$$\begin{aligned} E_{11} &= \frac{\bar{\gamma}_{11} + x_3 \kappa_2 - x_2 \kappa_3 + \lambda\psi' + \psi k_1 (x_3 \lambda_2 - x_2 \lambda_3)}{\sqrt{g}} \\ E_{12} = E_{21} &= \frac{2\bar{\gamma}_{12} - x_3 \kappa_1 + \lambda_2 \psi\sqrt{g} + \lambda\psi(\kappa_3 + k_3)}{2\sqrt{g}} \\ E_{13} = E_{31} &= \frac{2\bar{\gamma}_{13} + x_2 \kappa_1 + \lambda_3 \psi\sqrt{g} - \lambda\psi(\kappa_2 + k_2)}{2\sqrt{g}} \\ E_{22} &= E_{33} = E_{23} = E_{32} = 0 \end{aligned} \tag{47}$$

Components of the antisymmetric matrix $\tilde{\phi}$ are obtained from equations (26), (33), and (45):

$$\begin{aligned} \tilde{\phi}_{12} &= -\tilde{\phi}_{21} = -\phi_3 = \frac{-2\bar{\gamma}_{12} + x_3 \kappa_1 + \lambda_2 \psi\sqrt{g} - \lambda\psi(\kappa_3 + k_3)}{2\sqrt{g}} \\ \tilde{\phi}_{13} &= -\tilde{\phi}_{31} = \phi_2 = \frac{-2\bar{\gamma}_{13} - x_2 \kappa_1 + \lambda_3 \psi\sqrt{g} + \lambda\psi(\kappa_2 + k_2)}{2\sqrt{g}} \\ \tilde{\phi}_{11} &= \tilde{\phi}_{22} = \tilde{\phi}_{33} = 0; \quad \tilde{\phi}_{23} = \tilde{\phi}_{32} = \phi_1 = 0 \end{aligned} \tag{48}$$

From equation (32) the strain components for the small local rotation theory are the elements of the matrix E. The strain components for the moderate local rotation theory can now be obtained directly by substitution of E and $\tilde{\phi}$ into the second of equations (33). Note that the matrix $\tilde{\phi}$ contains some terms of the order of strains (i.e., $\bar{\gamma}_{1\alpha}$). Care should be taken to discard these terms when squared and when multiplied by any of the terms of matrix E. Note that it is not necessary, however, to introduce any *ad hoc* arguments to remove terms of the order of squares and products of the strain components. It may be desirable to make some simplifying assumptions about the magnitude of the initial curvatures, which affect the order of magnitude of the quantity $\sqrt{g} - 1$.

The elements of E have clear physical significance. We see that E_{11} is the extensional strain for the beam; $\bar{\gamma}_{11}$ is the strain of the reference line, terms involving κ_α are the bending strains, and the remaining terms are extensional strains related to warping. The off-diagonal terms $E_{1\alpha}$ are shear strains; $\bar{\gamma}_{1\alpha}$ is the transverse shear of the reference line and the remaining terms concern shear strain due to torsion and warp. The direction cosine matrix C^{Rr} (and thus κ_i) are taken as given in the present analysis. They may be expressed in a variety of ways as discussed by Hodges (1987a).

The present strain expressions for the small local rotation theory are very similar to those obtained by Wempner (1981). The last term in E_{11} is missing from Wempner's equations (8–29). This term was shown by Hodges (1980) to be important in correctly predicting the untwist of pretwisted beams under an axial tension force. The terms in $E_{1\alpha}$ involving $\lambda\psi\kappa_\beta$ are missing from Wempner's final expressions but are probably not very important anyway. It is unknown if there are any further differences in predictive capability between Wempner's theory and our small local rotation theory. Moreover, most of the nonlinear terms in equation (33) of the moderate local rotation theory are not included in Wempner's book.

Perhaps as significant as any differences in the results is the number of approximations invoked in Wempner's arguments in order to obtain his final result. The quadratic terms not shown in his equations (8–25) are neglected. The gradual change of the cross section strains is neglected (the underlined terms of equations (8–25)). Further approximations are made based on the thinness of the beam. Although the present approach involves fewer approximations, the results are simpler.

The simplicity of the present analysis, despite the generality of the example problem, is noteworthy. Indeed, the present

[3] This assumption is made strictly for illustrative purposes. The general theory does not require such an assumption. Nonclassical effects such as transverse normal strains and distortion shear can be treated by assumption of a more general displacement field.

Downloaded 03 May 2010 to 171.66.16.27. Redistribution subject to ASME license or copyright; see http://www.asme.org/terms/Terms_Use.cfm

expressions for strain were obtained with effort comparable to that expended by Hodges (1980) in an analysis involving only initial twist, extension, and torsion. Like Wempner, Hodges had to invoke several *ad hoc* approximations in order to simplify his result.

6 Conclusion

The analysis was based solely on the two assumptions that the strain components can be neglected compared to unity and that the local rotation components are no larger than the square root of the strain. If local rotation components are allowed to be as small as the strains, which might be the case for a beam with a closed or thick cross section, a very simple theory results. Unlike previous analyses, the removal of higher-order terms based on subjective criteria is unnecessary.

The theory was applied to a slender, precurved, pretwisted beam undergoing bending, torsion, and extension, as well as shear deformation and warping of arbitrary amplitude, which could be important for composite beams. The strain components are explicitly functions of x_α and depend implicitly upon seven functions of x_1 alone: $\tilde{\gamma}_{1i}$, κ_i, and ψ. These could be used as the generalized strains of a complete engineering beam theory. Such a theory will be developed in a later paper.

Acknowledgments

The first author was supported by the Naval Postgraduate School Foundation Research Program while on leave at the Aeroflightdynamics Directorate, US Army Aviation Research and Technology Activity (AVSCOM), Ames Research Center, Moffett Field, California (April–June, 1986). The authors thank Howard E. Hinnant of the Rotorcarft Dynamics Division, Aeroflightdynamics Directorate, who helped design the figure.

References

Budiansky, B., 1983, "Tensor Analysis," *Handbook of Applied Mathematics*, Pearson, C. E., ed., Van Nostrand Reinhold, Chapter 4.

Hodges, D. H., 1980, "Torsion of Pretwisted Beams Due to Axial Loading," ASME JOURNAL OF APPLIED MECHANICS, Vol. 47, pp. 393–397.

Hodges, D. H., 1987a, "Finite Rotations and Nonlinear Beam Kinematics," *Vertica*, Vol. 11, No. 1–2, p. 297–307.

Hodges, D. H., 1987b, "Nonlinear Beam Kinematics for Small Strains and Finite Rotations," *Vertica*, Vol. 11, No. 3, to be published.

Kane, T. R., Likins, P. W., and Levinson, D. A., 1983, *Spacecraft Dynamics*, McGraw-Hill, Chapter 1.

Love, A. E. H., 1944, *A Treatise on the Mathematical Theory of Elasticity*, Dover, Chapter 18.

Ogden, R. W., 1984, *Non-Linear Elastic Deformations*, Ellis Horwood, Chichester, Section 2.2.

Reissner, E., 1973, "On One-Dimensional Large-Displacement Finite-Strain Beam Theory," *Studies in Applied Mathematics*, Vol. 52, No. 2, pp. 87–95.

Sedov, L. I., 1966, *Foundations of the Non-linear Mechanics of Continua*, Pergamon Press, Chapter 1.

Simmonds, J. G., and Danielson, D. A., 1970, "Nonlinear Shell Theory with A Finite Rotation Vector," *Proceedings, Koninkl. Nederl. Akademie Van Wetenschappen*, Series B, Vol. 73, No. 5, pp. 460–478.

Simmonds, J. G., and Danielson, D. A., 1972, "Nonlinear Shell Theory with Finite Rotation and Stress-Function Vectors," ASME JOURNAL OF APPLIED MECHANICS, Vol. 39, pp. 1085–1090.

Simmonds, J. G., 1982, *A Brief on Tensor Analysis*, Springer-Verlag, Chapter 2.

Timoshenko, S. P., 1983, *History of Strength of Materials*, Dover.

Wempner, G. A., 1981, *Mechanics of Solids with Application to Thin Bodies*, Sijthoff and Noordhoff, The Netherlands, Chapters 6, 8, and 10.

Downloaded 03 May 2010 to 171.66.16.27. Redistribution subject to ASME license or copyright; see http://www.asme.org/terms/Terms_Use.cfm

Design of Material Properties That Yield a Prescribed Global Buckling Response

S. S. Antman[1]
Department of Mathematics,
University of Maryland,
College Park, MD 20742

C. L. Adler[1]
Department of Physics,
Brown University,
Providence, RI 02912

In the context of the large buckling of a nonlinearly elastic column under end thrust, this paper treats the design of (constitutive) functions appearing in bifurcation problems so as to produce a prescribed first bifurcating branch (e.g., a branch having a prescribed number of wiggles, which produce a prescribed pattern of hysteresis with snap bucklings in loading-unloading processes). The solution of this design problem also yields a method for determining a constitutive function from a single buckling experiment. A dual variational formulation is used to reduce the design problem to the solution of a linear Volterra integral equation of the first kind with a singular kernel. Effective numerical methods for the solution of such ill-posed equations are described and then applied to some physically interesting examples. Generalizations are discussed.

1 Introduction

Important information about large buckled states of structures is furnished by a bifurcation diagram, which relates an amplitude of stress or deformation to the applied load. For example, if the bifurcation is subcritical at the lowest buckling load, then it may give a misleadingly high estimate to the actual buckling load in a real structure, because imperfections could cause the structure to suffer a snap-buckling at a load well below the lowest buckling load. The safest estimate for the actual buckling load is furnished by the smallest load corresponding to the nontrivial stable equilibrium state. Such a load can only be determined from a bifurcation diagram (or from equivalent mathematical statements). If the first bifurcating branch has several wiggles, then in certain quasistatic loading-unloading processes, the structure exhibits hysteresis with snap bucklings. It is important to design many structures so that such bucklings, which can be dangerous, do not occur. There are, however, instances in which such buckling processes are beneficial, as in the operations of switches and sensors (cf Savage and Spano, 1982).

Thus a central problem of global bifurcation theory is to determine the detailed properties of bifurcation diagrams. In this paper we treat the problem inverse to this, namely, how to determine material properties for which the bifurcating branch emanating from the lowest buckling load has a prescribed global form. Our results could be used in the actual design of switches and sensors. Moreover, they furnish a way to determine material properties from experimental data (corresponding to a bifurcation diagram) for a buckling problem.

To make our presentation as transparent as possible, we treat the simplest case of the buckling of an elastica with a nonlinear moment-curvature equation. We describe generalizations in Section 5.

Various inverse problems related to ours have been studied. Urabe (1967, Chap. 13) gave a comprehensive treatment (with full bibliographic references) of the design of the elastic properties of an oscillator with one degree of freedom to ensure that the amplitude of response have a prescribed relation to the frequency. A related analysis of problems lacking a trivial solution was carried out by Cohen and Hansen (1971). In each case these authors treated semilinear equations of the form

$$u''(s)+\lambda f(u(s))=0 \tag{1.1}$$

subject to periodicity conditions or boundary conditions. (Here and below the prime denotes the derivative with respect to the independent variable s.) They sought f to ensure that λ have a prescribed dependence on an amplitude of u. For an appropriate choice of this amplitude, f can be determined by the explicit solution of Abel's integral equation.

In contrast, the physical situation we examine forces us to treat the quasilinear equation (2.1). We require a fair amount of preliminary work to convert the design problem to the solution of a linear Volterra integral equation of the first kind, which has a small body of mathematical theory, but has no known solution in closed form. In Section 3, we give the numerical solution of these equations for some physically interesting situations.

2 Formulation of the Boundary Value Problem and of the Inverse Problem

Let s, lying in [0, 1], be the scaled arc length parameter of a

[1] Also at the Naval Surface Weapons Center, Silver Spring, MD 20903-5000.

Contributed by the Applied Mechanics Division for publication in the JOURNAL OF APPLIED MECHANICS.

Discussion on this paper should be addressed to the Editorial Department, ASME, United Engineering Center, 345 East 47th Street, New York, N.Y. 10017, and will be accepted until two months after final publication of the paper itself in the JOURNAL OF APPLIED MECHANICS. Manuscript received by ASME Applied Mechanics Division, July 7, 1986; final revision October 27, 1986.

Copyright © 1987 by ASME
Downloaded 03 May 2010 to 171.66.16.27. Redistribution subject to ASME license or copyright; see http://www.asme.org/terms/Terms_Use.cfm

naturally straight (inextensible, unshearable) uniform elastica. We study the planar deformation of this elastica when it is clamped at end $s = 0$ and is subject to a compressive force (acting parallel to the initial straight state) of scaled magnitude λ applied at end $s = 1$. The end $s = 1$ is subject to zero bending couple. Let $\theta(s)$ be the angle between the tangent to the elastica at (the material point) s and the straight line describing the natural straight state. Let $M(\mu)$ be the couple needed to produce curvature μ (at any point of this elastica). Then the equilibrium states of this elastica are governed by

$$M(\theta'(s))' + \lambda \sin \theta(s) = 0, \tag{2.1}$$

$$\theta(0) = 0,\ M(\theta'(1)) = 0. \tag{2.2}$$

We require that the constitutive function M satisfy the physically reasonable restrictions

$$M(0) = 0,\ M_\mu(\mu) > 0,\ M(\mu) \to \infty \text{ as } \mu \to \infty. \tag{2.3}$$

Here the subscript μ denotes the derivative of M with respect to its argument. We use an analogous notation in the sequel. Properties (2.3) ensure that M has an inverse $\hat{\mu}$, so that

$$m = M(\mu) \text{ is equivalent to } \mu = \hat{\mu}(m), \tag{2.4}$$

with

$$\hat{\mu}(0) = 0,\ \hat{\mu}_m(m) > 0,\ \hat{\mu}(m) \to \infty \text{ as } m \to \infty. \tag{2.5}$$

$\hat{\mu}(m)$ is the curvature produced by the bending couple m. We define the stored (bending) energy of the elastica by

$$W(\mu) \equiv \int_0^\mu M(\xi)d\xi, \text{ so that } M(\mu) = W_\mu(\mu). \tag{2.6}$$

Then equations (2.3) and (2.6) imply that

$$W(0) = 0,\ W_\mu(0) = 0,\ W_{\mu\mu}(\mu) > 0,\ W(\mu) \to \infty \text{ as } \mu \to \infty. \tag{2.7}$$

We now introduce the Legendre transform V of W by

$$V(m) \equiv m\hat{\mu}(m) - W(\hat{\mu}(m)). \tag{2.8}$$

Then relations (2.4)-(2.8) imply that

$$\hat{\mu}(m) = V_m(m), \tag{2.9}$$

$$V(0) = 0,\ V_m(0) = 0,\ V_{mm}(m) > 0,\ V(m) \to \infty \text{ as } m \to \infty. \tag{2.10}$$

In view of equation (2.9) we can now replace equations (2.1), (2.2) by the equivalent system

$$\theta'(s) = V_m(m(s)), \tag{2.11}$$

$$m'(s) = -\lambda \sin \theta(s), \tag{2.12}$$

$$\theta(0) = 0,\ m(1) = 0. \tag{2.13}$$

The system (2.11), (2.12) has the Hamiltonian $V(m) - \lambda \cos \theta$ and therefore has the "energy" integral

$$V(m(s)) = \lambda[\cos \theta(s) - 1] + V(m(0)). \tag{2.14}$$

We now replace $\cos \theta$ in equation (2.14) with $\pm[1 - (m'/\lambda)^2]^{1/2}$, obtained from equation (2.11), and rearrange the resulting expression to get

$$[m'(s)]^2 = [V(m(0)) - V(m(s))]\{2\lambda - [V(m(0)) - V(m(s))]\}. \tag{2.15}$$

We study the first buckling mode (bifurcating branch) of equations (2.11)-(2.13), for which

$$0 \le \theta(s) < \pi,\ m'(s) < 0 \text{ for } s > 0,\ m(s) > 0 \text{ for } s < 1. \tag{2.16}$$

(That $\theta(s)$ cannot attain the limiting value π is a consequence of a simple phase-plane analysis of equations (2.1), (2.2), or of equations (2.11)-(2.13). The negativity of m' and the positivity of m then follow from equation (2.12).) Then equation (2.15) yields

$$1 = \int_{m(0)}^0 \frac{ds}{dm}\,dm = \int_0^{m(0)} \{[V(m(0)) - V(m)]\{2\lambda - [V(m(0)) - V(m)]\}\}^{-1/2} dm. \tag{2.17}$$

Now properties (2.10) ensure that V has an inverse Q for $m \ge 0$, so that

$$m = Q(v) \text{ is equivalent to } v = V(m) \text{ (for } m \ge 0). \tag{2.18}$$

Moreover, conditions (2.10) imply that $Q(v)$ behaves like const $\sqrt{v}$ for small v. We accordingly set

$$Q_v(v) = F(v)v^{-1/2}. \tag{2.19}$$

Setting

$$t = V(m(0)) \tag{2.20}$$

we readily reduce equation (2.17) to

$$1 = \int_0^t \frac{F(v)dv}{[v(t-v)(2\lambda - t + v)]^{1/2}}. \tag{2.21}$$

We now prescribe

$$\lambda = \Lambda(t), \tag{2.22}$$

substitute it into equation (2.21) and seek F to satisfy the resulting equation for all $t \ge 0$. (From F we can reconstruct M, as we explain below.) Equation (2.21) with λ given by equation (2.22) is a *linear* Volterra integral equation of the first kind with a singular kernel. In order that the integrand in equation (2.21) make sense, we require that

$$\Lambda(t) > t/2. \tag{2.23}$$

(This condition could be obtained directly from (2.14). In fact, we can get sharper restrictions from equation (2.14) when θ is confined to a subinterval of $(0,\pi)$.)

The prescription (2.22) corresponds to the first bifurcating branch for our buckling problem. We have chosen as amplitude the quantity t of equation (2.20), which is the maximum of the conjugate energy V. We could have alternatively chosen $m(0)$ as a measure of amplitude, but in this case we would have to solve the *nonlinear* Volterra integral equation (2.17) for V when λ is a given function of $m(0)$. If we were to take $\theta(1)$ as amplitude, then we could relate it to $m(0)$ by equation (2.14) and encounter the same difficulty. The important feature we wish to study is the number of wiggles that λ has as an amplitude increases. This number determines the number of equilibrium states there are for a fixed λ. This number is independent of any "reasonable" choice of amplitude (as is suggested by the foregoing considerations, which are typical of results for nonlinear Sturm-Liouville problems).

To find M from F we first use equation (2.19) to obtain

$$Q(v) = \int_0^v F(z)z^{-1/2}dz, \tag{2.24}$$

which is the bending couple corresponding to the conjugate energy v. From equation (2.18) we obtain $V_m(m) = [Q_v(V(m))]^{-1}$. Hence equations (2.9), (2.19) yield

$$\hat{\mu}(m) = \sqrt{V(m)}/F(V(m)), \tag{2.25}$$

which equations (2.18) and (2.4), respectively, convert to

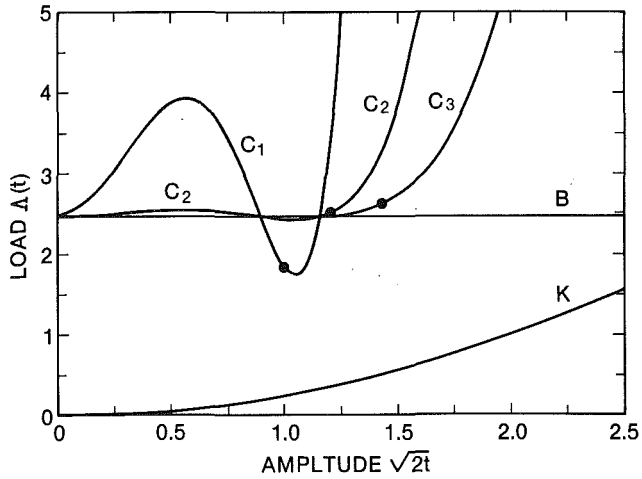
$$\hat{\mu}(Q(v)) = \sqrt{v}/F(v), \tag{2.26}$$

$$Q(v) = M(\sqrt{v}/F(v)). \tag{2.27}$$

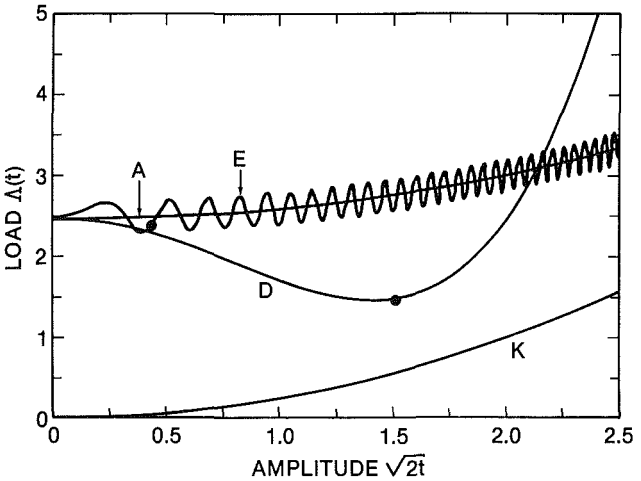
Equations (2.24) and (2.27) give alternative representations for $Q(v)$, which must agree. Note that $\hat{\mu}(Q(v))$ is the curvature corresponding to the conjugate energy v. We find a typical entry in the table of values of m versus μ, which defines the function M, by choosing some v, computing μ from the right-hand side of equation (2.26) and computing m from the right-hand side of equation (2.24).

There is one difficulty obstructing the solution of equations (2.21), (2.22) for F. There is no provision built into our numerical procedure, described in Section 4, to ensure that F corresponds to an M satisfying $M_\mu > 0$ (cf relations (2.3)) or any of its equivalent versions, which include $Q_{vv} = [F(v)v^{-1/2}]_v < 0$. In other words, it may not be possible to

Downloaded 03 May 2010 to 171.66.16.27. Redistribution subject to ASME license or copyright; see http://www.asme.org/terms/Terms_Use.cfm



(a)



(b)

Fig. 1 Bifurcation diagrams. The large dots correspond to the largest values of $\sqrt{2}t$ for which solutions of (2.21) exist. At the curvature corresponding to these values of t, the functions M cease to increase. K represents the curve given by $\Lambda(t) = t^2/2$.

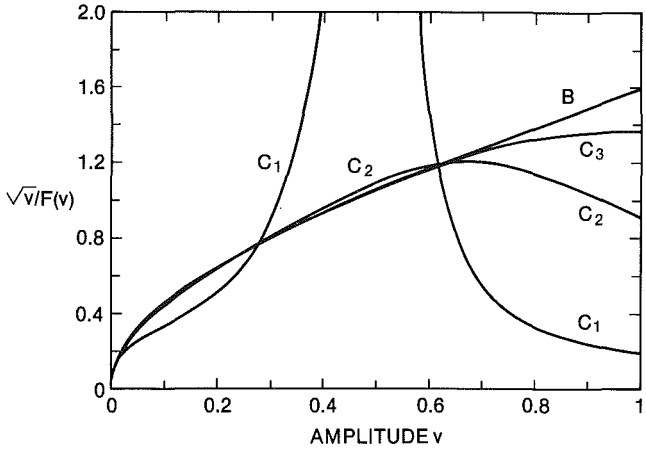


Fig. 2 Plots of $\sqrt{v}/F(v)$ as functions of v for cases B, C_1, C_2, C_3. The corresponding expressions from (3.1) are proportional. The maximum permissible values of v are those at which $\sqrt{v}/F(v)$ ceases to increase.

produce a given bifurcation diagram with a material meeting this natural restriction. We handle this problem in our numerical study by simply monitoring the slope of $F(v)v^{-1/2}$.

We note that by the results given by Linz (1985, pp. 75–76)), our problem (2.21), (2.22) has a unique continuous solution F. Since this problem in general has no known closed-form solution, we must resort to numerical methods for its solution. (Note that equations (2.21), (2.22) are convolution equations only if Λ is constant. But even for this very interesting problem, the inverse Laplace transform of the solution cannot be evaluated in closed form.) Since integral equations of the first kind are often ill-posed in the sense that small changes in data can produce large changes in solutions (cf Linz, 1985, Chap. 9, and Tikhonov and Arsenin, 1974), numerical studies must be done with care. In Section 3 we describe our numerical results and in Section 4 we outline the numerical methods used to produce them.

3 Solutions of Specific Problems

We determine M for the following choices for $\Lambda(t) - \pi^2/4$:

(3.1) Case A: $\dfrac{t}{4}+\dfrac{3t^2}{32\pi^2}$,

Case B: 0,

Case C_1: $20t-80t^2+75t^3$,

Case C_2: $t-4t^2+3.75t^3$,

Case C_3: $0.2t-0.8t^2+0.75t^3$,

Case D: $-2t+t^2$,

Case E: $\dfrac{t}{4}+\dfrac{3t^2}{32\pi^2}+0.2\sin(60t)$.

Case A corresponds to the Λ that represents the bifurcation diagram for equations (2.1), (2.2) when $M(\mu) = \mu$. The expression for Λ comes from a polynomial approximation to the actual Λ expressed in terms of an elliptic integral. The expression shown agrees with the exact solution to five significant figures for

$t = 1.76$ (or $\theta'(0) = 1.88$, $\theta(1) = 66^0$)

to three significant figures for

$t = 4.56$ (or $\theta'(0) = 3.02$, $\theta(1) = 102^0$)

and to an error of 2.24 percent for

$t = 11.96$ (or $\theta'(0) = 4.89$, $\theta(1) = 143^0$).

This Case A was designed to yield a check on the accuracy of our numerical procedures. Case B corresponds to the isochronous problem for vibrations discussed by Urabe (1967, Chap. 13). Cases C_1, C_2, C_3 have bifurcation diagrams with two wiggles and can therefore give rise to snap bucklings and hysteresis. The corresponding terms exhibited in (3.1) are proportional. Case D describes a subcritical bifurcation. Case E describes a highly oscillatory perturbation of Case A. Note that Case B, in particular, violates (2.23) for t sufficiently large.

In Fig. 1 we plot $\Lambda(t)$ versus $\sqrt{2}t$. (Since t is the maximum value of the conjugate energy, the quantity $\sqrt{2}t$, which is just $\theta'(0)$ in Case A, corresponds more closely to the usual variables for amplitudes than does t itself.)

In Fig. 2 we plot $F(v)/\sqrt{v}$ for a few related cases. These plots show where solutions break down, i.e., where $F(v)/\sqrt{v}$ ceases to increase. This information is incorporated directly into Fig. 1 and indirectly (via equation (2.14)) into Fig. 3.

In Fig. 3 we show the solutions M for all the cases of (3.1) together with their artificial continuations beyond the maximum permissible curvatures corresponding to the maximum t's. Note that the solutions break down by becoming multivalued. It would be interesting to determine whether there is

Downloaded 03 May 2010 to 171.66.16.27. Redistribution subject to ASME license or copyright; see http://www.asme.org/terms/Terms_Use.cfm

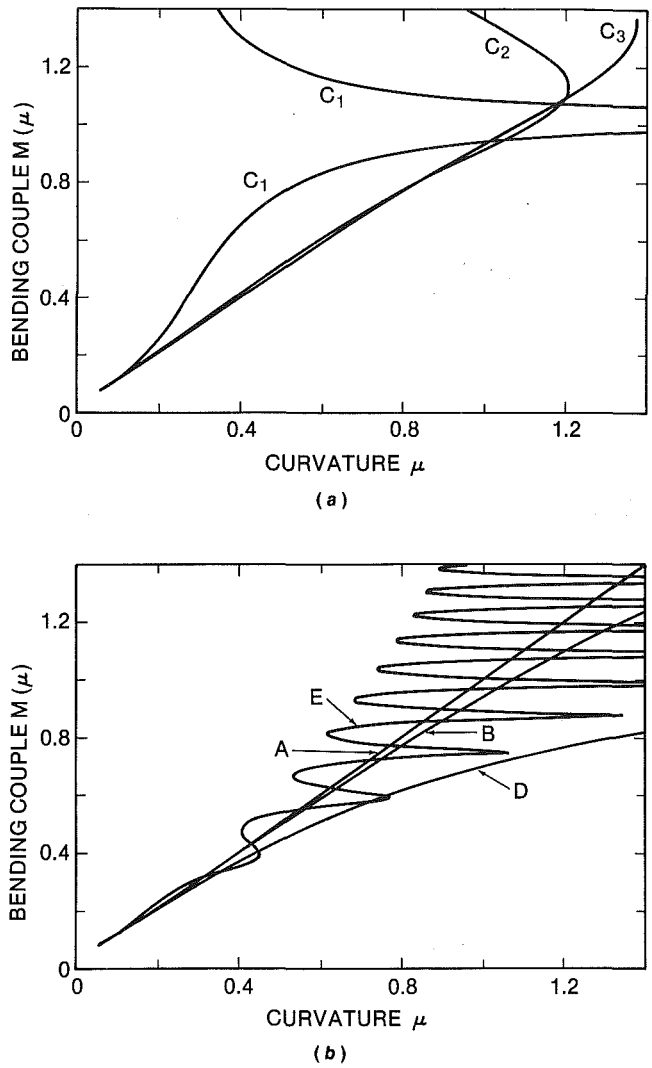


Fig. 3 Moment-curvature plots for solutions in all the cases of (3.1). The solutions cease to exist where these curves become multi-valued.

any physical significance to the upper and lower monotone envelopes of these curves, e.g., that of Case E.

It is worth noting that the maximum values of t increases as the size of the terms in Cases C_1–C_3 decrease. In Case C_1, the maximum t is too small for Λ to show all its wiggles. This problem does not occur in Case C_3. It might therefore appear that interesting bifurcation diagrams must be small in some sense. Such a conclusion would be incorrect. The relationship between the maximum t and the amplitudes shown in (3.1) is strongly influenced by the system of scalings we have employed. In particular the bifurcation point $\Lambda(0) = \pi^2/4$ for all the terms in (3.1). By letting this bifurcation point vary, we can handle quite large deviations in Λ.

The solution for Case A yields a graph for $M(\mu)$ that is indistinguishable from $M(\mu) = \mu$ for values of μ up to 4, at which the validity of Λ as an approximation to the exact bifurcation curve for $M(\mu) = \mu$ begins to break down. Thus we may conclude that our numerical techniques are very accurate.

Our results indicate a simple pattern, which is entirely to be expected on physical grounds. If one Λ grows faster than another, then the corresponding moment curvature diagram of the first grows at a faster rate than the second, i.e., it corresponds to a material whose stiffness increases at a faster rate.

4 Numerical Implementation

We treat the (ill-posed) problem (2.21), (2.22) by direct numerical approximation of the integral. But rather than using a higher-order approximation scheme, such as Simpson's rule, we use a very primitive scheme with a fine mesh. This approach enables us to avoid inaccuracies due to the inherent instability of the problem (cf Linz, 1985, Chap. 9). Since there apparently are no error estimates for solutions of equations like (2.21), (2.22), we must rely on indirect evidence to evaluate the efficacy of our procedure. This evidence is supplied by our results for Case A.

In fact, the use of Case A for testing accuracy is typical of an approach that works in general. Once M is found for a given Λ, we could compute the first branch for (2.1), (2.2) (or equivalently, for equations (2.11)–(2.13)) with this M by using now standard numerical techniques. If the resulting computed function Λ is close to the initially prescribed function, we may presume that the procedure is accurate. (There are convergence results for integral equations of Abel's type that are simpler than ours. Cf Weiss and Anderssen (1972), e.g. A symptom of the difficulty with equation (2.21) is that the 1 on the left-hand side does not approach 0 as t approaches 0, while the right-hand side is a (necessarily singular) integral over $[0,t]$.)

Since the kernel of equation (2.21) is singular at $v = 0$ and $v = t$, we employ product integration, which is based on the representation of the integral of equations (2.21), (2.22) as (the Riemann-Stieltjes integral)

$$\int_0^t \frac{F(v)}{[2\Lambda(t)-t+v]^{1/2}}\, d\sin^{-1}\left(\frac{2v-t}{t}\right). \tag{4.1}$$

Let h be the reciprocal of a large positive integer. (In our computations we take $h = 1/300$.) Let n be a positive integer. Then for $t = nh$ we approximate (4.1) by

$$\sum_{k=1}^{n} \frac{F((k+1/2)h)}{[2\Lambda(nh)-nh+(k+1/2)h]^{1/2}}\left\{\sin^{-1}\left(\frac{2(k+1)-n}{n}\right)\right.$$

$$\left.-\sin^{-1}\left(\frac{2k-n}{n}\right)\right\}. \tag{4.2}$$

(Note that the term in braces in (4.2) does not depend on the mesh size h, in consequence of the singular nature of the integrator. It is this feature that prevents the right-hand side of equation (2.21) from approaching 0 as $t \to 0$ and thereby rendering equation (2.21) meaningless.)

We seek an approximate solution of equations (2.21), (2.22) on the bounded t-interval $[0,Nh]$ where N is a fixed integer (taken to equal 300 in our computations). For each $n = 1,2,\ldots,N$ we equate (4.2) to 1, thereby obtaining a linear system of N equations for the N numbers $F((k+1/2)h)$, $k = 0,\ldots,N-1$. Since this system is in lower triangular form, it is cheaply inverted by Gaussian elimination.

In the reconstruction of M from F, we assign values nh, $n = 0, 1, \ldots, N$ to v and approximate the integral of equation (2.24) also by product integration:

$$2\sum_{k=1}^{n} F((k+1/2)h)\{[(k+1)h]^{1/2}-[kh]^{1/2}\}. \tag{4.3}$$

(It would of course be possible to replace the approximation (4.3) with something like Simpson's rule, but such sophistication would not be in keeping with the primitive approximation (4.2) and might require additional data).

5 Generalizations

We could have treated equations (2.1), (2.2), and (2.22) directly without introducing the conjugate formulation (2.11)–(2.13) in terms of the Legendre transformation (2.8).

Downloaded 03 May 2010 to 171.66.16.27. Redistribution subject to ASME license or copyright; see http://www.asme.org/terms/Terms_Use.cfm

We obtain in place of equation (2.14) the equivalent energy integral

$$\theta'(s)W_\mu(\theta'(s)) - W(\theta'(s)) + \lambda[1-\cos\theta(s)] = \theta'(0)W_\mu(\theta'(0)) - W(\theta'(0)) = \lambda[1-\cos\theta(1)]. \quad (5.1)$$

The properties of W given in relations (2.7) enable us to introduce

$$r = \mu^2/2,\ U(r) = W(\mu),$$

$$G(r) = \mu W_\mu(\mu) - W(\mu) = 2rU_r(r) - U(r) \text{ for } \mu \geq 0. \quad (5.2)$$

(If W were assumed to be even, then equation (5.2) would hold for all μ. But restriction (2.16) obviates the need for such an assumption.) Therefore,

$$G_r(r) = U_r(r) + 2r\,U_{rr}(r) = W_{\mu\mu}(\mu) > 0. \quad (5.3)$$

Note that equation (2.8) implies that $G(r) = V(M(\mu))$. Since both r and $M(\mu)$ approach ∞ if and only if $|\mu|$ approaches ∞, we find that $G(r) \to \infty$ as $r \to \infty$. This condition and equation (5.3) ensure that G has an inverse H defined on $[0,\infty)$ and therefore equation (5.1) is equivalent to

$$\theta'(s)^2 = 2H(\lambda[\cos\theta(s) - \cos\theta(1)]). \quad (5.4)$$

We now treat this equation as we treated equation (2.15), obtaining

$$1 = \int_0^{\theta(1)} \{2H(\lambda[\cos\theta - \cos\theta(1)])\}^{-1/2} d\theta = \int_0^{2\lambda\sin^2(\theta(1)/2)} \lambda^{-1}\{1 - [\chi/\lambda + \cos\theta(1)]^2\}^{-1/2} H(\chi)^{-1/2} d\chi, \quad (5.5)$$

the second form coming from the change of variables $\chi = \lambda[\cos\theta - \cos\theta(1)]$. If λ is now prescribed as a function of the amplitudes $\theta(1)$ or $\sin^2(\theta(1)/2)$, then the second form of (5.5) is also a linear Volterra integral equation of the first kind for $H^{-1/2}$. The first form of (5.5), like equation (2.17), is a nonlinear Volterra integral equation for which there are no readily available existence and uniqueness theorems. (We can regard our various reformulations as providing precisely those tools necessary to yield such theorems for nonlinear equations.)

We have assumed that the bifurcating branch is expressed by (2.22) in which λ is a given function of t. More generally we could prescribe λ and t to lie on an arbitrary curve in the (λ,t)-plane given parametrically by

$$\lambda = \lambda^\#(\xi),\ t = t^\#(\xi). \quad (5.6)$$

Then in place of equations (2.21), (2.22) we would have to solve

$$\int_0^{t^\#(\xi)} \frac{F(v)dv}{\{v[t^\#(\xi) - v][2\lambda^\#(\xi) - t^\#(\xi) + v]\}^{1/2}} = 1. \quad (5.7)$$

The numerical treatment of this linear equation would be only slightly more complicated than that described in Section 4.

We could jointly generalize equations (1.1) and (2.1) by studying autonomous Euler-Lagrange equations of the form

$$L_{\theta'}(\theta(s), \theta'(s), \lambda)' - L_\theta(\theta(s), \theta'(s), \lambda) = 0 \quad (5.8)$$

(Such equations arise as the generalization of equation (2.1) to describe nonlinearly elastic rods that can suffer extension and shear, as well as flexure. Cf Antman, 1974, Antman and Rosenfeld, 1978.) If $L_{\theta'\theta'} > 0$ and if $L_{\theta'}(\theta, \theta', \lambda) \to \infty$ as $\theta' \to \infty$ (possibly for λ restricted to some interval), then we can introduce the Legendre transform

$$V(\theta, m, \lambda) \equiv m\hat{\mu}(\theta, m, \lambda) - L(\theta, \hat{\mu}(\theta,m,\lambda), \lambda) \text{ where } L_{\theta'}(\theta, \hat{\mu}(\theta, m, \lambda), \lambda) = m, \quad (5.9)$$

and thus reduce equation (5.8) to the Hamiltonian system

$$\theta' = V_m(\theta, m, \lambda),\ m' = -V_\theta(\theta, m, \lambda) \quad (5.10a,b)$$

having the integral

$$V(\theta, m, \lambda) = \text{const.} \quad (5.11)$$

Alternatively we could multiply equation (5.8) by θ' to obtain the integral

$$\theta' L_{\theta'}(\theta, \theta', \lambda) - L(\theta, \theta', \lambda) = \text{const.} \quad (5.12)$$

We could treat equation (5.11) like (2.14) and equation (5.12) like (5.1). In either case we must isolate the dependence of V or L on λ so that we can formulate a meaningful design problem for a single function of a single variable. For example, solving equation (5.12) for $(\theta')^2/2$ we obtain

$$\theta'(s)^2 = 2H(\theta, \lambda, \text{const}). \quad (5.13)$$

To proceed further we might assume that $H(\theta,\lambda, \text{const})$ has the form $\hat{H}(J(\theta),\lambda, \text{const})$ where $\hat{H}$ is given and J is to be found. This procedure has a simple interpretation for rods that are flexible, extensible, and shearable: Assuming that the dependence of the stored energy on the extension and shear is given, we seek its dependence on the bending strain θ' when λ is a prescribed function of an amplitude of θ or θ'.

The situation for problems with many bifurcation parameters is not so satisfactory. (An example of such a problem from mechanics is the buckling in space of a rod under combined thrust and torque applied to one of its ends; cf Antman and Kenney, 1981.) As an example, consider the model problem

$$u''(s) + \lambda f_u(u(s)) + \sigma g_u(u(s)) = 0,\ u(0) = 0,\ u'(1) = 0 \quad (5.14)$$

where $f_u(0) = 0 = g_u(0)$. From the energy integral of this equation we obtain

$$1 = \int_0^{u(1)} \{\lambda[f(u) - f(u(1))] + \sigma[g(u) - g(u(1))]\}^{-1/2} du. \quad (5.15)$$

A bifurcation diagram for problem (5.14) is a surface in $(\lambda,\sigma,u(1))$ -space. Suppose we wish to prescribe this surface and suppose for simplicity that this surface intersects the plane $\sigma = 0$. Then the prescription of λ as a function of $u(1)$ on the plane $\sigma = 0$ enables us to determine f from equation (5.15). If we further require the bifurcating surface to have a prescribed shape where it intersects a plane of the form $\lambda = \text{const}$, then we can determine g from equation (5.15). Any further restriction on the bifurcating surface is likely to be incompatible. In short, if we have two functions to be determined, we can permit the bifurcating surface to pass through two prescribed curves. Generalizations of this rule are immediate.

Small solutions of bifurcation problems like equation (2.1) can be studied by perturbation methods: θ and λ can be expressed rigorously as finite Taylor polynomials in a suitable amplitude variable (cf Iooss and Joseph, 1980; Keller, 1969). The usual analysis gives the dependence of the first few Taylor coefficients of λ on the first few derivatives of M at the trivial state (cf Antman and Rosenfeld, 1978). But this process is readily reversed to handle the design problem for small amplitudes (i.e., in the so-called post-buckling range). Moreover, this perturbation method can treat many bifurcation problems, albeit only locally. An open problem is to develop effective global methods to handle equations more complicated than those we treated.

Much of our analysis exploited the convexity of energy functions. Recently, problems with nonconvex energies have been intensively studied (e.g., by James, 1981). Design problems for such energies would provide some interesting challenges.

Acknowledgment

The research reported here was supported by the Independent Research Fund of the Naval Surface Weapons Center and

Downloaded 03 May 2010 to 171.66.16.27. Redistribution subject to ASME license or copyright; see http://www.asme.org/terms/Terms_Use.cfm

the ONR-Navy Dynamics Institute Program. The work of S. S. Antman was also supported by NSF Grant DMS 8503317.

References

Antman, S. S., 1974, "Qualitative Theory of the Ordinary Differential Equations of Nonlinear Elasticity," *Mechanics Today*, Vol. 1, Nemat-Nasser, S., ed., Pergamon Press, pp. 58–101.

Antman, S. S., and Kenney, C. S., 1981, "Large Buckled States of Nonlinearly Elastic Rods Under Torsion, Thrust, and Gravity," *Arch. Rational Mech. Anal.*, Vol. 76, pp. 289–338.

Antman, S. S., and Rosenfeld, G., 1978, "Global Behavior of Buckled States of Nonlinearly Elastic Rods," *SIAM Rev*, Vol. 20, pp. 513–566. Corrections and additions, ibid, Vol. 22, 1980, pp. 186–187.

Cohen, D., and Hansen, E., 1971, "Inverse Problems Connected with Two-Point Boundary Value Problems," *SIAM J. Appl. Math.*, Vol. 20, pp. 413–425.

Iooss, G., and Joseph, D. D., 1980, *Elementary Stability and Bifurcation Theory*, Springer-Verlag.

James, R. D., 1981, "The Equilibrium and Post-Buckling Behavior of an Elastic Curve Governed by a Non-Convex Energy," *J. Elasticity*, Vol. 11, pp. 239–269.

Keller, J. B., 1969, "Bifurcation Theory for Ordinary Differential Equations," *Bifurcation Theory and Nonlinear Eigenvalue Problems*, Keller, J. B., and Antman, S., eds., Benjamin, pp. 17–48.

Linz, P., 1985, *Analytical and Numerical Methods for Volterra Equations*, SIAM.

Savage, H. T., and Spano, M. L., 1982, "Theory and Application of Highly Magnetoelastic Metglas 2605SC," *J. Appl. Phys.*, pp. 8092–8097.

Tikhonov, A. N., and Arsenin, V. Ya., 1974, *Methods of Solution of Incorrect Problems*, Nauka, in Russian. French translation, 1976, Mir.

Urabe, M., 1967, *Nonlinear Autonomous Oscillations*, Academic Press.

Weiss, R., and Anderssen, R. S., 1972, "A Product Integration Method for a Class of Singular First Kind Volterra Equations," *Numer. Math.*, Vol. 18, pp. 442–456.

Downloaded 03 May 2010 to 171.66.16.27. Redistribution subject to ASME license or copyright; see http://www.asme.org/terms/Terms_Use.cfm

General Solutions for the Inelastic Behavior of Pressurized Membranes

K. W. Neale
Assoc. Mem. ASME

E. Chater
Faculty of Applied Science,
University of Sherbrooke,
Sherbrooke, Québec, Canada J1K 2R1

The small-deflection behavior of inelastic membranes supported along arbitrary contours and subjected to lateral pressure is considered. Hill and Storåkers' (1980) solution for isotropic power-law hardening membranes is extended to a wide class of anisotropic material response. Applications to circular membranes are given for anisotropic materials characterized by Budiansky's (1984) general transversely isotropic yield function. Specific results corresponding to the yield functions proposed by Hill (1979) and Bassani (1977) are also presented.

1 Introduction

The behavior of plane membranes subjected to lateral pressure has been the subject of numerous investigations in the past. A renewed interest in this problem has surfaced lately as evidenced by the recent studies of Hill and Storåkers (1980), Chater and Neale (1983a, b), and Storåkers (1983a, b, c). This interest is due in part to the need for a more complete understanding of the mechanics of the bulge test, and its applicability for determining the material properties and formability characteristics of new sheet materials.

Among the studies carried out to date, the one presented by Hill and Storåkers (1980) is especially noteworthy. It is a comprehensive investigation for pressurized diaphragms supported along arbitrary boundaries and accounts for both viscoplastic (creep) as well as time-independent plastic behavior. Their analysis applies to isotropic power-law hardening membranes in the small-deflection range, and leads to an exact solution for circular membranes. Hill and Storåkers also establish a general correspondence principle relating viscoplastic and time-independent plastic solutions, as well as a variational principle which they use in an approximate analysis for elliptical membranes.

Hill and Storåkers show that the pressure-dependence of the solution within the small-deflection approximation is separable under power-law hardening. This implies that each element of the membrane undergoes a proportional stressing path. Consequently, nonlinear elastic or deformation theory relations of plasticity can rigorously be substituted for the flow theory relations if the loading is monotonic. Hill and Storåkers exploit this simplification in a thorough investigation of isotropic membranes.

In this study the work of Hill and Storåkers (1980) is extended to include a wide class of anisotropic material behavior. The small-deflection approximations (as specified by Hill and Storåkers) and nonlinear elastic representation are adopted. As in their work, our analysis encompasses both viscoplastic and time-independent plastic behavior. We show first that Hill and Storåkers' solution can readily be applied to any material whose stress dependence on strain or strain-rate is a homogeneous function. We examine the circular membrane in detail and present solutions for anisotropic materials characterized by Budiansky's (1984) general transversely isotropic yield function, as well as results corresponding to the recent yield functions proposed by Hill (1979) and Bassani (1977).

2 Basic Equations and General Analysis

We consider a plane membrane clamped around a simply-connected, but otherwise arbitrary, contour and subjected to a uniform lateral pressure p. The basic equations, within the context of the small-deflection approximation, have been given by Hill and Storåkers (1980). With respect to a Cartesian reference system x-y in the plane of the undeformed membrane, the strain components are

$$e_x = \frac{\partial u}{\partial x} + \frac{1}{2}\left(\frac{\partial w}{\partial x}\right)^2, \quad e_y = \frac{\partial v}{\partial y} + \frac{1}{2}\left(\frac{\partial w}{\partial y}\right)^2$$
$$e_{xy} = \frac{1}{2}\left(\frac{\partial u}{\partial y} + \frac{\partial v}{\partial x} + \frac{\partial w}{\partial x}\frac{\partial w}{\partial y}\right) \tag{2.1}$$

where u, v, w are the displacements in the x, y and normal directions, respectively. Equilibrium is governed by the following equations

$$\frac{\partial \sigma_x}{\partial x} + \frac{\partial \sigma_{xy}}{\partial y} = 0, \quad \frac{\partial \sigma_{xy}}{\partial x} + \frac{\partial \sigma_y}{\partial y} = 0$$
$$\sigma_x \frac{\partial^2 w}{\partial x^2} + 2\sigma_{xy}\frac{\partial^2 w}{\partial x \partial y} + \sigma_y \frac{\partial^2 w}{\partial y^2} = -\frac{p}{t} \tag{2.2}$$

where σ_x, σ_y, σ_{xy} are the membrane stress components and t is the (uniform) initial thickness of the membrane.

As in Hill and Storåkers (1980), we introduce dimensionless "reduced displacements" $\tilde{u}$, $\tilde{v}$, $\tilde{w}$ and "reduced stresses" $\tilde{\sigma}_x$,

Contributed by the Applied Mechanics Division for publication in the JOURNAL OF APPLIED MECHANICS.
Discussion on this paper should be addressed to the Editorial Department, ASME, United Engineering Center, 345 East 47th Street, New York, N.Y. 10017, and will be accepted until two months after final publication of the paper itself in the JOURNAL OF APPLIED MECHANICS. Manuscript received by ASME Applied Mechanics Division, July 10, 1986; final revision December 1, 1986.

Copyright © 1987 by ASME
Downloaded 03 May 2010 to 171.66.16.27. Redistribution subject to ASME license or copyright; see http://www.asme.org/terms/Terms_Use.cfm

$\tilde{\sigma}_y$, $\tilde{\sigma}_{xy}$ in order to obtain separable field equations. Here the reduced variables are defined as follows:

$$\frac{u}{\ell\tilde{u}}=\frac{v}{\ell\tilde{v}}=\left(\frac{w}{\ell\tilde{w}}\right)^2=f(\tau)$$
$$\frac{\sigma_x}{k\tilde{\sigma}_x}=\frac{\sigma_y}{k\tilde{\sigma}_y}=\frac{\sigma_{xy}}{k\tilde{\sigma}_{xy}}=g(\tau) \tag{2.3}$$

where k is a constant having units of stress, ℓ is a representative linear dimension of the undeformed membrane (e.g., mean radius), and $f(\tau)$, $g(\tau)$ are as yet unspecified functions of a time-like variable τ. These reduced variables depend on $\tilde{x}$, $\tilde{y}$ = x/ℓ, y/ℓ, and are independent of p, if the material has a plane-stress constitutive law of the general form

$$e_{\alpha\beta}=F(\sigma_{\alpha\beta}),\quad \sigma_{\alpha\beta}=G(e_{\alpha\beta}),\quad \alpha,\beta=1,2 \tag{2.4}$$

with F, G homogeneous of degree N, $\bar{N}$ = $1/N$ in $\sigma_{\alpha\beta}$, $e_{\alpha\beta}$, respectively.

From equations (2.1) and (2.3) we have

$$e_x=f\tilde{e}_x,\quad e_y=f\tilde{e}_y,\quad e_{xy}=f\tilde{e}_{xy} \tag{2.5}$$

where the "reduced strains" $\tilde{e}_x$, $\tilde{e}_y$, $\tilde{e}_{xy}$ are defined in terms of $\tilde{u}$, $\tilde{v}$, $\tilde{x}$, $\tilde{y}$ in the same manner as equations (2.1). From equations (2.3)–(2.5) and the homogeneity property of F it follows that

$$f=g^N,\quad \tilde{e}_{\alpha\beta}=\tilde{F}(\tilde{\sigma}_{\alpha\beta}) \tag{2.6}$$

where

$$\tilde{F}(\tilde{\sigma}_{\alpha\beta})=k^N F(\tilde{\sigma}_{\alpha\beta})=\frac{1}{g^N}F(\sigma_{\alpha\beta}) \tag{2.7}$$

Furthermore, the equilibrium equations (2.2) become

$$\frac{\partial\tilde{\sigma}_x}{\partial\tilde{x}}+\frac{\partial\tilde{\sigma}_{xy}}{\partial\tilde{y}}=0,\quad \frac{\partial\tilde{\sigma}_{xy}}{\partial\tilde{x}}+\frac{\partial\tilde{\sigma}_y}{\partial\tilde{y}}=0$$
$$\tilde{\sigma}_x\frac{\partial^2\tilde{w}}{\partial\tilde{x}^2}+2\tilde{\sigma}_{xy}\frac{\partial^2\tilde{w}}{\partial\tilde{x}\partial\tilde{y}}+\tilde{\sigma}_y\frac{\partial^2\tilde{w}}{\partial\tilde{y}^2}=-\left[\frac{p\ell}{kt g\sqrt{f}}\right] \tag{2.8}$$

If all reduced variables and field equations (2.6), (2.8) in these reduced variables are to be independent of p, the bracketed term on the right side of equations (2.8) must also be independent of p. Thus, we put

$$g\sqrt{f}=\frac{p\ell}{kt} \tag{2.9}$$

and the third of equations (2.8) becomes

$$\tilde{\sigma}_x\frac{\partial^2\tilde{w}}{\partial\tilde{x}^2}+2\tilde{\sigma}_{xy}\frac{\partial^2\tilde{w}}{\partial\tilde{x}\partial\tilde{y}}+\tilde{\sigma}_y\frac{\partial^2\tilde{w}}{\partial\tilde{y}^2}=-1 \tag{2.10}$$

In view of equations (2.6) and (2.9) we have

$$f=\left(\frac{p\ell}{kt}\right)^{\frac{2N}{N+2}},\quad g=\left(\frac{p\ell}{kt}\right)^{\frac{2}{N+2}} \tag{2.11}$$

This result is precisely that derived by Hill and Storåkers (1980) for power-law hardening isotropic membranes.

The problem now consists of solving for the reduced variables $\tilde{u}$, $\tilde{\sigma}_x$, $\tilde{e}_x$, etc., in terms of $\tilde{x}$, $\tilde{y}$ given the stress-strain relations $\tilde{e}_{\alpha\beta}$ = $\tilde{F}(\tilde{\sigma}_{\alpha\beta})$ and contour of the membrane boundary. The boundary conditions are $\tilde{u}$ = $\tilde{v}$ = $\tilde{w}$ = 0 on the boundary. Once the reduced variables have been obtained, the actual variables u, σ_x, e_x, etc., at any pressure p are obtained directly from equations (2.3), (2.5), and (2.11).

As noted by Hill and Storåkers, the solution in terms of reduced variables also applies to certain types of rate-dependent material response. For example, with strain-rates

$$\epsilon_{\alpha\beta}=\dot{e}_{\alpha\beta}=\dot{f}\tilde{e}_{\alpha\beta} \tag{2.12}$$

and a constitutive law of the form

$$\epsilon_{\alpha\beta}=F(\sigma_{\alpha\beta}) \tag{2.13}$$

the relations analogous to equations (2.6) become

$$\dot{f}=g^N,\quad \tilde{\epsilon}_{\alpha\beta}=\tilde{F}(\tilde{\sigma}_{\alpha\beta}) \tag{2.14}$$

with $\tilde{F}(\tilde{\sigma}_{\alpha\beta})$ satisfying (2.7), if F is homogeneous function of degree N in $\sigma_{\alpha\beta}$. Instead of equations (2.11) we now have

$$\dot{f}f^{N/2}=\left(\frac{p\ell}{kt}\right)^N \tag{2.15}$$

so that

$$[f(\tau)]^{\frac{N+2}{2}}=\frac{N+2}{2}\int_0^\tau\left(\frac{p\ell}{kt}\right)^N d\tau+[f(0)]^{\frac{N+2}{2}} \tag{2.16}$$

This correspondence principal is identical to that established by Hill and Storåkers for the isotropic membrane, and can be exploited in the manner indicated by them to analyze creep-type deformations.

Since the pressure-dependence is separable in the above solutions, proportional stressing and straining occurs for each element of the membrane. Thus, for time-independent plastic behavior flow theory constitutive relations and corresponding total deformation theory relations lead to identical results. A valid law for this behavior is

$$e_{\alpha\beta}=\frac{\partial\sigma_e}{\partial\sigma_{\alpha\beta}}e_e \tag{2.17}$$

where σ_e is the effective stress, assumed to be a homogeneous function of degree one in $\sigma_{\alpha\beta}$. The surface σ_e = const. defines the current yield locus and, in uniaxial tension, σ_e is equal to the uniaxial stress σ_u. The equivalent-work postulate $\sigma_e e_e$ = $\sigma_{\alpha\beta}e_{\alpha\beta}$ can be used together with equation (2.17) and Euler's theorem to define the effective strain e_e. It becomes equal to the axial strain e_u for uniaxial tension, is homogeneous of degree one in e_{ij}, and is related to σ_e through e_e = $\sigma_e/E_s(\sigma_e)$. Here, E_s denotes the uniaxial secant modulus, computed from the uniaxial stress-strain curve at the current level σ_u = σ_e. This constitutive theory implies a power-law hardening relation of the form

$$\sigma_e=ke_e^{\bar{N}} \tag{2.18}$$

The constitutive law (2.17) can also be expressed as follows

$$e_{\alpha\beta}=\frac{\partial W}{\partial\sigma_{\alpha\beta}} \tag{2.19}$$

where the potential function

$$W=\frac{k}{N+1}\left(\frac{\sigma_e}{k}\right)^{N+1} \tag{2.20}$$

is homogeneous of degree $N+1$ in $\sigma_{\alpha\beta}$. The inverse of equation (2.19) is

$$\sigma_{\alpha\beta}=\frac{\partial U}{\partial e_{\alpha\beta}},\quad U=\sigma_{\alpha\beta}e_{\alpha\beta}-W \tag{2.21}$$

where the potential function U is homogeneous of degree $\bar{N}+1$ in $e_{\alpha\beta}$. (Recall $\bar{N}$ = $1/N$.)

The previous solution can be shown to be valid for a rate-dependent material law of the form

$$\epsilon_{\alpha\beta}=\dot{e}_{\alpha\beta}=\frac{\partial\sigma_e}{\partial\sigma_{\alpha\beta}}\epsilon_e,\quad \epsilon_e=\dot{e}_e \tag{2.22}$$

where σ_e and ϵ_e are homogeneous of degree one in $\sigma_{\alpha\beta}$ and $\epsilon_{\alpha\beta}$, respectively. (Thus, $\sigma_{\alpha\beta}\epsilon_{\alpha\beta}$ = $\sigma_e\epsilon_e$.) We assume the effective strain-rate to be a function of total effective strain e_e and effective stress as follows:

$$\epsilon_e=G(\sigma_e)H(e_e) \tag{2.23}$$

with $G(\sigma_e)$ homogeneous of degree s in σ_{ij} and $H(e_e)$ homogeneous of degree q in e_{ij}. We then have, from (2.12) and the above,

$$\dot{f}=g^s f^q\quad \text{or}\quad g=f^{-\frac{q}{s}}\dot{f}^{\frac{1}{s}} \tag{2.24}$$

Downloaded 03 May 2010 to 171.66.16.27. Redistribution subject to ASME license or copyright; see http://www.asme.org/terms/Terms_Use.cfm

and

$$\tilde{\epsilon}_{\alpha\beta}=\frac{\partial\tilde{\sigma}_e}{\partial\tilde{\sigma}_{\alpha\beta}}\,\tilde{\epsilon}_e,\quad \tilde{\epsilon}_e=\tilde{G}(\tilde{\sigma}_e)\tilde{H}(\tilde{e}_e) \tag{2.25}$$

$$\tilde{G}(\tilde{\sigma}_e)=k^s G(\tilde{\sigma}_e)=\frac{1}{g^s}\,G(\sigma_e),\quad \tilde{H}(\tilde{e}_e)=\frac{1}{f^q}\,H(e_e) \tag{2.26}$$

Equation (2.9) still holds, so that

$$g\sqrt{f}=f^{\left(\frac{1}{2}-\frac{q}{s}\right)}\dot{f}^{\frac{1}{s}}=\frac{p\ell}{kt} \tag{2.27}$$

For an effective stress-strain-strain rate relation of the type

$$\sigma_e=k e_e^{\bar{M}}\epsilon_e^{\bar{N}} \tag{2.28}$$

we have $s=1/\bar{N}$, $q=-\bar{M}/\bar{N}$ so that

$$g=\dot{f}^{\bar{N}}f^{\bar{M}},\quad \dot{f}^{\bar{N}}f^{\left(\bar{M}+\frac{1}{2}\right)}=\frac{p\ell}{kt} \tag{2.29}$$

This result (2.29) was derived previously by Hill and Storåkers for isotropic membranes characterized by the specific uniaxial relation (2.28). As shown there, this leads to the relation

$$[f(\tau)]^{\frac{2(\bar{M}+\bar{N})+1}{2\bar{N}}}=\frac{2(\bar{M}+\bar{N})+1}{2\bar{N}}\int_0^\tau\left(\frac{p\ell}{kt}\right)^{\frac{1}{\bar{N}}}d\tau+[f(0)]^{\frac{2(\bar{M}+\bar{N})+1}{2\bar{N}}} \tag{2.30}$$

With $H(e_e)=1$, $q=0$ (or $\bar{M}=0$ in 2.28), the above solution describes steady-creep deformations and reduces to the expressions (2.14)–(2.16). Alternatively, with $\bar{N}=0$ in equation (2.28) we recover the rate-independent result (2.6)–(2.11) where now $\bar{M}=1/N$. Furthermore, for the rigid-plastic (rate-independent) limit $\bar{M}\to 0$, equations (2.29) gives

$$g=1,\quad f=\left(\frac{p\ell}{kt}\right)^2 \tag{2.31}$$

3 Solution for Circular Membranes

As an example of application of the previous general analysis, we consider the axisymmetric deformation of a pressurized circular membrane of radius a. Polar coordinates (r, Φ) are used as a reference. The principal strains are

$$e_r=\frac{du}{dr}+\frac{1}{2}\,\theta^2,\quad e_\Phi=\frac{u}{r} \tag{3.1}$$

where u is the radial displacement, $\theta=-dw/dr$ is the slope of the deformed membrane and w again denotes the transverse displacement. The equilibrium equations replacing equations (2.2) are (Hill and Storåkers, 1980)

$$\sigma_\Phi=\frac{p}{2t}\,\frac{d}{dr}\left(\frac{r^2}{\theta}\right),\quad \sigma_r=\frac{p}{2t}\,\frac{r}{\theta} \tag{3.2}$$

where σ_Φ and σ_r are the circumferential and radial membrane stress components.

We shall limit attention to constitutive laws of the form (2.17) and power-law hardening of the type (2.18). In view of equations (2.3), (2.5), and (2.11), and the choice $\ell=a$, the reduced variables are defined as follows (Hill and Storåkers, 1980):

$$\begin{aligned}
&\frac{u}{a\tilde{u}}=\left(\frac{\theta}{\tilde{\theta}}\right)^2=\left(\frac{pa}{kt}\right)^{\frac{2}{2\bar{N}+1}}\\
&\frac{e_r}{\tilde{e}_r}=\frac{e_\Phi}{\tilde{e}_\Phi}=\frac{e_e}{\tilde{e}_e}=\left(\frac{pa}{kt}\right)^{\frac{2}{2\bar{N}+1}}\\
&\frac{\sigma_r}{k\tilde{\sigma}_r}=\frac{\sigma_\Phi}{k\tilde{\sigma}_\Phi}=\frac{\sigma_e}{k\tilde{\sigma}_e}=\left(\frac{pa}{kt}\right)^{\frac{2\bar{N}}{2\bar{N}+1}}
\end{aligned} \tag{3.3}$$

The reduced strains satisfy

$$\tilde{e}_r=\frac{d\tilde{u}}{d\tilde{r}}+\frac{1}{2}\,(\tilde{\theta})^2,\quad \tilde{e}_\Phi=\frac{\tilde{u}}{\tilde{r}} \tag{3.4}$$

where $\tilde{r}=r/a$. Furthermore, we have $\tilde{\sigma}_e=\tilde{e}_e^{\bar{N}}$. As a result, equations (3.2) become

$$\tilde{\sigma}_r=\frac{1}{2}\,\frac{\tilde{r}}{\tilde{\theta}},\quad \tilde{\sigma}_\Phi=\frac{1}{2}\,\frac{d}{d\tilde{r}}\left(\frac{\tilde{r}^2}{\tilde{\theta}}\right) \tag{3.5}$$

As expected, all of the reduced variables are functions of $\tilde{r}$ and $\bar{N}$, and are independent of the applied pressure p.

The general, transversely isotropic yield function proposed by Budiansky (1984) will be used to derive the plastic stress-strain relations. This theory assumes isotropy in the plane of the membrane. In terms of the principal stresses $\sigma_1=\sigma_\Phi$, $\sigma_2=\sigma_r$ the current yield locus is prescribed parametrically in the polar coordinate form

$$\frac{\sigma_2+\sigma_1}{2\sigma_b}=\rho(\psi)\cos\psi,\quad \frac{\sigma_2-\sigma_1}{2\sigma_s}=\rho(\psi)\sin\psi \tag{3.6}$$

where $\rho(0)=\rho(\pi/2)=1$, and σ_b, σ_s denote the yield stresses in equibiaxial tension and pure shear, respectively. Symmetry of the (continuous) yield locus about $\psi=0$ implies that $\rho'(0)=0$. Explicit representations for the stresses are

$$\begin{aligned}
&\frac{\sigma_\Phi}{\sigma_e}=\frac{\tilde{\sigma}_\Phi}{\tilde{\sigma}_e}=-\frac{X\rho\sin(\psi-\psi_u)}{\sin\psi_u}\\
&\frac{\sigma_r}{\sigma_e}=\frac{\tilde{\sigma}_r}{\tilde{\sigma}_e}=\frac{X\rho\sin(\psi+\psi_u)}{\sin\psi_u}
\end{aligned} \tag{3.7}$$

where $X=\sigma_b/\sigma_u$, $\sigma_u=\sigma_e$ is the yield stress in uniaxial tension and $\psi_u=\tan^{-1}(\sigma_b/\sigma_s)$. The plastic constitutive relations equivalent to equation (2.17) are (Budiansky, 1984)

$$\begin{aligned}
&\frac{e_\Phi}{e_e}=\frac{\tilde{e}_\Phi}{\tilde{e}_e}=\frac{[\rho\sin(\psi+\psi_u)]'}{2X\rho^2\cos\psi_u}\\
&\frac{e_r}{e_e}=\frac{\tilde{e}_r}{\tilde{e}_e}=\frac{[\rho\sin(\psi-\psi_u)]'}{2X\rho^2\cos\psi_u}
\end{aligned} \tag{3.8}$$

where the prime denotes differentiation with respect to ψ. (Note that equations (3.7), (3.8) satisfy the equivalent-work postulate $\sigma_e e_e=\sigma_r e_r+\sigma_\Phi e_\Phi$.)

The above equations can be arranged as follows

$$\begin{aligned}
&\tilde{e}_e\,\frac{[\rho\sin(\psi+\psi_u)]'}{2X\rho^2\cos\psi_u}=\frac{\tilde{u}}{\tilde{r}}\\
&\tilde{e}_e\,\frac{[\rho\sin(\psi-\psi_u)]'}{2X\rho^2\cos\psi_u}=\frac{d\tilde{u}}{d\tilde{r}}+\frac{1}{2}\,(\tilde{\theta})^2\\
&\tilde{e}_e^{\bar{N}}\,\frac{X\rho\sin(\psi+\psi_u)}{\sin\psi_u}=\frac{1}{2}\left(\frac{\tilde{r}}{\tilde{\theta}}\right)\\
&-\tilde{e}_e^{\bar{N}}\,\frac{X\rho\sin(\psi-\psi_u)}{\sin\psi_u}=\frac{d}{d\tilde{r}}\left(\frac{\tilde{r}^2}{2\tilde{\theta}}\right)
\end{aligned} \tag{3.9}$$

These are to be solved for $\tilde{u}(\tilde{r})$, $\tilde{\theta}(\tilde{r})$, $\tilde{e}_e(\tilde{r})$ and $\psi(\tilde{r})$, subject to the following boundary conditions:

$$\begin{aligned}
&\tilde{e}_r(0)=\tilde{e}_\Phi(0)\quad\text{or}\quad\tilde{\sigma}_r(0)=\tilde{\sigma}_\Phi(0)\\
&\tilde{u}(1)=0
\end{aligned} \tag{3.10}$$

In view of equations (3.7)–(3.9), the boundary conditions become

$$\begin{aligned}
&\psi(0)=0,\quad \frac{\tilde{u}(0)}{\tilde{r}}=\frac{\tilde{e}_e(0)}{2X},\quad \frac{\tilde{\theta}(0)}{\tilde{r}}=\frac{1}{2X}\,[\tilde{e}_e(0)]^{-\bar{N}}\\
&\tilde{u}(1)=0,\quad \psi(1)=\psi^*
\end{aligned} \tag{3.11}$$

where ψ^* is the root of $[\rho\sin(\psi+\psi_u)]'=0$ (except for the limiting case of zero hardening ($\bar{N}=0$) where $\psi=0$ for $0\le\tilde{r}$

Downloaded 03 May 2010 to 171.66.16.27. Redistribution subject to ASME license or copyright; see http://www.asme.org/terms/Terms_Use.cfm

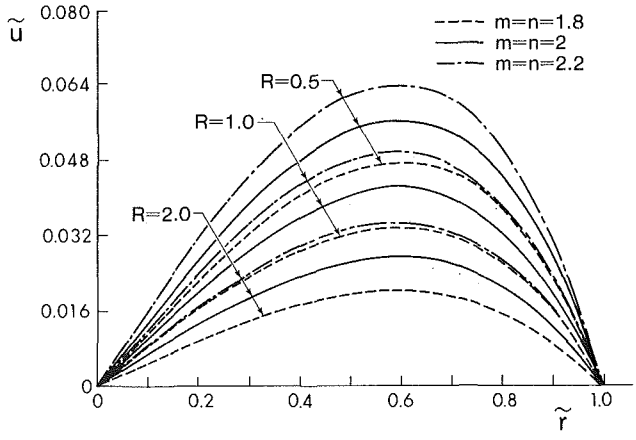


Fig. 1 Distributions of reduced radial displacement $\tilde{u}$ for $\bar{N} = 0.2$

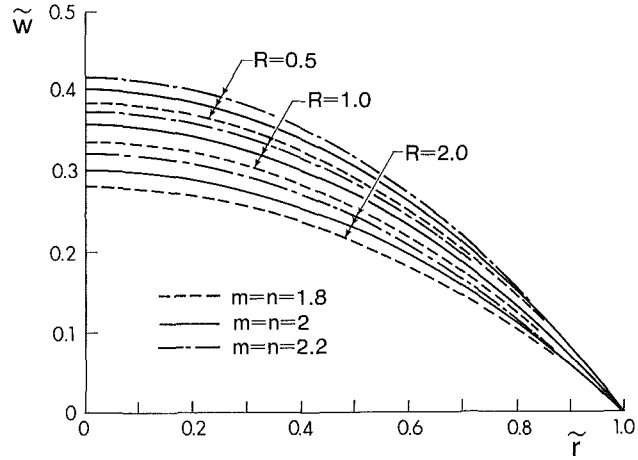


Fig. 2 Distributions of reduced transverse displacement $\tilde{w}$ for $\bar{N} = 0.2$

≤ 1). For this case ($\bar{N} = 0$) the following analytic solution, given by Hill and Storåkers for isotropic membranes, applies

$$\tilde{u} = \frac{1}{16X^2}\,\tilde{r}(1-\tilde{r}^2), \qquad \tilde{\theta} = \frac{1}{2X}\,\tilde{r}$$
$$\tilde{e}_e = \frac{1}{8X}\,(1-\tilde{r}^2), \qquad \psi = 0 \tag{3.12}$$

The state of stress is uniform throughout the membrane and is such that $\sigma_r = \sigma_\Phi = kX$. The actual displacements, as determined from equations (3.3) and (3.12), are

$$u = \frac{hrw}{a^2}, \quad w = h\left(1-\frac{r^2}{a^2}\right) \tag{3.13}$$

where the maximum deflection h is given by

$$\frac{h}{a} = \frac{1}{4X}\left(\frac{pa}{kt}\right) \tag{3.14}$$

The von Mises yield function corresponds to the choice $\rho(\psi) = X = 1$, $\psi_u = \tan^{-1}(\sqrt{3})$ in Budiansky's general representation. In this case the above equations (3.9) and boundary conditions (3.11) reduce to those given by Hill and Storåkers (1980). Other more general yield functions of the form

$$\rho(\psi) = [|\cos\psi|^m + |\sin\psi|^m]^{-\frac{1}{m}} \tag{3.15}$$

and

$$|\rho(\psi)\sin\psi|^m + |\rho(\psi)\cos\psi|^n = 1 \tag{3.16}$$

have been proposed in turn by Hill (1979) and Bassani (1977). When $\bar{N} \neq 0$, the associated system of equations (3.9) must be solved numerically. This has been done for the von Mises material by Hill and Storåkers (1980) using a Runge-Kutta technique. A similar method will be used here to obtain numerical solutions for other yield functions $\rho(\psi)$.

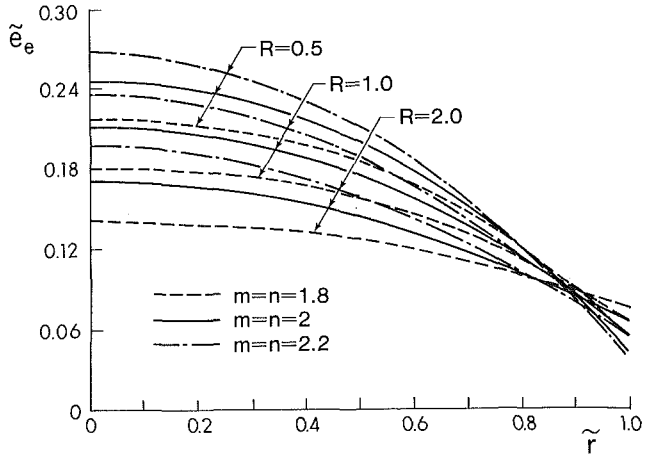


Fig. 3 Distributions of reduced effective strain $\tilde{e}_e$ for $\bar{N} = 0.2$

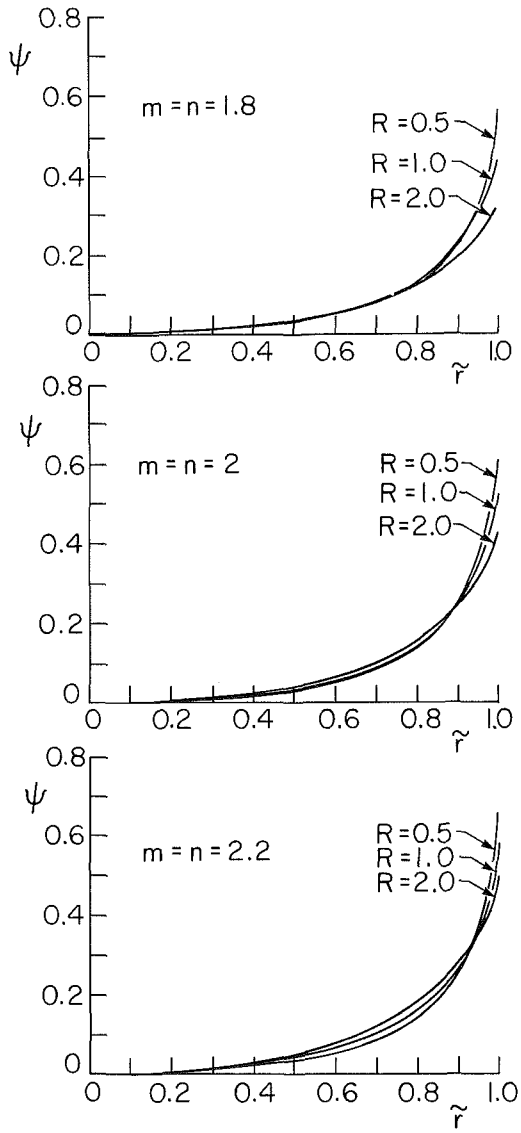


Fig. 4 Distributions of parametric angle ψ for $\bar{N} = 0.2$

Downloaded 03 May 2010 to 171.66.16.27. Redistribution subject to ASME license or copyright; see http://www.asme.org/terms/Terms_Use.cfm

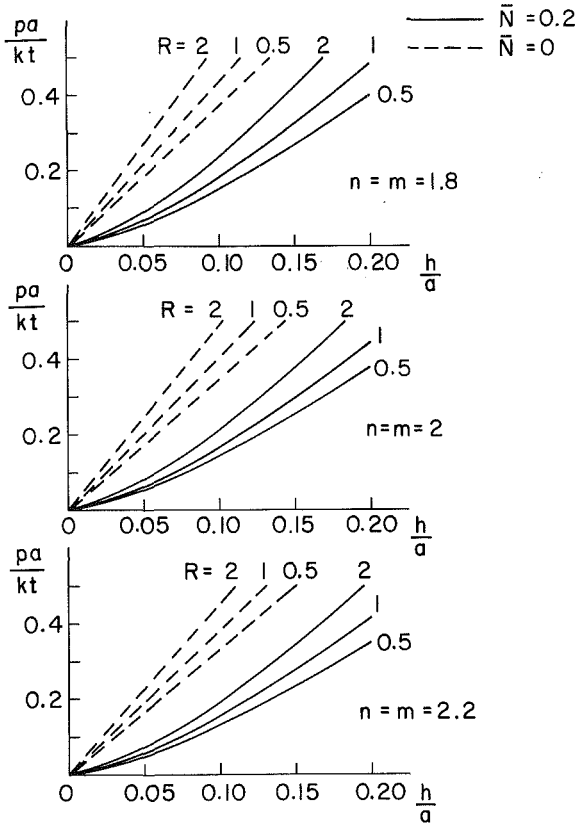


Fig. 5 Normalized pressure-deflection curves for anisotropic membranes

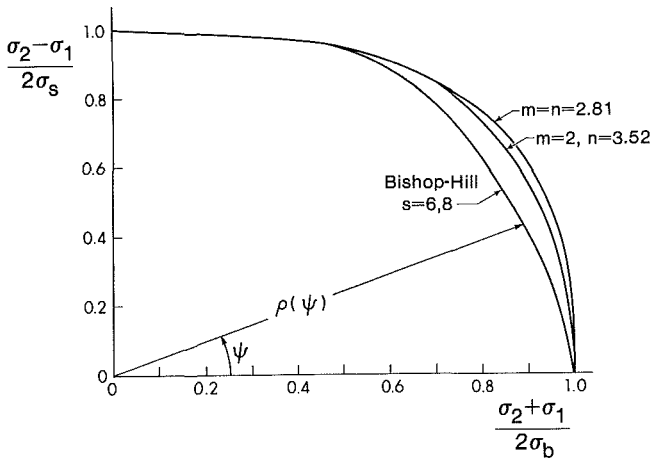


Fig. 6 Bishop-Hill yield locus and approximate representations of Hill, Bassani, and Budiansky

We note finally that, when the constitutive law is of the general form (2.21), the variational principle established by Hill and Storåkers (1980) can be used to provide approximate solutions for noncircular membranes. Their principle states that

$$\delta\iint(tU-pw)\,dx\,dy=0 \tag{3.17}$$

and they have shown its applicability for elliptic membranes. Other variational formulations and bounding principles have also been given by Storåkers (1983c) for membranes characterized by the constitutive law (2.21). These can be exploited for anisotropic membranes in the ways illustrated by Storåkers (1983c).

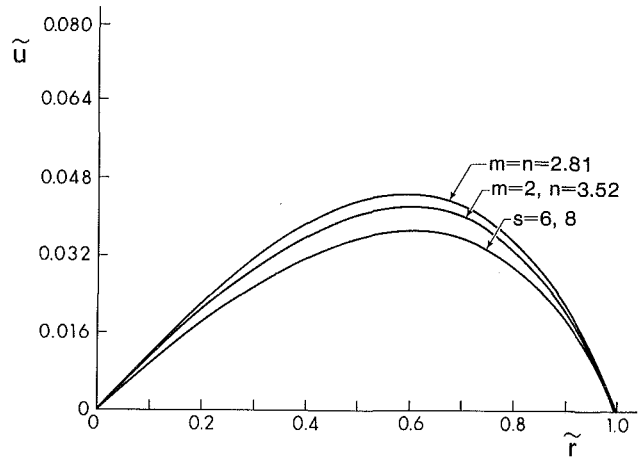


Fig. 7 Distributions of reduced radial displacement $\tilde{u}$ for $\bar{N}$ = 0.2

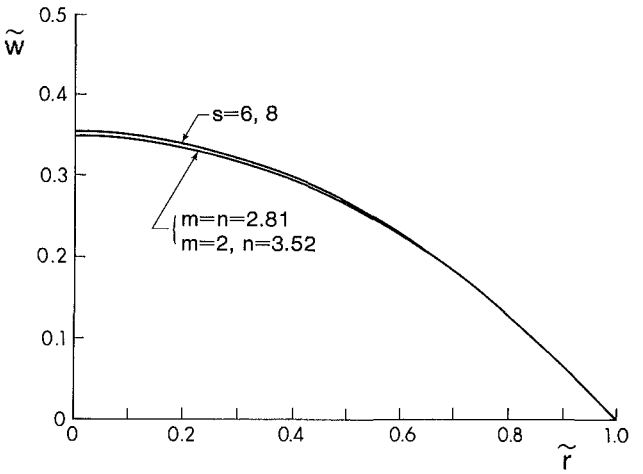


Fig. 8 Distributions of reduced transverse displacement $\tilde{w}$ for $\bar{N}$ = 0.2

4 Numerical Results and Discussion

Numerical solutions to the system of equations (3.9) have been obtained using a slightly modified version of the Runge-Kutta technique employed by Hill and Storåkers (1980). Here an integration of the two differential equations in (3.9) is initiated at the pole $\tilde{r}=0$, beginning with a trial guess for $\tilde{e}_e(0)$, to produce solutions for $\tilde{u}$ and $\tilde{\theta}$. At each step of the integration process, the remaining two nonlinear algebraic equations are solved for $\tilde{e}_e$ and ψ. This process is repeated iteratively until the assumed value of $\tilde{e}_e(0)$ furnishes a solution which satisfies the boundary conditions (3.11) at $\tilde{r}=1$.

Results are first given for Hill's (1979) two-parameter yield function (3.15) (or, equivalently, equation (3.16) with $m=n$) in Figs. 1–4. These results correspond to a hardening value of $\bar{N}=0.2$. Here R is the parameter commonly used to characterize sheet metal anisotropy. It is related to m, n and $X=\sigma_b/\sigma_u$ as follows (Budiansky, 1984)

$$R=\frac{1}{2}\left\{\frac{m}{n}\left[(2X)^n-1\right]-1\right\} \tag{4.1}$$

and represents the ratio of in-plane transverse plastic strain to the plastic strain in the thickness direction for in-plane uniaxial tension. The case $R=1$, $m=n=2$ ($X=1$) corresponds to the isotropic, von Mises material treated by Hill and Storåkers (1980).

Figures 1 and 2 show the effects of anisotropy on the reduced displacements $\tilde{u}$ and $\tilde{w}$. They indicate that these displacements increase if the parameter R is reduced or the parameter $m=n$ is increased. The same observation is gener-

Downloaded 03 May 2010 to 171.66.16.27. Redistribution subject to ASME license or copyright; see http://www.asme.org/terms/Terms_Use.cfm

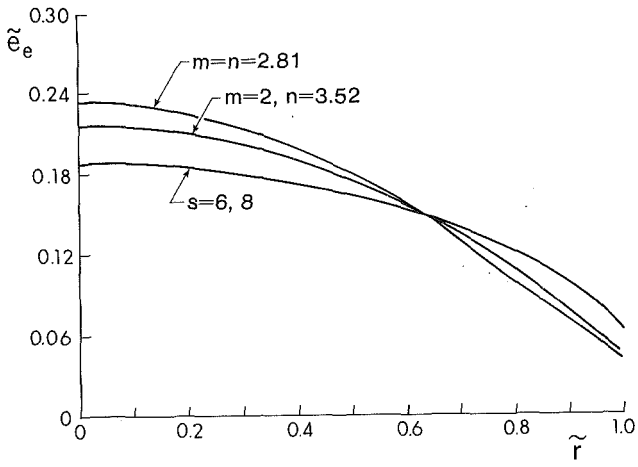


Fig. 9 Distributions of reduced effective strain $\tilde{e}_e$ for $\bar{N} = 0.2$

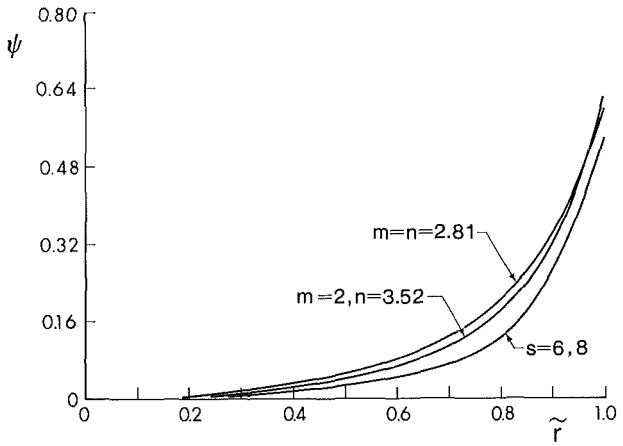


Fig. 10 Distributions of parametric angle ψ for $\bar{N} = 0.2$

ally true for the effective strain distribution $\tilde{e}_e$ (Fig. 3). The distributions of ψ, however, are rather insensitive to variations in R and $m = n$ (Fig. 4), except in the vicinity of $\tilde{r} = 1$ where the values of ψ are dictated by the boundary condition (3.11).

A comparison of the numerical results for $\bar{N} = 0.2$ and the exact analytical solution (3.12)–(3.14) for $\bar{N} = 0$ illustrates the combined effects of strain-hardening and anisotropy on the behavior of the membrane. For example, the maximum bulge deflection h is given by

$$\frac{h}{a} = \tilde{w}(0)\left(\frac{pa}{kt}\right)^{\frac{1}{2\bar{N}+1}}$$

which reduces to equation (3.14) for the case of zero hardening. Plots of nondimensional pressure (pa/kt) as a function of h/a are displayed in Fig. 5 for the two cases $\bar{N} = 0, 0.2$. They show first that, for a given pressure, the bulge height increases as R is reduced or $m = n$ is increased, as mentioned above. These results are consistent with those obtained by Chater and Neale (1983a) for the large-strain behavior of anisotropic membranes having similar anisotropic properties. Figure 5 also indicates that the bulge height increases as the strain-hardening exponent $\bar{N}$ increases, as observed by Hill and Storåkers (1980) for the Mises material ($n = m = 2$, $R = 1$) and Chater and Neale (1983a) for large-deformation anisotropic behavior.

In Figs. 6–10 we examine the effects of the detailed shape of the anisotropic yield function on the predicted results. Figure 6 shows a yield locus that Bassani (1977) computed for a textured polycrystal using the Bishop-Hill procedure. For this case $R = 2.7$, $X = 1.02$, and $\sigma_b/\sigma_s = 1.94$. Also shown here are two approximate fits ($m = n = 2.81$; $m = 2$, $n = 3.52$) to the Bishop-Hill locus that Bassani obtained using Hill's (1979) yield function (3.15), and his own three-parameter representation (3.16), respectively. We further considered the following parametric form suggested by Budiansky (1984)

$$\rho(\psi) = \sum_{i=0}^{s} a_i \cos(2i\psi) \tag{4.3}$$

and attempted to produce curves identical to the Bishop-Hill locus. Figure 6 shows the best fits of equation (4.3) obtained with $s = 6, 8$.

The computed results for the various yield loci are plotted in Figs. 7–10 for the case $\bar{N} = 0.2$. It can be seen that $\tilde{u}$, $\tilde{e}_e$, and ψ vary somewhat as the yield function is altered, but that small changes in the detailed shape of the yield locus have a negligible influence on the bulge profile $\tilde{w}$. For a zero-hardening material, the overall shape of the yield surface has no influence whatsoever on the behavior of the membrane; only the parameter $X = \sigma_b/\sigma_u$ enters in the analytic solution (3.12). In contrast, the predicted conditions for localized necking in sheet metals based on the above yield functions have been found to be strongly dependent on the detailed shape of the yield surface (Bassani et al., 1979).

Acknowledgments

This work was supported in part by the Natural Sciences and Engineering Research Council of Canada (NSERC) and the Government of the Province of Québec (Programme FCAR).

References

Bassani, J. L., 1977, "Yield Characterization of Metals With Transversely Isotropic Plastic Properties," *International Journal of Mechanical Sciences*, Vol. 19, pp. 651–660.

Bassani, J. L., Hutchinson, J. W., and Neale, K. W., 1979, "On the Prediction of Necking in Anisotropic Sheets," *Metal Forming Plasticity*, Lippmann, H., ed., Springer-Verlag, New York, pp. 1–13.

Budiansky, B., 1984, "Anisotropic Plasticity of Plane-Isotropic Sheets," *Mechanics of Material Behavior*, Dvorak, G. J., and Shield, R. T., eds., Elsevier Science Publishers, Amsterdam, pp. 15–29.

Chater, E., and Neale, K. W., 1983a, "Finite Plastic Deformation of a Circular Membrane Under Hydrostatic Pressure – I. Rate-Independent Behaviour," *International Journal of Mechanical Sciences*, Vol. 25, pp. 219–233.

Chater, E., and Neale, K. W., 1983b, "Finite Plastic Deformation of a Circular Membrane Under Hydrostatic Pressure – II. Strain-Rate Effects," *International Journal of Mechanical Sciences*, Vol. 25, pp. 235–244.

Hill, R., 1979, "Theoretical Plasticity of Textured Aggregates," *Mathematical Proceedings of the Cambridge Philosophical Society*, Vol. 85, pp. 179–191.

Hill, R., and Storåkers, B., 1980, "Plasticity and Creep of Pressurized Membranes: A New Look at the Small-Deflection Theory," *Journal of the Mechanics and Physics of Solids*, Vol. 28, pp. 27–48.

Storåkers, B., 1983a, "Small Deflections of Linear Elastic Circular Membranes Under Lateral Pressure," ASME JOURNAL OF APPLIED MECHANICS, Vol. 50, pp. 735–739.

Storåkers, B., 1983b, "A Viscoelastic Correspondance Principle for Plane Membranes Subjected to Lateral Pressure," ASME JOURNAL OF APPLIED MECHANICS, Vol. 50, pp. 740–742.

Storåkers, B., 1983c, "Variation Principles and Bounds for the Approximate Analysis of Plane Membranes Under Lateral Pressure," ASME JOURNAL OF APPLIED MECHANICS, Vol. 50, pp. 743–749.

Downloaded 03 May 2010 to 171.66.16.27. Redistribution subject to ASME license or copyright; see http://www.asme.org/terms/Terms_Use.cfm

A Sixth-Order Plate Theory—Derivation and Error Estimates

Z. Rychter
Institute of Architecture,
Technical University of Bialystok,
15-875 Bialystok, Poland

Two consistent variants of a sixth-order theory for elastic plate bending are developed together with corresponding three-dimensional statically and kinematically admissible solutions. The relative mean square error of these solutions as compared with exact elasticity solutions is found to be proportional to the thickness squared in analogy with previous estimates for Reissner's theory, but the contribution to the error governed by transverse shear deformability is reduced and shown to be of the order of the thickness cubed, this contribution being decisive in composite plates.

1 Introduction

There is an increasing number of two-dimensional theories for elastic plate bending, beginning with the Kirchhoff classical fourth-order theory (here we have in mind the order of the governing differential equations), through various sixth-order theories taking account of transverse shear and sometimes transverse normal strains, through less popular higher-than sixth-order theories which include contributions of stresses self-equilibrating over the thickness, and ending with formal nth-order theories based on diverse polynomial expansions with respect to the thickness coordinate. As these theories are comprehensively covered in the literature, to name a monograph by Panc (1975) or recent papers by Reddy (1984), Rehfield and Valisetty (1984), and Reissner (1985), we may dispense with their review here.

Being only approximations to the three-dimensional theory of elasticity, plate theories require validation which as a rule is restricted to solving simple examples where exact elasticity solutions are known. Since the pioneering works of Prager and Synge (1947) and Synge (1957) a more fundamental and rigorous approach towards accuracy analysis has become available which is based on the hypersphere theorem and related energy inequalities. The method provides global mean square error bounds in terms of statically and kinematically admissible approximations. There have been only a few applications of this approach. Nordgren (1971) was the first to study the accuracy of Kirchhoff's plate theory, his result being refined by Simmonds (1971) and Nordgren (1972), where the relative error was found to be of the order of the plate thickness squared. The same order error was also obtained by Nordgren (1972) for Reissner's sixth-order theory. In a recent study, Rychter (1984), the present writer derived an error bound for a "component" fourth-order theory due to Panc (1975), giving particular attention to anisotropic plates which have increased transverse shear deformability.

This report studies a recent sixth-order theory by Levinson (1980). The theory is remarkable in that it may be regarded as a complement to Reissner's theory insofar as geometric boundary conditions are concerned; in the later theory, the kinematic variables are weighted averages of the thickness distributions of displacements, while the former theory introduces pointwise lateral deflection and rotations of normals to the middle plane of the plate. The simplicity of Levinson's theory makes it appealing from a practical viewpoint, but several questions must be answered, relating to its consistency and accuracy, before it can be safely used. First, in his elementary derivation Levinson adopted the conventional equations of equilibrium known from the classical and Reissner theories. In a recent paper Reddy (1984) argues that such equilibrium equations are variationally inconsistent with the cubic tangential displacement distribution over the plate thickness assumed by Levinson. Unfortunately, Reddy's consistent theory turns out to be of the eighth order, thus requiring the prescription of four static or geometric quantities at each edge of the plate whereas usually only three quantities can be determined. Further, Levinson has validated his equations by making a comparison with Reissner's and elasticity theories for the torsion of a rectangular plate. Although a good fit was found, the problem considered hardly represents common plate applications as elements subject to bending under transverse loads and, consequently, no general conclusions pertaining to the range of applicability of Levinson's theory can be made. What is more, Levinson provides no means for obtaining from his two-dimensional theory three-dimensional distributions of stresses which are usually needed. Finally, one may ask whether Levinson's theory can be simplified without loss of accuracy so that there would be only one unknown deflection of the middle plane present, similar to simplified versions of Reissner's theory due to Speare and Kemp (1977), and of Ambartsumyan's theory due to Shirakawa (1983).

Contributed by The Applied Mechanics Division for publication in the JOURNAL OF APPLIED MECHANICS.

Discussion on this paper should be addressed to the Editorial Department, ASME, United Engineering Center, 345 East 47th Street, New York, N.Y. 10017, and will be accepted until two months after final publication of the paper itself in the JOURNAL OF APPLIED MECHANICS. Manuscript received by ASME Applied Mechanics Division, September 26, 1986.

Copyright © 1987 by ASME
Downloaded 03 May 2010 to 171.66.16.27. Redistribution subject to ASME license or copyright; see http://www.asme.org/terms/Terms_Use.cfm

In the present paper, all of these problems are solved in a general, rigorous, and systematic way. Levinson's theory is derived here in parallel with corresponding three-dimensional statically and kinematically admissible solutions which are shown to be close approximations to unknown exact elasticity solutions. We start with Levinson's cubic distribution of tangential displacement over the thickness, yet his assumption of constancy of the lateral deflection over the thickness is replaced by a fourth-degree polynomial in the thickness coordinate. Another departure is that we assume a transversely isotropic material rather than an isotropic one, since Levinson's theory takes account of transverse shear deformation which is much more pronounced in anisotropic plates, such as those made of modern composites. Apart from Levinson's version of plate theory, a simplified variant is derived in which all static and kinematic variables are expressed in terms of the lateral deflection of the middle plane. Both variants are shown to be of essentially the same accuracy—they provide three-dimensional approximations whose mean square error is found to be proportional to the thickness squared. Importantly, the contribution to the error which comes from transverse shear deformability is proportional to the thickness cubed, such a contribution being crucial in composite plates. In this respect our estimates are better than those of Nordgren (1972) for Reissner's theory where the shear part of the error was proportional to the thickness squared. This improvement is attributed to the fact that our statically admissible three-dimensional solution incorporates stresses self-equilibrating over the thickness, similar to those in Reissner (1975), Reissner (1985), and Rehfield and Valisetty (1984). Our analysis proves that Levinson's theory is consistent and precise, just as Reissner's theory, despite the reservations by Reddy (1984). As a by-product, that value 2/3 is found to be the correct shear factor for Levinson's theory, similar to the value 5/6 established by Nordgren (1972) for Reissner's theory.

2 Derivation of Levinson's Theory

As is well known, an exact elasticity solution can be approached using statically admissible stresses σ' and kinematically admissible stresses σ'', their difference being a measure for the closeness of approximation. Here we shall construct a pair of such stress fields which will entirely depend on the variables of Levinson's plate theory and will be sufficiently close to each other for our purposes.

The statically admissible field σ' (x_i, z), where x_i $(i=1, 2)$ are Cartesian coordinates on the middle plane and $z=x_3$ is normal distance from that plane, is expected to satisfy the equations of equilibrium with zero body forces

$$\sigma'_{ij,j}+\sigma'_{i3,3}=0 \tag{1}$$

$$\sigma'_{i3,i}+\sigma'_{33,3}=0 \tag{2}$$

where primes indicate partial differentiation and the standard summation convention on repeated indices is adopted. Additionally, σ' is subject to the traction boundary conditions on the faces

$$\sigma'_{i3}(x_j, z=\pm h)=0 \tag{3}$$

$$\sigma'_{33}(x_j, z=-h)=0 \quad \sigma'_{33}(x_j, z=h)=p(x_j) \tag{4}$$

according to which the upper face carries a distributed lateral load p; $2h$ denotes the thickness of the plate which is assumed constant.

As for the kinematically admissible stress field $\sigma''(x_i, z)$, it is only required to be generated from the displacement field $\mathbf{u}''(x_i, z)$ via the constitutive equations

$$\sigma''_{ij}=D[(1-\nu)u''_{(i,j)}+\nu\delta_{ij}u''_{k,k}]+C\delta_{ij}\sigma''_{33} \tag{5}$$

$$\sigma''_{i3}=2G'u''_{(i,3)} \tag{6}$$

$$\sigma''_{33}=(u''_{3,3}+Cu''_{i,i})E'(1-\nu)/(1-\nu-2\nu'^2E/E') \tag{7}$$

where

$$D=E/(1-\nu^2) \qquad C=\nu'E/(1-\nu)E' \tag{8}$$

δ_{ij} being the Kronecker delta and a pair of indices enclosed in parentheses indicating symmetrization. The material has been taken to be homogeneous and transversely isotropic so that the planes $z=$ const are the planes of isotropy. The five elastic constants involved are Young's modulus E and Poisson's ratio ν in planes of isotropy, and Young's modulus E', the shear modulus G' and Poisson's ratio ν' in transverse planes. In our development, we take into account the fact that the ratio E/G' may be large compared to unity which is common for composite plates.

The initial kinematical hypothesis about the displacement distribution over the thickness reads

$$u''_i(x_j, z)=zb_i(x_j)+z^3f_i(x_j) \tag{9}$$

$$u''_3(x_j, z)=w(x_j)+z^2g(x_j)+z^4r(x_j) \tag{10}$$

these relations being consistent with

$$b_i(x_j)=u''_{i,3}(x_j, z=0) \tag{11}$$

$$w(x_j)=u''_3(x_j, z=0) \tag{12}$$

According to equations (11) and (12), b_i and w are interpreted as rotations of normals and lateral deflection evaluated at the middle surface of the plate. This is the major departure from Reissner's theory where b_i and w are weighted averages of displacements. In what follows, b_i and w are regarded as the main kinematic variables of Levinson's theory—the remaining two-dimensional functions in equations (9) and (10), f, g, and r, will be found in terms of b_i and w.

Guided by the fact that Levinson's theory neglects transverse normal stress, we assume that

$$\sigma''_{33}=0 \tag{13}$$

Introducing equations (9) and (10) into (7), equation (13) is seen to be satisfied when

$$g=-(1/2)Cb_{i,i} \qquad r=-(1/4)Cf_{i,i} \tag{14}$$

Substitution of equations (9), (10), and (13) into (5) yields kinematically admissible surface parallel stresses,

$$\sigma''_{ij}=zD[(1-\nu)b_{(i,j)}+\nu\delta_{ij}b_{k,k}]+z^3D[(1-\nu)f_{(i,j)}+\nu\delta_{ij}f_{k,k}] \tag{15}$$

Since our general idea is to have σ' close to σ'', we take

$$\sigma'_{ij}=zD[(1-\nu)b_{(i,j)}+\nu\delta_{ij}b_{k,k}]+z^3D[(1-\nu)f'_{(i,j)}+\nu\delta_{ij}f'_{k,k}] \tag{16}$$

f'_i being an approximation to f_i. Now the moments M_{ij} of plate theory are defined as resultants of σ'_{ij} through

$$M_{ij}=\int_{-h}^{h}\sigma'_{ij}z\,dz \tag{17}$$

which, after substituting from equation (16), yield the constitutive equations of Levinson's theory

$$M_{ij}=(2/3)h^3D[(1-\nu)b_{(i,j)}+\nu\delta_{ij}b_{k,k}]+(2/5)h^5D[(1-\nu)f'_{(i,j)}+\nu\delta_{ij}f'_{k,k}] \tag{18}$$

With equation (18), the stresses in equation (16) may be brought into the form

$$\sigma'_{ij}=(3z/2h^3)M_{ij}+(D/5)(5z^3-3h^2z)[(1-\nu)f'_{(i,j)}+\nu\delta_{ij}f'_{k,k}] \tag{19}$$

Introduction of equation (19) into the equation of equilibrium

Downloaded 03 May 2010 to 171.66.16.27. Redistribution subject to ASME license or copyright; see http://www.asme.org/terms/Terms_Use.cfm

(1) and integration in the latter with respect to z under the boundary conditions (3) furnishes the statically admissible transverse shear stresses

$$\sigma'_{i3} = (3/4h)(1 - z^2/h^2)M_{ij,j} - (D/20)(5z^4 - 6h^2z^2 + h^4)[(1-\nu)f'_{(i,j)j} + \nu f'_{j,ji}] \quad (20)$$

The shear forces Q_i are defined as resultants of σ'_{i3} through

$$Q_i = \int_{-h}^{h} \sigma'_{i3} dz \quad (21)$$

Substituting here form equation (20) gives the first equilibrium equation of Levinson's theory

$$Q_i = M_{ij,j} \quad (22)$$

Further, introduction of equation (20) with (22) into the equation of equilibrium (2) and integration in the latter with respect to z under the boundary conditions (4) gives the transverse normal stress

$$\sigma'_{33} = (1/4h^3)(z^3 - 3h^2z - 2h^3)Q_{i,i} + (D/20)(z^5 - 2h^2z^3 + h^4z)f'_{j,jii} \quad (23)$$

To satisfy the boundary conditions (4), it is required that

$$Q_{i,i} = -p \quad (24)$$

which represents the second equilibrium equation of Levinson's theory.

To have σ' close to σ'', we adopt Levinson's constitutive equations for the shear forces

$$Q_i = (4/3)G'h(b_i + w_{,i}) \quad (25)$$

and specify the functions f_i and f'_i to be

$$f_i = -g_{,i}/3 - (b_i + w_{,i})/3h^2 \quad (26)$$

$$f'_i = -(b_i + w_{,i})/3h^2 \quad (27)$$

which with equation (25) may also be rewritten as

$$f_i = -g_{,i}/3 - Q_i/4G'h^3 \quad (28)$$

$$f'_i = -Q_i/4G'h^3 \quad (29)$$

Substitution of equations (9) and (10) into the constitutive equations (6) and use of equations (25)–(27) gives

$$\sigma''_{i3} = (3/4h)(1 - z^2/h^2)Q_i + z^4G'r_{,i} \quad (30)$$

Finally, comparison between equations (16), (20), (23), and equations (15), (30), (13), with use of equations (22), (26), and (27), yields

$$\sigma'_{ij} - \sigma''_{ij} = (z^3D/3)[(1-\nu)g_{,ij} + \nu\delta_{ij}g_{,kk}] \quad (31)$$

$$\sigma'_{i3} - \sigma''_{i3} = -z^4G'r_{,i} - (D/20)(5z^4 - 6h^2z^2 + h^4)[(1-\nu)f'_{(i,j)j} + \nu f'_{j,ji}] \quad (32)$$

$$\sigma'_{33} - \sigma''_{33} = (1/4h^3)(z^3 - 3h^2z - 2h^3)Q_{i,i} + (D/20)(z^5 - 2h^2z^3 + h^4z)f'_{j,jii} \quad (33)$$

In summary, we have arrived at the following result. The two-dimensional Levinson's plate theory consists of the equilibrium equations (22) and (24) and the constitute relations (18), (25), with f'_i given in equation (27). The theory incorporates the moments M_{ij}, shear forces Q_i, rotations b_i, and midsurface deflection w. The governing equations in terms of b_i and w are readily verified to constitute a sixth-order system of partial differential equations. At the same time, we have constructed the three-dimensional displacement and stress fields $\mathbf{u}''$, $\boldsymbol{\sigma}''$, and $\boldsymbol{\sigma}'$, defined entirely through the dependent variables of Levinson's theory, which may be used for the computation of stress and displacement distributions over the thickness of the plate once b_i and w have been found. When specified for isotropic materials, the plate theory developed above coincides with Levinson's equations. The three-dimensional displacements $\mathbf{u}''$, however, are significantly different from those in Levinson (1980) in that they incorporate contributions contained in the functions g and r. What's more, the stresses $\boldsymbol{\sigma}'$ are entirely new, these being not considered by Levinson. In this way, Levinson's theory has been put here in its proper three-dimensional perspective.

Our approach does not lead in a natural way to a correct formulation of the boundary conditions on the cylindrical edge surface of the plate. Guided by previous research on sixth-order plate theories, we take the traction boundary conditions to involve the prescription of the moments $M_{ij}n_j$ and shear force Q_in_i, and the kinematic boundary conditions, the prescription of the rotations b_i, and deflection w, where n_i is the outward unit normal vector to the edge. It can only be said that such boundary conditions comply with our thickness distributions of the kinematically admissible displacements $\mathbf{u}''$ and statically admissible stresses $\boldsymbol{\sigma}'$.

3 Error Estimates

What remains to be seen here is that the three-dimensional solutions of the preceding section are valid approximations to exact elasticity solutions consisting of displacements $\mathbf{u}$ and stresses $\boldsymbol{\sigma}$. Formally, the proof is based on the following inequalities:

$$\|\boldsymbol{\sigma}' - \boldsymbol{\sigma}\| / \|\boldsymbol{\sigma}'\| \leqq e' \quad (34)$$

$$\|\boldsymbol{\sigma}''(\mathbf{u}'') - \boldsymbol{\sigma}(\mathbf{u})\| / \|\boldsymbol{\sigma}''(\mathbf{u}'')\| \leqq e'' \quad (35)$$

where

$$e' = \|\tilde{\boldsymbol{\sigma}}\| / \|\boldsymbol{\sigma}'\| \quad e'' = \|\tilde{\boldsymbol{\sigma}}\| / \|\boldsymbol{\sigma}''\| \quad \tilde{\boldsymbol{\sigma}} = \boldsymbol{\sigma}' - \boldsymbol{\sigma}'' \quad (36)$$

derived by Synge (1957), see also Pecknold (1973). Here $\|\bullet\|$ denotes a mean square norm based on elastic energy, which for our transversely isotropic plate reads

$$\|\boldsymbol{\sigma}^*\|^2 = \int_{-h}^{h}\int_F [(1+\nu)\sigma^*_{ij}\sigma^*_{ij} - \nu\sigma^*_{ii}\sigma^*_{jj} - (2\nu'E/E')\sigma^*_{ii}\sigma^*_{33} + (E/G')\sigma^*_{i3}\sigma^*_{i3} + (E/E')\sigma^*_{33}\sigma^*_{33}]dFdz \quad (37)$$

$\boldsymbol{\sigma}^*$ being an arbitrary symmetric stress field and F being the region occupied by the midplane. The norm in equation (37) for stresses defines a norm for displacements, say $\mathbf{u}^*$, via the relation $\|\boldsymbol{\sigma}^*(\mathbf{u}^*)\|$, provided that rigid-body motions are deleted, where the stresses $\boldsymbol{\sigma}^*$ are obtained from the displacements $\mathbf{u}^*$ through the constitutive equations (5)–(7). In view of relations (34)–(36), the statically admissible stresses $\boldsymbol{\sigma}'$ and kinematically admissible displacements $\mathbf{u}''$ approach the exact stresses $\boldsymbol{\sigma}$ and displacements $\mathbf{u}$ with a relative error not exceeding e' and e'', respectively, where e' and e'' depend only on the approximate solutions $\boldsymbol{\sigma}'$ and $\boldsymbol{\sigma}''$, and decrease as the difference $\boldsymbol{\sigma}' - \boldsymbol{\sigma}''$ is decreased.

The quantities in equations (36) are aggregate measures of error, as they comprise all components of the stresses involved. For our purposes it is expedient to isolate portions which depend on transverse shear and tranverse normal deformability. Thus we split $\tilde{\boldsymbol{\sigma}}$ as follows:

$$\tilde{\boldsymbol{\sigma}} = \tilde{\boldsymbol{\sigma}}_s + \tilde{\boldsymbol{\sigma}}_n \quad (38)$$

and using the triangle inequality for $\|\tilde{\boldsymbol{\sigma}}_s + \tilde{\boldsymbol{\sigma}}_n\|$ find instead of equations (36)

$$e' \leqq e'_s + e'_n \qquad e'' \leqq e''_s + e''_n \quad (39)$$

where

Downloaded 03 May 2010 to 171.66.16.27. Redistribution subject to ASME license or copyright; see http://www.asme.org/terms/Terms_Use.cfm

$$e_s' = \|\tilde{\sigma}_s\|/\|\sigma'\| \qquad e_n' = \|\tilde{\sigma}_n\|/\|\sigma'\|$$
$$e_s'' = \|\tilde{\sigma}_s\|/\|\sigma''\| \qquad e_n'' = \|\tilde{\sigma}_n\|/\|\sigma''\| \tag{40}$$

The next step should be to calculate the e in equations (40), but this will not be done in view of the complexity of the resulting formulas. Rather, we restrict ourselves to some simple order-of-magnitude considerations.

First observe that the stresses in equations (40) are all expressible in terms of the rotations b_i and their derivatives. Thus we introduce the notation

$$b_{i,j} \sim b \qquad b_{i,jk} \sim b/L \qquad b_{i,jkl} \sim b/L^2 \tag{41}$$

where b and L may be interpreted as the amplitude of the midplane curvature and characteristic wavelength of deformation. Further, major simplifications result when the material properties are restricted as follows:

$$G' \lesssim E' \lesssim E \qquad 1-\nu \sim 1 \quad E/G' < L^2/h^2 \tag{42}$$

The first group above is met in well designed anisotropic plates where more stressed planes (parallel to the midplane) have larger elastic moduli, the second relation simply means that in-plane Poisson's ratio is not very close to unity (for the material considered, ν may take values such that $|\nu| < 1$), the third, inequality, relation, as will be seen later, is necessary for the plate theory to give meaningful results. Using these assumptions, we have for the quantities in equations (8)

$$D \sim E \qquad C \sim \nu' E/E' < (E/E')^{1/2} \tag{43}$$

the inequality relation being a consequence of the stipulated positive definiteness of elastic energy (see Lempriere, 1969). Using equations (41)–(43), it is found from equations (14), (18), (22), (28), and (29) that

$$Q_i \sim Eh^3 b/L \qquad f_i \sim f_i' \sim (E/G')b/L$$
$$g \sim (E/E')^{1/2} b \qquad r \sim (E/G')(E/E')^{1/2} b/L^2 \tag{44}$$

Now with the notation in equations (36), the stresses in equations (31)–(33) have estimates of the form

$$\tilde{\sigma}_{ij} \sim (E/E')^{1/2} Ebh^3/L^2$$
$$\tilde{\sigma}_{i3} \sim (E/G')Ebh^4/L^3 \qquad \tilde{\sigma}_{33} \sim Ebh^3/L^2 \tag{45}$$

The transverse shear part $\tilde{\sigma}_s$ of this, as defined in equation (38), consists of $\tilde{\sigma}_{i3}$, while the remainder constitutes $\tilde{\sigma}_n$. Thus, introducting (45) into (37) yields

$$\|\tilde{\sigma}_s\|^2 \sim h^9 (E/G')^3 FE^2 b^2/L^6$$
$$\|\tilde{\sigma}_n\|^2 \sim h^7 (E/E')FE^2 b^2/L^4 \tag{46}$$

F now being the area of the midplane. Further, from equation (37) with (44) the statically and kinematically admissible stresses in equations (16), (20), (23), and (15), (30), (13) are seen to have norms of the order

$$\|\sigma'\|^2 \sim \|\sigma''\|^2 \sim h^3 FE^2 b^2 \tag{47}$$

Introduction of equations (46) and (47) into (40) finally gives

$$e_s' \sim e_s'' \sim [(E/G')h^2/L^2]^{3/2}$$
$$e_n' \sim e_n'' \sim (E/E')^{1/2} h^2/L^2 \tag{48}$$

This means that our statically and kinematically admissible three-dimensional solutions $\tilde{\sigma}'$, $\mathbf{u}''$, and σ'', constructed from the variables of Levinson's theory, approximate exact elasticity solutions with a relative error bounded by a quantity porprotional to the thickness squared, because of e_n in (48), but, importantly, the shear-deformation portion e_s of the error is proportional to the thickness cubed. The later fact represents a definite improvement over Nordgren's (1972) result for Reissner's theory where the quantity that corresponds to e_s does not contain the exponent 3/2, as in (48), thus being proportional to h^2. To achieve this improvement, we have introduced the z^4 term in the distribution (10) of the lateral deflection over the thickness, and the nonlinear z^3 term in the distribution of the statically admissible surface parallel stresses in equation (16). Observe that for the plate theory to be applicable, we must require that e_s, $e_n << 1$ which in conjunction with (48) roughly determine the range of applicability of Levinson's theory in terms of the degree of anisotropy (E/G' and E/E') and the ratio h/L characterizing deformation variation over the midplane.

4 Simplified Plate Theory

Motivated by previous results due to Speare and Kemp (1977) and Shirakawa (1983) for other sixth-order theories, Levinson's theory will now be expressed entirely in terms of the lateral deflection. Most of the equations of Section 2 are valid here, so only necessary modifications will be indicated and results of practical interest recorded.

To begin with, expressions (25)–(29) are deleted and replaced by

$$b_i = -(1 + \Delta h^2 D/2G')w_{,i} \tag{49}$$
$$f_i = (1/6)(D/G' - C)\Delta w_{,i} \tag{50}$$
$$f_i' = (D/6G')\Delta w_{,i} \tag{51}$$

$\Delta w = w_{,ii}$ being the two-dimensional Laplace operator. Using equations (49) and (51) in (18), the moments become

$$M_{ij} = -(2/3)h^3 D(1 + 2h^2 \Delta D/5G') \times$$
$$[(1-\nu)w_{,ij} + \nu\delta_{ij}\Delta w] \tag{52}$$

Introducing this into equation (22) gives the shear forces

$$Q_i = -(2/3)h^3 D(1 + 2h^2 \Delta D/5G')\Delta w_{,i} \tag{53}$$

which, when substituted into equation (24), yield the sixth-order governing differential equation for the deflection w

$$(1 + 2h^2 \Delta D/5G')\Delta\Delta w = 3p/2Dh^3 \tag{54}$$

The statically admissible solution σ' in equations (16), (20), and (23) may be used with the present theory provided that b_i, f_i', and M_{ij} are taken from equations (49), (51), and (52). Likewise, the displacement field $\mathbf{u}''$ in equations (9) and (10) may also be utilized taking g and r from equations (14) with b_i and f_i specified now as in equations (49) and (50). Knowing the displacements $\mathbf{u}''$, the corresponding kinematically admissible stresses σ'' may be determined from the constitutive equations (5)–(7). Further, the error analysis of Section 3 may be repeated giving again upper bounds on the relative error as in (48).

Conclusions

This presentation is believed to have some elements of novelty of theoretical and practical interest. Levinson's theory, originally developed using an intuitive approach, has now been put on a firm mathematical foundation. Our analysis shows that the theory is consistent and precise, clearly indicating the error involved. The three-dimensional statically and kinematically admissible solutions which were developed to study the accuracy of Levinson's theory are of interest as such and may be used in computing displacement and stress distributions in the plate with high accuracy. The error estimates obtained are the best known so far for sixth-order theories, specifically, they improve those for Reissner's theory found by Nordgren (1972). Finally, a simplified plate theory has been presented, having the same accuracy as the original Levinson theory.

Downloaded 03 May 2010 to 171.66.16.27. Redistribution subject to ASME license or copyright; see http://www.asme.org/terms/Terms_Use.cfm

References

Lempriere, B. M., 1969, "Poisson's Ratio in Orthotropic Materials," *AIAA Journal*, Vol. 6, pp. 2226–2227.

Levinson, M., 1980, "An Accurate, Simple Theory of the Statics and Dynamics of Elastic Plates," *Mech. Res. Commun.*, Vol. 7, pp. 343–350.

Nordgren, R. P., 1971, "A Bound on the Error in Plate Theory," *Quart. Appl. Math.*, Vol. 28, pp. 587–595.

Nordgren, R. P., 1972, "A Bound on the Error in Reissner's Theory of Plates," *Quart. Appl. Math.*, Vol. 29, pp. 551–556.

Panc, V., 1975, *Theories of Elastic Plates*, Noordhoff, Leyden.

Pecknold, D. A., 1973, "Error Bounds for Approximate Solutions for Bending of Unsymmetrically Laminated Plates," *J. Struct. Mech.*, Vol. 2, pp. 281–299.

Prager, W., and Synge, J. L., 1947, "Approximations in Elasticity Based on the Concept of Function Space, *Quart. Appl. Math.*, Vol. 5, pp. 241–269.

Reddy, J. N., 1984, "A Simple Higher-Order Theory for Laminated Composite Plates," ASME JOURNAL OF APPLIED MECHANICS, Vol. 51, pp. 745–751.

Rehfield, L. W., and Valisetty, R. R., 1984, "A Simple, Refined Theory for Bending and Stretching of Homogeneous Plates," *AIAA Journal*, Vol. 22, pp. 90–95.

Reissner, E., 1975, "On Transverse Bending of Plates Including the Effect of Transverse Shear Deformation," *Int. J. Sol. Struct.*, Vol. 11, pp. 569–573.

Reissner, E., 1985, "Reflections on the Theory of Elastic Plates," *Appl. Mech. Rev.*, Vol. 38, pp. 1453–1464.

Rychter, Z., 1984, "A Bound on the Error in the Linear Theory of Transversely Isotropic Plate Bending," *Acta Mech.*, Vol. 54, pp. 121–126.

Shirakawa, K., 1983, "Bending of Plates Based on Improved Theory," *Mech. Res. Commun.*, Vol. 10, pp. 205–211.

Simmonds, J. G., 1971, "An Improved Estimate for the Error in the Classical, Linear Theory of Plate Bending," *Quart. Appl. Math.*, Vol. 29, pp. 439–447.

Speare, P. R. S., and Kemp, K. O., 1977, "A Simplified Reissner Theory for Plate Bending," *Int. J. Sol. Struct.*, Vol. 13, pp. 1073–1079.

Synge, J. L., 1957, *The Hypercircle in Mathematical Physics: A Method for the Approximate Solution of Boundary Value Problems*, University Press, Cambridge.

Downloaded 03 May 2010 to 171.66.16.27. Redistribution subject to ASME license or copyright; see http://www.asme.org/terms/Terms_Use.cfm

On Boundary Layers in a Pressurized Mooney Cylinder

L. A. Taber
Department of Mechanical Engineering,
University of Rochester,
Rochester, NY 14627

Asymptotic expansions are developed for the equations governing large axisymmetric deformation of a circular cylindrical shell composed of a Mooney material. The shell equations allow large normal strains and thickness changes but ignore transverse shear deformation. For a pressurized cylinder with rigid end plugs, results are presented to illustrate the development of a primary and a secondary boundary layer as generalizations of those that occur in small-strain shell theory. The form of the WKB-type expansion divides the secondary layer into bending and stretching components, which lie within the wider primary boundary layer. While the bending component of the secondary layer can become significant when strains are still small, the stretching component emerges as a consequence of large geometry changes in the edge zone, becoming significant as strains grow large and material nonlinearity becomes important.

Introduction

This paper extends earlier work concerning large elastic deformation of a circular plate (Taber, 1987) to a cylindrical shell. Here, the main focus of attention is on the boundary layers that occur near the edges of a pressurized rubber-like (Mooney) cylinder clamped to rigid end plugs. Based on shell equations valid for large displacements, rotations, and normal strains, but neglecting transverse shear strains, a WKB-type asymptotic expansion reveals the existence of a primary boundary layer and two components of a secondary boundary layer, one contributing bending and the other membrane stresses.[1] As the load increases, the primary layer widens while the secondary layer narrows.

For the most part, these boundary layers have been studied previously for axisymmetric deformation of thin shells of revolution within the limits of small strain. In their classic paper based on the equations for moderate rotations of an initially curved membrane, Bromberg and Stoker (1945) first identified the primary boundary layer, which supplements the linear membrane solution to enable the satisfaction of displacement boundary conditions. Nonlinear influence coefficients for the secondary layer, which allows enforcement of a zero rotation condition in a generalization of the familiar behavior given by linear shell bending theory, were computed by Reissner (1959a), Van Dyke (1966), and Ranjan and Steele (1980). In addition, Reissner (1959b) showed that, for a sufficiently steep clamped spherical cap with internal pressure, both of these boundary layers are contained in his nonlinear shell equations. On the other hand, while both layers can occur when strains are small, the membrane component of the secondary layer is mainly a phenomenon of large strain behavior (Taber, 1987). Consequently, material nonlinearity and the coupling between bending and stretching (Libai and Simmonds, 1981) are important factors.

Although a flat plate does not exhibit the primary boundary layer, the bending component of the secondary layer develops at large deflections, when the plate begins to resemble a shallow shell (Bromberg, 1956; Taber, 1985b), and the membrane component develops as the strains grow large (Taber, 1987). For large deformation of a steep shell, such as a cylinder, all of these effects occur. At *very* large pressures, a membrane of any initial shape becomes spherical except near the edges, where another type of boundary layer forms (Wu and Perng, 1972). However, since conventional shell theories would break down for the corresponding small deformation wavelengths (relative to the thickness) near a clamped edge, this layer is not considered in the present study.

Governing Equations

Consider a circular cylinder of undeformed radius R, length L, and thickness t loaded by an internal pressure p (Fig. 1(*a*)). For the subsequent asymptotic analysis, the basic shell equations, as given by specializing those of Reissner (1950, 1969, 1972), Simmonds (1986), and Taber (1985a), will be expressed in nondimensional form at the outset. Nondimensional quantities, to be identified during the discussion to follow, are taken as

$$x,y,z,r,h,L = R^{-1}(\bar{x},\bar{y},\bar{z},\bar{r},\bar{h},\bar{L})$$

$$N_i,Q,H,V = (pR)^{-1}(\bar{N}_i,\bar{Q},\bar{H},\bar{V})$$

$$\kappa_i = R\bar{\kappa}_i, \qquad M_i = \bar{M}_i/Ct^2 \tag{1}$$

$$W = \bar{W}/Ct, \qquad \Pi = \bar{\Pi}/CR^2t, \quad \Delta V = \Delta\bar{V}/R^3$$

[1] In Taber (1987), the bending and stretching components of the secondary boundary layer mistakenly were referred to as separate boundary layers in themselves.

Contributed by the Applied Mechanics Division for presentation at the 1987 Applied Mechanics, Biomechanics, and Fluids Engineering Conference, Cincinnati, OH, June 14–17, 1987, of the American Society of Mechanical Engineers.

Discussion of this paper should be addressed to the Editorial Department, ASME, United Engineering Center, 345 East 47th Street, New York, N.Y. 10017, and will be accepted until two months after final publication of the paper itself in the JOURNAL OF APPLIED MECHANICS. Manuscript received by ASME Applied Mechanics Division, August 15, 1986; final revision, October 13, 1986. Paper No. 87-APM-27.

Copyright © 1987 by ASME
Downloaded 03 May 2010 to 171.66.16.27. Redistribution subject to ASME license or copyright; see http://www.asme.org/terms/Terms_Use.cfm

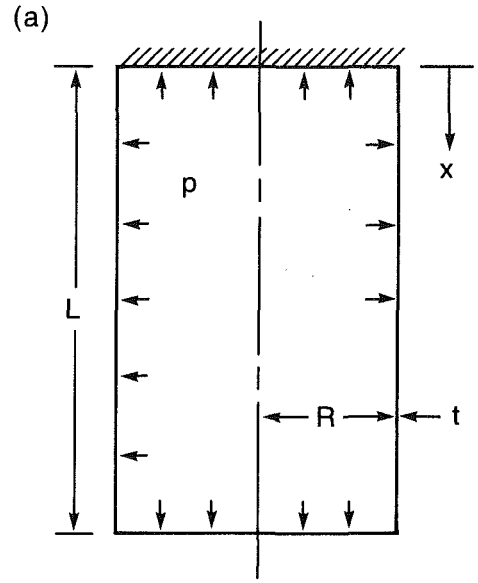


Fig. 1(a) Undeformed shell geometry

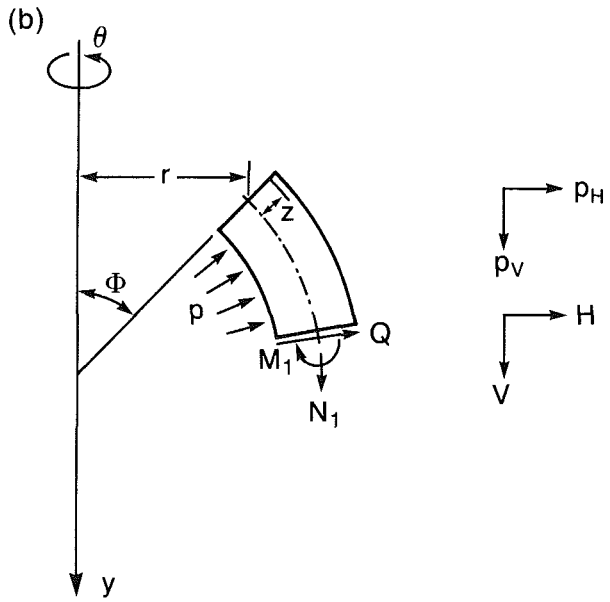


Fig. 1(b) Geometry and forces for deformed shell element

where bars indicate dimensional quantities and C is a material constant (with units of stress). Also, we define here the parameters

$$\alpha = pR/Ct, \quad \beta = (R/t)\alpha. \tag{2}$$

Geometry. For axisymmetric deformation (Fig. 1(*b*)), a point on the reference surface originally located at the coordinates $(R,\theta,\bar{x})$ moves to $(\bar{r},\theta,\bar{y})$. The motions of points off the reference surface are assumed to be governed by a relaxed Kirchhoff hypothesis, whereby normals to this surface remain straight and normal but can change in length. In addition, transverse shear strains that arise from the gradient of the deformed shell thickness are neglected. Under these and other assumptions commonly employed in thin shell theory, approximate stretch ratios are (Taber, 1985a)

$$\Lambda_i = \lambda_i + z\kappa_i \quad (i=1,2). \tag{3}$$

With $\Lambda_3 = \partial z/\partial z_0$, the material incompressibility condition $\Lambda_1\Lambda_2\Lambda_3 = 1$ determines the deformed transverse coordinate z in terms of the undeformed coordinate z_0, and the subscripts 1 and 2 indicate the deformed Φ and θ directions, respectively. The stretch ratios at the reference surface are

$$\lambda_1 = -r'/\phi, \quad \lambda_2 = r \tag{4}$$

where prime denotes differentiation with respect to the undeformed meridional coordinate x, and the curvature change measures are

$$\kappa_1 = \phi'/\eta, \quad \kappa_2 = \eta - \lambda_1\lambda_2^2 \tag{5}$$

in which

$$\phi = \sin\omega, \quad \eta = \cos\omega = (1-\phi^2)^{1/2} \tag{6}$$

with $\omega = \Phi - \pi/2$ being the rotation.

Equilibrium. For a pressurized cylinder with closed ends, vertical and horizontal force equilibrium and moment equilibrium yield

$$V = r^2/2, \quad H' - N_2 + \lambda_1\lambda_2\eta = 0$$
$$\beta^{-1}(M_1' + \phi M_2) - \lambda_1 Q = 0 \tag{7}$$

where the membrane stress resultants N_i, transverse shear Q, and moment resultants M_i are defined per unit *undeformed* length of the reference surface, acting in the deformed coordinate directions (Fig. 1(*b*)). In addition, the geometry gives

$$N_1 = -H\phi + V\eta, \quad Q = H\eta + V\phi \tag{8}$$

with H and V being the horizontal and vertical force components.

Constitutive Relations. Based on equations (3), appropriate constitutive relations for a hyperelastic shell material are

$$N_i = \alpha^{-1}\partial W/\partial\lambda_i, \quad M_i = (\beta/\alpha)\partial W/\partial\kappa_i \quad (i=1,2) \tag{9}$$

where W is the strain energy density function per unit undeformed area of the reference surface. Since the three-dimensional strain energy function generally cannot be integrated over the shell thickness to obtain W in closed form, approximations for W have been the focus of much recent study. A major simplification was found by Simmonds (1985), who showed that, for moderately large bending of thin shells of revolution (bending strains $t\kappa_i/2$ up to 0.15–0.2), the form of W is essentially independent of the undeformed geometry, and so it is sufficient to work out W for a flat plate. Taking advantage of this strategy, Simmonds (1986) computed the first approximation

$$W = \lambda_1^2 + \lambda_2^2 + 1/\lambda_1^2\lambda_2^2 - 3$$
$$+ (\alpha^2/12\beta^2)(\lambda_1\lambda_2)^{-6}[(3+\lambda_1^4\lambda_2^2)\lambda_2^2\kappa_1^2 + 4\lambda_1\lambda_2\kappa_1\kappa_2$$
$$+ (3+\lambda_1^2\lambda_2^4)\lambda_1^2\kappa_2^2] \tag{10}$$

for a Mooney (neo-Hookean) shell; a better approximation must include transverse shear strains. The coupling between bending and stretching evident in equations (9) and (10) is examined in detail by Libai and Simmonds (1981) and Taber (1985a).

Boundary Conditions. This paper considers a pressurized cylinder with both edges clamped to rigid end plates. With one end plate held fixed, the other is free to move axially, giving the boundary conditions (Fig. 1(*a*))

$$x=0: \quad r=1, \; y=0, \quad \omega=0$$
$$x=1: \quad r=1, \; V=1/2, \; \omega=0. \tag{11}$$

Equations (4), (5), (7), (9), and (11) represent the basic equations for large axisymmetric (torsionless) deformation of a circular cylindrical shell.

Asymptotic Solution for Small Strain

For small strain, the equations of the previous section

Downloaded 03 May 2010 to 171.66.16.27. Redistribution subject to ASME license or copyright; see http://www.asme.org/terms/Terms_Use.cfm

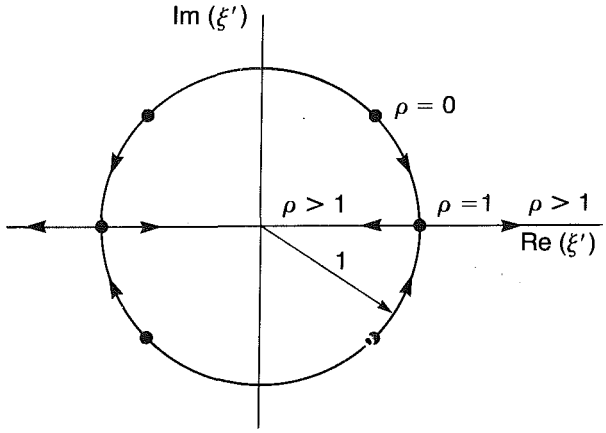


Fig. 2 Movement of characteristic shell roots in the complex ξ'-plane as ρ increases

reduce to those of Reissner (1950). Using a matrix formulation of the Reissner equations for a general shell of revolution, Ranjan and Steele (1980) developed a WKB-type asymptotic solution which is valid for moderately large rotations. The edge zone solution for radial displacement of a cylinder has the form

$$h = \mathrm{Re}\{Ae^{\mu\xi(x)}\} \tag{12}$$

where A can be taken as a complex constant within the boundary layer, and

$$\xi' = \pm[\rho \pm (\rho^2 - 1)^{1/2}]^{1/2} \tag{13}$$

provides the decay function $\xi(x)$. For a neo-Hookean shell material with Young's modulus $E = 6C$, $\mu^2 = 3R/t$ and $\rho = \beta/8$ with β given by equation (2). Note that equation (13) contains four roots to enable the satisfaction of two boundary conditions at each shell edge.

The character of the edge zone solution depends on the value of ρ, which increases as the pressure increases or the shell grows thinner. For $\rho << 1$, $\xi' \cong \pm(1 \pm i)/\sqrt{2}$ (Fig. 2), giving the familiar bending boundary layer behavior of the linear shell equations. As ρ increases but remains less than unity, ξ' moves toward the real axis along the unit circle in the complex ξ'-plane, and equation (12) exhibits the pressurization effects studied by Ranjan and Steele (1980), with stretching interacting with the bending boundary layer. For $\rho > 1$, all roots are real, with two approaching and two moving away from the origin (Fig. 2), giving separate membrane (primary) and bending (secondary) boundary layers as discussed below.

The behavior for real ξ' is readily discerned on examination of the limiting cases for large ρ. For $\rho >> 1$, the roots inside the unit circle give

$$(\mu\xi)_M \cong \pm 2(3/\alpha)^{1/2}x, \tag{14a}$$

corresponding to the nonlinear membrane boundary layer discussed by Bromberg and Stoker (1945) and Reissner (1959b). (The plus and minus signs provide the solutions near the edges $x = L$ and $x = 0$, respectively.) On the other hand, the roots outside the unit circle give

$$(\mu\xi)_B \cong \pm\frac{1}{2}(3\beta^2/\alpha)^{1/2}x, \tag{14b}$$

which corresponds to the bending boundary layer discussed by Reissner (1959b) for shells and by Bromberg (1956) and Taber (1985b) for a flat plate. As equations (2) and (14) show, the membrane boundary layer widens while the bending layer narrows with increasing pressure. The present work examines the realm of large strain, which falls in the range $\rho > 1$, or $\beta > 8$, where all values of ξ' are real and the algebra is somewhat simpler. Furthermore, for this range of loading, the solution for a cylinder is very similar to that for a plate (Taber, 1987).

Asymptotic Expansions for Large Strain

The present analysis follows that of Taber (1987). Of primary interest is the loading range where $\alpha = 0(1)$, which corresponds to the regime of moderately large bending and membrane strains (of the order of 20 percent). Then, by equation (2), $\beta >> 1$ for a thin shell, making the form of equations (4)–(10) suitable for asymptotic analysis.

A WKB-type asymptotic solution is obtained by expanding each dependent variable in a series of the form (Ranjan and Steele, 1980)

$$\{a(x), \kappa_i(x)\} = \sum_{m=0}^{\infty}\sum_{n=0}^{\infty} \beta^{-m} e^{n\beta\xi(x)} \{a^{(mn)}(x), \beta\kappa_i^{(mn)}(x)\} \tag{15}$$

where $a = r, \phi, \eta, \lambda_i, N_i, Q, H, V, M_i$, the $a^{(mn)}(x)$ and $\kappa_i^{(mn)}(x)$ are assumed to be 0(1), and $\xi(x)$ is the decay function. The $n = 0$ terms give the interior solution, and the exponential terms ($n > 0$) provide the edge zone solution. As in the solution for a clamped circular plate, the main features of the shell behavior are given by including terms only up through $n = 2$ (Taber, 1987).

After substitution of equations (15) into equations (4)–(10), coefficients of like powers of β, $\beta e^{\beta\xi}$, etc., are equated in the usual manner. Note that, by working with the basic equations individually instead of combining them into a reduced system of more complex equations, we relegate the heaviest algebra to the post-expansion phase of the analysis. In this way, multiplication of series is minimized, many intermediate simplifications become apparent, and the physical meaning of various terms is sometimes easier to see. In addition, this approach facilitates application to shells with other forms of strain energy density function, and, since equation (10) is valid for a general shell of revolution, the expansions of the constitutive relations are independent of geometry.

As will be shown shortly, the asymptotic expansions provide the first-approximation solution

$$\begin{aligned}
r &= r^{(00)} \\
\phi &= \phi^{(00)} + e^{\beta\xi}\phi^{(01)} + e^{2\beta\xi}\phi^{(02)} \\
N_i &= N_i^{(00)} + e^{2\beta\xi}N_i^{(02)} \\
Q &= e^{\beta\xi}Q^{(01)} \\
M_i &= \beta^{-1}M_i^{(10)} + e^{\beta\xi}M_i^{(01)} \qquad (i = 1,2)
\end{aligned} \tag{16}$$

in which only the nonzero terms are displayed. These expressions clearly illustrate the nonlinear membrane solution (00 terms), which contains the primary boundary layer, and separate bending (01 terms) and membrane (02 terms) components of the secondary boundary layer. It will be shown that, while the primary layer widens, the secondary layer narrows as the load increases. In addition, while the first-order interior bending moments vanish as for a membrane in the classical sense ($M_i^{(00)} = 0$), the change in curvature of the membrane solution gives the second-order bending moments $M_i^{(10)}$, which are generally small but may not be negligible for a relatively thick shell at large deflections.

With equations (16), the boundary conditions of vanishing radial displacement and rotation (equation (11)) give

$$x = 0, L: \quad r^{(00)} = 1, \quad \phi^{(00)} + \phi^{(01)} + \phi^{(02)} = 0. \tag{17}$$

The first of these equations is satisfied by the nonlinear membrane solution, but the second requires the edge zone solution. Details are given in Taber (1987). Furthermore, the condition on V in equation (11) is satisfied by the vertical equilibrium equation $(7)_1$, and the condition on y is taken care of when the deformed profile is computed from the geometrical relations

Downloaded 03 May 2010 to 171.66.16.27. Redistribution subject to ASME license or copyright; see http://www.asme.org/terms/Terms_Use.cfm

$$r(x) = 1 - \int_0^x \lambda_1 \phi \, dx, \quad y(x) = \int_0^x \lambda_1 \eta \, dx. \tag{18}$$

In the following discussion, details of the solution for each boundary layer are presented and illustrated separately. As specified, results are based on either the nonlinear membrane solution or the total approximate solution of equation (16).

Interior Solution and the Primary Boundary Layer

Basic Equations. The first-order terms in β provide the system of equations

$$\begin{aligned}
&\kappa_1^{(00)} = \kappa_2^{(00)} = M_1^{(00)} = M_2^{(00)} = 0 \\
&Q^{(00)} = H^{(00)}\eta^{(00)} + V^{(00)}\phi^{(00)} = 0 \\
&\lambda_1^{(00)} = -r^{(00)\prime}/\phi^{(00)}, \quad \lambda_2^{(00)} = r^{(00)}, \quad \eta^{(00)} = (1-\phi^{(00)2})^{1/2} \\
&N_1^{(00)} = 2\alpha^{-1}\lambda_1^{(00)}(1-\lambda_1^{(00)-4}\lambda_2^{(00)-2}) = -H^{(00)}\phi^{(00)} + V^{(00)}\eta^{(00)} \\
&N_2^{(00)} = 2\alpha^{-1}\lambda_2^{(00)}(1-\lambda_1^{(00)-2}\lambda_2^{(00)-4}) \\
&V^{(00)} = r^{(00)2}/2 \\
&H^{(00)\prime} - N_2^{(00)} + \lambda_1^{(00)}\lambda_2^{(00)}\eta^{(00)} = 0
\end{aligned} \tag{19}$$

which are the governing relations of nonlinear membrane theory (Adkins and Rivlin, 1952). A solution of these equations for pressurized cylinders was presented by Kydoniefs and Spencer (1969). The equations for $N_1^{(00)}$ and $Q^{(00)}$ imply the membrane conditions

$$V^{(00)} = N_1^{(00)}\eta^{(00)}, \quad H^{(00)} = -N_1^{(00)}\phi^{(00)}, \tag{20}$$

and the second-order β terms contribute the bending moments

$$M_i^{(10)} = \frac{\alpha}{6}\frac{1}{\lambda_i^{(00)6}\lambda_j^{(00)5}}[(3+\lambda_i^{(00)4}\lambda_j^{(00)2})\lambda_j^{(00)}\kappa_i^{(10)} + 2\lambda_i^{(00)}\kappa_j^{(10)}],$$

$$(i=1, j=2 \text{ and } i=2, j=1). \tag{21}$$

For a steep shell, unlike the case of a flat plate, the membrane equations (19) can, in themselves, exhibit boundary layer phenomena (the primary boundary layer) for small to moderate strain levels. But as deflections increase, the shell eventually reaches a point where the edge zone dissipates. In solving these equations, therefore, two approaches are explored: an asymptotic and a strain energy method.

Asymptotic Solution. Bromberg and Stoker (1945) first described the boundary layer that occurs near the edge of a curved membrane with internal pressure. Using nonlinear equations for small strain and moderate rotations, they showed that an edge-effect correction to the linear membrane solution enables the satisfaction of zero displacement at a fixed edge. Here, we seek a similar solution that includes a first-order correction for large strains. Since this boundary layer narrows as the pressure (α) decreases, the membrane equations (19) must be recast in a form appropriate to an asymptotic analysis valid for $\alpha \to 0$.

As $\alpha \to 0$, the solution variables should approach zero, and so the radial displacement and elongations

$$h^{(00)} = r^{(00)} - 1, \quad E_i^{(00)} = \lambda_i^{(00)} - 1 \tag{22}$$

are introduced. In terms of the new nondimensional quantities

$$\begin{aligned}
&\hat{h} = h^{(00)}/\epsilon^2, \quad \hat{\phi} = \phi^{(00)}/\epsilon, \quad \hat{\eta} = \eta^{(00)} \\
&\hat{E}_i = E_i^{(00)}/\epsilon^2, \quad \hat{N}_i = N_i^{(00)}, \quad \hat{H} = H^{(00)}/\epsilon, \quad \hat{V} = V^{(00)}
\end{aligned} \tag{23}$$

where $\epsilon^2 = \alpha$, equations (19) become

Table I

(mn)	(00)	(20)	(01)	(21)
$\hat{E}_1$	0	0.0104	0.0625	-0.0104
$\hat{E}_2$	0.125	0.0339	-0.125	-0.0339
$\hat{h}$	0.125	0.0339	-0.125	-0.0339
$\hat{\phi}$	0	0	-0.433	-0.117
$\hat{\eta}$	1	0	0	0
$\hat{N}_1$	0.5	0.125	0	-0.125
$\hat{N}_2$	1	0.125	-0.750	-0.0312
$\hat{H}$	0	0	0.217	0.113
$\hat{V}$	0.5	0.125	0	-0.125

$$\begin{aligned}
&\hat{H}\hat{\eta} + \hat{V}\hat{\phi} = 0 \\
&\epsilon\hat{h}' + \hat{\phi}(1+\epsilon^2\hat{E}_1) = 0, \quad \hat{E}_2 = \hat{h}, \quad \hat{\eta}^2 + \epsilon^2\hat{\phi}^2 = 1 \\
&\hat{N}_1 = 2\epsilon^{-2}(1+\epsilon^2\hat{E}_1)[1-(1+\epsilon^2\hat{E}_1)^{-4}(1+\epsilon^2\hat{E}_2)^{-2}] \\
&\quad = \hat{V}\hat{\eta} - \epsilon^2\hat{H}\hat{\phi} \\
&\hat{N}_2 = 2\epsilon^{-2}(1+\epsilon^2\hat{E}_2)[1-(1+\epsilon^2\hat{E}_1)^{-2}(1+\epsilon^2\hat{E}_2)^{-4}] \\
&\hat{V} = (1+\epsilon^2\hat{h})^2/2 \\
&\epsilon\hat{H}' - \hat{N}_2 + (1+\epsilon^2\hat{E}_1)(1+\epsilon^2\hat{E}_2)\hat{\eta} = 0.
\end{aligned} \tag{24}$$

These equations show that large strain effects are $0(\epsilon^2)$ and that a boundary layer will occur for $\epsilon \to 0$.

A solution to equations (24) is sought in the form

$$\hat{a}(x) = \sum_{m=0,2,\ldots}^{\infty} \sum_{n=0}^{\infty} \epsilon^m e^{n\hat{\xi}(x)/\epsilon}\hat{a}^{(mn)}(x) \tag{25a}$$

where $\hat{a} = \hat{h}, \hat{\phi}, \hat{\eta}, \hat{E}_i, \hat{N}_i, \hat{H}, \hat{V}$, and substitution into equations (24) reveals that terms with $n > 1$ vanish. Here, the (00) terms provide the linear membrane solution, the (01) terms give the nonlinear (primary) boundary layer of Bromberg and Stoker (1945) for small strain, and the $m = 2$ terms provide a first-order correction for large strain. With the decay function computed as $\hat{\xi} = \pm 2\sqrt{3}\,x$, in agreement with the small strain solution of equation (14*a*), Table I gives values of the solution variables for the approximation (valid for a fixed edge)

$$\hat{a} \cong \hat{a}^{(00)} + \epsilon^2\hat{a}^{(20)} + e^{\hat{\xi}(x)/\epsilon}(\hat{a}^{(01)} + \epsilon^2\hat{a}^{(21)}). \tag{25b}$$

Strain Energy Solution. Although the asymptotic analysis illustrates the essence of the primary boundary layer, this solution loses accuracy as the load increases. Therefore, a Ritz solution was also computed, based on the method presented by Tielking and Feng (1974).

The nondimensional total potential energy for the cylindrical membrane is

$$\Pi = 2\pi\int_0^L W\,dx - \alpha\Delta V \tag{26}$$

in which W is given by equation (10) with $\beta \to \infty$ and the internal volume change is

$$\Delta V = \pi\int_0^L r^2 y'\,dx - \pi L. \tag{27}$$

On substitution of

$$\lambda_1 = (r'^2 + y'^2)^{1/2}, \quad \lambda_2 = r, \tag{28}$$

Π becomes a function only of the deformed coordinates r and y with the load α given. Then, the series

$$r = \sum_{n=1}^{N_1} a_n\alpha_n(x), \quad y = \sum_{n=1}^{N_2} b_n\beta_n(x) \tag{29}$$

Downloaded 03 May 2010 to 171.66.16.27. Redistribution subject to ASME license or copyright; see http://www.asme.org/terms/Terms_Use.cfm

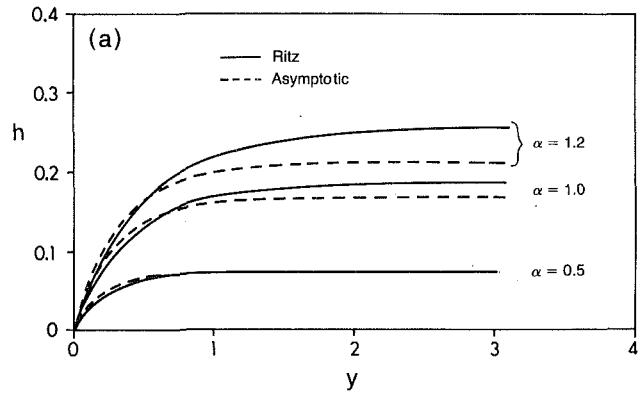


Fig. 3(*a*) Comparison of deformed cylindrical membrane profiles for asymptotic and Ritz solutions

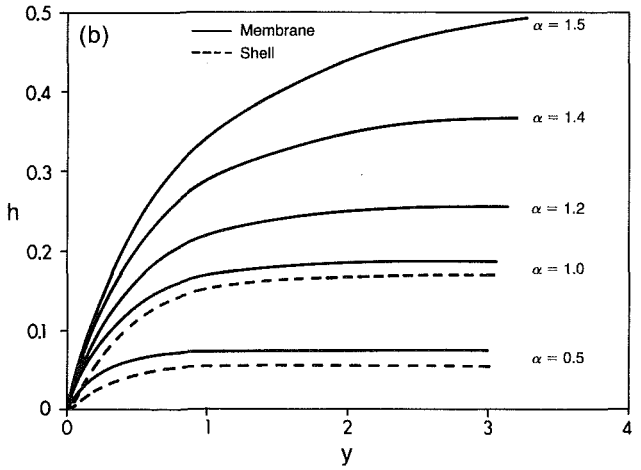


Fig. 3(*b*) Deformed profiles for cylindrical membrane and shell ($R/t = 20$, $L = 10$)

form the basis for a Ritz solution, with the unknown constants a_n and b_n computed by minimizing Π. Since the shape functions, the α_n could be chosen as simple sine functions if displacements alone were of interest. But then, the meridional curvature, and thus the bending moment, would vanish at the shell edges, when, in fact, the curvature in the membrane boundary layer can be significant. Therefore, with equation (25) as a guide, the shape functions are taken as

$$\alpha_n = (1 + e^{-\mu L} - e^{-\mu x} - e^{\mu(x-L)}) \cos \frac{n\pi x}{L}, \quad n = 0,2,4, \ldots$$

$$\beta_0 = x, \quad \beta_n = \sin \frac{n\pi x}{L}, \quad n = 2,4, \ldots \tag{30}$$

which satisfy symmetry and the displacement boundary conditions of equation (11). With $\mu = 2\sqrt{3}/\epsilon$, the first term of the r series provides the asymptotic solution of the previous section.

Comparison of Results. Comparison of deflection profiles from the asymptotic and Ritz ($N_1 = N_2 = 10$) membrane solutions for a cylinder with $L = 10$ (Fig. 3(*a*)) illustrates the widening boundary layer with increasing α. As expected, agreement is excellent for relatively small values of α and is not bad even for $\alpha = 1$. For larger values of α, however, the accuracy of the asymptotic solution worsens rapidly, especially outside the boundary layer.

Load-deflection curves of the Ritz solution (Fig. 4), which demonstrate the validity of the assumption $\alpha = 0(1)$, reveal an instability that is encountered often during the inflation of

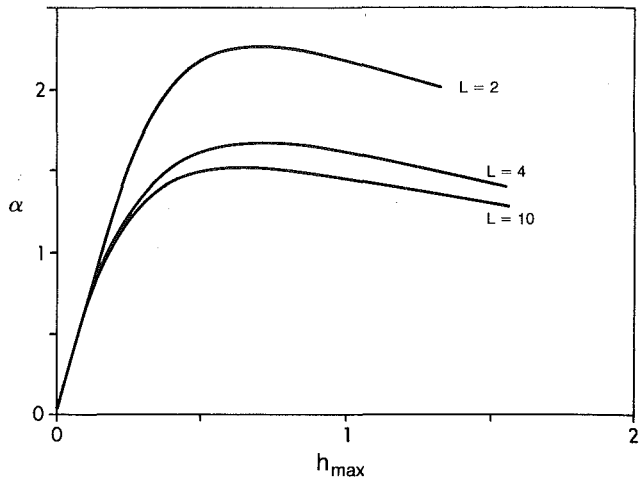


Fig. 4 Load versus maximum deflection curves for pressurized cylindrical membrane

Mooney membranes (Adkins and Rivlin, 1952; Kydoniefs and Spencer, 1969). These results show that, although the peak load increases substantially for short cylinders, the corresponding critical deflection changes little. But, more significantly, comparison of Figs. 3(*b*) and 4 for $L = 10$ shows that the primary boundary layer rapidly loses its form as the critical load ($\alpha \cong 1.5$) is approached. (Actually, it may be somewhat surprising that the edge zone retains its form for the relatively large values of α shown in Fig. 3(*a*)). Other than those in Fig. 3(*a*), therefore, all results in this paper employ the Ritz membrane solution.

The Secondary Boundary Layer

In a previous section, it was shown that, as the pressure grows large, separate membrane (primary) and bending (secondary) boundary layers form. This section will show that, as strains grow large, the secondary layer itself divides into separate bending and stretching components.

Bending Component. The first-order $e^{\beta\xi}$ terms are

$$r^{(01)} = \lambda_1^{(01)} = \lambda_2^{(01)} = \kappa_2^{(01)} = N_1^{(01)} = N_2^{(01)} = V^{(01)} = H^{(01)} = 0$$

$$\kappa_1^{(01)} = \xi' \phi^{(01)}/\eta^{(00)}, \quad \eta^{(01)} = -\phi^{(00)}\phi^{(01)}/\eta^{(00)}$$

$$Q^{(01)} = H^{(00)}\eta^{(01)} + V^{(00)}\phi^{(01)} = N_1^{(00)}\phi^{(01)}/\eta^{(00)} \tag{31}$$

$$M_1^{(01)} = (\alpha/6)(3 + \lambda_1^{(00)4}\lambda_2^{(00)2})\lambda_1^{(00)-6}\lambda_2^{(00)-4}\kappa_1^{(01)}$$

$$M_2^{(01)} = (\alpha/3)(\lambda_1^{(00)}\lambda_2^{(00)})^{-5}\kappa_1^{(01)}$$

along with the decay function

$$\xi(x) = \int_1^x \left[\frac{6}{\alpha} \frac{\lambda_1^{(00)7}\lambda_2^{(00)4}}{(3 + \lambda_1^{(00)4}\lambda_2^{(00)2})} N_1^{(00)}\right]^{1/2} dx. \tag{32}$$

For small strain, $\beta\xi(x) \to (\mu\xi)_B$ as given by equation (14*b*), indicating a bending-type boundary layer, which actually represents the bending component of the secondary boundary layer. This fact is confirmed by equations (31), which show contributions to the bending moments and transverse shear, but not to the membrane stress resultants.

Once the membrane solution and $\phi^{(01)}$ are determined, the boundary layer solution of equations (31) and (32) is complete. The function $\phi^{(01)}(x)$ can be computed from the second-order $e^{\beta\xi}$ terms (Taber, 1987) at the expense of considerable algebra. However, if β is large, giving a narrow edge zone, $\phi^{(01)}$ will vary only slightly within the boundary layer and so, in approximation, can be set equal to a constant to be determined from the boundary conditions (here, the condition of zero rotation). For further details, see Taber (1987), where it is

Downloaded 03 May 2010 to 171.66.16.27. Redistribution subject to ASME license or copyright; see http://www.asme.org/terms/Terms_Use.cfm

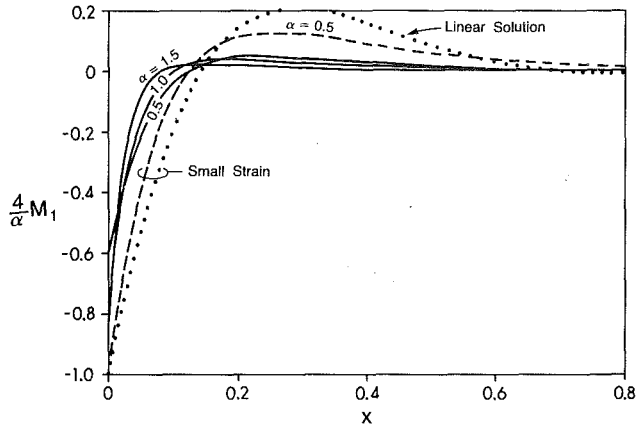


Fig. 5 Bending moment distributions near edge of clamped cylindrical shell ($R/t = 20$, $L = 10$)

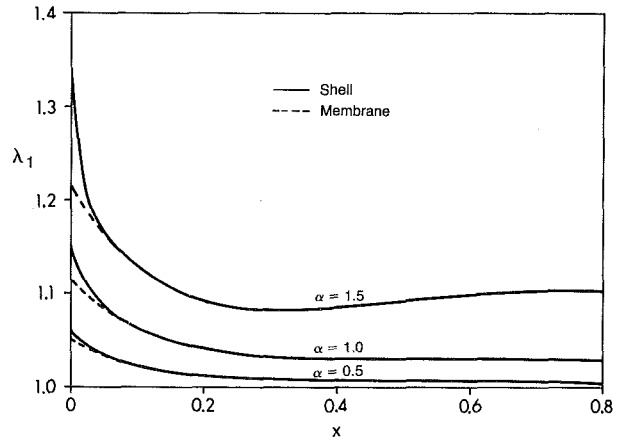


Fig. 6 Reference surface stretch ratio distributions near edges of clamped cylindrical shell and membrane ($R/t = 20$, $L = 10$)

shown that this approximation leads to little error for a clamped circular plate, even for relatively small values of β.

Both the primary boundary layer and the bending component of the secondary boundary layer are illustrated by the deformed shapes for the shell (Fig. 3(*b*)). Although the edge effect due to satisfying the condition of zero rotation is quite narrow, it produces a fairly uniform decrease in deflection over the shell interior. Note that these and subsequent results are based on the total first-approximation solution of equations (16).

Plots of bending moment distributions (Fig. 5) reveal a more detailed view of the bending behavior within the secondary boundary layer. First of all, the decreasing width of this layer with increasing load is evident in the large strain curves. Also shown are the small strain solutions for $\alpha << 1$ (the linear solution) and for $\alpha = 0.5$ (equation (12)). (Note that, for small strain, $4M_1/\alpha = -1$ at the edge for all α.) Although these latter results also show a narrowing boundary layer with increasing pressure, the strong coupling between bending and stretching contained in equation (10) for the strain energy density function makes this effect much more pronounced in the large strain curves. As shown by the high powers of the stretch ratios in the expressions for $M_1^{(01)}$ and ξ (equations (31) and (32)), relatively small reference surface elongations lead to significant reductions in bending moment resultants and the width of the boundary layer, respectively. And the stretch ratio distributions (Figs. 3 and 6) indicate significant levels in λ_1 or $\lambda_2 = 1 + h$ or both throughout the shell.

Stretching Component. Even when strains are small, the boundary layer effects discussed in the previous sections can be present. The interaction between these layers has been studied extensively by Reissner (1959b). For large strain, an additional stretching effect appears (Taber, 1987).

The $e^{2\beta\xi}$ terms give

$$r^{(02)} = \lambda_2^{(02)} = V^{(02)} = H^{(02)} = \kappa_1^{(02)} = \kappa_2^{(02)} = M_1^{(02)} = M_2^{(02)} = 0$$

$$Q^{(02)} = H^{(00)}\eta^{(02)} + V^{(00)}\phi^{(02)} = 0$$

$$\lambda_1^{(02)} = \frac{\alpha^2}{24}\left(\frac{15 + \lambda_1^{(00)4}\lambda_2^{(00)2}}{3 + \lambda_1^{(00)4}\lambda_2^{(00)2}}\right)\frac{\kappa_1^{(01)2}}{\lambda_1^{(00)3}\lambda_2^{(00)2}}$$

$$\phi^{(02)} = -(\phi^{(00)}/2\eta^{(00)2})\phi^{(01)2}, \quad \eta^{(02)} = -\phi^{(01)2}/2\eta^{(00)} \tag{33}$$

$$N_1^{(02)} = -H^{(00)}\phi^{(02)} + V^{(00)}\eta^{(02)} = -(N_1^{(00)}/2\eta^{(00)2})\phi^{(01)2}$$

$$N_2^{(02)} = \frac{4}{\alpha}\frac{\lambda_1^{(02)}}{(\lambda_1^{(00)}\lambda_2^{(00)})^3} - \frac{\alpha}{6}(1 + 6\lambda_1^{(00)-4}\lambda_2^{(00)-2})\frac{\kappa_1^{(01)2}}{\lambda_1^{(00)2}\lambda_2^{(00)3}}$$

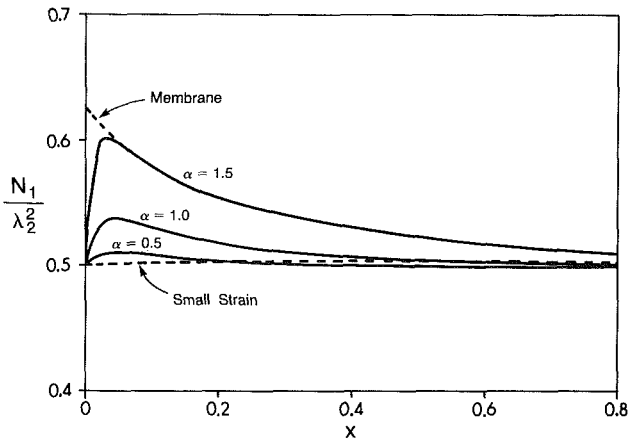


Fig. 7 Membrane stress resultant distributions near edge of clamped cylindrical shell ($R/t = 20$, $L = 10$)

which contribute to the membrane stress resultants but not to the bending moments and transverse shear stress, thus giving the stretching component of the secondary boundary layer. The width of this component is half that of the bending component.

The expression for $N_1^{(02)}$ in equation (33) indicates that the secondary membrane component arises from the geometry of deformation. The physical basis for this effect can be seen quite easily in a pressurized cylinder by examining the behavior of the stress resultant N_1 (Fig. 7). Where the rotation is zero, i.e., at the clamped edges and at the midpoint of the cylinder, $N_1 = V$. And since the vertical equilibrium equation $(7)_1$ gives $V/r^2 = V/\lambda_2^2 = 0.5$, then $N_1/\lambda_2^2 = 0.5$ at $x = 0$, $L/2$, L. This condition poses no problem for the case of small strains, in which $N_1 = N_1^{(00)} \cong 0.5$ everywhere (Table I). But, obviously, at large strains the nonlinear membrane solution cannot satisfy this condition at an edge; in fact, as shown in Fig. 7, the primary boundary layer produces a steadily increasing N_1 as the edge is approached. Thus, an edge zone correction to N_1 is necessary. Since $N_1^{(01)} = 0$ (equation (31)), the bending component of the secondary boundary layer is of no help here, and so $N_1^{(02)}$ of equation (33) is required. Consequently, *satisfaction of vertical force equilibrium at a clamped edge of a pressurized cylindrical shell undergoing large strains requires a secondary stretching in addition to that provided by the primary boundary layer*. The development of this effect within the primary membrane layer is shown vividly in Fig. 7.

Although geometry dictates the formation of the secondary stretching component, the details of the shell behavior within

Downloaded 03 May 2010 to 171.66.16.27. Redistribution subject to ASME license or copyright; see http://www.asme.org/terms/Terms_Use.cfm

the boundary layer depend on the constitutive relations. As shown in Fig. 7 and equation (33), $N_1^{(02)}$ must be negative for $N_1^{(00)}$ positive. In a linear material, this can be accomplished by a simple compression of the reference surface. But due to the coupling between bending and stretching during large strain (equation (10)), the strong bending at the edge in itself induces a significant compressive membrane stress resultant which actually overcorrects N_1. Therefore, as shown by the positive $\lambda_1^{(02)}$ given by equation (33) and the distributions of λ_1 of Fig. 6, the reference surface actually stretches additionally in the boundary layer, just enough to make the net $N_1/\lambda_2^2 = 0.5$ at the shell edge (Fig. 7).[2]

As a final note, the maximum bending strains ($t\kappa_1/2$) for the relatively thick shell considered here ($R/t = 20$) are 0.074, 0.244, and 0.601 for $\alpha = 0.5$, 1.0, and 1.5, respectively. Therefore, the approximation for W of equation (10), which is valid for moderately large bending strains, is not accurate quantitatively for the largest deflections considered in this work. This limitation in the constitutive relations should be kept in mind during studies of the shell behavior near a critical load (Fig. 4).

Acknowledgment

The author thanks Professor J. G. Simmonds for his helpful comments on the manuscript. This work was supported by the National Science Foundation under Grant No. MEA-8319996.

References

Adkins, J. E., and Rivlin, R. S., 1952, "Large Elastic Deformations of Isotropic Materials IX. The Deformation of Thin Shells," *Philosophical Transactions of the Royal Society of London*, Vol. 244, Series A, pp. 505–531.

Bromberg, E., 1956, "Nonlinear Bending of a Circular Plate Under Normal Pressure," *Communications on Pure and Applied Mathematics*, Vol. 9, pp. 633–659.

Bromberg, E., and Stoker, J. J., 1945, "Non-linear Theory of Curved Elastic Sheets," *Quarterly of Applied Mathematics*, Vol. 3, pp. 246–265.

Kydoniefs, A. D., and Spencer, A. J. M., 1969, "Finite Axisymmetric Deformations of an Initially Cylindrical Elastic Membrane," *Quarterly Journal of Mechanics and Applied Mathematics*, Vol. 22, pp. 87–95.

Libai, A., and Simmonds, J. G., 1981, "Large-Strain Constitutive Laws for the Cylindrical Deformation of Shells," *International Journal of Non-Linear Mechanics*, Vol. 16, pp. 91–103.

Ranjan, G. V., and Steele, C. R., 1980, "Nonlinear Corrections for Edge Bending of Shells," ASME Journal of Applied Mechanics, Vol. 47, pp. 861–865.

Reissner, E., 1950, "On Axisymmetrical Deformations of Thin Shells of Revolution," *Proceedings, Symposia in Applied Mathematics*, Vol. 3, American Mathematical Society, pp. 27–52.

Reissner, E., 1959a, "On Influence Coefficients and Nonlinearity for Thin Shells of Revolution," ASME Journal of Applied Mechanics, Vol. 26, pp. 69–72.

Reissner, E., 1959b, "The Edge Effect in Symmetric Bending of Shallow Shells of Revolution," *Communications on Pure and Applied Mathematics*, Vol. 12, pp. 385–398.

Reissner, E., 1969, "On Finite Symmetrical Deflections of Thin Shells of Revolution," ASME Journal of Applied Mechanics, Vol. 36, pp. 267–270.

Reissner, E., 1972, "On Finite Symmetrical Strain in Thin Shells of Revolution," ASME Journal of Applied Mechanics, Vol. 39, pp. 1137–1138.

Simmonds, J. G., 1985, "The Strain Energy Density of Rubber-Like Shells," *International Journal of Solids and Structures*, Vol. 21, pp. 67–77.

Simmonds, J. G., 1986, "The Strain Energy Density of Rubber-Like Shells of Revolution Undergoing Torsionless, Axisymmetric Deformation (Axishells)," ASME Journal of Applied Mechanics, Vol. 53, pp. 593–596.

Taber, L. A., 1985a, "On Approximate Large Strain Relations for a Shell of Revolution," *International Journal of Non-Linear Mechanics*, Vol. 20, pp. 27–39.

Taber, L. A., 1985b, "Nonlinear Asymptotic Solution of the Reissner Plate Equations," ASME Journal of Applied Mechanics, Vol. 52, pp. 907–912.

Taber, L. A., 1987, "Asymptotic Expansions for Large Elastic Strain of a Circular Plate," *International Journal of Solids and Structures*, in press.

Teilking, J. T., and Feng, W. W., 1974, "The Application of the Minimum Potential Energy Principle to Nonlinear Axisymmetric Membrane Problems," ASME Journal of Applied Mechanics, Vol. 41, pp. 491–496.

Van Dyke, P., 1966, "Nonlinear Influence Coefficients for a Spherical Shell and Pressure Loading," *AIAA Journal*, Vol. 4, pp. 2045–2047.

Wu, C.-H., and Perng, D. Y. P., 1972, "On the Asymptotically Spherical Deformations of Arbitrary Membranes of Revolution Fixed Along an Edge and Inflated by Large Pressures—A Nonlinear Boundary Layer Phenomenon," *SIAM Journal of Applied Mathematics*, Vol. 23, pp. 133–152.

[2] In fact, for $\alpha = 1.0$, $N_1 = N_1^{(00)} + N_1^{(02)} = 0.502$ at the shell edge, indicating that higher-order exponential terms in equation (15) would contribute only small corrections.

Downloaded 03 May 2010 to 171.66.16.27. Redistribution subject to ASME license or copyright; see http://www.asme.org/terms/Terms_Use.cfm

G. W. Brodland
Department of Civil Engineering,
University of Waterloo,
Waterloo, Ontario, Canada
N2L 3G1

H. Cohen
Head,
Department of Civil Engineering,
University of Manitoba,
Winnipeg, Manitoba, Canada
R3T 2N2

Large-Strain Axisymmetric Deformation of Cylindrical Shells

Nonlinear equations are derived for the axisymmetric deformation of thin, cylindrical shells made of Mooney-Rivlin materials and subject to arbitrarily large strains and rotations. These equations are then implemented numerically using an energy minimization technique. Finally, an extensive parametric analysis is done of cylindrical shells which are clamped at one end and loaded with either a radial force or an edge moment uniformly distributed along the circumference of the other end.

Introduction

Much of the research on axisymmetric deformation of shells of revolution is based on sets of equations, such as those of Reissner (1959), which apply when strains are small and the material response is linear. In order to extend the current understanding of nonlinear shell behavior, an alternative approach which accommodates nonlinear as well as linear material response, and which does not restrict the magnitudes of strains and rotations, is presented.

This paper develops energy-form, large-strain constitutive equations for the axisymmetric deformation of thin, cylindrical shells made of Mooney-Rivlin materials. No limitations are placed on the magnitude of strains. It is only required that a relaxed form of the Kirchhoff hypothesis apply; i.e., fibers remain straight and normal to the middle surface during deformation, but may change in length. A variational principle is used to find the deformed configuration. Numerical implementation of the equations circumvents the need to restrict strains and rotations.

The axisymmetric behavior of a cylindrical shell of length ℓ, radius a, and thickness h, which is clamped at one end and loaded with either a radial load Q or an edge moment M at the other is then investigated (see Fig. 1). The full range of geometries and deformations consistent with thin-shell theory is considered. Limiting cases of this problem include the well-known linear solution, when loads are small; and the highly nonlinear cantilever elastica solution (Frish-Fay, 1962; Wang, 1981), when the cylinder is very short and hoop effects are negligible. By considering a full range of loads and geometries, the domain over which linear theory is applicable is ascertained, and the ranges of so-called short, moderate, and long cylindrical shell behavior are identified.

Analysis

The middle surface of an axisymmetrically deformed, cylindrical shell is described in cylindrical coordinates by

$$\mathbf{r} = r(s)\mathbf{e}_r(\phi) + z(s)\mathbf{e}_z \tag{1}$$

where $\mathbf{r}$ is the position of a point whose surface coordinates (s, ϕ) are the arc length measured along a meridian from the loaded end of the shell, and the angle measured along a parallel circle, respectively. An arbitrary point $\mathbf{x}$ initially located at position N away from the middle surface is given by

$$\mathbf{x} = \mathbf{r} + n(N)\mathbf{n} \tag{2}$$

where $\mathbf{n}$ is, according to the Kirchhoff-Love hypothesis, normal to the deformed middle surface. This hypothesis, commonly used in the formulation of thin-shell theories, precludes shear-induced deformations. Note also that the *deformed middle surface* is defined to be the (deformed) image of the undeformed middle surface. When deformations are not infinitesimal, it will not, in general, correspond to the middle surface of the deformed configuration. The *undeformed* shell is also represented by equations (1) and (2), and is distinguished from the deformed configuration by the use of upper case symbols. Thus, the undeformed configuration is given by

$$R = a,\ Z = \ell - S,\ \Theta = \pi/2 \tag{3}$$

for $0 \le S \le \ell$, where Θ (θ in the deformed configuration) is the angle between the surface normal $\mathbf{n}$ and the axis of symmetry $\mathbf{e}_z$.

Since the deformation is axisymmetric, the principal stretches λ_α and curvatures k_α, where $\alpha = 1, 2$, are in the meridian and parallel directions, respectively. They are given by

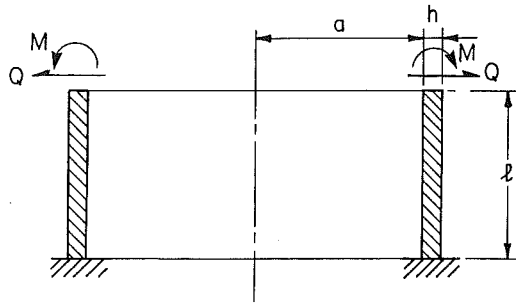


Fig. 1 Clamped cylindrical shell

Contributed by the Applied Mechanics Division for presentation at the 1987 Applied Mechanics, Biomechanics, and Fluids Engineering Conference, Cincinnati, OH, June 14–17, 1987, of the American Society of Mechanical Engineers.
Discussion of this paper should be addressed to the Editorial Department, ASME, United Engineering Center, 345 East 47th Street, New York, N.Y. 10017, and will be accepted until two months after final publication of the paper itself in the JOURNAL OF APPLIED MECHANICS. Manuscript received by ASME Applied Mechanics Division, July 31, 1986; final revision, November 1, 1986.
Paper No. 87-APM-35.

Copyright © 1987 by ASME
Downloaded 03 May 2010 to 171.66.16.27. Redistribution subject to ASME license or copyright; see http://www.asme.org/terms/Terms_Use.cfm

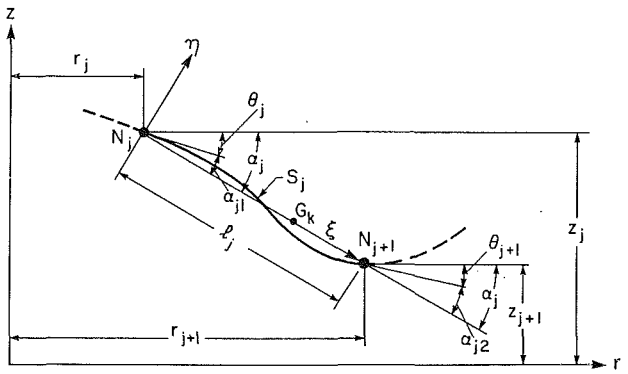


Fig. 2 Segmental representation

$$\lambda_1 = ds/dS, \quad \lambda_2 = r/R \tag{4}$$

and

$$k_1 = d\theta/ds, \quad k_2 = (\sin\theta)/r. \tag{5}$$

In the undeformed configuration, $K_1 = 0$ and $K_2 = 1/a$. Principal stretches v_i are given by

$$v_1 = (1 + k_1 n)\lambda_1, \quad v_2 = \frac{(1 + k_2 n)}{(1 + N/a)}\lambda_2, \quad v_3 = \frac{dn}{dN}. \tag{6}$$

The ratio $(g/G)^{1/2}$ of corresponding volume elements is given by

$$(g/G)^{1/2} = \frac{(1 + (k_1 + k_2)n + k_1 k_2 n^2)}{(1 + K_2 N)} v_3 (a/A)^{1/2} = v_1 v_2 v_3 \tag{7}$$

where

$$(a/A)^{1/2} = \lambda_1 \lambda_2 \tag{8}$$

is the ratio of middle surface areas. Since we are concerned with *incompressible* materials,

$$(g/G)^{1/2} = 1. \tag{9}$$

An explicit relation for n can be obtained by a suitable substitution of equations $(6)_3$, (8), and (9) into (7), followed by integration of equation (7) through the shell thickness. By involving approximations common to thin-shell theory throughout this process, we have

$$n = (N/\lambda_1\lambda_2) + [\lambda_1\lambda_2 K_2 - (k_1 + k_2)](N/\lambda_1\lambda_2)^2/2 - \left\{(k_1 + k_2)[\lambda_1\lambda_2 K_2 - (k_1 + k_2)] + \frac{2}{3}k_1 k_2\right\}(N/\lambda_1\lambda_2)^3/2. \tag{10}$$

We assume the material to be *hyperelastic*; that is, we assume that it has a strain energy density function ϵ which depends only on the current local strain state. The mechanical properties of the material are thus incorporated into the problem through ϵ. The Mooney-Rivlin strain energy function

$$\epsilon = C_1(I_1 - 3) + C_2(I_2 - 3) \tag{11}$$

where C_1 and C_2 are material constants,

$$I_1 = v_1^2 + v_2^2 + v_3^2, \quad I_2 = v_1^2 v_2^2 + v_2^2 v_3^2 + v_3^2 v_1^2, \tag{12}$$

and

$$v_3 = 1/v_1 v_2, \tag{13}$$

adequately describes many incompressible, rubber-like materials, and will be assumed here. When constants C_1, C_2 are set to $5E/24$ and $-E/24$, respectively (Brodland, 1985), the response of an incompressible *linear* material ($\nu = 0.5$) can be modelled – a feature which will allow results obtained here to be compared with the results for linear materials contained in the literature.

We wish to cast the problem in terms of total potential energy P. The strain energy component E of P is given by

$$E = \int_S \sigma d(A^{1/2}) = \int_V \epsilon d(G^{1/2}) \tag{14}$$

where S denotes the undeformed shell area and V denotes its undeformed volume. Using arguments now standard in continuum mechanics we have

$$\sigma = \int_{-h/2}^{h/2} \epsilon\{v_\alpha(N)\}(1 + N/a)dN \tag{15}$$

where equation (13) is used to eliminate v_3. Substitution of equations (6), (10), (11), and (12) into equation (15) followed by simplifications common to the thin-shell theory yields

$$\begin{aligned}\sigma = {} & C_1\{[\lambda_1^2 + \lambda_2^2 + \lambda_1^{-2}\lambda_2^{-3} - 3]h \\ & + [a_1^2(1 + 3\lambda_1^{-4}\lambda_2^{-2}) + 4a_1 a_2 \lambda_1^{-3}\lambda_2^{-3} \\ & + a_2^2(1 + 3\lambda_1^{-2}\lambda_2^{-4})]h^3/12\} \\ & + C_2\{[\lambda_1^2 - a_1^2 h^2/4)^{-1} \\ & + (\lambda_2^2 - a_2^2 h^2/4)^{-1} + \lambda_1^2\lambda_2^2 - 3]h \\ & + [\lambda_2^2 a_1^2 + 4\lambda_1\lambda_2 a_1 a_2 + \lambda_1^2 a_2^2]h^3/12\}\end{aligned} \tag{16}$$

where

$$a_1 = k_1/\lambda_2, \quad a_2 = k_2/\lambda_1 - \lambda_2/a. \tag{17}$$

The details of the calculations are given in Brodland (1985). We acknowledge the work of Libai and Simmonds (1981) and Simmonds (1986) who utilize similar procedures to analyze shell problems. Note that the possibility of middle surface shear deformation has been precluded by equation (2). As a result, equation (16) contains no terms associated with shear.

The *total potential energy* of the deformed shell is given by

$$P = E - W \tag{18}$$

where W, the potential of the external loads, is

$$W = Q(r_o - R_o) \text{ or } W = M(\theta_o - \Theta_o) \tag{19}$$

for applied radial load Q or applied moment M, respectively, and the subscript o indicates that quantities are measured at the loaded end ($S = s = 0$). The deformed equilibrium configuration is determined using the variational principle that *deformed equilibrium configurations correspond to local stationary values of total potential energy P*. It is not, in general, possible to use even the simplified integral $(14)_1$ in conjunction with equation (18) and the variational principle to analytically determine the deformed meridian. Appropriate numerical techniques, however, solve this problem easily.

Numerical Implementation

Let the meridian be broken into a series of discrete pieces as shown in Fig. 2. The n segmental functions S_j are pieced together between the $n + 1$ nodes to satisfy the radial, axial and angular positions r_j, z_j, and θ_j of the nodes. Specification of segmental functions S_j by

$$\eta_j(\xi) = \{\gamma_{j1}\xi(1 - 2\xi + \xi^2) + \gamma_{j2}\xi(-\xi + \xi^2)\}\ell_j \tag{20}$$

in terms of local Cartesian coordinates η, ξ using

$$\alpha_j = \tan^{-1}\{-(z_{j+1} - z_j)/(r_{j+1} - r_j)\} \tag{21}$$

$$\ell_j = \{(r_{j+1} - r_j)^2 + (z_{j+1} - z_j)^2\}^{1/2} \tag{22}$$

and

$$\gamma_{j1} = \alpha_j - \theta_j, \quad \gamma_{j2} = \alpha_j - \theta_{j+1} \tag{23}$$

provides a piecewise cubic representation of the meridian, and allows the problem to be cast in terms of the $3(n + 1)$ nodal positions r_j, z_j, and θ_j ($j = 1$ to $n + 1$) or X_i ($i = 1$ to $3(n + 1)$). Since the *local* transverse displacement $\eta_j(\xi)$ can be assumed small compared with ℓ_j, the meridian angle θ and curvature k_1 are given by

$$\theta(\xi) = \alpha_j - \frac{1}{\ell_j}\frac{d\eta_j(\xi)}{d\xi} \tag{24}$$

and

Downloaded 03 May 2010 to 171.66.16.27. Redistribution subject to ASME license or copyright; see http://www.asme.org/terms/Terms_Use.cfm

$$k_1 = -\frac{1}{\ell_j^2}\frac{d^2\eta(\xi)}{d_\xi^2}. \tag{25}$$

Radial and axial positions, principal stretches, and parallel curvature are given by

$$r(\xi) = r_j(1-\xi) + r_{j+1}(\xi) + \eta(\xi)\sin\alpha_j, \tag{26}$$

$$z(\xi) = z_j(1-\xi) + z_{j+1}(\xi) + \eta(\xi)\cos\alpha_j, \tag{27}$$

$$\lambda_1 = \ell_j/L_j,\ \lambda_2 = r(\xi)/R(\xi) \tag{28}$$

and

$$k_2 = \sin\theta(\xi)/r(\xi). \tag{29}$$

The total strain energy integral (14) is one-dimensional under axisymmetric deformations and can be written as

$$E = 2\pi\int_o^s R\sigma ds. \tag{30}$$

This integral can be evaluated in terms of nodal displacements X_i using equations (20) to (29) and Gaussian quadrature, which for p Gauss points takes the form

$$E = 2\pi\sum_{j=1}^{m}\sum_{k=1}^{p} R(G_k) f_k \sigma(G_k), \tag{31}$$

where f_k are Gaussian weighting factors.

Substitution of equations (19) and (31) into equation (18) yields a total potential energy of the form

$$P = P(X_i) = P(\mathbf{X}). \tag{32}$$

The problem is thus reduced to a *nonlinear programming problem* in that an objective function P, which cannot be written as a bilinear form in $\mathbf{X}$, is to be minimized. A host of techniques exist for the solution of this problem. A sequential gradient technique of the form

$$\mathbf{d} = -\mathbf{H}^{-1}\mathbf{g}^T \tag{33}$$

where

$$\mathbf{g} = \text{grad } W,\ \mathbf{H} = \text{grad}^2 W, \tag{34}$$

and $\mathbf{d}$ is a calculated displacement vector to a better estimate $\mathbf{x}+\mathbf{d}$ for $\mathbf{X}$, works satisfactorily. The process can be accelerated by using a displacement $\alpha\mathbf{d}$ where α is chosen to minimize W along $\mathbf{X}+\alpha\mathbf{d}$. This *line search* procedure is numerically efficient, as multiple evaluation of $W(\mathbf{x}+\alpha\mathbf{d})$ requires considerably less computer time than does the calculation of $\mathbf{d}$.

Results and Discussion

An axisymmetric, cylindrical shell is completely described by two dimensionless geometric parameters:

$$\lambda\ell = [3(1-\nu^2)/a^2h^2]^{1/4}\ell \tag{35}$$

and h/ℓ. The parameter h/ℓ does not appear in the linear solutions and does not have a significant effect on the numerical solution for the range $h/\ell \le 0.1$ considered here. Shear deformations become significant for larger values of this parameter, and, hence, the thin-shell theory developed here would not be accurate.

It is convenient to define load and deflection parameters, respectively, as $Q\ell^2/D$ and $wD/Q\ell^3$ for a radial load, and as $M\ell/D$ and $wD/M\ell^2$ for an edge moment where

$$D = Eh^3/12(1-\nu^2). \tag{36}$$

Note that the deflection parameters can be thought of as the product of w/ℓ and the inverse of their respective load parameters; e.g., $wD/Q\ell^3 = (w/\ell)(Q\ell^2/D)^{-1}$.

Figure 3 shows the radial edge deflections produced by various *radial edge loads* $Q\ell^2/D$. Note that *log-log* axes are used. It is convenient, for purposes of interpretation, to think of the abscissa $\lambda\ell$ as being varied by changing the radius a,

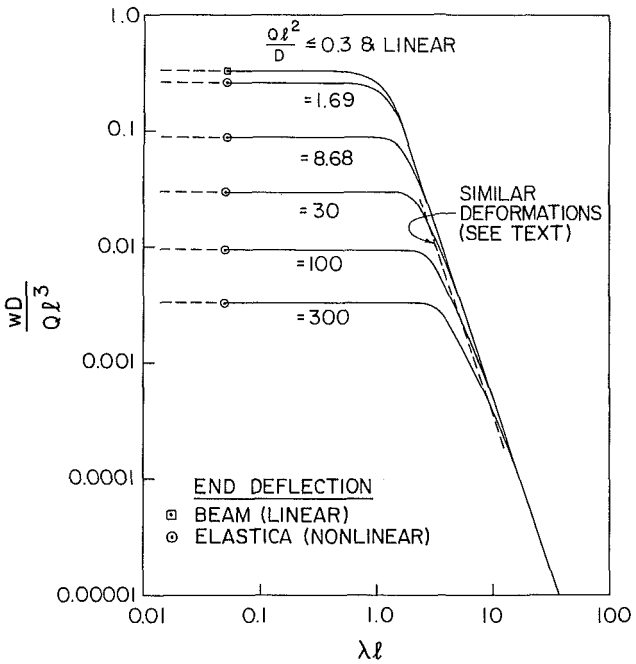


Fig. 3 Radial edge deflection due to radial load

keeping ℓ and h constant, and noting that $\lambda\ell$ is proportional to $a^{-1/2}$. This interpretation keeps the load parameter $Q\ell^2/D$ and the scaling $D/Q\ell^3$ of the deflection w constant. For large $\lambda\ell$, the radius a is small and the action of strong hoop effects "dampens" significant deflections within a region which is shorter than the length of the cylindrical shell. The deflection of the loaded end therefore does not depend on the actual length of the shell. Such shells are known as *long*, and deflections, as shown by Fig. 3, are characterized by constant

$$\frac{wD\lambda^3}{Q} = \frac{wD}{Q\ell^3}(\lambda\ell)^3. \tag{37}$$

As radius a is increased ($\lambda\ell$ reduced), there comes a point when significant deflections are not confined to a region shorter than the shell length, and an interaction occurs with the clamped boundary. Cylindrical shells of this kind are said to be of *intermediate* or *moderate* length, and are the most difficult to study analytically.

With sufficient further increase in a ($\lambda\ell$ less than about 0.5), deflection is governed by the beam action of the shell meridian; hoop effects are negligible. This is reasonable, as strains ϵ produced by radial displacement δ of the meridian are given by $\epsilon \approx \delta/a$, where a is large. Cylindrical shells of this type are called *short*. Since one end of the shell is clamped, the meridian behaves like a cantilever beam with a transverse end load. (When less severe edge restraints are present, short shells tend to deform so that the meridian shape does not change (Seide, 1975).) When loads are small, deflections of

$$w = Q\ell^3/3D \text{ or } \frac{wD}{Q\ell^3} = \frac{1}{3} \tag{38}$$

are produced. For higher loads ($Q\ell^2/D > 0.3$), large deflections occur, and elastica theory must be used to calculate deformation. This theory (Frish-Fay, 1962), gives deflections of the form

$$\frac{wD}{Q\ell^3} = f\left(\frac{Q\ell^2}{D}\right) \tag{39}$$

where f is a nonlinear function. As shown in Fig. 3, end deflections calculated by elastica theory and, where applicable, beam theory, agree very well with the results obtained here.

For loads of $Q\ell^2/D \le 0.3$, the radial end deflections ob-

Downloaded 03 May 2010 to 171.66.16.27. Redistribution subject to ASME license or copyright; see http://www.asme.org/terms/Terms_Use.cfm

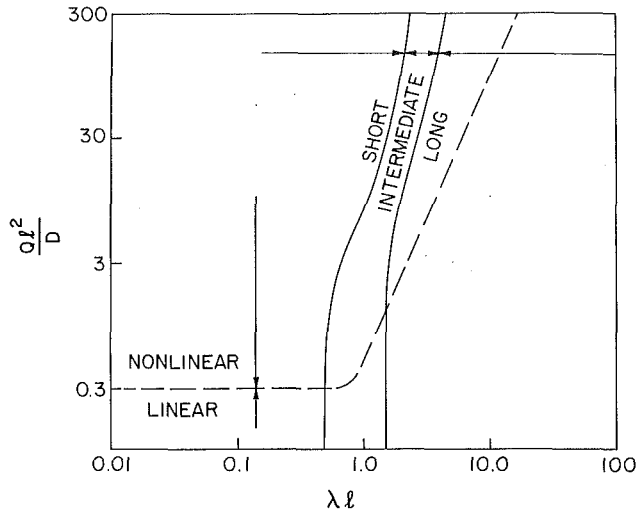


Fig. 4 Behavior domains (radial load)

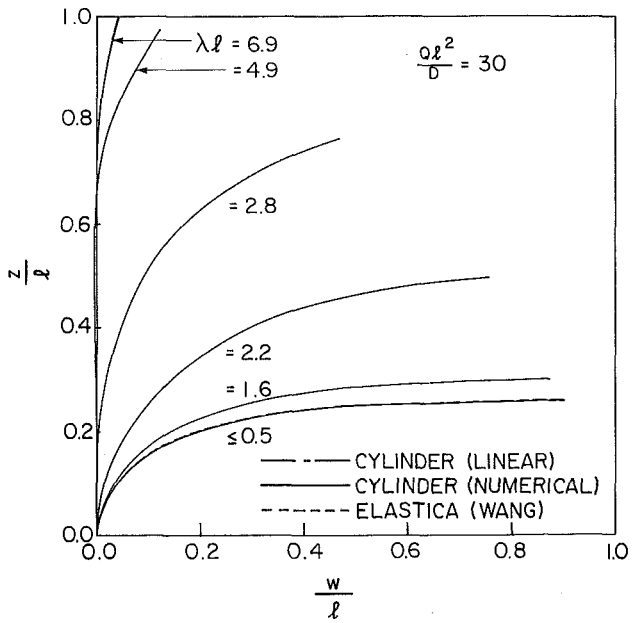


Fig. 5 Meridian contours (radial load)

tained here are indistinguishable from those calculated by linear theory. For larger loads, however, deflections diverge from the linear solution with decreasing $\lambda\ell$, since hoop effects are no longer sufficient to keep deflections small. Figure 4 shows the domains of linear and nonlinear behavior. It also shows the domains associated with short, intermediate and long cylindrical shell behavior. For linear deflections, the upper bound of $\lambda\ell \approx 0.5$ indicated is the same as the bound given by Seide (1975), and is similar to the value of $\pi/4$ given by Hetenyi (1946) for the mathematically equivalent problem of a beam on an elastic foundation. Their lower bounds of 3 and π, respectively, on long cylindrical shell behavior, are, however, more stringent than the value $\lambda\ell \approx 1.5$ indicated in Fig. 4. Geometric domains are seen to depend slightly on load $Q\ell^2/D$ when deflections are nonlinear.

Figure 5 shows typical meridian contours. The numerically deterimined curve for $\lambda\ell = 6.9$ differs from the contour predicted by linear theory only in the axial components of the displacement. This is typical and is to be expected, as the

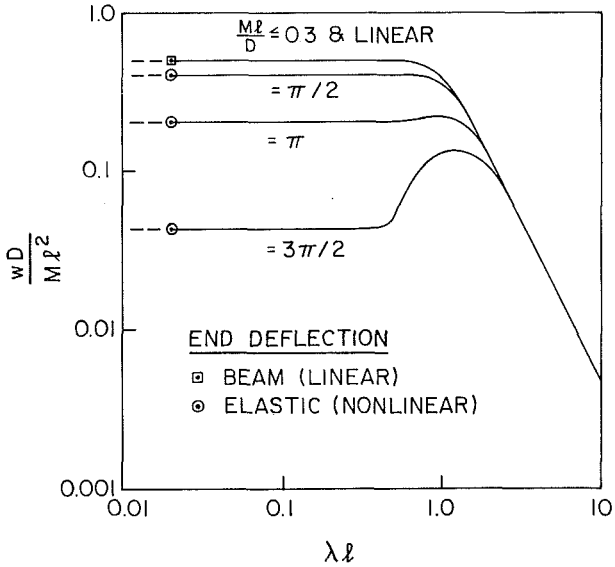


Fig. 6 Radial edge deflection due to edge moment

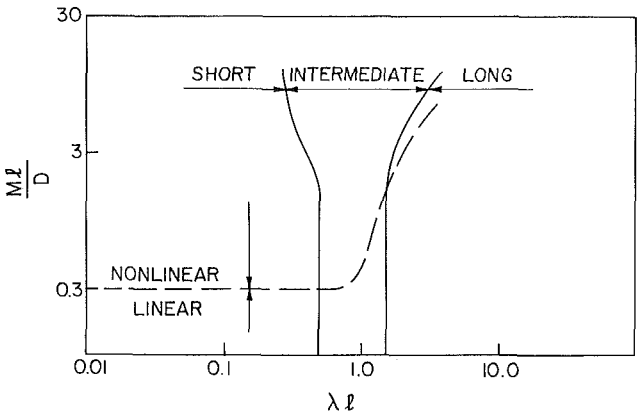


Fig. 7 Behavior domains (edge moment)

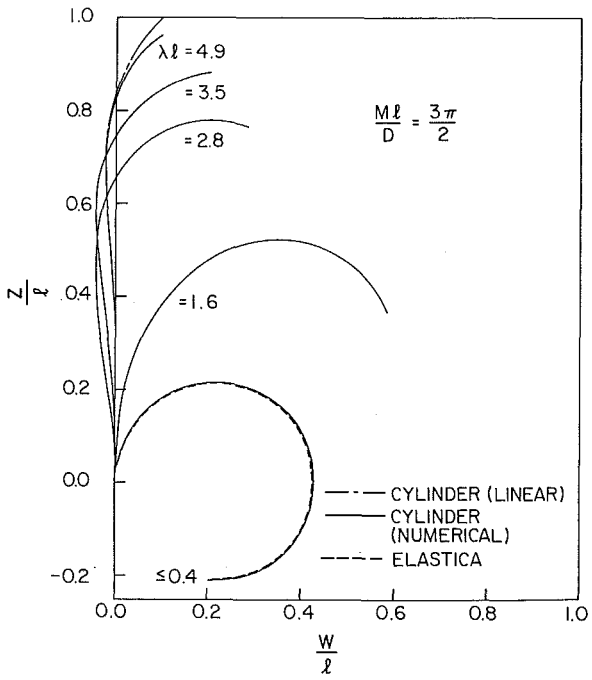


Fig. 8 Meridian contours (edge moment)

Downloaded 03 May 2010 to 171.66.16.27. Redistribution subject to ASME license or copyright; see http://www.asme.org/terms/Terms_Use.cfm

linear radial approximation $\sin\theta \approx \theta$ used in the linear analysis is valid over a wider range than is the linear axial approximation $\cos\theta \approx 1$. The contour for $\lambda\ell = 2.8$ illustrates highly nonlinear long shell behavior – significant deformation is confined to the region $0.1 < z/\ell < 1.0$. This contour is, in fact, produced at the loaded end in all the states through which the diagonal dashed line in Fig. 3 passes. For $\lambda\ell \leq 0.5$, short shell behavior is evident. The deformed contour is very close to the elastica contour calculated using the scheme proposed by Wang (1981).

Cylindrical shells loaded with an *edge moment* exhibit generally similar behavior. Figure 6 shows load versus end-deflection curves for cylindrical shells subjected to an edge moment. The curves for $M\ell/D = \pi$ and $M\ell/D = 3\pi/2$ are not monotonic since the radial displacement of the loaded edge actually decreases with increasing moment as the meridian wraps around. See also Fig. 8.

Figure 7 shows the domains of linear and nonlinear behavior for short, intermediate and long cylindrical shells. Figure 8 gives meridian contours for shells loaded with $M\ell/D = 3\pi/2$. For short cylindrical shells ($\lambda\ell \leq 0.4$), the meridian takes the form of a 3/4 circle.

Acknowledgments

The authors gratefully acknowledge the financial support of the Natural Sciences and Engineering Research Council of Canada.

References

Brodland, G. W., 1985, "Large Axisymmetric Deformation of Thin Shells of Revolution," Ph.D. Thesis, Department of Civil Engineering, University of Manitoba, Winnipeg, Manitoba.

Frisch-Fay, R., 1962, *Flexible Bars*, Butterworths, London.

Hetenyi, M., 1946, *Beams on Elastic Foundations*, University of Michigan Press.

Libai, A., and Simmonds, J. G., 1981, "Large-Strain Constitutive Laws for the Cylindrical Deformation of Shells," *Int. J. Non-Linear Mech.*, Vol. 16, No. 2, pp. 91–103.

Reissner, E., 1959, "On Axisymmetric Deformations of Thin Shells of Revolution," *Proc. Symp. in Appl. Math.*, Vol. 3, pp. 27–52.

Seide, P., 1975, *Small Elastic Deformations of Thin Shells*, Noordhoff Publishing, The Netherlands.

Simmonds, J. G., 1986, "The Strain-Energy Density of Rubber-Like Shells of Revolution Undergoing Torsionless, Axisymmetric Deformation (Axishells)," ASME Journal of Applied Mechanics, Vol. 53, pp. 593–596.

Wang, C. Y., 1981, "Large Deflections of an Inclined Cantilever with an End Load," *Int. J. Non-Linear Mech.*, Vol. 16, No. 2, pp. 155–164.

Downloaded 03 May 2010 to 171.66.16.27. Redistribution subject to ASME license or copyright; see http://www.asme.org/terms/Terms_Use.cfm

Imperfection-Sensitivity of Long Antisymmetric Cross-Ply Cylindrical Panels Under Shear Loads

David Hui
Mem. ASME

I. H. Y. Du

The Ohio State University,
Department of Engineering Mechanics,
Columbus, Ohio 43210

This paper examines the theoretical postbuckling behavior and imperfection-sensitivity of antisymmetrically laminated open, long, cylindrical panels under shear loads. The longitudinal edges may be simply-supported or clamped. It is found that the cylindrical panels may be sensitive to the presence of geometric imperfections depending primarily on the reduced-flatness parameter and Young's modulus ratio. The shear buckling load and the postbuckling coefficients are plotted as a function of the shell geometry, number of layers, and material parameters. The paper is the first in the literature to examine the postbuckling behavior of open laminated cylindrical panels under shear loads.

1 Introduction

Due to increasing use of light-weight, high-strength composite materials in the aerospace and mechanical engineering applications, shear buckling of laminated plates has received increased attention over the past twenty years. Ashton and Love (1969), Whitney (1969), Chamis (1971), Housner and Stein (1975), and Hui (1984b), among others, have studied shear buckling of composite rectangular plates. Excellent reviews on this subject were written by Johns (1971) and Leissa (1985). The "postbuckling" behavior of laminated rectangular plates under shear loads has also been examined by a number of authors. For example, Agarwal (1981), Sumihara et al. (1981), Zhang and Matthews (1981, 1984), and Stein (1985a,b) have examined these postbuckling problems in recent years and some experiments on diagonal tension behavior of shear panels were performed by Kaminski and Ashton (1971). Stein (1985a,b) found that laminated long plates may carry loads which are considerably higher than the classical shear buckling loads. The effects of the direction of shear load on the postbuckling behavior of these anisotropic rectangular plates were studied by Zhang and Matthews (1981, 1984). General computer codes were written by Viswanathan et al. (1974) and Bauld and Satyamurthy (1979).

Shear buckling of generally laminated open "cylindrical" panels have been examined by Zhang and Matthews (1983a) using beam functions. The effects of shear loads on antisymmetrically laminated cross-ply cylindrical panels simply-supported along all four edges were presented by Hui (1987). Zhang and Matthews (1983b) also investigated the postbuckling behavior of laminated cylindrical panels under axial compression but not shear load. Surprisingly, it appears that thorough theoretical studies on the postbuckling behavior of laminated open cylindrical panels under shear loads have not been reported in the open literature, even in the important special case of isotropic-homogeneous cylindrical panels. Based on some experiments (Rafel, 1943) and preliminary calculations on isotropic-homogeneous cylindrical panels under shear loads, it may be conjectured that cylindrical panels are still sensitive to the presence of geometric imperfections as in the case of axial load (Koiter, 1956; Stephens, 1971; Hui et al., 1981; Hui, 1985) but possibly to a lesser extent. Thus it is of interest to study the postbuckling and imperfection-sensitivity of laminated cylindrical panels under shear loads.

The objective of this paper is to examine the postbuckling behavior and imperfection-sensitivity of laminated open cylindrical panels under shear loads. Koiter's theory of elastic stability is employed and the analysis is based on a solution of the nonlinear Donnell-type equilibrium and compatibility equations. Using Koiter's perturbation technique, a sequence of linear ordinary differential equations are derived for the buckling and postbuckling state, using the simplifying assumption that the cylindrical panels are infinitely long, thus permitting a separable form of the solution. The buckling differential equations are discretized using a central difference scheme and the resulting eigenvalue problem is solved using the shifted inverse power method. Likewise, the second order ordinary differential equations are discretized and solved us-

Contributed by the Applied Mechanics Division for presentation at the 1987 Applied Mechanics, Biomechanics, and Fluids Engineering Conference, Cincinnati, OH, June 14-17, 1987, of the American Society of Mechanical Engineers.
Discussion of this paper should be addressed to the Editorial Department, ASME, United Engineering Center, 345 East 47th Street, New York, N.Y. 10017, and will be accepted until two months after final publication of the paper itself in the JOURNAL OF APPLIED MECHANICS. Manuscript received by ASME Applied Mechanics Division, April 1, 1986; final revision, October 6, 1986.
Paper No. 87-APM-28.

Copyright © 1987 by ASME
Downloaded 03 May 2010 to 171.66.16.27. Redistribution subject to ASME license or copyright; see http://www.asme.org/terms/Terms_Use.cfm

ing Gaussian elimination. The shear buckling load and the associated postbuckling coefficients are presented as a function of the geometric and material parameters of the laminated cylindrical panels. Example problems are chosen from antisymmetrically laminated cross-ply long cylindrical panels, simply-supported or clamped along the longitudinal edges. Parameter variation involving the geometry of the shell specified by the simplified-flatness parameter and the material parameter involving Young's modulus ratio will be presented. Particular attention will be given to Boron-epoxy and isotropic-homogeneous cylindrical panels.

It is found that open laminated cylindrical panels under shear loads have stable postbuckling behavior (not sensitive to geometric imperfections) for sufficiently small values of the simplified-flatness parameter. For larger values of the reduced-flatness parameter, the shear buckling loads of the cylindrical panels are found to be sensitive to the presence of geometric imperfections. This is especially true for Young's modulus ratio close to unity. Long cylindrical panels with clamped edges are less imperfection-sensitive than those with simply-supported edges.

2 Governing Differential Equations and Classical Buckling Load

The governing Donnell-type nonlinear equilibrium and compatibility equations for generally laminated cylindrical panels are, in nondimensional form, respectively, Hui (1985, 1986b)

$$L_{d^*}(w)+L_{b^*}(f)+f_{,xx} = f_{,yy}w_{,xx}+f_{,xx}w_{,yy}-2f_{,xy}w_{,xy} \tag{1}$$

$$L_{a^*}(f)-L_{b^*}(w)-w_{,xx}=(w_{,xy})^2-w_{,xx}w_{,yy} \tag{2}$$

where,

$$w=W/h,\ f=F/(E_2h^3),\ (x,y)=(X,Y)/(Rh)^{1/2}$$
$$a^*_{ij}=(E_2h)A^*_{ij},\ b^*_{ij}=B^*_{ij}/h,\ d^*_{ij}=D^*_{ij}/(E_2h^3) \tag{3}$$

In the above, W is the out-of-plane displacement (positive outwards), F is the stress function, R is the shell radius, h is the total thickness of the laminated shell, E_2 is the Young's modulus in the in-plane transverse direction, and the $L_{a^*}(\,)$, $L_{b^*}(\,)$, and $L_{d^*}(\,)$ are the nondimensional linear differential operators defined by Hui (1985, 1986) and Tennyson et al. (1971).

Using Koiter's (1945) theory of elastic stability, the total displacement and the total stress function can be expanded in the perturbed form,

$$w=w_p+\xi w_I+\xi^2 w_{II}$$
$$f=f_p+\xi f_I+\xi^2 f_{II} \tag{4}$$

where ξ is the amplitude of the normalized buckling mode. The axial compressive load σ, the lateral pressure p and the torsional load τ are related to the prebuckling stress function f_p by,

$$(\sigma,p,\tau)=(f_{p,yy},f_{p,xx},-f_{p,xy})=(N_x,N_y,N_{xy})R/(E_2h^2) \tag{5}$$

where N_x, N_y, and N_{xy} are the membrane stress resultants.

Substituting the total displacement and stress function into the governing nonlinear differential equations and collecting terms which involve ξ, one obtains,

$$L_{d^*}(w_I)+L_{b^*}(f_I)+f_{I,xx}+\sigma_x w_{I,xx}+\sigma_y w_{I,yy}-2\tau w_{I,xy}-w_{p,xx}f_{I,yy}-w_{p,yy}f_{I,xx}+2w_{p,xy}f_{I,xy}=0 \tag{6}$$

$$L_{a^*}(f_I)-L_{b^*}(w_I)-w_{I,xx}-2w_{p,xy}w_{I,xy}+w_{p,xx}w_{I,yy}+w_{p,yy}w_{I,xx}=0 \tag{7}$$

For an antisymmetric cross-ply laminate, the nondimensional linear operators are defined to be

$$L_{a^*}(\,)=a^*_{22}(\,)_{,xxxx}+(2a^*_{12}+a^*_{66})(\,)_{,xxyy}+a^*_{11}(\,)_{,yyyy}$$
$$L_{b^*}(\,)=b^*_{21}(\,)_{,xxxx}+(b^*_{11}+b^*_{22}-2b^*_{66})(\,)_{,xxyy}+b^*_{12}(\,)_{,yyyy}$$
$$L_{d^*}(\,)=d^*_{11}(\,)_{,xxxx}+(2)(d^*_{12}+2d^*_{66})(\,)_{,xxyy}+d^*_{22}(\,)_{,yyyy}$$

Assuming that the cylindrical panel is sufficiently long so that the boundary conditions at the two curved edges can be neglected, the buckling mode can be written in the separable form,

$$w_I(x,y)=w_c(y)\cos(Mx)+w_s(y)\sin(Mx)$$
$$f_I(x,y)=f_c(y)\cos(Mx)+f_s(y)\sin(Mx) \tag{8}$$

The wave number M is defined as,

$$M=m\pi(Rh)^{1/2}/L \quad \text{or} \quad M=(m\pi/\theta_s)(B/L) \tag{9}$$

where B is the curved distance between the two longitudinal edges and the simplified-flatness parameter θ_s is,

$$\theta_s=B/(Rh)^{1/2} \tag{10}$$

Substituting the separable form of the buckling mode $w_I(x,y)$ and $f_I(x,y)$ into the equilibrium equation for the buckling state, and collecting terms which involve cos (Mx) and sin (Mx), one obtains, respectively,

$$\begin{aligned}&d^*_{22}w_c(y)_{,yyyy}+[\sigma_y-2M^2(d^*_{12}+2d^*_{66})]w_c(y)_{,yy}\\&+(-\sigma_xM^2+d^*_{11}M^4)w_c(y)+(4d^*_{26}M)w_s(y)_{,yyy}\\&-(4d^*_{16}M^3+2\tau M)w_s(y)_{,y}+b^*_{12}f_c(y)_{,yyyy}\\&-[(b^*_{11}+b^*_{22}-2b^*_{66})(M^2)+w_{p,xx}]f_c(y)_{,yy}\\&+(-M^2+b^*_{21}M^4+M^2w_{p,yy})f_c(y)\\&+(2b^*_{16}-b^*_{62})Mf_s(y)_{,yyy}+[(2b^*_{26}-b^*_{61})(-M^3)\\&+2Mw_{p,xy}]f_s(y)_{,y}=0\end{aligned} \tag{11}$$

$$\begin{aligned}&d^*_{22}w_s(y)_{,yyyy}+[\sigma_y-(2M^2)(d^*_{12}+2d^*_{66})]w_s(y)_{,yy}\\&+(d^*_{11}M^4-M^2\sigma_x)w_s(y)-(4M)d^*_{26}w_c(y)_{,yyy}\\&+(4d^*_{16}M^3+2\tau M)w_c(y)_{,y}+b^*_{12}f_s(y)_{,yyyy}\\&+[(b^*_{11}+b^*_{22}-2b^*_{66})(-M^2)-w_{p,xx}]f_s(y)_{,yy}\\&+(b^*_{21}M^4-M^2+w_{p,yy}M^2)f_s(y)\\&+(2b^*_{16}-b^*_{62})(-M)f_c(y)_{,yyy}+[(2b^*_{26}-b^*_{61})(M^3)\\&-(2M)w_{p,xy}]f_c(y)_{,y}=0\end{aligned} \tag{12}$$

Similarly, collecting terms involving cos (Mx) and sin (Mx) in the compatibility equation for the buckling state, one obtains, respectively,

$$\begin{aligned}&a^*_{11}f_c(y)_{,yyyy}+(2a^*_{12}+a^*_{66})(-M^2)f_c(y)_{,yy}\\&+a^*_{22}M^4f_c(y)-2a^*_{16}Mf_s(y)_{,yyy}+2a^*_{26}M^3f_s(y)_{,y}\\&-b^*_{12}w_c(y)_{,yyyy}+[(b^*_{11}+b^*_{22}-2b^*_{66})M^2\\&+w_{p,xx}]w_c(y)_{,yy}+[-b^*_{21}M^4+M^2-w_{p,yy}M^2]w_c(y)\\&-(2b^*_{16}-b^*_{62})(M)w_s(y)_{,yyy}\\&+[(2b^*_{26}-b^*_{61})M^3-2Mw_{p,xy}]w_s(y)_{,y}=0\end{aligned} \tag{13}$$

$$\begin{aligned}&a^*_{11}f_s(y)_{,yyyy}+(2a^*_{12}+a^*_{66})(-M^2)f_s(y)_{,yy}\\&+a^*_{22}M^4f_s(y)-(2a^*_{16})(-M)f_c(y)_{,yyy}\\&-(2a^*_{26})(M^3)f_c(y)_{,y}-b^*_{12}w_s(y)_{,yyyy}\\&+[(b^*_{11}+b^*_{22}-2b^*_{66})M^2+w_{p,xx}]w_s(y)_{,yy}\\&+(-b^*_{21}M^4+M^2-M^2w_{p,yy})w_s(y)\\&+(2b^*_{16}-b^*_{62})(M)w_c(y)_{,yyy}\\&-(2b^*_{26}-b^*_{61})M^3w_c(y)_{,y}=0\end{aligned} \tag{14}$$

The boundary conditions at the two longitudinal edges of a laminated cylindrical panel are taken to be identical. The possible in-plane boundary conditions are

Downloaded 03 May 2010 to 171.66.16.27. Redistribution subject to ASME license or copyright; see http://www.asme.org/terms/Terms_Use.cfm

$$U(y=0)=0 \quad \text{or} \quad N_{xy}(y=0)=0$$
$$V(y=0)=0 \quad \text{or} \quad N_y(y=0)=0 \tag{15}$$

However, in all the example problems chosen, the following three boundary conditions are enforced (weakest in-plane conditions),

$$f_{,xy}(y=0)=0$$
$$f_{,xx}(y=0)=0$$
$$w(y=0)=0 \tag{16}$$

For clamped edges, one obtains, $w_{,y}(y=0) = 0$ whereas for simply-supported edges, the condition is $M_y(y=0) = 0$. The zero-amount condition implies

$$-b_{12}^* f_{,yy}(y=0) - b_{22}^* f_{,xx}(y=0)$$
$$+ b_{62}^* f_{,xy}(y=0) - d_{22}^* w_{,yy}(y=0)$$
$$- 2d_{26}^* w_{,xy}(y=0)=0 \tag{17}$$

For an antisymmetric cross-ply laminated panel ($b_{62}^* = 0$, $d_{26}^* = 0$) under pure shear, the membrane prebuckling state satisfies the above zero-moment condition. Likewise, for an antisymmetric angle-ply panel ($b_{12}^* = 0$, $b_{22}^* = 0$, $d_{26}^* = 0$) under axial compression or biaxial compression, the membrane prebuckling state also satisfies the $M_y(y=0) = 0$ requirement. The boundary conditions for the buckling state can be easily obtained by substituting the separable form of the buckling mode $w_I(x, y)$ and $f_I(x, y)$ into equations (16) and (17). The above four coupled linear ordinary differential equations with four unknown variables $w_s(y)$, $w_c(y)$, $f_s(y)$, and $f_c(y)$ and the associated boundary conditions are discretized using a central finite difference scheme using approximately 200 integration points between the two longitudinal edges (only 100 integration points are used for small θ_s). The resulting system of homogeneous linear algebraic equations can be expressed in matrix form,

$$[A]\vec{x} = \tau[B]\vec{x} \tag{18}$$

which can be solved using a "shifted" inverse power method (Hui and Hansen (1982)). Similar to the case of shear buckling of antisymmetric cross-ply simply-supported rectangular plates (Hui 1984b), the buckling load is independent of the direction of the applied shear loads. Thus, the smallest eigenvalue occurs in positive and negative pairs so that the standard power method fails and it is necessary to use the "shifted" technique. The classical buckling load is obtained by searching for the smallest eigenvalue for all possible values of the "continuous" wave number M. The corresponding buckling mode is normalized such that the largest magnitude of the displacement is one, that is,

$$[w_s(y)^2 + w_c(y)^2]^{1/2} = 1 \tag{19}$$

3 Second Order Fields

Substituting the total displacement and stress function (equations (4)) into the governing nonlinear partial differential equations and collecting terms which involve ξ^2, the equilibrium and compatibility equations for the second order fields are, respectively,

$$L_{d^*}(w_{II}) + L_{b^*}(f_{II}) + f_{II,xx} + \sigma_x w_{II,xx}$$
$$+ \sigma_y w_{II,yy} - 2\tau w_{II,xy} - w_{p,xx} f_{II,yy}$$
$$- w_{p,yy} f_{II,xx} + 2w_{p,xy} f_{II,xy}$$
$$= f_{I,yy} w_{I,xx} + f_{I,xx} w_{I,yy} - 2f_{I,xy} w_{I,xy} \tag{20}$$

$$L_{a^*}(f_{II}) - L_{b^*}(w_{II}) - 2w_{p,xy} w_{II,xy}$$
$$+ w_{p,xx} w_{II,yy} + w_{p,yy} w_{II,xx} - w_{II,xx}$$
$$= (w_{I,xy})^2 - w_{I,xx} w_{I,yy} \tag{21}$$

Upon substitution of the separable form of the buckling mode $w_I(x,y)$ and $f_I(x,y)$ into the right-hand sides of the equilibrium and compatibility equations for the second order fields, it is clear that $w_{II}(x,y)$ and $f_{II}(x,y)$ can be written in the separable form

$$w_{II}(x,y) = w^*(y) + w_A(y)\cos(2Mx) + w_B(y)\sin(2Mx)$$
$$f_{II}(x,y) = f^*(y) + f_A(y)\cos(2Mx) + f_B(y)\sin(2Mx) \tag{22}$$

Substituting the separable forms of $w_I(x,y)$, and $f_I(x,y)$ and $w_{II}(x,y)$, $f_{II}(x,y)$ into the partial differential equations for the second order fields, one obtains two coupled ordinary differential equations in $w^*(y)$ and $f^*(y)$ and four uncoupled ordinary differential equations in $w_A(y)$, $w_B(y)$, $f_A(y)$, and $f_B(y)$. The two coupled equilibrium and compatibility equations for $w^*(y)$ and $f^*(y)$ are, respectively,

$$d_{22}^* w^*(y)_{,yyyy} + b_{12}^* f^*(y)_{,yyyy}$$
$$= (-M^2/2)\{[w_s(y)f_s(y)]_{,yy} + [w_c(y)f_c(y)]_{,yy}\} \tag{23}$$

$$a_{11}^* f^*(y)_{,yyyy} - b_{12}^* w^*(y)_{,yyyy}$$
$$= (M^2/2)\{[w_s(y)w_s(y)_{,y}]_{,y} + [w_c(y)w_c(y)_{,y}]_{,y}\} \tag{24}$$

The four coupled ordinary differential equations are, from the equilibrium equations collecting terms involving sin ($2Mx$), respectively,

$$L_{11}(w_A, w_B, f_A, f_B) = (-M^2/2)\{[w_s(y)f_c(y)_{,yy}$$
$$+ w_s(y)_{,yy} f_c(y) - 2w_s(y)_{,y} f_c(y)_{,y}]$$
$$+ [w_c(y)f_s(y)_{,yy} + w_c(y)_{,yy} f_s(y)$$
$$- 2w_c(y)_{,y} f_s(y)_{,y}]\} \tag{25}$$

$$L_{12}(w_A, w_B, f_A, f_B) = (-M^2/2)\{[w_s(y)f_s(y)]_{,yy}$$
$$+ [w_c(y)f_c(y)]_{,yy}\} + (M^2/2)\{[w_s(y)f_s(y)_{,yy}$$
$$+ w_s(y)_{,yy} f_s(y) - 2w_s(y)_{,y} f_s(y)_{,y}]$$
$$- [w_c(y)f_c(y)_{,yy} + w_c(y)_{,yy} f_c(y)$$
$$- 2w_c(y)_{,y} f_c(y)_{,y}]\} \tag{26}$$

and from the compatibility equation by collecting terms involving sin ($2Mx$) and cos ($2Mx$), respectively,

$$L_{13}(w_A, w_B, f_A, f_B) = (M^2/2)[w_s(y)w_c(y)_{,yy}$$
$$+ w_c(y)w_s(y)_{,yy} - 2w_s(y)_{,y} w_c(y)_{,y}] \tag{27}$$

$$L_{14}(w_A, w_B, f_A, f_B) = (M^2/2)[w_s(y)_{,y}{}^2$$
$$- w_s(y)w_s(y)_{,yy} - w_c(y)_{,y}{}^2$$
$$+ w_c(y)w_c(y)_{,yy}] \tag{28}$$

In the above, $L_{11}(w_A, w_B, f_A, f_B)$, $L_{12}(w_A, w_B, f_A, f_B)$, $L_{13}(w_A, w_B, f_A, f_B)$, and $L_{14}(w_A, w_B, f_A, f_B)$ are obtained from the left-hand sides of the buckling ordinary differential equations (equations (11), (12), (13), and (14)) by replacing $w_c(y)$, $w_s(y)$, $f_c(y)$, $f_s(y)$ by $w_A(y)$, $w_B(y)$, $f_A(y)$, $f_B(y)$; further, the wave number M is replaced by $2M$ and τ is replaced by the classical buckling load τ_c. Since the in-plane boundary conditions for the second order fields do not involve $f^*(y)$ nor its derivative, an additional condition is needed to solve the (w^*, f^*) problem. The average second order longitudinal stress is set to zero (Hui, 1984a)

$$\int_{y=0}^{\theta_s} \int_{x=0}^{\infty} N_{x_{II}}(x,y)\,dx\,dy = 0 \tag{29}$$

which implies

$$f_{,y}^*(y=0)=0 \quad \text{and} \quad f_{,y}^*(y=\theta_s)=0 \tag{30}$$

Since the postbuckling coefficient (see next section) and the differential equation do not depend explicitly on $f^*(y)$ or $f^*(y)_{,y}$, it is only necessary to solve for $f^*(y)_{,yy}$. That is, a constant shift in $f^*(y)$ has no effect on the postbuckling coefficient so that one may arbitrarily set,

$$f^*(y=0)=0, \quad f^*(y=\theta_s)=0 \tag{31}$$

Downloaded 03 May 2010 to 171.66.16.27. Redistribution subject to ASME license or copyright; see http://www.asme.org/terms/Terms_Use.cfm

The remaining boundary conditions for the clamped conditions at the longitudinal edges are,

$$w^*(y=0)=0, \qquad w^*_{,y}(y=0)=0,$$
$$w^*(y=\theta_s)=0, \qquad w^*_{,y}(y=\theta_s)=0, \tag{32}$$

For a simply-supported cylindrical panel, the above zero-slope conditions are replaced by the zero-moment condition,

$$-b^*_{12}f^*_{,yy}(y=0)-d^*_{22}w^*_{,yy}(y=0)=0 \tag{33}$$

with the same condition at $y = \theta_s$. Since the cylindrical panels are "open," the single-valuedness of the displacements need not, and in fact, should not be enforced.

The boundary conditions for the (w_A, w_B, f_A, f_B) problem are obtained from equations (16) and (17) by substituting the appropriate separable forms for the second order fields. The coupled ordinary differential equations and the associated boundary conditions are discretized using a central finite difference scheme and solved using a Gaussian elimination equation solver LINPACK (Dongarra et al., 1979).

4 Initial Postbuckling Behavior

The initial postbuckling behavior of a laminated cylindrical panel subjected to shear loads is examined using Koiter's (1945) theory of elastic stability. Koiter's theory was reformulated in terms of the mixed formulation involving the stress function by Budiansky and Hutchinson (1964). Within the assumptions employed by Koiter for a single-mode system, the structure will be able to carry the applied shear loads in the initial postbuckling stage (that is, not sensitive to geometric imperfections) if the postbuckling b coefficent is positive whereas the opposite is true if b is negative. The degree of imperfection-sensitivity is measured by the magnitude of the b coefficient. In passing, an alternative approach to measure imperfection-sensitivity is to compute the initial postbuckling slope (Stein 1968); however, this method will not be used in this paper.

The b coefficient is defined as (Hutchinson and Amazigo, 1967)

$$b=(R_1+R_2)/|d_1| \tag{34}$$

where,

$$R_1=(2)\int_{y=0}^{\theta_s}\int_{x=0}^{\infty}[(f_{I,xx}w_{I,y})w_{II,y} + (f_{I,yy}w_{I,x})w_{II,x}-f_{I,xy}(w_{I,x}w_{II,y} + w_{I,y}w_{II,x})]dx\,dy \tag{35}$$

$$R_2=\int_{y=0}^{\theta_s}\int_{x=0}^{\infty}[f_{II,xx}(w_{I,y})^2+f_{II,yy}(w_{I,x})^2 - 2f_{II,xy}(w_{I,x}w_{I,y})]dx\,dy \tag{36}$$

$$d_1=\int_{y=0}^{\theta_s}\int_{x=0}^{\infty}[\sigma_y(w_{I,y})^2+\sigma_x(w_{I,x})^2 - 2\tau w_{I,x}w_{I,y}]dx\,dy \tag{37}$$

Substituting the separable forms of $w_I(x, y)$, $f_I(x, y)$ and $w_A(x, y)$, $w_B(x, y)$, $f_A(x, y)$, $f_B(x, y)$ into the above expressions, one obtains,

$$\begin{aligned}R_1=(M^2)\int_{y=0}^{\theta_s}\{&[-w^*(y),_y][f_s(y)w_s(y),_y\\ &+f_c(y)w_c(y),_y]-(1/2)w_B(y),_y[f_s(y)w_c(y),_y\\ &+f_c(y)w_s(y),_y]-(1/2)w_A(y),_y[-f_s(y)w_s(y),_y\\ &+f_c(y)w_c(y),_y]+w_B(y)[f_s(y),_{yy}w_c(y)\\ &+f_c(y),_{yy}w_s(y)]+w_A(y)[-f_s(y),_{yy}w_s(y)\\ &+f_c(y),_{yy}w_c(y)]-w^*(y),_y[f_s(y),_yw_s(y)\\ &+f_c(y),_yw_c(y)]+(1/2)w_B(y),_y[f_c(y),_yw_s(y)\\ &+f_s(y),_yw_c(y)]+(1/2)w_A(y),_y[-f_s(y),_yw_s(y)\\ &+f_c(y),_yw_c(y)]-w_B(y)[f_c(y),_yw_s(y),_y\\ &+f_s(y),_yw_c(y),_y]+w_A(y)[f_s(y),_yw_s(y),_y\\ &-f_c(y),_yw_c(y),_y]\}dy\end{aligned} \tag{38}$$

$$\begin{aligned}R_2=(M^2)\int_{y=0}^{\theta_s}\{&(-2)f_B(y)[w_s(y),_yw_c(y),_y]\\ &-f_A(y)[-w_s(y),_y{}^2+w_c(y),_y{}^2]\\ &+(1/2)f^*(y),_{yy}[w_s(y)^2+w_c(y)^2]\\ &-(1/2)f_B(y),_{yy}w_s(y)w_c(y)\\ &+(1/4)f_A(y),_{yy}[w_s(y)^2-w_c(y)^2]\\ &-f_B(y),_y[w_s(y)w_c(y),_y+w_c(y)w_s(y),_y]\\ &+f_A(y),_y[w_s(y)w_s(y),_y-w_c(y)w_c(y),_y]\}dy\end{aligned} \tag{39}$$

$$\begin{aligned}d_1=(1/2)\int_{y=0}^{\theta_s}\{&(\sigma_y)[w_s(y),_y{}^2+w_c(y),_y{}^2]\\ &+(\sigma_x)(M^2)[w_s(y)^2+w_c(y)^2]-(2\tau)(M)[w_s(y)w_c(y),_y\\ &-w_c(y)w_s(y),_y]\}dy\end{aligned} \tag{40}$$

The integrations are performed using Simpson's rule with approximately 200 integration points from $y=0$ to $y=\theta_s$.

5 Discussion of Results

The aim of this section is to present results for the initial postbuckling behavior of laminated cylindrical panels under shear loads. The cylindrical panels are assumed to be sufficiently long such that the boundary conditions at the two curved edges may be neglected. Example problems are chosen from Boron-epoxy laminated panels with the material parameters (Chia, 1980).

$$E_1/E_2=10, \quad G_{12}/E_2=1/3, \quad \nu_{12}=0.22 \tag{41}$$

The isotropic homogeneous special case can be obtained by setting,

$$E_1/E_2=1, \quad G_{12}/E_2=1/[2(1+\nu)], \quad \nu=0.3 \tag{42}$$

Within the assumptions of Donnell's shell theory, the present results are valid for all values of the radius to thickness ratio.

Figure 1(a) shows a graph of the nondimensional classical shear buckling load versus the simplified-flatness parameter for long isotropic homogeneous cylindrical panels simply-supported or clamped at the longitudinal edges. It should be noted that the variable τ^* is defined as,

$$\tau^*=\tau_c\theta^2 \qquad \text{for } \theta<1$$
$$\tau^*=\tau_c \qquad \text{for } \theta\geq 1 \tag{43}$$

The dimensional shear buckling load of a long flat plate is approximately the same as that for a cylindrical panel with a small curvature defined by $\theta_s < 1$. For large simplified-flatness parameter, the classical shear buckling load tends to level out (Hui, 1985). The optimum axial wave number ranges from ($M = 2.39\pi$, $\theta_s = 0.5$) to ($M = 0.082\pi$, $\theta_s = 8.0$) for clamped shells and from ($M = 1.59\pi$, $\theta_s = 0.5$) to ($M = 0.078\pi$, $\theta_s = 8.0$) for simply-supported shells.

Figure 1(b) shows a plot of the corresponding postbuckling b coefficient versus the simplified-flatness parameter for isotropic homogeneous, long cylindrical panels. As in the case of axial compression examined by Koiter (1956) and Stephens (1971), the b coefficient is positive for sufficiently small panel curvature. The transition values at which the b coefficient is zero occurs at approximately $\theta_s = 2.65$ (or $\theta = 0.766$) for simply-supported cylindrical panel and at $\theta_s = 2.90$ (or $\theta = 0.839$) for clamped panel where according to Koiter (1956)

$$\theta=\theta_s(2c)^{1/2}/(2\pi), \quad c=[3(1-\nu^2)]^{1/2} \tag{44}$$

The cylindrical panel appears to be most imperfection-

Downloaded 03 May 2010 to 171.66.16.27. Redistribution subject to ASME license or copyright; see http://www.asme.org/terms/Terms_Use.cfm

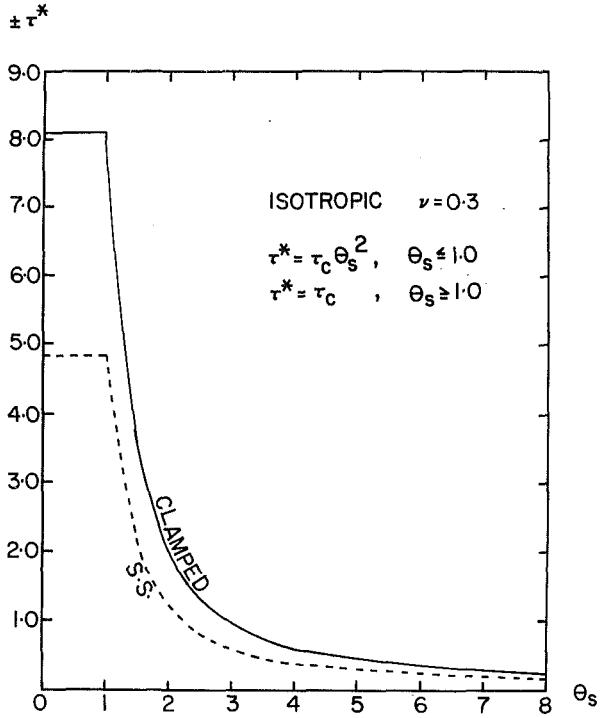


Fig. 1(*a*) Shear buckling load versus the reduced-flatness parameter for isotropic-homogeneous open cylindrical panels (ν = 0.3)

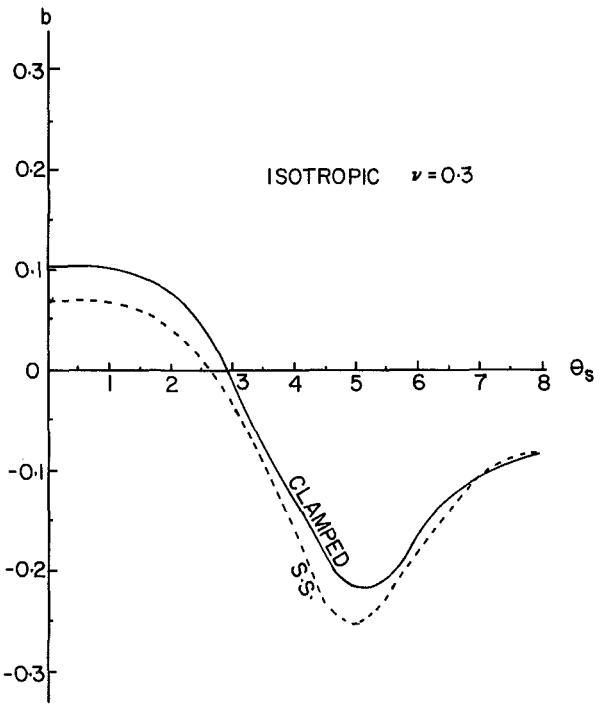


Fig. 1(*b*) Postbuckling *b* coefficient versus the reduced-flatness parameter for isotropic-homogeneous open cylindrical panels (ν = 0.3)

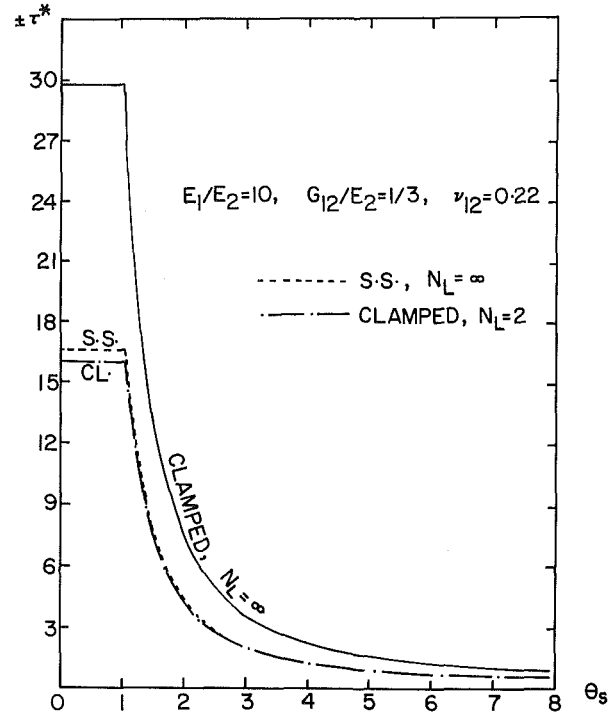


Fig. 2(*a*) Shear buckling load versus the reduced-flatness parameter for antisymmetric cross-ply boron-epoxy cylindrical panels (ν = 0.3)

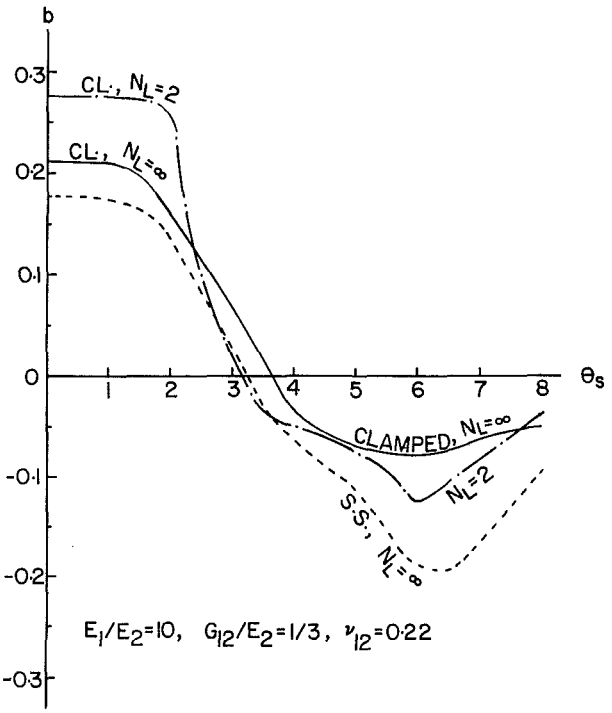


Fig. 2(*b*) Postbuckling *b* coefficient versus the reduced-flatness parameter for antisymmetric cross-ply boron-epoxy cylindrical panels

sensitive near θ_s = 5.0 for both the simply-supported or the clamped cases. The cylindrical panels are slightly sensitive to geometric imperfections for large values of θ_s.

Figure 2(*a*) shows a graph of the classical shear buckling load versus the simplified-flatness parameter for antisymmetrically laminated cross-ply cylindrical panels. The behavior is similar to the isotropic homogeneous case except that the classical buckling load is much higher. Significant reductions in τ_c are found by comparing the two-layer design (N_L = 2) with the infinite-layer (N_L = infinite) orthotropic cylindrical panels. The shear buckling loads are in qualitative agreement with that presented by Hui (1986b). The optimum axial wave number M ranges from (M = 2.80, θ_s = 0.5) to (M = 0.19, θ_s = 8.0) for clamped shells with N_L = ∞ and (M = 2.00, θ_s = 0.5) to (M = 0.054, θ_s = 8.0) for simply-supported shells with N_L = ∞. For clamped shells with N_L = 2, M varies from (M = 2.40, θ_s = 0.05) to (M = 0.20, θ_s = 8.0).

The corresponding postbuckling *b* coefficient is depicted in Fig. 2(*b*). The *b* coefficient, for Boron-epoxy cylindrical panels are generally much more positive than that for isotropic homogeneous cylindrical panels, especially for small values of

Downloaded 03 May 2010 to 171.66.16.27. Redistribution subject to ASME license or copyright; see http://www.asme.org/terms/Terms_Use.cfm

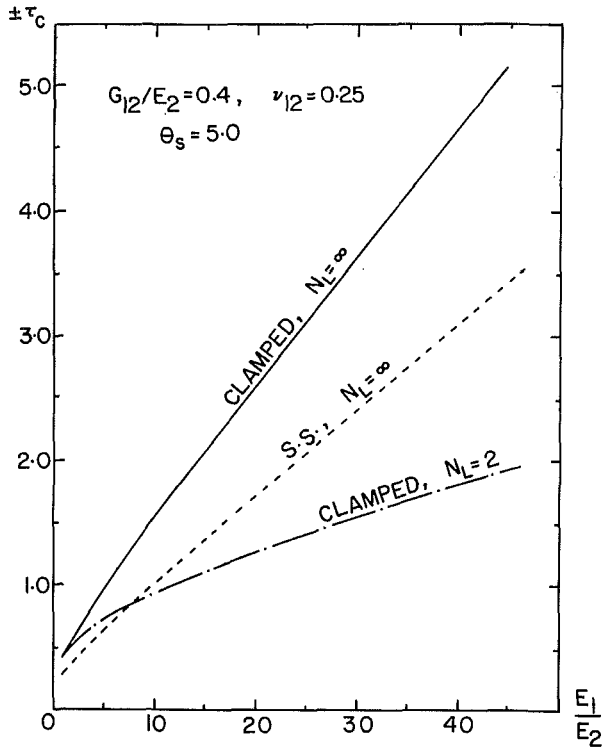


Fig. 3(*a*) Shear buckling load versus Young's modulus ratio for antisymmetric cross-ply cylindrical panels with $\theta_s = 5.0$

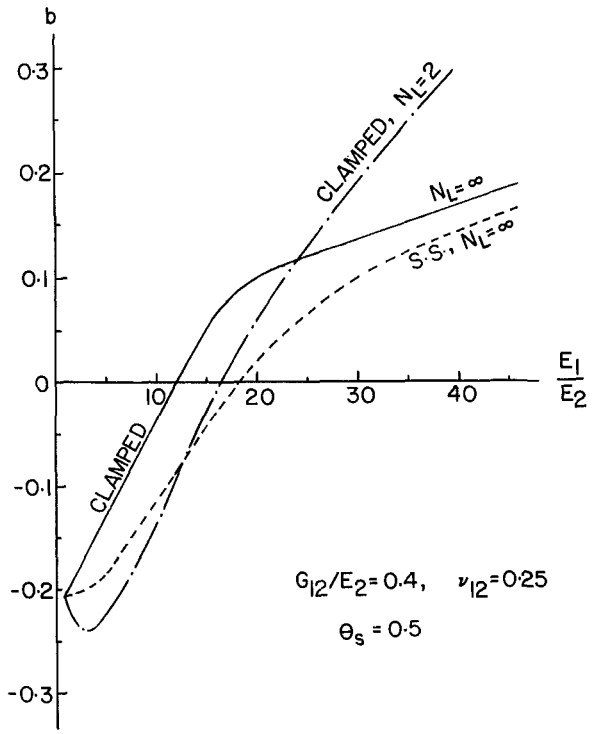


Fig. 3(*b*) Postbuckling *b* coefficient versus Young's modulus for antisymmetric cross-ply cylindrical panels with $\theta_s = 5.0$

θ_s. The transition values of the simplified-flatness parameters which correspond to $b = 0$ occur at $\theta_s = 3.7$ for (N_L = infinite, clamped), $\theta_s = 3.4$ for ($N_L = 2$ clamped) or (N_L = infinite, simply-supported). The cylindrical panel is most imperfection-sensitive near $\theta_s = 6.0$. Finally, it should be noted that the classical shear buckling loads and the postbuckling b coefficients are the same (within plotting accuracy) between the two-layered designs with (0 deg inside, 90 deg outside) or (90 deg inside, 0 deg outside). It should be noted that shear buckling loads of "symmetrically laminated" graphite-epoxy angle-ply cylindrical panels simply supported along all four edges depend a great deal on the direction of application of the shear load (Whitney, 1984). However, for the present "antisymmetrically laminated" cross-ply cylindrical panels, the sign of the shear loads has no effect on the buckling and postbuckling problems.

Finally, a plot of the classical shear buckling load versus Young's modulus ratio is depicted in Fig. 3(*a*). The fixed parameters are,

$$G_{12}/E_2 = 0.4, \quad \nu_{12} = 0.25, \quad \theta_s = 5.0 \tag{45}$$

The shear buckling load is roughly proportional to the Young's modulus ratio over most of the range of E_1/E_2 being considered. Again, the shear buckling loads are found to reduce significantly for a two-layer design due to bending-stretching coupling behavior of the laminated panel.

The corresponding postbuckling b coefficient versus E_1/E_2 is shown in Fig. 3(*b*). It appears that the increase in the shear buckling load due to higher values of E_1/E_2 is "not" accompanied by a higher degree of imperfection-sensitivity. In fact, the b coefficients are positive for E_1/E_2. Surprisingly, the $N_L = 2$ design corresponds to a relatively large value of the postbuckling b coefficient for sufficiently large values of E_1/E_2.

Concluding Remarks

The postbuckling and imperfection-sensitivity of long, antisymmetric cross-ply cylindrical panels (simply-supported or clamped at the longitudinal edges) under shear loads have been examined. The shear buckling loads of typical laminated cylindrical panels have been computed as a function of the reduced-flatness parameter and Young's modulus ratio. For sufficiently small values of the reduced-flatness parameter, the shear buckling loads of cylindrical panels are not sensitive to the presence of geometric imperfections. This agrees qualitatively with the postbuckling results of long laminated rectangular plates investigated by Stein (1985a, b). Over most of the practical range of the reduced-flatness parameter, especially for Young's modulus ratio relatively close to unity, the cylindrical panels are found to be postbuckling-unstable, hence imperfection-sensitive. This paper is the first to present a rigorous theoretical postbuckling analysis of laminated cylindrical panels under shear loads and this topic has not been dealt with in the open literature, even in the typical case of isotropic-homogeneous cylindrical panels.

Acknowledgment

The authors would like to acknowledge the generous use of the computer resources through ADML in the Ohio State University Robinson Laboratory Graphic Facilities.

References

Agarwal, B. L., 1981, "Postbuckling Behavior of Composite Shear Webs," *AIAA Journal*, Vol. 19, No. 7, pp. 933-939.

Ashton, J. E., and Love, T. S., 1969, "Shear Stability of Laminated Anisotropic Plates, Composite Materials: Testing and Design," American Society of Testing and Materials, ASTM-STP 460, pp. 352-361.

Bauld, N. R., Jr., and Satyamurthy, K., 1979, "Collapse Load Analysis for Plates and Panels," Air Force Flight Dynamics Lab., AFFDL-TR-79-3038, May.

Budiansky, B., and Hutchinson, J. W., 1964, "Dynamic Buckling of Imperfection-Sensitive Structures," *Proc. of the 11th International Congress of Applied Mechanics*, Munich, W. Germany, Gortler, H., ed., Springer-Verlag, 1966, pp. 636-651.

Chamis, C. C., 1971, "Theoretical Buckling Loads of Boron/Aluminum and Graphite/Resin Fiber Composite Anisotropic Plates," NASA TN D-6572, Dec.

Chia, C. Y., 1980, *A Nonlinear Analysis of Plates*, McGraw-Hill, New York.

Dongarra, J. J., Bunch, J. R., Moler, C. B., and Stewart, G. W., 1979, "LINPACK User's Guide," published by Society of Industrial and Applied

Downloaded 03 May 2010 to 171.66.16.27. Redistribution subject to ASME license or copyright; see http://www.asme.org/terms/Terms_Use.cfm

Math., Philadelphia; see also Argonne National Lab. Report TM-313, Aug. 1977.

Housner, J. M., and Stein, M., 1975, "Numerical Analysis and Parameter Studies of the Buckling of Composite Orthotropic Comp. and Shear Panels," NASA TN D-7996.

Hui, D., and Hansen, J. S., 1982, "Effect of Stringer Torsional Rigidity on Buckling of Integrally Stiffened Angle Ply Plates," *Fibre Science and Technology*, Vol. 16, No. 1, pp. 39–42.

Hui, D., Tennyson, R. C., and Hansen, J. S., 1981, "Mode Interaction of Axially Stiffened Cylindrical Shells: Effects of Stringer Axial Stiffness, Torsional Rigidity and Eccentricity," ASME JOURNAL OF APPLIED MECHANICS, Vol. 48, No. 4, pp. 915–922.

Hui, D., 1984b, "Effects of Mode Interaction on Collapse of Short, Imperfect Thin-Walled Columns,' ASME JOURNAL OF APPLIED MECHANICS, Vol. 50, No. 3, pp. 566–573.

Hui, D., 1984b, "Shear Buckling of Antisymmetric Cross-Ply Rectangular Plates," *Fibre Science and Technology*, Vol. 21, No. 4, pp. 327–340.

Hui, D., 1985, "Asymmetric Postbuckling of Symmetrically Laminated Cross Ply, Short Cylindrical Panels under Compression," *Composite Structures*, Vol. 3, pp. 81–95.

Hui, D., 1986, "Imperfection Sensitivity of Axially Compressed Laminated Flat Plates due to Bending-Stretching Coupling," *International Journal of Solids and Structures*, Vol. 22, No. 1, pp. 13–22.

Hui, D., 1987, "Effects of Shear Loads on Vibration and Buckling of Antisymmetic Cross-Ply Cylindrical Panels," *International Journal of Non-Linear Mechanics*, in press.

Hutchinson, J. W., and Amazigo, J. C., 1967, "Imperfection-Sensitivity of Eccentrically Stiffened Cylindrical Shells," *AIAA Journal*, Vol. 5, pp. 392–401.

Johns, D. J., 1971, "Shear Buckling of Isotropic and Orthotropic Plates – A Review," British Aeronautical Research Council, Rep. Memo R. and M. No. 3677.

Kaminski, B. E., and Ashton, J. E., 1971, "Diagonal Tension Behavior of Boron/Epoxy Shear Panels," *Journal of Composite Materials*, Vol. 5, Oct., pp. 553–558.

Koiter, W. T., 1945, "On the Stability of Elastic Equilibrium," Doctoral Thesis, Delft, The Netherlands, English Translation: NASA-TT-F10, 833, 1967, and AFFDL-TR-70-25, 1970.

Koiter, W. T., 1956, "Buckling and Post-Buckling Behaviour of Cylindrical Panel under Axial Compression," National Aeronautical Research Institute, Amsterdam, Report S-476, May, 14 pp.

Leissa, A. W., 1985, "Buckling of Laminated Composite Plates and Shell Panels," Air Force Wright Aeronautical Lab., AFWAL-TR-85-3069, 454 pp.

Rafel, N., 1943, "Effect of Normal Pressure on the Critical Shear Stress of Curved Sheet," NACA Wartime Report L-416, originally issued Jan. 1943 as restricted bulletin.

Stein, M., 1968, "Some Recent Advances in the Investigation of Shell Buckling," *AIAA Journal*, Vol. 6, No. 12, pp. 2339–2345.

Stein, M., 1985a, "Postbuckling of Long Orthotropic Plates in Combined Shear and Compression," *AIAA Journal*, Vol. 23, No. 5, pp. 788–794.

Stein, M., 1985b, "Analytical Results for Post-Buckling Behaviour of Plates in Compression and in Shear," Aspects of the Analysis of Plate Structures, a volume in honour of W. H. Wittrick, Dawe, D. J., Horsington, R. W., Kamtekar, A. G., and Little, G. H., eds., University of Birmingham, Clarendon Press, Oxford, pp. 205–223.

Stephens, W. B., 1971, "Imperfection-Sensitivity of Axially Compressed Stringer Reinfored Cylindrical Panels under Internal Pressure," *AIAA Journal*, Vol. 9, No. 9, pp. 1713–1719.

Sumihara, K., Kobayashi, S., and Koyama, K., 1981, "Shear Buckling Strength of CFRP Laminated Panels, 1st Report," *Journal of the Japan Society for Aeronautical and Space Sciences*, Vol. 29, June, pp. 321–332.

Tennyson, R. C., Chan, K. H., and Muggeridge, D. B., 1971, "The Effect of Axisymmetric Shape Imperfections on the Buckling of Laminated Anisotropic Circular Cylinders," *Canadian Aeronautics and Space Institute (CASI) Transactions*, Vol. 4, No. 2, Sept., pp. 131–139.

Viswanathan, A. V., Tamekuni, M., and Baker, L. L., 1974, "Elastic Stability of Laminated, Flat and Curved, Long Rectangular Plates Subjected to Combined Inplane Loads," NASA CR-2330, June.

Whitney, J. M., 1969, "Shear Buckling of Unsymmetrical Cross-Ply Plates," *Journal of Composite Materials*, Vol. 3, pp. 359–363.

Whitney, J. M., 1984, "Buckling of Anisotropic Laminated Cylindrical Plates," *AIAA Journal*, Vol. 22, No. 11, pp. 1641–1645.

Zhang, Y., and Matthews, F. L., 1981, "Postbuckling Behaviour of Cylindrically Curved Panels of Generally Layered Composite Materials with Small Initial Imperfections of Geometry," *Composite Structures*, Marshall, I. H., ed., Applied Science Publisher, London, England, pp. 428–441.

Zhang, Y., and Matthews, F. L., 1983a, "Initial Buckling of Curved Panels of Generally Layered Composite Materials," *Composite Structures*, Vol. 1, No. 1, pp. 3–30.

Zhang, Y., and Matthews, F. L., 1983b, "Postbuckling Behaviour of Curved Panels of Generally Layered Composite Materials," *Composite Structures*, Vol. 1, No. 2, pp. 115–135.

Zhang, Y., and Matthews, F. L., 1984, "Postbuckling Behavior of Anisotropic Laminated Plates under Pure Shear and Shear Combined with Compressive Loading," *AIAA Journal*, Vol. 22, No. 2, pp. 281–286.

Downloaded 03 May 2010 to 171.66.16.27. Redistribution subject to ASME license or copyright; see http://www.asme.org/terms/Terms_Use.cfm

Natural Frequencies of a Railroad Track[1]

S. P. Patil
A. M., ASME
Ascociation of American Railroads,
Transportation Test Center,
Pueblo, CO 81001
Assoc. Mem. ASME

The natural frequency of an infinite railroad track was first determined by Timoshenko as $\omega_R = \sqrt{k/m}$, *where* k *is the constant for the massless Winkler foundation and* m *is the mass per unit length of the rail. The natural frequencies of the track are determined here by modeling the track as a beam resting on a 3-D inertial elastic layer. It is shown that the mass of the supporting foundation has a significant effect on the natural frequencies of a railroad track. Finally, the concept of "added mass" is introduced in order to determine the natural frequency in a desired mode of vibration, by modeling the track as a beam on the massless Winkler foundation and adding the mass of the foundation to the beam.*

1 Introduction

The natural frequency of a railraod track was first determined by Timoshenko (1926). He modeled the track as a beam resting on a massless Winkler foundation. He arrived at a simple expression for the natural frequency $\omega_R = \sqrt{k/m}$, where k is the Winkler constant and m is the mass per unit length of the beam. Various other investigations (Hryniewicz, 1980) about the vibrations of footings supported on bases have shown that the mass of the base has a significant effect on the dynamic response of the footing. Hence, it is essential to consider the mass of the supporting foundation for determining the natural frequencies of a railroad track. More recent investigations (Hryniewicz, 1981; Oien, 1971) were about the vibrations of a rigid infinite strip attached to an inertial half-space. As expected, the analyses did not reveal any natural frequencies. Gazetas and Roesset (1979) analyzed the vibrations of the rigid strip attached to an inertial layer, overlaying a semi-infinite elastic mass (special case is the rigid base as assumed in this paper). The natural frequencies depend on the properties of the layer as well as the underlying mass.

The track is modeled as a beam resting on a three-dimensional inertial elastic layer. As shown in Fig. 1, a beam of width b, bending stiffness B, and mass per unit length m rests on a 3-D layer of depth H, elastic properties λ, μ, and mass density ρ.

The beam is subject to a concentrated oscillating load $P\cos\omega_0 t$. It is assumed that the contact between the beam and the foundation is smooth, hence the shear stresses τ_{xz} and τ_{yz} are zero at the surface of contact. It is further assumed that the beam equations can be applied at the surface of contact without any appreciable error. It is also assumed that the layer is attached to a rigid base at $z = 0$, but, for simplicity, is allowed to slide against it. Therefore, the vertical displacement w and the shear stresses τ_{xz} and τ_{yz} are zero at $z = 0$. The beam displacement is denoted by w_1 and the resulting mixed boundary value problem may be solved by matching beam and layer responses at $z = -H$. The method suggested by Filippov (1961) is followed for the analysis.

2 Solution of Equations of Motion for a 3-D Elastic Layer

The response of the layer in terms of the vertical displacement and the normal stress at its top surface is determined here. The equations of motion for the layer are given as

$$\mu\nabla^2\bar{u} + (\lambda+\mu)\frac{\partial\theta}{\partial x} = \rho\frac{\partial^2\bar{u}}{\partial t^2}$$

$$\mu\nabla^2\bar{v} + (\lambda+\mu)\frac{\partial\theta}{\partial y} = \rho\frac{\partial^2\bar{v}}{\partial t^2} \qquad (1)$$

$$\mu\nabla^2\bar{w} + (\lambda+\mu)\frac{\partial\theta}{\partial z} = \rho\frac{\partial^2\bar{w}}{\partial t^2}$$

where $\bar{u}(x, y, z, t)$ is the displacement in the x direction, $\bar{v}(x, y, z, t)$ is the displacement in the y direction, $\bar{w}(x, y, z, t)$ is the displacement in the z direction, $\theta = \partial\bar{u}/\partial x + \partial\bar{v}/\partial y + \partial\bar{w}/\partial z$ is the dilatation, λ, μ are Lamé constants for the layer, and ρ is the mass density of the layer.

It is assumed that the displacements can be expressed in the following form

$$\bar{u}(x,y,z,t) = u(x,y,z)\cos\omega_0 t$$

$$\bar{v}(x,y,z,t) = v(x,y,z)\cos\omega_0 t \qquad (2)$$

$$\bar{w}(x,y,z,t) = w(x,y,z)\cos\omega_0 t$$

Substitution of the above equation into equation (1) results in the elimination of the variable t.

[1]Research partially supported by a fellowship from Association of American Railroads, Chicago, and NSF Grant # CEE-8308919, based on part of Ph.D. dissertation submitted to University of Delaware.

Contributed by the Applied Mechanics Division for presentation at the 1987 Applied Mechanics, Biomechanics, and Fluids Engineering Conference, Cincinnati, OH, June 14–17, 1987, of the American Society of Mechanical Engineers.

Discussion of this paper should be addressed to the Editorial Department, ASME, United Engineering Center, 345 East 47th Street, New York, N.Y. 10017, and will be accepted until two months after final publication of the paper itself in the JOURNAL OF APPLIED MECHANICS. Manuscript received by ASME Applied Mechanics Division, April 23, 1986; final revision, September 26, 1986.

Paper No. 87-APM-32.

Copyright © 1987 by ASME
Downloaded 03 May 2010 to 171.66.16.27. Redistribution subject to ASME license or copyright; see http://www.asme.org/terms/Terms_Use.cfm

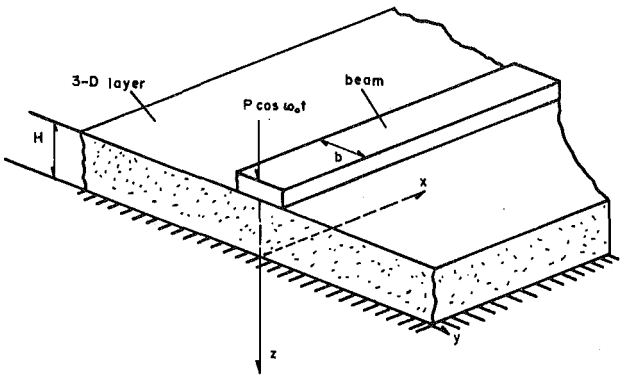


Fig. 1 Beam resting on a 3-D layer

$$\mu\nabla^2 u+(\lambda+\mu)\frac{\partial\theta}{\partial x}=-\rho\omega_0^2 u$$

$$\mu\nabla^2 v+(\lambda+\mu)\frac{\partial\theta}{\partial y}=-\rho\omega_0^2 v \tag{3}$$

$$\mu\nabla^2 w+(\lambda+\mu)\frac{\partial\theta}{\partial z}=-\rho\omega_0^2 w$$

Defining the displacement components u, v, and w as

$$u=u_1+\frac{\partial\Phi}{\partial x}$$

$$v=v_1+\frac{\partial\Phi}{\partial y} \tag{4}$$

$$w=w_1+\frac{\partial\Phi}{\partial z}$$

and substituting them into equation (3) results in the following equations which Φ, u_1, v_1, and w_1 must satisfy

$$\nabla^2\Phi+h^2\Phi=0$$

$$\nabla^2 u_1+k^2 u_1=0$$

$$\nabla^2 v_1+k^2 v_1=0$$

$$\nabla^2 w_1+k^2 w_1=0 \tag{5}$$

$$\frac{\partial u_1}{\partial x}+\frac{\partial v_1}{\partial y}+\frac{\partial w_1}{\partial z}=0$$

where,

$$h^2=\frac{\rho\omega_0^2}{\lambda+2\mu},\ \text{and}\ k^2=\frac{\rho\omega_0^2}{\mu}$$

Assuming that the layer is held fixed at the bottom and it is allowed to slide along the rigid base, we have the following boundary conditions at $z=0$

$$w(x,y,0)=0 \tag{6a}$$

$$\tau_{xz}(x,y,0)=0 \tag{6b}$$

$$\tau_{yz}(x,y,0)=0 \tag{6c}$$

Next, assuming the solutions for u_1, v_1, w_1 and Φ in the form of double Fourier integrals, such as

$$u_1=\int_0^\infty\int_0^\infty C_1\cosh\gamma_2 z\sin\alpha x\cos\beta y d\alpha d\beta$$

$$v_1=\int_0^\infty\int_0^\infty C_2\cosh\gamma_2 z\cos\alpha x\sin\beta y d\alpha d\beta$$

$$w_1=\int_0^\infty\int_0^\infty A_3\sinh\gamma_2 z\cos\alpha x\cos\beta y d\alpha d\beta \tag{7}$$

$$\Phi=\int_0^\infty\int_0^\infty C_4\cosh\gamma_1 z\cos\alpha x\cos\beta y d\alpha d\beta$$

they are found to satisfy equations (5) and the boundary conditions (6) if

$$\gamma_1^2=\alpha^2+\beta^2-h^2,\ \text{and}\ \gamma_2^2=\alpha^2+\beta^2-k^2 \tag{8}$$

Now, all but one constant in equation (7) may be eliminated using the last condition in equation (5) and the following conditions for smooth contact at the surface of the layer ($z=-H$),

$$\tau_{xz}=\mu\left(\frac{\partial w}{\partial x}+\frac{\partial u}{\partial z}\right)_{z=-H}=0$$

$$\tau_{yz}=\mu\left(\frac{\partial w}{\partial y}+\frac{\partial v}{\partial z}\right)_{z=-H}=0 \tag{9}$$

This procedure results in the expressions for the vertical displacement w and the potential Φ. They are

$$\Phi=\int_0^\infty\int_0^\infty C_4\cosh\gamma_1 z\cos\alpha x\cos\beta y d\alpha d\beta$$

$$w=-\frac{k^2}{2}\int_0^\infty\int_0^\infty\frac{C_4\gamma_1\sinh\gamma_1 z\cos\alpha x\cos\beta y}{\alpha^2+\beta^2-k^2/2}d\alpha d\beta \tag{10}$$

Considering equation (6d), the expression for dilatation is written as

$$\theta=\nabla^2\Phi=-h^2\int_0^\infty\int_0^\infty C_4\cosh\gamma_1 z\cos\alpha x\cos\beta y d\alpha d\beta \tag{11}$$

Using equations (10) and (11) the displacement w and the normal stress ($\sigma_z=\lambda\theta+2\mu\partial w/\partial z$) at the top surface of the layer are found as

$$w(x,y,-H)=\frac{k^2}{2}\int_0^\infty\int_0^\infty\frac{C_4\gamma_1\sinh\gamma_1 H\cos\alpha x\cos\beta y}{\alpha^2+\beta^2-k^2/2}d\alpha d\beta \tag{12a}$$

$$\sigma_z(x,y,-H)=2\mu\int_0^\infty\int_0^\infty\frac{C_4\sinh\gamma_1 H}{\alpha^2+\beta^2-k^2/2}\times\left[\begin{matrix}(\alpha^2+\beta^2-k^2/2)^2\coth\gamma_1 H\\-\gamma_1\gamma_2(\alpha^2+\beta^2)\coth\gamma_2 H\end{matrix}\right]\cos\alpha x\cos\beta y d\alpha d\beta \tag{12b}$$

3 Matching the Beam Response With the Response of the Layer

Next, the constant C_4 is determined by matching the response of the beam with the response of the elastic layer. The equation of motion for the beam is given as

$$B\frac{\partial^4\bar{w}_1}{\partial x^4}+m\frac{\partial^2\bar{w}_1}{\partial t^2}=P\delta(x)\cos\omega_0 t-\bar{p}(x,t) \tag{13}$$

where, w_1 is the deflection of the beam, B is the bending stiffness of the beam, m is the mass per unit length of the beam, P is the oscillating load on the beam, and p is the pressure exerted on the beam by the layer.

Assuming the deflection and pressure distribution in the following form

$$\bar{w}_1(x,t)=w_1(x)\cos\omega_0 t$$

$$\bar{p}(x,t)=p(x)\cos\omega_0 t \tag{14}$$

substitution of it into equation (13) results in

$$B\frac{d^4 w_1}{dx^4}-m\omega_0^2 w_1=P\delta(x)-p(x) \tag{15}$$

Downloaded 03 May 2010 to 171.66.16.27. Redistribution subject to ASME license or copyright; see http://www.asme.org/terms/Terms_Use.cfm

It is assumed that the pressure beneath the beam is uniform across its width b. Hence

$$p(x) = -b\sigma_z(x,0,-H) \tag{16}$$

The response of the beam as well as the pressure distribution, is assumed in the form of a single Fourier integral. That is

$$p(x) = \frac{1}{\pi}\int_0^\infty A(\alpha)\cos\alpha x d\alpha \tag{17a}$$

$$w_1(x) = \int_0^\infty C(\alpha)\cos\alpha x d\alpha \tag{17b}$$

Substituting the first expression into equation (16), the pressure which acts on the beam is written as

$$\sigma_z(x,0,-H) = -\frac{1}{\pi}\int_0^\infty A^*(\alpha)\cos\alpha x d\alpha \tag{18}$$

where $A^*(\alpha) = -bA(\alpha)$. Assuming an even rectangular pressure distribution under the beam in the y direction, the above expression for the entire x-y plane may be written as the following Fourier integral

$$\sigma_z(x,y,-H) = \frac{2}{\pi}\int_0^\infty \cos\beta y d\beta \int_0^\infty f_e(\lambda)\cos\beta\lambda d\lambda \int_0^\infty A^*\cos\alpha x d\alpha \tag{19}$$

$$f_e(\lambda) = \sigma_z(x,0,-H) \text{ if } y \le b/2$$

where, $$f_e(\lambda) = 0 \text{ if } y > b/2 \tag{20}$$

After integrating equation (19) with respect to λ and substituting equation (20), the pressure upon the beam is obtained as

$$\sigma_z(x,0,-H) = -\frac{2}{\pi^2}\int_0^\infty \int_0^\infty \frac{A^*(\alpha)\cos\alpha x \sin\frac{\beta b}{2}}{\beta} d\alpha d\beta \tag{21}$$

Matching the above pressure expression with equation (12b) a relationship between A^* and C_4 is obtained as

$$\frac{C_4 \sinh\gamma_1 H}{\alpha^2+\beta^2-k^2/2} = \frac{A^*\sin\frac{\beta b}{2}}{\mu\pi^2\beta[(\alpha^2+\beta^2-k^2/2)^2\coth\gamma_1 H - \gamma_1\gamma_2(\alpha^2+\beta^2)\coth\gamma_2 H]} \tag{22}$$

Substitution of the above relation into equation (12a) results in the expression for the vertical displacement under the beam as

$$w(x,0,-H) = -\frac{k^2}{2\mu\pi^2}\int_0^\infty \int_0^\infty \frac{A^*\gamma_1 \sin\frac{\beta b}{2}\cos\alpha x}{\beta[(\alpha^2+\beta^2-k^2/2)^2\coth\gamma_1 H - \gamma_1\gamma_2(\alpha^2+\beta^2)\coth\gamma_2 H]} d\alpha d\beta \tag{23}$$

Defining

$$\tau = \beta/\alpha,\ q = \alpha b/2,\ k^* = kb/2,\ h^* = hb/2, \text{ and } R = b/H \tag{24}$$

the expression in equation (23) is rewritten as

$$w(x,0,-H) = \frac{k^{*2}b}{4\mu\pi^2}\int_0^\infty A^*T(q)\cos\alpha x d\alpha \tag{25}$$

where,

$$T(q) = -\int_0^\infty \tau \left[\begin{array}{c} \sqrt{q^2+q^2\tau^2-h^{*2}}\sin q\tau d\tau \\ \hline (q^2+q^2\tau^2-k^{*2}/2)^2\coth\frac{2}{R}\sqrt{q^2+q^2\tau^2-h^{*2}} \\ -q^2(1+\tau^2)\sqrt{q^2+q^2\tau^2-h^{*2}}\sqrt{q^2+q^2\tau^2-k^{*2}}\coth\frac{2}{R}\sqrt{q^2+q^2\tau^2-k^{*2}} \end{array}\right] \tag{26}$$

The expression for $C(\alpha)$ is obtained next by substituting equation (17) into equation (15). It is

$$C(\alpha) = \frac{P-bA^*(\alpha)}{\pi B(\alpha^4 - m\omega_0^2/B)} \tag{27}$$

Use of the above expression for $C(\alpha)$ in equation (17b) results in the deflection of the beam as

$$w_1(x,0,-H) = \int_0^\infty \frac{(P-bA^*)\cos\alpha x}{\pi B(\alpha^4 - m\omega_0^2/B)} d\alpha \tag{28}$$

The expression for A^* is obtained by comparing equations (25) and (28). It is

$$A^* = \frac{P}{b[1+\epsilon T(q)[q^4-\delta]]} \tag{29}$$

where,

$$\epsilon = \frac{4Bk^{*2}}{\pi\mu b^4}$$

$$\delta = \frac{m\omega_0^2 b^4}{16B} \tag{30}$$

Substitution of equation (29) into equation (25) results in the deflection of the beam as

$$w(x,0,-H) = \frac{Pk^{*2}}{2\pi^2\mu b}\int_0^\infty \frac{T(q)\cos\frac{2qx}{b}}{1+\epsilon T(q)[q^4-\delta]} dq \tag{31}$$

The deflection of the beam under the load is given as

$$w(0,0,-H,t) = \frac{Pk^{*2}\cos\omega_0 t}{2\pi^2\mu b}\int_0^\infty \frac{T(q)}{1+\epsilon T(q)[q^4-\delta]} dq \tag{32}$$

The integral in equation (32) is difficult to evaluate in closed form. Since our main interest is only to determine the natural frequencies, the frequencies at which the integral I,

$$I = \int_0^\infty \frac{T(q)}{1+\epsilon T(q)[q^4-\delta]} dq \tag{33}$$

becomes singular, are determined.

It has been noted that for vibration of layers the resulting integral becomes singular near the left-end point. Therefore, it is of interest to study the behavior of the integral I, in the neighborhood of the left-end point $q = 0$. The integral I as a function of a small quantity ξ, is written as

$$I(\xi) = \int_0^\xi \frac{T(q)}{1+\epsilon T(q)[q^4-\delta]} dq \tag{34}$$

For small values of ξ, the above equation reduces to

Downloaded 03 May 2010 to 171.66.16.27. Redistribution subject to ASME license or copyright; see http://www.asme.org/terms/Terms_Use.cfm

$$I(\xi)=\frac{\xi T(\xi)}{1+\epsilon T(\xi)[\xi^4-\delta]} \tag{35}$$

Taking the limit as $\xi \to 0$, we have

$$\lim_{\xi\to 0} I(\xi)=\begin{cases} 0(\xi), & \text{if } \epsilon\delta T(0)\neq 1; \\ 0\left(\frac{1}{\xi^3}\right), & \text{if } \epsilon\delta T(0)=1 \end{cases} \tag{36}$$

From the above equation, it is evident that the integral I (hence the displacement under the load) may become infinite if the following frequency equation is satisfied.

$$\epsilon\delta T(0)=1 \tag{37}$$

Substituting for the values of ϵ and δ (ref. equation (30)), the frequency equation reduces to

$$T(0)=\frac{4\pi\mu}{m\omega_0^2 k^{*2}} \tag{38}$$

In order to determine $T(0)$, equation (26) is rewritten for small values of q, by neglecting the terms in q which are small compared to other terms, as

$$T(q)=\frac{8h^{*3}}{Hhq^2k^{*4}}\int_0^\infty \frac{\sin q\tau}{\tau\left[1+\tau^2+\frac{2h^{*2}\cot(hH)}{hHq^2}\right]}\,d\tau \tag{39}$$

The integral in the above equation may be integrated, using Tables of integrals, to give

$$T(q)=\frac{4\pi h^{*3}}{hHq^2k^{*4}}\,\frac{1-e^{-q\sqrt{1+\frac{2h^{*2}\cot(hH)}{hHq^2}}}}{1+\frac{2h^{*2}\cot(hH)}{hHq^2}} \tag{40}$$

Taking the limit as $q \to 0$, we have

$$T(0)=\lim_{q\to 0} T(q)=\frac{2\pi h^*}{\cot(hH)k^{*4}}\left[1-e^{-h^*\sqrt{\frac{2\cot(hH)}{hH}}}\right] \tag{41}$$

Substitution of the above equation into equation (38) results, after some rearrangememt, in the following frequency equation

$$M^*f=\frac{\cot(f)}{1-e^{-h^*\sqrt{\frac{2\cot(f)}{f}}}} \tag{42}$$

where

$f=hH$ is the nondimensional frequency
$M^*=m/\rho bH$ is the mass ratio

In terms of the other nondimensional parameters h^* and M^{**}, equation (42) may be written as

$$2M^{**}h^*=\frac{\cot(2h^*/R)}{1-e^{-h^*\sqrt{\frac{R\cot(2h^*/R)}{h^*}}}} \tag{43}$$

where $M^{**}=m/\rho b^2$ is the mass ratio.

If mass of the beam is negligible as compared to the mass of the foundation, i.e., $M^*=0$, then equation (42) reduces to

$$\cot(f)=0 \tag{44}$$

which is identical with the equation for determining the natural frequencies of a rod of length H, fixed at the bottom and free at the top.

4 Beam on a 3-D Noninertial Layer

In order to determine the effect of the mass of the foundation on the natural frequencies of the beam, the fundamental natural frequency is compared with the resonant frequency of the beam on a noninertial layer. The equation for determination of the natural frequencies, remains the same as equation (38). However, it is written again as

$$T(0)=\frac{4\pi\mu}{m\omega_0^2k^{*2}} \tag{45}$$

where, the value of $T(q)$ may be evaluated by a proper limiting process of setting the mass density of the layer ρ, to zero. Therefore,

$$T(q)=\lim_{\rho\to 0}\ -\int_0^\infty \frac{\sqrt{q^2+q^2\tau^2-h^{*2}}\sin q\tau}{\tau\left[\begin{array}{c}(q^2+q^2\tau^2-k^{*2}/2)^2\coth\frac{2}{R}\sqrt{q^2+q^2\tau^2-h^{*2}} \\ -q^2(1+\tau^2)\sqrt{q^2+q^2\tau^2-h^{*2}}\sqrt{q^2+q^2\tau^2-k^{*2}}\coth\frac{2}{R}\sqrt{q^2+q^2\tau^2-k^{*2}}\end{array}\right]}\,d\tau \tag{46}$$

For small values of ρ, the above equation, after rearrangement of the terms may be written as

$$T(q)=\lim_{\rho\to 0}\int_0^\infty \frac{\sin q\tau}{q^3\tau(1+\tau^2)^{3/2}[\sqrt{1-k'^2}\coth z_0\sqrt{1-h'^2}-\sqrt{1-h'^2}\coth z_0\sqrt{1-k'^2}]}\,d\tau \tag{47}$$

where,

$$z_0=\frac{2q\sqrt{1+\tau^2}}{R},\quad k'^2=\frac{k^{*2}}{q^2(1+\tau^2)},\quad \text{and}\quad h'^2=\frac{h^{*2}}{q^2(1+\tau^2)} \tag{48}$$

Noting the identity $[(1-h^2/k^2)=1/2(1-\nu)]$, it is fairly simple to see that

Downloaded 03 May 2010 to 171.66.16.27. Redistribution subject to ASME license or copyright; see http://www.asme.org/terms/Terms_Use.cfm

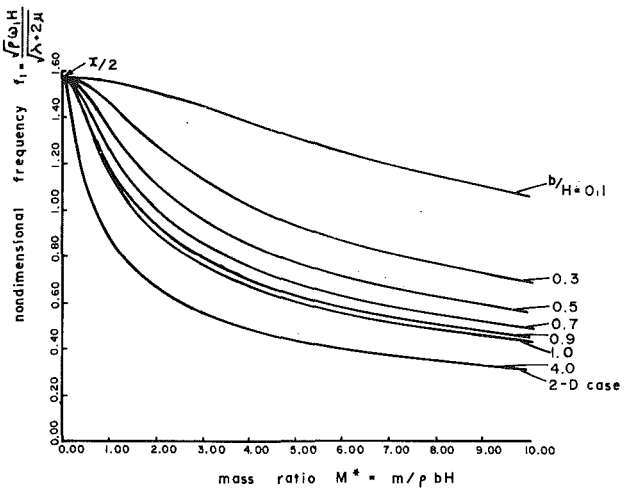


Fig. 2 Fundamental natural frequency of a beam on an inertial layer

$$\lim_{\rho\to 0}\begin{bmatrix}\sqrt{1-k'^2}\coth z_0\sqrt{1-h'^2} \\ -\sqrt{1-h'^2}\coth z_0\sqrt{1-k'^2}\end{bmatrix}$$

$$=\frac{k^{*2}}{4q^2(1-\nu)(1+\tau^2)}\left[z_0(1-\coth^2 z_0)-\coth z_0\right] \tag{49}$$

Substitution of the above equation into equation (47) results in

$$T(q)=-\frac{4(1-\nu)}{k^{*2}}\int_0^\infty \frac{\sin q\tau}{q\tau\sqrt{1+\tau^2}[z_0(1-\coth^2 z_0)-\coth z_0]}\,d\tau \tag{50}$$

For small values of q, hence z_0, noting the following limit,

$$\lim_{z_0\to 0} z_0(1-\coth^2 z_0)-\coth z_0=-\left(z_0+\frac{2}{z_0}\right) \tag{51}$$

equation (50) simplifies to

$$T(0)=\lim_{q\to 0}\frac{4(1-\nu)}{k^{*2}}\times$$

$$\int_0^\infty \frac{\sin q\tau}{q\tau\sqrt{1+\tau^2}\left[\dfrac{2q\sqrt{1+\tau^2}}{R}+\dfrac{R}{q\sqrt{1+\tau^2}}\right]}\,d\tau \tag{52}$$

After rearrangement of the terms, the above equation is rewritten as

$$T(0)=\lim_{q\to 0}\frac{2R(1-\nu)}{q^2k^{*2}}\int_0^\infty \frac{\sin q\tau}{\tau(1+\tau^2+R^2/2q^2)}\,d\tau \tag{53}$$

The integral in equation (53) may be evaluated using Tables of integrals. Taking the limit as $q\to 0$, we have

$$T(0)=\frac{2\pi(1-\nu)H}{bk^{*2}}\left[1-e^{-\frac{R}{\sqrt{2}}}\right] \tag{54}$$

Substitution of the above equation into equation (46) results in the resonant frequency (only one) of a beam resting on a 3-D noninertial layer as

$$\omega_R=\sqrt{\frac{2\mu b}{mH(1-\nu)\left[1-e^{-\frac{R}{\sqrt{2}}}\right]}} \tag{55}$$

5 Discussion of Results and the Concept of Added Mass

For the case of an inertial foundation, Fig. 2 shows the variation of the fundamental nondimensional natural frequency $f_1=\omega_1 H\sqrt{\rho}/(\lambda+2\mu)$ with respect to the mass ratio $M^*=(m/\rho bH)$, for various values of the depth ratio R (b/H) (ref. equation (42)). It is evident from the figure that when the mass of the beam is negligible as compared to the mass of the layer, i.e., $M^*=0$, then for all the values of the depth ratio b/H, the frequency f_1 converges to a single value of $\pi/2$, which is the fundamental natural frequency of the layer.

For increasing values of the mass ratio M^*, the magnitude of the fundamental frequency decreases as expected. For the case when $M^*\to\infty$, i.e., when the beam rests on a noninertial layer, all the natural frequencies converge to the resonant frequency given by equation (55).

An increase in the depth ratio b/H, results in the decrease in the magnitude of the frequency f_1. Hence, extending the foundation beyond the width of the beam results in an increase in the magnitude of the frequency f_1. When $b\to\infty$ the frequency curve for a 3-D case reduces to the frequency curve for a 2-D plane strain problem.

In the past many researchers have used noninertial foundation models for determination of the resonant frequency of a beam resting on them. A specific example of a railroad track is evaluated here to demonstrate the effect of the foundation mass on the fundamental natural frequency of the track.

The assumed track and the foundation parameters are: mass per unit length of the rails and the ties $m=80$ kg/m, mass density of the layer $\rho=200$ kg/m^3, modulus of elasticity for the layer $E=1.0*10^7$ kg/m^2, Poisson's ratio for the layer $\nu=0.3$, the width of the ties $b=2.75$ m, the depth of the layer $H=10$ m. Hence, the depth ratio $R=b/H=0.275$ and the mass ratio $M^{**}=m/\rho b^2=0.053$.

For the parameters $R=0.275$ and $M^{**}=0.053$, equation (43) gives the fundamental nondimensional frequency as $h^*=0.216$ or $f_1=\pi$. From equations (24) and (5) the fundamental frequency is obtained as $\omega_1=40.75$ rad/s. If the inertia of the foundation is neglected then the resonant frequency of the beam on a noninertial layer is given by equation (55). Substitution of the above parameters results in the resonant frequency as $\omega_R=462$ rad/s.

Thus, the fundamental frequency of a beam resting on an inertial layer is substantially lower than the resonant frequency of a beam resting on a noninertial layer. From the above example it shoud be noted that for a railroad track, $M^{**}=0.053$ (mass of the rail-tie structure is 5 percent of the mass of the foundation directly beneath the ties). Therefore, the mass of the track is generally insignificant as compared to the mass of the supporting foundation and the natural frequencies are independent of rail and tie parameters and mainly depend on the foundation parameters. Hence, the involved mathematical analysis seems unnecessary. However, for heavy strip footings where M^{**} could be a large number, it is necessary to use equation (43) or Fig. 3 to determine the fundamental natural frequency.

Since many railroad engineers model the railroad track as a beam on a Winkler foundation, it is of interest to modify the expression for the resonant frequency in order to predict the natural frequencies correctly. To achieve this aim a portion of the foundation mass is added to the mass of the rail-tie structure. In order to determine the value of this added mass, the resonant frequency of the beam (with added mass) on a noninertial layer is compared with the natural frequency of the beam on an inertial layer in the desired mode of vibration. It is of interest to note that the amount of "added mass" is different for different modes of vibration.

With this "added mass"' the resonant frequency of the track is given by equation (55) as

$$\omega_n=\sqrt{\frac{2\mu b}{(1-\nu)m_{tn}H\left[1-e^{-\frac{R}{\sqrt{2}}}\right]}} \tag{56}$$

Downloaded 03 May 2010 to 171.66.16.27. Redistribution subject to ASME license or copyright; see http://www.asme.org/terms/Terms_Use.cfm

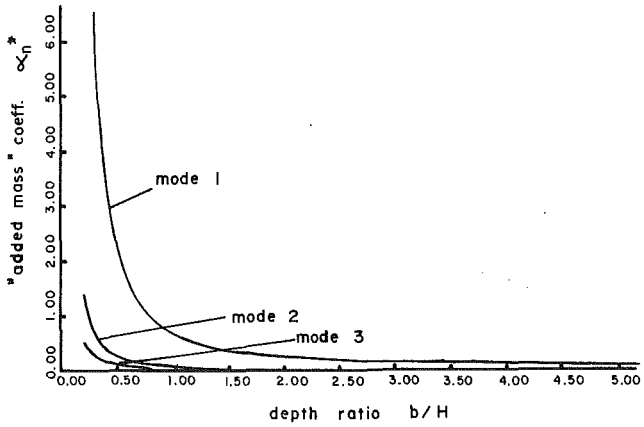


Fig. 3 Added mass coefficient for the first three modes of vibration

in which m_{tn} is the mass of the track including the "added mass" of the foundation in the nth mode of vibration. The expression for m_{tn} is

$$m_{tn} = m + \alpha_n^* \rho b^2 \tag{57}$$

where α_n^* is the coefficient for determining the added mass depending on the mode of vibration. Substitution of the above equation into equation (56) results in

$$\omega_n = \sqrt{\frac{2\mu b}{(1-\nu)H(m+\alpha_n^*\rho b^2)\left[1-e^{-\frac{R}{\sqrt{2}}}\right]}} \tag{58}$$

If the root of equation (43) is given as κ_n for nth mode of vibration, then the corresponding natural frequency is given as

$$\omega_n = \frac{2\kappa_n}{b}\sqrt{\frac{\lambda+2\mu}{\rho}} \tag{59}$$

Comparison of equations (58) and (59) results in the expression for the added mass coefficient α_n^*, for the nth mode of vibration as

$$\alpha_n^* = \frac{\mu R}{2\kappa_n^2(\lambda+2\mu)(1-\nu)\left[1-e^{-\frac{R}{\sqrt{2}}}\right]} - M^{**} \tag{60}$$

For the given track parameters the value of M^{**} is negligibly small and the corresponding value of κ_n is given as (from equation (43))

$$\kappa_n = \frac{(2n-1)\pi R}{4} \tag{61}$$

Substitution of the above equation into equation (60) results in

$$\alpha_n^* = \frac{4(1-2\nu)}{\pi^2 R(2n-1)^2(1-\nu)^2\left[1-e^{-\frac{R}{\sqrt{2}}}\right]} \tag{62}$$

Substitution of the above expression into equation (58) results in Timoshenko type expression for the natural frequencies of the railroad track, as

$$\omega_n = \sqrt{\frac{k}{m_{tn}}} \tag{63}$$

where,

m_{tn} is the mass of the beam and the foundation in the nth mode of vibration $\doteq \alpha_n^* \rho b^2$, ω_n is the nth natural frequency, k is the Winkler constant determined by comparing equation (55) with the expression $\omega_R = \sqrt{k/m}$.

$$k = \frac{2\mu b}{(1-\nu)H\left[1-e^{-\frac{R}{\sqrt{2}}}\right]} \tag{64}$$

Figure 3 shows the variation of the "added mass" coefficient α_n^*, in the first three modes of vibration, with respect to the depth ratio b/H. From the figure it is obvious that for higher modes of vibration the amount of "added mass" is negligible, which agrees with the fact that a negligible amount of foundation mass vibrates with the rail-tie structure at high frequencies of excitation.

For the example of the railroad track considered earlier, α_1^* may be found using equation (62) as $\alpha_1^* = 6.808$. Therefore, the total mass per unit length is given as $m_{t1} = 10297$ kg/m. The Winkler constant is found using equation (64) as $k = 1.71*10^7$ kg/m^2. Substitution of these parameters into equation (63) results in the fundamental natural frequency of the railroad track as $\omega_1 = 40.75$ rad/s, which is the same as obtained earlier.

6 Conclusions

If the track is modeled as a beam resting on a 3-D elastic layer with inertia then the mass of the layer has a significant effect on the natural frequencies of the track. For the given track parameters, the mass of the rail-tie structure is insignificant as compared to the mass of the foundation, hence the natural frequencies depend mainly on the foundation parameters.

There are an infinite number of natural frequencies of the track and they are of the same form as those of a rod in axial vibration, fixed at the base and free at the top. The magnitude of the natural frequencies increases due to extending the foundation beyond the width of the ties.

The concept of "added mass" is introduced in order to determine the natural frequency in a desired mode of vibration, by modeling the track as a beam on a simple massless Winkler foundation and adding the mass of the foundation to the beam.

Acknowledgment

The author wishes to thank Dr. Arnold D. Kerr of University of Delaware for his guidance in the writing of this paper.

References

Filippov, A. P., 1961, "Steady State Vibrations of an Infinite Beam on an Elastic Half-Space Subjected to a Moving Load," *Izvestia, an SSSR OTN Merhanika i Mashinostroenie*, Vol. 6.

Gazetas, G., and Roesset, M., 1979, "Vertical Vibrations of Machine Foundations," *ASCE Journal of the Geotechnical Division*, Vol. 105, pp. 1435–1454.

Gradshteyn, I. S., and Ryzhik, I. M., 1979, *Table of Integrals, Series and Products*, Academic Press, New York.

Hryniewicz, Z., 1980, "Vibrations of a Rigid Body on a Elastic Half-Plane," *Computer Methods in Applied Mechanics and Engineering*, Vol. 24, pp. 113–123.

Hryniewicz, Z., 1981, "Dynamic Response of a Rigid Strip on an Elastic Half-Space," *Computer Methods in Applied Mechanics and Engineering*, Vol. 25, pp. 355–364.

Oien, M. A., 1971, "Steady Motion of a Rigid Strip Bonded to an Elastic Half-Space," ASME JOURNAL OF APPLIED MECHANICS, Vol. 38, pp. 328–334.

Patil, S. P., 1984, "Vibrations of Railroad Tracks Subject to Oscillating and Moving Loads," Ph.D. Thesis, University of Delaware, Newark, DE.

Timoshenko, S. P., 1926, "Method of Analysis of Statical and Dynamical Stresses in Rails," *2nd International Congress of Applied Mechanics*, Zurich, pp. 407–420.

Downloaded 03 May 2010 to 171.66.16.27. Redistribution subject to ASME license or copyright; see http://www.asme.org/terms/Terms_Use.cfm

Effects of Nonconstant Spin Rate on the Vibration of a Rotating Beam

D. C. Kammer
Senior Project Engineer,
Structural Dynamics Research Corporation,
San Diego, CA 92121

A. L. Schlack, Jr.
Professor,
Department of Engineering Mechanics,
University of Wisconsin—Madison,
Madison, Wisconsin 53706

The effects of a time-dependent angular velocity upon the vibration of a rotating Euler beam are presented. It is assumed that the angular velocity can be expressed as the sum of a steady-state value and a relatively small periodic perturbation. Equations of motion are derived for a beam oriented parallel to the spin axis. Terms with time-dependent coefficients appear in the equations of motion due to the nonconstant spin rate resulting in a nonautonomous system possessing parametric instabilities. A perturbation technique called the KBM method is used to derive general expressions for approximate solutions and instability region boundaries. A simple perturbation function is assumed for the purpose of illustrating the use of the derived general expressions.

Introduction

Recently, a new interest in rotating beam dynamics has arisen due to the trend toward extremely high speeds in rotating machinery. Additionally, the vibration of rotating flexible bodies is of great interest due to the complexity and flexibility of modern-day spin-stabilized satellites. In many instances, these satellites possess flexible booms and antennas which can be accurately modeled by beams.

In past work on rotating beam dynamics such as Sutherland (1949), Houbolt (1958), Renard (1970), and Hodges (1981), the simplifying assumption was made that the beam rotated with a constant angular velocity. A time-dependent spin rate would not only be more general but more physically realistic due to external perturbations upon the system. A nonconstant angular velocity was first considered by Kammer and Schlack (accepted for publication) for a beam oriented radially with respect to the spin axis. This paper presents an investigation of the vibration and stability of an Euler beam rotating with a nonconstant angular velocity and mounted parallel to the axis of rotation. The spin rate is characterized as a periodic perturbation superimposed upon a steady state value.

Due to the time dependence of the spin rate, the equations of motion possess nonautonomous terms that are not found in the literature. These terms result in the appearance of parametric instabilities characterized by regions within which the amplitude of vibration grows exponentially with time even in the presence of system damping.

The nonautonomous equations of motion cannot be solved in general. However, if the time-dependent terms can be considered as small in comparison to other terms, perturbation techniques can be used to construct approximate solutions. The present work utilizes the Krylov-Bogoliubov-Mitropolsky (KBM) method to recursively construct periodic solutions and derive boundaries for the regions of instability for the nonautonomous or perturbed system.

Results presented in this paper can be used as a valuable engineering design tool to avoid damaging parametric resonances. In addition, the general equations presented can be used in conjunction with measured test data. The initially unknown periodic angular velocity of a structure can be measured, resulting in a time history which can be converted to a Fourier series representation. The Fourier series can then be used in the general relations to determine the response of the perturbed structure.

The authors wish to emphasize that the phenomena investigated and presented in this paper are not limited to rotating beams but can also appear in other structures such as cylindrical shells. It is believed by the authors that parametric instabilities are fundamental to many elastic systems which rotate with a nonconstant angular velocity.

Formulation of Equations of Motion

The general configuration investigated in this paper, illustrated in Fig. 1, consists of a long slender beam attached to the perimeter of a rigid body which rotates with a time-dependent angular velocity ω about a fixed axis. The beam is mathematically represented using Euler-Bernoulli beam theory. An expression for the kinetic energy is derived using the general relation

$$T = 1/2 \iiint \rho [\dot{r}\mathbf{e}_r + \omega x \mathbf{r}] \cdot [\dot{r}\mathbf{e}_r + \omega x \mathbf{r}] dx\, dy\, dz \qquad (1)$$

where ρ is the mass density of the beam and $\dot{r}$ is the total time derivative of the amplitude of the position vector $\mathbf{r}$ locating a general point within the beam relative to point $0'$ on the spin axis. The vector $\mathbf{r}$ is given by the relation

Contributed by the Applied Mechanics Division for publication in the JOURNAL OF APPLIED MECHANICS.

Discussion on this paper should be addressed to the Editorial Department, ASME, United Engineering Center, 345 East 47th Street, New York, N.Y. 10017, and will be accepted until two months after final publication of the paper itself in the JOURNAL OF APPLIED MECHANICS. Manuscript received by ASME Applied Mechanics Division, April 29, 1986; final revision October 16, 1986.

Copyright © 1987 by ASME
Downloaded 03 May 2010 to 171.66.16.27. Redistribution subject to ASME license or copyright; see http://www.asme.org/terms/Terms_Use.cfm

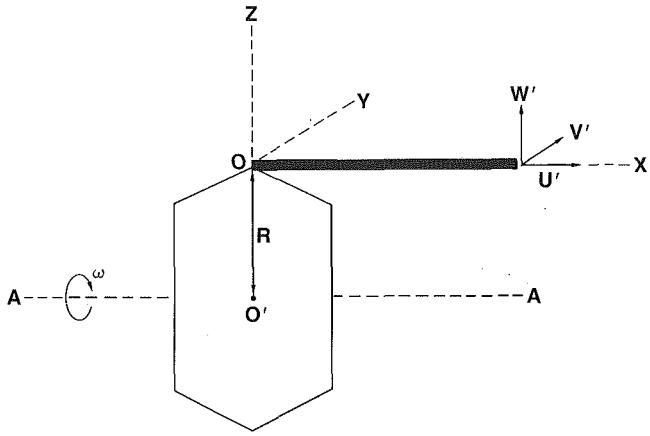


Fig. 1 General configuration consisting of an elastic beam mounted to a rigid body rotating with a nonconstant angular velocity about an axis fixed in space

$$\mathbf{r} = (x+u'-zw'_{,x}-yv'_{,x})\mathbf{i}+(y+v')\mathbf{j}+(z+w'+R)\mathbf{k} \quad (2)$$

in which u', v', and w' are general displacements of the elastic axis relative to the rotating xyz coordinate system and R is the distance between the root of the beam and the spin axis.

In the present case, the general displacements can be expressed in the form

$$\begin{aligned} u'(x,t) &= u(x,t) \\ v'(x,t) &= v(x,t) \\ w'(x,t) &= w_o(x) + w(x,t) \end{aligned} \quad (3)$$

where w_o is a steady state deflection and u, v, and w represent displacements away from the steady state position. It is assumed that the beam material obeys Hooke's Law and the strains and rotations are small compared to unity. The potential energy expression for the beam is derived using the equation

$$V = 1/2E\iiint[u'_{,x}-zw'_{,xx}-yv'_{,xx}]^2 dx\,dy\,dz \quad (4)$$

where E is the elastic modulus.

Equations of motion describing beam vibration are derived using the extended Hamilton's principle with the inclusion of linear viscous damping forces proportional to velocities measured relative to the rotating coordinate system. The angular velocity ω is assumed to be expressible in the form

$$\omega = \omega_o + f(t) \quad (5)$$

in which the function $f(t)$ is a time-dependent perturbation on the steady state spin rate ω_o. If the axial deflection u is small with respect to the transverse displacements v and w, the equations of motion for transverse vibration are given by the relations

$$\begin{aligned} &mv_{,tt}+cv_{,t}+2mw_{,t}\omega_o-m\omega_o{}^2v+[EI_zv_{,xx}]_{,xx} = \\ &\quad -m\dot{f}\,[w_o+R]+m[2\omega_of+f^2]v-m\dot{f}w-2mfw_{,t} \end{aligned} \quad (6)$$

$$\begin{aligned} &mw_{,tt}+cw_{,t}-2m\omega_ov_{,t}-mw\omega_o{}^2+[EI_yw_{,xx}]_{,xx} = \\ &\quad m[2\omega_of+f^2][w_o+R]+2mfv_{,t}+m\dot{f}v+m[2\omega_of+f^2]w \end{aligned} \quad (7)$$

in which m is the mass per unit length of the beam, c is a constant damping coefficient, and I_z and I_y are centroidal area moments of inertia about the z and y axes, respectively. Equations of motion for an arbitrary orientation of the beam have been previously presented by Kammer (1983).

The left sides of equations (6) and (7) agree with results derived by Likins et al. (1973), Vigneron (1975), Laurenson (1976), and Bauer (1980). Terms on the right side of each equation are due to the time dependence of the angular velocity. This paper presents an investigation into the form and stability properties of the solution to the homogeneous portion of equations (6) and (7) given by

$$\begin{aligned} &mv_{,tt}+cv_{,t}+2m\omega_ow_{,t}-m\omega_o{}^2v+[EI_zv_{,xx}]_{,xx} = \\ &\quad m[2\omega_of+f^2]v-m\dot{f}w-2mfw_{,t} \end{aligned} \quad (8)$$

$$\begin{aligned} &mw_{,tt}+cw_{,t}-2m_ov_{,t}-m\omega_o{}^2w+[EI_yw_{,xx}]_{,xx} = \\ &\quad m[2\omega_of+f^2]w+m\dot{f}v+2mfv_{,t}. \end{aligned} \quad (9)$$

It may be noted that equations (8) and (9) are independent of the parameter R, which is the distance between the root of the beam and the spin axis. Therefore, the equations also represent motion for a spinning shaft.

Solution Method

Initially the space dependence must be eliminated from equations (8) and (9), resulting in a set of ordinary differential equations in time which can be solved for system response. Space and time are separated by assuming that the solution can be expressed as a linear combination of eigenfunctions Ψ_i corresponding to the system's space differential operator multiplied by generalized coordinates s_i. For the present case the operator takes on the form associated with a nonrotating beam and the associated eigenvalue problem can be solved for an infinite number of eigenvalues and eigenfunctions. The specific method used to formulate the eigenvalue problem is dependent upon the relationship between I_y and I_z. For the general case where $I_y \neq I_z$, the stiffness of the beam in the two bending planes is dissimilar, and the eigenvalue problem can be solved using the method put forth by Ariaratnam (1965).

If the beam is assumed to be uniform and the damping coefficient c is constant, the derived eigenfunctions are orthogonal in an ordinary sense. The series expansions

$$v = \sum_{i=1}^{\infty}\Psi_i s_{2i}; \quad w = \sum_{i=1}^{\infty}\Psi_i s_{1i} \quad (10)$$

can be used to discretize equations (8) and (9), resulting in an infinite set of uncoupled pairs of coupled ordinary differential equations in time of the form

$$\begin{aligned} &\ddot{s}_{1i}+2\alpha\dot{s}_{1i}-2\omega_o\dot{s}_{2i}+\lambda_{1i}{}^2s_{1i} \\ &\quad = [2\omega_of+f^2]s_{1i}+2\dot{f}s_{2i}+f\dot{s}_{2i} \end{aligned} \quad (11)$$

$$\begin{aligned} &\ddot{s}_{2i}+2\alpha\dot{s}_{2i}+2\omega_o\dot{s}_{1i}+\lambda_{2i}{}^2s_{2i} \\ &\quad = [2\omega_of+f^2]s_{2i}-2\dot{f}s_{1i}-f\dot{s}_{1i} \end{aligned} \quad (12)$$

where $\alpha = c/2m$ and $\lambda_{1i}{}^2$ and $\lambda_{2i}{}^2$ are the eigenvalues corresponding to the ith equation pair.

Equations (11) and (12) represent a coupled nonautonomous system which possesses no general closed-form solution. However, it is assumed that the function f representing the time dependence of the angular velocity is a small periodic perturbation upon the steady state spin rate ω_o. This assumption renders the right side of equations (11) and (12) small compared to terms on the left side. The system is said to be weakly nonautonomous, and a parameter ϵ which is small in comparison to unity can be associated with the nonautonomous terms. The perturbation f can be expressed by the Fourier series

$$f(t) = \sum_{k=-p}^{p} f_k e^{jk\beta t} \quad (13)$$

in which β is the perturbation frequency and $j = (-1)^{1/2}$.

The KBM method described by Bogoliubov and Mitrolpolsky (1961) is used as the mode of solution of equations (11) and (12) in this investigation. The method is an extension of the variation of parameters technique to higher order approximations using asymptotic expansions in the small parameter ϵ.

Downloaded 03 May 2010 to 171.66.16.27. Redistribution subject to ASME license or copyright; see http://www.asme.org/terms/Terms_Use.cfm

Solution in the Case of Nonresonance

The case of nonresonance is characterized by the assumption that the perturbation frequency and the natural frequency are related such that the full phase of the natural oscillation is not appreciably influenced by the phase of the perturbation.

Before proceeding with the solution, equations (11) and (12) are put in a form that is more congruous with the solution method. Initially, the small parameter ϵ is identified in the right side of the system. Function f is small compared to the steady state angular velocity ω_o; therefore, each Fourier coefficient f_k is also small in magnitude with respect to ω_o. For the purposes of this investigation, ϵ is defined as $\epsilon = |f_{-p}|/\omega_o$ which, due to the above observation, is small with respect to one.

In addition, the time scale is changed such that the differential equations are in terms of dimensionless time $\tau = t\omega_o$. These changes transform a representative pair of equations from (11) and (12) into the form

$$s_1'' + 2\bar{\alpha}s_1' - 2s_2' + \bar{\lambda}_1^2 s_1 = \epsilon[2\bar{f} + \epsilon\bar{f}^2]s_1 + \epsilon\bar{f}s_2' + \epsilon 2\bar{f}'s_2 \tag{14}$$

$$s_2'' + 2\bar{\alpha}s_2' + 2s_1' + \bar{\lambda}_2^2 s_2 = \epsilon[2\bar{f} + \epsilon\bar{f}^2]s_2 - \epsilon\bar{f}s_1' - \epsilon 2\bar{f}'s_1 \tag{15}$$

in which $\bar{\alpha}$ and $\bar{\lambda}$ are determined by dividing α and λ by ω_o, respectively, and $'$ denotes a derivative with respect to dimensionless time τ. Terms $\bar{f}$ and $\bar{f}_k$ are defined by the relations

$$\bar{f} = \sum_{k=-p}^{p} \bar{f}_k e^{jk\theta} \quad \text{and} \quad \bar{f}_k = f_k/|f_{-p}|$$

where $\theta = \beta\tau/\omega_o$.

If $\epsilon = 0$, the right sides of equations (14) and (15) vanish, resulting in the unperturbed system

$$s_1'' + 2\bar{\alpha}s_1' - 2s_2' + \bar{\lambda}_1^2 s_1 = 0 \tag{16}$$

$$s_2'' + 2\bar{\alpha}s_2' + 2s_1' + \bar{\lambda}_2^2 s_2 = 0. \tag{17}$$

Minorsky (1947) states that parametric excitation is not possible in a system which is over- or critically damped. In order to investigate this phenomenon later, it is assumed that the system is asymptotically stable. Therefore, the characteristic equation corresponding to the unperturbed system yields the two roots $\delta_1 = -\bar{\alpha}_1 + j\bar{\Omega}_1$ and $\delta_2 = -\bar{\alpha}_2 + j\bar{\Omega}_2$ as well as their complex conjugates. The solution of the unperturbed system is given by

$$s_{10} = Ae^{-\bar{\alpha}_1\tau}\cos\psi_1 + Be^{-\bar{\alpha}_2\tau}\cos\psi_2 \tag{18}$$

$$s_{20} = Ae^{-\bar{\alpha}_1\tau}[K_{11}\cos\psi_1 + K_{12}\sin\psi_1] + Be^{-\bar{\alpha}_2\tau}[K_{21}\cos\psi_2 + K_{22}\sin\psi_2] \tag{19}$$

where

$$K_{11} = \bar{\alpha} - \frac{\bar{\alpha}_1}{2} - \frac{\bar{\lambda}_1^2\bar{\alpha}_1}{2(\bar{\alpha}_1^2 + \bar{\Omega}_1^2)} \tag{20}$$

$$K_{12} = -\frac{\bar{\Omega}_1}{2} + \frac{\bar{\lambda}_1^2\bar{\alpha}_1}{2(\bar{\alpha}_1^2 + \bar{\Omega}_1^2)}. \tag{21}$$

The full phase ψ_1 is defined as $\psi_1 = \bar{\Omega}_1\tau + \phi_1$ in which $\bar{\Omega}_1$ is the damped natural frequency and ϕ_1 is the corresponding phase angle. Expressions for K_{21}, K_{22}, and ψ_2 can be obtained from equations (20), (21), and the relation for ψ_1 by replacing the subscript 1 with 2.

Due to the linearity of the system being investigated, solutions to the unperturbed and perturbed problems can be separated into two subsolutions, one in the harmonic ψ_1 and one in the harmonic ψ_2. Each subsolution is itself a homogeneous solution of the same form. Therefore, only the subsolution containing the harmonic ψ_1 is presented in this paper.

An approximate solution to the perturbed system (14) and (15) in the neighborhood of the unperturbed solution s_{10} and s_{20} is derived using the assumed form

$$s_1 = s_{10} + \epsilon u_1(A,\psi_1,\theta) + \epsilon^2 u_2 + \epsilon^3 u_3 + \ldots \tag{22}$$

$$s_2 = s_{20} + \epsilon v_1(A,\psi_1,\theta) + \epsilon^2 v_2 + \epsilon^3 v_3 + \ldots \tag{23}$$

Amplitude A and phase ψ_1 are determined by the relations

$$A' = \epsilon A_1(A) + \epsilon^2 A_2 + \epsilon^3 A_3 + \ldots \tag{24}$$

$$\psi_1' = \bar{\Omega}_1 + \epsilon C_1(A) + \epsilon^2 C_2 + \epsilon^3 C_3 + \ldots \tag{25}$$

in which the coefficients A_i and C_i are functions of amplitude A only.

First through nth order approximations to the system solution are derived by substituting relations (22) through (25) into equations (14) and (15). Each side of the resulting two relations is expanded, and terms containing equal powers of ϵ are equated, resulting in pairs of coupled partial differential equations in u_i and v_i of the form

$$\begin{aligned} &u_{i,\tau\tau} + 2\bar{\Omega}_1 u_{i,\psi_1\tau} + \bar{\Omega}_1^2 u_{i,\psi_1\psi_1} + 2\bar{\alpha}\bar{\Omega}_1 u_{i,\psi_i} + 2\bar{\alpha}u_{i,\tau} - 2\bar{\Omega}_1 v_{i,\psi_1} - 2v_{i,\tau} + \bar{\lambda}_1^2 u_i \\ &= R_{(i-1)1} + 2[A_i(\bar{\alpha}_1 - \bar{\alpha} + K_{11}) + AC_i(\bar{\Omega}_1 + K_{12})]e^{-\bar{\alpha}_1\tau}\cos\psi_1 \\ &\quad + 2[A_i(\bar{\Omega}_1 + K_{12}) + AC_i(\bar{\alpha} - \bar{\alpha}_1 - K_{11})]e^{-\bar{\alpha}_1\tau}\sin\psi_1 \end{aligned} \tag{26}$$

$$\begin{aligned} &v_{i,\tau\tau} + 2\bar{\Omega}_1 v_{i,\psi_1\tau} + \bar{\Omega}_1^2 v_{i,\psi_1\psi_1} + 2\bar{\alpha}\bar{\Omega}_1 v_{i,\psi_1} + 2\bar{\alpha}v_{i,\tau} + 2\bar{\Omega}_1 u_{i,\psi_1} + 2u_{i,\tau} + \bar{\lambda}_2^2 v_i \\ &= R_{(i-1)2} + 2\{A_i[K_{11}(\bar{\alpha}_1 - \bar{\alpha}) - \bar{\Omega}_1 K_{12} - 1] + AC_i[K_{12}(\bar{\alpha}_1 - \bar{\alpha}) + \bar{\Omega}_1 K_{11}]\}e^{-\bar{\alpha}_1\tau}\cos\psi_1 \\ &\quad + 2\{A_i[K_{12}(\bar{\alpha}_1 - \bar{\alpha}) + \bar{\Omega}_1 K_{11}] + AC_i[1 + K_{11}(\bar{\alpha} - \bar{\alpha}_1) + \bar{\Omega}_1 K_{12}]\}e^{-\bar{\alpha}_1\tau}\sin\psi_1 \end{aligned} \tag{27}$$

in which the subscript i denotes the order of the approximation and $R_{(i-1)r}$ is a function of A, ψ_1, and θ. Equations (26) and (27) are solved by assuming that u_i, v_i, $R_{(i-1)1}$, and $R_{(i-1)2}$ can be written as Fourier series of the form

$$u_i = e^{-\bar{\alpha}_1\tau}\sum_{\substack{n=-ip \\ n\neq 0}}^{ip} g^i{}_{n1}e^{j(n\theta+\psi_1)} + g^i{}_{n(-1)}e^{j(n\theta-\psi_1)} \tag{28}$$

$$v_i = e^{-\bar{\alpha}_1\tau}\sum_{\substack{n=-ip \\ n\neq 0}}^{ip} h^i{}_{n1}e^{j(n\theta+\psi_1)} + h^i{}_{n(-1)}e^{j(n\theta-\psi_1)} \tag{29}$$

$$R_{(i-1)1} = e^{-\bar{\alpha}_1\tau}\sum_{n=-ip}^{ip} r^i{}_{1n1}e^{j(n\theta+\psi_1)} + r^i{}_{1n(-1)}e^{j(n\theta-\psi_1)} \tag{30}$$

$$R_{(i-1)2} = e^{-\bar{\alpha}_1\tau}\sum_{n=-ip}^{ip} r^i{}_{2n1}e^{j(n\theta+\psi_1)} + r^i{}_{2n(-1)}e^{j(n\theta-\psi_1)}. \tag{31}$$

Substitution of these series into equations (26) and (27) results in a pair of coupled algebraic equations which can be solved by Cramer's rule for the Fourier coefficients of u_i and v_i, yielding the general expressions

$$g^i{}_{n1} = \{r^i{}_{1n1}[\nabla_n^2 + 2\bar{\alpha}\nabla_n + \bar{\lambda}_2^2] + 2r^i{}_{2n1}\nabla_n\}/D(\nabla_n) \tag{32}$$

$$h^i{}_{n1} = \{r^i{}_{2n1}[\nabla_n^2 + 2\bar{\alpha}\nabla_n + \bar{\lambda}_1^2] - 2r^i{}_{1n1}\nabla_n\}/D(\nabla_n) \tag{33}$$

where

$$\nabla_n \equiv -\bar{\alpha}_1 + j(n\bar{\beta} + \bar{\Omega}_1)$$

$$D(\nabla_n) = -n\bar{\beta}(n\bar{\beta} + 2\bar{\Omega}_1)[\bar{\alpha}_2 - \bar{\alpha}_1 + j(n\bar{\beta} + \bar{\Omega}_1 - \bar{\Omega}_2)][\bar{\alpha}_2 - \bar{\alpha}_1 + j(n\bar{\beta} + \bar{\Omega}_1 + \bar{\Omega}_2)]$$

and $\bar{\beta} = \beta/\omega_0$.

Downloaded 03 May 2010 to 171.66.16.27. Redistribution subject to ASME license or copyright; see http://www.asme.org/terms/Terms_Use.cfm

The Fourier coefficients for the functions u_i and v_i become infinite when the expression for $D(\nabla_n)$ vanishes; therefore, the zeros of $D(\nabla_n)$ correspond to the parametric resonances that exist in the system. For a beam with unequal principal moments of inertia, parametric resonances of the fractional-order type are given by the expression $\bar{\Omega}_1 = q\,\bar{\beta}/2$ where q is an integer variable. These resonances are equivalent to those found for a radial beam by Kammer and Schlack (accepted for publication). In the damped case, $\bar{\alpha}_1 \neq \bar{\alpha}_2$ for any combination of system physical parameters due to Coriolis effects. Therefore, the solution given by equations (32) and (33) remains finite at combination type resonances given by $q\bar{\beta} = \bar{\Omega}_1 \pm \bar{\Omega}_2$. Combination resonances are not considered in this paper.

Functions A_i and C_i in equations (24) and (25) are determined by eliminating terms with vanishing denominators (resonant terms) from the expressions for u_i and v_i (28, 29). In the case of nonresonance, this corresponds to the elimination of all the fundamental harmonics of ψ_1 ($n=0$). Expressions $P_{(i-1)1}$ and $P_{(i-1)2}$ are defined as functions which contain all the resonant terms which must be eliminated from the "forcing" functions $R_{(i-1)1}$ and $R_{(i-1)2}$, respectively. These terms can be written as

$$P_{(i-1)1} = e^{-\bar{\alpha}_1\tau}[p^i{}_{11}e^{j\psi_1} + p^i{}_{1(-1)}e^{-j\psi_1}] \tag{34}$$

$$P_{(i-1)2} = e^{-\bar{\alpha}_1\tau}[p^i{}_{21}e^{j\psi_1} + p^i{}_{2(-1)}e^{-j\psi_1}]. \tag{35}$$

Each of the coefficients $p^i{}_{sk}$ in equations (36) and (37) can be expressed in terms of its real and imaginary parts as $p^i{}_{sk} = p^i{}_{skR} + jp^i{}_{skI}$.

Elimination of the resonant terms leads to general expressions for A_i and C_i of the form

$$\begin{aligned} A_i = \{&H_1[-p^i{}_{11R}(\bar{\alpha}_1{}^2 - \bar{\Omega}_1{}^2 - 2\bar{\alpha}\bar{\alpha}_1 + \bar{\lambda}_2{}^2) + 2\bar{\alpha}_1 p^i{}_{21R} \\ &+ 2\bar{\Omega}_1(\bar{\alpha}-\bar{\alpha}_1)p^i{}_{11I} + 2\bar{\Omega}_1 p^i{}_{21I}] + H_2[p^i{}_{11I}(\bar{\alpha}_1{}^2 \\ &- \bar{\Omega}_1{}^2 - 2\bar{\alpha}\bar{\alpha}_1 + \bar{\lambda}_2{}^2) - 2\bar{\alpha}_1 p^i{}_{21I} + 2\bar{\Omega}_1(\bar{\alpha}-\bar{\alpha}_1)p^i{}_{11R} \\ &+ 2\bar{\Omega}_1 p^i{}_{21R}]\}/[H_1{}^2 + H_2{}^2] \end{aligned} \tag{36}$$

$$\begin{aligned} C_i = \{&H_1[-p^i{}_{11I}(\bar{\alpha}_1{}^2 - \bar{\Omega}_1{}^2 - 2\bar{\alpha}\bar{\alpha}_1 + \bar{\lambda}_2{}^2) + 2\bar{\alpha}_1 p^i{}_{21I} \\ &- 2\bar{\Omega}_1(\bar{\alpha}-\bar{\alpha}_1)p^i{}_{11R} - 2\bar{\Omega}_1 p^i{}_{21R}] + H_2[-p^i{}_{11R}(\bar{\alpha}_1{}^2 \\ &- \bar{\Omega}_1{}^2 - 2\bar{\alpha}\bar{\alpha}_1 + \bar{\lambda}_2{}^2) + 2\bar{\alpha}_1 p^i{}_{21R} + 2\bar{\Omega}_1(\bar{\alpha}-\bar{\alpha}_1)p^i{}_{11I} \\ &+ 2\bar{\Omega}_1 p^i{}_{21I}]\}/[H_1{}^2 + H_2{}^2]A \end{aligned} \tag{37}$$

in which the constants H_1 and H_2 are defined as

$$\begin{aligned} H_1 = {}&[\bar{\alpha}_1 - \bar{\alpha} + K_{11}](\bar{\alpha}_1{}^2 - \bar{\Omega}_1{}^2 - 2\bar{\alpha}_1\bar{\alpha} + \bar{\lambda}_2{}^2) \\ &- 2\bar{\Omega}_1{}^2(\bar{\alpha}_1 - \bar{\alpha} - K_{11}) + 2\bar{\alpha}_1[1 - K_{11}(\bar{\alpha}_1 - \bar{\alpha}) + \bar{\Omega}_1 K_{12}] \\ H_2 = {}&[\bar{\Omega}_1 + K_{12}](\bar{\alpha}_1{}^2 - \bar{\Omega}_1{}^2 - 2\bar{\alpha}_1\bar{\alpha} + \bar{\lambda}_2{}^2) \\ &- 2\bar{\alpha}_1{}^2[K_{12}(\bar{\alpha}_1 - \bar{\alpha}) + \bar{\Omega}_1 K_{11}] + 2\bar{\Omega}_1[1 + (\bar{\alpha}_1 - \bar{\alpha})^2 + \bar{\Omega}_1 K_{12}]. \end{aligned} \tag{38}$$

In the first approximation, terms of order ϵ and larger are retained in the assumed solution. The integer variable i is set to the value 1 in the general relations (26) through (33). Increasingly higher approximations to the solution can be derived by successively solving higher order equations using the general expressions given. The functions $R_{(i-1)1}$ and $R_{(i-1)2}$ found in each of the successive solutions depend only on terms already determined in lower order approximations.

As an example of the application of the general equations, the perturbation function f is taken to be $f = a\cos\theta$ in which a is assumed to be small compared to ω_0. If the parameter ϵ is assumed in the form $\epsilon = a/\omega_0$, function $\bar{f}$ is given by Fourier series $\bar{f} = 1/2\,(e^{j\theta} + e^{-j\theta})$ with Fourier coefficients given by $\bar{f}_1 = 1/2$ and $\bar{f}_{-1} = 1/2$. The integer variable p found in equations (28) through (31) has the value 1 for this example.

A resonance appears in the first approximation due to the presence of a zero in the denominators of several of the coefficients for the first order corrections u_1 and v_1. The singular denominators are given by the expression

$$\begin{aligned} D(\nabla_{-1}) = {}&\bar{\beta}(2\bar{\Omega}_1 - \bar{\beta})[(\bar{\alpha}_2 - \bar{\alpha}_1) + j(\bar{\Omega}_1 - \bar{\Omega}_2 - \bar{\beta})] \\ &[(\bar{\alpha}_2 - \bar{\alpha}_1) + j(\bar{\Omega}_1 + \bar{\Omega}_2 - \bar{\beta})]. \end{aligned} \tag{39}$$

Functions u_1 and v_1 become infinite when the perturbation frequency $\bar{\beta}$ is twice the natural frequency $\bar{\Omega}_1$. This singularity is termed a primary parametric resonance since it appears in the first approximation. Due to the symmetry of the solution in both the harmonics ψ_1 and ψ_2, a primary resonance will also appear at $\bar{\Omega}_2 = \bar{\beta}/2$. Second and third order approximations to the solution result in the appearance of secondary resonances $\bar{\Omega}_1 = \bar{\beta}$ and $\bar{\Omega}_2 = \bar{\beta}$, and tertiary resonances $\bar{\Omega}_1 = (3/2)\bar{\beta}$ and $\bar{\Omega}_2 = (3/2)\bar{\beta}$. Higher order solutions yield still higher order resonances.

Solution in the Case of Resonance

Due to the nonautonomous nature of equations (11) and (12), parametric resonances can occur in the system when $\bar{\Omega}_1 = q\bar{\beta}/2$. The resonance domain is investigated by assuming that the natural frequency $\bar{\Omega}_1$ is sufficiently close to $q\bar{\beta}/2$ such that the detuning $\Delta = \bar{\Omega}_1 - q\bar{\beta}/2$ is of the first order in ϵ. Therefore, the phase difference between the natural oscillation and the perturbation action will have an appreciable influence upon the rate of change of both the amplitude and frequency. The assumed solution is still taken in the form of equations (22) and (23); however, the resonance condition demands that the amplitude A and the phase ϕ_1 be determined using the expressions

$$A' = \epsilon A_1(A,\phi_1) + \epsilon^2 A_2 + \epsilon^3 A_3 + \ldots \tag{40}$$

$$\phi_1' = \bar{\Omega}_1 - q\bar{\beta}/2 + \epsilon C_1(A,\phi_1) + \epsilon^2 C_2 + \epsilon^3 C_3 + \ldots \tag{41}$$

where the coefficients A_i and C_i are now dependent on both the amplitude and phase.

The solution process in the resonant case is analogous to that used for nonresonance. Series forms for $R_{(i-1)1}$, $R_{(i-1)2}$, u_i, and v_i are unchanged. Fourier coefficients in the expressions for u_i and v_i are determined by the general equations (32) and (33) with $\nabla_n = -\bar{\alpha}_1 + j(n+q/2)\bar{\beta}$. The denominators of the coefficients are given by

$$\begin{aligned} D(\nabla_n) = {}&-n\bar{\beta}^2(n+q)\{(\bar{\alpha}_2 - \bar{\alpha}_1) + j[(n+q/2)\bar{\beta} - \bar{\Omega}_2]\} \\ &\{(\bar{\alpha}_2 - \bar{\alpha}_1) + j[(n+q/2)\bar{\beta} + \bar{\Omega}_2]\}. \end{aligned} \tag{42}$$

Equation (42) illustrates which terms will lead to resonances. All harmonics $n\theta + \psi_1$ where $n=0, -q$ and all harmonics $n\theta - \psi_1$ where $n = 0, q$ must be eliminated and are therefore included in the expressions for $P_{(i-1)1}$ and $P_{(i-1)2}$. Functions A_i and C_i are determined by relations (36) and (37) with the substitution $\bar{\Omega}_1 = q\bar{\beta}/2$.

The perturbation function $f = a\cos\bar{\beta}\tau$ is again used as an example in the case of resonance with $\epsilon = a/\omega_0$. In the work performed in the nonresonant case, the primary resonance was determined to be $\bar{\Omega}_1 = \bar{\beta}/2$. Therefore, the integer variable q will have a value of 1 in the general expressions. This resonance is of prime interest due to the fact that it alone appears in the first approxiamtion and is, therefore, the most dangerous of the resonances which could be considered. Only the solution in the first approximation ($i = 1$) is considered.

Fourier coefficients $g^1{}_{11}$ and $h^1{}_{11}$ are of the form

$$\begin{aligned} g^1{}_{11} = {}&\{r^1{}_{111}[(-\bar{\alpha}_1 + j3\bar{\beta}/2)^2 + 2\bar{\alpha}(-\bar{\alpha}_1 + j3\bar{\beta}/2) + \bar{\lambda}_2{}^2] \\ &+ 2(-\bar{\alpha}_1 + j3\bar{\beta}/2)r^1{}_{211}\}/D(-\bar{\alpha}_1 + j3\bar{\beta}/2) \end{aligned} \tag{43}$$

$$\begin{aligned} h^1{}_{11} = {}&\{r^1{}_{211}[(-\bar{\alpha}_1 + j3\bar{\beta}/2)^2 + 2\bar{\alpha}(-\bar{\alpha}_1 + j3\bar{\beta}/2) + \bar{\lambda}_1{}^2] \\ &- 2(-\bar{\alpha}_1 + j3\bar{\beta}/2)r^1{}_{111}\}/D(-\bar{\alpha}_1 + j3\bar{\beta}/2). \end{aligned} \tag{44}$$

Coefficients $g^1{}_{1(-1)}$ and $h^1{}_{1(-1)}$ are given by the complex conjugates of $g^1{}_{11}$ and $h^1{}_{11}$, respectively.

If the coefficients A_{1k} and C_{1k} are defined by the expressions

Downloaded 03 May 2010 to 171.66.16.27. Redistribution subject to ASME license or copyright; see http://www.asme.org/terms/Terms_Use.cfm

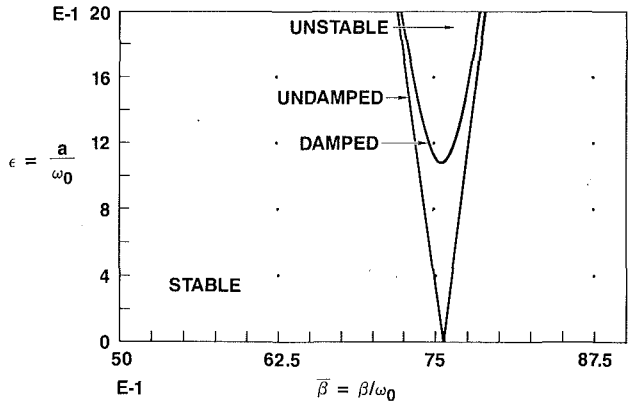


Fig. 2 Primary parametric instability region $\bar{\Omega}_1 = \bar{\beta}/2$ (first approximation)

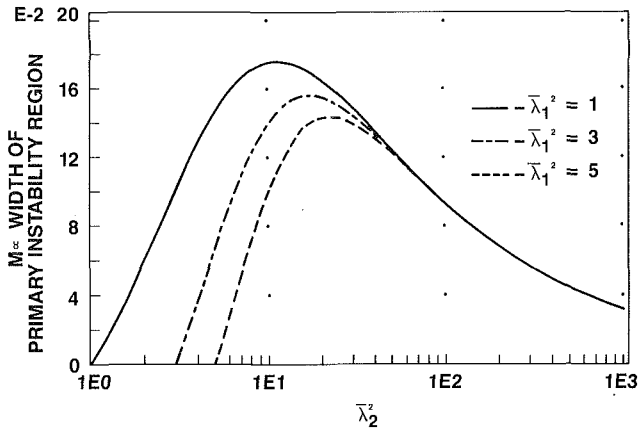


Fig. 3 Width of primary parametric instability region as a function of system eigenvalues

$$A_1 = A_{10} + A_{11}\cos 2\phi_1 + A_{12}\sin 2\phi_1$$
$$AC_1 = AC_{10} + A_{12}\cos 2\phi_1 - A_{11}\sin 2\phi_1$$

the amplitude A and the phase ϕ_1 are determined by solving the coupled nonlinear differential system

$$\dot{A} = (a/\omega_0)A_{11}\cos 2\phi_1 + (a/\omega_0)A_{12}\sin 2\phi_1 \quad (45)$$

$$\dot{\phi}_1 = \bar{\Omega}_1 - \bar{\beta}/2 + [(a/\omega_0)A_{12}\cos 2\phi_1 - (a/\omega_0)A_{11}\sin 2\phi_1]/A. \quad (46)$$

The substitution

$$\bar{u} = A\cos\phi_1; \quad \bar{v} = A\sin\phi_1$$

transforms the nonlinear equations into a linear system with the solution

$$\bar{u} = D_1 e^{\gamma\tau} + D_2 e^{-\gamma\tau}$$

$$\bar{v} = D_1 \frac{\gamma - \epsilon C_{12}}{\epsilon C_{11} - \bar{\Omega}_1 + \bar{\beta}/2} e^{\gamma\tau} - D_2 \frac{\gamma + \epsilon C_{12}}{\epsilon C_{11} - \bar{\Omega}_1 + \bar{\beta}/2} e^{-\gamma\tau} \quad (47)$$

$$A = [\bar{u}^2 + \bar{v}^2]; \quad \phi_1 = \mathrm{Tan}^{-1}(\bar{v}/\bar{u})$$

in which $\gamma = \pm [-(\bar{\Omega}_1 - \bar{\beta}/2)^2 + \epsilon^2(C_{11}^2 + C_{12}^2)]^{1/2}$ are the eigenvalues of the transformed system, D_1 and D_2 are constants determined by initial conditions, and C_{11} and C_{12} are given by $C_{11} = A_{12}/A$ and $C_{12} = -A_{11}/A$.

The stability of the solution given by equation (47) is determined by the parameter $\zeta = -\bar{\alpha}_1 + \gamma$. For instability to occur, ζ must be real and positive. This requirement leads to a condition for instability in the first approximation of the form

$$2\bar{\Omega}_1 - 2\epsilon[(C_{11}^2 + C_{12}^2) - (\bar{\alpha}_1/\epsilon)^2]^{1/2} < \bar{\beta} < 2\bar{\Omega}_1 + 2\epsilon[(C_{11}^2 + C_{12}^2) - (\bar{\alpha}_1/\epsilon)^2]^{1/2}. \quad (48)$$

Equation (48) defines a region of instability rather than merely a discrete spectrum as in the case of ordinary resonance, and, in this regard, a parametric resonance is much more dangerous. For the instability condition to be physically attainable, the damping coefficient $\bar{\alpha}_1$ must satisfy the inequality $\bar{\alpha}_1 \leq \epsilon(C_{11}^2 + C_{12}^2)^{1/2}$. Therefore, the system damping must be of the first order in ϵ for parametric excitation to take place at the primary resonance.

The primary instability region described by equation (48) is illustrated in Fig. 2 for the specific physical parameters $\bar{\lambda}_1^2 = 1$, $\bar{\lambda}_2^2 = 10$, and $\bar{\alpha} = 0.1$ which result in the system characteristics $\bar{\Omega}_1 = 3.789$, $\bar{\Omega}_2 = 0.8331$, $\bar{\alpha}_1 = -0.1294$, and $\bar{\alpha}_2 = -0.0706$. The figure illustrates that damping caused the instability region to shrink in accordance with theory as described by Bolotin (1964). Within the region of parametric instability, the derived solution grows exponentially. On the boundaries of the region, the amplitude A and phase ϕ_1 are constant, and the vibration is purely periodic and synchronous. Exterior to the instability region, the amplitude and phase are themselves periodic functions of time, and the oscillation is periodic and asynchronous. Higher order approximations will refine the existing instability boundaries and reveal higher order resonances resulting in a series of instability regions comparable to those found in the Strutt diagram for the Mathieu equation.

If the system is considered to be undamped, an interesting observation can be made concerning the width of the primary parametric instability region for the perturbation function being considered. The width of the region for any value of ϵ is of the form $W = \epsilon 2M$ where M is a function given by

$$M = \frac{\bar{\lambda}_1^2 - \bar{\lambda}_2^2}{\bar{\Omega}_1(\bar{\Omega}_2^2 - \bar{\Omega}_1^2)}. \quad (49)$$

Equation (49) illustrates that the width of the instability region is proportional to the difference in the two principal stiffnesses. If the cross section of the beam has two identical principal area moments of inertia, the primary instability region vanishes and parametric resonance is not possible.

Function M is plotted in Fig. 3 for various values of $\bar{\lambda}_1$ and $\bar{\lambda}_2$. The figure illustrates that for each value of $\bar{\lambda}_1$ there exists a value of $\bar{\lambda}_2$ which maximizes the width of the instability region. A relation such as equation (62) cannot be determined for the general case of a damped system due to the lack of an explicit expression relating the system variables $\bar{\lambda}_1$, $\bar{\lambda}_2$, $\bar{\alpha}$, $\bar{\alpha}_1$, $\bar{\alpha}_2$, $\bar{\Omega}_1$, and $\bar{\Omega}_2$. Further investigation presented by Kammer (1983) using energy considerations showed that all possible parametric resonances vanish when the two principal area moments of inertia for the beam are equal, regardless of the form of the perturbation function. Therefore, parametric resonance is not possible for a beam with a cross section having equal principal moments and longitudinal axis parallel to the spin axis.

Conclusion

Equations of motion have been presented for a beam rotating with nonconstant angular velocity oriented parallel to the spin axis. The nonstationarity of the angular velocity resulted in terms with time-dependent coefficients which are not found in equations derived in the literature. General solutions were derived using the KBM method in which the angular velocity was expressed as the sum of a steady state term and a relatively small arbitrary periodic perturbation.

Solutions which were derived assuming a nonresonant condition revealed singularities called parametric resonances of the form $\bar{\Omega}_1 = q\bar{\beta}/2$ which would not be apparent if the simplifying assumption of constant angular velocity had been made. These resonances were investigated assuming a condition of resonance to determine the boundaries of the instability regions. It was shown that these regions vanish if the cross

Downloaded 03 May 2010 to 171.66.16.27. Redistribution subject to ASME license or copyright; see http://www.asme.org/terms/Terms_Use.cfm

section of the beam possesses two identical principal area moments of inertia. A simple perturbation function $f = a\cos\bar{\beta}\tau$ was considered to demonstrate the use of derived general expressions.

References

Ariaratnam, S. T., 1965, "The Vibration of Unsymmetrical Rotating Shafts," ASME JOURNAL OF APPLIED MECHANICS, pp. 157–162.

Bauer, H. F., 1980, "Vibration of a Rotating Uniform Beam, Part I: Orientation in the Axis of Rotation," *Journal of Sound and Vibration*, Vol. 72, No. 2, pp. 177–189.

Bogoliubov, N. N., and Mitropolsky, Y. A., 1961, *Asymptotic Methods in the Theory of Nonlinear Oscillations*, Gordan and Breach Science Publishers, New York.

Bolotin, V. V., 1964, *Dynamic Stability of Elastic Systems*, Holden-Day, Inc., San Francisco, Calif.

Hodges, D. H., and Rutkowski, J., 1981, "Free-Vibration Analysis of Rotating Beams by Variable-Order Finite Element Method," *AIAA Journal*, Vol. 19, No. 11, pp. 1459–1466.

Houbolt, J. C., and Brooks, C. W., 1958, "Differential Equations of Motion for Combined Flapwise Bending, Chordwise Bending and Torsion of Twisted Non-Uniform Rotor Blades," National Advisory Committee for Aeronautics Report 1346.

Kammer, D. C., 1983, "Dynamic Response of Rotating Beams with Nonconstant Angular Velocity," Ph.D. Thesis, University of Wisconsin, Madison.

Kammer, D. C., and Schlack, A. L., "Dynamic Response of a Radial Beam With Nonconstant Angular Velocity," accepted for publication in the *Journal of Vibration, Acoustics, Stress, and Reliability in Design*.

Laurenson, R. M., 1976, "Modal Analysis of Rotating Structures," *AIAA Journal*, Vol. 14, No. 10, pp. 1444–1450.

Likins, P. W., Barbera, F. J., and Baddeley, V., 1973, "Mathematical Modeling of Spinning Elastic Bodies for Modal Analysis," *AIAA Journal*, Vol. 11, No. 9, pp. 1251–1258.

Minorsky, N., 1947, *Introduction to Nonlinear Mechanics*, Ann Arbor, Michigan.

Renard, M. L., and Rakowski, J. E., 1970, "Equatorial Vibrations of a Long Flexible Boom on a Spin-Stabilized Satellite of Non-Zero Radius," *21st Congress of the International Astronautical Federation*, Mar Del Plata, Argentina, pp. 35–53.

Sutherland, R. L., 1949, "Bending Vibration of a Rotating Blade Vibrating in the Plane of Rotation," ASME JOURNAL OF APPLIED MECHANICS, pp. 389–394.

Vigneron, F. R., 1975, "Comment on 'Mathematical Modeling of Spinning Elastic Bodies for Modal Analysis'," *AIAA Journal*, Vol. 13, No. 1, pp. 126–127.

Downloaded 03 May 2010 to 171.66.16.27. Redistribution subject to ASME license or copyright; see http://www.asme.org/terms/Terms_Use.cfm

D. Storti
Mem. ASME

Y. Aboelnaga
Student Mem. ASME

Department of Mechanical Engineering,
University of Washington,
Seattle, WA 98195

Bending Vibrations of a Class of Rotating Beams with Hypergeometric Solutions[1]

We study the transverse deflections of a straight tapered symmetric beam attached to a rotating hub as a model for the bending vibration of blades in turbomachinery. A broad class of blade shapes is obtained for which the equation of motion can be solved analytically in terms of hypergeometric functions. Based on this analytic solution, an algorithm for computing the natural bending frequencies and mode shapes as a function of setting angle and rotation rate is presented and applied to an example.

Introduction

In this paper, we study the bending vibrations of a beam attached to a rotating hub (see Fig. 1 after Lo et al., 1960) as a model for the behavior of a turbomachine blade. We present a method to analytically determine the bending modes for a class of variable cross-section rotating beams as a function of setting angle and rotation rate. These results can be useful in determining resonance and detuning criteria at operating speeds. Our model includes the effects of variable cross section in addition to finite hub radius and staggered mounting angle which were treated by Schilhansl (1958). The analysis involves factoring the fourth-order linear differential operator which appears in the equation of motion into a pair of commuting second-order operators as introduced by Cranch and Adler (1955) for stationary beams. The resulting second-order differential equations are solved in terms of hypergeometric functions. This is similar to the work of Wang (1957), but now the differential operator is more complicated due to the inclusion of centrifugal effects. While our methods apply only to a specific class of beam shapes which will be specified below, this class is quite broad and includes a wide variety of cross-sections and thickness variations. Two important characteristics of these beams are that they have a vanishing thickness at the tip (which simplifies the treatment of the boundary conditions) and that they are doubly symmetric so that torsion is uncoupled from bending. The bending stiffness about the major principle axis of inertia of the section is assumed to be sufficiently large that bending in that direction can be neglected. Thus, the model presented here does not include the effects of pretwist and camber or allow for twisting vibrations or bending vibtations about the major principal

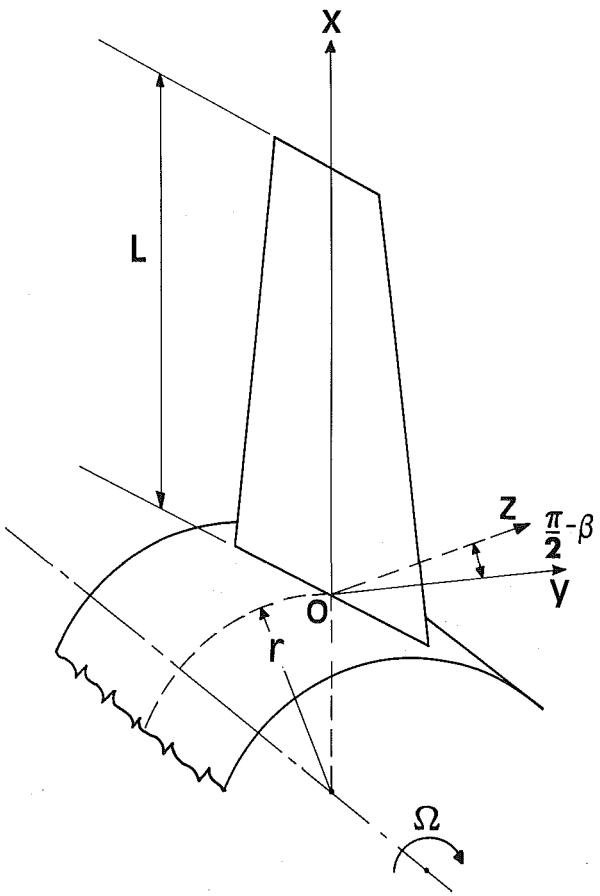


Fig. 1 Beam on a rotating disk as a model of a turbomachinery blade

[1]This research was partially supported by a grant from the University of Washington Graduate School Research Fund.

Contributed by the Applied Mechanics Division for presentation at the 1987 Applied Mechanics, Biomechanics, and Fluids Engineering Conference, Cincinnati, OH, June 14–17, 1987, of the American Society of Mechanical Engineers.

Discussion of this paper should be addressed to the Editorial Department, ASME, United Engineering Center, 345 East 47th Street, New York, N.Y. 10017, and will be accepted until two months after final publication of the paper itself in the JOURNAL OF APPLIED MECHANICS. Manuscript received by ASME Applied Mechanics Division, February 24, 1986; final revision, July 24, 1986.

Paper No. 87-APM-21.

Copyright © 1987 by ASME
Downloaded 03 May 2010 to 171.66.16.27. Redistribution subject to ASME license or copyright; see http://www.asme.org/terms/Terms_Use.cfm

axis of inertia. These factors have been included in studies of stationary beams by Gere and Lin (1958) and Krenk (1983).

Equation of Motion and the Factorization Method

The equation of motion governing the free transverse vibrations of an elastic beam rigidly mounted with setting angle β on a hub rotating with constant angular velocity Ω is given by Lo et al. (1960) as

$$\frac{\partial^2}{\partial x^2}\left(EI\frac{\partial^2\chi}{\partial x^2}\right)-\frac{\partial}{\partial x}\left(N\frac{\partial\chi}{\partial x}\right)+\rho A\frac{\partial^2\chi}{\partial t^2}-\rho A\Omega^2\chi\sin^2\beta=0 \tag{1}$$

where χ is the bending displacement about the minor principal axis (in the y direction), ρ and E are the mass density and elastic modulus of the beam material, A is the area of the cross section, and I is the area moment of inertia. The centrifugal force N is given by

$$N=\Omega^2\int_x^L \rho A(\zeta+r)d\zeta. \tag{2}$$

By separating variables, we find that the motion is harmonic and that the mode shape, $Z(x)$, and natural frequency, ω, are determined by the fourth-order linear ordinary differential equation with variable coefficients

$$\rho A\mathbf{L}(Z)=\frac{d^2}{dx^2}\left(EI\frac{d^2Z}{dx^2}\right)-\frac{d}{dx}\left(N\frac{dZ}{dx}\right)$$

$$-\rho A(\omega^2+\Omega^2\sin^2\beta)Z=0 \tag{3}$$

subject to fixed-free boundary conditions

$$Z(0)=Z'(0)=0,\ [EI\,Z''(x)]_{x=L}=[(EI\,Z''(x))']_{x=L}=0. \tag{4}$$

We seek solutions of equation (3) by factoring the fourth-order operator into a pair of commuting second-order operators, $\mathbf{L}_1$ and $\mathbf{L}_2$, and solving the two associated second order equations, $\mathbf{L}_1(Z)=0$ and $\mathbf{L}_2(Z)=0$. Based on the form used by Cranch and Adler (1955), we write the second-order operators as

$$\mathbf{L}_1=\frac{1}{R}\frac{d}{dx}\left(S\frac{d}{dx}\right)-p \tag{5}$$

$$\mathbf{L}_2=\frac{1}{R}\frac{d}{dx}\left(S\frac{d}{dx}\right)+\frac{1}{p}(\omega^2+\Omega^2\sin^2\beta) \tag{6}$$

where p is a parameter, and R and S are functions of x yet to be determined. To obtain the desired operator $\mathbf{L}$, the following conditions must be satisfied

$$\rho A=R,\ EI=S^2/R \tag{7}$$

$$N=\left[-\frac{1}{p}(\omega^2+\Omega^2\sin^2\beta)+p-\frac{d}{dx}\left(\frac{1}{R}\frac{dS}{dx}\right)\right]S$$

$$=\Omega^2\int_x^L(\zeta+r)R(\zeta)d\zeta. \tag{8}$$

If ρA and EI are specified independently, then equations (7) determine S and R, but equations (8) cannot generally be satisfied. However, for the following forms of the functions R and S (Storti and Aboelnaga, 1986), these conditions can be simultaneously satisfied:

$$R=\rho A_0\left[\frac{1-q\xi}{1-q}\right]^m\xi^n \tag{9}$$

$$S=\sqrt{(\rho A_0 EI_0)}\left[\frac{1-q\xi}{1-q}\right]^{m+1}\xi^{n+1} \tag{10}$$

where subscript zero indicates the value at the root ($x=0$), m and n are free parameters (with the restriction $n\geq 1$), $\xi=(1-x/L)$, and $q=[(n+1)L/(n+m+2)(L+r)]$. Substituting into equation (8) then gives

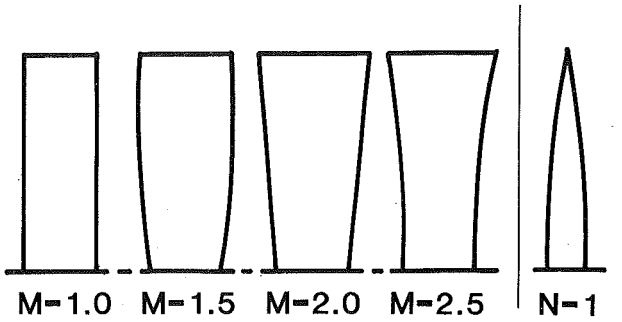


Fig. 2 An example of admissable beam shapes. A beam with parabolically varying thickness corresponding to $n=1$ (shown at right) is accompanied by four possible width profiles ($m=1.0$, $m=1.5$, $m=2.0$, and $m=2.5$, respectively).

$$(\omega/k)^2=(p/k)\,[(p/k)-(\Omega/k)^2+1]-(\Omega/k)^2\sin^2\beta \tag{11}$$

$$\text{where } k=\frac{(m+n+2)q}{(1-q)}\left[\frac{EI_0}{\rho A_0 L^4}\right]^{1/2} \tag{12}$$

and p will be determined from the boundary conditions.

If the blade cross section is symmetric about both the major and minor principal axes (e.g., circular, elliptical, rectangular, or wedge-shaped), then the maximum thickness h and chord length l are given by

$$h=h_0\left[\frac{1-q\xi}{1-q}\right]\xi \tag{13}$$

$$l=l_0\left[\frac{1-q\xi}{1-q}\right]^{m-1}\xi^{n-1},\ n\geq 1. \tag{14}$$

By varying m and n, a large family of blade geometries admitting the factorization can be specified. (See Fig. 2 for some examples.)

Solution in Terms of Hypergeometric Functions

Let us now introduce the dimensionless variables

$$s=q(1-x/L),\ z=qZ/L. \tag{15}$$

Substituting into $\mathbf{L}_1(Z)=0$ and $\mathbf{L}_2(Z)=0$ yields

$$s(1-s)\frac{d^2z}{ds^2}+[(n+1)-(n+m+2)s]\frac{dz}{ds}$$

$$-(n+m+2)\frac{p}{k}z=0 \tag{16}$$

$$s(1-s)\frac{d^2z}{ds^2}+[(n+1)-(n+m+2)s]\frac{dz}{ds}$$

$$+(n+m+2)\left(\frac{p}{k}-\frac{\Omega^2}{k^2}+1\right)z=0. \tag{17}$$

These can be recognized as hypergeometric differential equations (Abramowitz and Stegun, 1965) whose general form is given by

$$s(1-s)\frac{d^2z}{ds^2}+[c-(a+b+1)s]\frac{dz}{ds}-ab\,z=0. \tag{18}$$

The hypergeometric function is defined by

$$F(a,b;c;s)=1$$

$$+\sum_{n=1}^{\infty}\frac{a(a+1)\ldots(a+n-1)b(b+1)\ldots(b+n-1)}{n!c(c+1)\ldots(c+n-1)}s^n \tag{19}$$

which converges for $|s|<1$ (which is the region of interest for this problem) whenever c is not zero or a negative integer. If c is not an integer, then equation (18) has the general solution

$$z(s)=KF(a,b;c;s)+K's^{1-c}F(a-c+1,b-c+1;2-c;s) \tag{20}$$

Downloaded 03 May 2010 to 171.66.16.27. Redistribution subject to ASME license or copyright; see http://www.asme.org/terms/Terms_Use.cfm

while if $c-1$ is a positive integer, the general solution contains a logarithmic term (Abramowitz and Stegun, 1965, p. 564, equation 15.5.19)

$$z(s) = KF(a,b;c;s) + K'\{F(a,b;c;s)\ln s + \ldots\}. \quad (21)$$

In either case, we must choose $K' = 0$ to ensure that the solution remains bounded at the blade tip where $s = 0$.

To treat equations (16) and (17), we make the identifications

$$c = n+1 \quad (22)$$

$$a_1 = \left(\frac{m+n+1}{2}\right)\left(1+\left[1-\frac{4(m+n+2)}{(m+n+1)^2}\frac{p}{k}\right]^{1/2}\right)$$

$$b_1 = \left(\frac{m+n+1}{2}\right)\left(1-\left[1-\frac{4(m+n+2)}{(m+n+1)^2}\frac{p}{k}\right]^{1/2}\right) \quad (23)$$

$$a_2 = \left(\frac{m+n+1}{2}\right)\left(1+\left[1+\frac{4(m+n+2)}{(m+n+1)^2}\left(\frac{p}{k}-\frac{\Omega^2}{k^2}+1\right)\right]^{1/2}\right)$$

$$b_2 = \left(\frac{m+n+1}{2}\right)\left(1-\left[1+\frac{4(m+n+2)}{(m+n+1)^2}\left(\frac{p}{k}-\frac{\Omega^2}{k^2}+1\right)\right]^{1/2}\right) \quad (24)$$

and the general solution of $\mathbf{L}(z) = 0$ satisfying the boundary conditions at the tip becomes

$$z(s) = K_1 F(a_1,b_1;c;s) + K_2 F(a_2,b_2;c;s). \quad (25)$$

Applying the boundary conditions at the root gives the condition for the existence of a nontrivial solution

$$\frac{F'(a_1,b_1;c;q)}{F(a_1,b_1;c;q)} = \frac{F'(a_2,b_2;c;q)}{F(a_2,b_2;c;q)}. \quad (26)$$

Recalling that a_1 and b_1 depend on the parameter p/k while a_2 and b_2 depend on $(-1 + \Omega^2/k^2 - p/k)$, let us define $Y = F'/F$ so that equation (26) becomes

$$Y(p/k) = Y(-1+\Omega^2/k^2 - p/k). \quad (27)$$

This allows for the following graphical determination of the natural frequencies of bending vibration. Begin by making a plot of $Y(p/k)$. Then construct a plot of $Y(-1+\Omega^2/k^2 - p/k)$ by moving the origin of the horizontal axis to $-1+\Omega^2/k^2$ and reflecting about the vertical axis. The intersections of these two curves determine values of p/k, and the corresponding bending frequency ω is found using equation (11).

The hypergeometric function $F(a_1,b_1;c;q)$ is computed using the series definition given by equation (19). Let the jth term in the sum be named T_j, so that

$$F(a_1,b_1;c;q) = \sum_{j=0}^{\infty} T_j \quad (28)$$

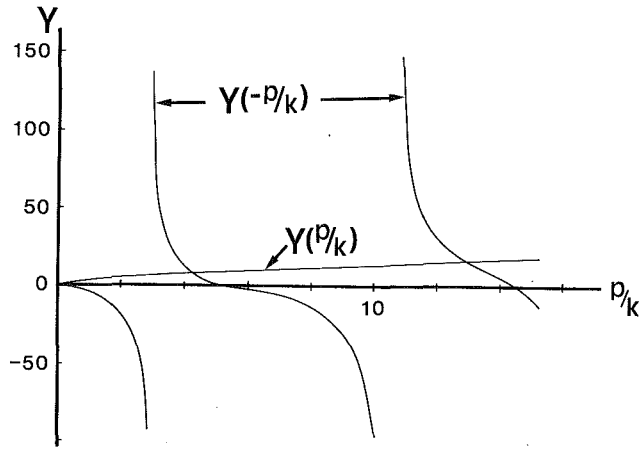


Fig. 3 $Y(p/k)$ for $n = m = 1$, $r = L$

where $T_0 = 1$ and the succeeding terms are given by the recursion relation

$$T_j = \left[\frac{(a_1+j-1)(b_1+j-1)q}{(c+j-1)j}\right]T_{j-1} \quad (29a)$$

$$= \left[\frac{\{(n+m+2)(p/k) + (n+m+1)(j-1) + (j-1)^2\}q}{(n+j)j}\right]T_{j-1}. \quad (29b)$$

Since this series is convergent for $q < 1$ (which is always true when n and m are positive) and each term in the series has a continuous derivative with respect to q, we can find the series for F' by differentiating term by term (Abramowitz and Stegun, 1965; Wylie and Barrett, 1982). If we denote the terms in the series for F' by T_j', then

$$F' = \sum_{j=1}^{\infty} T_j', \quad T_j' = (j/q)T_j. \quad (30)$$

An Example

To demonstrate the calculation of $Y = F'/F$ and the determination of the bending modes, we consider an example consisting of a type 304 stainless steel blade ($E = 18.92\times10^{10}$ N-m^{-2}, $\rho = 8.03\times10^3$ kg-m^{-3}) of length $L = 0.5$m mounted on a hub of radius $r = 0.5$m so that $r/L = 1$. The blade has constant chord length $l = l_0 = 0.2$m and $n = m = 1$ so that $q = 1/4$, and the thickness varies according to

$$h = h_0(1 + x/3L)(1 - x/L) \quad (31)$$

(as shown in Fig. 2) where the half-thickness at the blade root is $h_0 = 0.025$m. The recursion relations become

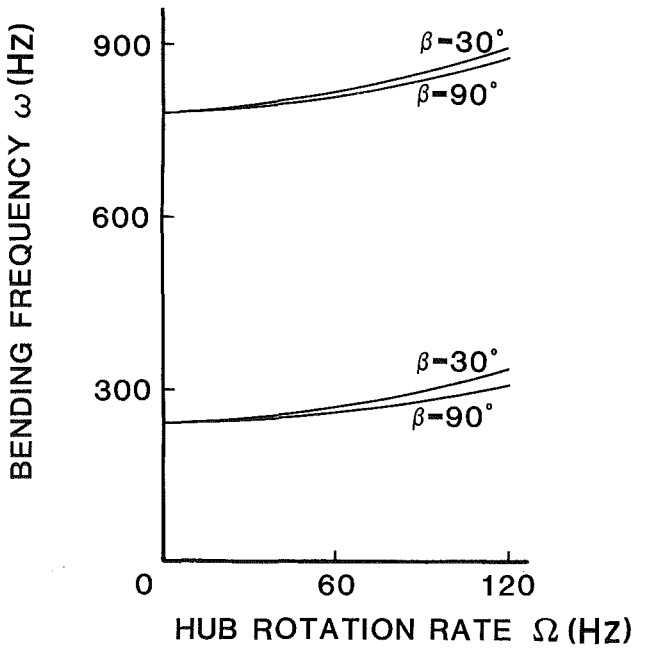


Fig. 4 First and second bending frequencies as a function of rotation rate for 30 deg and 90 deg mounting angles

Downloaded 03 May 2010 to 171.66.16.27. Redistribution subject to ASME license or copyright; see http://www.asme.org/terms/Terms_Use.cfm

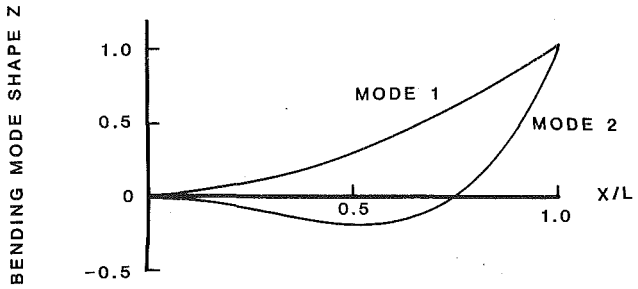


Fig. 5 Mode shapes for the first two bending modes

$$T_j = \left[\frac{(j+2)(j-1)+4(p/k)}{4j(j+1)}\right] T_{j-1},\ T_1 = 1 \tag{32}$$

$$T_j' = 4j\ T_j \tag{33}$$

where $k = 186$ rad/s, and the resulting graph of $Y(p/k)$ is shown in Fig. 3. $Y(-1+\Omega^2/k^2-p/k)$ is constructed by shifting the curve horizontally and reflecting about the vertical axis. The intersection points determine the values of p/k corresponding to the bending modes. The modal frequencies as a function of the mounting angle β are then determined by equation (11). Figure 4 shows the resulting frequencies for the first two bending modes as functions of rotation frequency for various mounting angles. Figure 5 shows the corresponding mode shapes which are virtually unchanged as the rotation rate varies from 0 to 372 rad/s (or approximately 3500 rpm). This calculation can be easily adapted for any suitable choice of parameters.

Conclusion

In this paper we have described a method for analytically finding the bending modes of a large family of variable cross-section rotating beams as described in equations (13)–(14). To implement the method, the function $Y(p/k)$ must be calculated by summing convergent series obtained by substituting the appropriate parameters into equations (29)–(30). The bending frequencies and mode shapes are found using a simple graphical technique and equations (11), (25), and (26). This method applies for beams mounted at any setting angle, and work aimed at extending this technique to other blade geometries is currently in progress.

References

Aboelnaga, Y. S., 1982, "Bending Vibrations of a Cantilever Beam on a Rotating Disc," M.S. Thesis, New Jersey Institute of Technology, Newark, N.J.

Abramowitz, M., and Stegun, I., 1965, *Handbook of Mathematical Functions*, Dover, New York, pp. 556–566.

Cranch, E. T., and Adler, A. A., 1955, "Bending Vibrations of Variable Section Beams," ASME JOURNAL OF APPLIED MECHANICS, Vol. 78, pp. 103–108.

Gere, J. M., and Lin, Y. K., 1958, "Coupled Vibrations of Thin-Walled Beams of Open Cross Section," ASME JOURNAL OF APPLIED MECHANICS, Vol. 80, pp. 373–378.

Krenk, S., 1983, "A Linear Theory for Pretwisted Elastic Beams," ASME JOURNAL OF APPLIED MECHANICS, Vol. 50, pp. 137–142.

Lo, H., Goldberg, J. E., and Bogdanoff, J. L., 1960, "Effect of Small Hub-Radius Change on Bending Frequencies of a Rotating Beam," ASME JOURNAL OF APPLIED MECHANICS, Vol. 82, pp. 548–551.

Schilhansl, M. J., 1958, "Bending Frequencies of a Rotating Cantilevered Beam," ASME JOURNAL OF APPLIED MECHANICS, Vol. 80, pp. 28–20.

Storti, D. W., and Aboelnaga, Y. S., 1986, "Beam Shapes which Allow Factorization of the Rotating Beam Equation," Applied Mathematics Technical Report 86-6, University of Washington, Seattle.

Wang, H. C., 1967, "Generalized Hypergeometric Function Solutions on the Transverse Vibration of a Class of Nonuniform Beams," ASME JOURNAL OF APPLIED MECHANICS, Vol. 89, pp. 702–708.

Wylie, C. R., and Barrett, L. C., 1982, *Advanced Engineering Mathematics*, McGraw-Hill, N.Y.

Downloaded 03 May 2010 to 171.66.16.27. Redistribution subject to ASME license or copyright; see http://www.asme.org/terms/Terms_Use.cfm

Large Amplitude Oscillations of Thin Circular Rings

S. P. Maganty

W. B. Bickford

Department of Mechanical and Aerospace Engineering, Arizona State University, Tempe, AZ 85287

Using an intrinsic formulation, an accurate set of geometrically nonlinear equations of motion is derived for the large amplitude oscillations of a thin circular ring. Nondimensionalization of the equations of motion and the compatibility conditions indicates clearly that certain terms involving the extensional deformation, the shear deformation, and the rotatory inertia are relatively small and can be discarded. The resulting equations of motion are analyzed by the method of multiple scales with a single bending mode approximation to the linear problems indicating a softening type of nonlinearity for both the in-plane and the out-of-plane problems with the out-of-plane flexural motion experiencing a greater degree of softening when compared to that of the in-plane flexural motion. The results for the nonresonant case indicate that the frequency of an out-of-plane bending mode is significantly reduced by the presence of a nonzero in-plane bending amplitude, whereas the results for the resonant case indicate the presence of unsteady oscillations with an exchange of energy between the in-plane and the out-of-plane modes.

Introduction

Large amplitude in-plane flexural motions of thin circular rings were analyzed for periodic motions by [1, 2, 7, 8, 10]. Evensen [1] specialized the shallow shell equations to the case of a circular ring and subsequently reduced the equations of motion to ordinary differential equations through a Galerkin procedure by assuming linear vibration modes. For periodic motions, the simple amplitude-frequency relation presented by Evensen [1] indicates a softening type of nonlinearity with the theoretical results for the correction to the linear frequency shown to be in good agreement with the experimental results for mode number $n=4$. Maewal [7] solved the equations of motion derived by Evensen [1] using an asymptotic analysis without going through the Galerkin procedure and indicated a correction to the amplitude-frequency relation obtained by Evensen.

Simmonds [10] derived a set of three nonlinear differential equations governing the large amplitude in-plane motions of a circular ring in terms of rotation and force resultant components rather than in terms of the displacement components as reported in the work of previous investigators. The effects of extensional strain, shearing strain, and rotatory inertia were included in the formulation and are shown to be of $0(n^2h^2/a^2)$ where n is the number of circumferential waves, h is the radial thickness of the ring, and a is the centroidal radius of the ring. The equations of motion obtained are shown to be considerably simpler than those that would result from an exact formulation in terms of the displacement components. The perturbation solution for periodic oscillations presented in [10] indicates discrepancies with Maewal's result even to the lowest order. For low values of n, the correction to the linear natural frequency differs substantially from that of Maewal's [7] and Evensen's [1] who used shallow shell type approximations in obtaining their results. Maewal and Nachbar [8] starting with an energy functional expressed in terms of the displacement components with quartic terms retained, arrived at the same amplitude – frequency relation for periodic motions as that obtained by Simmonds [10].

Ho, Scott, and Eisley [4] examined the large amplitude flexural motions in two perpendicular planes of a straight simply supported beam using the method of multiple scales. With a single bending mode approximation in each plane, the equations governing the amplitude and the phase modulations of both the resonant (internal resonance) and the nonresonant case indicate the presence of coupling between the two modes. Rogers and Warner [9] using the equations of motion presented by Love in [6] and neglecting the nonlinear curvature and inertia effects investigated the dynamic out-of-plane stability of a circular rod due to in-plane excitation and indicated that the out-of-plane motion may become unstable at a lower frequency of excitation than the in-plane motion.

In this paper, an accurate set of six equations of motion is derived for the general oscillations of a thin circular ring in terms of the dimensionless axial froce F_T, the in-plane shearing force F_N, the in-plane flexural rotation α, the out-of-plane shearing force F_B, the out-of-plane flexural rotation ψ, and the torsional rotation ϕ. The effects of extensional strain, shearing strains, and rotatory inertia are included. Subsequent nondimensionalization of the equations of motion and of the compatibility conditions indicates clearly that certain terms involving the extensional deformation, the shear deformation, and the rotatory inertia are of higher order and can be neglected. The method of multiple scales is used to analyze

Contributed by the Applied Mechanics Division for publication in the JOURNAL OF APPLIED MECHANICS.
Discussion on this paper should be addressed to the Editorial Department, ASME, United Engineering Center, 345 East 47th Street, New York, N.Y. 10017, and will be accepted until two months after final publication of the paper itself in the JOURNAL OF APPLIED MECHANICS. Manuscript received by ASME Applied Mechanics Division, June 23, 1986; final revision, October 20, 1986.

Copyright © 1987 by ASME
Downloaded 03 May 2010 to 171.66.16.27. Redistribution subject to ASME license or copyright; see http://www.asme.org/terms/Terms_Use.cfm

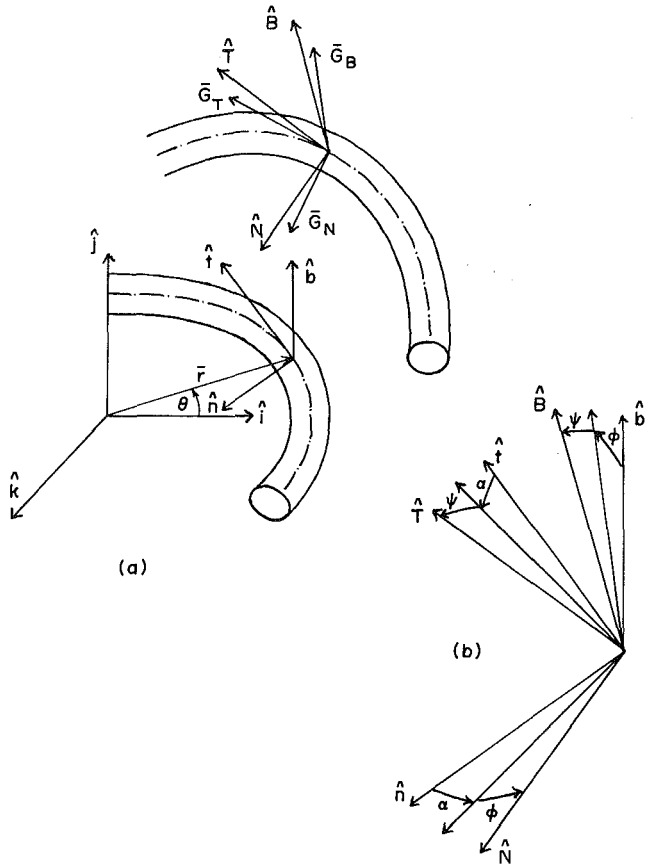


Fig. 1 (a) Geometry of the undeformed and the deformed ring segment; (b) the three Euler angle rotations

nonresonant and resonant free oscillations. The first order differential equations for obtaining the amplitude and phase modulations are presented and indicate the presence of coupling between the in-plane flexural mode and the out-of-plane flexural mode for both the nonresonant and the resonant motions. For the nonresonant case of a circular cross-section ring, the result for the correction $\Delta\omega_m$ to the linear out-of-plane natural frequency with zero initial condition on the in-plane flexural rotation α, can be specialized to

$$\Delta\omega_m = -(\beta a_{D0})^2 m[25.86m^{18} + 56.24m^{16} - 68.93m^{14} - 383.02m^{12} - 707.60m^{10} - 81.05m^8 + 408.66m^6 + 224.03m^4 + 59.41m^2 - 1.65]/\{56.13(m^2-1)(0.769m^2+1)^{7/2}[9.23m^6 + 15.23m^4 - 8.77m^2 + 0.23]\} \quad (1)$$

where a_{D0} is the initial amplitude of the out-of-plane bending rotation ψ, m is the wave number associated with the out-of-plane mode, and β is the perturbation parameter which can be set to unity for small amplitudes of oscillation.

Finally, numerical studies are carried out to determine the effect of the initial out-of-plane and in-plane amplitudes on the linear in-plane and out-of-plane frequencies, respectively. Also, the coupling between the in-plane and the out-of-plane motions under resonance conditions is investigated numerically.

Equations of Motion

With reference to Fig. 1(*a*), let $\hat{n}$, $\hat{b}$, and $\hat{t}$ denote the unit normal, binormal, and tangent vectors to the centerline of the undeformed ring. The position vector of a particle on the undeformed centerline is

$$\bar{r}(\theta) = a(\cos\theta\hat{i} + \sin\theta\hat{j}) = -a\hat{n}. \quad (2)$$

The tangent vector could be expressed as

$$\hat{r}'(\theta) = a(-\sin\theta\hat{i} + \cos\theta\hat{j}) = a\hat{t} \quad (3)$$

where $(\,)' \equiv \dfrac{\partial}{\partial\theta}$.

Assume the deformation process to carry the undeformed frame ($\hat{t}$, $\hat{n}$, $\hat{b}$) into the deformed frame ($\bar{G}_T$, $\bar{G}_N$, $\bar{G}_B$) which could be constructed as follows. First, the frame ($\hat{t}$, $\hat{n}$, $\hat{b}$) is rigidly rotated through three successive Euler angle rotations α, ϕ, and ψ as shown in Fig. 1(*b*) about $\hat{b}$, $\hat{t}^1$, and $\hat{n}^2$, respectively, where $\hat{t}^1$ is the new position of $\hat{t}$ after the first rotation α about $\hat{b}$, while $\hat{n}^2$ is the final position of $\hat{n}$ after two successive rotations α and ϕ about $\hat{b}$ and $\hat{t}^1$. This intermediate frame is shown in Fig. 1(*a*) as $\hat{T}$, $\hat{N}$, $\hat{B}$. Next, the frame $\hat{T}$, $\hat{N}$, $\hat{B}$ is given an additional rigid body rotation representing the shearing strains γ_i and γ_o (see [5] for more details) bringing the vectors $\hat{N}$ and $\hat{B}$ into coincidence with $\bar{G}_N$ and $\bar{G}_B$, respectively. Finally, stretching of the $\hat{T}$ axis corresponding to the extensional strain Γ brings $\hat{T}$ into coincidence with $\bar{G}_T$. Hence, the tangent to the deformed centerline for small strains is given as

$$\bar{R}'(\theta,t) = a[(1+\Gamma)\hat{T} + \gamma_i\hat{N} - \gamma_o\hat{B}] \quad (4)$$

where

$$\hat{T} = +(\cos\alpha\cos\psi - \sin\alpha\sin\phi\sin\psi)\hat{t} + (\sin\alpha\cos\psi + \cos\alpha\sin\phi\sin\psi)\hat{n} - (\cos\phi\sin\psi)\hat{b} \quad (5a)$$

$$\hat{N} = -(\sin\alpha\cos\phi)\hat{t} + (\cos\alpha\cos\phi)\hat{n} + (\sin\phi)\hat{b} \quad (5b)$$

$$\hat{B} = +(\cos\alpha\sin\psi + \sin\alpha\sin\phi\cos\psi)\hat{t} + (\sin\alpha\sin\psi - \cos\alpha\sin\phi\cos\psi)\hat{n} + (\cos\phi\cos\psi)\hat{b}. \quad (5c)$$

For the complete ring to suffer no dislocation,

$$\int_o^{2\pi} \bar{R}'\,d\theta = a\int_o^{2\pi} [(1+\Gamma)\hat{T} + \gamma_i\hat{N} - \gamma_o\hat{B}]d\theta = 0 \quad (6)$$

Substituting for $\hat{T}$, $\hat{N}$, $\hat{B}$ in terms of $\hat{i}$, $\hat{j}$, $\hat{k}$ from equations (2), (3), (5) into equation (6), results in the following compatibility conditions.

$$\int_o^{2\pi} [(1+\Gamma)(-\sin\theta\cos\alpha\cos\psi + \sin\theta\sin\alpha\sin\phi\sin\psi - \cos\theta\sin\alpha\cos\psi - \cos\theta\cos\alpha\sin\phi\sin\psi) + \gamma_i(\sin\theta\sin\alpha\cos\phi - \cos\theta\cos\alpha\cos\phi) + \gamma_o(\sin\theta\cos\alpha\sin\psi + \sin\theta\sin\alpha\sin\phi\cos\psi + \cos\theta\sin\alpha\sin\psi - \cos\theta\cos\alpha\sin\phi\cos\psi)]d\theta = 0 \quad (7a)$$

$$\int_o^{2\pi} [(1+\Gamma)(\cos\theta\cos\alpha\cos\psi - \cos\theta\sin\alpha\sin\phi\sin\psi - \sin\theta\sin\alpha\cos\psi - \sin\theta\cos\alpha\sin\phi\sin\psi) - \gamma_i(\cos\theta\sin\alpha\cos\phi + \sin\theta\cos\alpha\cos\phi) + \gamma_o(-\cos\theta\cos\alpha\sin\psi - \cos\theta\sin\alpha\sin\phi\cos\psi + \sin\theta\sin\alpha\sin\psi - \sin\theta\cos\alpha\sin\phi\cos\psi)]d\theta = 0 \quad (7b)$$

$$\int_o^{2\pi} [-(1+\Gamma)\cos\phi\sin\psi + \gamma_i\sin\phi - \gamma_o\cos\phi\cos\psi]d\theta = 0 \quad (7c)$$

The equations of motion (49) and (50) of [11] with the effects of rotatory inertia restored from equation (20) of [11] become

$$\bar{F}' = ma\ddot{\bar{R}} \quad (8a)$$

$$\bar{M}' + \bar{R}' \times \bar{F} = \dot{\bar{H}} \quad (8b)$$

where

$$\bar{F} = F_T\hat{T} + F_N\hat{N} + F_B\hat{B} \quad (9a)$$

and

Downloaded 03 May 2010 to 171.66.16.27. Redistribution subject to ASME license or copyright; see http://www.asme.org/terms/Terms_Use.cfm

$$\bar{M}=M_T\hat{T}+M_N\hat{N}+M_B\hat{B} \tag{9b}$$

are, respectively, the force and moment resultants acting over the cross section, m is the mass per length of the undeformed ring, and $\dot{(\ )}\equiv\partial/\partial t$. $\bar{H}$ is the angular momentum vector expressed as

$$\bar{H}=I_T\omega_T\hat{T}+I_N\omega_N\hat{N}+I_B\omega_B\hat{B} \tag{10}$$

where ω_T, ω_N, and ω_B are the components of the angular velocity vector $\bar{\omega}$ of the $(\hat{T}, \hat{N}, \hat{B})$ frame and I_T, I_N, and I_B are the principal mass moments of inertia. In terms of the time derivatives of the kinematical variables α, ϕ, and ψ the angular velocity $\bar{\omega}$ can be readily obtained from the coordinate transformation rules, resulting in the following expressions.

$$\omega_T=-\dot{\alpha}\cos\phi\sin\psi+\dot{\phi}\cos\psi \tag{11a}$$

$$\omega_N=\dot{\alpha}\sin\phi+\dot{\psi} \tag{11b}$$

$$\omega_B=\dot{\alpha}\cos\phi\cos\psi+\dot{\phi}\sin\psi \tag{11c}$$

In order to obtain six scalar equations of motion from equations (8), the following differentiation formulas are needed.

$$\hat{T}'=+[\phi'\sin\psi+(1+\alpha')\cos\phi\cos\psi]\hat{N}-[\psi'+(1+\alpha')\sin\phi]\hat{B} \tag{12a}$$

$$\hat{N}'=+[-\phi'\sin\psi-(1+\alpha')\cos\phi\cos\psi]\hat{T}+[\phi'\cos\psi-(1+\alpha')\cos\phi\sin\psi]\hat{B} \tag{12b}$$

$$\hat{B}'=+[\psi'+(1+\alpha')\sin\phi]\hat{T}+[-\phi'\cos\psi+(1+\alpha')\cos\phi\sin\psi]\hat{N} \tag{12c}$$

$$\begin{aligned}\bar{T}''=&-[\psi'^2+2\psi'(1+\alpha')\sin\phi+\phi'^2\sin^2\psi\\&+(1+\alpha')^2\sin^2\phi+2\phi'(1+\alpha')\cos\phi\sin\psi\cos\psi\\&+(1+\alpha')^2\cos^2\phi\cos^2\psi]\hat{T}\\&+[\phi''\sin\psi+2\phi'\psi'\cos\psi-2\psi'(1+\alpha')\cos\phi\sin\psi\\&-(1+\alpha')^2\sin\phi\cos\phi\sin\psi+\alpha''\cos\phi\cos\psi]\hat{N}\\&+[\phi'^2\sin\psi\cos\psi+\phi'(1+\alpha')\cos\phi\cos2\psi\\&-\psi''-(1+\alpha')^2\cos^2\phi\sin\psi\cos\psi\\&-\phi'(1+\alpha')\cos\phi-\alpha''\sin\phi]\hat{B}\end{aligned} \tag{12d}$$

$$\begin{aligned}\hat{N}''=&[-\phi''\sin\psi+2\phi'(1+\alpha')\sin\phi\cos\psi\\&-\alpha''\cos\phi\cos\psi-(1+\alpha')^2\sin\phi\cos\phi\sin\psi]\hat{T}\\&+[-\phi'^2-(1+\alpha')^2\cos^2\phi]\hat{N}\\&+[2\phi'(1+\alpha')\sin\phi\sin\psi+\phi''\cos\psi\\&-\alpha''\cos\phi\sin\psi+(1+\alpha')^2\sin\phi\cos\phi\cos\psi]\hat{B}\end{aligned} \tag{12e}$$

$$\begin{aligned}\hat{B}''=&[\phi'^2\sin\psi\cos\psi+\phi'(1+\alpha')\cos\phi\cos2\psi\\&+\psi''+\alpha''\sin\phi+\phi'(1+\alpha')\cos\phi\\&-(1+\alpha')^2\cos^2\phi\sin\psi\cos\psi]\hat{T}\\&+[-\phi''\cos\psi+2\phi'\psi'\sin\psi+\alpha''\cos\phi\sin\psi\\&+2\psi'(1+\alpha')\cos\phi\cos\psi\\&+(1+\alpha')^2\sin\phi\cos\phi\cos\psi]\hat{N}\\&+[-\phi'^2\cos^2\psi+2\phi'(1+\alpha')\cos\phi\sin\psi\cos\psi\\&-\psi'^2-2\psi'(1+\alpha')\sin\phi-(1+\alpha')^2\sin^2\phi\\&-(1+\alpha')^2\cos^2\phi\sin^2\psi]\hat{B}\end{aligned} \tag{12f}$$

Time derivatives of $\hat{T}$, $\hat{N}$, $\hat{B}$ can be readily obtained from equations (12) by replacing the space derivatives with time derivatives. Also, $\dot{\alpha}$ is substituted for $1+\dot{\alpha}$ since $\dot{t}=\dot{n}=0$. To present the equations of motion in terms of α, ϕ, ψ, F_T, F_N, and F_B the constitutive relations are assumed in the following form.

$$F_T=AE\Gamma \qquad F_N=AG\gamma_i \qquad F_B=AG\gamma_o \tag{13a}$$

$$M_T=GJ_T\kappa_T \qquad M_N=EJ_N\kappa_N \qquad M_B=EJ_B(\kappa_B-\kappa_o) \tag{13b}$$

where E – Young's Modulus, G – shear Modulus, A – area of cross-section, J_T – torsional constant, J_N, J_B are the area moments of inertia about the $\hat{n}$ and $\hat{b}$ axes, respectively, while κ_T, κ_N, and κ_B are the curvature components along $\hat{T}$, $\hat{N}$, and $\hat{B}$, respectively, and $\kappa_o=1/a$.

By making use of Kirchhoff's kinetic analogy [3],

$$\kappa_T=\frac{1}{a}[-(1+\alpha')\cos\phi\sin\psi+\phi'\cos\psi] \tag{14a}$$

$$\kappa_N=\frac{1}{a}[(1+\alpha')\sin\phi+\psi'] \tag{14b}$$

$$\kappa_B=\frac{1}{a}[(1+\alpha')\cos\phi\cos\psi+\phi'\sin\psi] \tag{14c}$$

Finally, using equations (4), (8–14) and the indicated time derivatives of $\hat{T}$, $\hat{N}$, and $\hat{B}$, the six scalar equations of motion can be obtained. The following dimensionless variables are defined.

$$\begin{aligned}(F_T,F_N,F_B)&=\left(\frac{EJ_B}{a^2}\right)(\tilde{F}_T,\tilde{F}_N,\tilde{F}_B)\\(k_T,k_N,k_B)&=h(\tilde{k}_T,\tilde{k}_N,\tilde{k}_B)\\\epsilon&=\frac{h}{a},\quad t=\frac{\tilde{t}}{(EJ_B/ma^4)^{1/2}}\\\delta_1&=k_T^2/k_B^2,\quad \delta_2=k_N^2/k_B^2,\quad \delta_3=G/E\end{aligned} \tag{15}$$

where k_T, k_N, k_B are, respectively, the radii of gyration for the second moments of area about the $\hat{T}$, $\hat{N}$, and $\hat{B}$ axes. In what follows, $\dot{(\ )}$ will represent $\partial/\partial\tilde{t}$ and the tildes will be dropped. After discarding terms of order $0(n^2h^2/a^2)$, $0(m^2h^2/a^2)$ or $0(nmh^2/a^2)$, where n and m are the circumferential wave numbers, the equations of motion in nondimensionalized form can be written as:

Force equation along $\hat{T}$.

$$\begin{aligned}&F_T''+2F_N'[-\phi'\sin\psi-(1+\alpha')\cos\phi\cos\psi]+2F_B'[\psi'\\&+(1+\alpha')\sin\phi]+F_T[-\phi'^2\sin^2\psi-2\phi'(1+\alpha')\cos\phi\\&\sin\psi\cos\psi-\psi'^2-2\psi'(1+\alpha')\sin\phi-(1+\alpha')^2\cos^2\phi\\&\cos^2\psi-(1+\alpha')^2\sin^2\phi]+F_N[-\phi''\sin\psi+2\phi'(1\\&+\alpha')\sin\phi\cos\psi-\alpha''\cos\phi\cos\psi-(1+\alpha')^2\sin\phi\cos\phi\\&\sin\psi]+F_B[\phi'^2\sin\psi\cos\psi+\phi'(1+\alpha')\cos\phi\cos2\psi\\&+\psi''+\alpha''\sin\phi+\phi'(1+\alpha')\cos\phi\\&-(1+\alpha')^2\cos^2\phi\sin\psi\cos\psi]\\&=[-2\dot{\alpha}\dot{\phi}\cos\phi\sin\psi\cos\psi-\dot{\alpha}^2\sin^2\phi-\dot{\alpha}^2\cos^2\phi\cos^2\psi\\&-\dot{\phi}^2\sin^2\psi-\dot{\psi}^2-2\dot{\alpha}\dot{\psi}\sin\phi]\end{aligned} \tag{16a}$$

Force equation along $\hat{N}$

$$\begin{aligned}&F_N''+2F_T'[\phi'\sin\psi+(1+\alpha')\cos\phi\cos\psi]+2F_B'[-\phi'\cos\psi\\&+(1+\alpha')\cos\phi\sin\psi]+F_T[\phi''\sin\psi+2\phi'\psi'\cos\psi\\&-2\psi'(1+\alpha')\cos\phi\sin\psi-(1+\alpha')^2\sin\phi\cos\phi\sin\psi\\&+\alpha''\cos\phi\cos\psi]+F_N[-\phi'^2-(1+\alpha')^2\cos^2\phi]\\&+F_B[-\phi''\cos\psi+2\phi'\psi'\sin\psi+2\psi'(1+\alpha')\cos\phi\cos\psi\\&+\alpha''\cos\phi\sin\psi+(1+\alpha')^2\sin\phi\cos\phi\cos\psi]\\&=[\ddot{\alpha}\cos\phi\cos\psi-2\dot{\alpha}\dot{\psi}\cos\phi\sin\psi+\ddot{\phi}\sin\psi+2\dot{\phi}\dot{\psi}\cos\psi\\&-\dot{\alpha}^2\sin\phi\cos\phi\sin\psi]\end{aligned} \tag{16b}$$

Force equation along $\hat{B}$

$$\begin{aligned}&F_B''+2F_T'[-\psi'-(1+\alpha')\sin\phi]+2F_N'[\phi'\cos\psi\\&-(1+\alpha')\cos\phi\sin\psi]+F_T[\phi'^2\sin\psi\cos\psi+\phi'(1\\&+\alpha')\cos\phi\cos2\psi-\psi''-(1+\alpha')^2\cos^2\phi\sin\psi\cos\psi\end{aligned}$$

Downloaded 03 May 2010 to 171.66.16.27. Redistribution subject to ASME license or copyright; see http://www.asme.org/terms/Terms_Use.cfm

$$-\phi'(1+\alpha')\cos\phi-\alpha''\sin\phi]+F_N[2\phi'(1+\alpha')\sin\phi\sin\psi+\phi''\cos\psi-\alpha''\cos\phi\sin\psi+(1+\alpha')^2\sin\phi\cos\phi\cos\psi]+F_B[-\phi'^2\cos^2\psi+2\phi'(1+\alpha')\cos\phi\sin\psi\cos\psi-\psi'^2-2\psi'(1+\alpha')\sin\phi-(1+\alpha')^2\sin^2\phi-(1+\alpha')^2\cos^2\phi\sin^2\psi]$$
$$=[-\dot\alpha^2\cos^2\phi\sin\psi\cos\psi-\ddot\psi-\ddot\alpha\sin\phi+\dot\alpha\dot\phi\cos\phi\cos2\psi+\dot\phi^2\sin\psi\cos\psi-\dot\alpha\dot\phi\cos\phi] \quad (16c)$$

Moment equation along $\hat{T}$.

$$\delta_1\delta_3[-\alpha''\cos\phi\sin\psi+\phi'(1+\alpha')\sin\phi\sin\psi-\psi'(1+\alpha')\cos\phi\cos\psi+\phi''\cos\psi-\phi'\psi'\sin\psi]+\delta_2[-\phi'(1+\alpha')\sin\phi\sin\psi-(1+\alpha')^2\sin\phi\cos\phi\cos\psi-\phi'\psi'\sin\psi-\psi'(1+\alpha')\cos\phi\cos\psi]+[\psi'(1+\alpha')\cos\phi\cos\psi+(1+\alpha')^2\sin\phi\cos\phi\cos\psi+\phi'\psi'\sin\psi+\phi'(1+\alpha')\sin\phi\sin\psi-\psi'-(1+\alpha')\sin\phi]=0 \quad (16d)$$

Moment equation along $\hat{N}$

$$\delta_2[\alpha''\sin\phi+\phi'(1+\alpha')\cos\phi+\psi'']+\delta_1\delta_3[-\phi'(1+\alpha')\cos\phi\sin^2\psi-(1+\alpha')^2\cos^2\phi\sin\psi\cos\psi+\phi'^2\sin\psi\cos\psi+\phi'(1+\alpha')\cos\phi\cos^2\psi]+[-\phi'(1+\alpha')\cos\phi\cos^2\psi+(1+\alpha')^2\cos^2\phi\sin\psi\cos\psi-\phi'^2\sin\psi\cos\psi+\phi'(1+\alpha')\cos\phi\sin^2\psi+\phi'\cos\psi-(1+\alpha')\cos\phi\sin\psi]-F_B=0 \quad (16e)$$

Moment equation along $\hat{B}$

$$[\alpha''\cos\phi\cos\psi-\phi'(1+\alpha')\sin\phi\cos\psi-\psi'(1+\alpha')\cos\phi\sin\psi+\phi''\sin\psi+\phi'\psi'\cos\psi]+\delta_1\delta_3[\psi'(1+\alpha')\cos\phi\sin\psi+(1+\alpha')^2\sin\phi\cos\phi\sin\psi-\phi'\psi'\cos\psi-\phi'(1+\alpha')\sin\phi\cos\psi]+\delta_2[\phi'(1+\alpha')\sin\phi\cos\psi-(1+\alpha')^2\sin\phi\cos\phi\sin\psi+\phi'\psi'\cos\psi-\psi'(1+\alpha')\cos\phi\sin\psi]+F_N=0 \quad (16f)$$

The terms which have been discarded from equations (16) are associated with the extensional deformation, the shear deformation, and the rotatory inertia. Additionally, as was pointed out in [10] the purely radial mode of oscillation has been eliminated as a result of discarding the higher order terms.

Similarly, expressing equations (7*a–c*) in terms of the dimensionless variables F_T, F_N, and F_B and discarding terms of relative order ϵ^2 results in the following reduced compatibility equations.

$$\int_o^{2\pi}[-\sin\theta\cos\alpha\cos\psi+\sin\theta\sin\alpha\sin\phi\sin\psi-\cos\theta\sin\alpha\cos\psi-\cos\theta\cos\alpha\sin\phi\sin\psi]d\theta=0 \quad (17a)$$

$$\int_o^{2\pi}[\cos\theta\cos\alpha\cos\psi-\cos\theta\sin\alpha\sin\phi\sin\psi-\sin\theta\sin\alpha\cos\psi-\sin\theta\cos\alpha\sin\phi\sin\psi]d\theta=0 \quad (17b)$$

$$\int_o^{2\pi}[-\cos\phi\sin\psi]d\theta=0 \quad (17c)$$

Perturbation Solution

For small, but finite amplitudes of oscillation of order β (perturbation parameter), an approximate solution to the equations of motion is obtained by the method of multiple scales. To this end, one fast scale $T_o=t$ and two slow scales $T_1=\beta t$ and $T_2=\beta^2 t$ are defined. F_T, α, ϕ, ψ are assumed to take the following forms.

$$F_T=\beta F_{T1}(\theta,T_0,T_1,T_2)+\beta^2F_{T2}(\theta,T_0,T_1,T_2)+\beta^3F_{T3}(\theta,T_0,T_1,T_2)+\ \ldots \quad (18a)$$

$$\alpha=\beta\alpha_1(\theta,T_0,T_1,T_2)+\beta^2\alpha_2(\theta,T_0,T_1,T_2)+\beta^3\alpha_3(\theta,T_0,T_1,T_2)+\ \ldots \quad (18b)$$

$$\phi=\beta\phi_1(\theta,T_0,T_1,T_2)+\beta^2\phi_2(\theta,T_0,T_1,T_2)+\beta^3\phi_3(\theta,T_0,T_1,T_2)+\ \ldots \quad (18c)$$

$$\psi=\beta\psi_1(\theta,T_0,T_1,T_2)+\beta^2\psi_2(\theta,T_0,T_1,T_2)+\beta^3\psi_3(\theta,T_0,T_1,T_2)+\ \ldots \quad (18d)$$

Partial derivatives with respect to t are transformed according to

$$\frac{\partial}{\partial t}=D_0+\beta D_1+\beta^2D_2+\ \ldots$$

$$\frac{\partial^2}{\partial t^2}=D_0^2+2\beta D_0D_1+\beta^2(D_2+2D_0D_2)+\ \ldots$$

where

$$D_n=\frac{\partial}{\partial T_n},\quad n=0,\ 1,\ 2,\ \ldots$$

Substituting (18) into (16) and (17), the following sets of equations result when F_N and F_B are eliminated and the coefficients of equal powers of β are equated.

Order β

$$F_{T1}''-F_{T1}+2\alpha_1'''=0 \quad (19a)$$

$$2F_{T1}'-\alpha_1^{IV}+\alpha_1''-D_0^2\alpha_1=0 \quad (19b)$$

$$(\delta_2+\delta_1\delta_3)\phi_1'''+\delta_2\psi_1^{IV}-\delta_1\delta_3\psi_3''+D_0^2\psi_1=0 \quad (19c)$$

$$\delta_1\delta_3\phi_1''-\delta_2\phi_1-(\delta_2+\delta_1\delta_3)\psi_1'=0 \quad (19d)$$

$$\int_o^{2\pi}-\alpha_1\sin\theta d\theta=0;\ \int_o^{2\pi}\alpha_1\cos\theta d\theta=0;\ \int_o^{2\pi}-\psi_1 d\theta=0 \quad (19e,f,g)$$

Order β^2

$$F_{T2}''-F_{T2}+2\alpha_2'''=$$
$$+\underline{\phi_1''\phi_1}(-4\delta_2+2)+\underline{\phi_1'\phi_1'}(-4\delta_2+2)+\underline{\psi_1'\psi_1'}(2\delta_2+2)$$
$$-2\underline{\phi_1'''\psi_1}+\underline{\phi_1''\psi_1'}(-4\delta_2-4)+\underline{\psi_1''\psi_1}(3\delta_2-\delta_1\delta_3+2)$$
$$+\underline{\phi_1'\psi_1''}(-5\delta_2+\delta_1\delta_3-2)+\underline{\phi_1'\psi_1}(3\delta_2+\delta_1\delta_3)$$
$$+\underline{\phi_1\psi_1'}(2\delta_2)-2\alpha_1'\alpha_1'''-2\delta_2\underline{\psi_1'''\phi_1}-2\delta_2\underline{\psi_1'''\psi_1'}$$
$$+2F_{T1}\alpha_1'-\alpha_1''\alpha_1''-\delta_1\delta_3\underline{\psi_1\psi_1}-\delta_2\underline{\psi_1''\psi_1''}$$
$$-D_0\alpha_1D_0\alpha_1-\underline{D_0\psi_1D_0\psi_1} \quad (20a)$$

$$2F_{T2}'-\alpha_2^{IV}+\alpha_2''-D_0^2\alpha_2=$$
$$+\underline{\phi_1'''\phi_1}(\delta_2-\delta_1\delta_3-1)+\underline{\phi_1''\phi_1'}(6\delta_2-3)$$
$$+\underline{\psi_1'''\psi_1}(-3\delta_2+\delta_1\delta_3-1)+\underline{\psi_1''\psi_1'}(-5\delta_2+3\delta_1\delta_3-3)$$
$$+\underline{\phi_1^{IV}\psi_1}+\underline{\phi_1'''\psi_1'}(\delta_2-\delta_1\delta_3+3)$$
$$+\underline{\phi_1''\psi_1''}(3\delta_2-2\delta_1\delta_3+3)+\underline{\psi_1'''\phi_1'}(3\delta_2-\delta_1\delta_3+1)$$
$$+\underline{\phi_1''\psi_1}(-3\delta_2-2\delta_1\delta_3-1)+\underline{\phi_1'\psi_1'}(-5\delta_2-\delta_1\delta_3-1)$$
$$+\underline{\phi_1\psi_1''}(-2\delta_2+\delta_1\delta_3)-2F_{T1}'\alpha_1'$$
$$+\underline{\psi_1'\psi_1}(3\delta_1\delta_3+\delta_2+1)-\alpha_1''F_{T1}$$

Downloaded 03 May 2010 to 171.66.16.27. Redistribution subject to ASME license or copyright; see http://www.asme.org/terms/Terms_Use.cfm

$$+\underline{\phi_1'\phi_1}(-2\delta_2+1)+\underline{\phi_1\psi_1}(\delta_2)-2\alpha_1'\alpha_1''$$
$$+2D_0D_1\alpha_1+\underline{\psi_1 D_0{}^2\phi_1}+2\underline{(D_0\phi_1)D_0\psi_1)} \tag{20b}$$

$$(\delta_2+\delta_1\delta_3)\phi_2'''+\delta_2\psi_2{}^{IV}-\delta_1\delta_3\psi_2''+D_0{}^2\psi_2=$$
$$-\delta_2\alpha_1{}^{IV}\phi_1+\alpha_1'''\phi_1'(-\delta_1\delta_3-3\delta_2+3)$$
$$+\alpha_1''\phi_1''(-2\delta_1\delta_3-3\delta_2+3)+\alpha_1'\phi_1'''(-\delta_1\delta_3-\delta_2+1)$$
$$+\alpha_1'''\psi_1(2\delta_1\delta_3-3)+\alpha_1''\psi_1'(4\delta_1\delta_3-2)$$
$$+\alpha_1'\psi_1''(2\delta_1\delta_3-1)+2F_{T1}'\psi_1'+2F_{T1}'\phi_1$$
$$+F_{T1}\psi_1''+F_{T1}\psi_1+\alpha_1''\phi_1-2D_0D_1\psi_1-\phi_1D_0{}^2\alpha_1 \tag{20c}$$

$$\delta_1\delta_3\phi_2''-\delta_2\phi_2-(\delta_1\delta_3+\delta_2)\psi_2'=$$
$$\delta_1\delta_3\alpha_1''\psi_1+\alpha_1'\psi_1'(\delta_1\delta_3+\delta_2-1)+\alpha_1'\phi_1(2\delta_2-1) \tag{20d}$$

$$\int_o^{2\pi}\left[-\left(\frac{\alpha_1{}^2+\psi_1{}^2}{2}\right)\cos\theta-\alpha_2\sin\theta-\phi_1\psi_1\sin\theta\right]d\theta=0 \tag{20e}$$

$$\int_o^{2\pi}\left[-\left(\frac{\alpha_1{}^2+\psi_1{}^2}{2}\right)\sin\theta+\alpha_2\cos\theta+\phi_1\psi_1\cos\theta\right]d\theta=0 \tag{20f}$$

$$\int_o^{2\pi}[-\psi_2]d\theta=0 \tag{20g}$$

The equations at order β^3 are extremely lengthy and are not presented here.

Examining the terms in the order β^2 problem indicates that the large amplitude in-plane oscillations can exist independently without exciting the out-of-plane motion where as the large amplitude out-of-plane oscillations are necessarily accompanied by in-plane motions as indicated by the underlined terms in (20*a*, *b*). This result is expected in view of the fact that for a thin circular ring undergoing large amplitude out-of-plane motions, the in-plane motions are practically unavoidable in a situation where the extensional strains are small.

Assuming n and m to represent the mode numbers of the dominant modes in the in-plane and the out-of-plane motions, respectively, the solution to the order β problem can be written as follows.

$$F_{T1}=[A(T_1,T_2)e^{i\omega_nT_o}+cc]\cos n\theta \tag{21a}$$
$$\alpha_1=[B(T_1,T_2)e^{i\omega_nT_o}+cc]\sin n\theta \tag{21b}$$
$$\phi_1=[C(T_1,T_2)e^{i\omega_mT_o}+cc]\cos m\theta \tag{21c}$$
$$\psi_1=[D(T_1,T_2)e^{i\omega_mT_o}+cc]\sin m\theta \tag{21d}$$

where cc represents the corresponding complex conjugate terms. As is usual in the method of multiple scales, the dependence of the complex quantities A, B, C, and D on T_1 and T_2 is determined at higher levels of approximation and also homogeneous solutions at all higher orders are taken to be zero. Let ω_n and ω_m denote the linear natural frequencies of the nth in-plane and the mth out-of-plane modes, respectively. Then, from equations (19) and (21), it follows that

$$\omega_n^2=\frac{n^2(n^2-1)^2}{(1+n^2)};\qquad \frac{A}{B}=-\frac{2n^3}{1+n^2};$$
$$n=2,3,\ldots \tag{22a}$$

$$\omega_m^2=\frac{\delta_1\delta_2\delta_3m^2(m^2-1)^2}{\delta_2+m^2\delta_1\delta_3};\qquad \frac{C}{D}=-\frac{(\delta_2+\delta_1\delta_3)m}{\delta_2+m^2\delta_1\delta_3};$$
$$m=2,3,\ldots \tag{22b}$$

Note that, the $n=0$ case is excluded because purely radial motions are neglected, while the $n=1$ condition is excluded by (19*e*). Similarly, the $m=0$ and $m=1$ cases are dropped since they represent a purely torsional and a rigid body motion, respectively. As expected, the expressions for the linear natural frequencies coincide with those given by Love [6].

For rings with circular cross-section, $\delta_1=2$; $\delta_2=1$; $\delta_3=1/[2(1+\nu)]$ where ν is Poisson's ratio. Equations (22) indicate that $\omega_n\approx\omega_m$ for $n=m=2,3\ldots$ Hence, in what follows nonresonant ($\omega_n\neq\omega_m$) and resonant ($\omega_n\approx\omega_m$) motions are treated separately.

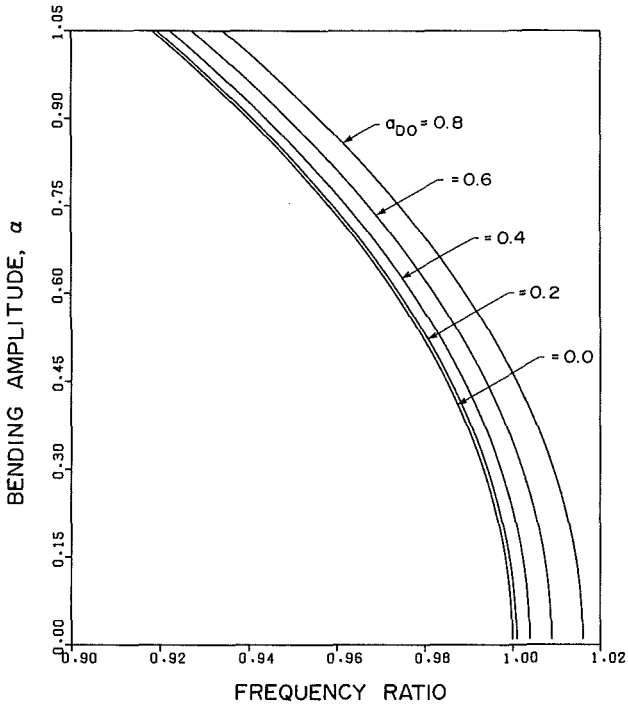


Fig. 2 In-plane amplitude-frequency curves for $n=2$ and $m=3$

Case a: Nonresonant Motions ($\omega_n\neq\omega_m$ and $n\neq m$). Substituting the solution to the order β problem given by equations (21) into equations (20), the following solvability conditions at order β^2 are obtained.

$$\frac{\partial B}{\partial T_1}=0,\qquad \frac{\partial D}{\partial T_1}=0 \tag{23a,b}$$

The solution to the order β^2 problem may then be written as

$$F_{T2}=D\bar{D}G_1+B\bar{B}G_2+D\bar{D}G_3\cos2m\theta+B\bar{B}G_4\cos2n\theta$$
$$+DDG_5e^{2i\omega_mT_o}+BBG_6e^{2i\omega_nT_o}+DDG_7e^{2i\omega_mT_o}\cos2m\theta$$
$$+BBG_8e^{2i\omega_nT_o}\cos2n\theta+cc \tag{24a}$$

$$\alpha_2=D\bar{D}H_1\sin2m\theta+B\bar{B}H_2\sin2n\theta+DDH_3e^{2i\omega_mT_o}\sin2m\theta$$
$$+BBH_4e^{2i\omega_nT_o}\sin2n\theta+cc \tag{24b}$$

$$\psi_2=BDJ_1e^{i(\omega_n+\omega_m)T_o}\sin(n+m)\theta+BDJ_2e^{i(\omega_n+\omega_m)T_o}\sin(n-m)\theta$$
$$+B\bar{D}J_3e^{i(\omega_n-\omega_m)T_o}\sin(n+m)\theta$$
$$+B\bar{D}J_4e^{i(\omega_n-\omega_m)T_o}\sin(n-m)\theta+cc \tag{24c}$$

$$\phi_2=BDI_1e^{i(\omega_n+\omega_m)T_o}\cos(n+m)\theta+BDI_2e^{i(\omega_n+\omega_m)T_o}\cos(n-m)\theta$$
$$+B\bar{D}I_3e^{i(\omega_n-\omega_m)T_o}\cos(n+m)\theta$$
$$+B\bar{D}I_4e^{i(\omega_n-\omega_m)T_o}\cos(n-m)\theta+cc \tag{24d}$$

The coefficients G_j, H_j, I_j, and J_j are defined in Appendix A. Using equations (21), (24) and the indicated equations for the order β^3 problem, the solvability conditions at this order with B, D being replaced by $a_je^{i\theta_j}/2$, $j=B$, D could be written as

$$\frac{da_B}{dT_2}=0;\quad a_B\frac{d\theta_B}{dT_2}=[K_1a_B{}^3+K_2a_D{}^2a_B] \tag{25a,b}$$

$$\frac{da_D}{dT_2}=0;\quad a_D\frac{d\theta_D}{dT_2}=[K_3a_D{}^3+K_4a_B{}^2a_D] \tag{25c,d}$$

The constants K_j, which are lengthy combination of the con-

Downloaded 03 May 2010 to 171.66.16.27. Redistribution subject to ASME license or copyright; see http://www.asme.org/terms/Terms_Use.cfm

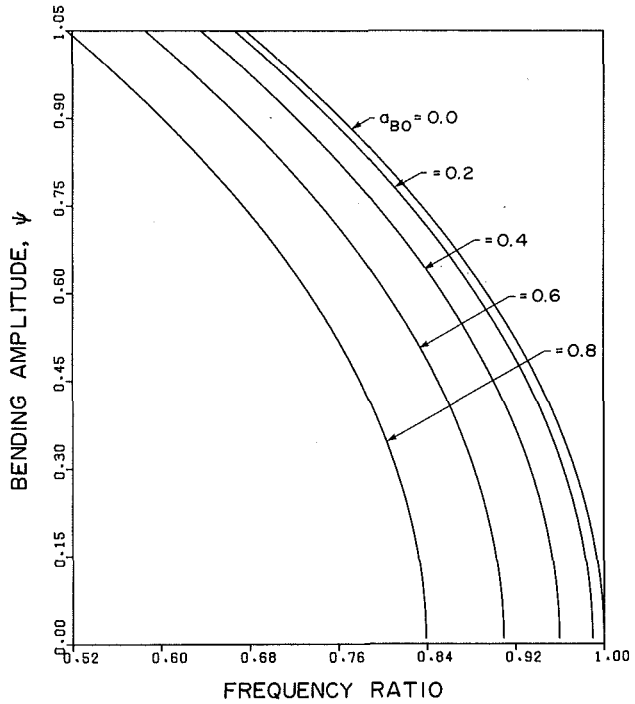


Fig. 3 Out-of-plane amplitude-frequency curves for $n=3$ and $m=2$

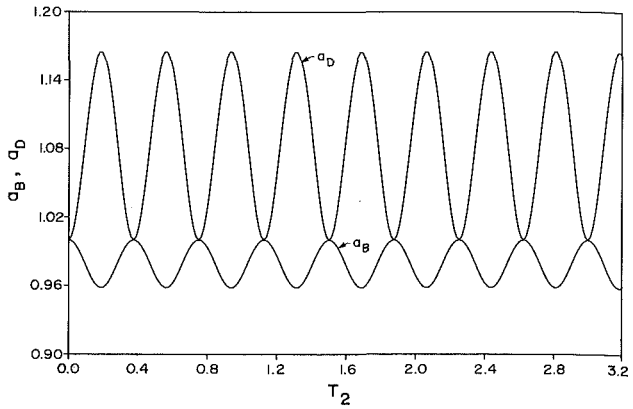


Fig. 4 Variation of the in-plane and the out-of-plane amplitudes with slow time scale T_2 for $n=m=2$

stants defined in Appendix A are not presented here. Equations (25) are of the same form as the corresponding equations obtained by Ho, Scott, and Eisley [4] for a straight beam undergoing coupled flexural oscillations in two perpendicular planes. These equations (25) indicate that the phases and hence the frequencies of the two modes are dependent on both the amplitudes of oscillation.

The correction $\Delta\omega_n$ given by θ_B/t and obtained by integrating equations (25*a*, *b*, *c*) is used to plot the in-plane "amplitude-frequency" curves for different values of the initial out-of-plane amplitude as shown in Fig. 2 for the case $n=2$ and $m=3$. Similarly, $\Delta\omega_m$ given by θ_D/t and obtained by integrating (25*a*, *c*, *d*) is used to plot the out-of-plane "amplitude-frequency" curves for various values of the initial in-plane amplitude as shown in Fig. 3 for the case $n=3$ and $m=2$. The abscissas in Figs. 2 and 3 are normalized with respect to the linear in-plane and the linear out-of-plane natural frequencies, respectively. For all calculations, δ_1 was taken to be 2.0, δ_2 to be 1.0, and δ_3 to be 1/2.6 corresponding to $\nu=0.3$. The expression for $\Delta\omega_n$, when specialized to the in-plane problem reduces to equation (4) of [10], while the corresponding expression for $\Delta\omega_m$ upon specializing to the out-of-plane problem reduces to equation (1) given previously in the introduction.

The use of the phrase "amplitude-frequency" in the preceding paragraph and in Figs. 2 and 3 needs clarification. Only when $a_{D0}=0$ in Fig. 2 or when $a_{B0}=0$ in Fig. 3 is there a periodic motion and a single identifiable frequency of oscillation. The other curves which are presented in Fig. 2 for nonzero out-of-plane bending amplitudes are meant to indicate that the qualitative effect of the large in-plane amplitudes can still be considered to be softening in nature and analogously for Fig. 3.

Case b: Resonant Motions ($\omega_m=\omega_n+\beta\sigma_1+\beta^2\sigma_2$, $n=m$). With the solution to the order β problem given by equations (21), the solvability conditions at the order β^2 for this case are still given by equation (23). As a result σ_1 is zero (for a nonzero σ_1, the solvability conditions at order β^3 will contradict the condition imposed by equations (23)). Subsequently, in the solution to the order β^2 problem, equations (24*c*) and (24*d*) are modified according to,

$$\psi_2 = BDJ_1 e^{i(\omega_n+\omega_m)T_0}\sin(n+m)\theta + B\bar{D}J_3^* e^{-i\sigma_2 T_2}\sin(n+m)\theta + cc \qquad (26a)$$

$$\phi_2 = BDI_1 e^{i(\omega_n+\omega_m)T_0}\cos(n+m)\theta + BDI_2^* e^{i(\omega_n+\omega_m)T_0} + B\bar{D}I_3^* e^{-i\sigma_2 T_2}\cos(n+m)\theta + B\bar{D}I_4^* e^{-i\sigma_2 T_2} + cc \qquad (26b)$$

Again, I_j^* and J_j^* are defined in Appendix A. For the resonant case the corresponding solvability conditions at order β^3 result in the following nonlinear, first order coupled equations.

$$\frac{da_B}{dT_2} = K_5 a_B a_D{}^2 \sin(2\theta_D - 2\theta_B + 2\sigma_2 T_2) \qquad (27a,b)$$

$$a_B\frac{d\theta_B}{dT_2} = K_6 a_B{}^3 + [K_7 - K_5\cos(2\theta_D - 2\theta_B - 2\sigma_2 T_2)]a_D{}^2 a_B$$

$$\frac{da_D}{dT_2} = K_8 a_B{}^2 a_D \sin(2\theta_B - 2\theta_D - 2\sigma_2 T_2) \qquad (27c,d)$$

$$a_D\frac{d\theta_D}{dT_2} = K_9 a_D{}^3 + [K_{10} - K_8\cos(2\theta_B - 2\theta_D - 2\sigma_2 T_2)]a_B{}^2 a_D$$

Again, the constants $K_5 - K_{10}$ which are lengthy combinations of those defined in Appendix A are not presented. Equations (27) above have the same general form as equations (39)–(42) presented by Ho, Scott, and Eisley [4] for the resonant case. To examine the nature of coupling between the in-plane and the out-of-plane motions, the coupled set (27) is integrated numerically with initial conditions of order β. The results for a_B and a_D are plotted against the slow scale T_2 for the case $n=2$ and $m=2$ as shown in Fig. 4.

Discussion and Conclusions

For nonresonant oscillations, the amplitude-frequency curves as shown in Fig. 2 for the case $n=2$ and $m=3$ indicate the softening effect of the nonlinearities. The effect of the initial out-of-plane amplitude a_{D0} is to shift the curves marginally to the right. This was observed to be true for all cases with n less than m. On the other hand, when n is greater than m the curves were slightly shifted to the left with increasing values of a_{D0}. In all cases, for a given n and a_{D0}, it was observed that the magnitude of the shift progressively decreased with increasing values of m. For the case $n=3$ and $m=2$ the amplitude-frequency curves as shown in Fig. 3 also indicate the presence of a softening type of nonlinearity. For n greater than m, the effect of the initial in-plane amplitude a_{B0} is to shift the curves to the left thereby lowering the flexural frequency of the out-of-plane bending mode. For the cases with n less than m the curves were shifted marginally to the right for increasing

Downloaded 03 May 2010 to 171.66.16.27. Redistribution subject to ASME license or copyright; see http://www.asme.org/terms/Terms_Use.cfm

values of a_{B0}. It was found that the magnitude of the shift for a given value of m and a_{B0} increased with increasing values of n before ultimately reaching a nearly constant value.

For resonant oscillations, the variation of the in-plane and the out-of-plane amplitudes with the slow time scale T_2 as shown in Fig. 4 for the case $n=2$ and $m=2$ indicates an exchange of energy between the in-plane coordinate α and the out-of-plane coordinate ψ. As expected, the growth in amplitude of ψ depends on the detuning parameter σ_2. If should be noted that $\sigma_2=0$ requires that δ_1 be $1/\delta_3$ and δ_2 be unity which in general may not lead to cross-sections which could be realized in practice.

In conclusion, an accurate set of equations of motion including the effects of extensional strain, shearing strains, and rotatory inertia is derived for a thin circular ring. As a result of the subsequent nondimensionalization of the equations of motion, it is clear that the relative contributions of certain terms involving the extensional strain, the shearing strains, and the rotatory inertia are of higher order and are thus neglected. An asymptotic solution is obtained by the method of multiple scales. It is shown that large amplitude in-plane motions of a circular ring can exist with no corresponding out-of-plane motion occurring, but that the large amplitude out-of-plane motions are necessarily accompanied by the corresponding in-plane motions. The corrections to the linear natural frequency of the in-plane and the out-of-plane bending modes are obtained for the nonresonant case. For the nonresonant motions, the initial out-of-plane amplitude was shown to have a marginal effect on the in-plane oscillations whereas the effect of the initial in-plane amplitude on the out-of-plane oscillations was shown to be more significant. For the resonant case, the presence of unsteady oscillations with an exchange of energy between the in-plane and the out-of-plane motions is indicated.

Acknowledgment

The authors are indebted to the reviewer for his appropriate comments and suggestions.

References

1 Evensen, D. A., 1964, "Nonlinear Flexural Vibrations of Thin Circular Rings," Ph.D. thesis, California Institute of Technology.

2 Evensen, D. A., 1966, "Nonlinear Flexural Vibrations of Thin Circular Rings," ASME Journal of Applied Mechanics, Vol. 33, pp. 553-560.

3 Frisch-Fay, R., 1962, *Flexible Bars*, Butterworths, London.

4 Ho, C. H., Scott, R. A., and Eisley, J. G., 1976, "Non-Planar, Non-Linear Oscillations of a Beam. II. Free Motions," *Journal of Sound and Vibration*, Vol. 47, pp. 333-339.

5 Libal, A., and Simmonds, J. G., 1983, "Nonlinear Elastic Shell Theory," *Advances in Applied Mechanics*, Academic Press, Vol. 23, pp. 271-371.

6 Love, A. E. H., 1944, *A Treatise on the Mathematical Theory of Elasticity*, Fourth Edition, Dover, New York.

7 Maewal, A., 1978, "Nonlinear Flexural Vibrations of an Elastic Ring," ASME Journal of Applied Mechanics, Vol. 45, pp. 428-429.

8 Maewal, A., and Nachbar, W., 1978, "Lyapunov-Schmidt Method for Analysis of Postbuckling Behavior and Steady Harmonic Oscillations of Conservative Structures," *Eighth U.S. National Congress on Applied Mechanics*, Los Angeles.

9 Rodgers, L. C., and Warner, W. H., 1973, "Dynamic Stability of Out-of-Plane Motion of Elastic Rods," *SIAM Journal of Applied Mathematics*, Vol. 24, No. 1, pp. 36-43.

10 Simmonds, J. G., 1979, "Accurate Nonlinear Equations and a Perturbation Solution for the Free Vibrations of a Circular Elastic Ring," ASME Journal of Applied Mechanics, Vol. 46, pp. 156-160.

11 Simmonds, J. G., and Danielson, D. A., 1972, "Nonlinear Shell Theory With Finite Rotation and Stress-Function Vectors," ASME Journal of Applied Mechanics, Vol. 39, pp. 1085-1090.

APPENDIX A

Here, the coefficients in the solution to the order β^2 problem are defined.

$$G_1=\left[\frac{\delta_1\delta_2\delta_3(m^2-1)^2}{(\delta_2+m^2\delta_1\delta_3)}\right]\ ;\ G_2=[n^2]$$

$$G_3=-G_1\qquad ;\ G_4=-G_2$$

$$G_5=\left[\frac{-G_1(2m^2-1)}{2}\right]\ ;\ G_6=\left[\frac{-n^2(2n^4-5n^2+1)}{2(1+n^2)}\right]$$

$$\begin{aligned}G_7=\{&-\delta_1\delta_2\delta_3(m^2-1)^2[\delta_1{}^2\delta_2\delta_3{}^2(2m^8-3m^6+m^2)\\&+\delta_1{}^2\delta_3{}^2(-8m^8+22m^6-5m^4)\\&+\delta_1\delta_2{}^2\delta_3(-6m^6+13m^4-8m^2+1)\\&+\delta_1\delta_2\delta_3(-8m^6+28m^4-2m^2)\\&+\delta_2{}^2(-4m^4+14m^2-1)]\}/\{2(\delta_1\delta_3m^2+\delta_2)^2\\&[\delta_1\delta_2\delta_3(4m^6-7m^4+2m^2+1)\\&+\delta_1\delta_3(-16m^6+8m^4-m^2)+\delta_2(-16m^4+8m^2-1)]\}\end{aligned}$$

$$G_8=\left[\frac{-n^2(2n^2-1)(n^2+5)}{2(4n^4+5n^2-3)}\right]$$

$$\begin{aligned}H_1=&[(\delta_1{}^2\delta_3{}^2+2\delta_1\delta_2\delta_3)(m^4+m^2)+\delta_2{}^2(3m^2-1)\\&+2\delta_1\delta_2{}^2\delta_3(m^4-2m^2+1)]/[4m(\delta_1\delta_3m^2+\delta_2)^2]\end{aligned}$$

$$H_2=\left[\frac{n}{2(1+n^2)}\right];\quad H_4=\left[\frac{(4n^4-1)}{4n(4n^4+5n^2-3)}\right]$$

$$\begin{aligned}H_3=&[\delta_1{}^2\delta_3{}^2(-16m^8+24m^6+15m^4-m^2)\\&+\delta_1{}^2\delta_2\delta_3{}^2(24m^8-44m^6+16m^4+4m^2)\\&+\delta_1\delta_2{}^2\delta_3(-16m^8+60m^6-74m^4+32m^2-2)\\&+\delta_1\delta_2\delta_3(-32m^8+48m^6+30m^4-2m^2)\\&+\delta_2{}^2(-16m^6+48m^4-11m^2+1)]/\\&\{8m(\delta_1\delta_3m^2+\delta_2)[\delta_1\delta_2\delta_3(4m^6-7m^4+2m^2+1)\\&+\delta_1\delta_3(-16m^6+8m^4-m^2)+\delta_2(-16m^4+8m^2-1)]\}\end{aligned}$$

$$\begin{aligned}I_1=\frac{-1}{2\Delta_1(n+m,\omega_n+\omega_m)}&[\Delta_2(n+m)\{X_2(\Phi_1+\Phi_2)+\Phi_3+\Phi_4\\&+X_1(\Phi_5+\Phi_6)+X_1X_2\Phi_7\}+\Delta_3(n+m,\omega_n+\omega_m)\\&\{X_2\Phi_8-\Phi_9+\Phi_{10}\}]\end{aligned}$$

$$\begin{aligned}I_2=\frac{-1}{2\Delta_1(n-m,\omega_n+\omega_n)}&[\Delta_2(n-m)\{X_2(\Phi_1-\Phi_2)+\Phi_3-\Phi_4\\&+X_1(\Phi_5-\Phi_6)+X_1X_2\Phi_7\}+\Delta_3(n-m,\omega_n+\omega_m)\\&\{X_2\Phi_8+\Phi_9+\Phi_{10}\}]\end{aligned}$$

$$\begin{aligned}I_3=\frac{-1}{2\Delta_1(n+m,\omega_n-\omega_m)}&[\Delta_2(n+m)\{X_2(\Phi_1+\Phi_2)+\Phi_3+\Phi_4\\&+X_1(\Phi_5+\Phi_6)+X_1X_2\Phi_7\}+\Delta_3(n+m,\omega_n-\omega_m)\\&\{X_2\Phi_8-\Phi_9+\Phi_{10}\}]\end{aligned}$$

$$\begin{aligned}I_4=\frac{-1}{2\Delta_1(n-m,\omega_n-\omega_m)}&[\Delta_2(n-m)\{X_2(\Phi_1-\Phi_2)+\Phi_3-\Phi_4\\&+X_1(\Phi_5-\Phi_6)+X_1X_2\Phi_7\}+\Delta_3(n-m,\omega_n-\omega_m)\\&\{X_2\Phi_8+\Phi_9+\Phi_{10}\}]\end{aligned}$$

$$\begin{aligned}J_1=\frac{1}{2\Delta_1(n+m,\omega_n+\omega_m)}&[\Delta_4(n+m)\{X_2\Phi_8-\Phi_9+\Phi_{10}\}\\&+\Delta_5(n+m)\{X_2(\Phi_1+\Phi_2)+\Phi_3+\Phi_4+X_1(\Phi_5+\Phi_6)\\&+X_1X_2\Phi_7\}]\end{aligned}$$

$$\begin{aligned}J_2=\frac{1}{2\Delta_1(n-m,\omega_n+\omega_m)}&[\Delta_4(n-m)\{X_2\Phi_8+\Phi_9+\Phi_{10}\}\\&+\Delta_5(n-m)\{X_2(\Phi_1-\Phi_2)+\Phi_3-\Phi_4+X_1(\Phi_5-\Phi_6)\\&+X_1X_2\Phi_7\}]\end{aligned}$$

$$J_3=\frac{1}{\Delta_1(n+m,\omega_n-\omega_m)}[J_1\Delta_1(n+m,\omega_n+\omega_m)]$$

$$J_4=\frac{1}{\Delta_1(n-m,\omega_n-\omega_m)}[J_2\Delta_1(n-m,\omega_n+\omega_m)]$$

Downloaded 03 May 2010 to 171.66.16.27. Redistribution subject to ASME license or copyright; see http://www.asme.org/terms/Terms_Use.cfm

$$I_2^* = \frac{-1}{2\delta_2}[-\delta_1\delta_3 n^2 + (\delta_1\delta_3 + \delta_2 - 1)nm + X_2(2\delta_2 - 1)n]$$

$$I_3^* = \frac{-1}{2\Delta_1(n+m,0)}[\Delta_2(n+m)\{X_2(\Phi_1 + \Phi_2) + \Phi_3 + \Phi_4 + X_1(\Phi_5 + \Phi_6) + X_1X_2\Phi_7\} + \Delta_3(n+m,0)\{X_2\Phi_8 - \Phi_9 + \Phi_{10}\}]$$

$$I_4^* = \frac{-1}{2\delta_2}[-\delta_1\delta_3 n^2 + (\delta_1\delta_3 + \delta_2 - 1)nm + X_2(2\delta_2 - 1)n]$$

$$J_3^* = \frac{1}{\Delta_1(n+m,0)}[J_1\Delta_1(n+m,\omega_n + \omega_m)]$$

where Δ_1 through Δ_5, X_1, X_2, and Φ_1 through Φ_{10} are defined as follows.

$$\Delta_1(x,y) = \delta_1\delta_2\delta_3 x^2(x^2-1)^2 - y^2(\delta_1\delta_3 x^2 + \delta_2)$$

$$\Delta_2(x) = x(\delta_1\delta_3 + \delta_2); \Delta_3(x,y) = \delta_2 x^4 + \delta_1\delta_3 x^2 - y^2$$

$$\Delta_4(x) = x^3(\delta_1\delta_3 + \delta_2); \Delta_5(x) = \delta_1\delta_3 x^2 + \delta_2$$

$$X_1 = -2n^3/(1+n^2); \quad X_2 = -m(\delta_1\delta_3 + \delta_2)/(\delta_1\delta_3 m^2 + \delta_2)$$

$$\Phi_1 = -\delta_2 n^4 + (-2\delta_1\delta_3 - 3\delta_2 + 3)n^2m^2 - n^2 + {\omega_n}^2$$

$$\Phi_2 = (-\delta_1\delta_3 - 3\delta_2 + 3)n^3 m + (-\delta_1\delta_3 - \delta_2 + 1)nm^3$$

$$\Phi_3 = (-4\delta_1\delta_3 + 2)n^2 m; \quad \Phi_4 = (-2\delta_1\delta_3 + 3)n^3 - (2\delta_1\delta_3 - 1)nm^2$$

$$\Phi_5 = -2nm; \Phi_6 = -m^2 + 1; \Phi_7 = -2n; \Phi_8 = (2\delta_2 - 1)n$$

$$\Phi_9 = -\delta_1\delta_3 n^2; \Phi_{10} = (\delta_1\delta_3 + \delta_2 - 1)nm$$

Downloaded 03 May 2010 to 171.66.16.27. Redistribution subject to ASME license or copyright; see http://www.asme.org/terms/Terms_Use.cfm

An Evaluation of Recent Developments in Hardening and Flow Rules for Rate-Independent, Nonproportional Cyclic Plasticity

D. L. McDowell
Assistant Professor,
George W. Woodruff School of Mechanical Engineering,
Georgia Institute of Technology,
Atlanta, GA 30332
Assoc. Mem. ASME

The Mroz kinematic hardening rule has previously demonstrated superior capability to correlate cyclically stable nonproportional stress-strain response. In this paper, recently proposed kinematic hardening rules for single and multiple surface cyclic plasticity models are evaluated. Significant improvement over the Mroz rule, without loss of generality, is achieved with a deviatoric stress rate-dominated rule proposed by Tseng and Lee for two surface theory. Recent approaches for correlation of the modulus function and isotropic hardening are discussed. The norm of the Mroz distance vector is found to uniquely correlate the variation of plastic hardening modulus through a cycle; it is necessary to include a measure of instantaneous nonproportionality, however, to properly normalize the modulus function. A new evolution equation is offered to correlate the additional isotropic hardening observed during nonproportional loading, and several contemporary approaches are also considered.

Introduction

With increasing emphasis on lightweight, high performance structures, there has been a corresponding rise of interest in constitutive equations for cyclic plasticity. For example, this is true for the turbine and rocket engine, and for the nuclear and ground vehicle industries. Historically the complexity of cyclic plasticity models increased as more experimentally observed effects were reported. There has been a relatively recent emphasis (Dafalias and Popov, 1975; Dafalias, 1981; Krieg, 1975; Lamba and Sidebottom, 1978a, 1978b; McDowell, 1985a, 1985b; Nouailhas et al., 1983; Tanaka et al., 1985; Tseng and Lee, 1983) on the formulation of models for multiaxial loading. This includes consideration of nonproportional variation of the components of stress and strain referenced to material axes (nonproportional loading).

Lamba and Sidebottom (1978a, 1978b) produced data from nonproportional cyclic axial-torsional tests on OFHC copper, and showed that the kinematic hardening rule of Mroz (1967) was far superior to that of Ziegler (1959) or Prager (1956) for correlating stress-strain response during nonproportional loading. Lamba also reported a significant increase in cyclic hardening under sinusoidal out-of-phase loading, a finding that since has been reported for other materials for similar loading conditions (McDowell, 1983a; Kanazawa et al., 1979; Krempl and Lu, 1984). Prediction of the direction of plastic strain rate in general depends greatly on the kinematic hardening rule for nonproportional loading. Likewise, isotropic hardening during nonproportional loading can no longer be represented as a function of accumulated plastic strain or plastic work; it is also a function of changes in the direction of the plastic strain rate vector over a loading history (McDowell, 1985c). Since both the direction of the plastic strain rate vector and the additional hardening during nonproportional loading are of first order importance, it is not extravagant but absolutely necessary to account for them in the cyclic plasticity model.

In this paper, experimental data from axial torsional, strain controlled, cyclic nonproportional loading tests is examined in detail for type 304 stainless steel at room temperature. Within the context of von Mises yield and loading surfaces, recently proposed approaches for kinematic hardening will be evaluated. More accurate rules are developed where necessary. Second invariant plasticity theory (i.e., von Mises) is selected as the basis for evaluation since it is of extreme practical importance to the computational plasticity community. Likewise, studies of isotropic hardening and modulus function will be based on this framework.

Results of three strain-controlled axial torsional histories are considered in this paper. All tests were conducted at room temperature. The initial values of Young's modulus and shear modulus were determined as $E = 188$ GPa and $G = 77$ GPa, respectively. A summary of the three test histories appears in Table I, including the effective strain rate and controlled axial

Contributed by the Applied Mechanics Division for presentation at the 1987 Applied Mechanics, Biomechanics, and Fluids Engineering Conference, Cincinnati, OH, June 14-17, 1987, of the American Society of Mechanical Engineers.
Discussion of this paper should be addressed to the Editorial Department, ASME, United Engineering Center, 345 East 47th Street, New York, N.Y. 10017, and will be accepted until two months after final publication of the paper itself in the JOURNAL OF APPLIED MECHANICS. Manuscript received by ASME Applied Mechanics Division, March 25, 1986; final revision, August 11, 1986.
Paper No. 87-APM-37.

Copyright © 1987 by ASME
Downloaded 03 May 2010 to 171.66.16.27. Redistribution subject to ASME license or copyright; see http://www.asme.org/terms/Terms_Use.cfm

Table I Complex strain histories

Complex Strain Histories
Block Number

Specimen Identification	$\dot{\bar{\epsilon}}(\text{sec}^{-1})$	1	2	3	4
SS01	0.003	endpoint sequence: 0 $\epsilon=\gamma=0$ 1 $\epsilon=0.0041$ $\gamma=0.006$ 2 $\epsilon=-0.0041$ $\gamma=-0.006$ return to $\epsilon=\gamma=0$	endpoint sequence: 0 $\epsilon=\gamma=0$ 1 $\epsilon=0.0041$ $\gamma=-0.006$ 2 $\epsilon=-0.0041$ $\gamma=0.006$ return to $\epsilon=\gamma=0$	endpoint sequence: 0 $\epsilon=\gamma=0$ 1 $\epsilon=0.0041$ $\gamma=0.006$ 2 $\epsilon=0.0041$ $\gamma=-0.006$ 3 $\epsilon=-0.0041$ $\gamma=0.006$ 4 $\epsilon=-0.0041$ $\gamma=-0.006$ return to $\epsilon=\gamma=0$	
		25 cycles	25 cycles	25 cycles	
SS09	0.001	Incremental Step Test: $\epsilon_a^{max}=0.007$ $\gamma_a^{max}=0.0105$	*$\epsilon_a=0.005$ $\gamma_a=0.0075$ $\beta=0$	*$\epsilon_a=0.005$ $\gamma_a=0.0075$ $\beta=30^0$	*$\epsilon_a=0.005$ $\gamma_a=0.0075$ $\beta=60^0$
		10 cycles	16 cycles	25 cycles	25 cycles
SS04	0.002	0 $\epsilon=\gamma=0$ 1 $\epsilon=0,\gamma=0.0085$ 2 $\epsilon=0,\gamma=-0.0085$ 3 $\epsilon=-.0039,\gamma=0.0057$ 4 $\epsilon=0.0039,\gamma=-0.0057$ 5 $\epsilon=-0.0046,\gamma=0.0039$ 6 $\epsilon=0.0046,\gamma=-0.0039$ 7 $\epsilon=0.0051,\gamma=0$ 8 $\epsilon=-0.0051,\gamma=0$ 9 $\epsilon=0.0046,\gamma=0.0039$ 10 $\epsilon=-0.0046,\gamma=-0.0039$ 11 $\epsilon=0.0039,\gamma=0.0057$ 12 $\epsilon=-0.0039,\gamma=-0.0057$ return to $\epsilon=\gamma=0$			
		50 cycles			

*Denotes sinusoidal loading with $\epsilon = \epsilon_a \sin\omega t$, $\gamma = \gamma_a \sin(\omega t - \beta)$.

and shear strain endpoint sequence of each block within each history. Details of the experimental procedures and more in-depth discussion of the experiments appear elsewhere (McDowell, 1983a, 1983b, 1985d).

Studies of kinematic hardening will be limited to consideration of essentially stable cyclic response observed in the latter cycles of each block. In this case, the kinematic hardening rules may be examined in the absence of isotropic hardening. In a later section, isotropic hardening effects and the modulus function will also be examined.

Kinematic Hardening Rules

Previous work (Lamba and Sidebottom, 1978a, 1978b; McDowell, 1985d) has demonstrated the lack of correlation obtained with the use of either a Prager or Ziegler kinematic hardening rule for nonproportional cyclic loading, i.e.,

$$\dot{\alpha} = \mu \dot{\epsilon}^P \tag{1}$$

or

$$\dot{\alpha} = \dot{\eta}(\mathbf{s} - \alpha) \tag{2}$$

where $\mathbf{s}$ is the deviatoric stress tensor, α is the backstress, and μ and $\dot{\eta}$ are scalar multipliers.

The superiority of a Mroz-type hardening rule, based on the concept of nested yield and loading surfaces, has been previously demonstrated. For computationally efficient two-surface models with a yield surface f and enclosing limit surface f^* of the form $f(\mathbf{s}-\alpha, R) = 0$ and $f^*(\mathbf{s}-\alpha^*, R^*) = 0$, the Mroz rule may be stated as

$$\dot{\alpha} = \mu_m (\mathbf{s}^* - \mathbf{s}) \tag{3}$$

where $\mathbf{s}^*$ is the similar point on the limit surface as shown in Fig. 1 defined by

$$\mathbf{s}^* = \alpha^* + (R^*/R)(\mathbf{s} - \alpha) \tag{4}$$

where R and R^* are the yield and limit surface radii, respectively.

Other kinematic hardening rules have been proposed recently which would also conceptually apply to the nonproportional loading case. Tseng and Lee (1983) proposed that the yield surface translation is related to the deviatoric stress rate direction. Their theory was motivated chiefly by the predominance of stress rate in translation of the yield locus observed in the experiments of Phillips et al. (1974, 1979). In their theory, for a stationary limit surface,

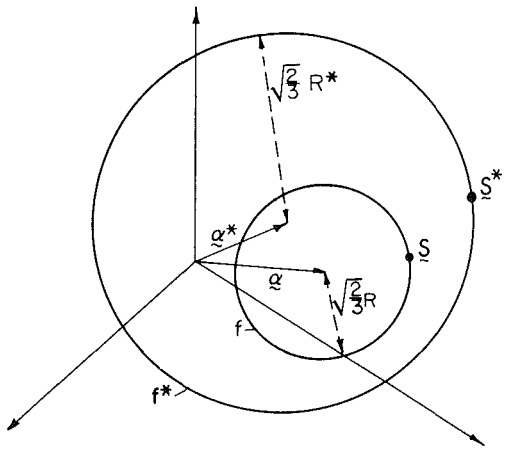


Fig. 1 Surfaces f and f^* in deviatoric stress space

$$\dot{\alpha} = \mu_T \nu \tag{5}$$

where

$$\nu = \frac{\left[\sqrt{\frac{2}{3}}(R^* - R)\lambda - \alpha\right]}{\left\|\sqrt{\frac{2}{3}}(R^* - R)\lambda - \alpha\right\|} \tag{6}$$

$$\lambda = \frac{\mathbf{s} + \delta_s \dot{\mathbf{s}}/\|\dot{\mathbf{s}}\|}{\|(\mathbf{s} + \delta_s \dot{\mathbf{s}}/\|\dot{\mathbf{s}}\|)\|} \tag{7}$$

Downloaded 03 May 2010 to 171.66.16.27. Redistribution subject to ASME license or copyright; see http://www.asme.org/terms/Terms_Use.cfm

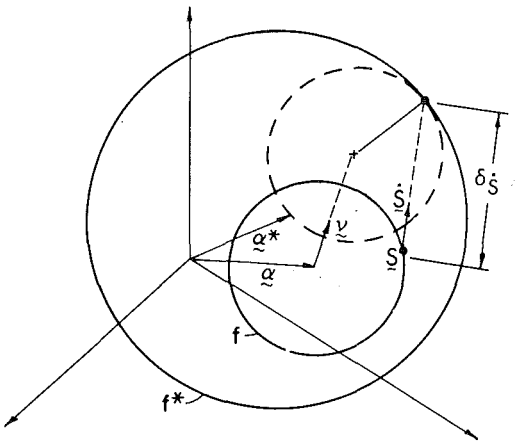


Fig. 2 Tseng-Lee kinematic hardening rule for nonzero α^*

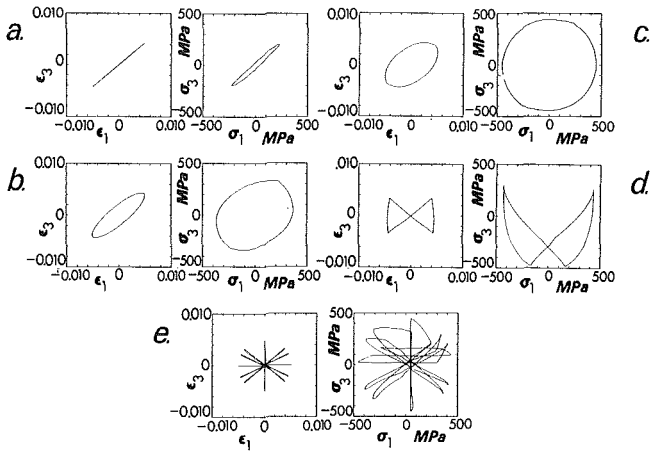


Fig. 3 Imposed ϵ_1 versus ϵ_3 strain paths and resulting cyclically stable stress subspace responses for: (*a*) block 2, specimen SS09; (*b*) block 3, specimen SS09; (*c*) block 4, specimen SS09; (*d*) block 3, specimen SS01; and (*e*) block 1, specimen SS04

$$\delta_{\dot{s}} = -\mathbf{s}:\dot{\mathbf{s}}/\|\dot{\mathbf{s}}\| + \left[(\mathbf{s}:\dot{\mathbf{s}}/\|\dot{\mathbf{s}}\|)^2 + \left(\frac{2}{3}(R^*)^2 - \|\mathbf{s}\|^2\right)\right]^{1/2} \tag{8}$$

where the scalar product is defined by $\mathbf{s}:\dot{\mathbf{s}} = s_{ij}\dot{s}_{ij}$ for example. The norm of a second order tensor $\mathbf{s}$ is denoted by $\|\mathbf{s}\| = (\mathbf{s}:\mathbf{s})^{1/2}$.

Here, $\delta_{\dot{s}}$ is the norm of the vector from the current stress point to the intersection of the deviatoric stress rate direction relative to the current stress point with the stationary limit surface f^* of the form

$$f^*(\mathbf{s},R^*) = (3/2)\mathbf{s}:\mathbf{s} - (R^*)^2 \tag{9}$$

Note that $\boldsymbol{\alpha}^* = \mathbf{0}$ in their formulation. Equations (5)–(9) are meant to apply to von Mises yield and limit surfaces. Note also that the rule guarantees tangency of the surfaces as $\delta_{\dot{s}} \to 0$ as in the Mroz rule.

Outside of the context of a multiple surface plasticity theory, one could generalize the assumed dominance of deviatoric stress rate direction with the rule

$$\dot{\boldsymbol{\alpha}} = \mu_s \dot{\mathbf{s}} \tag{10}$$

Another rule which has been introduced in the context of rate-dependent state variable or unified creep-plasticity theory is due to Chaboche et al. (1979),

$$\dot{\boldsymbol{\alpha}} = C[a'\dot{\boldsymbol{\epsilon}}^P - \boldsymbol{\alpha}\|\dot{\boldsymbol{\epsilon}}^P\|] \tag{11}$$

where a' is a constant and C is a scalar. In Chaboche's formulation, both C and a' can be functions of the accumulated plastic strain, $\bar{\epsilon}^P$. In equation (11), C is determined by consistency, leaving a' freely specified. The second term, widely regarded as a dynamic recovery term, in principle can account for nonproportional loading effects since an additional directional index $\boldsymbol{\alpha}$ is appended to the otherwise Prager-type rule. It should be noted that other investigators have proposed similar forms (Lindholm et al., 1985). It should also be noted that neither of equations (10)–(11) requires a multiple surface formulation.

The Tseng-Lee Rule in equations (5)–(8) was motivated by observation that the yield surface movement was related to deviatoric stress rate. In their implementation of this observation, however, Tseng and Lee were constrained to ensure nesting of the yield and limit surfaces as $\delta_{\dot{s}} \to 0$. Hence, the deviatoric stress rate direction and that of $\boldsymbol{\nu}$ in the Tseng-Lee Rule in equation (6) are not equivalent, though $\boldsymbol{\nu}$ follows the deviatoric stress rate direction much more closely than the Mroz rule in equation (3) for nonproportional loading.

The Tseng-Lee rule may be extended to the case of a translating limit surface by referencing to $\boldsymbol{\alpha}^*$ rather than the origin. The Tseng-Lee rule with nonzero $\boldsymbol{\alpha}^*$ is illustrated in Fig. 2.

It is possible to evaluate these rules via numerical differentiation of data from strain-controlled, axial torsional tests on thin-walled tubular specimens (McDowell, 1985d). It is convenient to make these comparisons in the axial torsional subspace.

The definition of the axial torsional subspace follows as a subspace of Ilyushin's five-dimensional deviatoric vector space (McDowell, 1985d). Define the stress vector as

$$\boldsymbol{\sigma} = \sigma_1 \mathbf{n}_1 + \sigma_3 \mathbf{n}_3 \tag{12}$$

where

$$\sigma_1 = \sigma_{zz} = \sigma, \quad \sigma_3 = \sqrt{3}\sigma_{z\theta} = \sqrt{3}\tau$$

and $\mathbf{n}_1$ and $\mathbf{n}_3$ are orthonormal base vectors in the stress plane. Here, z and θ denote the tube longitudinal and circumferential directions, respectively. Likewise, the plastic strain vector is defined by

$$\boldsymbol{\epsilon}^P = \epsilon_1^P \mathbf{n}_1 + \epsilon_3^P \mathbf{n}_3 \tag{13}$$

where

$$\epsilon_1^P = \epsilon_{zz}^P, \quad \text{and} \quad \epsilon_3^P = (2/\sqrt{3})\epsilon_{z\theta}^P.$$

Note that the plastic strain rate vector is defined as

$$\dot{\boldsymbol{\epsilon}}^P = \dot{\epsilon}_1^P \mathbf{n}_1 + \dot{\epsilon}_3^P \mathbf{n}_3 \tag{14}$$

The effective stress $\bar{\sigma}$ and plastic strain rate $\dot{\bar{\epsilon}}^P$ (normalized to the axial case) are recognized as

$$\bar{\sigma} = |\boldsymbol{\sigma}| = (\boldsymbol{\sigma}\cdot\boldsymbol{\sigma})^{1/2} = (\sigma_1^2 + \sigma_3^2)^{1/2} \tag{15}$$

$$\dot{\bar{\epsilon}}^P = |\dot{\boldsymbol{\epsilon}}^P| \tag{16}$$

The total strain vector is heuristically defined as

$$\boldsymbol{\epsilon} = \epsilon_1 \mathbf{n}_1 + \epsilon_3 \mathbf{n}_3 \tag{17}$$

where $\epsilon_1 = \epsilon_{zz} = \epsilon$ and $\epsilon_3 = (2/\sqrt{3})\epsilon_{z\theta} = \gamma/\sqrt{3}$. The effective strain rate reported in Table I is then $\dot{\bar{\epsilon}} = |\dot{\boldsymbol{\epsilon}}|$ since $\gamma = 2\epsilon_{z\theta}$.

The plastic strain rate vector in the subspace was computed by numerical differentiation of data (McDowell, 1985d).

The axial torsional subspace can also be considered a deviatoric subspace since the second invariant of deviatoric stress can be related to $\boldsymbol{\sigma}\cdot\boldsymbol{\sigma}$

$$\bar{\sigma} = (\boldsymbol{\sigma}\cdot\boldsymbol{\sigma})^{1/2} = \sqrt{\frac{3}{2}\,\mathbf{s}:\mathbf{s}} = \sqrt{3J_2'} \tag{18}$$

Hence, a von Mises yield surface also is circular in the subspace, i.e.,

$$f = (\boldsymbol{\sigma} - \tilde{\boldsymbol{\alpha}})\cdot(\boldsymbol{\sigma} - \tilde{\boldsymbol{\alpha}}) - R^2 \tag{19}$$

Downloaded 03 May 2010 to 171.66.16.27. Redistribution subject to ASME license or copyright; see http://www.asme.org/terms/Terms_Use.cfm

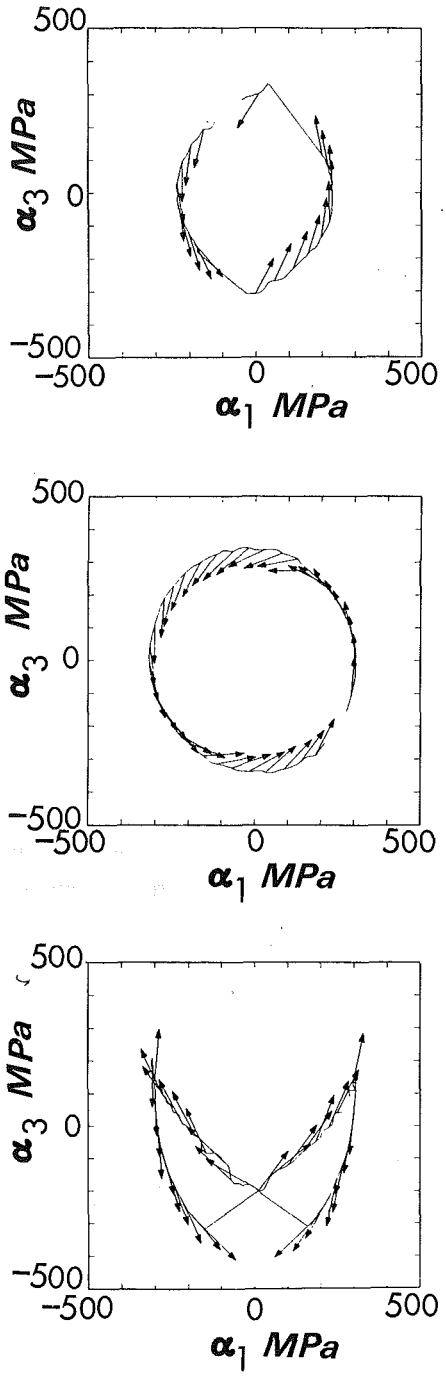


Fig. 4 Correlation achieved by Mroz rule for stable cycles from (top) block 3, specimen SS09, (center) block 4, specimen SS09, and (bottom) block 3, specimen SS01

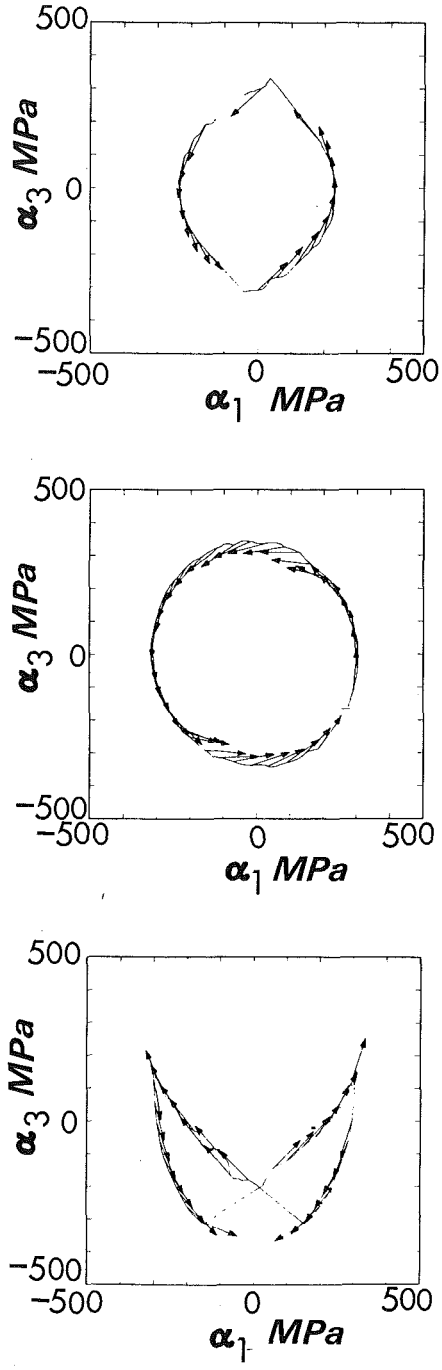


Fig. 5 Correlation achieved by Tseng-Lee rule for stable cycles from (top) block 3, specimen SS09, (center) block 4, specimen SS09, and (bottom) block 3, specimen SS01

where R is the uniaxial yield stress and $\bar{\alpha}$ is the backstress in the subspace. The associated flow rule in the subspace is given for $f = 0$ by

$$\dot{\epsilon}^P = \frac{1}{h} \langle \dot{\sigma} \cdot \mathbf{n} \rangle \mathbf{n} \tag{20}$$

where $\mathbf{n} = (\sigma - \bar{\alpha})/|\sigma - \bar{\alpha}|$ and h is the hardening modulus. The Macauley bracket is defined by $\langle M \rangle = M$ if $M \geq 0$ and $\langle M \rangle = 0$ if $M < 0$. Hence, $\dot{\epsilon}^P$ is collinear with $(\sigma - \bar{\alpha})$ for the von Mises case. A stationary limit surface f^* in the subspace, required by two surface theories, is given by

$$f^* = \sigma^* \cdot \sigma^* - (R^*)^2 \tag{21}$$

where σ^* is a point on the limit surface.

Referring to equations (19)–(21), it is apparent that if R and $\mathbf{n}$ $(= \dot{\epsilon}^P/|\dot{\epsilon}^P|)$ are known, then $\bar{\alpha}$ can be computed directly from

$$\bar{\alpha} = \sigma - R\mathbf{n} \tag{22}$$

for each point in the plastic range under conditions of stable or pure kinematic hardening (R = constant). Figure 3 illustrates the imposed ϵ_1 versus ϵ_3 strain paths and resulting stable cycles of σ_1 versus σ_3 in the axial torsional subspace for the histories in this study, which are fully described in Table I.

In Figs. 4–7, the backstress path based on equation (22) is plotted as a solid line for essentially stable cycles of three nonproportional histories. In addition, vectors are plotted along these paths which represent the direction of backstress evolu-

Downloaded 03 May 2010 to 171.66.16.27. Redistribution subject to ASME license or copyright; see http://www.asme.org/terms/Terms_Use.cfm

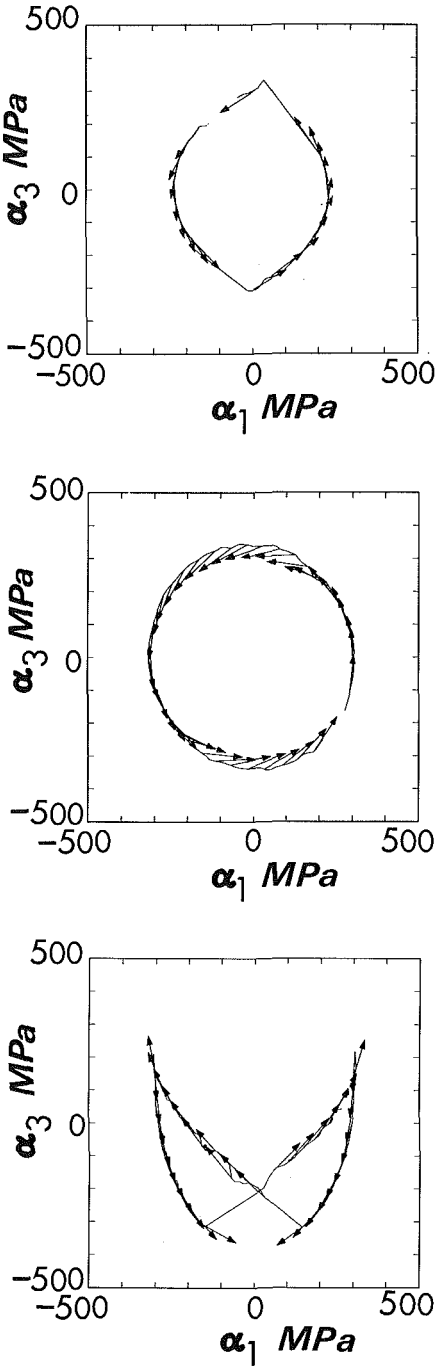


Fig. 6 Correlation achieved by deviatoric stress rate rule for stable cycles from (top) block 3, specimen SS09, (center) block 4, specimen SS09, and (bottom) block 3, specimen SS01

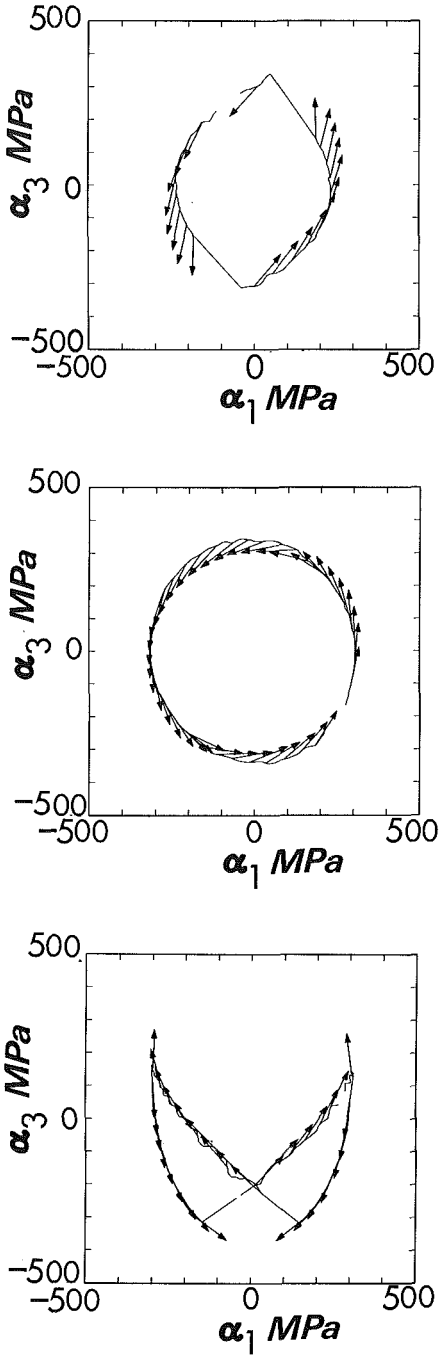


Fig. 7 Correlation achieved by Chaboche rule for stable cycles from (top) block 3, specimen SS09, (center) block 4, specimen SS09, and (bottom) block 3, specimen SS01

tion predicted by the models of Mroz, Tseng-Lee, deviatoric stress rate, and that of Chaboche. These models are stated in the axial torsional subspace as

Mroz: $$\dot{\tilde{\alpha}} = \tilde{\mu}_m (\sigma^* - \sigma) \tag{23}$$

where $$\sigma^* = (R^*/R)(\sigma - \tilde{\alpha}) \tag{24}$$

Tseng-Lee: $$\dot{\tilde{\alpha}} = \tilde{\mu}_T \nu^s \tag{25}$$

where

$$\nu^s = \frac{(R^* - R)\lambda - \tilde{\alpha}}{|(R^* - R)\lambda - \tilde{\alpha}|} \tag{26}$$

$$\lambda = \frac{\sigma + \delta_{\dot{\sigma}} \dot{\sigma}/|\dot{\sigma}|}{|\sigma + \delta_{\dot{\sigma}} \dot{\sigma}/|\dot{\sigma}||} \tag{27}$$

and

$$\delta_{\dot{\sigma}} = -\sigma \cdot \dot{\sigma}/|\dot{\sigma}| + [(\sigma \cdot \dot{\sigma}/|\dot{\sigma}|)^2 + ((R^*)^2 - |\sigma|^2)]^{1/2} \tag{28}$$

Deviatoric stress rate: $$\dot{\tilde{\alpha}} = \mu_\sigma \dot{\sigma} \tag{29}$$

Chaboche: $$\dot{\tilde{\alpha}} = c[a(\sigma - \tilde{\alpha}) - \tilde{\alpha}]|\dot{\epsilon}^P| \tag{30}$$

It should be noted that the Mroz and Tseng-Lee models require specification of R^*, the limit surface radius. Several values of R^*, including the maximum effective stress in a cycle, were used in evaluating these models. Also, in the Chaboche model, constant a was selected as $a = 2.3$ to provide the best fit to the data from specimen SS01, block 3. Note

Downloaded 03 May 2010 to 171.66.16.27. Redistribution subject to ASME license or copyright; see http://www.asme.org/terms/Terms_Use.cfm

that the limit surface is stationary in both the Mroz and Tseng-Lee models.

Referring to Figs. 4–7, it is noted that degree of tangency of the vectors to the path of $\bar{\alpha}$ provides the measure of accuracy of each model.

As discussed later, it was found that the yield surface dimension does not experience significant change, assuming J_2' flow theory and a deviation from linearity definition of yield. Hence, a constant yield surface radius of $R = 160$ MPa was used in all calculations for the backstress path. In contrast, the limit surface radii required for the Mroz and Tseng-Lee rules experienced significant dependence on nonproportional loading. In Figs. 4–5 it was assumed that $R^* = \max|\sigma| + 30$ MPa where $\max|\sigma|$ is the maximum cyclically stable value of effective stress in each loading block.

From Figs. 4–7, it is clear that some models provide a good correlation for one history, but poor correlation for others. Interestingly, the hardening rules of Mroz and Chaboche are significantly less accurate than the rules associated with deviatoric stress rate. The hardening rule of Chaboche is less accurate for the sinusoidal loading paths than the deviatoric stress rate rules. The tremendous improvement of the Chaboche rule over the Prager (1956) or Ziegler (1959) rules indicates strongly that a dynamic recovery term must be included in a single surface (Drucker and Palgen, 1981) or state variable approach (Chan et al., 1984) which uses Prager-type hardening.

It is noted that there are some differences between the directions of yield surface translation given by the Tseng-Lee rule of equation (25) and the deviatoric stress rate. The deviatoric stress rate direction provides an overall superior correlation of the backstress rate direction.

However, use of deviatoric stress rate does not ensure nesting of yield and limit surfaces in a multiple surface model. Hence, the data indicates that the Tseng-Lee rule is superior to the Mroz rule for two surface theories, yet still invokes the desired nesting feature for both proportional and nonproportional loading.

Modulus Function. Accurate assignment of the hardening modulus function H in the flow rule

$$\dot{\epsilon}^P = \frac{1}{H}\langle \dot{\mathbf{s}}:\mathbf{n}\rangle \mathbf{n} \tag{31}$$

expressed in deviatoric stress space is extremely important for modeling nonproportional cyclic stress-strain response. In the axial torsional subspace, equation (20) is appropriate where $H = (2/3)h$. Modulus function h may be computed from experimental data since

$$h = \frac{(d\sigma/ds)\cdot\mathbf{n}}{(d\epsilon^P/ds)\cdot\mathbf{n}} \tag{32}$$

and $d\sigma/ds$, $d\epsilon^P/ds$, and $\mathbf{n}$ are known from numerical differentiation of data (McDowell, 1985d), where $s = \int(d\sigma\cdot d\sigma)^{1/2}$ is the effective stress arc length along the path.

McDowell (1985d) showed that dependence of h on the Mroz distance vector for a two surface theory

$$\delta_m = |\sigma^* - \sigma| \tag{33}$$

offered better correlation with nonproportional cyclic loading data than dependence on effective stress $\sqrt{3J_2'}$. Since dependence of h on δ_m is assumed in two surface models with Mroz-type kinematic hardening rules, it is not surprising that such models have consistently demonstrated superior accuracy for nonproportional cyclic plasticity.

Recent advances and close examination of experimental data, however, suggest that the correlation for h can be improved. In this work, several recently proposed independent variables will be considered and compared to the performance of δ_m.

It is now recognized (McDowell, 1985c, 1985d; Nouailhas et al., 1983) that for cyclic loading, the accumulation of inelastic strain in the history is not a sufficient independent variable for h or H. For nonproportional loading, it is clear that accumulation of plastic strain from the most recent point of elastic unloading, as suggested in earlier works (Eisenberg, 1976; Wu and Yip, 1981), is not sufficient.

For cyclic plasticity models which employ only a yield surface, nonproportionality effects can be included in the modulus function

$$H = F(\eta) + \frac{2}{3}\left(\frac{dR}{d\bar{\epsilon}^P}\right) \tag{34}$$

where $F(\eta)$ can be a history functional of the plastic strain trajectory, including path length and direction (Dafalias, 1984), i.e.,

$$F(\eta) = \mathbf{n}(\eta):\frac{d}{d\eta}\int_0^\eta \zeta(\eta-\eta')\mathbf{n}(\eta')d\eta' \tag{35}$$

where

$$d\eta = g(\bar{\epsilon}^P)d\bar{\epsilon}^P \tag{36}$$

and $\zeta(\eta - \eta')$ is an unspecified function.

It is noted that $F(\eta)$ is related to the kinematic hardening rule in the general rate-independent model structure given by Dafalias (1984) for a von Mises yield surface, i.e.,

$$f = \frac{3}{2}(\mathbf{s}-\boldsymbol{\alpha}):(\mathbf{s}-\boldsymbol{\alpha}) - R^2 = 0 \tag{37}$$

$$L = \frac{1}{H}(\dot{\mathbf{s}}:\mathbf{n}) \tag{38}$$

$$\dot{\boldsymbol{\alpha}} = \langle L\rangle F(\eta)\boldsymbol{\xi}/(\boldsymbol{\xi}:\mathbf{n}) \tag{39}$$

$$\dot{R} = \langle L\rangle\sqrt{\frac{2}{3}}\,dR/d\bar{\epsilon}^P \tag{40}$$

and the flow rule stated in equation (31). The reader can verify that the consistency condition is met by equations (31), (34), and (37)–(40). In equation (39), $\boldsymbol{\xi}$ is a unit vector representing the direction of translation of the yield surface.

As pointed out by Dafalias (1984), there are two very different procedures of assigning H in equation (34). One may define $F(\eta)$ which specifies H when $dR/d\bar{\epsilon}^P$ is known. This is indeed a very difficult task for nonproportional loading. An alternative route is offered by the multiple loading surface approaches (Lamba and Sidebottom, 1978; Dafalias and Popov, 1975; McDowell, 1985a, 1985b; Tseng and Lee, 1983; Mroz, 1967; Tanaka et al., 1985; Dafalias, 1981) in which H is specified and $F(\eta)$ is computed by invoking the consistency condition since $dR/d\bar{\epsilon}^P$ is known.

The recent theory offered by Krieg and Key for nonproportional loading (Krieg and Key, 1984) is an example of the first approach. In their model,

$$\dot{\epsilon}^P = \frac{(\mathbf{s}-\boldsymbol{\alpha}):\dot{\epsilon}}{\frac{2}{3}R^2[1 + (Z(\beta) + B)/3G]}(\mathbf{s}-\boldsymbol{\alpha}) \tag{41}$$

Since

$$\dot{\epsilon} = \dot{\mathbf{s}}/2G + \dot{\epsilon}^P + (1/3)(\dot{\epsilon}:\mathbf{I})\mathbf{I} \tag{42}$$

where $\mathbf{I}$ is the identity tensor, one can show that

$$H = \frac{2}{3}[Z(\beta) + B] \tag{43}$$

where β in this case is defined as the scalar product of the backstress and plastic strain rate direction, i.e.,

Downloaded 03 May 2010 to 171.66.16.27. Redistribution subject to ASME license or copyright; see http://www.asme.org/terms/Terms_Use.cfm

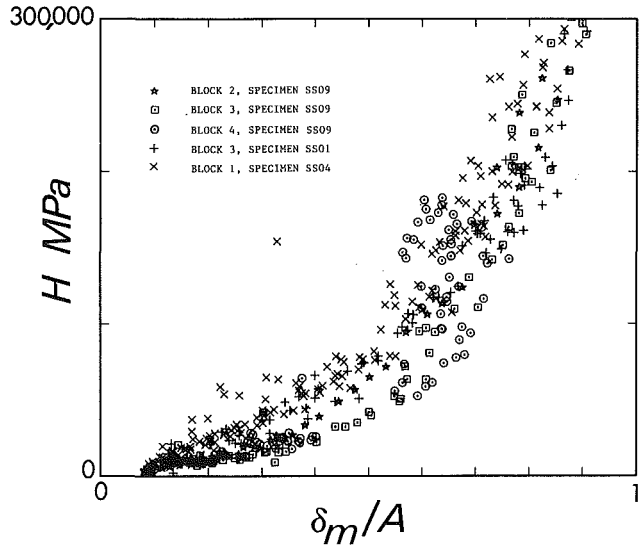


Fig. 8 Correlation of H versus δ/A for Mroz definition of δ. Stars, squares, circles, plus signs and x's correspond to data from stable cycles of block 2-4 of specimen SS09, block 3 of specimen SS01, and block 1 of specimen SS04, respectively.

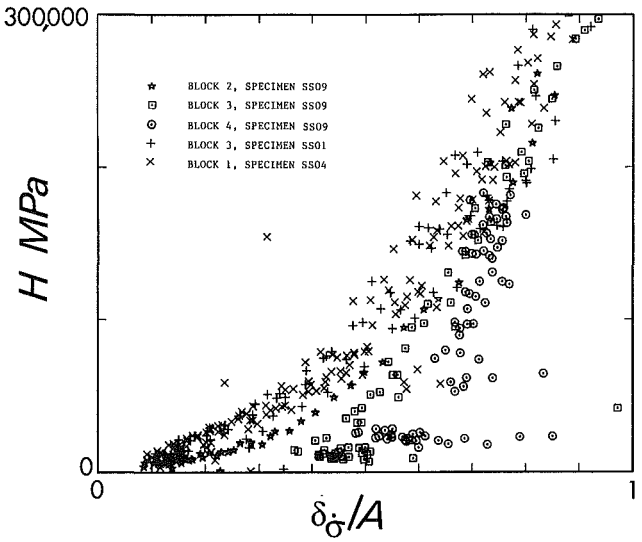


Fig. 9 Correlation of H versus δ/A for Tseng-Lee definition of δ

$$\beta = \alpha : \mathbf{n} \tag{44}$$

Parameter B is defined as the asymptotic slope of the stress-plastic strain curve. Hence, evaluation of this approach can be made by determining the correlative capability of the β parameter in equations (43)–(44).

The latter approach, in which H is specified, is exemplified by the Mroz or other multiple surface approaches. This paper will investigate the capability of several parameters within the context of a two surface theory. Denoting by δ some measure of distance from the current stress point to a point on the limit or bounding surface (i.e., asymptotic stress-strain response), H may be written as

$$H = H(\delta, \delta_{in}, H^*) \tag{45}$$

where δ_{in} is the value of δ at initiation of the yielding process. According to Dafalias (1981, 1984), δ_{in} provides a discrete memory parameter of the most recent unloading-reloading event. Parameter H^* is the asymptotic value of H reached at high levels of plastic strain accumulated since the most recent loading reversal. Use of δ_{in} is necessary in a two surface model to provide a memory of prior excursions in the plastic range; in multiple surface models, this memory is provided by the presence of a series of loading surfaces, each possessing an independent backstress and radius.

Table II Values of A for modulus parameter normalization

	Two Surface δ Parameters			Krieg-Key*	
	A (MPa)			A (MPa)	
History	δ_m	$\delta_{\dot{\sigma}}$	R^* (MPa)	max|σ|	max $(\bar{\alpha}\cdot n)$
SS09, Block #2	440	440	338	308	140
SS09, Block #3	530	360	429	399	230
SS09, Block #4	530	330	500	470	300
SS04, Block #1	465	470	494	464	300
SS01, Block #3	480	530	555	525	360

*R = 160 MPa

A general property of the modulus function is that $H \to H^*$ as $\delta/\delta_{in} \to 0$ and H is large ($\to \infty$) as $\delta/\delta_{in} \to 1$. There exists a multitude of possible forms for δ. First consider the axial torsional subspace forms

$$\delta = \delta_m \tag{46}$$

$$\delta = \delta_{\dot{\sigma}} \tag{47}$$

In Figs. 8–9, the correlative capability of δ/A for each of equations (46)–(47) with cyclically stable data from five loading blocks is shown. Here, A is a parameter used to normalize δ between 0 and 1. Parameter A is analogous to δ_{in} as discussed above. In these three plots, A was independently selected for each form of δ and each history to match the value of δ/A from proportional history block 2 of specimen SS09 at H = 300,000 MPa. Table II lists the values of A selected to normalize each history. Hence, the data is normalized at high modulus values for comparison. Again, a stationary limit surface with radius

$$R^* = \max|\sigma| + 30\ \text{MPa} \tag{48}$$

was used for determining these δ parameters, where max $|\sigma|$ is the maximum effective stress in a stable cycle for each history. Analysis of the data for widely varying values of R^*, as in an earlier paper (McDowell, 1985d), showed that the accuracy of each of these δ parameters is very weakly dependent on R^*.

To determine the relative performance of these two measures of δ, one can compare their ability to correlate data from several nonproportional cyclic paths. The measure of correlative capability is the uniqueness of the functional form independent of path. All data are obtained from cyclically stable cycles, so the hardening can be assumed purely kinematic, i.e., $dR/d\bar{\epsilon}^P = 0$. On the same basis, the Krieg-Key modulus function in equation (43) may be evaluated, considering the function $(\bar{\alpha}\cdot\mathbf{n})/A$.

Referring to Figs. 8–9, it is clear that the correlation achieved by the Mroz definition of δ is superior to the Tseng-Lee δ parameter. The Tseng-Lee definition of δ exhibits a very pronounced lack of correlation in the low modulus regime. The correlative capability of both δ parameters, though, cannot be judged entirely on the basis of Figs. 8–9 without consideration of the A values required for normalization. From Table II, it is seen that the A values are certainly not constant for each δ parameter for all histories. In fact, there does not appear to be any relationship between A and R^* for each parameter. This result for these *completely reversed* nonproportional loading histories is somewhat disturbing since A and δ_{in} mentioned in equation (45) should be essentially equivalent in this case. To further exemplify this point, δ_m/A was plotted versus H with $A = 2R^*$; a unique correlation was not obtained. It should be noted that several previous models

Downloaded 03 May 2010 to 171.66.16.27. Redistribution subject to ASME license or copyright; see http://www.asme.org/terms/Terms_Use.cfm

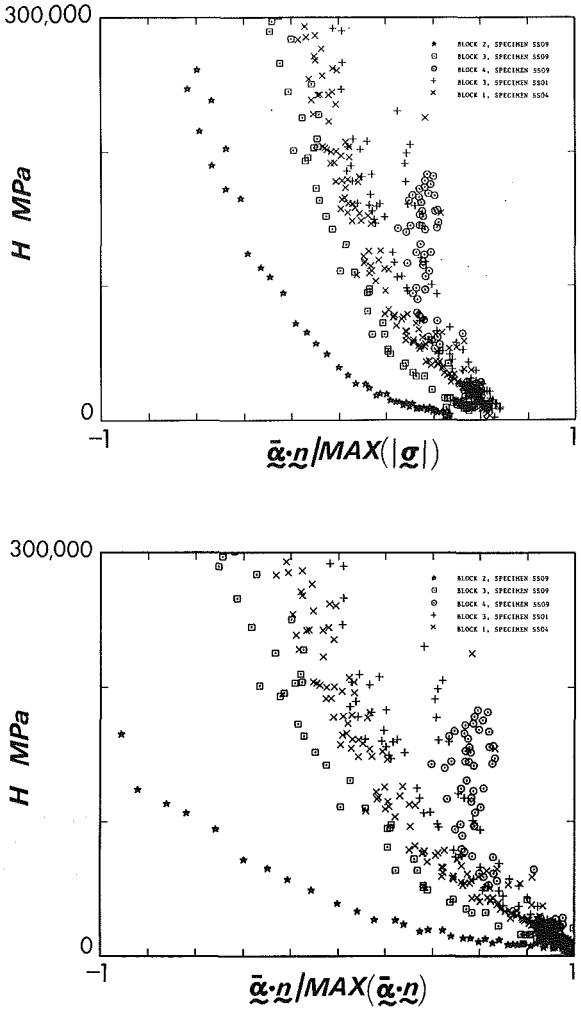


Fig. 10 Correlation of H versus Krieg-Key modulus parameter $(\bar{\alpha}\cdot\underline{n})/A$ for (top) A = max $|\underline{\sigma}|$ in cycle and (bottom) A = max $(\bar{\alpha}\cdot\underline{n})$ in cycle

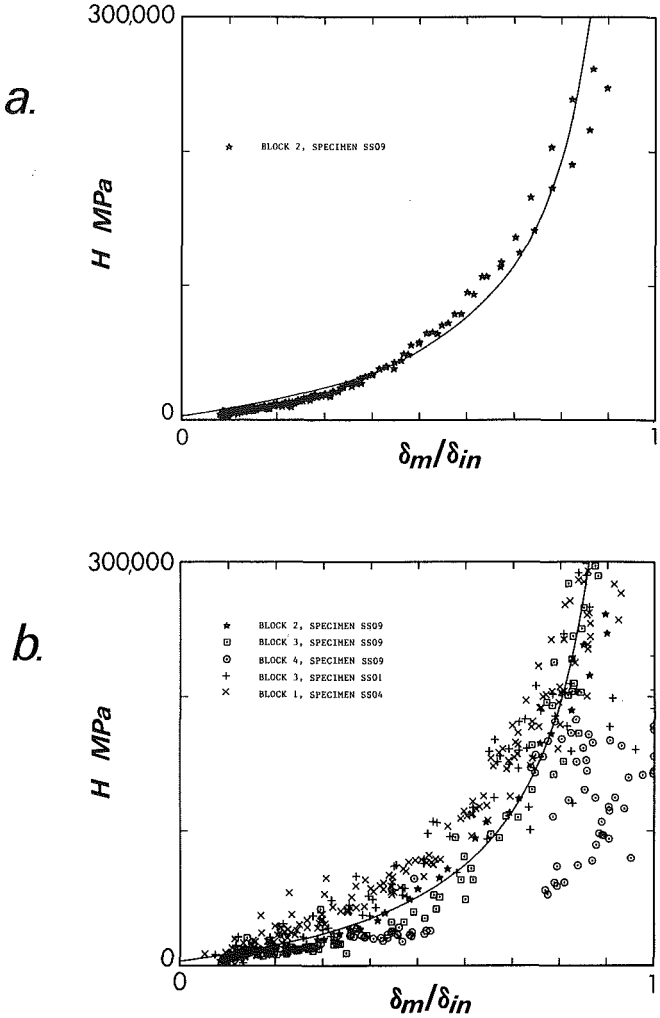


Fig. 11 Dafalias modulus function with $\delta = \delta_m$ (*a*) fit to proportionally loaded, stable cycle from block 2, specimen SS09, and (*b*) resulting correlation of data from other nonproportional histories with this function

for nonproportional loading based on the Mroz δ have employed this somewhat inaccurate normalization (Lamba and Sidebottom, 1978; McDowell et al., 1982).

The correlative capability of the Krieg-Key modulus function is shown in Fig. 10, where two different definitions of A are used to normalize the data. Both definitions appear in Table II. A value of R = 160 MPa was assumed in calculation of the backstress. Obviously, correlation of the data is very poor using this parameter. It should be noted that the correlation is not improved when a value of R = 300 MPa is used to compute backstress via equation (22).

Having evaluated the capability of several proposed parameters to correlate modulus variation during nonproportional loading, we turn to possible specific forms of equation (45) since the multiple surface (two surface, in this case) plasticity models have demonstrated superior correlation of modulus if δ is properly selected. It has already been established in this work that normalization of δ by a constant or by R^* or maximum effective stress will not produce satisfactory correlation. Hence, we must seek forms for H which employ a normalizing parameter which is a function of the history of loading.

Dafalias (1981, 1984) has proposed a specific form of equation (45), i.e.,

$$H = \left[1 + g(\delta_{in})\left(\frac{\delta/\delta_{in}}{1-\delta/\delta_{in}}\right)\right]H^* \tag{49}$$

where $g(\delta_{in})$ controls the slope of the stress-strain curve. Though rather elaborate rules can be devised to properly assign δ_{in} for unloading-reloading events, such rules will be unnecessary in this work since only completely reversed, nonproportional cyclic loading will be considered. Again, note that the precise form for δ is left unspecified in equation (49). In fact, Tseng and Lee have used equation (49) for H along with their definition of $\delta = \delta_{\dot{s}}$ from equation (8).

Equation (49) has the property that $H \to \infty$ as $\delta \to \delta_{in}$, i.e., at initial yielding. Also, $H \to H^*$ as $\delta \to 0$, i.e., approaching the limit surface.

In Fig. 11(*a*), the Dafalias modulus function is fit to proportional loading history SS09, block 2 with $\delta = \delta_m$, g = 16, δ_{in} = 417 MPa, R^* = 338 MPa, and H^* = 3000 MPa. It should be noted that a better fit could be obtained if the modulus function were nonlinear in (δ_m/δ_{in}) / $(1-\delta_m/\delta_{in})$. The best measure of usefulness of any modulus function, of course, is the capability to extend uniaxial or proportional loading test results to the nonproportional case. Figure 11(*b*) shows the correlation obtained for all histories of this study using the Dafalias function with g = constant; the solid line is reproduced from Fig. 11(*a*), representing proportional cycling. In all cases, δ_{in} was defined as the maximum value of δ_m during plastic flow for each history.

From Fig. 11, it is apparent that the correlation is satisfactory for all histories except SS09, block 4 (i.e., 60 degree out-of-phase sinusoidal loading). This history does not exhibit

Downloaded 03 May 2010 to 171.66.16.27. Redistribution subject to ASME license or copyright; see http://www.asme.org/terms/Terms_Use.cfm

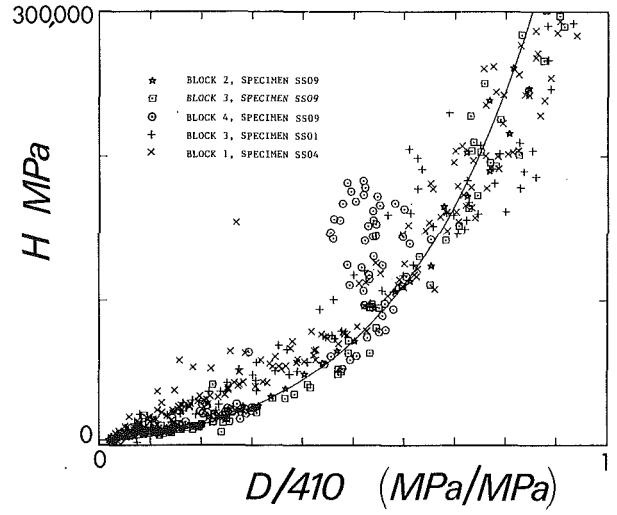


Fig. 12 Correlation of H versus D. Solid line is that obtained by fitting proportional loading data from specimen SS09, block 2.

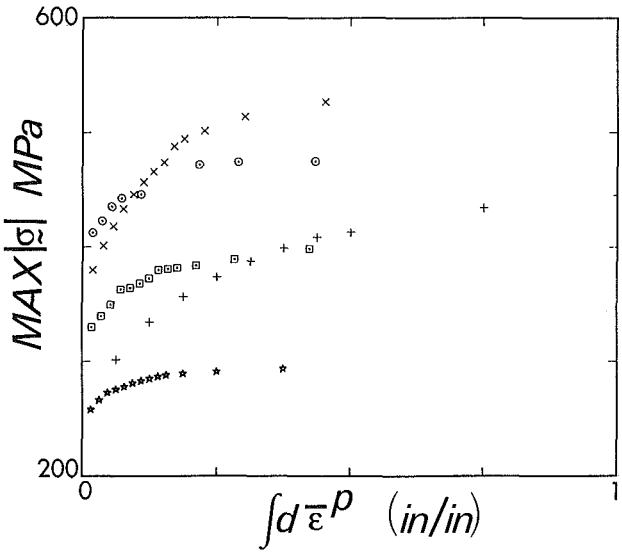


Fig. 13 Maximum effective stress in each cycle versus accumulated plastic strain for several loading blocks including block 3, specimen SS09 (squares), block 4, specimen SS09, (circles), block 1, specimen SS04 (plus signs), block 1, specimen SS01 (stars), and block 3, specimen SS01 (x's)

unloading response; hence, the normalizing parameter δ_{in} is likely more properly determined from a reversal prior to this history. The value of δ_{in} = 545 MPa obtained for history SS09, block 3 is close to the value of A = 530 MPa required for correlation with δ_m as reported in Table II. This history points out a difficulty with a normalization procedure that depends on the initiation of yielding for nonproportional loading. In particular, it is very difficult to assign a proper definition of δ_{in} for such histories. Also, it is important that the modulus function fit proportional cycling data well. Other models (Chan et al., 1984) have employed an exponential or hyperbolic sine fit.

To obviate the difficulty associated with use of δ_{in} as a normalizing parameter, another was sought which depended on current state rather than prior history. Examination of the data indicated that the quantity $(\mathbf{n}\cdot\mathbf{n}_{\delta m})$, representative of the noncollinearity of the loading increment, is essential to obtaining good correlation of data in addition to a distance parameter. The best correlation is achieved by employing this quantity as a modifier of the normalizing parameter, i.e.,

$$H = H^*[1 + G(\delta_{in})\{\sinh(k_1 D)\}^{k_2}] \tag{50}$$

where

$$D = \left\{\frac{\delta_m}{2 - |\mathbf{n}\cdot\mathbf{n}_{\delta m}|}\right\} \tag{51}$$

k_1 and k_2 are constants, and $\mathbf{n}_{\delta m} = (\sigma^* - \sigma)/\delta_m$.

Here, $G(\delta_{in})$ is a memory repository intended to account for unloading-reloading effects. In the axial torsional subspace, assuming $G(\delta_{in})$ = constant for these histories under consideration, the relationship

$$H = 3000[1 + 16\{\sinh(0.005D)\}^{1.75}]\text{MPa} \tag{52}$$

is determined by fitting the response from the proportional loading block 2 of specimen SS09. All other histories are plotted in Fig. 12 using equation (52) with R^* = max $|\sigma|$ + 30 MPa in each case. Excellent correlation of the data is obtained. Furthermore, the constants are determined only from uniaxial or equivalent proportional loading tests.

It must be stated that no claim is made here regarding the generality of any specific approach for all metals. It is important to realize, though, thay any truly promising modulus function must exhibit good correlation of various nonproportional loading paths for *at least one* material. In this regard, the fact that one modulus function produced good correlation in this study is encouraging. Other materials, of course, must be studied to provide more perspective. The author is not aware of similar detailed evaluation of modulus functions for nonproportional cyclic loading of other materials.

Isotropic Hardening. It is now widely recognized (McDowell, 1983; Kanazawa et al., 1979; Krempl and Lu, 1984) that the extent of isotropic hardening may depend on the nonproportionality of loading. Austenitic stainless steels, for example, exhibit a tremendous cumulative increase in flow stress under nonproportional biaxial loading relative to stable uniaxial cycling. This effect is certainly evident in the biaxial histories of this study, as presented elsewhere (McDowell, 1983). In fact, 90 degree out-of-phase sinusoidal, axial torsional, strain-controlled loading results in nearly a 100 percent increase in effective flow stress over the uniaxial case at the same effective plastic strain range.

McDowell (1985a, 1985b) introduced a measure of nonproportionality of loading ϕ which entered into the isotropic hardening rule for a scalar variable, κ, i.e.,

$$\dot{\kappa} = \bar{\mu}(\bar{\kappa}(\phi, q) - \kappa)(\dot{\epsilon}^P : \dot{\epsilon}^P)^{1/2} \tag{53}$$

Note that the cyclically stable state, $\bar{\kappa}$, is dependent upon the nonproportionality of the loading path and plastic strain range, reflected by ϕ and q, respectively.

This measure of nonproportionality resulted in good correlation of sinusoidal nonproportional biaxial loading (McDowell, 1985b). It results in ϕ values of $0 \le \phi \le 1$ such that $\phi = 0$ for proportional straining, and $\phi = 1$ for 90 degree out-of-phase sinusoidal, axial torsional straining with a shear to axial strain amplitude ratio of $\gamma_a/\epsilon_a = (1+\nu)$. There are several reservations which require development of another approach. First, this approach applies only to cases where the principal axes of strain continuously rotate at some point during the loading cycle. Secondly, this approach does not provide good correlation of square loading paths or nonproportional loading paths other than sinusoidal. Thirdly, calculation of ϕ is based on total strain and strain rate; from a mechanistic viewpoint, nonproportionality of plastic strain rate should more closely relate to increased activation and interaction of slip systems and, hence, additional isotropic hardening.

Several alternate approaches for nonproportional isotropic hardening have been suggested recently. Bodner and Partom (Lindholm et al., 1985) and Walker (Lindholm et al., 1985) have introduced isotropic hardening rules intended to account

Downloaded 03 May 2010 to 171.66.16.27. Redistribution subject to ASME license or copyright; see http://www.asme.org/terms/Terms_Use.cfm

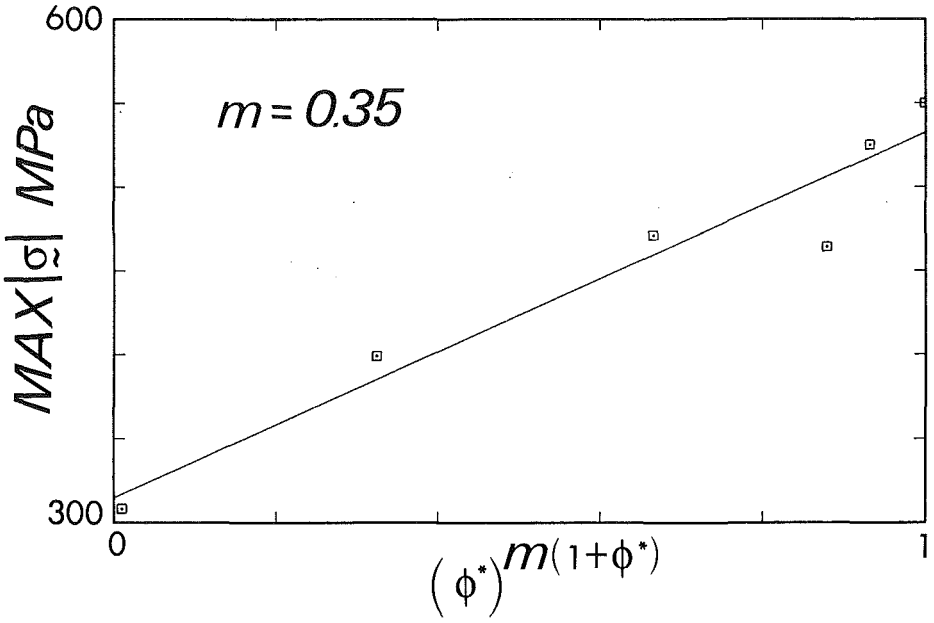


Fig. 14 Correlation of isotropic hardening achieved using state variable ϕ^* for several nonproportional loading blocks. The value of max $|\underset{\sim}{\sigma}| \simeq 550$ MPa was reported by Krempl and Lu (1984) for 90 deg out-of-phase loading (i.e. $\phi^* = 1$).

for additional nonproportional hardening. Both approaches, however, assume a unique cyclically stable state independent of the degree of nonproportionality of the path. This prediction of saturation to a single limiting value of κ is not supported by experiments (McDowell, 1983; Kanazawa et al., 1979; Krempl and Lu, 1984). In Fig. 13, the maximum effective stress in each cycle, max $|\sigma|$, is plotted versus the accumulated plastic strain $\int(d\epsilon^P \cdot d\epsilon^P)^{1/2}$ for loading blocks from each of the three histories of this study. It is noted that the cyclically stable state depends greatly on the nonproportionality of the loading path. This behavior is the key feature of nonproportional loading.

We now turn to development of an appropriate isotropic hardening rule which includes dependence of the hardening rate and final state on the nonproportionality of the loading history. For correlation of the final state a number of parameters were investigated, including $(\mathbf{n}:\dot{\mathbf{s}}/\|\dot{\mathbf{s}}\|)$, $((\mathbf{s}/\|\mathbf{s}\|) : (\dot{\mathbf{s}}/\|\dot{\mathbf{s}}\|))$ (e.g., Bodner et al., Lindholm et al., 1985) and $(\mathbf{n}:\mathbf{s}/\|\mathbf{s}\|)$. None demonstrated correlation of data with the exception of $(\mathbf{N}:\mathbf{n})$, where $\mathbf{N}$ is the unit normal vector in the direction of ϵ^P at the point of maximum plastic strain excursion in the current loading block. We may unambiguously define a loading block as a repeated assemblage of identical cycles or combination of cycles and subcycles. Careful examination of data led to the folllwing plastic strain-based parameter:

$$\phi^* = \left(\frac{\pi}{\pi-2}\right)\left|\left(\frac{\pi-2}{\pi}\right) - \left|\Lambda - \frac{2}{\pi}\right|\right| \tag{54}$$

where

$$\Lambda = \frac{1}{\int_{t_B}^{t} \|\dot{\epsilon}^P\| dt} \int_{t_B}^{t} |\mathbf{N}:\dot{\epsilon}^P| dt \tag{55}$$

and $\mathbf{N} = \epsilon^{P^*}/\|\epsilon^{P^*}\|$ where ϵ^{P^*} is the plastic strain at the maximum value of $\|\epsilon^P\|$ in the current loading block. The time at the initiation of the current loading block is given by t_B. Similar to ϕ, it can be shown that $\phi^* = 0$ for proportional loading and $\phi^* = 1$ for 90 degree out-of-phase sinusoidal, axial-torsional loading with $\gamma_a/\epsilon_a = \sqrt{3}$ and $\nu = 1/2$. From a physical viewpoint, Λ represents the plastic strain averaged component of the inelastic strain rate in the maximal plastic strain direction. Since it is defined as an averaged noncollinearity of plastic strain, it should relate more fundamentally to isotropic hardening micro-mechanisms.

An appropriate evolution equation for an isotropic hardening variable κ is

$$\dot{\kappa} = \mu_o[\kappa_o + K(\phi^*)^{m(1+\phi^*)} - \kappa](\dot{\epsilon}^P:\dot{\epsilon}^P)^{1/2} \tag{56}$$

where μ_o and m are constants, and K is at most a function of plastic strain range (McDowell, 1985a). Parameter κ_o, also a function of plastic strain range, is the uniaxial cyclically stable value of κ. Note the nonlinear dependence of the final state ($\kappa_o + K\ (\phi^*)^{m(1+\phi^*)}$) on ϕ^*.

Figure 14 demonstrates the correlation obtained for the various loading blocks of this study between the cyclically stable value of maximum effective stress in a cycle, max $|\sigma|$, and $(\phi^*)^{m(1+\phi^*)}$; the implicit assumption in this plot that K = constant is justifiable since the effective plastic strain ranges for all these histories are nearly equivalent. The correlation is quite good considering the differences in nonproportional loading paths considered.

In Fig. 15, assuming κ = max $|\sigma|$ in each cycle, the values of κ from the histories of this study are normalized and plotted versus accumulated plastic strain, $\int|\dot{\epsilon}^P|dt$, in each associated loading block. The normalization of max $|\sigma|$ in Fig. 15 is made between the initial and final values of max $|\sigma|$ in each cycle for each loading block. Interestingly, most of the histories essentially follow the hardening response observed for the proportional straining of initially annealed material in block 1 of history SS01. This is true of histories for which the principal strain directions rotate continuously (e.g., block 3 of SS01, blocks 3-4 of SS09). However, the rate of hardening observed for specimen SS04 in Fig. 15 is significantly lower than that of the other blocks. This behavior can possibly be related to the fact that plastic strain is accumulated in this history along discrete sets of principal directions. Hence, the hardening rate may be dependent on directional accumulation of plastic strain. It should be noted that this hardening rate behavior could not be correlated with either of the Bodner-

Downloaded 03 May 2010 to 171.66.16.27. Redistribution subject to ASME license or copyright; see http://www.asme.org/terms/Terms_Use.cfm

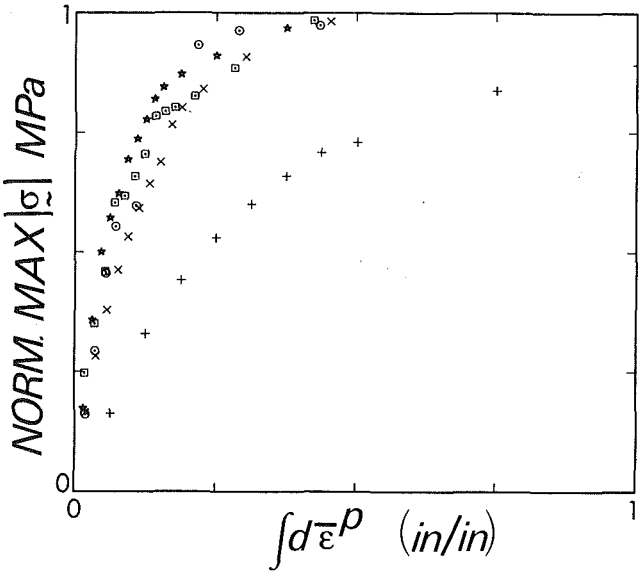


Fig. 15 Normalized maximum effective stress in each cycle versus accumulated plastic strain for several loading blocks. Normalization is between the initial and stable values of max $|\sigma|$ for each loading block. Symbols correspond to the same histories as in Fig. 13.

Partom or Walker rate approaches. In fact, none of the parameters mentioned earlier in conjunction with the correlation of the level of isotropic hardening were viable in correlating the reduced hardening rate of specimen SS04. In view of the correlation which can be achieved for the other histories via the simple approach in equation (56) and the fact that hardening rate is a second order effect compared to the extent of hardening, it may not be necessary to include dependence of the hardening rate coefficient on the nonproportionality of loading. Certainly, more data is desirable to include such dependence.

As a final point, it should be noted that in general it is necessary to allow continuous evolution of **N** between successive loading blocks. An example would be a number of cycles of axial loading followed by torsional cycling. Experimentally, some additional hardening is observed in such cases (McDowell, 1983; Krempl and Lu, 1984). Instantaneous redefinition of **N** to the current proportional cycling block would be incompatible with this observation. From a micromechanical viewpoint, the values of the resolved shear stresses on slip planes within each grain have certainly changed, and a latent hardening effect is quite reasonably expected.

Isotropic Hardening – Evolution of Yield Surface or Modulus Function?

The maximum effective stress in a cycle relates closely to R^*, the radius of a limit surface in a two surface theory. In general, both the yield and limit surfaces can isotropically harden. Isotropic hardening of the yield surface is usually associated with changes in the small offset yield strength after accounting for kinematic hardening. Likewise, isotropic hardening of the limit surface is associated with changes in the flow stress at relatively large plastic strain levels.

It is interesting to consider that the modulus function H can also be a repository for isotropic hardening. In fact, it is difficult to separate changes in the modulus function from growth of the yield surface defined by a plastic strain offset on the basis of uniaxial tests. Nonproportional cyclic loading tests are quite helpful in this regard since it is possible to determine the position of the center of any assumed yield surface form by backward extrapolation of the plastic strain rate direction after abrupt changes in loading direction. Since for stable cycling hardening is purely kinematic, one should not observe abrupt changes in the yield surface center after an unloading-reloading sequence in a different direction for a simple von Mises yield surface. From plots of backstress for several nonproportional loading blocks it was observed that $R = 160$ MPa results in the smoothest path of $\tilde{\alpha}$. Since $R = 148$ MPa is the yield strength of the virgin annealed material, defined by a deviation from linearity (McDowell, 1985b), it is clear that very little of the isotropic hardening can be attributed to the growth of a small offset or deviation from linearity-defined yield surface; rather, it must be accommodated in the modulus function through an isotropic variable associated with limit, not yield, behavior. In a two surface theory this corresponds to growth of the limit surface. As a result, the kinematic hardening variable will exhibit increased magnitude during nonproportional hardening.

This result is of considerable importance for this material, since the extent of isotropic hardening is relatively exceptional. It is somewhat fortuitous from a modeling standpoint, since it infers that the domain of purely elastic behavior for a rate-independent material response is less influenced in magnitude by complex loading than the domain of plastic behavior. Again, perspective must be maintained since only one material has been analyzed. Certainly, though, this result warrants study in other materials under complex nonproportional loading.

Of course, the objection may be made that anisotropic deformation of the yield surface may lead to a perceived abrupt change in α as observed for larger assumed yield surface radii. However, it is observed that the anisotropic deformation of the yield surface (Shiratori et al., 1979; Hecker, 1976) is strongly a function of the offset plastic strain yield definition. Anistropy is much more pronounced for small offset definitions of yield. Since nearly all computational codes for initially isotropic, rate-independent metals employ a simple yield surface, usually of von Mises form, it is worthwhile to experimentally investigate the integrity and extension of such an approach; the bounding surface approach, in particular, offers the capability to model anisotropic plastic flow via the modulus function although the yield surface is a simple form.

Conclusions

Analysis of nonproportional cyclic loading data for type 304 stainless steel at room temperature has revealed some interesting results.

1 The kinematic hardening rule for von Mises yield and limit surfaces is prescribed more accurately by a deviatoric stress rate rule which provides for nesting than by a Mroz rule.

2 If a Prager-type kinematic hardening rule is used in either a state variable or single loading surface theory, a dynamic recovery term must be included to correlate nonproportional data. The accuracy of such an approach, though, was found inferior to that of the two-surface theory with a deviatoric stress rate-type rule.

3 A modulus function based on the distance from the current stress point to the limit surface in the direction of deviatoric stress rate does not correlate nonproportional loading data uniquely.

4 A modulus function based on a Mroz distance vector can be improved by including in the normalization the scalar product of the plastic strain rate direction with the Mroz vector. Proper definition of δ_{in} as proposed by Dafalias appears to be a very difficult task for nonproportional loading.

5 A modulus function is proposed which correlates the data from several different nonproportional histories quite well. It is determined entirely from uniaxial or proportional loading tests.

6 A more general isotropic hardening rule is proposed

Downloaded 03 May 2010 to 171.66.16.27. Redistribution subject to ASME license or copyright; see http://www.asme.org/terms/Terms_Use.cfm

which correlates the observed additional hardening. It is found that, within the context of the second invariant plasticity theory, the isotropic hardening is predominantly associated with the growth of an isotropic limit surface rather than the yield surface.

Acknowledgments

The author wishes to acknowledge the National Science Foundation for support of this research.

References

Chaboche, J. L., Dang-Van, K., and Cordier, G., 1979, "Modelization of Strain Memory Effect on the Cyclic Hardening of 316 Stainless Steel," *Trans. 5th SMiRT*, L 11/3, Berlin.

Chan, K. S., Bodner, S. R., Walker, K. P., and Lindholm, U. S., 1984, "A Survey of Unified Constitutive Theories," *Proc. 2nd Symp. on Nonlinear Constitutive Relations for High Temperature Applications*, NASA Lewis Research Center, June 13–15.

Dafalias, Y. F., 1981, "The Concept and Application of the Bounding Surface in Plasticity Theory," Physical Non-Linearities in Structural Analysis, Hult, J., and Lemaitre, J., eds., *IUTAM Symposium*, Senlis, France, Springer Verlag, pp. 56–63.

Dafalias, Y. F., and Popov, E. P., 1975, "A Model of Nonlinearly Hardening Materials for Complex Loading," *Acta Mechanica*, Vol. 21, pp. 173–192.

Dafalias, Y. F., 1984, "Modeling Cyclic Plasticity: Simplicity Versus Sophistication," *Mechanics of Engineering Materials*, Desai and Gallagher, eds., Wiley, pp. 153–178.

Drucker, D. C., and Palgen, L., 1981, "On Stress-Strain Relations Suitable for Cyclic and Other Loading," ASME JOURNAL OF APPLIED MECHANICS, Vol. 48, pp. 479–485.

Eisenberg, M. A., 1976, "A Generalization of Plastic Flow Theory with Application to Cyclic Hardening and Softening Phenomena," ASME *Journal of Engineering Materials and Technology*, Vol. 98, pp. 221–228.

Hecker, S. S., 1976, "Experimental Studies of Yield Phenomena in Biaxially Loaded Metals," *Constitutive Equations in Viscoplasticity: Computational and Engineering Aspects*, AMD, ASME, Vol. 20, pp. 1–32.

Kanazawa, K., Brown, M. W., and Miller, K. J., 1979, "Cyclic Deformation of 1% Cr-Mo-V Steel Under Out-of-Phase Loads," *Fatigue of Engineering Materials and Structures*, Vol. 2, pp. 217–228.

Krempl, E., and Lu, H., 1984, "The Hardening and Rate-Dependent Behavior of Fully Annealed AISI Type 304 Stainless Steel Under Biaxial In-Phase and Out-of-Phase Strain Cycling at Room Temperature," ASME *Journal of Engineering Materials and Technology*, Vol. 106, pp. 376–382.

Krieg, R. D., 1975, "A Practical Two Surface Plasticity Theory," ASME JOURNAL OF APPLIED MECHANICS, Vol. 42, pp. 641–646.

Krieg, R. D., and Key, S. W., 1984, "On the Accurate Representation of Large Strain Non-Proportional Plastic Flow in Ductile Metals," *Proc. ASME Winter Annual Meeting, Constitutive Equations: Macro and Computational Aspects*, New Orleans, pp. 41–52.

Lamba, H. S., and Sidebottom, O. M., 1978a, "Cyclic Plasticity for Nonproportional Paths: Part 1—Cyclic Hardening, Erasure of Memory, and Subsequent Strain Hardening Experiments," ASME *Journal of Engineering Materials and Technology*, Vol. 100, pp. 96–103.

Lamba, H. S., and Sidebottom, O. M., 1978b, "Cyclic Plasticity for Nonproportional Paths:3Part 2—Comparison with Predictions of Three Incremental Plasticity Models," ASME *Journal of Engineering Materials and Technology*, Vol. 100, pp. 104–111.

Lindholm, U.S., Chan, K. S., Bodner, S. R., Weber, R. M., Walker, K. P., and Cassenti, B. N., 1985, "Constitutive Modeling for Isotropic Materials," NASA CR-174980, SwRI-7476/30.

McDowell, D. L., 1983a, "On the Path Dependence of Transient Hardening and Softening to Stable States Under Complex Biaxial Cyclic Loading," *Proceedings of the International Conference on Constitutive Laws for Engineering Materials*, Desai and Gallagher, eds., Tucson, AZ, pp. 125–132.

McDowell, D. L., 1983b, "Transient Nonproportional Cyclic Plasticity," Report No. 107, Design and Materials Division, Dept. of Mechanical and Industrial Engineering, University of Illinois at Urbana-Champaign.

McDowell, D. L., 1985a, "A Two Surface Model for Transient Nonproportional Cyclic Plasticity: Part I – Development of Appropriate Equations," ASME JOURNAL OF APPLIED MECHANICS, Vol. 52, pp. 298–302.

McDowell, D. L., 1985b, "A Two Surface Model for Transient Nonproportional Cyclic Plasticity: Part II – Comparison of Theory with Experiments," ASME JOURNAL OF APPLIED MECHANICS, Vol. 52, pp. 303–308.

McDowell, D. L., 1985c, "The Significance of Nonproportional Loading Tests for Characterization of Cyclic Response of Metals," *Proc. 1985 Spring Conference on Experimental Mechanics, Society for Experimental Stress Analysis*, Las Vegas, pp. 229–236.

McDowell, D. L., 1985d, "An Experimental Study of the Structure of Constitutive Equations for Nonproportional Cyclic Plasticity," ASME *Journal of Engineering Materials and Technology*, Vol. 107, pp. 307–315.

McDowell, D. L., Socie, D. F., and Lamba, H. S., 1982, "Multiaxial Nonproportional Cyclic Deformation," ASTM STP 770, pp. 500–518.

Mroz, Z., 1967, "An Attempt to Describe the Behaviour of Metals Under Cyclic Loads Using a More General Workhardening Model," *Acta Mechanica*, Vol. 7, pp. 199–212.

Nouailhas, D., Policella, H., and Kaczmarek, H., 1983, "On the Description of Cyclic Hardening Under Complex Loading Histories," *Proceedings of the International Conference on Constitutive Laws for Engineering Materials*, Desai and Gallagher, eds., Tucson, AZ, pp. 45–49.

Phillips, A., and and Lee, C. W., 1979, "Yield Surfaces and Loading Surfaces. Experiments and Recommendations," *International Journal of Solids and Structures*, Vol. 15, pp. 715–729.

Phillips, A., Tang, J. L., and Ricciuti, M., 1974, "Some New Observations on Yield Surfaces," *Acta Mechanica*, Vol. 20, pp. 23–39.

Prager, W., 1956, "A New Method of Analyzing Stresses and Strains on Work-Hardening Plastic Solids," ASME JOURNAL OF APPLIED MECHANICS, Vol. 23, pp. 493–496.

Shiratori, E., Ikegami, K., and Yoshida, F., 1979, "Analysis of Stress-Strain Relations by Use of an Anisotropic Hardening Plastic Potential," *Journal of the Mechanics and Physics of Solids*, Vol. 27, pp. 213–229.

Tanaka, E., Murakami, S., and Ooka, M., 1985, "A Constitutive Model of Cyclic Plasticity in Multiaxial Non-Proportional Loading," L 2/4, *SMiRT 8*.

Tseng, N. T., and Lee, G. C., 1983, "Simple Plasticity Model of the Two-Surface Type," *ASCE Journal of Engineering Mechanics*, Vol. 109, No. 3, pp. 795–810.

Wu, H. C., and Yip, M. C., 1981, "Endochronic Description of Cyclic Hardening Behavior for Metallic Materials," ASME *Journal of Engineering Materials and Technology*, Vol. 103, pp. 212–217.

Ziegler, H., 1959, "A Modification of Prager's Hardening Rule," *Quarterly of Applied Mathematics*, Vol. 17, pp. 55–60.

Downloaded 03 May 2010 to 171.66.16.27. Redistribution subject to ASME license or copyright; see http://www.asme.org/terms/Terms_Use.cfm

A. Chandra
Assistant Professor,
Aerospace and Mechanical Engineering Department,
University of Arizona,
Tucson, AZ 85721
Assoc. Mem. ASME

S. Mukherjee
Professor,
Department of Theoretical & Applied Mechanics,
Cornell University,
Ithaca, NY 14853
Mem. ASME

A Boundary Element Analysis of Metal Extrusion Processes

The subject of this paper is an analysis of metal extrusion processes by the boundary element method (BEM). It is demonstrated here that the BEM can be used to analyze, efficiently and accurately, this complicated class of problems including both material and geometrical nonlinearities. Numerical results for sample problems of plane extrusion of aluminum bars, obtained by the BEM, are presented and discussed in this paper. The BEM results are compared against FEM results for the same sample problems. The FEM results were reported by the authors in a previous publication.

Introduction

Metal forming processes such as extrusion, rolling, sheet metal forming, etc., generally subject the workpiece to finite-strains and displacements. The components of elastic strain, in these examples, are generally limited to about 10^{-3} since the elastic moduli of metals are typically about three orders of magnitude larger than the yield stress. Thus, the nonelastic strain components, which can be of the order of unity, greatly dominate the elastic strains.

A considerable body of literature (e.g., McMeeking and Rice, 1975; Lee et al., 1977; Dawson and Thompson, 1977; Oh et al., 1983; Onate and Zienkiewicz, 1983; Chandra and Mukherjee, 1984 a,b) exists where the finite element method has been used to analyze metal forming problems, using rigid plastic, elastic-plastic, flow type and elastic-viscoplastic material models. While the finite element method has been very successful in several engineering applications, it is quite sensitive to aspect ratios of individual elements. This requires remeshing where severe deformation is involved. Moreover, the secondary variables obtained through numerical differentiation in a finite element technique are inherently less accurate than the primary variables. In a typical displacement formulation, the secondary variables are stresses, and, in a problem involving both material and geometric nonlinearities, the stresses at the present time essentially drive the problem through future time steps. These are the two major limitations of typical FEM approaches, that stand in the way of robust and cost effective yet accurate FEM analyses of metal forming processes. The analyses of Oh et al. (1983), Dawson and Thompson (1977), and Onate and Zienkiewicz (1983) are cost effective, but all of them treat the metal forming process as viscous flow. Thus, very critical quantities like residual stresses cannot be recovered from such analyses. Also, the viscous flow approaches are more suitable for steady state processes.

Contributed by the Applied Mechanics Division for publication in the JOURNAL OF APPLIED MECHANICS.
Discussion on this paper should be addressed to the Editorial Department, ASME, United Engineering Center, 345 East 47th Street, New York, N.Y. 10017, and will be accepted until two months after final publication of the paper itself in the JOURNAL OF APPLIED MECHANICS. Manuscript received by ASME Applied Mechanics Division, December 9, 1986.

The boundary element method (BEM – also called the boundary integral equation method) is another powerful general purpose method (Banerjee and Butterfield, 1981; Mukherjee, 1982; Brebbia et al., 1984). It is far more tolerant of aspect ratio degradation than the FEM and can yield secondary variables as accurately as the primary ones. Recently, Chandra and Mukherjee (1984c, 1985), Mukherjee and Chandra (1984, 1986) have obtained a BEM formulation capable of incorporating both material and geometric nonlinearities. The BEM formulation of Chandra and Mukherjee is extended here to analyze practical metal forming problems. The elastic-viscoplastic state variable model originally proposed by Hart (1976) and later modified to include large strains (Chandra and Mukherjee, 1984a,b,c, 1985; Hart, 1982) is used here for material characterization.

This paper begins with a discussion of the boundary element formulation for 3-D and planar problems. A description of the numerical implementation for planar problems follows. Special attention is paid to the formulation of the load correlation matrix for general follower loads and modelling of friction boundary conditions at the die-workpiece interface. The process of plane strain extrusion is analyzed. The results obtained from the BEM are then compared to those obtained from the FEM with regard to computational effort and accuracy.

Boundary Element Formulation

Kinematics. A three-dimensional body is considered in this section. Referring to a set of spatially fixed rectangular Cartesian coordinates, a material particle in the body in a reference configuration is assumed to have coordinates X_i. The same particle has coordinates x_i in the current configuration. Unless otherwise indicated, the range of indices in this section is 1, 2, 3.

The displacement vector u_i is defined by the equation

$$x_i = X_i + u_i \tag{1}$$

The velocity of this material point during deformation is denoted by v_i. The deformation rate d_{ij} is the symmetric part of the velocity gradient.

Copyright © 1987 by ASME
Downloaded 03 May 2010 to 171.66.16.27. Redistribution subject to ASME license or copyright; see http://www.asme.org/terms/Terms_Use.cfm

$$d_{ij} = (1/2)\left(\frac{\partial v_i}{\partial x_j} + \frac{\partial v_j}{\partial x_i}\right), \tag{2}$$

whereas, the spin ω_{ij} is the antisymmetric part.

$$\omega_{ij} = (1/2)\left(\frac{\partial v_i}{\partial x_j} - \frac{\partial v_j}{\partial x_i}\right). \tag{3}$$

Constitutive Assumptions. The boundary element formulation presented next is valid for a wide range of elastic-viscoplastic models. It is valid for compressible as well as incompressible plasticity. While some details about these models are given later, the key assumptions used in the BEM formulation are presented here.

The first assumption is that the deformation rate tensor can be linearly decomposed into an elastic and a nonelastic part (Chandra and Mukherjee, 1984 a,b,c, 1985; Nemat-Nasser, 1982),

$$d_{ij} = d_{ij}^{(e)} + d_{ij}^{(n)}. \tag{4}$$

The next step relating $d_{ij}^{(e)}$ to the stress rate is very important. A hypoelastic material is one in which the components of a (proper) stress rate are homogeneous linear functions of the components of a (proper) rate of deformation. One form of such a law, under conditions of material isotropy (of the virgin specimen) can be written as,

$$\overset{*}{\sigma}_{ij} = \lambda d_{kk}^{(e)} \delta_{ij} + 2G d_{ij}^{(e)}, \tag{5}$$

where $\overset{*}{\sigma}_{ij}$ is the Jaumann rate of the Cauchy stress, λ and G are Lamé constants and δ_{ij} are the components of the Kronecker delta. The final step generally requires the determination of the material rate of stress from the Jaumann rate by taking account of rotations, i.e., from the equation

$$\dot{\sigma}_{ij} = \overset{*}{\sigma}_{ij} - \sigma_{ik}\omega_{kj} + \omega_{ik}\sigma_{kj}, \tag{6}$$

where the material rate is,

$$\dot{\sigma}_{ij} = \frac{\partial \sigma_{ij}}{\partial t} + \frac{\partial \sigma_{ik}}{\partial x_k} v_k \tag{7}$$

This is the approach used in the present paper. It has recently been reported in the literature that the use of equations (6)–(7) may lead to errors when large shear strains are involved along with induced anisotropy. A complete discussion of this problem together with a possible solution is available in a recent publication by Chandra and Mukherjee (1986).

It should be mentioned here that the nonelastic part of the deformation rate, $d_{ij}^{(n)}$, must be determined from an appropriate constitutive model. A discussion of such material models is presented later.

3-D BEM Formulation. A brief review of the BEM formulation for these problems is presented here. Further details are available in the earlier papers by Chandra and Mukherjee (1984c, 1985), Mukherjee and Chandra (1984, 1986).

The deformations and stresses in a body due to applied forces and displacements are analyzed at time t. An updated Lagrangian frame is used and the configuration of the body at time t is used as a reference configuration for the time step t to $t+\Delta t$.

The key to the BEM formulation is the identity of Chandra and Mukherjee (1984c, 1985) in the updated Lagrangian frame.

$$\int_B \overset{*}{\sigma}_{ij} \epsilon_{ij}^{(R)} dV = \int_B \sigma_{ij}^{(R)} d_{ij}^{(e)} dV \tag{8}$$

where $\sigma_{ij}^{(R)}$ and $\epsilon_{ij}^{(R)}$ are reference fields in an elastic body subjected to small strains and displacements.

Following Chandra and Mukherjee (1984c, 1985) it can be shown that the velocity v_j at a point p inside a structure undergoing small elastic strains but large nonelastic strains and rotations, may be written as

$$v_j(p) = \int_{\partial B^o} [U_{ij}(p,Q)\dot{\tau}_i(Q) - T_{ij}(p,Q)v_i(Q)]dS_Q^o + \int_{B^o} \rho_o U_{ij}(p,q)\dot{F}_i^o(q)dV_q^o + \int_{B^o} [\lambda U_{mj,m}(p,q)\delta_{ik}(q) + 2GU_{ij,k}(p,q)]d_{ik}^{(n)}(q)dV_q^o + \int_{B^o} U_{ij,m}(p,q)[G_{mik\ell}(q) + C_{mik\ell}(q)]v_{k,\ell}(q)dV_q^o \tag{9}$$

In the above, U_{ij} and T_{ij} are the usual two-point kernels of small strain elasticity that are given in many references (e.g., the books by Banerjee and Butterfield, 1981, or Mukherjee, 1982). The tensors **G** and **C** are

$$G_{ijk\ell} = \frac{1}{2}[\sigma_{ik}\delta_{j\ell} + \sigma_{j\ell}\delta_{ik} + \sigma_{jk}\delta_{i\ell} - \sigma_{i\ell}\delta_{jk}]$$

$$C_{ijk\ell} = -\sigma_{ij}\delta_{k\ell}$$

The traction components at a point on the boundary are denoted as τ_i, and ρ_o and $\dot{F}_i^o$ are the mass density and the body force rate, respectively, in the reference configuration. Also, p (or P) is a source point and q (or Q) is a field point with lower case letters denoting points inside the reference volume B^o and capital letters denoting points on the boundary ∂B^o. Finally, a comma denotes differentiation at a field point.

If the nonelastic deformation is incompressible, as is often the case for metals, $d_{kk}^{(n)} = 0$. In such cases it is also usual to assume that $v_{k,k} = 0$. Thus, in equation (9), the first term in the second domain integral and the second term in the last domain integral vanish for incompressible materials.

The first three integrals on the right-hand side of the above equation (9) are analogous to terms in the BEM formulation for viscoplasticity with small strains and displacements (Mukherjee, 1982). The traction rate term $\dot{\tau}_i$ requires special care, and is explained in detail in the next section. The last domain integral incorporates the effects of bulk deformation of the body. Iterations within each time step are now required because of the presence of the unknown velocity field in the last domain integral. These iterations, however, may be easily taken care of as demonstrated in several earlier publications by various researchers (e.g., Banerjee and Butterfield, 1981; Chandra and Mukherjee, 1984c, 1985).

Load Correction. The traction rate components $\dot{\tau}_i$ in the above equation are given by (Chandra and Mukherjee, 1984c, 1985)

$$\dot{\tau}_i = n_j \dot{s}_{ji} = \dot{t}_i - n_j \sigma_{jk}\omega_{ki} - n_j d_{jk}\sigma_{ki} = \dot{t}_i - n_j G_{jik\ell} v_{k,\ell} \tag{10}$$

where

$$\dot{t}_i = n_j \overset{*}{\tau}_{ji} = n_j \overset{*}{\sigma}_{ji} - n_j C_{jik\ell} v_{k,\ell} \tag{11}$$

It should be remembered that for incompressible materials

$$C_{ijk\ell} v_{k,\ell} = 0 \tag{12}$$

In the above equations (10)–(12), $\overset{*}{\sigma}_{ji} n_j$ may be interpreted as the components of the rate of the prescribed follower force, per unit deformed surface area, on the deforming boundary. The follower force moves with a boundary point and rotates with the normal to the boundary at that point. Equations (10)–(12) may be interpreted as the "load correction." Several researchers (e.g., Chandra and Mukherjee, 1984a,b; Yamada and Hirakawa, 1978) have discussed the "load correction" for extrusion and sheet metal forming problems using the FEM, and a similar technique is used here to analyze the metal extrusion problem by the BEM. The details of the implementations of the "load correction" equations for metal extrusion is discussed in the next section.

Boundary Displacement Rates. A boundary integral equa-

Downloaded 03 May 2010 to 171.66.16.27. Redistribution subject to ASME license or copyright; see http://www.asme.org/terms/Terms_Use.cfm

tion can be obtained from equation (9) in the usual way by taking the limit as $p \to P$. This gives,

$$c_{ij}v_i(P) = \int_{\partial B^o} [U_{ij}(P,Q)\dot{\tau}_i(Q) - T_{ij}(P,Q)v_i(Q)]dS_Q^o$$

$$+ \int_{B^o} \rho_o U_{ij}(P,q)\dot{F}_i^o(q)dV_q^o + \int_{B^o} [\lambda U_{mj,m}(P,q)\delta_{ik}(q)$$

$$+ 2GU_{ij,k}(P,q)]d_{ik}^{(n)}(q)dV_q^o + \int_{B^o} U_{ij,m}(P,q)[G_{mik\ell}(q)$$

$$+ C_{mik\ell}(q)]v_{k,\ell}(q)dV_q^o \tag{13}$$

The coefficients of c_{ij}, in general, depend on the location of a boundary node and on the local geometry at P. If the boundary is locally smooth at P, $c_{ij} = (1/2)\delta_{ij}$. Otherwise, it can be evaluated indirectly for three-dimensional problems (Mukherjee, 1982).

Stress Rates. The first step towards the determination of stress rates is the differentiation of the velocity field from equation (9) at an internal source point p. Thus,

$$v_{j,\bar{\ell}}(p) = \int_{\partial B^o} [U_{ij,\bar{\ell}}(p,Q)\dot{\tau}_i(Q) - T_{ij,\bar{\ell}}(p,Q)v_i(Q)]dS_Q^o$$

$$+ \int_{B^o} \rho_o U_{ij,\bar{\ell}}(p,q)\dot{F}_i^o(q)dV_q^o + \frac{\partial}{\partial x_{\bar{\ell}}}\int_{B^o} [\lambda U_{mj,m}(p,q)\delta_{ik}(q)$$

$$+ 2GU_{ij,k}(p,q)]d_{ik}^{(n)}(q)dV_q^o + \frac{\partial}{\partial x_{\bar{\ell}}}\int_{B^o} U_{ij,m}(p,q)[G_{mikn}(q)$$

$$+ C_{mikn}(q)]v_{k,n}(q)dV_q^o \tag{14}$$

where

$$,\bar{\ell} \equiv \frac{\partial}{\partial x_{\bar{\ell}}} \tag{14b}$$

denotes differentiation with respect to a source point. The kernel $U_{ij,k}$ has a singularity of the order r^{-2} (where r is the distance from a source to a field point) and cannot be directly differentiated under the integral sign. Several methods for evaluating such derivatives of the integrals are discussed by Mukherjee (1982).

Once the velocity gradients are known throughout the body at any time, equation (14) is used to find $d_{ij}^{(e)}$ and ($d_{ij}^{(n)}$ being known from the constitutive model) and $\overset{*}{\sigma}_{ij}$ is obtained from equation (5).

The above BEM equations are valid for three-dimensional problems. They must be somewhat modified for plane strain situations (Mukherjee and Chandra, 1986).

The above equations are now discretized to obtain appropriate algebraic equations of the form

$$[A]\{v\} + [B]\{\dot{\tau}\} = \{b\} \tag{15}$$

The details of this procedure are available in previous references (e.g., Banerjee and Butterfield, 1981; Mukherjee, 1982; Chandra and Mukherjee, 1984c, 1985).

Interface Modelling for Extrusion Problems. Interface conditions at the die-workpiece boundary are considered next for problems of plane strain extrusion. The assumptions made here are the same as those presented earlier for FEM analysis of the same problem (Chandra and Mukherjee, 1984a,b).

The assumptions are best explained in terms of a local coordinate system α,β,γ. The origin of this coordinate system is positioned on the die-workpiece interface. The α axis is tangential to the die surface and the β axis is the outward normal to the die surface.

A consequence of the assumption of plane strain is that

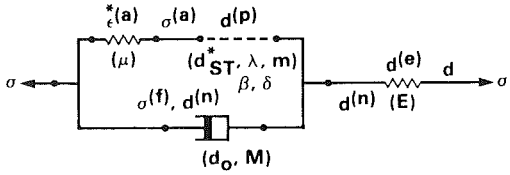


Fig. 1 Constitutive model in tension

$$v_\gamma = 0,\ \sigma_{\alpha\gamma} = \sigma_{\gamma\alpha} = \sigma_{\beta\gamma} = \alpha_{\gamma\beta} = 0$$

It is further assumed that the contact or lubricant layer adjacent to the die surface cannot provide any resistance to tensile or compressive deformation. Thus, the scheme is equivalent to having an interface or bond element with zero stiffness in the direction tangential to the contact surface. Therefore,

$$\sigma_{\alpha\alpha} = 0. \tag{16}$$

so that only pressures and shear loadings get transferred across the interface and the stretch or compression of either the die or the workpiece is not transferred to the other.

Another assumption made here is that the material is incompressible so that

$$d_{\alpha\alpha} + d_{\beta\beta} = 0 \qquad (\text{since } d_{\gamma\gamma} = 0) \tag{17}$$

Using the above assumptions, zero normal velocity ($v_\beta = 0$) and the fact that the normal has components (0,1,0) in the local coordinate system, equation (10) in the local coordinate system becomes

$$\dot{\tau}_\alpha = \overset{*}{\sigma}_{\alpha\beta} + \sigma_{\beta\beta}\omega_{\alpha\beta} + \sigma_{\alpha\beta}d_{\alpha\alpha} \tag{18}$$

The other traction component is assumed to vanish, i.e.,

$$\dot{t}_\beta = 0 \tag{19}$$

The final assumptions relate to friction

$$\overset{*}{\sigma}_{\alpha\beta} = \frac{G_s}{h}\mu v_\alpha \tag{20}$$

(where G_s and h are the shear modulus and the height of the interface element, respectively, and μ is the coefficient of friction), and

$$\omega_{\alpha\beta} = \kappa v_\alpha \tag{21}$$

where κ is the local curvature.

The rate of the traction component, $\dot{\tau}_\alpha$, has now been obtained in terms of the tangential velocity v_α, its gradient in the tangential direction $v_{\alpha,\alpha}$, and the nonzero stress components $\sigma_{\alpha\beta}$ and $\sigma_{\beta\beta}$.

Constitutive Model. The mathematical structure of the nonelastic constitutive models with state variables, that are of interest in this study can be summarized by the following equations (9,12,14–16)

$$d_{ij}^{(n)} = f_{ij}(\sigma_{ij}q_{ij}^{(k)}), \tag{22}$$

$$\overset{*}{q}_{ij}^{(k)} = g_{ij}^{(k)}(\sigma_{ij}, q_{ij}^{(0)}) \tag{23}$$

and for incompressible nonelastic deformation,

$$d_{kk}^{(n)} = 0, \tag{24}$$

which says that the history dependence of $d_{ij}^{(n)}$ at any time can be represented by the current value of the stress and suitably chosen state variables q_{ij} which can be scalars and tensors. Suitable evolution laws must be prescribed for these state variables. Equations (22)–(24) are valid for uniform temperature so that thermal strains and temperature effects are neglected. In the interest of brevity, further discussion of these equations is avoided here. A more detailed discussion of the small strain equations can be found in Mukherjee (1982).

The particular material model that has been used to generate the numerical results presented later is that due to Hart (1976) generalized to the case of large strains and rotations (Chandra and Mukherjee, 1984 a,b,c; Hart, 1982).

Downloaded 03 May 2010 to 171.66.16.27. Redistribution subject to ASME license or copyright; see http://www.asme.org/terms/Terms_Use.cfm

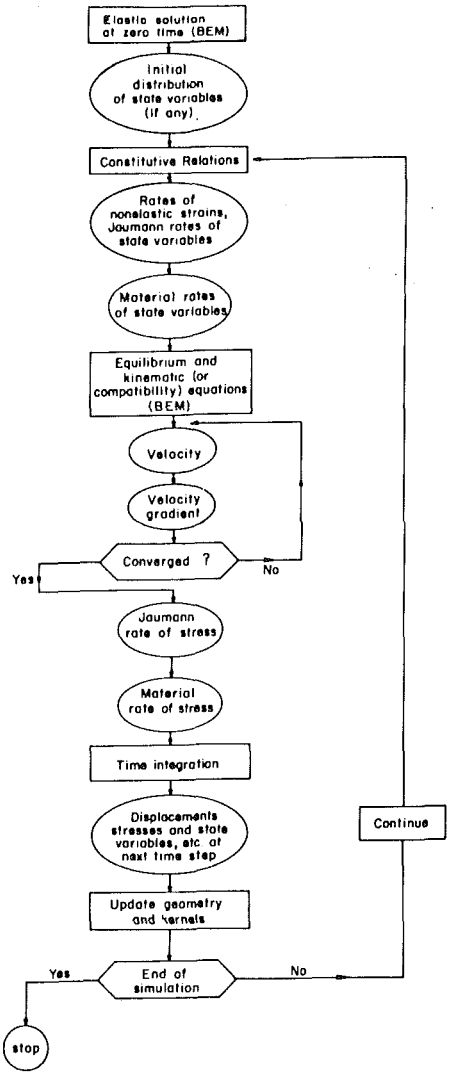


Fig. 2 Flow chart

The model in uniaxial tension is shown in Fig. 1. Material response in dilatation is assumed to be elastic. This model has two state variables, the anelastic strain $\epsilon_{ij}^{(a)}$, a stored strain which reflects the magnitude and direction of prior deformation history and is responsible for induced anisotropy, and a scalar state variable H, the hardness, which is analogous to an isotropic strain hardening parameter or current yield stress. One key point in the generalization of the small strain equations is the replacement of the equation

$$\dot{\epsilon}_{ij}^{(a)} = \dot{\epsilon}_{ij}^{(n)} - \dot{\epsilon}_{ij}^{(p)} \tag{25}$$

by the equation

$$\overset{*}{\epsilon}_{ij}^{(a)} = d_{ij}^{(n)} - d_{ij}^{(p)}, \tag{26}$$

where $d_{ij}^{(p)}$ represents the completely irrecoverable (permanent) path dependent deformation rate. Since $\epsilon_{ij}^{(a)}$ is a proper state variable, its Jaumann rate is used in equation (26).

Hart's model has the mathematical structure of equations (22)–(24). Thus, given the Cauchy stress and the state variables (hardness and anelastic strain) at any time, it delivers, among other things, $d_{ij}^{(n)}$ and the state variable rates $\dot{H}$ and $\overset{*}{\epsilon}_{ij}^{(a)}$ at that time. The BEM equations are then used to calculate $\overset{*}{\sigma}_{ij}$ etc. The detailed equations of Hart's model for large strain applications can be found in previous publications (e.g., Chandra and Mukherjee, 1984 a,b,c) and are not repeated here in the interest of brevity.

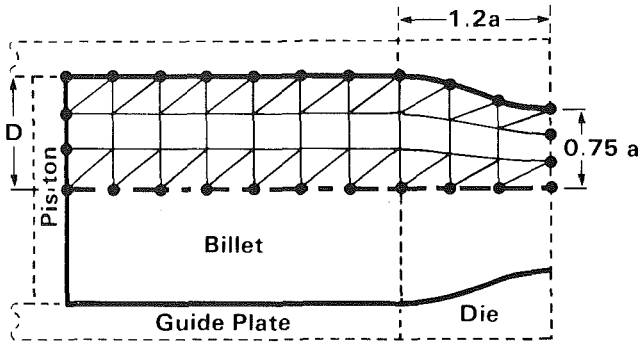


Fig. 3 Geometry of the extrusion problem

Numerical Results

Solution Strategy. The solution strategy, in essence, consists of marching forward in real time with suitable updating of the configuration of the body. The presence of velocity gradients in the boundary traction rates and in the last domain integral in equation (9) requires iteration within each time step. The strategy described here assumes $\dot{F}_i = 0$ for all time. This assumption, however, can be waived without any difficulty. The elasticity problem is solved first to obtain the initial distribution of the state variables. At each time step, an initial guess for the velocity gradient is fed in and iterated until convergence is achieved. Typically, the velocity gradient obtained at time $t - \Delta t$ is used as the initial guess at time t. The extrusion process is nearly steady state and fast convergence could be achieved for reasonable values of Δt. The flow chart shown in Fig. 2 shows the solution procedure in detail.

The BEM program uses straight boundary elements and polygonal internal cells. The velocity and traction rate are taken to be piecewise linear over the boundary elements while the nonelastic deformation rate and the velocity gradients are assumed to be piecewise constant over the internal cells. The values of the boundary variables are assigned at nodes which lie at the intersections of boundary segments. Possible discontinuities in tractions are taken care of by placing a "zero length" element between nodes and assigning different values of traction at each of those nodes.

All integrations of kernels are carried out analytically. The last two terms in equation (14) are evaluated by first performing the integration over an internal cell for an arbitrary source point p_m and then differentiating the integral at p_m (Mukherjee, 1982; Chandra and Mukherjee, 1984c, 1985).

The FEM analysis reported before (Chandra and Mukherjee, 1984a) used a piecewise quadratic description of velocities over triangular elements. Time integrations for both the BEM and FEM programs are carried out by an explicit Euler type method with automatic step control (Kumar et al., 1980). Hart's constitutive model for large strain problems is used to model material behavior. The material used is commercially pure aluminum at 24°C and the details of the material parameters may be found in Chandra and Mukherjee (1984a). The parameter $G_s/h = 1.268 \times 10^5$ MPa/m. The experimental basis of these parameters can also be found in Alexopoulos (1981).

Results for Plane Strain Extrusion. The primary purpose of obtaining the numerical results presented here is to demonstrate the ability of the boundary element method (BEM) in solving metal forming problems involving both geometric and material nonlinearities. Handling of the boundary conditions at the die interface requires special care for the extrusion problem. In the present BEM analysis, this can be incorporated quite easily through "load correction" (equations (10)–(12) and (16)–(21)).

Downloaded 03 May 2010 to 171.66.16.27. Redistribution subject to ASME license or copyright; see http://www.asme.org/terms/Terms_Use.cfm

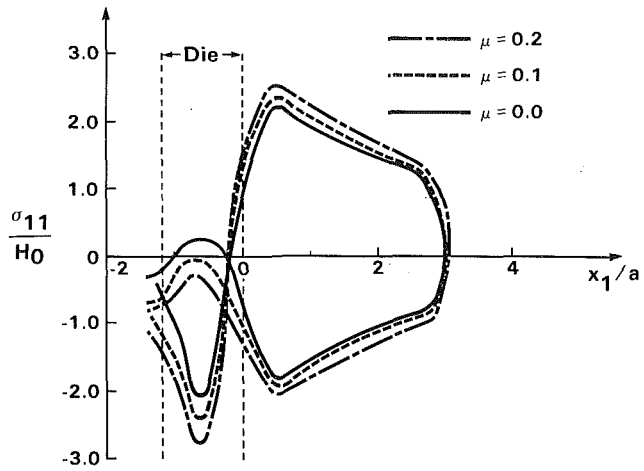


Fig. 4 Steady state distributions of σ_{11} at different piston velocities for two values of X_2 ($\mu = 0$)

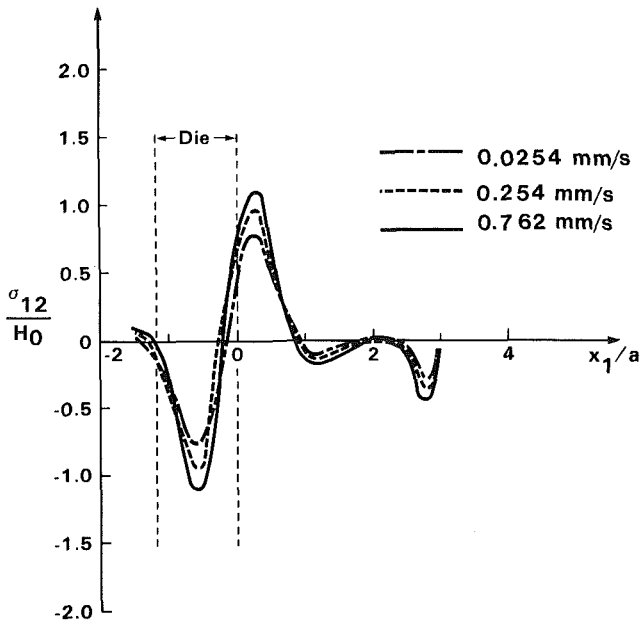


Fig. 5 Steady state distributions of σ_{12} as functions of piston velocity ($\mu = 0$)

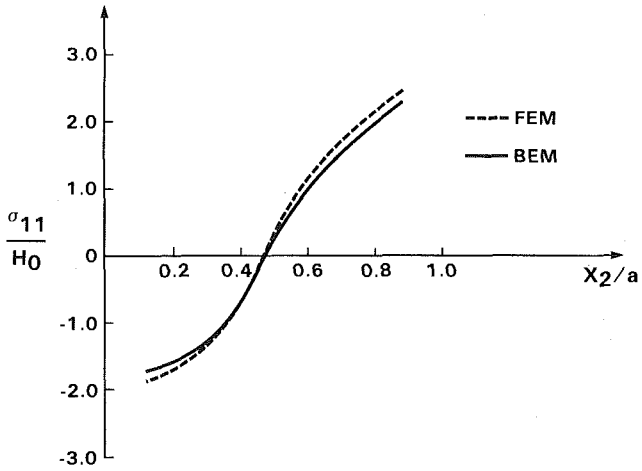


Fig. 6 Comparison of residual stress distributions from the BEM and FEM (piston velocity = 0.762 mm/s, $\mu = 0$)

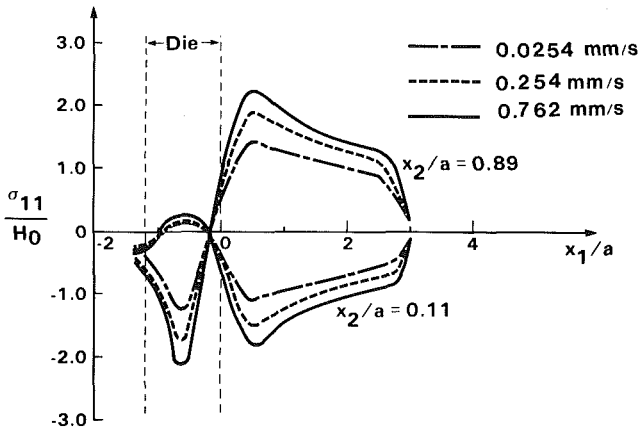


Fig. 7 Steady state distributions of σ_{11} as functions of friction coefficient for two values of X_2 (piston velocity = 0.762 mm/s)

The geometry of planar extrusion considered here is shown in Fig. 3 and numerical results are presented in Figs. 4–7. Figure 4 shows the steady state distributions of the longitudinal stress σ_{11} for three different velocities in the absence of friction. In particular, the center line of the workpiece is chosen to be the x_1 axis and the stress distributions are shown for material points in the deformed configuration which initially had the same relative ordinate ($x_2/a = 0.11$ and 0.89) in the billet. Maximum residual tensile stress in an extruded workpiece is of crucial importance in design, since this is the primary potential source for crack initiation and growth. It is seen from Fig. 3 that the rate dependence of this quantity is quite significant. As the piston velocity is tripled from 0.254 mm/s to 0.762 mm/s, the BEM analysis predicts a change of 15.5 percent in the maximum longitudinal tensile stress in the workpiece. This compares well with the 17 percent change predicted by the FEM analysis (Chandra and Mukherjee, 1984a). The faster the billet is forced through the die, the less time there is for stresses to relax at material points in the workpiece, as they move through the die. Consequently, the maximum longitudinal tensile stress upon exit from the die increases substantially with the speed of extrusion. Predictions of crucial effects like rate dependence of residual stresses is only possible through a detailed analysis using a realistic elastic-viscoplastic model for material behavior. It should be emphasized again that the material parameters for aluminum used in these calculations are those measured carefully by experiments (Alexopoulos, 1981).

Another important feature of elastic-viscoplastic analysis is that, following a peak value, the magnitude of σ_{11} decreases as a function of x_1 in most of the billet that has passed through the die. This is a result of stress relaxation in the workpiece after it is deformed, and the BEM predictions for such relaxations compare very well with those predicted by FEM analysis (Chandra and Mukherjee, 1984a).

The results for the steady state distributions of shearing stress σ_{12} are shown in Fig. 5. It is seen that there is a marked variation of shearing stress inside and in the neighborhood of the die. Residual longitudinal stress distribution over a cross-section ($x_1 = 0{\cdot}4a$ from the die exit), from the two methods, are shown in Fig. 6. It should be noted that these residual stress distributions must be self-equilibrating and for the residual stresses obtained from the current BEM analysis, the error in satisfying equilibrium is about 5 percent.

The effect of friction on the results is depicted in Fig. 7. Three different values of friction are chosen for a piston velocity of 0.762 mm/s. The presence of friction increases the longitudinal stress peaks significantly. Of course, the friction model with constant coefficient of friction, that is used here, is crude at best and much work remains to be done on modelling friction in metal forming processes. The present analysis does

Downloaded 03 May 2010 to 171.66.16.27. Redistribution subject to ASME license or copyright; see http://www.asme.org/terms/Terms_Use.cfm

show, however, the effects friction may have in metal extrusion processes. The predictions from the BEM analysis, once again, match quite well with the FEM predictions from Chandra and Mukherjee (1984a).

Conclusions

This paper is a first attempt at the prediction of stress and deformation histories in extrusion using a boundary element method (BEM) incorporating a realistic rate-dependent inelastic constitutive model. The problem is indeed a very challenging one, since it involves complicated interactions of geometrical and material nonlinearities. This paper uses an updated Lagrangian approach and the BEM formulation is based on the identity of Chandra and Mukherjee (1984c, 1985). The basic BEM methodology is then extended to take care of the complicated interface conditions in metal extrusion processes. This is achieved through the implementation of "load correction" terms. Thus, it is possible for the first time to predict stress and deformation histories in an extrusion process through the BEM.

Traditionally, the FEM has been used in such analyses and one of the main difficulties in solving any real-life problem is the amount of CPU time necessary. This is where the application of the BEM becomes advantageous. Because of the reduced matrix size and the capability of obtaining secondary variables accurately (Mukherjee, 1982; Chandra and Mukherjee, 1984c, 1985), the BEM analysis took only about 55 percent of the time required by a similar FEM analysis performed by the authors. Of course, much improvement is still needed in both the FEM and the BEM to make them a viable day to day design tool for metal forming operations. However, the present study shows the strength and the potential of BEM and warrants that active research be pursued in this area in order to take advantage of the potential benefits of the boundary element method.

Acknowledgments

Mukherjee's contribution to this research has been supported by Grant nos. CEE-8206344 and MSM-8609391 of the US National Science Foundation to Cornell University. A. Chandra's contribution to this research has been supported by Grant nos. DMC-8604410 and DMC-8657345 of the US National Science Foundation to the University of Arizona.

References

Alexopoulos, P. S., 1981, "An Experimental Investigation of Transient Deformation Based on a State Variable Approach," Ph.D. Thesis, Department of Materials Science and Engineering, Cornell University.

Banerjee, P. K., and Butterfield, R., 1981, *Boundary Element Methods in Engineering Science*, McGraw-Hill, U.K.

Brebbia, C. A., Telles, J. C. F., and Wrobel, L. C., 1984, *Boundary Element Techniques Theory and Applications in Engineering*, Springer-Verlag, Berlin.

Chandra, A., and Mukherjee, S., 1984b, "A Finite Element Analysis of Metal Forming Problems with an Elastic-Viscoplastic Material Model," *International Journal for Numerical Methods in Engineering*, Vol. 20, pp. 1613–1628.

Chandra, A., and Mukherjee, S., 1984a, "A Finite Element Analysis of Metal Forming Processes with Thermomechanical Coupling," *International Journal of Mechanical Sciences*, Vol. 26, pp. 661–676.

Chandra, A., and Mukherjee, S., 1984c, "Boundary Element Formulations for Large Strain-Large Deformation Problems of Viscoplasticity," *International Journal of Solids and Structures*, Vol. 20, pp. 41–53.

Chandra, A., and Mukherjee, S., 1985, "A Boundary Element Formulation for Sheet Metal Forming," *Applied Mathematical Modelling*, Vol. 9, pp. 175–182.

Chandra, A., and Mukherjee, S., 1986, "An Analysis of Large Strain Viscoplasticity Problems Including the Effects of Induced Material Anisotropy," ASME JOURNAL OF APPLIED MECHANICS, Vol. 53, pp. 77–82.

Dawson, P. R., and Thompson, E. G., 1977, "Steady State Thermomechanical Finite Element Analysis of Elasto-Viscoplastic Metal Forming Processes," *Numerical Manufacturing Processes*, ASME P.V.P.-P.B.-025, pp. 167–182.

Hart, E. W., 1976, "Constitutive Relations for the Non-elastic Deformation of Metals," ASME *Journal of Engineering Materials and Technology*, Vol. 98, pp. 193–202.

Hart, E. W., 1982, "The Effects of Material Rotations in Tension-Torsion Testing," *International Journal of Solids and Structures*, Vol. 18, pp. 1031–1042.

Kumar, V., Morjaria, M., and Mukherjee, S., 1980, "Numerical Integration of Some Stiff Constitutive Models of Inelastic Deformation," ASME *Journal of Engineering Materials and Technology*, Vol. 102, pp. 92–96.

Lee, E. H., Mallet, R. L., and Yang, W. H., 1977, "Stress and Deformation Analysis of Metal Extrusion Process," *Computational Methods in Applied Mechanics and Engineering*, Vol. 10, pp. 339–353.

McMeeking, M. C., and Rice, J. R., 1975, "Finite Element Formulation for Problems of Large Elastic-Plastic Deformation," *International Journal of Solids and Structures*, Vol. 11, pp. 601–616.

Mukherjee, S., 1982, *Boundary Element Methods in Creep and Fracture*, Elsevier Applied Science Publishers, Barking, Essex, U.K.

Mukherjee, S., and Chandra, A., 1984, "Boundary Element Formulations for Large Strain-Large Deformation Problems of Plasticity and Viscoplasticity," *Developments in Boundary Element Methods*, Vol. 3, Elsevier Applied Science Publishers, Barking, Essex, U.K., Chapter 2, pp. 27–58.

Mukherjee, S., and Chandra, A., 1986 (expected), "Nonlinear Solid Mechanics," *Boundary Element Methods in Mechanics*, North Holland Publishers, Amsterdam.

Nemat-Nasser, S., 1982, "On Finite Deformation Elasto-Plasticity," *International Journal of Solids and Structures*, Vol. 18, pp. 857–872.

Oh, S. I., Park, J. J., Kobayashi, S., and Altan, T., 1983, "Application of FEM Modelling to Simulate Metal Flow in Forging a Titanium Alloy Engine Disk," ASME *Journal of Engineering for Industry*, Vol. 105, pp. 251–258.

Onate, E., and Zienkiewicz, O. C., 1983, "A Viscous Shell Formulation for the Analysis of Thin Sheet Metal Forming," *International Journal of Mechanical Sciences*, Vol. 25, pp. 305–335.

Yamada, Y., and Hirakawa, H., 1978, "Large Deformation and Instability Analysis of Metal Forming Processes," *Numerical Modelling of Manufacturing Processes*, ASME, PVP-PB-025, pp. 19–33.

Downloaded 03 May 2010 to 171.66.16.27. Redistribution subject to ASME license or copyright; see http://www.asme.org/terms/Terms_Use.cfm

A Complementary Work Bounding Principle for Forward Integration Along the Path of Loading for Elasto-Plastic Bodies

J. B. Martin
Professor of Civil Engineering,
University of Cape Town,
Rondebosch, 7700, South Africa
Fellow ASME

The paper presents an extension of the complementary work bounding principle of Hodge (1966) for integration along the path of loading for a statically loaded elastic-plastic body. Using an internal variable framework, the concept of a piecewise holonomic constitutive equation, updated at discrete intervals along the loading path, is introduced. It is shown that the complementary work over the entire path decreases (or does not increase) each time the last interval is subdivided. The result has some interesting implications with regard to the formulation of a mechanical principle for time discretisation along the loading path, and these are explored.

Introduction

The solution of a boundary value problem in classical quasi-static time-independent plasticity is path dependent, i.e., the solution at time t depends on the initial state and the history of loading, although the time measure does not explicitly appear in the problem. In diagrammatic terms, we consider a body, shown in Fig. 1(*a*), which without loss in generality can be considered to be in its virgin state at time $t = 0$. The body is subjected to a loading history, shown in Fig. 1(*b*); time t can be any monotonically increasing parameter which measures the progress of the load point along the load path. We seek the solution for the displacements, reactions, strains, and stresses as a function of time t over the interval $[0, T]$.

In all but a limited number of cases, the solution to this problem must be found numerically. In order to achieve this, we must discretise the problem both in space and time. The spatial discretisation will not be a major concern in this paper, and we shall assume that we may work within the standard framework of finite element approximations. In the time discretisation, we effectively sample the load history at a number of points, as shown in Fig. 1(*c*). If the discrete external nodal load vector is denoted by $\mathbf{P}(t)$, a sampling which divides the load path into n intervals leads us to discrete load values $\mathbf{P}_0, \mathbf{P}_1, \ldots, \mathbf{P}_n$. Conventionally, we solve a sequence of problems in which we apply load increments

$$\Delta\mathbf{P}_1 = \mathbf{P}_1 - \mathbf{P}_0, \quad \Delta\mathbf{P}_2 = \mathbf{P}_2 - \mathbf{P}_1, \tag{1}$$

up to

$$\Delta\mathbf{P}_n = \mathbf{P}_n - \mathbf{P}_{n-1},$$

updating the solution at the end of each increment.

Our concern in this paper is the governing principle under which the incremental solution is carried out. Minimum principles for the rate problem (i.e., for increments which are infinitesimally small) have been known for some time (see, for example, Greenberg, 1949), and form the basis for a consistent spatial discretisation of the body and the formulation of a tangent stiffness matrix $\mathbf{K}_T$ at a particular instant. Thus, if the nodal displacement parameters are denoted by $\mathbf{u}(t)$, and at the end of the $(i-1)$th interval the solution sequence has provided displacements $\mathbf{u}_{i-1}$ for loads $\mathbf{P}_{i-1}$, we can write

$$\mathbf{K}_T^i\, \dot{\mathbf{u}} = \dot{\mathbf{P}} \tag{2}$$

where $\dot{\mathbf{u}}$, $\dot{\mathbf{P}}$ represent infinitesimal increments.

Various ad hoc time-marching schemes have been employed to move to the end of the next interval. In the earliest numerical solutions (see, for example, Marcal and King, 1967), an Euler forward difference scheme was used, with $\dot{\mathbf{P}}$, $\dot{\mathbf{u}}$ in equation (2) replaced by $\Delta\mathbf{P}_i$, $\Delta\mathbf{u}_i$. An algorithm for updating stresses and internal variables must also be adopted; this was also done on an ad hoc basis.

The simple Euler scheme introduces cumulative errors, even when the number of intervals is large. Subsequent developments led to implicit iterative forward integration schemes, based on Newton-Raphson methods (see, for example, Zienkiewicz, 1977; Owen and Hinton, 1980; Bathe, 1982). The tangent stiffness matrix is used as a predictor (and may be updated in each iteration within the increment), updated stresses and hence internal nodal forces are computed using some scheme for integrating the constitutive equations for the incremented strains, and a residual out of balance force vector is computed as the difference between the predicted forces and the desired load $\mathbf{P}_i$. The residual is then applied to the struc-

Contributed by the Applied Mechanics Division for publication in the JOURNAL OF APPLIED MECHANICS.
Discussion on this paper should be addressed to the Editorial Department, ASME, United Engineering Center, 345 East 47th Street, New York, N.Y. 10017, and will be accepted until two months after final publication of the paper itself in the JOURNAL OF APPLIED MECHANICS. Manuscript received by ASME Applied Mechanics Division, April 24, 1986.

Copyright © 1987 by ASME
Downloaded 03 May 2010 to 171.66.16.27. Redistribution subject to ASME license or copyright; see http://www.asme.org/terms/Terms_Use.cfm

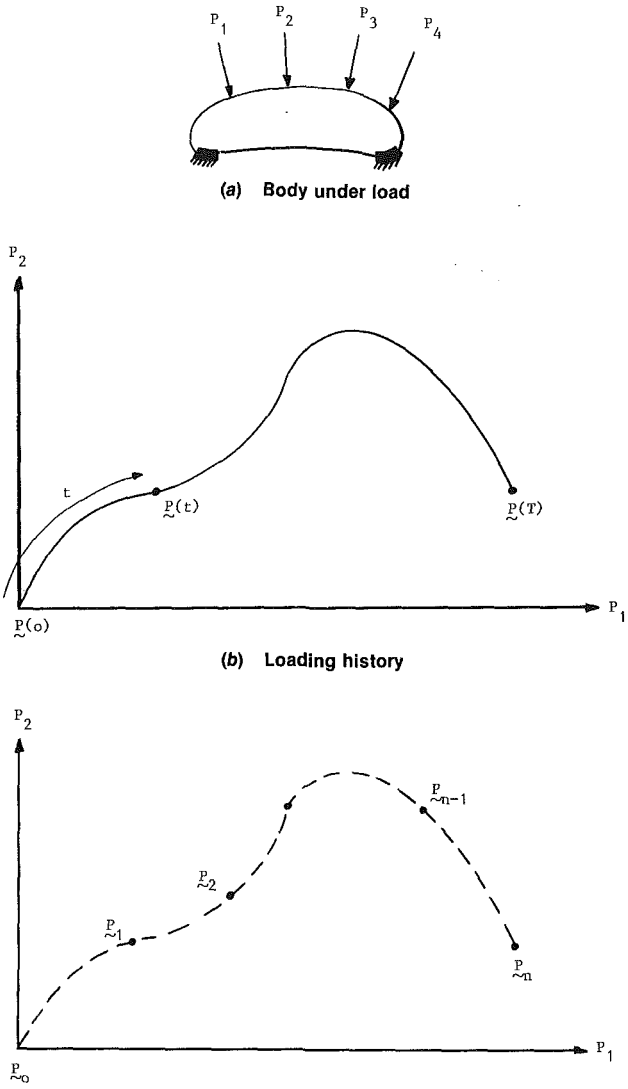


Fig. 1 Body and loading history

ture, and the iterations continue until the residual satisfies some predetermined tolerance.

These equilibrium iteration schemes are extremely effective in many problems; however, they embody a series of independent, and hence *ad hoc*, choices of algorithms to advance the solution in time. In particular, they do not permit us to answer, in a formal way, some fundamental questions. For example, although the answer may be intuitively obvious, we cannot easily define a measure of accuracy of the full solution (i.e., $\mathbf{u}_1, \mathbf{u}_2, \ldots, \mathbf{u}_n$), and demonstrate that according to this measure the solution improves as additional load history sample points are incorporated, thus subdividing any or all intervals.

In this paper we explore a mechanical principle which provides a partial answer to this question, and suggests that a formal way of treating both spatial and time discretisation may exist. Since the introduction of the time discretisation is the novel feature, our present discussion will focus on this aspect.

The essential feature is that the algorithm for the integration of the constitutive equations cannot be arbitrarily chosen. It was suggested in a recent paper (Martin, et al., 1984) that the form of the governing equations for plasticity dictates the choice of a backward difference algorithm for the internal variables (or loosely, the plastic strains). In mechanical terms, this leads to a holonomic problem for each load increment. Minimum principles for the holonomic incremental problem are well established (see Maier and Nappi, 1983; Martin et al., 1984). In principle, a solution can be obtained for each load value along the path within the increment. For the next increment the holonomic incremental constitutive equations are updated and the process is repeated. Thus, in principle, we have a solution for every load value on the entire loading path, even though we only compute it for the sample points $\mathbf{P}_0$, $\mathbf{P}_1$, $\mathbf{P}_2, \ldots, \mathbf{P}_n$.

Within this framework, we do not think of n as the number of load increments, but as the number of updatings of the holonomic constitutive equations, including the initial choice at time $t=0$.

The special case $n=1$, where no updating occurs after the holonomic constitutive equations are set at time $t=0$, is the case of what is conventionally referred to as deformation theory; this has been summarized by Martin (1975). It is this case that provides the key to the result we shall present in this paper: The deformation theory complementary work boundary principle (see Haar and von Karman, 1909; Hodge, 1966; Martin, 1966) states that the complementary work computed using a consistently formulated deformation theory is not less than the complementary work computed for the continuous solution. The deformation theory must be based on paths of minimum work or maximum complementary work (Ponter and Martin, 1972), which in turn corresponds to the choice of straight line paths in internal variable space (Carter and Martin, 1976), and to a backward difference algorithm for the internal variables (Martin et al., 1984).

Given that we can conceptually determine the entire response $\mathbf{u}(t)$ for a sequence of n incremental holonomic solutions, we can also determine the complementary work Ω as a function of time, where

$$\Omega(t) = \int_o^t \mathbf{u}^T \dot{\mathbf{P}}\, dt, \quad 0 \le t \le T. \tag{3}$$

We may plot $\Omega(t)$, as a function of time over the entire history of loading, $0 \le t \le T$. Further, we may compare this function for solutions involving increasing numbers of updates n. We show that, *provided that the additional update occurs in the last interval*,

$$[\Omega(t)]_{n=1} \ge [\Omega(t)]_{n=2} \ge [\Omega(t)]_{n=3} \ge \ldots\ldots \tag{4}$$

for all t, $0 \le t \le T$.

We shall refer to this as sequential updating; for $n=1$ we initialise the holonomic equations at $t=0$; for $n=2$ we update the constitutive equations at some time t_1, $0 < t_1 < T$; for $n=3$ we update at times t_1, t_2, $t_1 < t_2 < T$, and so on.

Structural Formulation

We adopt a structural formulation which is simple and conceptually general, in the form given by Martin (1981, 1984). The formulation is in spatially discrete terms, but can be readily identified with finite element approximations.

Nodal displacements are represented by the components of the vector $\mathbf{u}$, and internal slips in the structure by the components of the vector $\boldsymbol{\lambda}$. Strain quantities do not appear directly in the formulation, although the internal variables may be identified with the plastic strains for certain constitutive models.

The strain energy F of the structure is assumed to be a homogeneous, convex, quadratic function of the components of $\mathbf{u}$ and $\boldsymbol{\lambda}$. Small changes in the kinematic variables give

$$dF = d\mathbf{u}^T \frac{\partial F}{\partial \mathbf{u}} + d\boldsymbol{\lambda}^T \frac{\partial F}{\partial \boldsymbol{\lambda}}$$

$$= d\mathbf{u}^T \mathbf{R} - d\boldsymbol{\lambda}^T \mathbf{X}, \tag{5}$$

Downloaded 03 May 2010 to 171.66.16.27. Redistribution subject to ASME license or copyright; see http://www.asme.org/terms/Terms_Use.cfm

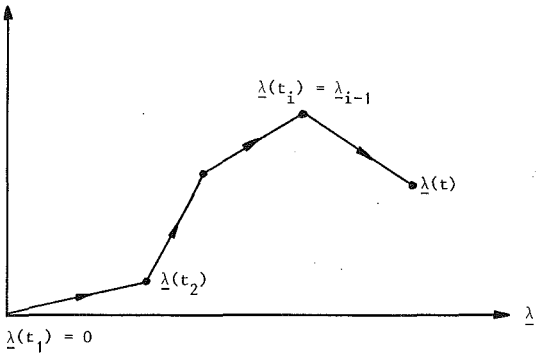


Fig. 2 Straight line path in $\underline{\lambda}$ space

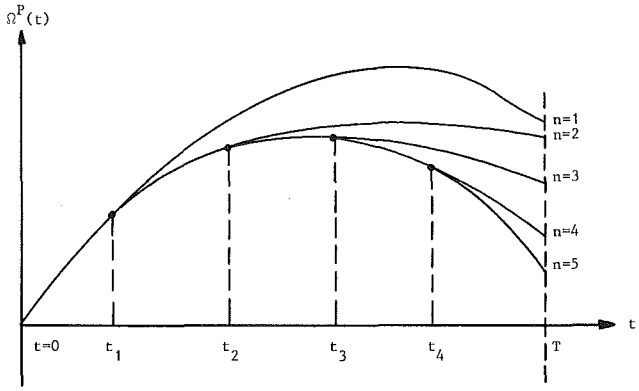


Fig. 3 Plastic complementary work history for sequential updates

and we identify the internal nodal forces $\mathbf{R}$ and the internal forces $\mathbf{X}$ acting on the slips,

$$\mathbf{R}=\frac{\partial F}{\partial \mathbf{u}}, \quad \mathbf{X}=-\frac{\partial F}{\partial \boldsymbol{\lambda}}. \tag{6}$$

Both $\mathbf{R}$ and $\mathbf{X}$ are homogeneous linear functions of $\mathbf{u}$ and $\boldsymbol{\lambda}$. Noting that $\partial^2 F/\partial \mathbf{u}\partial\boldsymbol{\lambda} = \partial^2 F/\partial\boldsymbol{\lambda}\partial\mathbf{u}$, we put

$$\begin{aligned} \mathbf{R}&=\mathbf{K}\,\mathbf{u}+\mathbf{L}\,\boldsymbol{\lambda}, \\ -\mathbf{X}&=\mathbf{L}^T\mathbf{u}+H\,\boldsymbol{\lambda}. \end{aligned} \tag{7}$$

Hence

$$\begin{aligned} F&=1/2\;\mathbf{u}^T\mathbf{K}\mathbf{u}+\mathbf{u}^T\mathbf{L}\boldsymbol{\lambda}+1/2\;\boldsymbol{\lambda}^T\mathbf{H}\boldsymbol{\lambda} \\ &=1/2\left\{\frac{u}{\lambda}\right\}^T\begin{bmatrix}K & L\\ L^T & H\end{bmatrix}\left\{\frac{u}{\lambda}\right\}. \end{aligned} \tag{8}$$

The rate of change of the internal slip vector $\boldsymbol{\lambda}$ is assumed to be governed by a rigid, perfectly plastic relation. We assume the existence of a dissipation function D which is homogeneous, convex, and of degree one in the components of $\dot{\boldsymbol{\lambda}}$, with

$$\mathbf{X}=\frac{\partial D}{\partial \dot{\boldsymbol{\lambda}}}. \tag{9}$$

To be consistent with thermodynamic requirements, $D \geq 0$ with $D = 0$ if and only if $\dot{\boldsymbol{\lambda}} = 0$. It follows that the derivatives of D are discontinuous at the origin. In addition, because $\partial D/\partial\dot{\boldsymbol{\lambda}}$ is homogenous and of degree zero in $\dot{\boldsymbol{\lambda}}$, derivatives of D may be discontinuous along lines which are radial on the $\dot{\boldsymbol{\lambda}}$ space. At a point on the D surface where $\partial D/\partial\dot{\boldsymbol{\lambda}}$ is discontinuous, equation (9) is interpreted as requiring that $\mathbf{X}$ should take some value within the domain bounded by adjacent values of $\partial D/\partial\dot{\boldsymbol{\lambda}}$.

Equations (7) and (9) define completely the mechanical behavior of the structure. If the external forces at the nodes are denoted by $\mathbf{P}$, equilibrium requires that

$$\mathbf{R}=\mathbf{P}, \tag{10}$$

and the governing equations can be conveniently written as

$$\mathbf{K}\mathbf{u}(t)+\mathbf{L}\boldsymbol{\lambda}(t)=\mathbf{P}(t), \tag{11}$$

$$\mathbf{L}^T\mathbf{u}(t)+\mathbf{H}\boldsymbol{\lambda}(t)=-\left[\frac{\partial D}{\partial\dot{\boldsymbol{\lambda}}}\right]_{\dot{\lambda}(t)}. \tag{12}$$

Initial conditions are assumed to be

$$\mathbf{u}(0)=0, \quad \boldsymbol{\lambda}(0)=0, \quad \mathbf{P}(0)=0, \tag{13}$$

and the loading history $\mathbf{P}(t)$ is defined over the interval $[0, T]$. These equations define a broad class of stable, quasi-static elastic-plastic problems.

For our present purpose, it is convenient to recast the governing equations to some extent. From equation (11)

$$\mathbf{u}=\mathbf{K}^{-1}\mathbf{P}-\mathbf{K}^{-1}\mathbf{L}\boldsymbol{\lambda}. \tag{14}$$

We may use this relation to define elastic displacements $\mathbf{u}^E$ and plastic displacements $\mathbf{u}^P$;

$$\mathbf{u} = \mathbf{u}^E+\mathbf{u}^P \tag{15a}$$

$$\mathbf{u}^E = \mathbf{K}^{-1}\mathbf{P} \tag{15b}$$

$$\mathbf{u}^P = -\mathbf{K}^{-1}\mathbf{L}\boldsymbol{\lambda}=\mathbf{N}\boldsymbol{\lambda} \tag{15c}$$

$$\mathbf{N} = -\mathbf{K}^{-1}\mathbf{L}. \tag{15d}$$

The governing equations may then be rewritten as

$$\mathbf{K}\mathbf{u}^E=\mathbf{P} \tag{16a}$$

$$-\mathbf{N}^T\mathbf{P}+\mathbf{Z}\boldsymbol{\lambda}=-\mathbf{X}=-\frac{\partial D}{\partial\dot{\boldsymbol{\lambda}}}, \tag{16b}$$

where

$$\mathbf{Z}=\mathbf{H}-\mathbf{L}^T\mathbf{K}^{-1}\mathbf{L}=\mathbf{H}-\mathbf{N}^T\mathbf{K}\mathbf{N}. \tag{17}$$

We note that $\mathbf{u}^P$ is a linear function of $\boldsymbol{\lambda}$; however, equation (15*c*) cannot in general be inverted. The matrix $\mathbf{K}$ will in general be positive definite, and equation (16*a*) describes the solution for a linear elastic material.

The matrix $\mathbf{Z}$ is not necessarily positive definite, but may only be positive semi-definite. This latter case is associated with structures in which flow may occur, that is, where changes in $\mathbf{u}^P$ may occur at fixed $\mathbf{P}$. We shall restrict ourselves to values of $\mathbf{P}$ which can be equilibrated.

The complementary work Ω is given by

$$\begin{aligned} \Omega(t)&=\int_o^t \mathbf{u}^T(\tau)\dot{\mathbf{P}}(\tau)d\tau \\ &=\int_o^t \mathbf{u}^{ET}(\tau)\dot{\mathbf{P}}(\tau)d\tau+\int_o^t \mathbf{u}^{PT}(\tau)\dot{\mathbf{P}}(\tau)d\tau \\ &=\Omega^E(t)+\Omega^P(t). \end{aligned} \tag{18}$$

From equation (16*a*) the elastic complementary work is

$$\Omega^E=\int_o^t \mathbf{P}^T\mathbf{K}^{-1}\dot{\mathbf{P}}\;dt=1/2\;\mathbf{P}^T(t)\mathbf{K}^{-1}\mathbf{P}(t). \tag{19}$$

This contribution is independent of the way in which the plastic part of the solution is advanced, and depends only on the current value of the load vector. Our concern is with the plastic complementary work, which can be written as

$$\begin{aligned} \Omega^P(t)&=\int_o^t \mathbf{u}^{PT}(\tau)\dot{\mathbf{P}}(\tau)d\tau \\ &=\int_o^t \boldsymbol{\lambda}^T(\tau)\{\mathbf{N}^T\dot{\mathbf{P}}(\tau)\}d\tau. \end{aligned} \tag{20}$$

This integral thus depends on the way in which $\boldsymbol{\lambda}$ changes with

Downloaded 03 May 2010 to 171.66.16.27. Redistribution subject to ASME license or copyright; see http://www.asme.org/terms/Terms_Use.cfm

$\mathbf{N}^T\mathbf{P}$. We shall consider this relation in further detail in the following sections.

In a similar manner, we can compute the work along the loading path

$$W(t)=\int_o^t \mathbf{P}^T(t)\dot{\mathbf{u}}(t)\,dt$$

$$=\int_o^t \mathbf{P}^T(t)\dot{\mathbf{u}}^E(t)\,dt+\int_o^t \mathbf{P}^T(t)\dot{\mathbf{u}}^P(t)\,dt$$

$$=W^E(t)+W^P(t). \tag{21}$$

From equation (15b) the elastic work W^E is

$$W^E(t)=\int_o^t \mathbf{u}^{ET}\mathbf{K}\,\dot{\mathbf{u}}^E dt=\frac{1}{2}\,\mathbf{u}^{ET}\mathbf{K}\,\mathbf{u}^E. \tag{22}$$

This contribution depends only on the instantaneous value of $\mathbf{u}^E$, and is thus history independent. The plastic work W^P is

$$W^P(t)=\int_o^t \mathbf{P}^T(t)\,\mathbf{N}\,\dot{\lambda}(t)\,dt$$

$$=\int_o^t (\mathbf{N}^T\mathbf{P})^T\dot{\lambda}\,dt. \tag{23}$$

Substituting for $\mathbf{N}^T\mathbf{P}$ from equation (16b), this becomes

$$W^P(t)=\int_o^t \left(\mathbf{Z}\,\lambda+\frac{\partial D}{\partial\dot{\lambda}}\right)^T\dot{\lambda}\,dt$$

$$=\frac{1}{2}\,\lambda^T(t)\mathbf{Z}\,\lambda(t)+\int_o^t D(\dot{\lambda})\,dt, \tag{24}$$

in view of the fact that D is homogeneous and of degree one. We note also that

$$W^P(t)+\Omega^P(t)=[\lambda^T(\tau)\mathbf{N}^T\mathbf{P}(\tau)]_o^t=\lambda^T(t)\mathbf{N}^T\mathbf{P}(t). \tag{25}$$

Constitutive Equations

The governing equation whose solution we seek is equation (16b):

$$\left(\frac{\partial D}{\partial\dot{\lambda}}\right)_{\dot{\lambda}(t)}+\mathbf{Z}\lambda(t)=\mathbf{N}^T\mathbf{P}(t). \tag{26}$$

The only term involving rates is the first term. For the ith increment we make use of a backward difference scheme, and write

$$\dot{\lambda}(t)=\frac{1}{\Delta t}\{\lambda(t)-\lambda_{i-1}\},\quad \Delta t=t-t_{i-1}\geq 0. \tag{27}$$

This also assumes that $\lambda(t)$ changes along a straight line path in λ space over the interval $[t_{i-1}, t]$, as shown diagrammatically in Fig. 2. Equation (27) implies that the constitituve equations are updated at time t_{i-1}, when $\lambda(t_{i-1})=\lambda_{i-1}$, and that we adopt a holonomic relation between $\{\lambda(t)-\lambda_{i-1}\}$ and $\mathbf{X}(t)$.

Because $\partial D/\partial\dot{\lambda}$ is homogeneous and of degree zero, we need not in fact distinguish between $\dot{\lambda}$ and $\dot{\lambda}\Delta t$. We may write

$$D=D(\Delta\lambda), \tag{28}$$

and may interpret D as the dissipated work associated with the change $\Delta\lambda=\lambda-\lambda_{i-1}$ along a straight line path in λ space. Equation (26) now becomes

$$\left(\frac{\partial D(\Delta\lambda)}{\partial\Delta\lambda}\right)_{\lambda(t)-\lambda_{i-1}}+\mathbf{Z}\lambda(t)=\mathbf{N}^T\mathbf{P}(t). \tag{29}$$

Evidently, we can replace $\partial D(\Delta\lambda)/\partial\Delta\lambda$ by $\partial D(\lambda)/\partial\lambda$; further we can write

$$\left(\frac{\partial D(\lambda)}{\partial\lambda}\right)_{\lambda(t)-\lambda_{i-1}}=\left(\frac{\partial D(\lambda-\lambda_{i-1})}{\partial\lambda}\right)_{\lambda(t)}. \tag{30}$$

Geometrically, we simply displace the origin of the potential function $D(\lambda)$ in the $D-\lambda$ space. The governing equation (29) then becomes

$$\left(\frac{\partial D(\lambda-\lambda_{i-1})}{\partial\lambda}\right)_{\lambda(t)}+\mathbf{Z}\,\lambda(t)=\mathbf{N}^T\mathbf{P}(t). \tag{31}$$

With the adoption of the backward difference algorithm, the plastic work W^P (equation (24)) can be simply expressed. Since $\dot{\lambda}(t)$ is constant within each time interval, equation (24) becomes

$$W^P(t)=\frac{1}{2}\,\lambda^T(t)\,\mathbf{Z}\,\lambda(t)+D(\lambda_1)+D(\lambda_2-\lambda_1)+\ldots$$
$$+D\{\lambda(t)-\lambda_{i-1}\},\ t_{i-1}\leq t\leq t_i. \tag{32}$$

This suggests that we may define a potential function

$$W_i^P(\lambda)=\frac{1}{2}\,\lambda^T\mathbf{Z}\,\lambda+D(\lambda_1)+D(\lambda_2-\lambda_1)+\ldots+D(\lambda-\lambda_{i-1}), \tag{33}$$

which can be regarded as a fixed surface in the $W^P-\lambda$ space. The surface is convex, since $\mathbf{Z}$ is semi-positive definite and D is convex. The solution at time t, $t_{i-1}\leq t\leq t_i$, is given by a state point on this surface identified by the condition, from equation (31), that

$$\mathbf{N}^T\mathbf{P}(t)=\left(\frac{\partial W_i^P}{\partial\lambda}\right)_{\lambda(t)}. \tag{34}$$

We can thus form a geometric analogy of the evolution of the solution. For the ith interval, $t_{i-1}\leq t\leq t_i$, the solution point moves on the fixed W_i^P surface, given in terms of $\mathbf{P}(t)$ through equation (34). At time t_i, when the next update occurs, we define a new surface

$$W_{i+1}^P(\lambda)=\frac{1}{2}\,\lambda^T\mathbf{Z}\lambda+D(\lambda_1)+D(\lambda_2)+\ldots+D(\lambda_1-\lambda_{i-1})$$
$$+D(\lambda-\lambda_{i-1}), \tag{35}$$

and the solution point moves on this surface during the $(i+1)$th interval, $t_i\leq t\leq t_{i+1}$.

It is clear that

$$W_i^P(\lambda_i)=W_{i+1}^P(\lambda_i), \tag{36}$$

and that the hyperplane $\mathbf{N}^T\mathbf{P}(t_i)$ is tangent to both surfaces at λ_i. Further, we note that

$$W_{i+1}^P-W_i^P=D(\lambda-\lambda_i)+D(\lambda_i-\lambda_{i-1})-D(\lambda-\lambda_{i-1}). \tag{37}$$

It follows from the convexity of D that

$$D(\lambda-\lambda_i)-D(\lambda-\lambda_{i-1})\geq\overline{(\lambda-\lambda_i}-\overline{\lambda-\lambda_{i-1}})\left(\frac{\partial D}{\partial\lambda}\right)_{\lambda-\lambda_{i-1}}$$

$$=-(\lambda_i-\lambda_{i-1})\left(\frac{\partial D}{\partial\lambda}\right)_{\lambda-\lambda_{i-1}}$$

$$\geq -D(\lambda_i-\lambda_{i-1}). \tag{38}$$

Hence,

$$W_{i+1}^P\geq W_i^P, \tag{39}$$

and the updated potential surface either coincides with or lies above the previous surface.

Complementary Work Bounding Principle

Since, from equation (25),

$$W^P(t)+\Omega^P(t)=\lambda^T(t)\mathbf{N}^T\mathbf{P}(t), \tag{40}$$

Downloaded 03 May 2010 to 171.66.16.27. Redistribution subject to ASME license or copyright; see http://www.asme.org/terms/Terms_Use.cfm

we may use a Legendre transform to define a potential function Ω_i^P $(\mathbf{N}^T\mathbf{P})$, and write the governing equation (34) as

$$\lambda(t) = \left(\frac{\partial \Omega_i^P}{\partial \mathbf{N}^T\mathbf{P}}\right)_{\mathbf{N}^T\mathbf{P}(t)} . \tag{41}$$

We can thus define a solution point within the ith interval which lies on a fixed complementary work surface; $\lambda(t)$ is given by the slope of this surface at the point $\mathbf{N}^T\mathbf{P}(t)$. This construction is easier to visualize since $\mathbf{N}^T\mathbf{P}$ is the independent variable in the loading program. When the constitutive equations are updated at time t_i, we form a new complementary work surface; the two surfaces touch with a common tangent at $\mathbf{N}^T\mathbf{P}(t_i)$.

We note that

$$\Omega_i^P(\mathbf{N}^T\mathbf{P}) = \max_{\lambda}\{\lambda^T\mathbf{N}^T\mathbf{P} - W_i^P(\lambda)\} \tag{42a}$$

$$\Omega_{i+1}^P(\mathbf{N}^T\mathbf{P}) = \max_{\lambda}\{\lambda^T\mathbf{N}^T\mathbf{P} - W_{i+1}^P(\lambda)\}. \tag{42b}$$

From the convexity of $D(\lambda)$, equation (38),

$$D(\lambda-\lambda_i) + D(\lambda_i-\lambda_{i-1}) \geq D(\lambda-\lambda_{i-1}), \tag{43}$$

and hence, for arbitrary $\mathbf{N}^T\mathbf{P}$,

$$\lambda^T\mathbf{N}^T\mathbf{P} - \frac{1}{2}\lambda^T\mathbf{Z}\lambda - D(\lambda-\lambda_i) - D(\lambda_i-\lambda_{i-1}) - \ldots - D(\lambda_i)$$

$$\leq \lambda^T\mathbf{N}^T\mathbf{P} - \frac{1}{2}\lambda^T\mathbf{Z}\lambda - D(\lambda-\lambda_{i-1}) - \ldots - D(\lambda_i). \tag{44}$$

It follows then that, referring to inequality (44),

$$\max_{\lambda}\{\text{LHS}\} \leq \{RHS\} \leq \max_{\lambda}\{\text{RHS}\}, \tag{45}$$

and hence that

$$\Omega_{i+1}^P(\mathbf{N}^T\mathbf{P}) \leq \Omega_i^P(\mathbf{N}^T\mathbf{P}). \tag{46}$$

We may interpret this result in the following way. For a given loading history $\mathbf{N}^T\mathbf{P}(t)$ over the period $o \leq t \leq T$, we may plot the value of $\Omega^P(\mathbf{N}^T\mathbf{P})$ as a function of time t. If the constitutive equation is not updated, the solution point lies on the Ω_o^P surface for the whole time period, shown diagrammatically in the case $n=1$ in Fig. 3. If we update at time $t_1 > 0$, the solution point moves on the surface Ω_1^P for $t \geq t_1$, and $\Omega_1^P \leq \Omega_o^P$, leading to the case $n=2$ in Fig. 3. If we further update at time t_2, $t_2 > t_1$, the solution point lies on the surface Ω_2^P for $t \geq t_2$, and $\Omega_2^P \leq \Omega_1^P \leq \Omega_o^P$, leading to the case $n=3$ in Fig. 3.

We can thus plot a function over the loading history which decreases or does not increase, each time an additional sequential update is effected. This indicates a type of convergence as the number of updates is increased. However, we may only introduce an additional update in the last interval, and this limits the applicability of the result.

Continuous Solution

In terms of the geometrical model of a solution point on the complementary work surface, a solution which is continuous in time is obtained by continuous updating of the complementary work surface. It can be shown rigorously that continuous updating leads to the equations of the rate problem; this point will be discussed in a separate paper.

It follows directly from the result given in the previous section that the plastic complementary work for the case $n=1$ is not less than the complementary work for the continuous solution, which can be regarded on an infinite number of sequential updates. Hence

$$[\Omega^P(t)]_{n=1} \geq [\Omega^P(t)]_{n\to\infty}. \tag{47}$$

This is a restatement of the complementary work bounding principle of Hodge (1966).

Conclusions

The result given in the paper indicates that, for an increasing number of sequential updates, the plastic complementary work does provide a basis for demonstrating consistent improvement of the solution. This suggests that there may exist procedures whereby the forward integration algorithm can be treated as part of the mechanical problem. The backward difference algorithm, in particular, has properties which are amenable to such analysis, and has gained popularity in elasto-plastic finite element calculations on a different rational basis (see, for example, Hughes, 1984).

However, the result formulated in this paper cannot be extended to nonsequential updates. This is the case of real interest, permitting us to compare solutions for n and $n+1$ updates over a time interval $(0, T)$, with the additional update chosen arbitrarily to subdivide any subinterval rather than the last interval. It is relatively easy to produce a counter-example to the conjecture that the result given in this paper may be extended.

Acknowledgments

The support of the Council for Scientific and Industrial Research of South Africa is gratefully acknowledged. The author is also indebted to B. D. Reddy, A. R. S. Ponter, and D. H. Martin for helpful discussions.

References

Bath, K-J., 1982, *Finite Element Procedures in Engineering Analysis*, Prentice Hall, NJ.

Carter, P., and Martin, J. B., 1976, "Work Bounding Functions for Plastic Materials," ASME Journal of Applied Mechanics, Vol. 43, pp. 434–438.

Greenberg, H. J., 1949, "Complementary Minimum Principles for an Elastic-Plasic Material," *Quarterly of Applied Mathematics*, Vol. 7, pp. 85–95.

Haar, A., and von Karman, T., 1909, "Zur Theorie der Spannungzustaende in Plastischen und Sandartigan Medien," Nachr. der Wiss. zu Gottingen, Math.-phys. Klasse, pp. 204–218.

Hodge, P. G., 1966, "A Deformation Bounding Theorem for Flow and Plasticity," *Quarterly of Applied Mathematics*, Vol. 24, pp. 171–174.

Hughes, T. J. R., 1984, "Numerical Implementation of Constitutive Models: Rate Independent Deviatoric Plasticity," *Theoretical Foundations for Large Scale Computations of Nonlinear Material Behaviour*, Nemat-Nasser, S., Asaro, R. J., and Hegemier, G. A., eds., Martinus Nijhoff Publishers.

Maier, G., and Nappi, A., 1983, "On the Unified Framework Provided by Mathematical Programming to Plasticity," *Mechanics of Material Behaviour*, Dvorak, G. J., and Shield, R. T., eds., Elsevier, pp. 253–273.

Marcal, P. V., and King, I. P., 1967, "Elastic-Plastic Analysis of Two-Dimensional Stress Systems by the Finite Element Method," *International Journal of Mechanical Science*, Vol. 9, pp. 143–155.

Martin, J. B., 1966, "Extended Displacement Bound Theorems for Work Hardening Continua Subjected to Dynamic Loading," *International Journal of Solids and Structures*, Vol. 2, pp. 9–26.

Martin, J. B., 1975, *Plasticity: Fundamentals and General Results*, MIT Press, Chapter 24.

Martin, J. B., 1981, "An Internal Variable Approach to the Formulation of Finite Element Problems in Plasticity," *Physical Nonlinearities in Structural Analysis*, Hult, J., and LeMaitre, J., eds., Springer Verlag, pp. 165–176.

Martin, J. B., 1984, "On Methods for the Estimation of Deformations of Elastic-Plastic Structures Subjected to Variable Loads," *Inelastic Structures under Variable Loads*, Polizzotto, C., and Sawczuk, A., eds., COGRAS (Palmermo), pp. 153–165.

Martin, J. B., Reddy, B. D., Griffin, T. B., and Bird, W. W., 1984, "Applications of Mathematical Programming Concepts to Incremental Elastic-Plastic Analysis," Technical Report No. 52, Applied Mechanics Research Unit, University of Cape Town, to appear in *Engineering Structures*.

Owen, D. R. J., and Hinton, E., 1980, *Finite Elements in Plasticity*, Pineridge Press.

Ponter, A. R. S., and Martin, J. B., 1972, "Some Extremal Properties and Energy Theorems for Inelastic Materials and Their Relationship to the Deformation Theory of Plasticity," *Journal of Mechanics and Physics of Solids*, Vol. 20, pp. 281–300.

Zienkiewicz, O. C., 1977, *The Finite Element Method*, McGraw-Hill, NY.

Downloaded 03 May 2010 to 171.66.16.27. Redistribution subject to ASME license or copyright; see http://www.asme.org/terms/Terms_Use.cfm

J. L. Ding
Assistant Professor,
Department of Mechanical Engineering,
Washington State University,
Pullman, WA 99164
Assoc. Mem. ASME

W. N. Findley
Professor,
Division of Engineering,
Brown University,
Providence, R.I. 02912
Fellow ASME

On Using Stress Relaxation Tests to Characterize Material Behavior

Stress relaxation tests, in which the gage length of the specimen was maintained constant by servocontrol, were performed on 2618-T61 aluminum. The test results, which were independent of the stiffness of the testing machine, were converted into a relation between stress and inelastic strain rate. It was found that the contribution by the anelastic component to the total stress relaxation was significant only in the initial stage. The validity of using the obtained stress versus inelastic-strain-rate relation to characterize the material behavior is also discussed. Results do not substantiate the concept of a "hardness" flow curve, but data were well predicted from the creep data by theory based on strain hardening and viscoelasticity.

Introduction

Stress relaxation is a time-dependent decrease of stress in a solid due to the conversion of elastic into inelastic strain. The stress relaxation test involves a time-dependent decrease in stress at constant total strain. Stress relaxation data have been used for engineering design in evaluating the constitutive relations governing material's inelastic behavior (see the book edited by Fox, 1979).

In a series of investigations by Hart, the use of the stress relaxation test was described for the constitutive modeling of material behavior. For a brief overall review see Hart (1979). Some related recent work is found in the paper by Alexopoulos et al. (1982).

In Hart (1976), the inelastic strain was decomposed into two components, anelastic strain (time-dependent, recoverable) and plastic strain (time-dependent, nonrecoverable). Similar decomposition was also used by Findley and Lai (1978) and Ding and Findley (1984 a and b), where these two components were termed as viscoelastic and viscous components, respectively. The formulation of the constitutive equation was based on a state-variable approach in which a tensor state variable was associated with the anelastic component, which accounted for the anisotropy induced by the deformation, and a scalar state variable called "hardness' associated with the plastic component, which accounted for isotropic hardening. An evolution rule was developed for each state variable in terms of deformation and metallurgical changes.

Stress relaxation tests were used by Hart et al. to characterize the scalar state variable. Test procedures used by Lee and Hart (1971), Hart and Solomon (1973), Yamada and Li (1973, 1974) were as follows. The specimen was loaded in an Instron testing machine at a specified crosshead speed to a point where a known amount of plastic strain was obtained. Then the crosshead was stopped and fixed in its position, and the load was recorded as a function of time. The load kept decreasing due to the continuous straining of the specimen by the residual load. The load versus time relation was then converted to a relation between stress and the inelastic strain rate taking into account the stiffnesses of both the testing machine and the specimen.

Woodford (1975) later performed similar tests on a Cr-Mo-V steel using a modified creep machine. In his test, smooth loading to the desired stress level was achieved in about 5 seconds at a strain rate of about 10^{-3}/s, and the loading wheel was then locked in position. Furthermore, an extensometer was used to measure the strain to eliminate the need to account for machine stiffness due to the significant discrepancies found between the computed strain and that measured on specimens after the test.

The idea behind these tests was that the accumulated strain-hardening during the stress relaxation was assumed to be very small, i.e., the value of the hardness didn't change much, and the obtained stress-inelastic strain rate relation could, therefore, be used for characterizing the current "hardness" of the material. For all the tests reported, it was found that there existed a scaling relation between the characteristic curves at different "hardness" levels, i.e., a master curve could be formed by translating all the characteristic curves along a particular direction; or, conversely, each curve was part of the master curve translated to a certain "hardness" level. This scaling relation was used to determine some of the material parameters used in the constitutive equation.

In the present paper, interest was focused on the role of the stress relaxation test as a tool for characterizing the material behavior. A different test method using direct strain control by servomechanism was employed to study the stress relaxation phenomenon of 2618-T61 aluminum alloy. The results were compared with the approach used by Hart et al.

Contributed by the Applied Mechanics Division for presentation at the 1987 Applied Mechanics, Biomechanics, and Fluids Engineering Conference, Cincinnati, OH, June 14–17, 1987, of the American Society of Mechanical Engineers.
Discussion of this paper should be addressed to the Editorial Department, ASME, United Engineering Center, 345 East 47th Street, New York, N.Y. 10017, and will be accepted until two months after final publication of the paper itself in the JOURNAL OF APPLIED MECHANICS. Manuscript received by ASME Applied Mechanics Division, March 25, 1986; final revision, September 22, 1986.
Paper No. 87-APM-25.

Copyright © 1987 by ASME
Downloaded 03 May 2010 to 171.66.16.27. Redistribution subject to ASME license or copyright; see http://www.asme.org/terms/Terms_Use.cfm

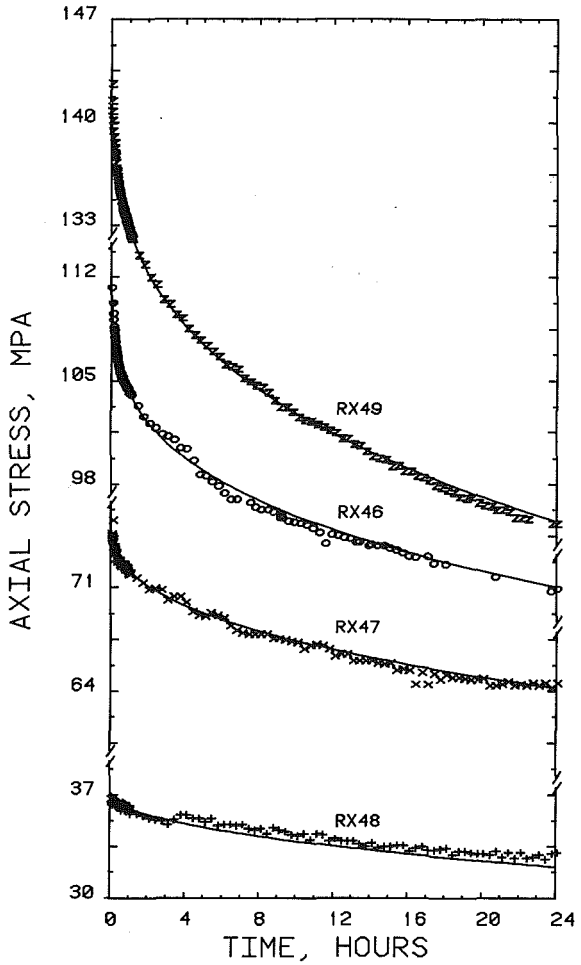


Fig. 1 The results of four stress relaxation tests: RX46, RX47, RX48, and RX49. The imposed strain for each test was 0.1725, 0.1150, 0.0575 and 0.23 percent, respectively. The solid lines represent equation (3).

Material and Specimen

The material used in the current work was 2618-T61 aluminum from the same batch as used in previous investigations for studying creep under complex stress states by Ding and Findley (1984 a, b, c; 1985; 1986).

The specimen was a thin-walled tube of circular cross-section with two ends enlarged for gripping purposes. The nominal outside diameter and wall thickness were 2.465 and 0.1524 cm (1.000 and 0.006 in), respectively. The total length of the specimen was 20.3 cm (8.0 in), and the gage length on the middle section of the tube, i.e., the distance between the gage points to which the extensometer was attached, was 10.16 cm (4.00 in).

Apparatus and Testing Procedure

The apparatus used in the present investigation was a combined tension and torsion creep machine. Since the present work only involved axial loading, a description of the torque capability is not given. Other details can be found in Findley and Gjelsvik (1962).

The relative axial displacement between the gage points was measured by a matched pair of linear variable differential transforms (LVDT) using an AC-null balance system. One LVDT was attached to the gage points through four invar rods and the other (reference LVDT) was connected to a micrometer. Before the test, the outputs of these two LVDT's cancelled each other, i.e., balanced. During the test some imbalance was induced, due to the relative displacement between the gage points, which could be balanced out again with the reference LVDT by turning the micrometer. The relative displacement could then be read from the micrometer.

In contrast with the creep tests in which the load was applied by dead weights, a servo hydraulic system was used for loading in the present tests. Before the test was started, the relative displacement between the gage points corresponding to the desired strain was calculated. The micrometer connected to the reference LVDT was then adjusted to the calculated desired displacement and an error signal was thus induced between the reference LVDT and extensometer LVDT. This error signal was used to drive the hydraulic system through the servocontroller until the error signal was balanced out. Thus the relative displacement between the gage points had also reached the desired value. The desired strain was imposed by adjusting the set point in the servocontroller very rapidly (in less than 10 s), but smoothly enough to eliminate any dynamic effect. The instant when the error signal was balanced out was considered as the starting point (zero time t_o) for the relaxation process. The load applied to the specimen was measured by two series-connected load cells whose outputs were recorded through a strip chart recorder and a digital printer, respectively. The printing interval was set to be 1 minute during the first one hour, then 20 minutes until the end of the test. The sensitivity of the load measuring system was 0.1 lb.

It should be noted that there is one important difference between the present test set-up and that used by Hart and coworkers. In their test, the crosshead was fixed so that the specimen kept straining during the relaxation stage and the load drop depended not only on the stiffness of the specimen but also the stiffness of the loading frame. In the present tests, the distance between the gage points was fixed (i.e., no further straining) and the load drop depended only on the stiffness of the specimen.

All the current tests were performed at a test temperature of 200°C, which is about 0.4~0.5 of the homologous temperature. The variation of temperature was within ±0.3°C both with the time and position within the gage length. The specimen was soaked at the test temperature for approximately 18 hours before the test started.

Experimental Results

Four tests are presented here as shown in Fig. 1. The imposed strains are 0.1725, 0.1150, 0.0575, and 0.23 percent for tests RX46, RX47, RX48, and RX49, respectively. These were the first parts of the data reported in Ding and Findley (1986), where they were used to evaluate some constitutive models for this material, not including work presented in the current paper. The solid lines are the data-fitting curves which will be discussed later.

In order to check if there was any permanent strain induced during the initial rapid loading stage, a plot of strain versus the stress at the starting time is shown in Fig. 2, where the slope of the solid line represents the reciprocal of the elastic modulus at the test temperature ($E = 6.50 \times 10^4$ MPa) obtained in previous creep tests by Ding and Findley (1984a). Figure 2 shows that the initial responses for all the four tests are elastic. This observation will be used in the later discussion.

Metallurgical Softening Effect

In order to make sure that the material was metallurgically stable during the test period, two aging tests were performed by Ding and Findley (1984a) in which two specimens were soaked at the test temperature (200°C) for 114 and 312 hours, respectively, prior to a creep test. The results were compared with those of creep tests under the same stress level but with the specimen soaked at the test temperature for only 18 hours. No significant differences were found among them.

Downloaded 03 May 2010 to 171.66.16.27. Redistribution subject to ASME license or copyright; see http://www.asme.org/terms/Terms_Use.cfm

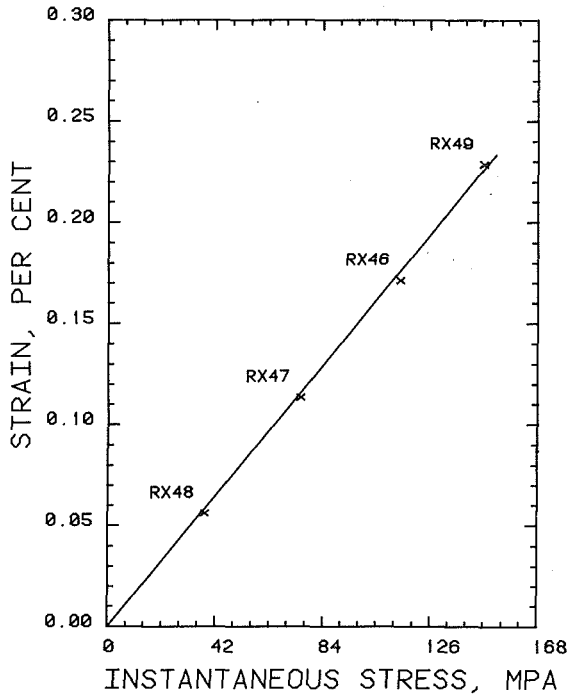


Fig. 2 Imposed axial strain versus instantaneous axial stress for the relaxation tests shown in Fig. 1. The slope of the solid line was obtained from the elastic modulus determined from creep tests, i.e., $E = 6.50 \times 10^4$ MPa.

Table 1 Constants in equation (3) for fitting the stress relaxation curves shown in Fig. 1

Test No.	σ_{11}°, MPa	σ_{11}^{+}, MPa/h^n	n
RX46	113.70	− 9.61	0.270
RX47	75.64	− 3.53	0.371
RX48	37.20	− 1.14	0.470
RX49	146.17	−13.53	0.283

Reduction of a Stress Versus Inelastic Strain Rate Relation From Stress Relaxation Data

The stress relaxation data could be converted to a relation between stress and inelastic strain rate. As mentioned earlier, because of the current test technique, this conversion did not involve the stiffness of the testing machine.

Considering ϵ_{11} to be composed of an elastic component (ϵ_{11}^E) and a time dependent inelastic component (ϵ_{11}^I), a stress versus inelastic strain rate relation was deduced from the stress relaxation data using the fact that ϵ_{11} is constant during a relaxation test, i.e.,

$$\epsilon_{11} = \epsilon_{11}^E + \epsilon_{11}^I = \text{constant}. \tag{1}$$

Differentiating equation (1) with respect to time and expressing $\dot{\epsilon}_{11}^I$ in terms of $\dot{\sigma}_{11}$ yielded the following expression:

$$\dot{\sigma}_{11}/E = -\dot{\epsilon}_{11}^I, \tag{2}$$

where E is the elastic modulus which is the same as the slope of the solid line in Fig. 2.

From relaxation data (σ_{11} versus t), $\dot{\sigma}_{11}$ was calculated at each instant. A σ_{11} versus $\dot{\epsilon}_{11}^I$ relation was thus obtained from equation (2).

In order to calculate $\dot{\sigma}_{11}$, the relaxation data was first fitted by a power function

$$\sigma_{11} = \sigma_{11}^{\circ} + \sigma_{11}^{+} t^n. \tag{3}$$

The resulting values of σ_{11}°, σ_{11}^{+} and n are listed in Table 1 and the fitting curves are shown in Fig. 1 as the solid lines.

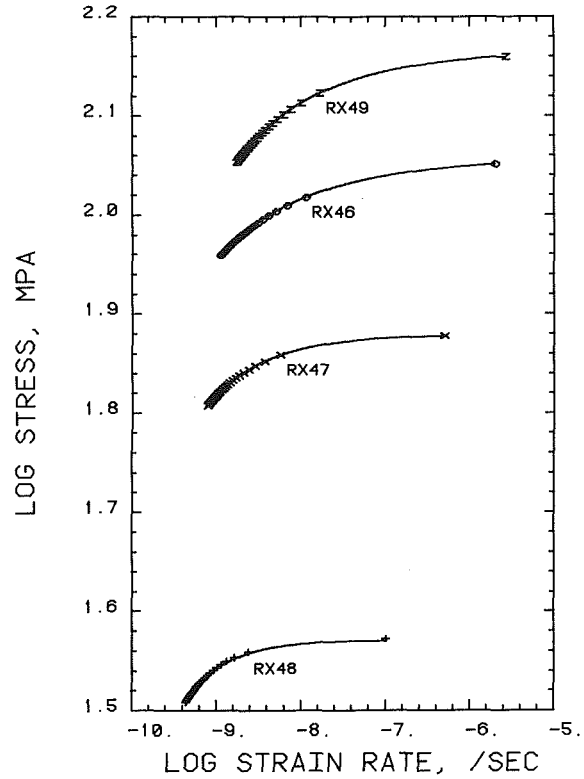


Fig. 3 Log of stress (MPa) versus log of inelastic strain rate (per second) deduced from the stress relaxation tests shown in Fig. 1 by means of equation (2) and (3)

Differentiating equation (3) with respect to time yielded $\dot{\sigma}_{11}$ and thus $\dot{\epsilon}_{11}^I$ by use of equation (2). A relation between stress and the inelastic strain rate was thus obtained and shown in Fig. 3 where the symbols represent the calculated values and the duration between consecutive symbols was 1 hour.

Interpretation of the Test Results

The curves shown in Fig. 3 look similar to those found in Hart and Solomon (1973), Yamada and Li (1973, 1974), and Woodford (1975). However, the interpretation of these curves is quite different. In their tests, the relaxation tests were preceded by a certain amount of plastic strain induced during the loading stage. Due to this amount of plastic strain, the material was said to be in a certain plastic state which was characterized by a scaler state variable "hardness." The stress-inelastic strain rate relation deduced from the relaxation tests was interpreted as the characteristic curve for this plastic state assuming that further work hardening was negligible and that the material was metallurgically stable during the relaxation tests.

However, in the current work, all the curves shown in Fig. 3 were obtained from the material with exactly the same histories because all the specimens were machined from the same batch of material and there was no plastic strain induced in any specimen during the loading stage as shown in Fig. 2. Therefore, if the stress-strain rate relation obtained from the relaxation tests could be used to characterize the state of the material, the curves shown in Fig. 3 are all supposed to be overlapped together in one continuous curve. This is because the specimen used for all the tests were essentially at the same "hardness" level. The results shown in Fig. 3 do not support this view. The stress corresponding to a particular strain rate was highly path-dependent, i.e., not uniquely determined by the strain rate.

Metallurgical instability during the test, as a possible reason for the differences between the test results, was ruled out as

Downloaded 03 May 2010 to 171.66.16.27. Redistribution subject to ASME license or copyright; see http://www.asme.org/terms/Terms_Use.cfm

discussed previously. Another possibility is the way the specimen was loaded during the loading stage. In the current tests, the loading may be considered as "rapid loading," while in Hart's tests, it was a loading under constant cross-head speed. Rapid loading was used by Woodford (1975). The speed of the loading could have some effects on the behavior of the anelastic component even though its contribution to the total stress relaxation could be significant only in the initial state as suggested by Hart et al. (1975). In order to clarify this point, an analysis was made in the following on the contribution to the total strain by each of the inelastic components, namely, plastic and anelastic. Since a stress relaxation test was used by Hart to characterize the plastic component only, even though both components are active during the test, this analysis may also be necessary in identifying the role played by the anelastic component.

The Contribution of the Anelastic Component to the Total Stress Relaxation

In a previous work by Ding and Findley (1984 a and b), a viscous-visco-elastic model was developed to describe the time-dependent behavior under complex stress states for 2618-T61 aluminum alloy. In this model, which originated from Findley and Lai (1978), the time-dependent strain was decomposed into viscoelastic and viscous components which are parallel to the anelastic and plastic components, respectively, used in Hart's constitutive equation. Even though this model had some limitation on predicting the material behavior under nonproportional loadings (Ding and Findley, 1984c, 1985), it worked excellently for proportional loadings (Ding and Findley, 1984b). In fact, all the stress relaxation curves shown in Fig. 1 were well described from creep tests by this model as reported by Ding and Findley (1986). However, no attention was paid in this prior paper to the contribution by each strain component to the total stress relaxation. In the present work, the same model will be used as follows to calculate the stress drop due to each component. Since relaxation tests are essentially uniaxial creep tests under continuously decreasing stress states, i.e., they belong to the category of proportional loading, the following calculated results give a reasonable estimation for the role played by each strain component during stress relaxation.

The constitutive equation for the viscoelastic component was based on the modified superposition principle. For a series of m steps in combined tension σ and torsion τ stress states, ϵ_{11}^{VE} is given as follows:

$$\epsilon_{11}^{\mathrm{VE}} = F^{\mathrm{VE}}(\sigma_1,\tau_1)[t^{n_1} - (t-t_1)^{n_1}] + \ldots$$
$$+ F^{\mathrm{VE}}(\sigma_{m-1},\tau_{m-1})[(t-t_{m-2})^{n_1} - (t-t_{m-1})^{n_1}]$$
$$+ F^{VE}(\sigma_m,\tau_m)(t-t_{m-1})^{n_1},\ t_{m-1} < t, \qquad (4)$$

where t is time, $t_1, \ldots, t_{m-1}$ are the times at which the stress was abruptly changed. $F^{VE}(\sigma,\tau) = F_1^+\sigma + F_3^+\sigma^3 + F_4^+\sigma\tau^2$ is the stress dependence of $\epsilon_{11}^{\mathrm{VE}}$ under constant stress states. Similarly, $\epsilon_{11}^{\mathrm{VE}}$ was obtained by replacing $F^{VE}(\sigma,\tau)$ by $G^{VE}(\sigma,\tau)$ in equation (4). Other details can be found in Ding and Findley (1984a, b).

The constitutive equation for the viscous component based on isotropic strain hardening is given by

$$\dot{\epsilon}_{ij}^{V} = \sigma_{ij}' n F(\tau_{\max})\{\tfrac{1}{2}\gamma_{\max})/[\tau_{\max}F(\tau_{\max})]\}^{(n-1)/n}, \qquad (5)$$

where σ_{ij}' is the stress deviator, $\tau_{\max}$ is maximum shear stress, and $\gamma_{\max}$ is maximum engineering shear strain. In fact, two other flow rules based on different hardening natures, namely, kinematic hardening and independent hardening were also studied in Ding and Findley (1984a, b, c; 1985; 1986). However, equation (5) was found to be the best one at least for proportional loadings.

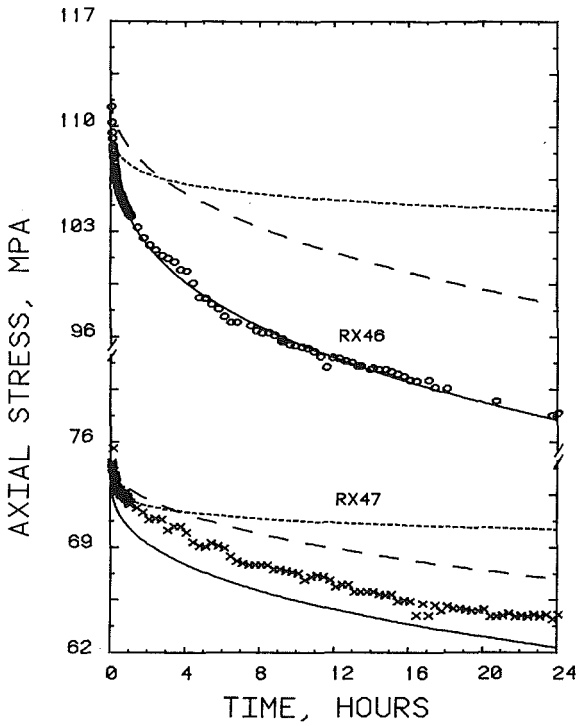


Fig. 4(a) Comparison of the experimental data for stress relaxation with the results calculated from a viscous-viscoelastic model for tests RX46 and RX47 using data from creep tests. Solid lines are the calculated total stress drop; dashed lines are the stress drop due to the viscous component; and dotted lines are the stress drop due to the viscoelastic component.

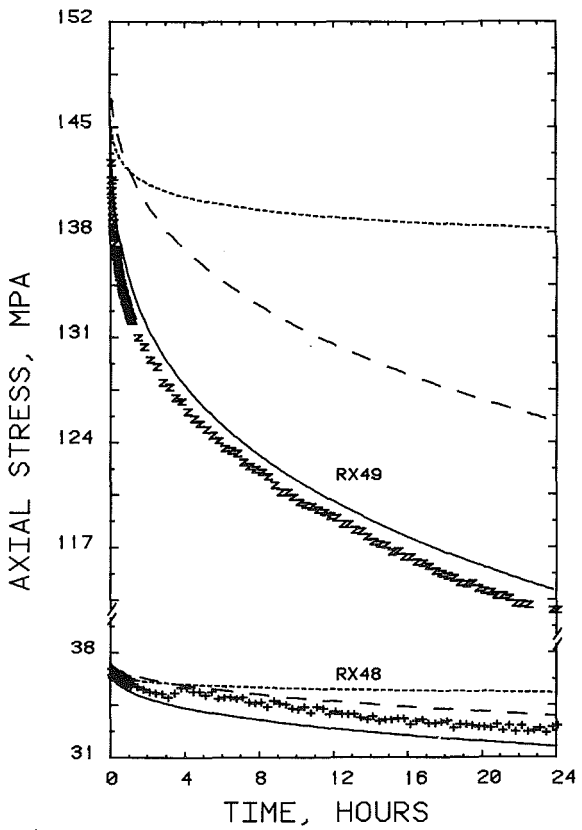


Fig. 4(b) Comparison of the experimental data for stress relaxation with the results calculated from a viscous-viscoelastic model for tests RX48 and RX49 using data from creep tests. Solid lines are the calculated total stress drop; dashed lines are the stress drop due to the viscous component; and dotted lines are the stress drop due to the viscoelastic component.

Downloaded 03 May 2010 to 171.66.16.27. Redistribution subject to ASME license or copyright; see http://www.asme.org/terms/Terms_Use.cfm

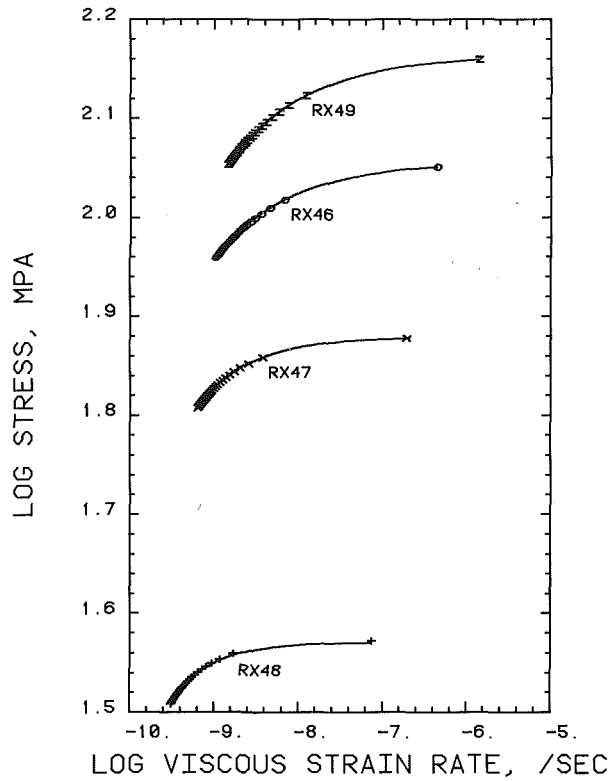


Fig. 5 Log of stress versus log of viscous strain rate deduced from the viscous-viscoelastic model corresponding to theory curves shown as long dash lines in Fig. 4

The results predicted by the viscous-viscoelastic model are shown in Fig. 4(*a*) and Fig. 4(*b*) in which the solid lines are the total stress drop which were also shown in Ding and Findley (1986), the long-dashed lines are the stress drop due to the viscous component, and the dotted lines are due to the viscoelastic component. From these two figures, it can be seen that the contribution by the viscoelastic component to the stress relaxation is indeed significant but only in the initial stage.

The accumulated viscous strain and viscous strain rate were also calculated from the viscous-viscoelastic model using constants from Ding and Findley (1984a). The relation between stress and viscous strain rate are shown in Fig. 5 in log-log coordinates. The results are very similar to those shown in Fig. 3.

Discussion

The path dependence of the test results discussed above was apparently due to the work-hardening effect induced by the viscous strain during the stress relaxation. The viscous strain accumulated in test RX49, of which the imposed strain was the largest among the four tests, was calculated to be 3.7×10^{-4}. The hardening effect induced by this small amount of strain did not seem negligible.

On the other hand, a stress relaxation test is actually a creep test under a continuously decreasing stress state. As discussed by Lai and Findley (1982), in a conventional creep test at constant stress, all three stress components are fixed. However, in a stress relaxation test under constant strain as performed in the current work, only one strain component is constant, the others are variable. Actually for the tests done by Hart et al., none of the strain components are constant. It seems questionable that much useful information could be obtained easily from a test in which all the test conditions are variable.

Conclusion

The stress relaxation is a path-dependent deformation process. The hardening effect due to the inelastic strain during the stress relaxation process is not negligible. Stress relaxation is equivalent to a creep test under continuously decreasing stress state and does not provide more constitutive information than a constant load creep test. Results of experiments on 2618-T61 aluminum do not support the concept of a "hardness" flow curve.

Acknowledgment

The tests reported in the current paper were performed at Brown University under the support of US Army Research Office, Grant No. DAAG29-81-K-0138. Analysis of the data and preparation of this manuscript was supported in part by funds provided by the Washington State University Research and Arts Committee and the National Science Foundation under Grant No. MEA-84029. Thanks are also due to Ms. Jo Ann Rattey for typing the manuscript and for Mr. Sang-Rok Lee for preparing the figures.

References

Alexopoules, P., Keusseyan, R. L., Wire, G. L. and Li, C.-Y., 1982, "Experimental Investigation of Nonelastic Deformation Emphasizing Transient Phenomena by Using a State Variable Approach," in *Mechanical Testing for Deformation Model Development*, ASTM STP 765, Rohde, R. W., and Swearengen, J. C., eds., pp. 148–184.

Ding, J. L., and Findley, W. N., 1984a, "48 Hour Multiaxial Creep and Creep Recovery of 2618 Aluminum Alloy at 200°C," ASME JOURNAL OF APPLIED MECHANICS, Vol. 51, pp. 125–132.

Ding, J. L., and Findley, W. N., 1984b, "Multiaxial Creep of 2618 Aluminum Under Proportional Loading Steps," ASME JOURNAL OF APPLIED MECHANICS, Vol. 51, pp. 133–140.

Ding, J. L., and Findley, W. N., 1984c, "Creep Experiments Under Nonproportional Loadings with Stress Reversals for 2618 Aluminum," ASME *Journal of Eng. Mater. Technol.*, Vol. 106, pp. 397–404.

Ding, J. L., and Findley, W. N., 1985, "Nonproportional Loading Steps in Multiaxial Creep of 2618 Aluminum," ASME JOURNAL OF APPLIED MECHANICS, Vol. 52, pp. 621–628.

Ding, J. L., and Findley, W. N., 1986, "Simultaneous and Mixed Stress Relaxation in Tension and Creep in Torsion of 2618 Aluminum," ASME JOURNAL OF APPLIED MECHANICS, Vol. 53, No. 3, pp. 529–535.

Findley, W. N., and Gjelsvik, A., 1962, "A Biaxial Testing Machine for Plasticity, Creep or Relaxation Under Variable Principle Stress Ratios," *Proceedings, ASTM*, Vol. 62, pp. 1103–1118.

Findley, W. N., and Lai, J. S., 1978, "Creep and Recovery of 2618 Aluminum Alloy Under Combined Stress with a Representation by a Viscous-Visco-elastic Model," ASME JOURNAL OF APPLIED MECHANICS, Vol. 45, pp. 507–514.

Fox, Alfred, ed., 1979, *Stress Relaxation Testing*, ASTM STP 676, American Society for Testing and Materials.

Hart, E. W., and Solomon, H. D., 1973, "Load Relaxation Studies of Polycrystalline High Purity Aluminum," *Acta Metallurgica*, Vol. 21, pp. 295–307.

Hart, E. W., Li, C-Y., Yamada, H., and Wire, G. L., 1975, "Phenomenological Theory: A Guide to Constitutive Relations and Fundamental Deformation Properties," in *Constitutive Equations in Plasticity*, Argon, A. S., ed., MIT Press, pp. 149–197.

Hart, E. W., 1976, "Constitutive Relations for the Nonelastic Deformation of Metals," *ASME J. Engr. Mater. and Technol.*, Vol. 98, pp. 193–202.

Hart, E. W., 1979, "Load Relaxation Testing and Material Constitutive Equations," in *Stress Relaxation Testing*, ASTM STP 676, Fox, A., ed., pp. 5–20.

Lai, J. S., and Findley, W. N., 1982, "Simultaneous Stress Relaxation in Tension and Creep in Torsion of 2618 Aluminum at Elevated Temperature," ASME JOURNAL OF APPLIED MECHANICS, Vol. 49, pp. 19–25.

Lee, D., and Hart, E. W., 1971, "Stress Relaxation and Mechanical Behavior of Metals," *Metallurgical Transactions*, Vol. 2, pp. 1245–1248.

Woodford, D. A., 1975, "Measurement of the Mechanical State of a Low Alloy Steel at Elevated Temperature," *Metallurgical Transactions*, Vol. 6A, pp. 1693–1697.

Yamada, H., and Li, C-Y., 1974, "Stress Relaxation and Mechanical Equation of State Austenitic Stainless Steel," *Metallurgical Transactions*, Vol. 4, pp. 2133–2136.

Yamada, H., and Li, C-Y., 1974, "Stress Relaxation and Mechanical Equation of State in B.C.C. Metals in Monotonic Loading," *Acta Metallurgica*, Vol. 22, pp. 249–253.

Downloaded 03 May 2010 to 171.66.16.27. Redistribution subject to ASME license or copyright; see http://www.asme.org/terms/Terms_Use.cfm

B. Budiansky
Division of Applied Sciences,
Harvard University,
Cambridge, MA 02138

E. Kimmel
Department of Mechanical Engineering,
Massachusetts Institute of Technology,
Cambridge, MA 02139

Elastic Moduli of Lungs

Macroscopic elastic moduli governing the incremental deformation of pressurized lungs are calculated on the basis of a micromechanical study of an individual lung element (alveolus). The spongy lung tissue (parenchyma) is presumed to be in an initial state of isotropic tension, and the lung alveolus is idealized as a pin-jointed truss in the shape of a regular dodecahedron. The analysis is based on a variational statement of nonlinear structural mechanics, and the results show how the moduli depend on the initial tension and the assumed constitutive behavior of the idealized truss members.

Introduction

The theory of lung elasticity has received much study during the last two decades, with particular attention directed to the establishment of overall constitutive relations between stress and strain in lung tissue. The most common approach (e.g., Lambert and Wilson, 1973; Frankus and Lee, 1974; Fung et al., 1978; Vawter et al., 1979; Lanir, 1983; Stamenovic and Wilson, 1985) has been to contemplate representative substructural lung elements, idealize their geometries, specify their elastic properties (often via strain-energy functions), assume that local and overall strains are identical, and, finally, get macroscopic constitutive relations by appropriate averages of the local stresses. The earlier work of Mead et al. (1970) and Wilson (1972) was more in line with the complementary approach of loading representative elements with the macroscopic stress, and computing their strains. In a recent paper, Kimmel et al. (1986) returned to this viewpoint, and studied the elastic behavior of pressurized lungs on the basis of a model in which a typical microstructural element of spongy lung tissue (parenchyma) was idealized as a regular, pin-jointed, dodecahedral space truss (Fig. 1(*a*)). An initial isotropic tension transmitted to the parenchyma by the surrounding pressurized pleural membrane was simulated by radial forces at each joint that produced identical tensile forces in the truss members. The model was then used in a calculation of linear, isotropic relations between subsequent small increments of macroscopic stress and strain in the parenchyma. The results showed the dependence of the elastic constants for incremental deformation on the initial hydrostatic tension, and on the tensile constitutive behavior of the idealized truss members. The elastic moduli found were in fairly good agreement with those inferred from available experimental data, but the calculations produced some anomalous results for small values of the stiffness of the element members.

In this paper the model of Kimmel et al. is reformulated, and a rigorous analysis, based on a general variational principle of nonlinear structural mechanics, is executed.

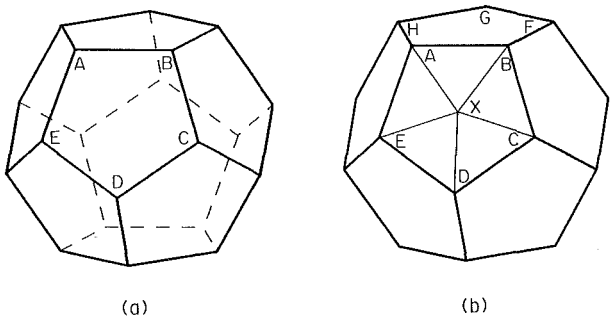


Fig. 1 (*a*) Regular dodecahedron, (*b*) subdivision of pentagonal faces

Model Formulation

The microscopic air sacs (alveoli) of which the spongy lung parenchyma is composed are roughly polyhedral in shape, and bounded by thin interfacial membranes. Besides alveoli, the parenchyma is also pervaded by blood vessels, by bronchioles emanating from the main bronchial tubes, by fibers surrounding openings in the alveolar walls, and by fibrous tissues extending from the surrounding pleural membrane (Wilson and Bachofen, 1982). We will pretend that the elastic effects of these extra constituents may be simulated simply by an appropriate thickness of the walls of an alveolar conglomeration. Since each alveolar wall is shared by two alveoli, we will regard the parenchyma as an aggregate of individual hollow polyhedra, the faces of which have *half* the actual average effective wall thickness. Then, in accordance with standard ideas of composite-material theory, we define the macroscopic strain produced by a prescribed macroscopic stress as the average of the strains experienced by the individual polyhedra in a large piece of parenchyma subjected to boundary tractions consistent with the given stress. When the lung is inflated, the alveolar openings allow the pressures in the alveoli to equalize, so that there are no net pressures across the individual alveolar walls, but a transpulmonary pressure P_0 is applied to the inside surface of the pleura. We will assume that, in turn, the pleural membrane transmits a hydrostatic tension $P < P_0$ to the parenchyma, that this initial hydrostatic stress produces a purely dilatational strain, and that subsequent stress and strain increments are then connected by isotropic constitutive relations.

Contributed by the Applied Mechanics Division for publication in the JOURNAL OF APPLIED MECHANICS.

Discussion on this paper should be addressed to the Editorial Department, ASME, United Engineering Center, 345 East 47th Street, New York, N.Y. 10017, and will be accepted until two months after final publication of the paper itself in the JOURNAL OF APPLIED MECHANICS. Manuscript received by ASME Applied Mechanics Division, June 30, 1986; final revision October 29, 1986.

Copyright © 1987 by ASME
Downloaded 03 May 2010 to 171.66.16.27. Redistribution subject to ASME license or copyright; see http://www.asme.org/terms/Terms_Use.cfm

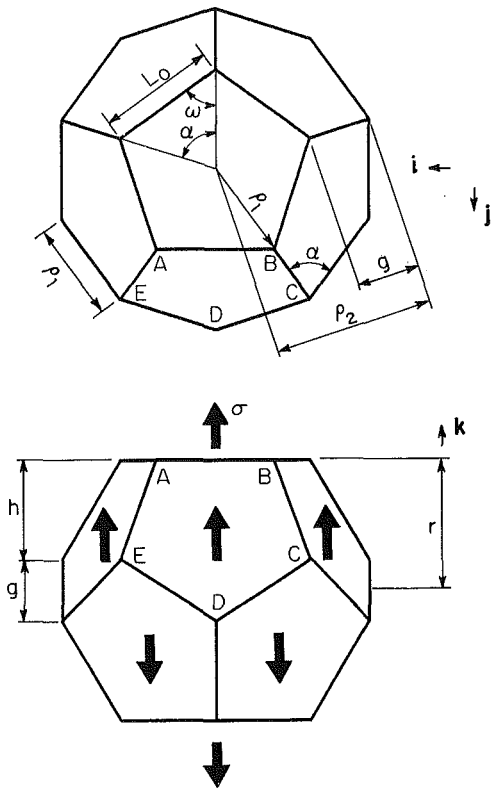


Fig. 2 Plan and elevation views; notation

In this paper, we will bypass the conceptual averaging process needed to determine the macroscopic strain produced by a given stress, and calculate instead the average strain experienced by a *single* hollow element in the shape of a regular dodecahedron. In this analysis, each face of the dodecahedron will be subjected to a traction consistent with the prescribed uniform stress but, at the same time, the surface displacements will be constrained in a way that keeps each face nearly flat. To be precise (see Fig. 1(*b*)), it will be assumed that (*i*) the vector displacement at the center of each pentagonal face is the mean of the displacements at its five corners; and that (*ii*) on each face the displacement varies linearly within each of the five constituent triangles that meet at the center. Accordingly, the five corner displacements suffice to specify the displacement within each pentagon. It is easily shown that for small displacements satisfying these kinematic assumptions the average mean curvature of each face vanishes.[1] By virtue of its symmetry, the isolated dodecahedron, when loaded and constrained in this way, is indeed an elastically isotropic structure, properly reflecting the isotropy of the random aggregate it is meant to represent.

Following Kimmel et al., we make a further simplification, in which we concentrate all of the in-plane load carrying capacity of the dodecahedral faces into elastic, pin-jointed rods along the edges, and adopt for these members the constitutive relation

$$\frac{\dot{T}}{T}=B\left(\frac{\dot{L}}{L}\right) \tag{1}$$

[1] For small deflection $w(x,y)$ normal to an initially flat surface of area A and boundary C, the local mean curvature is

$$\frac{1}{2A}\int_A \nabla^2 w\, dA=\frac{1}{2A}\int_C \frac{\partial w}{\partial n}\, ds$$

where $\partial w/\partial n$ is the normal derivative, and the line integral around the perimeter of the pentagon vanishes when the conditions (*i*), (*ii*) are imposed on w.

Here T and L are current values of member force and length, dots represent time derivatives, and B is a nondimensional stiffness that may itself depend on L.

We will first consider a uniform hydrostatic tension P applied normally to the faces of the dodecahedron, and calculate the incremental bulk modulus K defined by

$$K=\dot{P}/(\dot{V}/V) \tag{2}$$

where V is the enclosed volume. Then, with the hydrostatic tension kept constant and normal to the deforming faces, we will apply surface traction rates corresponding to a uniaxial stress σ (Fig. 2) and calculate the Young's modulus

$$E=\dot{\sigma}/\dot{\epsilon} \tag{3}$$

where $\dot{\epsilon}$ is the average strain rate in the direction of σ suffered by the dodecahedron. The standard connections for isotropic bodies will then give Poisson's ratio ν and the shear modulus G.

Bulk Modulus

The calculation of K that follows is essentially the same as that of Kimmel et al. Suppose that hydrostatic tension P produces identical forces T in the 30 members of the dodecahedron. Then, by the principle of virtual work, P produces rates-of-change of volume and length that satisfy

$$P\dot{V}=30T\dot{L} \tag{4}$$

Self-similar growth of the dodecahedron due to P implies that

$$\dot{V}/V=3\dot{L}/L \tag{5}$$

so that

$$PV=10TL \tag{6}$$

and

$$\dot{P}/P+\dot{V}/V=\dot{T}/T+\dot{L}/L \tag{7}$$

Eliminating $\dot{L}/L$ and $\dot{T}/T$ from equations (5), (7), and (1) gives

$$\dot{P}/P=\left(\frac{B-2}{3}\right)\dot{V}/V$$

and so by the definition (2)

$$K/P=(B-2)/3 \tag{8}$$

Young's Modulus

With the hydrostatic tension P maintained, we apply vertical tension σ to the 12 planar faces of the dodecahedron (Fig. 2 shows plan and elevation views of the loaded dodecahedron; geometrical relations are listed in the Appendix A). The nominal stress σ is specified as a force per unit horizontal projection of *original* surface area, i.e., the area corresponding to the presence of P alone.

While σ is applied, P is kept normal to the *current* surface orientations, and its magnitude in terms of force per unit *current* area is fixed. To begin the analysis of deformation due to σ, we assert the principle of virtual work

$$\sum_{i=1}^{30} T_i\delta\Delta_i=P\delta V+\delta\pi \tag{9}$$

where Δ_i represents the elongation of the ith member, T_i is the corresponding force, and π is the potential of the applied σ loading. (The procedure that follows was guided by an earlier development (Budiansky, 1969) of equations for the nonlinear analysis of space trusses.) The elongation Δ_i is defined as (L_i-L_0), where L_i is the current member length, and L_0 is the reference length corresponding to the initial state when only P is present. The virtual changes in volume δV and the virtual

Downloaded 03 May 2010 to 171.66.16.27. Redistribution subject to ASME license or copyright; see http://www.asme.org/terms/Terms_Use.cfm

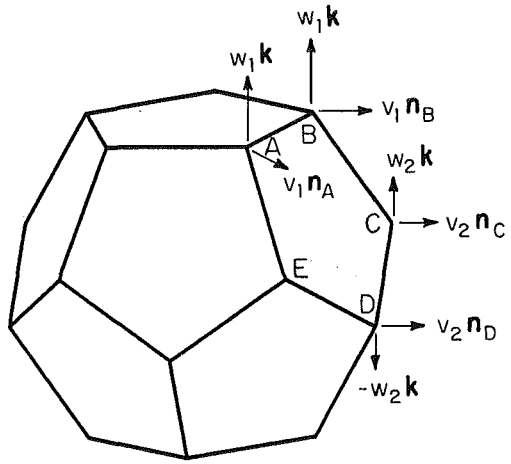


Fig. 3 Corner displacements produced by uniaxial tension

elongations $\delta\Delta_i$ must be compatible with changes in joint displacements at the corners of the dodecahedron and with the previously stated kinematic assumptions concerning the displacements within the faces of the dodecahedron.

Since there are only three distinct member responses when σ is applied, namely (see Fig. 2) those of (1) AB, (2) BC, and (3) CD, we can replace the internal-virtual-work sum in equation (9) by

$$10\sum_{i=1}^{3} T_i\Delta_i$$

Also, just four displacement variables suffice to specify the deformation. These are (see Figs. 2, 3) the vertical displacements w_1, w_2 in the direction of the unit vector $\mathbf{k}$ of the joints at A and C, respectively; and the outward displacements v_1, v_2 at B, C, in the horizontal direction $\mathbf{n}_B = \mathbf{n}_C$, pointing away from the vertical central axis of the dodecahedron. The joint displacements elsewhere follow by symmetry.

The $T\delta\Delta$ terms in equation (9) will be rewritten in terms of the Lagrangian strain defined by

$$\eta = \frac{1}{2}(L^2 - L_0^2)/L_0^2$$

$$= \Delta/L_0 + \frac{1}{2}(\Delta/L_0)^2 \tag{10}$$

and the modified force variable Q defined as

$$Q \equiv [L_0/(L_0+\Delta)]T \equiv (L_0/L)T \tag{11}$$

It follows that

$$\delta\eta = \delta\Delta/L_0 + \Delta\delta\Delta/L_0^2 = (L/L_0^2)\delta\Delta$$

and

$$T\delta\Delta = L_0 Q\delta\eta$$

so that the variational statement (9) may be transformed to

$$10L_0\sum_{k=1}^{3} Q_k\delta\eta_k = P\delta V + \delta\pi \tag{12}$$

Note that since $\dot{\eta} = L\dot{L}/L_0^2$, and $\dot{T}/T = \dot{Q}/Q + \dot{L}/L$, the constitutive relation (1) is equivalent to

$$\dot{Q}/Q = (B-1)\dot{L}/L$$

$$= (B-1)(L_0/L)^2\dot{\eta} \tag{13}$$

The advantage of η over Δ is that it is quadratic instead of irrational in the displacements.

It is convenient to introduce nondimensional displacements $y_i\,(i = 1,2,3,4)$ defined by

$$[y_1, y_2, y_3, y_4] = [w_1, v_1, w_2, v_2]/L_0 \tag{14}$$

Then, for three member types, the definition (10) leads to

$$\eta_k = a_{ki}y_i + \frac{1}{2}b_{kij}y_iy_j \quad (k=1,2,3) \tag{15}$$

in terms of coefficients a_{ki} and $b_{kij} = b_{kji}$ that are derived and listed in Appendix A. Here, and hereafter, we use summation convention, summing from 1 to 4 over repeated subscripts.

The deformed volume V of the dodecahedron can be expressed as a function of the joint displacements by (Appendix B)

$$V = V_0\left[1 + c_iy_i + \frac{1}{2}d_{ij}y_iy_j + O(y^3)\right] \tag{16}$$

Here V_0 is the original pressurized volume, and $d_{ij} = d_{ji}$. Finally, in Appendix C the potential of the applied tensile stresses is derived in the form

$$\pi = \sigma V_0[f_iy_i] \tag{17}$$

Substituting equations (15)–(17) into equation (12) and dividing by PV_0, puts the variational statement of equilibrium into the form

$$\left(\frac{1}{T_0}\right)\sum_{k=1}^{3} Q_k(a_{ki} + b_{kij}y_j)\delta y_i - [c_i + d_{ij}y_j + O(y^2)]\delta y_i = (\sigma/P)f_i\delta y_i \tag{18}$$

Here we used equation (6) to replace $PV_0/(10L_0)$ by T_0.

For $\sigma \to 0$, y_i vanishes and $Q_k \to T_0$, so that (18) becomes

$$\left\{\sum_{k=1}^{3} a_{ki} - c_i\right\}\delta y_i = 0 \tag{19}$$

Since equation (19) holds for arbitrary variations δy_i, we should have

$$\sum_{k=1}^{3} a_{ki} - c_i = 0 \quad (i=1,2,3,4) \tag{20}$$

and it can be verified that these four equations are indeed satisfied. This is consistent with the fact that equation (19) simply asserts the principle of virtual work at the initial state, and our special assumptions concerning the displacements ensures its validity.

Now we want to use (18) to get a variational statement governing the displacement rates $\dot{y}_i$. Differentiating (18) with respect to time (remembering that the δy_i's are variations that remain arbitrary) gives

$$\left(\frac{1}{T_0}\right)\sum_{k=1}^{3} [\dot{Q}_k(a_{ki} + b_{kij}y_j) + Q_k b_{kij}\dot{y}_j]\delta y_i - [d_{ij}\dot{y}_j + O(y\dot{y})]\delta y_i = (\dot{\sigma}/P)f_i\delta y_i \tag{21}$$

Now let $\sigma \to 0$, so that $y_i \to 0$, $L \to L_0$, and $Q_k \to T_0$; then

$$\left\{\frac{1}{T_0}\sum_{k=1}^{3}\dot{Q}_k a_{ki} + \sum_{k=1}^{3} b_{kij}\dot{y}_j - d_{ij}\dot{y}_j\right\}\delta y_i = (\dot{\sigma}/P)f_i\delta y_i \tag{22}$$

Here, by equation (13),

$$\dot{Q}_k = T_0(B-1)\dot{\eta}_k \tag{23}$$

where, by differentiation of equation (15), and letting $y_i \to 0$,

$$\dot{\eta}_k = a_{ki}\dot{y}_i \tag{24}$$

Hence equation (22) implies the four independent equations

$$[(B-1)q_{ij} + s_{ij} - d_{ij}]\dot{y}_j = (\dot{\sigma}/P)f_i \quad (i=1,2,3,4) \tag{25}$$

where

Downloaded 03 May 2010 to 171.66.16.27. Redistribution subject to ASME license or copyright; see http://www.asme.org/terms/Terms_Use.cfm

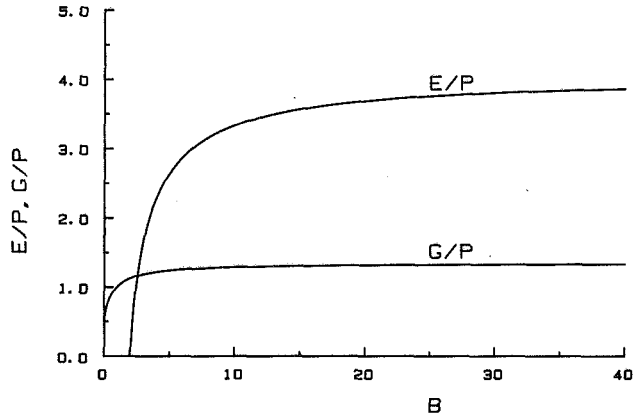


Fig. 4 Normalized Young's modulus E and shear modulus G

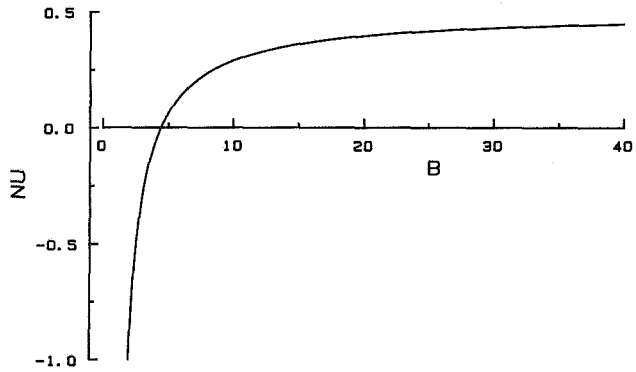


Fig. 5 Poisson's ratio ν

$$q_{ij} = \sum_{k=1}^{3} a_{ki} a_{kj} \tag{26}$$

and

$$s_{ij} = \sum_{k=1}^{3} b_{kij} \tag{27}$$

are listed in Appendix B. The dotted quantities in equations (25) now refer to the state at $\sigma = 0$, and these four equations constitute a symmetric system of four simultaneous, linear equations for $\dot{y}_j$ ($j = 1,2,3,4$). The results will, of course, be proportional to $\dot{o}/P$. Then, to define the average strain rate $\dot{\epsilon}$, we write

$$\dot{\pi} = \sigma V_O \dot{\epsilon} \tag{28}$$

and by equation (17) this gives

$$\dot{\epsilon} = f_i \dot{y}_i \tag{29}$$

The final result for Young's modulus, given by equation (3), is

$$E/P = \frac{\dot{o}/P}{(f_i \dot{y}_i)} \tag{30}$$

Thus the solution of equations (25) will provide E/P as a function of B. Then, with the use of equation (8) for K/P, the standard relations

$$E = 3K(1-2\nu) = 2G(1+\nu) \tag{31}$$

among Poisson's ratio ν, shear modulus G, E, and K for isotropic materials may be used to compute ν and G/P.

Results and Discussion

The results for E/P and G/P are plotted versus B in Fig. 4,

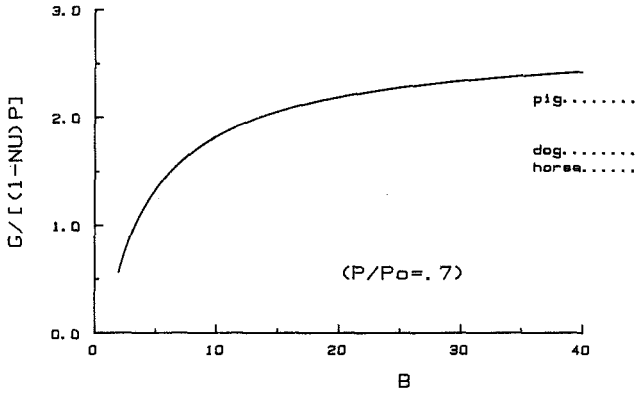


Fig. 6 Comparison of theory and experiment

and Poisson's ratio ν is shown in Fig. 5. It is shown in Appendix D that for $B \to \infty$, the limiting values become

$$\left.\begin{aligned} E/P &= 5(1+\sqrt{5})/4 \\ &= 4.045 \\ G/P &= 1.348 \\ \nu &= 1/2 \end{aligned}\right\} \tag{32}$$

For $B \to 2$, K vanishes, and $\nu \to -1$, because isotropic expansion dominates the strain-rate tensor induced by $\dot{o}$; hence $E/P \sim 9K \sim 3(B-2)$ for $B \to 2$. On the other hand, the shear modulus does not vanish at $B = 2$, where $G/P \approx 1.127$. But for $B < 2$, the structure is unstable, and the values for G/P would not be observable.

The limiting results for $B \to \infty$ shown in equations (32) are somewhat higher than those of Kimmel et al. (1986), who find $E/P \to 3.51$. But for B less than ~ 5, the results of Kimmel et al. deviate very markedly from the present ones, showing anomalous *increases* in both E/P and G/P as B decreases. This is probably due to the fact that the various engineering approximations made by Kimmel et al. do not cope adequately with a delicate balance of elastic responses as the instability point at $B = 2$ is approached.

To corroborate the isotropy of our model, an independent computation of Poisson's ratio was made by means of direct calculation of the average strain-rate tensor in the dodecahedron (Appendix E). An explicit formula (equation (*E*8)) derived for ν in terms of the y_i's was found to provide numerical results in perfect agreement with those calculated from E/P and K/P on the basis of the isotropy relations (31).

We also studied (Appendix F) the effect of imposing an additional constraint on the displacements, keeping each face of the dodecahedron perfectly flat during the imposition of σ. It turns out that for $B \to \infty$, this additional constraint makes no change at all in the limiting results (32). The reason for this is that inextensionality of the members enforces the planarity constraint automatically! Furthermore, the imposition of planarity produced only a tiny increase—less than 1/10 percent—in E/P over the full range $2 < \beta < \infty$, and the results in Figs. 4, 5 were barely changed.

Experiments on dog, pig, and horse lungs by Hajji et al. (1979), involving local external indentation of the pleural membrane of an inflated lung, were used by the investigators to extract values of $G/(1-\nu)$ for incremental straining. Based on the somewhat uncertain value of $P/P_0 = 0.7$ (Stamenovic and Wilson, 1985, suggest $P/P_0 \sim 3/4$) the results are shown in Fig. 6, where the experimental values of $G/[P(1-\nu)]$ found are compared with the predictions of the present theory. Theory and experiment are generally consistent for the range $B \sim 5$–20, but it should be noted that near the lower end of this range the theoretical values of ν (Fig. 5) become quite low.

Downloaded 03 May 2010 to 171.66.16.27. Redistribution subject to ASME license or copyright; see http://www.asme.org/terms/Terms_Use.cfm

Concluding Remarks

An important feature of the present theoretical approach is that by focusing on incremental stress-strain relations, the constitutive description of the lung substructure has conveniently been thrown into the single elastic parameter B, which, to be sure, may itself depend on the stress level. Not only is B supposed to represent the *effective* elasticity of a fairly complex structure, it can also be presumed to incorporate the effects of surface tension in the alveolar walls. (That is to say, the basic relation given by equation (1) can still be considered to apply, operationally, when surface tension is present.)

The finite limits approached by G/P and E/P for $B \to \infty$ are clearly consequences of the fact that the basic pin-jointed dodecahedron is a statically underdeterminate *mechanism* (rather than a *structure*) in the absence of hydrostatic tension. By the same token, it is clear that the use of a statically determinate (or indeterminate) truss model would have led to G/P, $E/P \to \infty$ for $B \to \infty$. Finally, we note that if, in contrast to the present approach, overall properties were calculated via the imposition of the macroscopic strain field all along each member, then $B \to \infty$ would imply unbounded stiffness for all models—underdeterminate or not.

Acknowledgment

This work was supported by a Bantrell Post-Doctoral Fellowship to E. Kimmel, by the Office of Naval Research (Contract N00014-84-K-0510), by the Division of Applied Sciences, Harvard University, and by the Department of Mechanical Engineering, Massachusetts Institute of Technology. Discussions of the theoretical model and of the results were amplified in the light of helpful comments by Dimitrije Stamenovic.

References

Budiansky, B., 1969, "Remarks on Theories of Solid and Structural Mechanics," *Problems of Hydrodynamics and Continuum Mechanics*, L. I. Sedov Sixtieth Birthday, SIAM, pp. 77–83.

Frankus, A., and Lee, G. C., 1974, "A Theory of Distortion Studies of Lung Parenchyma Based on Alveolar Membrane Properties," *Journal of Biomechanics*, Vol. 7, pp. 101–107.

Fung, Y. C., Tong, P., and Patitucci, P., 1978, "Stress and Strain and the Lung," *Engineering Mechanics*, ASCE, Vol. 104, pp. 201–224.

Hajji, M. A., Wilson, T. A., and Lai-Fook, S. J., 1979, "Improved Measurements of Shear Modulus and Pleural Membrane Tension of the Lung," *Journal of Applied Physiology: Respiratory and Environmental Exercise Physiology*, Vol. 47, pp. 175–181.

Kimmel, E., Kamm, R. D., and Shapiro, A. H., 1986, "A Cellular Model of Lung Elasticity," to be published in the *ASME Journal of Biomechanical Engineering*.

Lambert, R. K., and Wilson, T. A., 1973, "A Model for the Elastic Properties of the Lung and Their Effect on Expiratory Flow," *Journal of Applied Physiology*, Vol. 34, pp. 34–38.

Lanir, Y., 1983, "Constitutive Equations for the Lung Tissue," *ASME Journal of Biomechanical Engineering*, Vol. 105, pp. 374–380.

Mead, J., Takishima, T., and Leith, D., 1970, "Stress Distribution in Lungs: A Model of Pulmonary Elasticity," *Journal of Applied Physiology*, Vol. 28, pp. 596–608.

Stamenovic, D., and Wilson, T. A., 1985, "A Strain Energy Function for Lung Parenchyma," *ASME Journal of Biomechanical Engineering*, Vol. 107, pp. 81–86.

Vawter, D. L., Fung, Y. C., and West, J. B., 1979, "Constitutive Equation of Lung Tissue Elasticity," *ASME Journal of Biomechanical Engineering*, Vol. 101, pp. 38–45.

Wilson, T. A., 1972, "A Continuum Analysis of a Two-Dimensional Mechanical Model of the Lung Parenchyma," *Journal of Applied Physiology*, Vol. 33, pp. 472–478.

Wilson, T. A., and Bachofen, H., 1982, "A Model for the Mechanical Structure of the Alveolar Duct," *Journal of Applied Physiology*, Vol. 52, pp. 1069–1070.

APPENDIX A

Lagrangian Strains

The geometrical parameters of the regular dodecahedron shown in Fig. 2 satisfy the relations

$$\omega = 54^\circ$$

$$\alpha = 72^\circ$$

$$\sin\omega = \cos\frac{\alpha}{2} = (1+\sqrt{5})/4$$

$$4\sin^2\omega = 1 + 2\sin\omega$$

$$h = \rho_1 = L_0(\sec\omega)/2$$

$$\rho_2 = g + h = L_0\tan\omega$$

$$r = L_0\tan\omega\sin\omega$$

and the dihedral angle Ω between normals to adjacent planes is

$$\Omega = \arctan 2$$

These relations are useful in the calculations of this Appendix, as well as in those that follow.

Consider a bar PQ having initial length L_0, and let $\mathbf{t}_{PQ}$ represent a unit vector pointing from P to Q. Displacements $\mathbf{U}_P$, $\mathbf{U}_Q$ at P and Q produce the deformed length L_{PQ} satisfying

$$L_{PQ}^2 = \|L_0\mathbf{t} + \mathbf{U}_Q - \mathbf{U}_P\|^2 \tag{A1}$$

The Lagrangian strain (equation (10)) is then given by

$$\eta_{PQ} = \frac{\mathbf{t}_{PQ}\cdot(\mathbf{U}_Q - \mathbf{U}_P)}{L_0} + \frac{\|\mathbf{U}_Q - \mathbf{U}_P\|^2}{2L_0^2} \tag{A2}$$

We will now apply the generic relation (A2) to find the strains of members AB, BC, and CD (Fig. 3). The pertinent joint displacements are

$$\left.\begin{aligned}\mathbf{U}_A &= w_1\mathbf{k} + v_1\mathbf{n}_A\\ \mathbf{U}_B &= w_1\mathbf{k} + v_1\mathbf{n}_B\\ \mathbf{U}_C &= w_2\mathbf{k} + v_2\mathbf{n}_C\\ \mathbf{U}_D &= -w_2\mathbf{k} + v_2\mathbf{n}_D\end{aligned}\right\} \tag{A3}$$

Since

$$\mathbf{t}_{AB}\cdot\mathbf{k} = 0,\ \mathbf{t}_{AB}\cdot\mathbf{n}_B = -\mathbf{t}_{AB}\cdot\mathbf{n}_A = \cos\omega,$$

we get

$$\eta_1 \equiv \eta_{AB} = 2(v_1/L_0)\cos\omega + 2(v_1/L_0)^2\cos^2\omega \tag{A4}$$

The unit vector in the direction of CB satisfies

$$\mathbf{t}_{CB}\cdot\mathbf{k} = h/L_0 = (\sec\omega)/2$$

$$\mathbf{t}_{CB}\cdot\mathbf{n}_B = \mathbf{t}_{CB}\cdot\mathbf{n}_C = -g/L_0 = -(\csc 2\omega)/2$$

and so equation (A2) gives

$$\eta_2 \equiv \eta_{BC} = \frac{(w_1 - w_2)\sec\omega}{2L_0} + \frac{(v_2 - v_1)\csc 2\omega}{2L_0} + \frac{(w_1 - w_2)^2}{2L_0^2} + \frac{(v_1 - v_2)^2}{2L_0^2} \tag{A5}$$

Finally,

$$\mathbf{t}_{DC}\cdot\mathbf{k} = g/L_0 = \frac{1}{2}\csc 2\omega$$

$$\mathbf{t}_{DC}\cdot\mathbf{n}_C = -\mathbf{t}_{DC}\cdot\mathbf{n}_D = (\rho_1/L)\cos\alpha = \frac{1}{4}\csc 2\omega$$

and with $\|\mathbf{n}_C - \mathbf{n}_D\|^2 = 2(1 - \sin\omega)$, equation (A2) produces

$$\eta_3 \equiv \eta_{CD} = (w_2/L_0)\csc 2\omega + \frac{1}{2}(v_2/L_0)\csc 2\omega + 2(w_2/L_0)^2 + (1 - \sin\omega)(v_2/L_0)^2 \tag{A6}$$

Rewritten in terms of the y_i's equation (14), equations

Downloaded 03 May 2010 to 171.66.16.27. Redistribution subject to ASME license or copyright; see http://www.asme.org/terms/Terms_Use.cfm

(A4)–(A6) provide the following results for the coefficients a_{ki} in (15):

$$[a_{ki}] = \frac{1}{2}\begin{bmatrix} 0 & 4\cos\omega & 0 & 0 \\ \sec\omega & -\csc 2\omega & -\sec\omega & \csc 2\omega \\ 0 & 0 & 2\csc 2\omega & \csc 2\omega \end{bmatrix} \quad (A7)$$

The coefficients b_{1ij} vanish, except for

$$b_{122} = 4\cos^2\omega \quad (A8)$$

The matrix of coefficients b_{2ij} is

$$[b_{2ij}] = \begin{bmatrix} 1 & 0 & -1 & 0 \\ 0 & 1 & 0 & -1 \\ -1 & 0 & 1 & 0 \\ 0 & -1 & 0 & 1 \end{bmatrix} \quad (A9)$$

Finally, the only b_{3ij} that do not vanish are

$$b_{333} = 4$$
$$b_{344} = 2(1-\sin\omega) \quad (A10)$$

The coefficients q_{ij} and s_{ij} defined by equations (26) and (27) are

$$q_{ij} = \left(\frac{\sec^2\omega}{4}\right)\times \begin{bmatrix} 1 & -(\csc\omega)/2 & -1 & (\csc\omega)/2 \\ -(\csc\omega)/2 & 3(\csc^2\omega)/2 & (\csc\omega)/2 & -(\csc^2\omega)/4 \\ -1 & (\csc\omega)/2 & 9-8\sin\omega & (\csc^4\omega)/16 \\ (\csc\omega)/2 & -(\csc^2\omega)/4 & (\csc^4\omega)/16 & (\csc^2\omega)/2 \end{bmatrix} \quad (A11)$$

and

$$[s_{ij}] = \begin{bmatrix} 1 & 0 & -1 & 0 \\ 0 & 4-2\sin\omega & 0 & -1 \\ -1 & 0 & 5 & 0 \\ 0 & -1 & 0 & 3-2\sin\omega \end{bmatrix} \quad (A12)$$

APPENDIX B

Volume Change

Together with the assumptions made concerning the piecewise linear displacement patterns within each face, the corner displacements w_1, v_1, w_2, v_2 (Fig. 3) determine the configuration of the dodecahedron subjected to uniform tension. The deformed volume can be written as (Fig. 1(*b*))

$$V = 2V_{ABFGH} + 10[V_{AXB} + 2V_{BXC} + 2V_{CXD}] \quad (B1)$$

wherein each of the subscripted terms represents the volume of a pyramid with its apex at the center of the dodecahedron, and the subscript denotes the base. The *original* area of the pentagon *ABFGH* was

$$A_0 = (5/4)L_0^2\tan\omega \quad (B2)$$

and the altitude of the corresponding pyramid was (Fig. 2)

$$r = L_0\tan\omega\sin\omega$$

Hence the deformed volume is

$$V_{ABFGH} = 5(L_0\tan\omega\sin\omega + w_1)(L_0 + 2v_1\cos\omega)^2(\tan\omega)/12 \quad (B3)$$

To facilitate the calculation of the remaining terms in (*B*1), we use the orthogonal unit vectors (**i**,**j**,**k**) shown in Fig. 2 to write the original position vectors of *A*, *B*, *C*, *D*, *E* and *X* as

$$\left.\begin{aligned} \mathbf{A},\mathbf{B} &= [\pm\mathbf{i}/2 + \mathbf{j}(\tan\omega)/2 + \mathbf{k}\tan\omega\sin\omega]L_0 \\ \mathbf{C},\mathbf{E} &= [\mp\mathbf{i}\sin\omega + \mathbf{j}\tan\omega\sin\omega + \mathbf{k}(\csc 2\omega)/4]L_0 \\ \mathbf{D} &= [\mathbf{j}\tan\omega - \mathbf{k}(\csc 2\omega)/4]L_0 \\ \mathbf{X} &= [2\mathbf{j}+\mathbf{k}][\tan\omega(1+\sin\omega)]/5 \end{aligned}\right\} \quad (B4)$$

The displacement vectors are

$$\left.\begin{aligned} \mathbf{w}_A,\mathbf{w}_B &= \pm\mathbf{i}v_1\cos\omega + \mathbf{j}v_1\sin\omega + \mathbf{k}w_1 \\ \mathbf{w}_C,\mathbf{w}_E &= \mp\mathbf{i}v_2\cos\omega + \mathbf{j}v_2\sin\omega + \mathbf{k}w_2 \\ \mathbf{w}_D &= \mathbf{j}v_2 - \mathbf{k}w_2 \\ \mathbf{w}_X &= [\mathbf{w}_A + \mathbf{w}_B + \mathbf{w}_C + \mathbf{w}_D + \mathbf{w}_E]/5 \\ &= \mathbf{j}[2v_1\sin\omega + v_2(1+2\sin\omega)]/5 + \mathbf{k}[2w_1 + w_2]/5 \end{aligned}\right\} \quad (B5)$$

Then

$$V_{ABX} = [\mathbf{A}+\mathbf{w}_A]\times[\mathbf{X}+\mathbf{w}_X]\cdot[\mathbf{B}+\mathbf{w}_B]/6 \quad (B6)$$

and similarly for the remaining two pyramidal volumes in (*B*1). Carrying out the required straightforward but tedious calculations leads to

$$\begin{aligned} V = V_0 &+ [w_1(3+8\sin\omega)/2 + 2v_1(1+\sin\omega) + w_2(-1 \\ &+ 4\sin\omega)/2 + v_2(1+6\sin\omega)]L_0^2\tan\omega \\ &+ [v_1^2(2+\sin\omega) + v_2^2(2+3\sin\omega) + 2w_1v_1(3+2\sin\omega) \\ &+ w_1v_2(7+6\sin\omega) - 4w_2v_1 + 4v_1v_2\sin\omega \\ &+ w_2v_2(5+2\sin\omega)][2L_0\sin\omega]/3 \\ &+ [\text{cubic terms}] \end{aligned}$$

where the original volume V_0 is

$$V_0 = 5L_0^3\tan^2\omega\sin\omega \quad (B7)$$

The coefficients in the expansion in (16) for V/V_0 in terms of the nondimensional y's are then

$$\left.\begin{aligned} c_1 &= \cot\omega(3\csc\omega + 8)/10 \\ c_2 &= 2\cot\omega(\csc\omega + 1)/5 \\ c_3 &= \cot\omega(-\csc\omega + 4)/10 \\ c_4 &= \cot\omega(\csc\omega + 6)/5 \end{aligned}\right\} \quad (B8)$$

and

$$[d_{ij}] = (2\cot^2\omega/15)\times \begin{bmatrix} 0 & 6+4\sin\omega & 0 & 7+6\sin\omega \\ 6+4\sin\omega & 2(2+\sin\omega) & -4 & 4\sin\omega \\ 0 & -4 & 0 & 5+2\sin\omega \\ 7+6\sin\omega & 4\sin\omega & 5+2\sin\omega & 2(2+3\sin\omega) \end{bmatrix} \quad (B9)$$

Downloaded 03 May 2010 to 171.66.16.27. Redistribution subject to ASME license or copyright; see http://www.asme.org/terms/Terms_Use.cfm

APPENDIX C

Stress Potential

If the applied σ stresses in the $\mathbf{k}$ direction produce the surface displacements $\mathbf{u}$, then the potential of the stresses is

$$\pi = \int_S [\mathbf{n}\cdot\sigma\mathbf{k}\mathbf{k}\cdot\mathbf{u}]dS \qquad (C1)$$

where the integration is over the undeformed surface, and $\mathbf{n}$ is the unit normal to this surface. Our kinematic assumptions imply that (Fig. 1(b)) the face $ABFGH$ remains plane, as does its counterpart at the bottom of the dodecahedron. Hence the partial potential of the σ-stresses applied to these two faces is simply

$$[2\sigma A_0 w_1] \qquad (C2)$$

where A_0 is the original area of the pentagon.

In face $ABCDE$ (Fig. 1(b)), the midpoint vector displacement $\mathbf{w}_X$ is the mean of the five corner displacments, the average over each triangle of the linearly varying displacements within each triangle is the mean of its three corner displacements, and it follows that the average displacement over the pentagon is also $\mathbf{w}_X$. Hence the potential of the σ-stresses is just

$$(\mathbf{n}\cdot\sigma\mathbf{k}\mathbf{k}\cdot\mathbf{w}_X)A_0 \qquad (C3)$$

But (Fig. 3)

$$\mathbf{w}_X\cdot\mathbf{k} = (2w_1 + w_2)/5 \qquad (C4)$$

$$\mathbf{n}\cdot\mathbf{k} = \cos\Omega = 1/\sqrt{5} \qquad (C5)$$

and the contribution ($C3$) is

$$\sigma A_0 \cos\Omega(2w_1 + w_2)/5 \qquad (C6)$$

Adding 10 such contributions to ($C2$) gives the total potential

$$\pi = 2\sigma A_0[(1 + 2\cos\Omega)w_1 + w_2\cos\Omega]$$
$$= 2\sigma A_0[(1 + 2/\sqrt{5})w_1 + w_2/\sqrt{5}] \qquad (C7)$$

Hence, with the use of equations ($B2$) and ($B7$) for A_0 and V_0, which give

$$A_0 L_0/V_0 = (\cot\omega\csc\omega)/4 \qquad (C8)$$

the coefficients f_i in equation (17) become

$$\left.\begin{aligned} f_1 &= (\cot\omega)(\csc\omega)(1 + 2/\sqrt{5})/2 \\ f_2 &= 0 \\ f_3 &= (\cot\omega)(\csc\omega)/(2\sqrt{5}) \\ f_4 &= 0 \end{aligned}\right\} \qquad (C9)$$

APPENDIX D

Inextensional Limit, B→∞

For $B\to\infty$, the members become inextensional, and therefore the strain rates given by equation (24) must vanish:

$$a_{ki}\dot{y}_i = 0 \qquad (k = 1,2,3) \qquad (D1)$$

It follows that for $B\to\infty$,

$$\dot{y}_i = \beta_i c \qquad (D2)$$

where, in accordance with the a_{ki} matrix shown in ($A7$)

$$\beta_1 = \sqrt{5},\ \beta_2 = 0,\ \beta_3 = 1,\ \beta_4 = -2 \qquad (D3)$$

To evaluate the constant c, substitute ($D2$) into the variational statement (22) and choose $\delta y_i = \beta_i$. This gives

$$c[s_{ij} - d_{ij}]\beta_i\beta_j = (\dot{\sigma}/P)f_i\beta_i \qquad (D4)$$

and then the limiting value of E/P, from equation (30), becomes

$$E/P = (s_{ij} - d_{ij})\beta_i\beta_j/(f_k\beta_k)^2 \qquad (D5)$$

Substitution of the values of s_{ij}, d_{ij}, and f_k given in equations ($A12$), ($B9$), and ($C9$), respectively, provides the results (after considerable reduction)

$$E/P = 5\sin\omega$$
$$= 5(1 + \sqrt{5})/4 \qquad (D6)$$

and this was corroborated numerically via the solution of equations (25) for very large B.

APPENDIX E

Average Strain Rates

The average strain-rate tensor $\dot{\epsilon}$ in a body V_0 that suffers velocities $\dot{\mathbf{u}}$ on its boundary S is

$$\dot{\epsilon} = \left\{\int_S (\dot{\mathbf{u}}\,\mathbf{n} + \mathbf{n}\,\dot{\mathbf{u}})dS\right\}/(2V_0) \qquad (E1)$$

where $\mathbf{n}$ is the unit normal to S. If we let $\dot{\epsilon} = \mathbf{k}\cdot\dot{\epsilon}\cdot\mathbf{k}$ denote the strain rate in the $\mathbf{k}$ direction, ($E1$) gives

$$\dot{\epsilon} = \left\{\int_S (\mathbf{k}\cdot\dot{\mathbf{u}})(\mathbf{n}\cdot\mathbf{k})dS\right\}/V_0 \qquad (E2)$$

which, by ($C1$), is the same as $\dot{\pi}/(V_0\sigma) = f_i\dot{y}_i$. Hence, direct averaging to calculate E/P gives the same result as that found from the use of the energy definition (28) for $\dot{\epsilon}$. However, an independent calculation of Poisson's ratio can be based on the direct calculation of the mean transverse strain rate

$$\dot{\epsilon}_T \equiv (\mathbf{i}\cdot\dot{\epsilon}\cdot\mathbf{i} + \mathbf{j}\cdot\dot{\epsilon}\cdot\mathbf{j})/2 \qquad (E3)$$

Since $\mathbf{n}\cdot\mathbf{i} = 0$ on $ABCDE$ (see Fig. 2)

$$\dot{\epsilon}_T = 10\left\{\int_{ABCDE} (\mathbf{n}\cdot\mathbf{j})(\dot{\mathbf{u}}\cdot\mathbf{j})dS\right\}/(2V_0) \qquad (E4)$$

But

$$\mathbf{n}\cdot\mathbf{j} = \sin\Omega = 2/\sqrt{5} \qquad (E5)$$

and

$$\int_{ABCDE} (\dot{\mathbf{u}}\cdot\mathbf{j})dS = (\dot{\mathbf{w}}_X\cdot\mathbf{j})A_0$$
$$= [2\dot{v}_1\sin\omega + \dot{v}_2(1 + \sin\omega)]A_0/5 \qquad (E6)$$

where ($B5$) has been used for $\mathbf{w}_X$. Hence ($E4$) gives

$$\dot{\epsilon}_T = 2[2\dot{y}_2\sin\omega + \dot{y}_4(1 + 2\sin\omega)][A_0L_0]/(V_0\sqrt{5})$$
$$= [\dot{y}_2(1 + \sqrt{5}) + \dot{y}_4(3 + \sqrt{5})][\cot\omega\csc\omega]/(4\sqrt{5}) \qquad (E7)$$

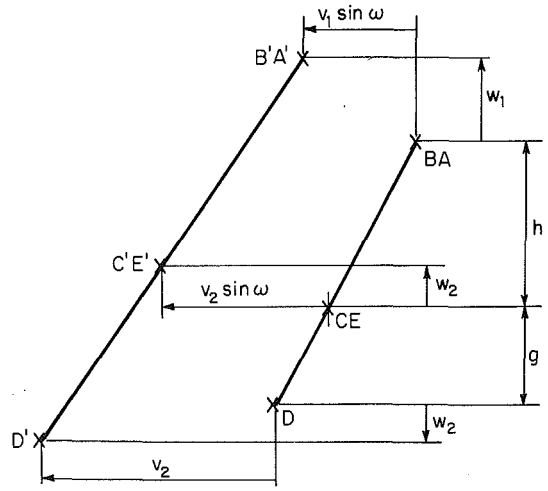


Fig. 7 Corner displacements constrained by planarity condition

Downloaded 03 May 2010 to 171.66.16.27. Redistribution subject to ASME license or copyright; see http://www.asme.org/terms/Terms_Use.cfm

Since $\dot{\epsilon}_T = -\nu\dot{\epsilon} = -\nu f_i \dot{y}_i$ we find, with equation (C8) for f_i,

$$\nu = -\frac{1}{2}\left[\frac{\dot{y}_2(1+\sqrt{5})+\dot{y}_4(3+\sqrt{5})}{\dot{y}_1(2+\sqrt{5})+\dot{y}_3}\right] \tag{E8}$$

APPENDIX F

Planarity Constraint

An edge view of the pentagon *ABCDE* (Fig. 3) is shown in Fig. 7. For the corners of the displaced pentagon $A'B'C'D'E'$ to remain coplanar, we must have

$$\frac{h+w_1-w_2}{h/2+(v_2-v_1)\sin\omega} = \frac{g+2w_2}{g/2+v_2(1-\sin\omega)} \tag{F1}$$

In terms of the nondimensional displacements y_i, this reduces to the condition

$$F \equiv g_i y_i + \frac{1}{2} h_{ij} y_i y_j = 0 \tag{F2}$$

where

$$\left.\begin{aligned} g_1 &= (\sec\omega)/2 \\ g_2 &= \tan\omega \\ g_3 &= -(\sec\omega)/2 - 2\tan\omega \\ g_4 &= -(\sec\omega)/2 \end{aligned}\right\} \tag{F3}$$

$$\left.\begin{aligned} h_{14} &= h_{41} = -1+2\sin\omega \\ h_{23} &= h_{32} = 2(1+2\sin\omega) \\ h_{34} &= h_{43} = -(1+6\sin\omega) \end{aligned}\right\} \tag{F4}$$

and all other h_{ij}'s vanish.

To impose the constraint (F2), we introduce the scalar Lagrangian multiplier λ, and add

$$\lambda\delta F \equiv \lambda(g_i + h_{ij}y_j)\delta y_i \tag{F5}$$

to the left side of the variational statement (18). It follows from this modified variational equation that if $\lambda \to \lambda_0$ for $\sigma \to 0$, then

$$\left\{\sum_{k=1}^{3} a_{ki} - c_i + \lambda_0 g_i\right\}\delta y_i = 0 \tag{F6}$$

and therefore (equation (20)) $\lambda_0 = 0$. If we now reproduce the steps that originally led to equation (25), the corresponding equations for the constrained problem become

$$[(B-1)q_{ij} + s_{ij} - d_{ij}]\dot{y}_j + \dot{\lambda}g_i = (\dot{\sigma}/P)f_i \qquad (i=1,2,3,4) \tag{F7}$$

where $\dot{\lambda}$ refers to the state at $\sigma = 0$. These four equations, together with the differentiated constraint relation

$$g_i\dot{y}_i = 0 \tag{F8}$$

that holds for $y_i = 0$, constitute a symmetric system of five linear equations for $\dot{y}_1$, $\dot{y}_2$, $\dot{y}_3$, $\dot{y}_4$ and $\dot{\lambda}$, and their numerical solution provided the results discussed in the text. The equations of inextensionality (D1) and the planarity condition (F8) are equivalent to the homogeneous relations

$$\begin{bmatrix} 0 & 1 & 0 & 0 \\ 2\sin\omega & -1 & -2\sin\omega & 1 \\ 0 & 0 & 2 & 1 \\ 1 & 2\sin\omega & -1-4\sin\omega & -1 \end{bmatrix}\begin{bmatrix} \dot{y}_1 \\ \dot{y}_2 \\ \dot{y}_3 \\ \dot{y}_4 \end{bmatrix} = 0 \tag{F9}$$

Remarkably, the matrix of coefficients is singular, so that the limiting solution (D2), (D3) for $\dot{y}_1$ in the limit $B \to \infty$ remains valid, as do the limiting results for the moduli. Thus, planarity, at least for small displacements, is a consequence of inextensionality.

Downloaded 03 May 2010 to 171.66.16.27. Redistribution subject to ASME license or copyright; see http://www.asme.org/terms/Terms_Use.cfm

The Normal Impact on an Elastic Half Space of an Elastic Rod-Mass System

H. A. Downey, Jr.
Graduate Student,[1]
Assoc. Mem. ASME

D. B. Bogy
Professor,
Mem. ASME

Department of Mechanical Engineering,
University of California,
Berkeley, CA 94720

The normal impact problem of a one-dimensional elastic rod with a lumped mass on the trailing end onto an elastic half space is solved for the time-dependent interface displacement and stress. This problem is reduced to an integral equation, whose kernel is the solution of a simpler auxiliary problem, which is solved in closed form. After examining the graph of the kernel it is found that a simple linear expression adequately represents its half space contribution. This approximation allows the integral equation to be solved in closed form and provides insight into its solution. Numerical results are presented, which display the impact and rebound of the rod, and illustrate the presence of major effects from the Rayleigh wave in the half space and the reflected wave from the trailing end of the rod. Results are presented for various half-space materials, rod lengths, and masses. It is found that in the absence of the mass the maximum contact stress depends entirely on the rod material, but with the lumped mass added the contact stress can become much greater and depends on the rod, the half space, and the mass.

Introduction

The motivation for considering this problem comes from the need for a better understanding of the dynamics of wire-matrix impact printing. In this much used printing technology, a thin wire, 0.2 to 0.35 mm in diameter, and 20 mm to 100 mm in length, and usually with some lumped mass on the driven end (part of the electromagnet) is employed. This wire is accelerated by an electromagnet, and then it impacts layers of ribbon and paper on a platen, which is either an elastomer covered roll or a metal bar of aluminum or steel.

The parameters of primary interest in printing are the contact force as a function of time, which effects the transfer of ink from the ribbon to the paper, and the total contact time, which limits the printing speed. It is important to analyze the effects of rod length, diameter, velocity, material, and the effects of the lumped mass and half space materials on the printing parameters. The question also arises as to how to model the ribbon, paper, and platen combination.

Various approaches to this problem have been taken in the literature. Naemura and Kobayashi (1979) made static and dynamic measurements of the force-displacement function, which they fit with a power law curve. Then they approximated the result by equivalent linear stiffnesses. Conway and Lee (1970) and Conway et al. (1970, 1972) took somewhat different approaches. They studied the impact of spheres on layers and indenters on plates to simulate the paper and ribbon response for general impact printing. Wang and Hall (1983) made experimental measurements using an actual printwire, and they also fit a power law response function to their measured results. The constants they obtained with this approach were quite different from those of Naemura and Kobayashi (1979), possibly because Wang and Hall's (1983) measurements included the effects of the wire deflection.

The analysis undertaken in this paper is a first step toward a more fundamental approach. Ultimately the problem should be posed with a layered half space having at least two layers, one viscoelastic layer representing the ribbon, and the other viscoelastic or plastic layer representing the paper. As an initial study we consider here only a homogeneous elastic half space.

Related half space problems have been solved, and the solutions are presented in the literature. Most of these are concerned with seismic studies or ultrasonic testing. Pekeris (1955) solved the problem of a surface pulse on a half space. Mitra (1964) solved for the surface displacements due to an impulsive uniform normal pressure over a circular region on the surface of a half space. Gutzwiller (1962) treated the problem of a rigid disk impacting a half space, but this solution is not easily adaptable to our problem because of its complexity.

The most applicable and closely related to our needs is the solution of Matsumoto et al. (1978). In that paper, the contact stress for a semi-infinite rod impacting a half space was obtained. Here we extend that solution to the case of a finite rod with a mass attached, and we also solve for the displacement

[1] Also Sr. Assoc. Engineer, IBM Corp., Charlotte, NC.

Contributed by the Applied Mechanics Division for presentation at the 1987 Applied Mechanics, Biomechanics, and Fluids Engineering Conference, Cincinnati, OH, June 14–17, 1987, of the American Society of Mechanical Engineers.
Discussion of this paper should be addressed to the Editorial Department, ASME, United Engineering Center, 345 East 47th Street, New York, N.Y. 10017, and will be accepted until two months after final publication of the paper itself in the JOURNAL OF APPLIED MECHANICS. Manuscript received by ASME Applied Mechanics Division, February 12, 1986; final revision, August 15, 1986.
Paper No. 87-APM-19.

Copyright © 1987 by ASME
Downloaded 03 May 2010 to 171.66.16.27. Redistribution subject to ASME license or copyright; see http://www.asme.org/terms/Terms_Use.cfm

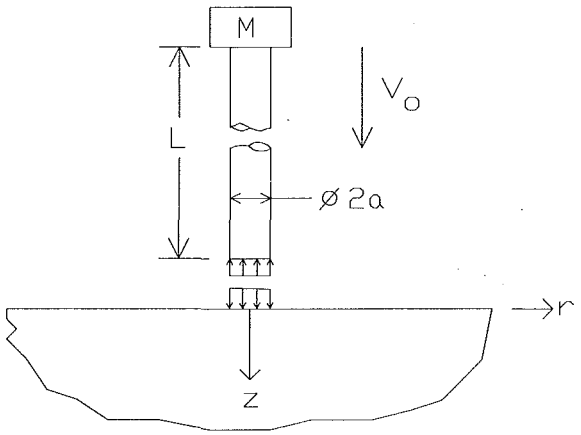


Fig. 1 Diagram of the problem

of the rod into the half space so that a study can be made of the bounce off as well as the force-displacement characteristics of the impact.

Formulation of the Problem

The impact problem under consideration is axisymmetric and torsionless, and the three-dimensional theory of elastic wave propagation is used to analyze the response of the half space. Since the length of the rod is much greater than its diameter, the simpler one-dimensional rod theory is used to describe the wave propagation in the rod.

Having made this simplification in the rod model, the question of how to treat the boundary conditions at the contact surface must be answered. The desired boundary conditions in the context of three-dimensional theory would be vanishing shearing tractions and matched normal displacements in the contact region. But one-dimensional rod theory does not describe variations of displacement or stress over the rod's cross-section. Thus, there are two choices: either we set the displacement of the half space in the contact region equal to the uniform displacement of the rod, and the normal traction on the rod equal to the average of the normal traction on the half space, or we set the displacement of the rod equal to the average displacement in the contact region of the half space, and the normal traction on the half space equal to the normal traction on the rod. The first would impose a uniform displacement over the contact region so that the end of the rod is effectively a rigid punch. This would yield stress singularities on the half space at the edge of the contact region. The second choice would require that the normal traction on the half space be uniform in the contact region. In our application the overall response of the half space is desired, rather than the local stress, therefore the second choice is used here. The rod is also assumed to be smooth, so that the shear tractions are set to zero on the surface of the half space.

The geometry and coordinate system are shown in Fig. 1. The rod has length L, radius a, and lumped mass M. The rod is described by coordinate z, which is positively oriented into the half space, with the contacting end of the rod at $z = 0$. The initial uniform rod velocity V_o is in the positive z direction. We use cylindrical polar coordinates for the half space (r,θ,z), with the origin at the center of the contact region. At time $t=0$ the rod contacts the half space.

The variables are all nondimensionalized, lengths with respect to a, time with respect to a divided by the longitudinal wave speed of the half space, the half-space stress with respect to the shear modulus of the half space, and the lumped mass with respect to $\pi\rho_o a^3$. The stress in the rod is normalized by the steady-state stress value for a rod impacting a rigid half space. They are as follows:

$$r^* = r/a,\ z^* = z/a,\ w^* = w/a,\ L^* = L/a,\ u_i^* = u_i/a,$$
$$t^* = c_1 t/a,\ \Phi^* = \Phi/a^2,\ \psi^* = \psi/a^2,\ \tau_{ij}^* = \tau_{ij}/2\mu,$$
$$\sigma_z^* = -c_o\sigma_z/E_o V_o,\ M^* = M/\pi\rho_o a^3. \tag{1}$$

For convenience, from now on the asterisks will be dropped, and all quantities will be in nondimensional form. The displacement vector in the half space is expressed in terms of potentials by

$$\mathbf{u} = \nabla\Phi + \nabla\times\psi. \tag{2}$$

In the axisymmetric case, there is no angular dependence, the θ component of displacement is zero, the only nonzero component of the vector potential ψ is the θ component, which we call Ψ, and thus equation (2) reduces to the two scalar equations,

$$u_r = \frac{\partial\Phi}{\partial r} - \frac{\partial\Psi}{\partial z},$$
$$u_z = \frac{\partial\Phi}{\partial z} + \frac{1}{r}\frac{\partial}{\partial r}(\Psi r). \tag{3}$$

The equations of motion for the half space in terms of potentials reduce to

$$\nabla^2\Phi = \frac{\partial^2\Phi}{\partial t^2},$$
$$\nabla^2\Psi - \frac{\Psi}{r^2} = \kappa^2\frac{\partial^2\Psi}{\partial t^2}, \tag{4}$$

where

$$\nabla^2 = \frac{\partial^2}{\partial r^2} + \frac{1}{r}\frac{\partial}{\partial r} + \frac{\partial^2}{\partial z^2},$$
$$\kappa^2 = c_1^2/c_2^2, \tag{5}$$

with c_1 and c_2 representing the longitudinal and shear wave velocities. These are given in terms of the Lamé constants and the density by

$$c_1^2 = (\lambda + 2\mu)/\rho,\ c_2^2 = \mu/\rho. \tag{6}$$

The half-space stress components related to traction in the contact region are

$$\tau_{zz} = \frac{\lambda}{2\mu}\nabla^2\Phi + \frac{\partial^2\Phi}{\partial z^2} + \frac{\partial^2\Psi}{\partial r\partial z} + \frac{1}{r}\frac{\partial\Psi}{\partial z},$$
$$\tau_{rz} = \frac{\partial^2\Phi}{\partial r\partial z} + \frac{1}{2}\left(\frac{\partial^2\Psi}{\partial r^2} + \frac{1}{r}\frac{\partial\Psi}{\partial r} - \frac{\partial^2\Psi}{\partial z^2} - \frac{\Psi}{r^2}\right). \tag{7}$$

The equation of motion and stress-strain relation for the bar are

$$\frac{\partial^2 w}{\partial z^2} = \kappa_o^2\frac{\partial^2 w}{\partial t^2},$$
$$\sigma_z = -\frac{c_o}{V_o}\frac{\partial w}{\partial z}, \tag{8}$$

where

$$\kappa_o^2 = c_1^2/c_o^2,\ c_o^2 = E_o/\rho_o. \tag{9}$$

c_o is the bar wave velocity, w is the longitudinal displacement, E_o is Young's modulus, and ρ_o is the density for the bar.

Boundary and Initial Conditions

In accordance with the assumptions made in the last section, the normal traction on the half space is uniform over the contact region and its resultant is equal to the normal force on the rod.

Downloaded 03 May 2010 to 171.66.16.27. Redistribution subject to ASME license or copyright; see http://www.asme.org/terms/Terms_Use.cfm

$$\tau_{zz}(r,0,t)=\begin{cases} -\dfrac{V_o}{E_1 c_1}\,\sigma_z(0,t) & 0\leqq r\leqq 1 \\ 0 & r\geqq 1 \end{cases} \tag{10}$$

where

$$E_1=2\mu/E_o\kappa_o. \tag{11}$$

The constants in the expression are due to the different nondimensionalization in the rod and the half space. The second stress boundary condition on the half space arises from the assumption of a smooth rod,

$$\tau_{rz}(r,0,t)=0. \tag{12}$$

The displacement of the rod into the half space is the average displacement of the half space in the contact region,

$$w(0,t)=\frac{1}{\pi}\int_0^1 u_z(r,0,t)2\pi r\,dr. \tag{13}$$

The boundary condition for the trailing end of the rod with the lumped mass is an expression of Newton's second law,

$$\left[\frac{\partial w}{\partial z}\right]_{z=-L}=M\kappa_o^2\left[\frac{\partial^2 w}{\partial t^2}\right]_{z=-L}. \tag{14}$$

Initially the half space is at rest before contact, and the rod has a uniform velocity directed toward the half space. These initial conditions are expressed by

$$\Phi=\frac{\partial\Phi}{\partial t}=\Psi=\frac{\partial\Psi}{\partial t}=w=0,$$

$$\frac{\partial w}{\partial t}=\frac{V_o}{c_1}\qquad \text{at } t=0. \tag{15}$$

Solution by Integral Transforms

The solution technique for the half space employs two integral transforms. The Laplace transform is first performed with respect to the time variable, denoted by an overbar on the time-dependent functions. Then a Hankel transform is used in the radial variable, designated by a superposed caret with the order indicated by a superscripted integer. Explicitly these are,

$$\bar{\phi}(r,z,s)=\int_0^\infty \phi(r,z,t)e^{-st}dt,$$

$$\hat{\phi}^\nu(\xi,z,t)=\int_0^\infty \phi(r,z,t)J_\nu(\xi r)r\,dr, \tag{16}$$

with the inversion formulas,

$$\phi(r,z,t)=\frac{1}{2\pi i}\int_{\gamma-i\infty}^{\gamma+i\infty}\bar{\phi}(r,z,s)e^{st}ds,$$

$$\phi(r,z,t)=\int_0^\infty \hat{\phi}^\nu(\xi,z,t)J_\nu(\xi r)\xi\,d\xi. \tag{17}$$

Both transforms are applied to the equations of motion for the displacement potentials (3), in which equation (3*a*) requires the zeroth order, and equation (3*b*) the first order Hankel transforms. The rod equation of motion is transformed in time only. The formal solutions of the resulting differential equations, after applying initial conditions and discarding the unbounded terms for the half space, are

$$\hat{\bar{\Phi}}^0 = \frac{f(\xi,s)}{\xi}e^{-\alpha z},\alpha=(\xi^2+s^2)^{1/2},$$

$$\hat{\bar{\Psi}}^1 = \frac{g(\xi,s)}{\xi}e^{-\beta z},\beta=(\xi^2+\kappa^2 s^2)^{1/2},$$

$$\bar{w} = A(s)e^{\kappa_o sz}+B(s)e^{-\kappa_o sz}+V_o/s^2c_1. \tag{18}$$

where α and β are multivalued functions of the complex variable ξ. The branch cuts in the slowness plane from the slownesses s_1 and s_2 are chosen to satisfy the radiation condition of outgoing waves in the half space at infinity.

The unknown parameters $f(\xi,s)$, $g(\xi,s)$, $A(s)$, and $B(s)$ now are to be determined from the boundary conditions. First $B(s)$ is eliminated from equation (18*c*), using the Laplace transform of boundary condition (14). The rod displacement solution then becomes

$$\bar{w}=A(s)\left[\frac{1-M\kappa_o s}{1+M\kappa_o s}e^{-\kappa_o s(2L+z)}+e^{\kappa_o sz}\right]+\frac{V_o}{s^2c_1}. \tag{19}$$

In order to determine $f(\xi,s)$ and $g(\xi,s)$ from the boundary conditions (10) and (12), both these and the stress equations (7) must be properly transformed to yield

$$\hat{\bar{\tau}}^0_{zz}=\left(\frac{\kappa^2 s^2}{2}+\xi^2\right)\hat{\bar{\Phi}}^0+\xi\frac{\partial\hat{\bar{\Psi}}^1}{\partial z},$$

$$\hat{\bar{\tau}}^1_{rz}=-\xi\frac{\partial\hat{\bar{\Phi}}^0}{\partial z}-\left(\frac{\kappa^2 s^2}{2}+\xi^2\right)\hat{\bar{\Psi}}^1,$$

$$[\hat{\bar{\tau}}^1_{rz}]_{z=0}=0,$$

$$[\hat{\bar{\tau}}^0_{zz}]_{z=0}=\left[\frac{\partial\bar{w}}{\partial z}\right]_{z=0}\frac{J_1(\xi)}{\xi E_1\kappa_o}. \tag{20}$$

Substitution of the transformed solutions $\hat{\bar{\Phi}}^0$ and $\hat{\bar{\Psi}}^1$ into the boundary conditions yields the following two equations,

$$\left(\xi^2+\frac{\kappa^2 s^2}{2}\right)f(\xi,s)-\beta\xi g(\xi,s)=\frac{sA(s)Q(s)J_1(\xi)}{E_1\xi},$$

$$-\alpha\xi f(\xi,s)+\left(\xi^2+\frac{\kappa^2 s^2}{2}\right)g(\xi,s)=0, \tag{21}$$

where

$$Q(s)=\left[1-\frac{1-M\kappa_o s}{1+M\kappa_o s}e^{-2\kappa_o Ls}\right]. \tag{22}$$

From these we obtain

$$f(\xi,s)=\frac{sA(s)J_1(\xi)(\xi^2+\kappa^2 s^2/2)Q(s)}{E_1R(\xi,s)},$$

$$g(\xi,s)=\frac{sA(s)J_1(\xi)\alpha\xi Q(s)}{E_1R(\xi,s)}, \tag{23}$$

where R is the Rayleigh function

$$R(\xi,s)=(\xi^2+\kappa^2 s^2/2)^2-\alpha\beta\xi^2. \tag{24}$$

The only remaining undetermined parameter is $A(s)$, and it is to be determined by the remaining boundary condition, (13), the one matching the rod and half space displacements. First use the Laplace transform of equation (3*b*) with equations (18) and (16), to express $\bar{u}_z$ as

$$\bar{u}_z=\int_0^\infty[-\alpha f(\xi,s)e^{-\alpha z}+\xi g(\xi,s)e^{-\beta z}]J_0(\xi r)d\xi. \tag{25}$$

Next, substitute this into the boundary condition (13), along with equations (23), and after carrying out the integration over r, we obtain for $A(s)$

$$A(s)=-\frac{E_1}{P(s)E_1+sQ(s)\bar{F}(s)}\frac{V_o}{s^2c_1}, \tag{26}$$

where

$$\bar{F}(s)=\kappa^2 s^2\int_0^\infty\frac{\alpha J_1^2(\xi)}{\xi R(\xi,s)}d\xi, \tag{27}$$

and

$$P(s)=\left[1+\frac{1-M\kappa_o s}{1+M\kappa_o s}e^{-2\kappa_o Ls}\right]. \tag{28}$$

Downloaded 03 May 2010 to 171.66.16.27. Redistribution subject to ASME license or copyright; see http://www.asme.org/terms/Terms_Use.cfm

The contact stress on the end of the rod (also the half space) is desired, as well as the displacement of the rod into the half space (the average displacement of the half space). Using the solution for $\bar{w}$, equation (19), the transformed constitutive equation for the rod from equations (8), and equation (26), we obtain the desired results in the Laplace transform domain as

$$\bar{\sigma}_o(s)[\bar{F}(s)+\bar{G}(s)]=E_1/s^2,$$
$$\bar{w}_o(s)[\bar{F}(s)+\bar{G}(s)]=(V_o/s^2c_1)\bar{F}(s), \tag{29}$$

where

$$\bar{\sigma}_z|_{z=0}\equiv\bar{\sigma}_o,\bar{w}|_{z=0}\equiv\bar{w}_o, \tag{30}$$

and where

$$\bar{G}(s)=\frac{E_1P(s)}{s\,Q(s)}. \tag{31}$$

What remains is the inversion of the Laplace transforms in equations (29) to obtain $\sigma_o(t)$ and $w_o(t)$. The main difficulty is caused by the function $\bar{F}(s)$, which is defined by an integral that is not easily handled. However, if $\bar{F}(s)$ and $\bar{G}(s)$ could be inverted separately, the desired solution could be obtained as the solution of a set of Volterra integral equations, by using the convolution theorem of Laplace transforms:

$$\int_0^t[F(t-\tau)+G(t-\tau)]\sigma_o(\tau)d\tau=E_1t,$$
$$\int_0^t[F(t-\tau)+G(t-\tau)]w_o(\tau)d\tau=\frac{V_o}{c_1}\int_0^tF(t-\tau)\tau d\tau. \tag{32}$$

Physical Significance of the Kernel

Before inverting the kernel of the integral equations, it is instructive to examine its physical significance. For this purpose consider the simpler problem of an impulsive normal pressure over a circular region of the half-space boundary, and solve for just the average surface displacement of the half space inside the load region. The surface displacements outside of the load region were presented by Mitra (1964) for this problem.

In terms of the same nondimensional quantities as used earlier, the boundary conditions for this problem are

$$\tau_{zz}|_{z=0}=\begin{cases}-\delta(t) & 0<r\leqq 1\\ 0 & r>1\end{cases},$$
$$\tau_{rz}|_{z=0}=0. \tag{33}$$

Using Laplace and Hankel transforms we again obtain for the potentials the results in equation (18), and the boundary conditions (33) become

$$\hat{\bar{\tau}}^0_{zz}|_{z=0}=-J_1(\xi)/\xi,\ \hat{\bar{\tau}}^1_{rz}|_{z=0}=0. \tag{34}$$

Applying these boundary conditions to determine f and g, we obtain

$$f(\xi,s)=-\frac{J_1(\xi)(\xi^2+\kappa^2s^2/2)}{R(\xi,s)},\ g(\xi,s)=-\frac{\xi\alpha J_1(\xi)}{R(\xi,s)}. \tag{35}$$

Using the displacement equation (25) and averaging over the contact region as indicated in equation (13), we obtain for the average normal surface displacement

$$avg(\bar{u}_z|_{z=0})=\frac{1}{\pi}\int_0^1\int_0^\infty\frac{\alpha\kappa^2s^2}{2R(\xi,s)}J_1(\xi)J_0(\xi r)d\xi\,2\pi r\,dr. \tag{36}$$

Upon performing the integration over r, we find that

$$\bar{F}(s)\equiv avg(\bar{u}_z|_{z=0}), \tag{37}$$

where $\bar{F}(s)$ is defined in equation (27). Therefore, the physical significance of the half-space portion of the kernel, $F(t)$ in equations (32) is obtained. It is the time response of the average surface displacement of a circular region of a half space subjected to a uniform impulsive load over that same region.

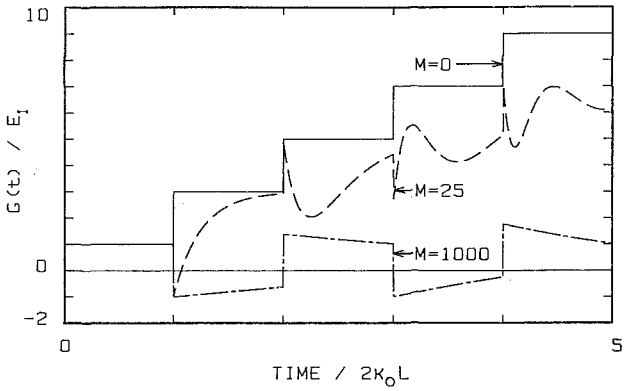


Fig. 2 Rod portion of the kernel for three lumped masses

The other portion of the kernel, $G(t)$, is similarly found to be the displacement response of the end of the rod, which is initially at rest, to an impulsive load of magnitude 2μ.

Inversion of the Kernel

The inversion of the rod portion of the kernel, $\bar{G}(s)$, is straightforward. From equation (31) with equations (22) and (28) we can express $\bar{G}(s)$ as

$$\bar{G}(s)=\frac{E_1}{s}\left(\frac{1+\dfrac{1-M\kappa_os}{1+M\kappa_os}e^{-2\kappa_oLs}}{1-\dfrac{1-M\kappa_os}{1+M\kappa_os}e^{-2\kappa_oLs}}\right). \tag{38}$$

For real $s>0$,

$$\left|\frac{1-M\kappa_os}{1+M\kappa_os}e^{-2\kappa_oLs}\right|<1, \tag{39}$$

so the function $\bar{G}(s)$ can be expanded in a geometric series that is absolutely convergent,

$$\bar{G}(s)=\frac{E_1}{s}\left[1+2\left(\frac{1-M\kappa_os}{1+M\kappa_os}\right)e^{-2\kappa_oLs}+2\left(\frac{1-M\kappa_os}{1+M\kappa_os}\right)^2e^{-4\kappa_oLs}+\ldots\right], \tag{40}$$

where the terms in this series represent reflections from the rod end.

The inversion can now be carried out term-by-term using partial fraction expansion and integral tables to obtain the result

$$G(t)=E_1\{1+[2-4e^{-(t-2\kappa_oL)/\kappa_oM}]H<t-2\kappa_oL>+[2-8(t-4\kappa_oL)/\kappa_oM\,e^{-(t-4\kappa_oL)/\kappa_oM}]H<t-4\kappa_oL>+\ldots\}. \tag{41}$$

Figure 2 shows this result for a small mass, a large mass, and the limiting case with no mass. For no mass, the step-like result is intuitive. The steps occur when the reflections arrive from the free end of the rod. The steps increase the magnitude because the free end reflects a wave with the same sign as the incident wave. When a large mass is present, the result approaches that for a rod with a fixed end, which is a square-wave response; the end on which the initial impulse is applied merely jumps back and forth as each new reflection arrives.

The inversion of the half-space portion of the kernel, $\bar{F}(s)$ has already been carried out by Matsumoto et al. (1978) in their study of a semi-infinite rod. The solution utilizes the Cagniard-de Hoop method after using appropriate integral representations for the Bessel functions. The result is in the

Downloaded 03 May 2010 to 171.66.16.27. Redistribution subject to ASME license or copyright; see http://www.asme.org/terms/Terms_Use.cfm

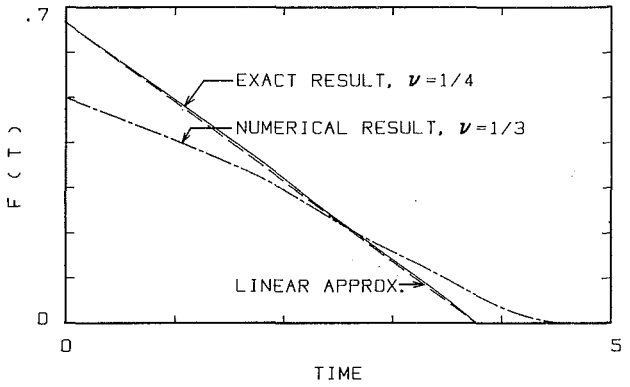


Fig. 3 Half space portion of the kernel

form of double finite integrals. For a half space with Poisson's ratio, $\nu = 1/4$, or $\kappa^2 = 3$, the integration was performed explicitly by using the method presented by Pekeris (1955). Both of these results are listed in the Appendix.

The solution is separated into three parts. The first part is valid until the longitudinal wave travels across the contact region along a diameter. The second holds until the shear wave travels across, and the last is valid until the Rayleigh surface wave travels across the contact region. After this time $F(t)$ is identically zero.

Figure 3 shows this result, from Matsumoto et al. (1978), for the case with Poisson's ratio equal to 1/4. In addition, the result for Poisson's ratio of 1/3, calculated using a numerical inversion technique, is shown. The character of the solution is the same, the displacement of the half space jumps initially and declines to zero almost linearly, reaching zero when the Rayleigh wave has traveled across the whole contact region. A straight line is also shown, so that the deviation from strict linearity is more evident.

An Approximate Analytical Solution

After examining the graph of $F(t)$ in Fig. 3, one may conclude that a linear approximation is sufficient to yield a useful approximate solution to the integral equation. We must also limit the rod portion of the kernel, $G(t)$, to that for a semi-infinite rod, or a finite rod with no mass, the cases for which it is also strictly linear. The linear approximation is

$$F(t) \simeq \begin{cases} \dfrac{1}{\kappa^2}\left(2-\dfrac{t}{\tau_R}\right), & t \leqq 2\tau_R, \\ 0, & t \geqq 2\tau_R, \end{cases} \tag{42}$$

where τ_R is the dimensionless Rayleigh wave slowness.

With this form for $F(t)$, the integral equations (32) can be differentiated twice to yield first order differential equations for the stress and displacement. The initial conditions are extracted after the first differentiation, and they amount to a jump in stress and zero initial displacement. Thus we obtain

$$\sigma_o'(t) - b\,\sigma_o(t) = -b\,\sigma_o(t-2\tau_R) - 2bE_1\tau_R\kappa^2[\sigma_o'(t-2\kappa_oL) + \sigma_o'(t-4\kappa_oL) + \ldots],$$

$$w_o'(t) - b\,w_o(t) = \begin{cases} -V_o b/c_1(t-2\tau_R), & 0 \leqq t \leqq 2\tau_R, \\ -b\,w_o(t-2\tau_R) & t \geqq 2\tau_R \\ -2bE_1\tau_R\kappa^2[w_o'(t-2\kappa_oL) + w_o'(t-4\kappa_oL) + \ldots], \end{cases} \tag{43}$$

where

$$b = 1/\tau_R(2+\kappa^2E_1) \tag{44}$$

with initial conditions

$$\sigma_o(0^+) = bE_1\tau_R\kappa^2, \qquad w_o(0^+) = 0. \tag{45}$$

After examining these differential equations, one can see that the solution must be obtained in time increments of $2\tau_R$ and $2\kappa_oL$. This is because the forcing term on the right-hand side is a multiple of the solution and its derivative for previous time increments. The more fundamental time increment is that involving the Rayleigh wave, since $2\kappa_oL$ is the time for the bar wave to travel away from the interface, reflect off the trailing end, and return, which is a much longer time. Since the half space is at rest before the impact, the interface stress and displacement are zero for negative time, and thus the forcing terms will correspondingly be zero. The stress equation in the first time increment is homogeneous, unlike the displacement equation, and the stress increases exponentially at first.

The time increment in the solution has a special physical significance. When impact occurs, axially symmetric surface waves start to propagate inward and outward from the boundary of the contact region. The surface waves traveling across this region of uniform stress are unimpeded until the other edge is reached at time $2\tau_R$. At this point the wave is scattered because of the discontinuity in the boundary conditions, and some portion of the incident surface wave is reflected back across the contact area. The reflected wave then affects the solution in the next time period. There is also the contribution from the bar wave reflected from the free end of the rod, which occurs much later at $2\kappa_oL$.

These approximate solutions, not including the rod reflections, (so they represent a semi-infinite rod, or a finite rod before the first reflection occurs) are

$$\sigma_o(t) = bE_1\tau_R\kappa^2e^{bt}\sum_{n=0}^{\infty}(-b)^n\frac{e^{-2b\tau_R}}{n!}(t-2n\tau_R)H<t-2n\tau_R>,$$

$$w_o(t) = \frac{V_oE_1\tau_R\kappa^2}{c_1}\left\{\left(1+\frac{t}{\tau_R\kappa^2E_1}-e^{bt}\right) + [1+b(t-(4\tau_R+E_1\kappa^2))e^{b(t-2\tau_R)}]H<t-2\tau_R> + \left[1-\frac{b^2}{2}(t^2-2\tau_R(6+\kappa^2E_1)t+2\tau_R^2(20+8E_1\kappa^2+E_1^2\kappa^4)) \cdot e^{b(t-4\tau_R)}\right]H<t-4\tau_R> + \ldots\right\}. \tag{46}$$

The accuracy of these approximate results can be seen in Fig. 4, where equations (46) are plotted along with the numerical solution of the exact integral equations, which is presented next. The contact stress is indistinguishable from the numerical result using the exact kernel, thus the approximation is very good in determining the stress. The displacement does not agree quite as well, understating the actual displacement at large time.

Numerical Solution of the Integral Equations

The numerical solution of the integral equations is straightforward once the kernel is known. There are no singularities in either the kernel or the solution. The solution technique follows that described by Baker (1977) for Volterra integral equations of the second kind.

The integrals are discretized by using numerical quadrature. Equal intervals are used, since this allows the kernel to be represented by a table, with trapezoidal weights. Twenty-six equally spaced values for the kernel were sufficient to give accurate and stable results, thus the time increment is one twenty-fifth of $2\tau_R$. If K represents the kernel, $\phi(t)$ the unknown, and $g(t)$ the right-hand side, then the discretized integral equation becomes

Downloaded 03 May 2010 to 171.66.16.27. Redistribution subject to ASME license or copyright; see http://www.asme.org/terms/Terms_Use.cfm

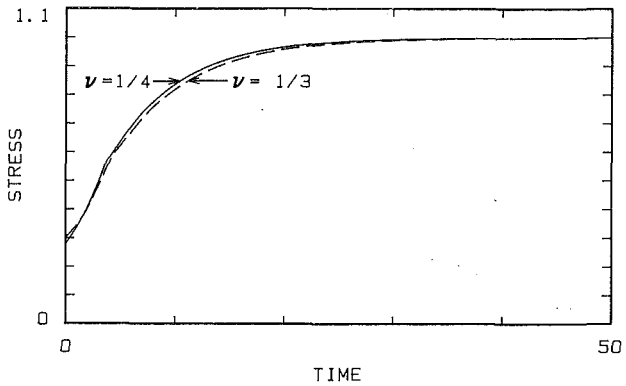


Fig. 4(*a*) Interface stress for steel semi-infinite rod, aluminum half space. Solid curve shows the numerical solution and approximate analytical solution, dashed curve is the numerical solution using a numerical half space kernel.

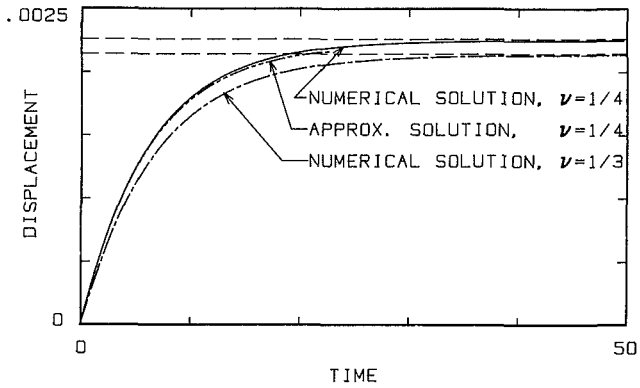


Fig. 4(*b*) Displacement of semi-infinite rod into half space. Dashed lines are the static solutions for the corresponding Poisson's ratio.

Table 1 Material properties

Material	Young's Modulus (Gpa)	Density (Kg/m^3)
Nylon	2.9	1.135×10^3
Material A	24.1	1.66×10^3
Material B	48.3	2.18×10^3
Aluminum	72.4	2.7×10^3
Steel	207	7.86×10^3

$$\sum_{j=0}^{k} w_{kj} K[(k-j)h]\phi(jh) = g(kh);\ k=1,2,\ldots \tag{47}$$

where the quadrature weights w_{kj} are

$$w_{i0}=h/2,\ w_{ij}=h\ (\text{for } i\neq j),\ w_{ii}=h/2. \tag{48}$$

Given the initial value of ϕ, there is only one unknown for each time step, and the solution marches forward in time. The solution is carried out until the contact stress reaches zero, which corresponds to the time at which the rod loses contact with the half space. Note that the contact displacement may not be zero at this time.

Numerical Results

For the numerical calculations, Table 1 shows the materials used and their properties. Arranged from softest to stiffest, the table includes two fictitious materials spaced equally between nylon and aluminum. Since the assumption was made that $\nu = 1/4$ for the half space, the Young's modulus of the actual materials was used, but not Poisson's ratio.

Figure 4(*a*) shows the dependence of the contact stress on time for a semi-infinite steel rod, and aluminum half space. The stress asymptotically approaches unity, which is the normalized value of the stress produced when a rod impacts a rigid half space. There is an initial jump in stress followed by the first portion of the curve which has positive curvature. Then there is a discontinuity in slope which occurs at the Rayleigh wave time $2\tau_R$. The contact stress for the same material with $\nu = 1/3$ is also shown. It shows a slightly larger initial jump, and then a slower rise.

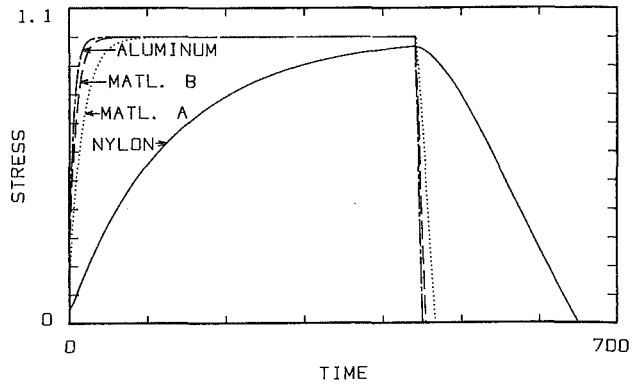


Fig. 5(*a*) Interface stress for rod of length 200 with no mass, impacting four half-space materials

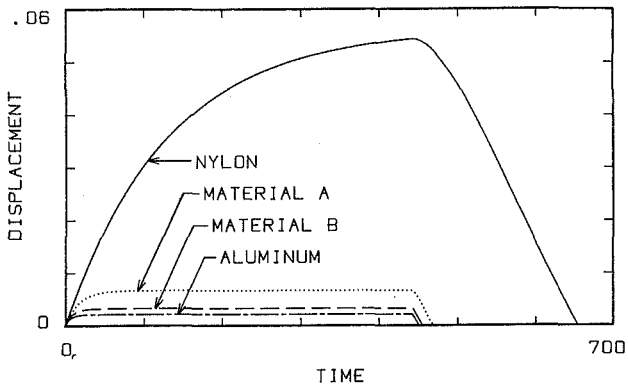


Fig. 5(*b*) Displacement of rod of length 200 with no mass into four half-space materials

The corresponding displacement is shown in Fig. 4(*b*). Here there is no initial jump, which is to be expected, and the displacement also approaches an asymptotic value. The result for $\nu = 1/3$ is also shown. It is very similar, rising to a steady value about six percent lower. The steady state value corresponds to the static elasticity result for the average displacement of a half space with a uniform pressure in a circular region. Using the solution presented in Gladwell (1980) with the asymptotic value for the stress, we find that this average displacement is

$$w_o = \frac{4V_o}{E_1 c_1}(1-\nu)(0.42617798). \tag{49}$$

Figures 5(*a*) and 5(*b*) show the stress and displacement for a finite length rod with no lumped mass, for four different half-space materials. The rod is steel, and the half-space materials are nylon, material A, material B, and aluminum. The stress rises more quickly for the stiffer half spaces, and reaches the asymptotic value sooner. The rod bounces off almost immediately after the first reflection arrives from the free end in the stiffer cases. The time scales have been adjusted so that all are normalized to the longitudinal wave speed of the stiffest half space. This is so that the reflected wave from the rod arrives at the same time in all cases.

Figures 6(*a*) and 6(*b*) show the effect of adding the lumped mass to the rod. The mass has no effect on the response until the first rod reflection arrives, causing the stress and displace-

Downloaded 03 May 2010 to 171.66.16.27. Redistribution subject to ASME license or copyright; see http://www.asme.org/terms/Terms_Use.cfm

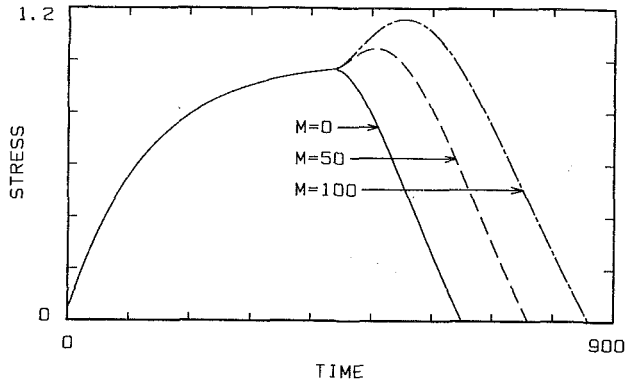


Fig. 6(a) Interface stress for rod of length 200 with three different lumped masses. Half space is nylon.

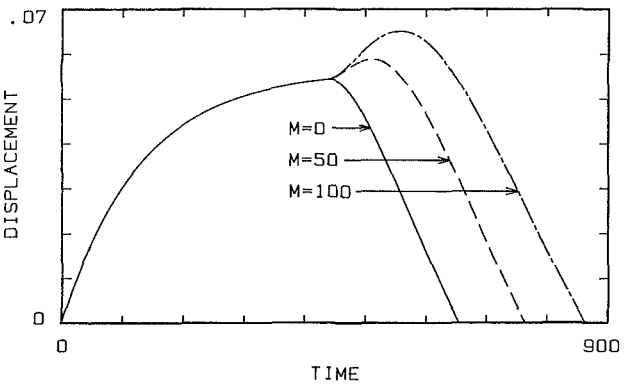


Fig. 6(b) Displacement of rod into nylon half space for three different lumped masses. Rod length 200.

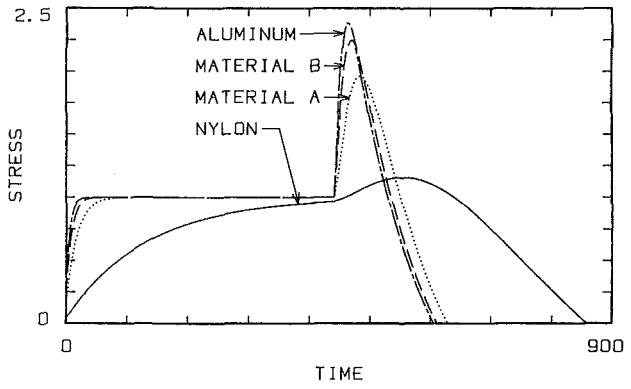


Fig. 7(a) Interface stress for rod of length 200, with lumped mass of 100, impacting four half-space materials.

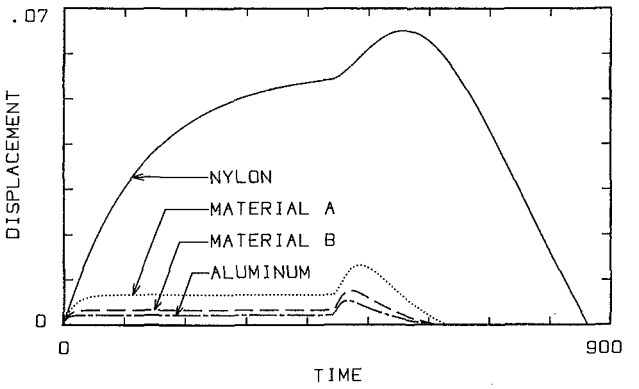


Fig. 7(b) Displacement of rod into four half-space materials. Rod length is 200, lumped mass is 100.

ment to increase beyond the infinite rod asymptotic values at first, and then decline to zero. A larger mass gives a correspondingly larger increase, and a longer contact time.

Figures 7(*a*) and 7(*b*) show the effects of the four different half-space materials when the lumped mass is present. The peak stress is related to the half space materials, with larger peaks corresponding to stiffer materials.

Finally, Fig. 8 shows contact displacement versus stress for the same four cases as in Figs. 7. These show a small amount of hysteresis, which is caused by energy propagating into the half space. In addition, when the impacting end of the rod leaves the half space, the rod does not have uniform velocity, since waves continue to propagate back and forth in the rod.

As pointed out by one reviewer, the near linearity of the stress-displacement curves in Fig. 8 suggests that the half space could be modeled by a linear spring, and that the other results in Figs. 4–7 would be reproduced with high accuracy. The solution for the rod-mass system impacting a linear spring was derived in order to evaluate this conjecture. The simplest result is for the case of a semi-infinite rod, corresponding to Fig. 4, in which the stress and displacement are given by:

$$\sigma_o(t) = 1 - e^{-kt}, w_o(t) = (V_o/kc_1)(1 - e^{-kt}), \qquad (50)$$

where k is determined such that the large time asymptotic value of $w_o(t)$ in equation (50) equals the value predicted by the static result in equation (49), that is,

$$k = E_1/4(1-\nu)(0.42617798). \qquad (51)$$

These results are not presented graphically, but they approximate the gross features of the half-space results in Fig. 4. The stress does not have an initial jump, nor does it have the initial positive curvature, but it has the same asymptotic value. Both the stress and displacement for the linear spring model approach the asymptotic value sooner than for the half space,

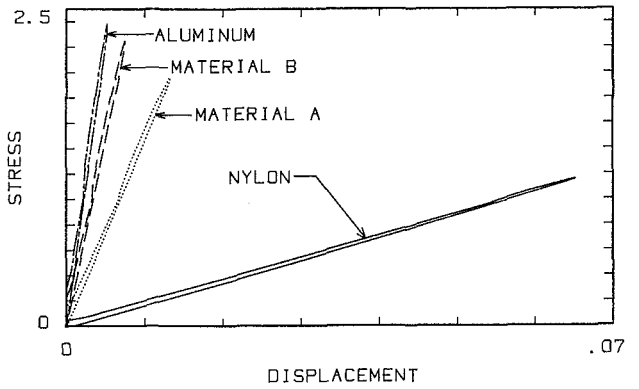


Fig. 8 Interface stress plotted against half space indentation, showing hysteresis, for the four cases in Fig. 7.

which is to be expected since the spring is massless. The spring model results corresponding to Fig. 7 were also computed for the stiffest (aluminum) case. The difference in rise time was negligible on the scale shown, but the stress peak due to the lumped mass was about four percent higher for the linear spring model. If stress were plotted against displacement as in Fig. 8, there would be no hysteresis, as expected.

Conclusion

Some interesting conclusions can be drawn from the analysis presented here. The half space material has a large effect on the rise time of the stress and displacement, but the maximum value, for a rod with no mass, depends entirely on the rod material. If a mass is added to the trailing end of the rod the maximum stress is larger, and it is affected by both the half space material and the size of the mass.

Downloaded 03 May 2010 to 171.66.16.27. Redistribution subject to ASME license or copyright; see http://www.asme.org/terms/Terms_Use.cfm

Contact times for rods without a mass are somewhat dependent on the half-space material, but are much more dependent on the length of the rod. The rod cannot bounce off until after the reflected wave arrives from the trailing end of the rod. In all cases the rod leaves before a second reflection occurs.

The stress-displacement curves show an almost linear response, with a small amount of energy loss. In this respect this simplified model does not agree with actual printing behavior, which usually shows much more loss, as well as more nonlinear stress-displacement behavior, as shown by Wang and Hall (1983).

Further work is planned to model more accurately the details of the actual printing process. The first improvement should model the half space as a material with losses, such as viscoelastic. Then it may be appropriate to include one or more layers on the half space to model more accurately the paper and ribbon.

Acknowledgment

This research has been partially supported by an IBM Departmental Grant to the Department of Mechanical Engineering at U. C. Berkeley. H. A. Downey would like to thank IBM in Charlotte, N. C., for its support under the IBM resident study program.

References

Baker, C. T. H., 1977, *The Numerical Treatment of Integral Equations*, Oxford University Press, Oxford, pp. 759–762.

Conway, H. D., and Lee, H. C., 1970, "Impact of an Indenter on a Large Plate," ASME JOURNAL OF APPLIED MECHANICS, Vol. 37, No. 1, pp. 234–235.

Conway, H. D., Lee, H. C., and Bayer, R. G., 1970, "The Impact Between a Rigid Sphere and a Thin Layer," ASME JOURNAL OF APPLIED MECHANICS, Vol. 37, No. 1, pp. 159–162.

Conway, H. D., Engel, P. A., and Lee, H. C., 1972, "Force-Time Investigations for the Elastic Impact Between a Rigid Sphere and a Thin Layer," *Int. J. Mech. Sci.*, Vol. 14, pp. 523–529.

Gladwell, G. M. L., 1980, *Contact Problems in the Theory of Elasticity*, Sijthoff & Noordhoff International Publishers, Germantown, Maryland, pp. 81–86.

Gutzwiller, M. C., 1962, "The Impact of a Rigid Circular Cylinder on an Elastic Solid," *Proc. Royal Society*, A255, pp. 153–191.

Matsumoto, H., Nakahara, I., and Matsuoka, Y., 1978, "The Impact of an Elastic Cylinder on an Elastic Solid," *Bulletin of the JSME*, Vol. 21, No. 154, pp. 579–586.

Mitra, M. Von, 1964, "Disturbance Produced in an Elastic Half-Space by Impulsive Normal Pressure," *Proc. Camb. Phil. Soc.*, Vol. 60, pp. 683–696.

Naemura, A., and Kobayashi, M., 1979, "Impact Printing Fundamental Properties," *Review of the Electrical Communication Laboratories, Tokyo*, Vol. 27, No. 9–10, pp. 864–875.

Pekeris, C. L., 1955, "The Seismic Surface Pulse," *Proceedings of the National Academy of Sciences, USA*, Vol. 41, pp. 469–480.

Wang, H. C., and Hall, S. A., 1983, "Paper-Function Model for Wire-Matrix Printing," *Proceedings of the Society for Information Display*, Vol. 24, No. 1, pp. 13–15.

APPENDIX

From Matsumoto et al. (1978), the following equations are the inverted form of $F(t)$:

For $0 \leqq t \leqq 2$

$$F(t) = \frac{2}{\kappa^2} + \frac{t}{\pi^2\kappa^2}\int_0^t \frac{1}{m}\sqrt{4-m^2}\,W_1(t,m)\,dm + \int_0^{t/\kappa} \frac{1}{m}\sqrt{4-m^2}\,W_2(t,m)\,dm \tag{52}$$

For $2 < t \leqq 2\kappa$

$$F(t) = \frac{2}{\kappa^2} + \frac{t}{\pi^2\kappa^2}\int_0^2 \frac{1}{m}\sqrt{4-m^2}\,W_1(t,m)\,dm + \int_0^{t/\kappa} \frac{1}{m}\sqrt{4-m^2}\,W_2(t,m)\,dm \tag{53}$$

For $t > 2\kappa$

$$F(t) = \frac{2}{\kappa^2} + \frac{t}{\pi^2\kappa^2}\int_0^2 \frac{1}{m}\sqrt{4-m^2}\,[W_1(t,m) + W_2(t,m)]\,dm \tag{54}$$

where

$$W_1(t,m) = \int_{1/\kappa}^{t/\kappa m} \frac{(1/2-u^2)^2\sqrt{u^2-1/\kappa^2}}{uR(u)\sqrt{t^2/\kappa^2m^2-u^2}}\,du$$

$$W_2(t,m) = \int_{1/\kappa}^{t/\kappa m} \frac{u(u^2-1/\kappa^2)\sqrt{u^2-1}}{R(u)\sqrt{t^2/\kappa^2m^2-u^2}}\,du$$

$$R(u) = (1/\kappa^2-1)u^6 + (3/2-1/\kappa^2)u^4 - u^2/2 + 1/16 \tag{55}$$

For the special case with $\kappa^2 = 3$, or $\nu = 0.25$, the integrals in equations (55) can be evaluated, to yield

for $0 \leqq t \leqq 2$

$$F(t) = \frac{2}{3\pi}\int_t^2 \sqrt{4-m^2}\,dm + \frac{t}{6\pi}\int_{t/\sqrt{3}}^t [f_1(t,m) + f_2(t,m)]\,dm + \frac{t}{3\pi}\int_{t/\tau_R}^{t/\sqrt{3}} f_2(t,m)\,dm \tag{56}$$

for $2 < t \leqq 2\sqrt{3}$

$$F(t) = \frac{t}{6\pi}\int_{t/\sqrt{3}}^2 [f_1(t,m) + f_2(t,m)]\,dm + \frac{t}{3\pi}\int_{t/\tau_R}^{t/\sqrt{3}} f_2(t,m)\,dm \tag{57}$$

for $2\sqrt{3} < t \leqq 2\tau_R$

$$F(t) = \frac{t}{3\pi}\int_{t/\tau_R}^{t/\sqrt{3}} f_2(t,m)\,dm \tag{58}$$

for $t > 2\tau_R$

$$F(t) \equiv 0 \tag{59}$$

where

$$f_1(t,m) = \sqrt{4-m^2}\left\{\frac{6}{\sqrt{4t^2-3m^2}} - \frac{\sqrt{2(\sqrt{3}-1)}}{\sqrt{4t^2-3(3-\sqrt{3})m^2}}\right\}$$

$$f_2(t,m) = \sqrt{4-m^2}\left\{\frac{\sqrt{2(\sqrt{3}+1)}}{\sqrt{4\tau_R^2m^2-4t^2}}\right\}$$

$$\tau_R^2 = \frac{3(3+\sqrt{3})}{4} \tag{60}$$

Downloaded 03 May 2010 to 171.66.16.27. Redistribution subject to ASME license or copyright; see http://www.asme.org/terms/Terms_Use.cfm

The Normal Impact of an Elastic Rod-Mass System on a Viscoelastic Half Space

H. A. Downey, Jr.,
Graduate Student,[1]
Assoc. Mem. ASME

D. B. Bogy
Professor,
Mem. ASME

Department of Mechanical Engineering,
University of California,
Berkeley, CA 94720

The normal impact of a one-dimensional elastic rod, with a lumped mass on the trailing end, onto a viscoelastic half space is considered and the problem is solved for the time dependent interface stress and displacement. The problem is reduced to an integral equation, whose two-part kernel consists of solutions of two simpler problems. One part pertains to the half space only and the other is for the rod-mass system. The half-space portion of the kernel is obtained through a numerical inversion of the Laplace transformed solution. Given the half-space kernel contribution, which depends only on the two viscoelastic parameters and Poisson's ratio, the integral equation is solved numerically for two families of half space materials. The viscoelastic effects on the half space are quite pronounced. Certain combinations of the parameters cause a large hysteresis in the impact, and softer half spaces require longer contact times before the rod leaves the surface.

Introduction

A wire-matrix printhead used in impact printing consists of an array of long thin wires, driven by electromagnets. These wires strike a layered stack of ribbon and paper (and often carbon paper) on a platen of elastic or viscoelastic material, forming characters as patterns of dots. The push for faster and better printing creates the need for more understanding of this impact. The two important parameters in the process are the total contact time, which governs the printing speed, and the contact stress as a function of time, which affects the quality of the image. The objective of our study is to understand some of the effects that the wire material and length, lumped mass, half space material, and paper and ribbon properties have on the printing parameters.

The solution presented here is an extension of our earlier analysis in Downey and Bogy (1987). That paper gave the solution for the same problem with an elastic (rather than viscoelastic) half space. The model employed is a substantial simplification of the actual impact problem. The platen and layers of paper and ribbon are modeled as a homogeneous viscoelastic half space. Ultimately, it may be necessary to include the layers in the model.

Here, as in the previous paper, we solved for the displacement of the rod into the half space and the contact stress. In the case of the elastic half space the problem was reduced to an integral equation, with a two-part kernel in an explicit form. The first portion of this kernel is the same as that arrived at by Matsumoto et al. (1978), who considered a semi-infinite rod impacting an elastic half space.

Formulation of the Problem

For simplicity, the rod is modeled using one-dimensional rod theory, since its length is much greater than its radius. Linear viscoelasticity theory is used for the half space, and the impact is assumed to be axisymmetric and torsionless.

The viscoelastic model we use is the two parameter standard linear solid, the simplest constitutive relation appropriate for viscoelastic solids. We also assume the same time dependence in the bulk and shear moduli, which implies that Poisson's ratio is constant. In differential form these constitutive equations are

$$\left(\frac{\partial}{\partial t}+\frac{1}{\tau_\sigma}\right) s_{ij}=2\tilde{\mu}\left(\frac{\partial}{\partial t}+\frac{\alpha}{\tau_\sigma}\right) e_{ij},$$

$$\left(\frac{\partial}{\partial t}+\frac{1}{\tau_\sigma}\right) \tau_{kk}=3\tilde{k}\left(\frac{\partial}{\partial t}+\frac{\alpha}{\tau_\sigma}\right) \epsilon_{kk}, \tag{1}$$

where s_{ij} and e_{ij} are the deviatoric components of the stress and strain tensors:

$$\begin{aligned} s_{ij} &= \tau_{ij}-1/3\ \tau_{kk}\ \delta_{ij}, \\ e_{ij} &= \epsilon_{ij}-1/3\ \epsilon_{kk}\ \delta_{ij}, \end{aligned} \tag{2}$$

τ_σ is the stress relaxation time, α is the ratio of the stress to strain relaxation times, which for stability must lie between zero and one, and $\tilde{\mu}$ and $\tilde{k}$ are the instantaneous shear and bulk moduli, respectively.

[1] Also Sr. Assoc. Engineer, IBM Corp., Charlotte, NC.

Contributed by the Applied Mechanics Division for presentation at the 1987 Applied Mechanics, Biomechanics, and Fluids Engineering Conference, Cincinnati, OH, June 14-17, 1987, of the American Society of Mechanical Engineers.
Discussion of this paper should be addressed to the Editorial Department, ASME, United Engineering Center, 345 East 47th Street, New York, N.Y. 10017, and will be accepted until two months after final publication of the paper itself in the JOURNAL OF APPLIED MECHANICS. Manuscript received by ASME Applied Mechanics Division, June 18, 1986; final revision, October 21, 1986.
Paper No. 87-APM-26.

Copyright © 1987 by ASME
Downloaded 03 May 2010 to 171.66.16.27. Redistribution subject to ASME license or copyright; see http://www.asme.org/terms/Terms_Use.cfm

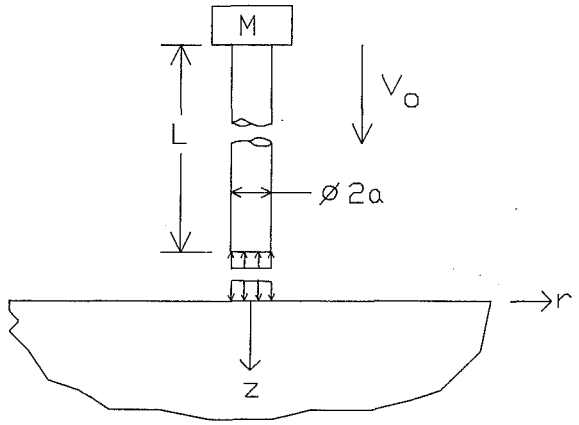


Fig. 1 Geometry and coordinate system

The boundary conditions for the contact region are the same as in Downey and Bogy (1987). We assume uniform normal traction in the contact region, and no shear traction on the surface of the half space. The displacement of the rod tip into the half space is set equal to the average displacement of the half space in the contact region.

Figure 1 illustrates the problem. The half space occupies the region $z > 0$, and the contact region is centered at the origin of the cylindrical polar coordinates (r, θ, z). The rod has length L, radius a, and a lumped mass M is attached at $z = -L$. Its initial velocity, V_o, is in the positive z direction.

All the variables used in the solution are to be nondimensionalized. These are self-explanatory with the exception of the stress in the rod, which is normalized to the steady-state stress value for a rod impacting a rigid half space. The dimensionless quantities, indicated by asterisks, are as follows:

$$r^* = r/a,\ z^* = z/a,\ w^* = w/a,\ L^* = L/a,\ u_i^* = u_i/a,$$
$$t^* = \tilde{c}_1 t/a,\ \Phi^* = \Phi/a^2,\ \psi^* = \psi/a^2,\ \tau_{ij}^* = \tau_{ij}/2\tilde{\mu},\ s_{ij}^* = s_{ij}/2\tilde{\mu},$$
$$\sigma_z^* = -c_o\sigma_z/E_oV_o,\ M^* = M/\pi\rho_o a^3,\ \tau_\sigma^* = \tilde{c}_1\tau_\sigma/a, \tag{3}$$

where $\tilde{c}_1$ is the longitudinal wave speed in the viscoelastic half space, and E_o and c_o are the Young's modulus and wave speed of the rod. For convenience, throughout the remainder of the paper, the asterisks will be deleted with the understanding that all quantities are dimensionless.

To obtain the solution to the viscoelastic impact problem we take advantage of the elastic-viscoelastic correspondence principle (Christensen, 1971), and start with the Laplace transformed solution to the corresponding elastic impact problem considered in Downey and Bogy (1987).

After application of the Laplace transform to the viscoelastic constitutive equations (1), we obtain

$$\bar{s}_{ij} = 2\tilde{\mu}\frac{(s+\alpha/\tau_\sigma)}{(s+1/\tau_\sigma)}\bar{e}_{ij} \equiv 2\bar{\mu}(s)\bar{e}_{ij},$$
$$\bar{\tau}_{kk} = 3\tilde{k}\frac{(s+\alpha/\tau_\alpha)}{(s+1/\tau_\sigma)}\bar{\epsilon}_{kk} \equiv 3\bar{k}(s)\bar{\epsilon}_{kk}, \tag{4}$$

where the superposed bar denotes the Laplace transform with respect to time. Comparing these to the Laplace transformed elastic constitutive equations, we see that the constants μ and k correspond to $\bar{\mu}(s)$ and $\bar{k}(s)$ in equations (4). In addition, λ corresponds to $\bar{\lambda}(s)$, defined by $\bar{\lambda}(s) = \bar{k}(s) - 2/3\,\bar{\mu}(s)$. According to the correspondence principle we make this substitution in the Laplace transformed elastic solution.

Unfortunately, the nondimensionalization introduces a complication. In the elastic case we used μ and c_1 to nondimensionalize the stress and time, and we must also use constants for this purpose in the viscoelastic case; instead of μ and c_1 we use here $\tilde{\mu}$ and $\tilde{c}_1$. This affects most of the equations in Downey and Bogy (1987), so we must repeat the key ones here.

Expressing the displacement of the elasticity solution in terms of the potentials Φ and ψ, there is only one nonzero component of the vector potential ψ, ψ_θ, which we will call Ψ. There are only two components of the displacement:

$$u_r = \frac{\partial\Phi}{\partial r} - \frac{\partial\Psi}{\partial z},$$
$$u_z = \frac{\partial\Phi}{\partial z} + \frac{1}{r}\frac{\partial}{\partial r}(\Psi r). \tag{5}$$

The equations of motion for the elastic half space become

$$\nabla^2\Phi = \frac{\tilde{c}_1^2}{c_1^2}\frac{\partial^2\Phi}{\partial t^2},$$
$$\nabla^2\Psi - \frac{\Psi}{r^2} = \kappa^2\frac{\partial^2\Psi}{\partial t^2}, \tag{6}$$

where

$$\kappa^2 = \tilde{c}_1^2/c_2^2,\ c_1^2 = (\lambda+2\mu)/\rho,\ \tilde{c}_1^2 = (\tilde{\lambda}+2\tilde{\mu})/\rho,\ c_2^2 = \mu/\rho,$$
$$\nabla^2 = \frac{\partial^2}{\partial r^2} + \frac{1}{r}\frac{\partial}{\partial r} + \frac{\partial^2}{\partial z^2}. \tag{7}$$

The half-space stress components pertinent to tractions in the contact region are

$$\tau_{zz} = \frac{\lambda}{2\tilde{\mu}}\nabla^2\Phi + \frac{\mu}{\tilde{\mu}}\left(\frac{\partial^2\Phi}{\partial z^2} + \frac{\partial^2\Psi}{\partial r\partial z} + \frac{1}{r}\frac{\partial\Psi}{\partial z}\right),$$
$$\tau_{rz} = \frac{\mu}{\tilde{\mu}}\frac{\partial^2\Phi}{\partial r\partial z} + \frac{\mu}{2\tilde{\mu}}\left(\frac{\partial^2\Psi}{\partial r^2} + \frac{1}{r}\frac{\partial\Psi}{\partial r} - \frac{\partial^2\Psi}{\partial z^2} - \frac{\Psi}{r^2}\right). \tag{8}$$

The equation of motion and constitutive relation for the rod are

$$\frac{\partial^2 w}{\partial z^2} = \kappa_o^2\frac{\partial^2 w}{\partial t^2},\ \sigma_z = -\frac{c_o}{V_o}\frac{\partial w}{\partial z}, \tag{9}$$

where

$$\kappa_o^2 = \tilde{c}_1^2/c_o^2,\ c_o^2 = E_o/\rho_o, \tag{10}$$

c_o is the bar wave speed, and w is the longitudinal displacement.

Boundary and Initial Conditions

These are the same as in Downey and Bogy (1987) with a few minor exceptions. From the assumptions of uniform normal contact traction and smooth contact we have

$$\tau_{zz}(r,0,t) = \begin{cases} -\dfrac{V_o}{E_1\tilde{c}_1}\sigma_z(0,t) & 0 \le r \le 1 \\ 0 & r \ge 1, \end{cases} \tag{11}$$
$$\tau_{rz}(r,0,t) = 0,$$

where

$$E_1 = 2\tilde{\mu}/E_o\kappa_o, \text{ a constant.} \tag{12}$$

The displacement of the rod tip is the average contact displacement of the half space:

$$w(0,t) = \frac{1}{\pi}\int_0^1 u_z(r,0,t)\,2\pi r\,dr. \tag{13}$$

The condition arising from the lumped mass on the trailing end of the rod is

$$\left[\frac{\partial w}{\partial z}\right]_{z=-L} = M\kappa_o^2\left[\frac{\partial^2 w}{\partial t^2}\right]_{z=-L}. \tag{14}$$

Downloaded 03 May 2010 to 171.66.16.27. Redistribution subject to ASME license or copyright; see http://www.asme.org/terms/Terms_Use.cfm

Finally the initial conditions on the half space and the rod are

$$\Phi=\frac{\partial\Phi}{\partial t}=\Psi=\frac{\partial\Psi}{\partial t}=w=0,$$

$$\frac{\partial w}{\partial t}=\frac{V_o}{\tilde{c}_1}, \text{ at } t=0. \tag{15}$$

Elastic Solution by Transforms

After applying Laplace transforms in time, and Hankel transforms in the radial variable to the above equations of elasticity, we obtain the following as solutions to the resulting differential equations,

$$\hat{\tilde{\Phi}}^0 = \frac{f(\xi,s)}{\xi}\, e^{-\alpha z},\ \alpha(\xi,s)=\left(\xi^2+\frac{\tilde{c}_1^2}{c_1^2}\, s^2\right)^{1/2}, \tag{16a}$$

$$\hat{\tilde{\Psi}}^1 = \frac{g(\xi,s)}{\xi}\, e^{-\beta z},\ \beta(\xi,s)=(\xi^2+\kappa^2 s^2)^{1/2}, \tag{16b}$$

$$\tilde{w} = A(s)\, e^{\kappa_o s z}+B(s)\, e^{-\kappa_o s z}+V_o/s^2\tilde{c}_1. \tag{16c}$$

The undetermined parameters are used to satisfy the boundary and initial conditions, and this yields

$$A(s) = -\frac{E_1}{P(s)E_1+sQ(s)\bar{F}(s)}\,\frac{V_o}{s^2\tilde{c}_1},$$

$$B(s) = A(s)\,\frac{(1-M\kappa_o s)}{(1+M\kappa_o s)}\, e^{-2\kappa_o L s},$$

$$f(\xi,s) = \frac{\tilde{\mu}sA(s)J_1(\xi)\,(\xi^2+\kappa^2 s^2/2)Q(s)}{\mu E_1 R(\xi,s)},$$

$$g(\xi,s) = \frac{\tilde{\mu}sA(s)J_1(\xi)\alpha\xi Q(s)}{\mu E_1 R(\xi,s)}, \tag{17}$$

where

$$P(s) = \left[1+\frac{1-M\kappa_o s}{1+M\kappa_o s}\, e^{-2\kappa_o L s}\right], \tag{18a}$$

$$Q(s) = \left[1-\frac{1-M\kappa_o s}{1+M\kappa_o s}\, e^{-2\kappa_o L s}\right], \tag{18b}$$

$$R(\xi,s) = (\xi^2+\kappa^2 s^2/2)^2-\xi^2\,\alpha(\xi,s)\beta(\xi,s), \tag{18c}$$

$$\bar{F}(s) = \frac{\tilde{\mu}\kappa^2 s^2}{\mu}\int_0^\infty \frac{\alpha J_1^2(\xi)}{\xi R(\xi,s)}\, d\xi. \tag{18d}$$

The parts of the solution we are interested in are the displacement of the rod into the half space, and the dependence of the interface traction on time. We use the solution for $\tilde{w}(s)$ in equation (16c) and substitute the transformed constitutive relation (9) and the parameters (17) to get the elastic solution in the Laplace domain as

$$\tilde{\sigma}_o(s)\,[\bar{F}(s)+\bar{G}(s)]=E_1/s^2,$$

$$\tilde{w}_o(s)\,[\bar{F}(s)+\bar{G}(s)]=(V_o/s^2\tilde{c}_1)\bar{F}(s), \tag{19}$$

where

$$\tilde{\sigma}_z|_{z=0}\equiv\tilde{\sigma}_o,\ \tilde{w}|_{z=0}\equiv\tilde{w}_o, \tag{20}$$

and

$$\bar{G}(s)=\frac{E_1 P(s)}{sQ(s)}. \tag{21}$$

The Viscoelastic Solution

At this point we can get the corresponding viscoelastic solution in the Laplace domain by substituting $\tilde{\lambda}(s)$ and $\tilde{\mu}(s)$ defined in equations (4) for λ and μ, respectively. Thus we have

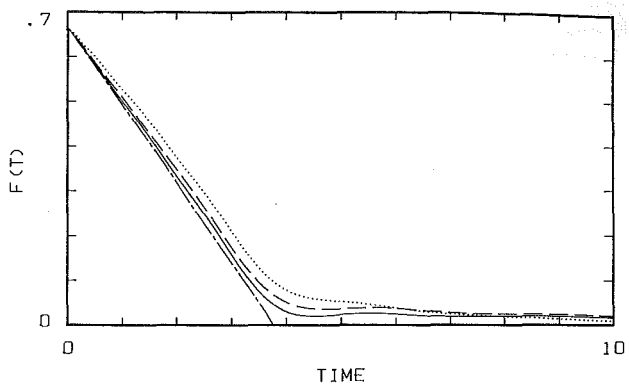


Fig. 2 Half-space portion of the kernel for $\alpha=0.75$. Dotted curve is for $\tau_\sigma=2$, dashed curve is for $\tau_\sigma=5$, solid curve is for $\tau_\sigma=10$ Chain-dashed curve is the elastic case.

$$\frac{\tilde{c}_1^2}{c_1^2} = \frac{(\tilde{\lambda}+2\tilde{\mu})}{[\tilde{\lambda}(s)+2\tilde{\mu}(s)]}=\frac{(s+1/\tau_\sigma)}{(s+\alpha/\tau_\sigma)},$$

$$\frac{\mu}{\tilde{\mu}} = \frac{\tilde{\mu}(s)}{\tilde{\mu}}=\frac{(s+\alpha/\tau_\sigma)}{(s+1/\tau_\sigma)},$$

$$\kappa^2 = \frac{\tilde{c}_1^2}{c_2^2}=\frac{(\tilde{\lambda}+2\tilde{\mu})}{\tilde{\mu}(s)}=\bar{\kappa}^2\,\frac{(s+1/\tau_\sigma)}{(s+\alpha/\tau_\sigma)},\ \bar{\kappa}^2\equiv\frac{\tilde{c}_1^2}{\tilde{c}_2^2}. \tag{22}$$

Then the only changes are in equations (18c), (18d), and $\alpha(\xi,s)$ and $\beta(\xi,s)$, which become

$$\bar{F}(s) = \bar{\kappa}^2 s^2\,\frac{(s+1/\tau_\sigma)^2}{(s+\alpha/\tau_\sigma)^2}\int_o^\infty \frac{\alpha(\xi,s)J_1^2(\xi)d\xi}{\xi R(\xi,s)},$$

$$\alpha(\xi,s) = \left(\xi^2+\frac{(s+1/\tau_\sigma)}{(s+\alpha/\tau_\sigma)}\, s^2\right)^{1/2},$$

$$\beta(\xi,s) = \left(\xi^2+\frac{\bar{\kappa}^2 s^2(s+1/\tau_\sigma)}{(s+\alpha/\tau_\sigma)}\right)^{1/2},$$

$$R(\xi,s) = \left(\xi^2+\frac{\bar{\kappa}^2 s^2(s+1/\tau_\sigma)}{2(s+\alpha/\tau_\sigma)}\right)^2-\alpha(\xi,s)\beta(\xi,s)\xi^2. \tag{23}$$

Now, provided $\bar{F}(s)$ and $\bar{G}(s)$ can be inverted, we can write the solution as a set of Volterra integral equations of the second kind, using the convolution theorem of Laplace transforms,

$$\int_o^t [F(t-\tau)+G(t-\tau)]\,\sigma_o(\tau)d\tau=E_1 t,$$

$$\int_o^t [F(t-\tau)+G(t-\tau)]\,w_o(\tau)d\tau=\frac{V_o}{\tilde{c}_1}\int_o^t F(t-\tau)\,\tau d\tau. \tag{24}$$

$G(t)$ has already been obtained by Downey and Bogy (1987), where we showed that it is the response of a rod to an impulsive load on the end opposite from the mass. Since this part depends only on the rod, it is unchanged. All that remains is to invert the other portion of the kernel $\bar{F}(s)$, which relates to the half space.

In the elastic case, $\bar{F}(s)$ was invertible in closed form using the method of Cagniard-de Hoop, but this approach does not go through in the viscoelastic case. Here it must be inverted using a numerical technique. In the previous paper, we showed that $F(t)$ represented the half space contribution in the kernel. In fact, we showed that it is the time response of the average surface displacement of a circular region of a half space subjected to a uniform impulsive normal load in the same region.

In the elastic case, as shown in Fig. 2, this average displacement $F(t)$ jumps after the impulse at $t=0$, then it declines almost linearly, reaching zero when the Rayleigh wave has traveled from one side of the contact region to the other. The

Downloaded 03 May 2010 to 171.66.16.27. Redistribution subject to ASME license or copyright; see http://www.asme.org/terms/Terms_Use.cfm

average displacement then remains at zero. For the viscoelastic case, we expect that the initial response will be identical, and then it should lag behind the elastic response.

It is important to realize that $F(t)$ depends only on three material parameters in the half space, Poisson's ratio and the two viscoelastic constants α and τ_σ. After $F(t)$ is determined for fixed values of these three parameters, it can be used in the integral equations for many different half-space moduli and densities, rod materials and density, and lumped masses. Thus only a few results for $F(t)$ are necessary to generate many solutions to our impact problem.

Numerical Inversion of $\bar{F}(s)$

The numerical technique used to invert the half-space portion of the kernel, $\bar{F}(s)$, is described by Doetsch (1971). Starting with the definition of the transform of $F(t)$,

$$\bar{F}(s) = \int_o^\infty F(t)e^{-st}dt, \tag{25}$$

we treat this as an integral equation for $F(t)$ given $\bar{F}(s)$ and we transform the infinite range of t to a finite interval with the substitution $t = y(\theta)$ defined by $e^{-pt} = \cos\theta$, where p is a positive parameter to be chosen. In addition we evaluate this at a sequence of s values, $s = (2n+1)p$. With these changes the integral equation becomes

$$p\bar{F}((2n+1)p) = \int_o^{\pi/2} \cos^{2n}\theta \sin\theta\, F(y(\theta))d\theta. \tag{26}$$

Then the unknown, $F(y(\theta))$ is expanded in a Fourier series of the functions $\sin(2m+1)\theta$, suggested by the fact that the kernel can be expressed as a linear combination of the same functions. The orthogonality of these functions is used to arrive at the following recursion formula for the Fourier coefficients:

$$[\binom{2n}{n} - \binom{2n}{n-1}]c_o + [\binom{2n}{k} - \binom{2n}{k-1}]c_{n-k} + \ldots + c_n = \frac{4^{n+1}}{\pi} p\bar{F}((2n+1)p). \tag{27}$$

We calculate these coefficients sequentially, first choosing p to provide the best results (for large t, p should be small and vice versa). Numerically it is only possible to compute about the first twenty coefficients, because of the cancellation errors introduced by the coefficients in equation (27) which become very large as n increases.

We also tried another method, described by Bellman et al. (1966), which is similar to the above technique but it employs Legendre polynomials after a different mapping. This was less suited to our problem, since it gave oscillatory results.

The major difficulty in implementing either method is the evaluation of $\bar{F}(s)$ for any s (equation (23a)). First, it is in the form of an infinite integral which converges like $(1/\xi^4)$, and second, the squared Bessel function in the integrand is highly oscillatory and always positive.

This leads to problems in the mapping onto a finite interval and also in carrying out the numerical integration. To overcome this we split the integration interval at some point q, and mapped each part separately onto [0, 1]. Thus

$$\int_o^\infty f(\xi)d\xi = \int_o^q f(\xi)d\xi + \int_q^\infty f(\xi)d\xi = \int_o^1 [qf(qx) + \frac{q}{x^2} f\left(\frac{q}{x}\right)]dx. \tag{28}$$

We see that the second part of the integrand used an inversion map, in which infinity maps to zero. With the proper choice of q this second part, which oscillates rapidly but is of small amplitude, gets added to the early large values from the first part, and they are relatively much less significant. The integration was performed satisfactorily with an eighty point Gauss-Legendre quadrature. The Bessel function was evaluated using its series representation for small arguments, and a rational approximation from Abramowitz and Stegun (1972) for large arguments.

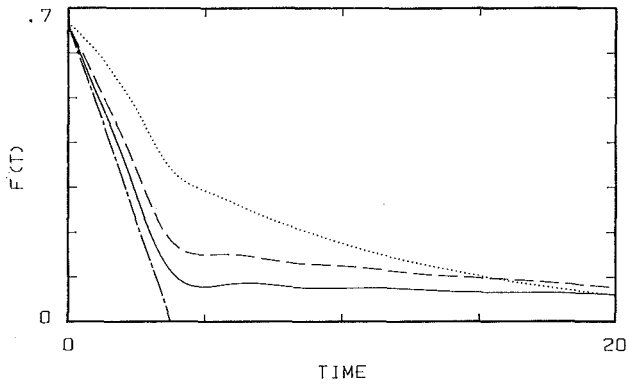


Fig. 3 Half-space portion of the kernel for $\alpha = 0.25$. Dotted curve is for $\tau_\sigma = 2$, dashed curve is for $\tau_\sigma = 5$, solid curve is for $\tau_\sigma = 10$. Chain-dashed curve is the elastic case.

Numerical Results for $F(t)$

Since the function $F(t)$ is the actual response of the simpler impulse-load half space problem described above, it is of interest in itself, providing physical insight into the effects of viscoelasticity on a half space.

All the numerical results obtained were for Poisson's ratio of 1/4, to allow comparison with the elastic results of Downey and Bogy (1987). $F(t)$ was calculated for nine cases using parameters from a matrix of three values each of the viscoelastic constants α and τ_σ. These were $\alpha = 0.75$, 0.5, 0.25, and $\tau_\sigma = 2$, 5, and 10.

The numerical inversion worked best for smaller stress relaxation times τ_σ. The small oscillations in the results (Figs. 2 and 3) are apparently caused by numerical inaccuracies, and they have been minimized by the proper choice of p. As a check on the accuracy of the numerical technique, we calculated $F(t)$ for the elastic solution, and found that it agreed with the closed form result of Matsumoto et al. (1978).

Figs. 2 and 3 show $F(t)$ corresponding to $\alpha = 0.75$ and 0.25, respectively, each with all three values of τ_σ. The elastic result is shown in both figures for comparison. The curves corresponding to $\alpha = 0.5$ are not presented, but they lie about midway between the two sets shown. One observes that as α approaches 1, which is the elastic limit, the results become closer to $F(t)$ of the elastic solution.

The initial jump in $F(t)$ after the impulse is the same in all cases, but it recovers slower for the viscoelastic than for the elastic half space, up until the Rayleigh wave time when the elastic result becomes identically zero. After this time, the viscoelastic half space shows a residual deflection that returns slowly to zero.

The Solution of the Integral Equations

Having obtained the values for the kernel functions, numerically solving the integral equations for the rod displacement and contact stress is quite straightforward. For this we use the method from Baker (1977). Having computed and stored the values for the kernel as described above, we use numerical quadrature for the integrals. This leads to a linear recursion relation that involves all previous solution values.

We show the results for two cases in Figs. 4 through 9. The first case has the half space Young's modulus and density

Downloaded 03 May 2010 to 171.66.16.27. Redistribution subject to ASME license or copyright; see http://www.asme.org/terms/Terms_Use.cfm

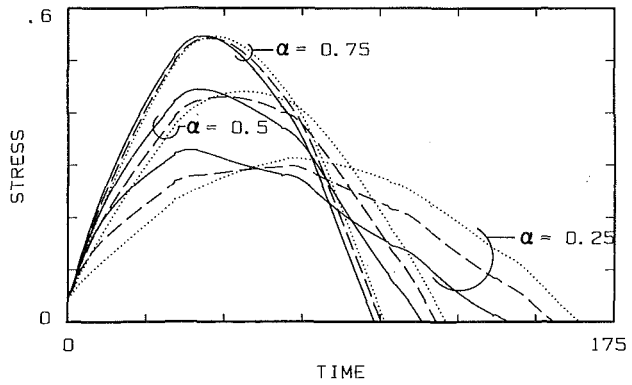


Fig. 4 Stress-time response for a rod with mass impacting a soft viscoelastic half space. Dotted curves are for $\tau_\sigma = 2$, dashed curves are for $\tau_\sigma = 5$, solid curves are for $\tau_\sigma = 10$. Three different α's are shown.

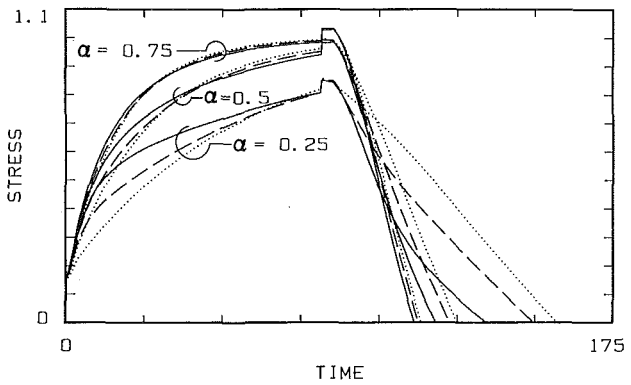


Fig. 7 Stress-time response for a rod with mass impacting a stiff viscoelastic half space. Dotted curves are for $\tau_\sigma = 2$, dashed curves are for $\tau_\sigma = 5$, solid curves are for $\tau_\sigma = 10$. Three different α's are shown.

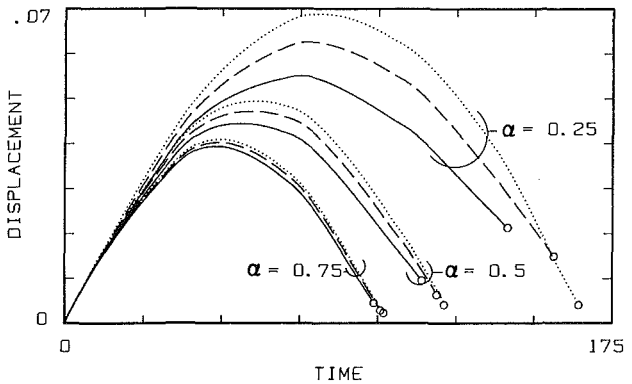


Fig. 5 Displacement-time response for a rod with mass impacting a soft viscoelastic half space. Dotted curves are for $\tau_\sigma = 2$, dashed curves are for $\tau_\sigma = 5$, solid curves are for $\tau_\sigma = 10$. Three different α's are shown.

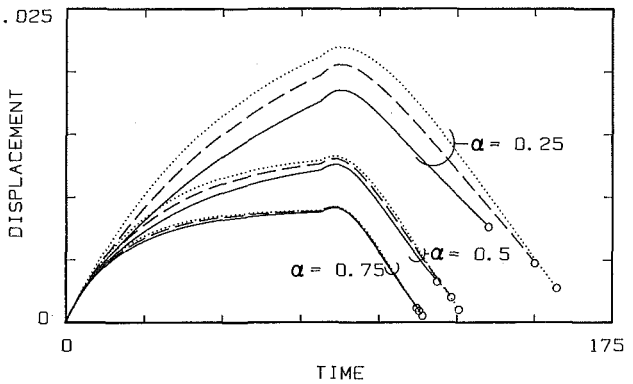


Fig. 8 Displacement-time response for a rod with mass impacting a stiff viscoelastic half space. Dotted curves are for $\tau_\sigma = 2$, dashed curves are for $\tau_\sigma = 5$, solid curves are for $\tau_\sigma = 10$. Three different α's are shown.

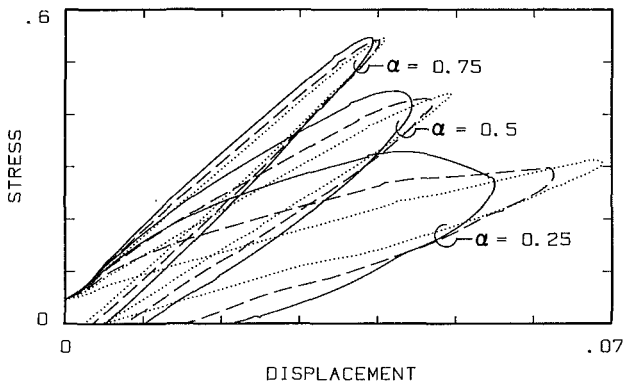


Fig. 6 Stress-displacement response for a rod with mass impacting a soft viscoelastic half space. Dotted curves are for $\tau_\sigma = 2$, dashed curves are for $\tau_\sigma = 5$, solid curves are for $\tau_\sigma = 10$. Three different α's are shown.

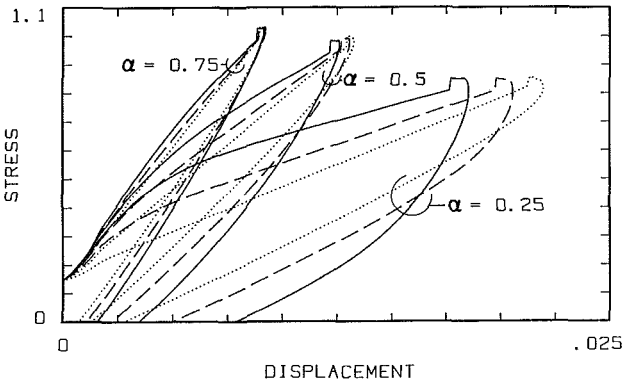


Fig. 9 Stress-displacement response for a rod with mass impacting a stiff viscoelastic half space. Dotted curves are for $\tau_\sigma = 2$, dashed curves are for $\tau_\sigma = 5$, solid curves are for $\tau_\sigma = 10$. Three different α's are shown.

equal to that of nylon ($E = 2.9$ GPa, and $\rho = 1135$ Kg/m^3), while Poisson's ratio is kept at 1/4. The rod material is steel, with a length of 50, and a lumped mass of 5 (ten percent of the rod mass).

The second case has a stiffer and more dense half space material for which $E = 24.1$ GPa and $\rho = 1666$ Kg/m^3. The rod and mass are unchanged. Each calculation is carried out until the contact stress becomes zero. At this time there is still some positive displacement of the rod, indicating the viscoelastic nature of the half-space recovery as the rod bounces off.

The first set of results are given in Figs. 4–6 and the second set in Figs. 7–9. Figures 4 and 7 present contact stress, Figs. 5 and 8 show contact displacement, and Figs. 6 and 9 show stress plotted against displacement to reveal the hysteresis in the contact history. The small kinks in the stress-time curves in Fig. 4 and somewhat larger ones in Fig. 7 occur when the wave front that is propagating back and forth in the rod arrives at the contact interface. The stiffer half space has only one rod reflection before bounce-off, as shown in Fig. 7, while the soft half space has up to four reflections, Fig. 4.

The results are very sensitive to the ratio, α, of stress relaxa-

Downloaded 03 May 2010 to 171.66.16.27. Redistribution subject to ASME license or copyright; see http://www.asme.org/terms/Terms_Use.cfm

tion time to strain relaxation time. For smaller values of α, the viscoelastic effects are larger, the peak stresses are smaller, and the displacements and the contact times are larger. If α is held constant, a change in the stress relaxation time, τ_σ, produces a less sensitive effect. A shorter τ_σ makes the half space somewhat softer, but the hysteresis is much greater when the stress relaxation time is longer.

The stress-time response of the stiff half space is much less sensitive to the parameters than the displacement-time result. This is associated with the fact that the stress approaches an asymptotic value. We showed (Downey and Bogy, 1987) that this asymptote is a function of just the rod material. Another interesting observaton for the stiff half space is the "jump" in stress when the first rod reflection arrives. This is due to the presence of the lumped mass, and it also appears in the elastic result.

The curves in Figs. 6 and 9 also show that smaller values of α give more hysteresis, but here changes in τ_σ have a much greater effect. The results for $\tau_\sigma = 10$ have much more hysteresis, and the combination of this and small α is the most dissipative.

Calculations performed for the soft half space, changing only the lumped mass on the rod to 12.5, gave results that are very similar in nature to Figs. 4–6 with slightly higher peak stress (about five percent), and longer contact times (about ten percent).

Conclusions

The solution obtained is in a quite satisfactory form, even though the half-space portion of the kernel must be obtained numerically. Since $F(t)$ depends only on Poisson's ratio and the two viscoelastic parameters, only a few cases need to be calculated to obtain solutions of the whole problem for a wide variety of materials and geometries. The integral equation is easy to solve numerically, having no singularities and requiring modest computer time.

The few cases we have presented here show that a broad range of responses can be obtained. For this reason it is hard to draw any general conclusions about the dependence of the results on all the parameters of interest. However, for a given geometry or material there are only a few parameters to vary, which allows useful conclusions to be drawn. For the cases we have considered, in which the rod material and geometry remained the same and only the half space material was varied, the trends are clear.

The viscoelastic parameters affected the results significantly, altering the effective stiffness and the losses, as shown in the hysteresis curves in Figs. 6 and 9. The combination of the two viscoelastic parameters that produce the most hysteresis, gives results that have some resemblance to measured force-displacement curves from wire matrix printing experiments (see Wang and Hall, 1983). The stress-time curves for the soft half space, Fig. 4, show much better agreement with those experiments than do the curves for the stiffer one, Fig. 7.

The results obtained here are promising, and appear to model actual wire-matrix printing behavior much better than the purely elastic half space. A logical next step is to solve the problem with a layer of viscoelastic material resting on an elastic half space.

Acknowledgment

This work was partially supported by an IBM Departmental Grant to the Department of Mechanical Engineering at UC Berkeley. H. A. D. would like to thank IBM in Charlotte, N. C., for its support under the IBM Resident Study Program.

References

Abramowitz, M., and Stegun, I. A., ed., 1972, *Handbook of Mathematical Functions*, Dover, New York, p. 370.

Baker, C. T. H., 1977, *The Numerical Treatment of Integral Equations*, Oxford University Press, Oxford, pp. 759-762.

Bellman, R., Kalaba, R. E., and Lockett, J. A., 1966, *Numerical Inversion of the Laplace Transform*, American Elsevier, New York, pp. 22-41.

Christensen, R. M., 1971, *Theory of Viscoelasticity*, Academic Press, New York, pp. 41-43.

Doetsch, G., 1971, *Guide to the Applications of the Laplace and Z-Transforms*, Van Nostrand-Reinhold, London, pp. 138-140.

Downey, H. A., and Bogy, D. B., 1987, "The Normal Impact on an Elastic Half Space of an Elastic Rod-Mass System," ASME JOURNAL OF APPLIED MECHANICS, to appear.

Matsumoto, H., Nakahara, I., and Matsuoka, Y., 1978, "The Impact of an Elastic Cylinder on an Elastic Solid," *Bulletin of the JSME*, Vol. 21, No. 154, pp. 579-586.

Wang, H. C., and Hall, S. A., 1983, "Paper-Function Model for Wire-Matrix Printing," *Proceedings of the Society for Information Display*, Vol. 24, No. 1, pp. 13-15.

Downloaded 03 May 2010 to 171.66.16.27. Redistribution subject to ASME license or copyright; see http://www.asme.org/terms/Terms_Use.cfm

M. Mayseless
Visiting Scholar.

W. Goldsmith
Professor,
Fellow ASME

S. P. Virostek
Research Assistant,
Assoc. Mem. ASME

Department of Mechanical Engineering,
University of California,
Berkeley, CA 94720

S. A. Finnegan
Engineering Science Division,
US Naval Weapons Center,
China Lake, CA 93555

Impact on Ceramic Targets

A series of approximately 150 tests were conducted on ceramic targets struck by cylindro-conical hard-steel projectiles at normal incidence up to velocities of about 1000 m/s. The primary objective was the determination of the effect of layering and the delineation of the ballistic limit of various combinations. In addition, a study of the erosive effect of the ceramic was executed. It was found that, on the basis of areal density, metal plates prefaced by ceramic materials are ballistically more inefficient than purely metallic targets in the low velocity range, while the reverse was found at speeds above 250 m/s. The eroded length was found to be related to the velocity of the projectile and the thickness of the ceramic layer. The projectile displacement data were found to be in very good accord with the results obtained from a previously utilized analytic force history taking into account the erosion process. The energy required to erode the projectile was found to be several orders of magnitude greater than that consumed in the fracture process of the frontal ceramic plate.

Introduction

A very large amount of effort has been devoted to the study of the problem of normal penetration of projectiles into homogeneous metal targets (Backman and Goldsmith, 1978). In contrast, only a limited amount of information has been published on the behavior of composite materials or combinations of these and other substances under impact conditions. It has been established that ceramic-faced targets represent a class of light armor that is highly efficient in reducing the penetrability of a given striker, but only a few publications are available on this subject, most of them dealing with experimental results, with some supplementation by computer analysis based on two-dimensional continuum-mechanics codes (Wilkins et al., 1969; Landingham and Casey, 1972; and Wilkins, 1978). This type of research was primarily aimed at delineating the principal mechanisms of response of such targets and to provide a limited data base for their application.

During the penetration process of cylindro-conical projectiles (which consist of a cylinder with a conical nose shape), the tip is significantly eroded because of the high amplitude stress wave generated as the result of the relatively large acoustic impedance of the ceramic and its much higher elastic compressive limit compared to hard steel. The ceramic is shattered in the vicinity of the impact point, with long radial fractures emanating from this region. Under certain circumstances, a set of concentric circumferential fractures also develops. In order to delay and minimize this breaking process, the ceramic should be backed by another plate. The most common materials previously utilized for this support are 6061-T6 aluminum and fiber glass. It was found that flexural strength and the ability to deflect without rupture both are fundamental requirements for the back-up plate (Wilkins et al. 1969). However, the investigation was limited to these two substances, and thus the effect of these mechanical properties was not quantitatively evaluated.

The objective of the present investigation is to provide some additional reliable data on the ballistic performance of the ceramic targets and the projectile erosion in order to create a basis for the development of an analytical model of the process. It is expected that such a model will incorporate the major features of the penetration process and will permit a prediction of the ballistic limit of the system and the final mass, length, and velocity of the projectile. However, the complexity of the phenomenon may require the conduct of additional tests before a reliable and comprehensive analytical representation of the event can be constructed.

Apparatus and Procedure

The present study involved the impact of 12.7 mm diameter hard-steel projectiles (oil hardened drill rod with a hardness of 60 R_c) with 60 deg conical tips at normal incidence. The projection devices consisted of a pneumatic gun limited to a velocity of 250 m/s and a powder gun with a range up to 1000 m/s for the projectiles employed which had an average mass of 30 g and a length of 38 mm. The ceramic targets consisted of alumina (AD-85 and AD-94) manufactured by Coors Corp. Backing materials employed included two types of aluminum, 2024-0 and 6061-T-6, two types of steel, SAE 1010 and 4130, as well as K29 Kevlar which was bonded under pressure in the laboratory with a polyester resin representing 43–47 percent of the composite volume, for a total specific gravity of 1.2. Three

Contributed by the Applied Mechanics Division for publication in the JOURNAL OF APPLIED MECHANICS.

Discussion on this paper should be addressed to the Editorial Department, ASME, United Engineering Center, 345 East 47th Street, New York, N.Y. 10017, and will be accepted until two months after final publication of the paper itself in the JOURNAL OF APPLIED MECHANICS. Manuscript received by ASME Applied Mechanics Division, June 23, 1986; final revision, October 20, 1986.

Copyright © 1987 by ASME
Downloaded 03 May 2010 to 171.66.16.27. Redistribution subject to ASME license or copyright; see http://www.asme.org/terms/Terms_Use.cfm

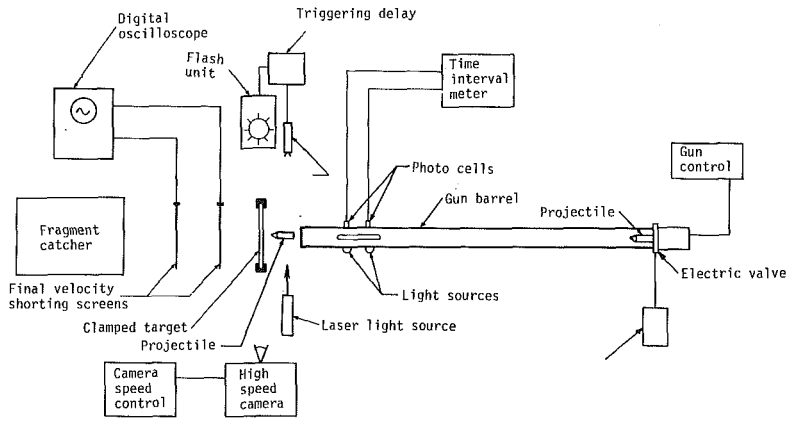


Fig. 1 Experimental arrangement

thicknesses of the ceramic were utilized: 3.18, 6.35, and 12.7 mm, while the backing ranged from 1.6 to 16 mm. The experimental arrangement is shown in Fig. 1. The initial velocity was measured by recording the signal produced by the interruption of two light beams passing through slits in the barrel. The terminal bullet speed was ascertained either by a similar device involving a laser net or by the shorting of an open circuit of a silver-painted grid, with a maximum error of about 2 percent. A high-speed framing camera with a capacity of 80 frames and rates up to 10^6 pictures per second or a 6-frame Kerr cell camera were employed to measure the kinematics of the projectile/target system. A substantial effort was made to prevent additional deformation or erosion of the striker after perforation; this was accomplished by decelerating the objects using soft materials such as clay or Celotex (Levy and Goldsmith, 1984; Goldsmith and Finnegan, 1971; and Liss and Goldsmith, 1984), after they passed through the targets.

The targets were clamped in a hard-steel holder either over the entire circumference or over 90 deg at the top and bottom in order to provide for photographic coverage. The clamping diameter was 114 mm; the diameter of the circular alumina plates was 130 mm, while that of the backing material was 140 mm. In all cases, the alumina was glued to its adjacent layers. The holder was constructed to permit an inclination of the target at increments of 10 deg; however, to avoid the likelihood of ricochet, the maximum angle was limited to 50 deg. The target holder was rigidly attached to a heavy stand and the center of the target was placed concentrically with the bore of the gun and approximately 380 mm in front of the muzzle. All fragments from the target combination remaining in the holder as well as those recovered in the surrounding area and catcher box were collected for later analysis. The bullet and all of its fragments were also retrieved and its terminal length and mass were recorded. The framing camera was operated at 2.5 - 10 μs intervals between exposures.

A total of 150 tests, primarily at normal incidence, involving either the ceramic by itself or various combinations were executed in the initial velocity range from 23 to 920 m/s. The majority of the experiments were carried out with 6.35 mm thick AD-85 ceramic. Force measurements using quartz crystals, previously executed for metallic plates (Levy and Goldsmith, 1984; and Liss and Goldsmith, 1984) were also performed in the present investigation, but will not be reported here, because they include the erosive effects and detailed wave structure that can be interpreted most effectively by a comprehensive model or computer code. Instead, the force history will be derived here from the displacement measurements using a simple model which ignores wave propagation and considers the mass loss of the projectile to be linear for the duration of the penetration.

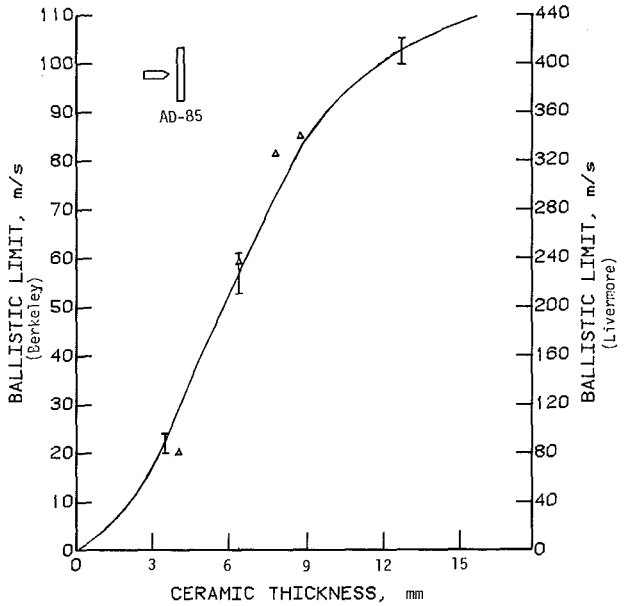


Fig. 2 Ballistic limit of AD-85 plates as a function of thickness for two cylindro-conical projectiles of 12.7 and 7.62 mm diameter: Symbol I: Berkeley data; triangles: Wilkins et al. (1969)

Results and Discussion

An initial series of shots was conducted to determine the ballistic limit (defined as the minimum velocity necessary to penetrate the target), of the AD-85 plates without any backing. The results are presented in Fig. 2 and compared with those extracted from Wilkins et al. (1969), with the origin of the data, Berkeley or Livermore, indicated on the axes. Both projectiles have the same general shape and are made from very similar steel, where the diameter of the projectile used by Livermore was 7.62 mm and its weight is 8.32 g. The solid line constitutes the optimal fit for the Berkeley results, and the triangular points constitute the information of Wilkins et al. (1969), either measured or extrapolated to zero backing thickness on the basis that the ballistic limit is linear with the thickness of the backing material below a value of 5 mm. This was demonstrated for the case of 6.35 mm thick plates of AD-85 (Wilkins et al., 1969). The results are virtually coincident when a factor of 4 is applied to the ballistic limit, as shown in the diagram. This factor is considered to be the result of the combination of the mass ratio of the two projectiles, which is equal to 3.5 and the 10 percent higher level of hardness of the Berkeley projectile, indicating that the major effect

Downloaded 03 May 2010 to 171.66.16.27. Redistribution subject to ASME license or copyright; see http://www.asme.org/terms/Terms_Use.cfm

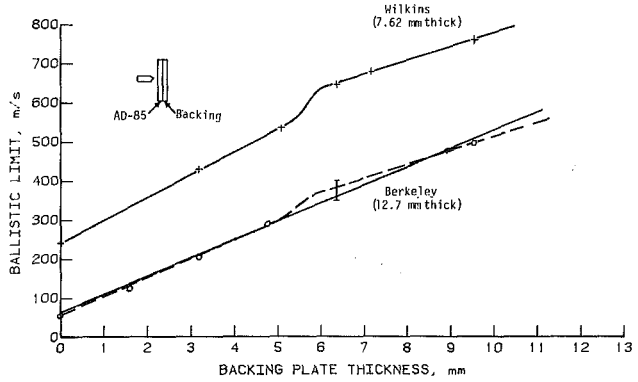


Fig. 3 Ballistic limit of 6.35 mm AD-85 aluminum as a function of 6061-T6 aluminum backing plate thickness: crosses: data from Wilkins et al., (1969); circles; current data. The results differ due to divergent bullet configurations.

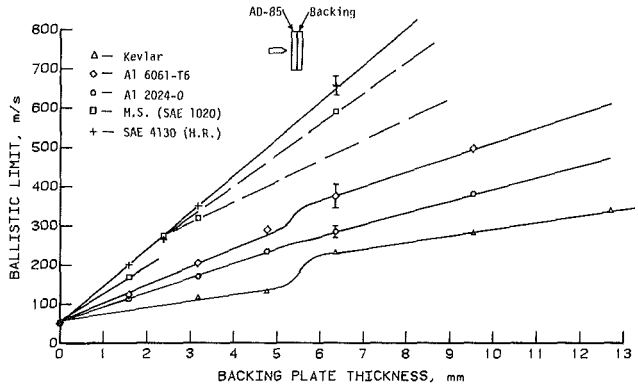


Fig. 4 Ballistic limit for the 6.35 mm thick AD-85 as a function of backing thickness for various materials

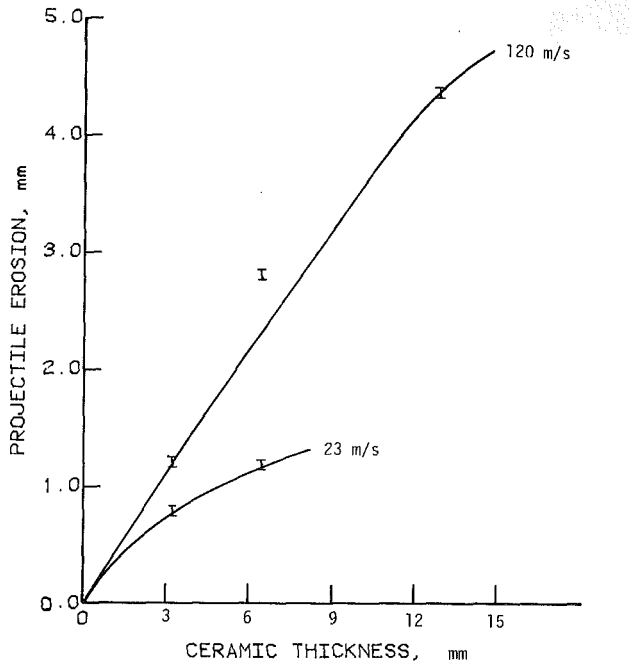


Fig. 5 Reduction of projectile length for the pure AD-85 ceramic as a function of thickness for two different initial velocities

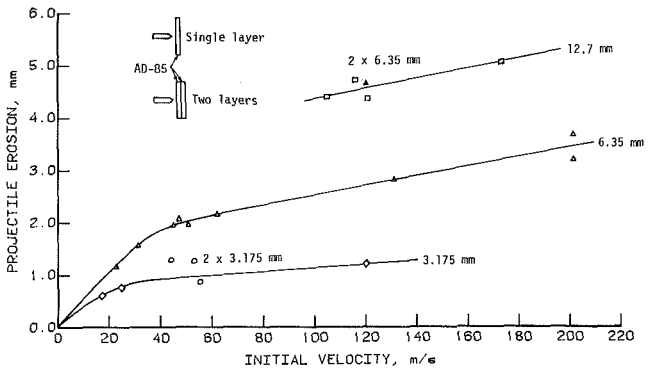


Fig. 6 Length reduction of the projectile for pure alumina targets as a function of striking velocity

on this ballistic limit is due primarily to the momentum of the striker.

The previous investigation (Wilkins et al., 1969) ascertained that the ballistic limit of combined ceramic/aluminum targets decreased linearly with the thickness of the ceramic for thicknesses of the 6061-T6 A1 rear plate from 5 to 7 mm. This was explained using the assumption that the ballistic limit of these targets is linearly proportional to the stress at the rear of the ceramic and that transmitted to the backup plate. The test results shown in Fig. 2 indicate that these observations of Wilkins et al. (1969) do not apply in the limit of zero-backing thickness and hence also probably not to large ratios of ceramic to rear-plate thickness.

A comparison of the results of the present investigation with that of Wilkins et al. (1969) for the case of a target composed of a 6.35 thick frontal layer of alumina backed by different thicknesses of 6061-T6 aluminum is presented in Fig. 3. In the Livermore case, an abrupt local change in the curve is noted when the backup plate thickness is between 5.5 and 6 mm. Due to some scattering in our experimental data for the same kind of backup material, it is not clear whether or not this kind of behavior is indicated by our results. However, it is clear that for Kevlar backup targets, we do see the so-called kink effect, as shown in Fig. 4. The previous work indicated that this kinking effect is diminished as the thickness of the ceramic is decreased. The present investigation shows that, in addition, this phenomenon also occurs with increased mass of the projectile. Furthermore, the location of the kink in Fig. 4 occurred at the same value of the backing thickness for two different projectile diameters, although Wilkins (1978) indicates that this position should scale with this parameter.

According to the momentum scaling the ballistic limit v is connected to the mass of the projectile m and the target thickness h through the scaling law $v_2/v_1 = (m_1/m_2)(h_2/h_1) = k$, where the subscripts 2 and 1 refer to two different cases. In the present instance, the simple momentum scaling that had been applied to targets composed solely of the ceramic appears to be valid only for very small back-up plate thicknesses, while this scaling appears to conform more nearly to an energy ratio where $v_2/v_1 = k^{1/2}$ in the vicinity of the kink. Above this regime, the ratio of the ballistic limits decreases still further. Extensive additional investigations are required to determine the reasons for the presence of the kink and the scaling factor over the entire range of backing plate and frontal layer thicknesses.

The effect of changing the material and thickness of the back-up plate for 6.35 mm thick alumina frontal layers is shown in Fig. 4. The ballistic limit increases with augmented tensile strength and acoustic impedance. The actual value of this parameter was estimated from shots that just barely penetrated or rebounded; this is indicated by the bar whenever the projectile was not embedded in the target. An examination of the Rockwell hardness of the mild steel layers used in the tests indicated that the 6.35 mm plate was 30 percent harder (on the Rockwell A scale) than those with smaller thicknesses

Downloaded 03 May 2010 to 171.66.16.27. Redistribution subject to ASME license or copyright; see http://www.asme.org/terms/Terms_Use.cfm

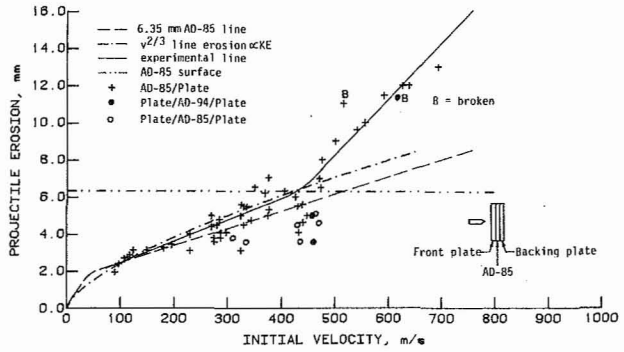


Fig. 7 Length reduction of the projectile for alumina targets as a function of a striking velocity. *B* denotes a broken projectile

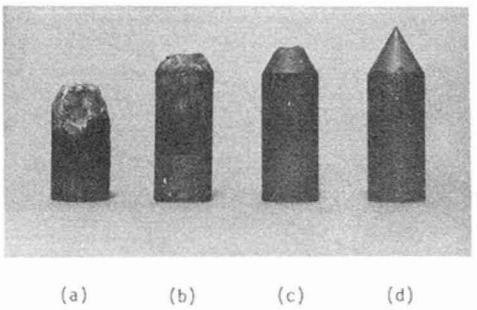


Fig. 8 Terminal projectile shapes showing erosion and comparison with original shape: *(a)* initial velocity: 690 m/s; 6.35 mm thick AD-85 backed by 6.35 mm hard steel; *(b)* initial velocity: 445 m/s; 6.35 mm thick AD-85 backed by 6.35 mm 2024-0 aluminum; *(c)*initial velocity: 120 m/s; 12.7 mm thick AD-85 with no backing; *(d)* original shape

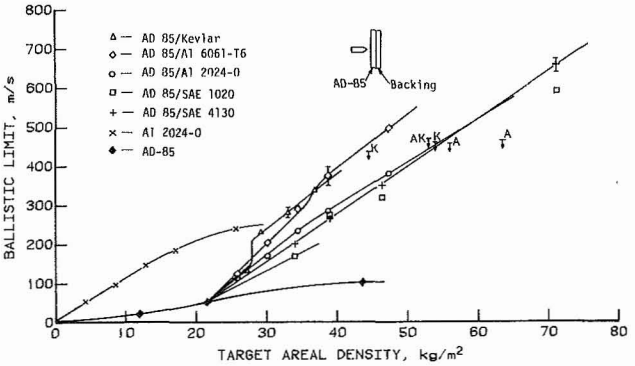


Fig. 9 Ballistic limit as a function of target areal density. Symbols *A* and *K* represent the soft aluminum and/or Kevlar frontal layers.

and its external appearance exhibited a much higher degree of brittleness. In consequence, this one value is questionable and this has been indicated by the presence of dashed lines. In general the hard steel resulted in a higher ballistic limit than for mild steel except for the 2.4 mm thickness; the reason for this aberration is currently unknown. This anomaly as well as the general trends exhibited in Fig. 4 will be further explored by the conduct of additional tests involving different thicknesses of the back-up plate and the ceramic, as well as the use of different types of materials and numbers of layers to provide the basis for a more comprehensive model of the process.

In order to better understand the erosion process and estimate the effectiveness of using the ceramic targets, the length and mass of the recovered projectiles were examined. The reduction in length due to erosion was found to be strongly dependent on the thickness of the ceramic as shown in Fig. 5 for pure ceramic targets struck at two different velocities. In the lower range of impact velocities, the amount of erosion is highly nonlinear in terms of the ceramic thickness, while exhibiting a more linear relation at higher velocities, at least up to 200 m/s. In an earlier investigation (Radin, 1987), it was found that layering of targets reduces the ballistic limit compared to monolithic plates of the same thickness. In order to assess the effect of layering of the ceramic on the erosion phase, tests were performed on two adjacent ceramic plates of the same thickness without either bonding or backing and compared with the results on a single plate of the same total thickness with the results shown in Fig. 6. It was found that the plates with a total thickness of 12.7 mm exhibited the same erosion characteristics as the single plate, whereas the two plates totalling 6.35 mm in thickness produced a substantially smaller erosion. It is believed that the reason for this behavior can be traced to the low tensile strength of the ceramic, and the substantially reduced bending stiffness of the thinner plate. In consequence, tensile waves reflected from the back surface will fracture the rear plate when sufficiently thin before the projectile has emerged from the target, thus reducing its ability to erode the bullet.

Figure 7 summarizes all the data on reduction in length of the projectile as the result of erosion produced by interaction with the ceramic-faced targets. The dashed line starting at the origin represents the data for bare 6.35 mm thick ceramic plates, duplicated from Fig. 6. It is evident that the general trend of the backing is to increase the erosion relative to that for the pure ceramic, since the integrity of the alumina is maintained for a longer period of time. A few points do not conform to this trend, perhaps due to either imperfections in the material or convexity between the mating surfaces.

All circled points comprise the data for sandwiched alumina components prefaced and backed by various materials. The open points define AD-85, while the solid circles represent AD-94. In all instances, this configuration reduced the eroded length compared to that produced by the pure ceramic or that with a backup. In a few instances, the impact also caused fracture of the projectile in which some sizeable pieces were separated, resulting in an overstatement of the actual eroded length, as indicated by the two data points labelled "B" in Fig. 7.

The dash-dot line in this diagram represents the hypothesis that the eroded volume of the projectile is proportional to its kinetic energy. During the diminution of the conical tip, this translates into a relation such that the eroded length varies with the 2/3 power of the velocity. On the other hand, in the cylindrical section, it is expected, according to this model, that the additional eroded length is proportional to the energy remaining after the erosion of the tip. This implies that the further reduction of the length in this region depends more strongly on initial velocity than in the frontal section. However, the experimental results indicate that the change in the velocity dependence occurs before the tip is fully eroded, corresponding to a point close to the thickness of the ceramic layer. Nevertheless, it was found that, at low velocities, the erosion produced a slightly concave crater that could, with good approximation, be considered plane; a transition occurred subsequently to generate convex terminal tip shapes as shown in Fig. 8. In consequence, at least one transition zone occurs during tip erosion, and a second change in the erosion dependence prevails in the transition from tip to shank due to geometric considerations.

The ballistic limit is also affected by the presence of a frontal layer, as shown in Fig. 9, as a function of areal density. All layered targets emanate from the line representing the pure ceramic. The Kevlar backing, which constituted the most inefficient barrier from the viewpoint of thickness, now is the most efficient rear layer based on density, rivalling that of the

Downloaded 03 May 2010 to 171.66.16.27. Redistribution subject to ASME license or copyright; see http://www.asme.org/terms/Terms_Use.cfm

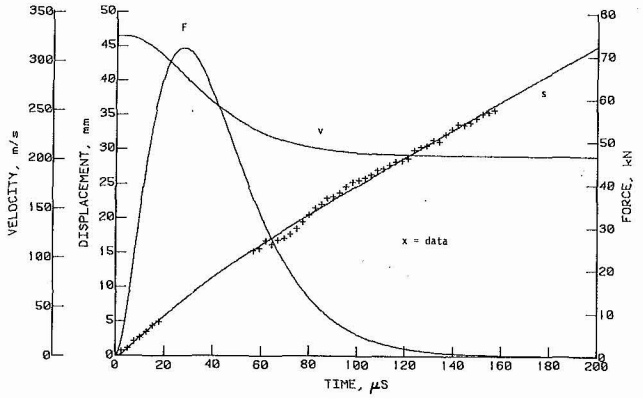


Fig. 10 Force *(F)*, velocity *(v)*, and displacement *(s)* computed from the force and mass models: impact velocity: 325 m/s; final measured velocity: 224 m/s; initial mass: 30.82 g; final mass: 30.58 g; τ = 45 μs

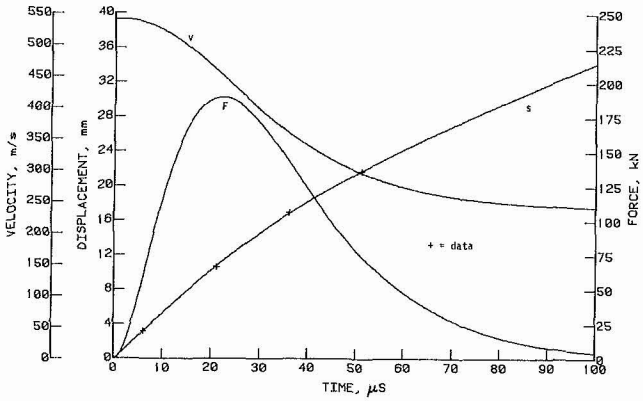


Fig. 11 Force *(F)*, velocity *(v)*, and displacement *(s)* computed from the force and mass models: impact velocity: 540 m/s; final estimated velocity: 220 m/s; initial mass: 29.9 g; final mass: 25.8 g; τ = 50 μs

hard aluminum. Up to a ballistic limit of 400 m/s, the soft aluminum is slightly more efficient than hard steel, but this trend is reversed above that level. The data represented by downward arrows constitute perforation events for the sandwiched targets so that the ballistic limit is lower than the peak level indicated. This indicates that the effect of sandwiching is to lower the ballistic limit relative to the areal density. A comparable phenomenon has been observed in the penetration of rotating projectiles of the same geometry (Yaziv et al., 1983). In our case this effect is due to smaller erosion of the projectile and probably earlier fracturing of the alumina caused by shock waves which precede the actual contact between the projectile and the ceramic. The curve also shows that, at low impact velocities, a metallic plate may be more efficient than either the pure ceramic or some ceramic-metal combinations.

High-speed camera data were accumulated for approximately twenty runs, and the corresponding displacement-time curves were plotted. In earlier investigations (Masket, 1949; and Calder and Goldsmith, 1971), it was found that the force history during penetration of plates could be reasonably approximated by the expression $F(t) = Ae^{-bt}t^2$, where A and b are constants. For a constant projectile mass, the corresponding acceleration can be integrated in closed form to obtain the displacement history. In the present case, the erosion process, but not wave propagation, was taken into account. The mass was represented by $m(t) = m_o - (\Delta m)\ t/\tau$ where m_o is the initial mass, $\Delta m = m_o - m_f$ is the mass lost by erosion, and τ is the erosion interval. The displacement is obtained by numerical evaluation of the ratio F/m, representing the instantaneous deceleration, with the constants optimally determined to provide the best fit with the displacement

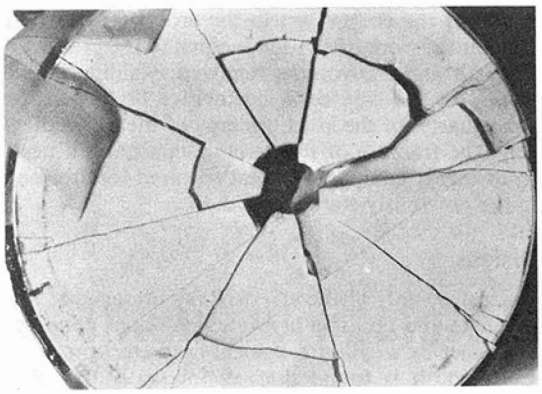


Fig. 12 Typical 6.35 mm thick AD-85 alumina frontal plate

measurements. The duration of contact, τ, is evaluated from the thickness of the ceramic layer, the terminal velocity, and the eroded length of the penetrator.

The high-speed camera typically provided seventy frames for the displacement determination, while the Kerr cell camera provided only six data points. Two representative results are depicted in Figs. 10 and 11 with the computed curves shown by solid lines. The targets for both runs involve a 6.35 mm AD 85 alumina plate prefacing a 6.35 mm thick Kevlar and 9.52 mm thick 6061-T6 A1 plate, respectively. In both cases, the calculated displacements are in very good accord with the mean value of the measured data. The small oscillation superposed on the average displacement in Fig. 10 was found to correspond to the double transit time of a longitudinal elastic wave in the projectile; this phenomenon cannot be observed in Fig. 11 due to the paucity of the data. The calculated final projectile velocity was within 10 percent of that measured for Fig. 10 and that estimated on the basis of the measured ballistic limit in Fig. 11. Consequently, the impulse exerted can be determined with a reasonable degree of accuracy. The ratio of the peak forces for these two cases is observed to correspond approximately to the square of the velocities, which is reasonable when the global behavior of the system is considered. The initial transient generated at the instant of impact, which consists of a very high stress of extremely short duration, cannot be determined with the optical equipment employed here, nor with force-measuring devices embedded in the rear of the projectile (Liss and Goldsmith, 1984). However, the overall phenomenon does not appear to be significantly affected by the presence of this first high-level pulse component; thus, it can be concluded that the impedance of the ceramic influences the event at most only in the first few microseconds due to the low strength of the ceramic and the conical shape of the striker.

The pulse width at the level of the average force corresponds very closely to the value calculated from the average projectile velocity and the total thickness of the target. For the case depicted in Fig. 10, the mean pulse duration was found to be 45 μs, compared to 48 μs obtained from the velocity calculation.

A typical ceramic plate reconstructed after impact is presented in Fig. 12. A conical region of crushed ceramic is invariably found directly behind the central hole. In addition, both radial and circumferential cracks are generated in the target. An estimate of the energy dissipated in these fracture processes is based on the assumption of a Mott distribution for the particle size within the conoid with the total surface area of these particles proportional to the two-thirds power of the total mass. For an estimated surface energy of the ceramic of 20 J/m^2 (A. Evans, Personal Communication), it was found that less than 2 J were consumed in the fracture of the

Downloaded 03 May 2010 to 171.66.16.27. Redistribution subject to ASME license or copyright; see http://www.asme.org/terms/Terms_Use.cfm

an estimate of the energy lost in the erosion process, it was assumed that the work of erosion is equal to the product of the yield strength and the volume removed, yielding a value of about 1 kJ for the case depicted in Fig. 11; this represents about one quarter of the kinetic energy of the projectile. Consequently, the fracture of the ceramic consumes a negligible amount of energy compared to that required for erosion, supporting the previously stated hypothesis.

Conclusions

An extensive study of the effect of the presence of alumina in both single and multiple layer targets under conditions of normal impact by a cylindro-conical hard-steel projectile has been executed. It is found that, at low velocities, a higher ballistic efficiency based on areal density is achieved by targets composed solely of one layer of metal, whereas at speeds above about 250 m/s, a higher efficiency is attained when a 6.35 mm thick layer of AD-85 alumina prefaces another layer of either metal or a fibrous composite. If another non-ceramic layer is placed in front of the alumina, the efficiency is once more reduced. The ballistic limit of the present tests is in agreement with scaled data obtained from smaller projectiles. The relation between the initial velocity and the ceramic layer thickness relative to the eroded length of the strikers was experimentally determined and was qualitatively found to be in agreement with a simple model of the process in the lower velocity range.

Acknowledgment

This work was sponsored by the Army Office of Research under Contract DAA629-80-K-052. The interest and assistance of The Ordnance Division of FMC Corporation in the conduct is appreciated.

References

Backman, M. E., and Goldsmith, W., 1978, "The Mechanics of Penetration of Projectiles into Targets," *International Journal of Engineering Science*, Vol. 16, pp. 1-99.

Calder, C. A., and Goldsmith, W., 1971, "Plastic Deformation and Perforation of Thin Plates Resulting from Projectile Impact," *International Journal of Solids Structures*, Vol. 7, 1971, pp. 863-881.

Goldsmith, W., and Finnegan, S. A., 1971, "Penetration and Peforation Processes in Metal Targets At and Above Ballistic Velocities," *International Journal of Mechanical Sciences*, Vol. 13, pp. 843-866.

Landingham, R. L., and Casey, A. W., 1972, "Final Report of the Light-Armor Materials Program," Lawrence Livermore National Laboratory, UCRL-51269.

Levy, N., and Goldsmith, W., 1984, "Normal Impact and Perforation of Thin Plates by Hemispherically-Tipped Projectiles – II. Experimental Results," *International Journal of Impact Engineering*, Vol. 2, pp. 299-334.

Liss, J., and Goldsmith, W., 1984, "Plate Perforation Phenomena Due to Normal Impact by Blunt Cylinders," *International Journal of Impact Engineering*, Vol. 2, pp. 37-64.

Masket, A. V., 1949, "The Measurement of Forces Resisting Armor Penetration," *Journal of Applied Physics*, Vol. 20, pp. 132-140.

Radin, J., 1985, "Normal Projectile Perforation of Layered Targets," Research Thesis, M. Sc., The Technion, Haifa, Israel, 1987.

Wilkins, M. L., 1978, "Mechanics of Penetration and Perforation," *International Journal of Engineering Science*, Vol. 16, pp. 793.

Wilkins, M. L., Cline, C. F., and Honodel, C. A., 1969, Light Armor," Lawrence Livermore National Laboratory, UCRL-71817.

Yaziv, D., Mayseless, M., Shevah, H., and Rosenberg, G., 1983, "Anomalous Effect in Perforation Shots of Lightweight Armor," *7th International Symposium on Ballistics*, The Hague, The Netherlands.

Downloaded 03 May 2010 to 171.66.16.27. Redistribution subject to ASME license or copyright; see http://www.asme.org/terms/Terms_Use.cfm

Plastic Stress Intensity Factors in Steady Crack Growth

P. Ponte Castañeda[1]
Division of Applied Sciences,
Harvard University,
Cambridge, MA 02138
Assoc. Mem. ASME

The asymptotic stress and deformation fields of a crack propagating steadily and quasi-statically into an elastic-plastic material, characterized by J_2-flow theory with linear strain-hardening, were first determined by Amazigo and Hutchinson (1977) for the cases of mode III and mode I (plane strain and plane stress). Their solutions were approximate in that they neglected the possibility of plastic reloading on the crack faces. This effect was taken into account by Ponte Castañeda (1987b), who also introduced a new formulation for the (eigenvalue) problem in terms of a system of first order O.D.E.'s in the angular variations of the stress and velocity components. The strength of the power-type singularity, serving as the eigenvalue, and the angular variations of the field were determined as functions of the hardening parameter.

The above analysis, however, does not determine the amplitude factor of these near-tip asymptotic fields, or plastic *stress intensity factor. In this work, a simple, approximate technique based on direct application of a variational statement of compatibility is developed under the assumption of small scale yielding. A trial function for the stress function of the problem, that makes use of the asymptotic information in the near-tip and far-field limits, is postulated. Such a trial function depends on arbitrary parameters that measure the intensity of the near-tip fields and other global properties of the solution. Application of the variational statement then yields optimal values for these parameters, and in particular determines the plastic stress intensity factor, thus completing the knowledge of the near-tip asymptotic fields. The results obtained by this novel method are compared to available finite element results.*

1 Introduction

In the propagation of cracks in ductile materials, a stage of stable crack growth, where the effects of inertia are unimportant, is often observed under continuously increasing external load, and immediately following the onset of crack growth. This phenomenon is intrinsic to the plastic deformation at the tip of a moving crack: as the crack propagates in an elastic-plastic material, it leaves behind a wake of residual plastic deformation, which typically accounts for all of the energy available from the external source, and thus reduces the tendency of the crack to grow unstably.

Under small scale yielding, which assumes that the size of the active plastic zone surrounding the crack tip is small compared to the crack size and the overall dimensions of the specimen in consideration, an appropriate measure of the external loading is the stress intensity factor of the enclosing elastic singularity fields. In accord with the discussion in the previous paragraph, it has been postulated that the graph of such elastic stress intensity factor versus the amount of crack growth, called the resistance curve, is a material property for small scale yielding.

Central to these notions, and to the continued development of fracture mechanics in general, is the knowledge of the stress and deformation fields near the tip of the advancing crack in elastic-plastic materials, and important advances have been made in recent years.

Most of the work, however, has been in the context of the ideal elastic-plastic solid. McClintock (1958) and McClintock and Irwin (1965) were the first to demonstrate that the key to stable crack growth lies in the nature of the plastic deformation, and found that the strains in the active plastic zone near the tip of the crack depend logarithmically on the radial distance from the crack tip, r. Later, Chitaley and McClintock (1971) gave the correct asymptotic solution to the problem of a steadily and quasi-statically mode III crack growing in an ideal elastic-plastic material with Mises yield criterion. Rice (1974) demonstrated that the same logarithmic dependence of the strains on r would be expected for the cases of plane stress and plane strain. Slepyan (1974) obtained the first correct asymptotic solution of the plane strain problem in modes I and II using a Tresca yield criterion. Rice et al. (1980), following Rice and Sorensen (1978), and Gao and Hwang (1980), independently, solved the plane strain problem in mode I using a Mises yield criterion, but the validity of their solution was restricted to the case of $\nu = 1/2$, where ν is Poisson's ratio. Somewhat later, Drugan et al. (1982) generalised the results to

[1] Currently at The Department of Mechanical Engineering, The Johns Hopkins University, Baltimore, MD 21218.

Contributed by the Applied Mechanics Division for publication in the JOURNAL OF APPLIED MECHANICS.

Discussion on this paper should be addressed to the Editorial Department, ASME, United Engineering Center, 345 East 47th Street, New York, N.Y. 10017, and will be accepted until two months after final publication of the paper itself in the JOURNAL OF APPLIED MECHANICS. Manuscript received by ASME Applied Mechanics Division, July 24, 1986; final revision, December 1, 1986.

Copyright © 1987 by ASME
Downloaded 03 May 2010 to 171.66.16.27. Redistribution subject to ASME license or copyright; see http://www.asme.org/terms/Terms_Use.cfm

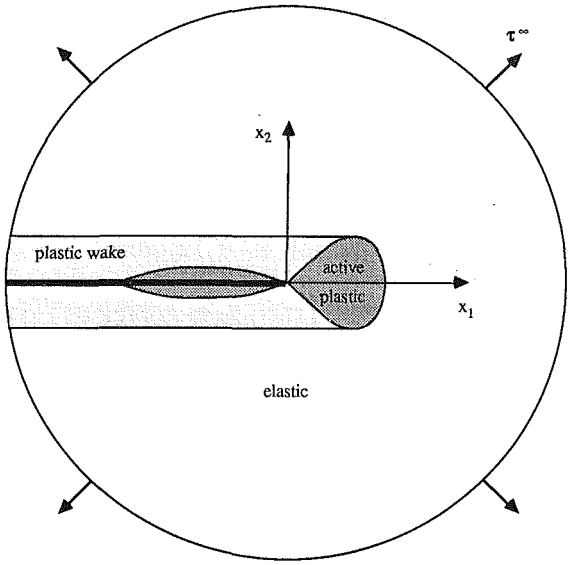


Fig. 1 Steadily-propagating crack in small scale yielding

the case of $\nu \neq 1/2$. The plane-stress mode I problem has remained most elusive, but recently, Ponte Castañeda (1986) produced a solution to the corresponding mode II problem, that also shed some light on the analytical difficulties of the mode I problem. In addition, a general discussion of the subject can be found in Rice (1982).

The corresponding work for the hardening elastic-plastic solid is at a less developed stage, and most of this work relates to the linear-hardening case. Slepyan (1973), using a modified J_2-deformation theory, produced the first asymptotic solution to the problem of a mode III crack propagating steadily in a linear-hardening material. Much later, Ponte Castañeda (1987a) extended Slepyan's work to the mode I case. Amazigo and Hutchinson (1977), using J_2-flow theory, produced steady-state asymptotic solutions for the moving crack in antiplane strain, as well as in plane strain and plane stress mode I. For a linear-hardening material, with Young's modulus, E, and tangent modulus, E_t, they found a variable-separable solution with stress and strain fields having a power singularity of strength, s, which is a function of the hardening ratio, $\alpha = E_t/E$, and vanishes in the perfectly-plastic limit. These solutions, however, neglected the possibility of plastic reloading on the crack flanks which is known to occur in the elastic-perfectly plastic solutions mentioned above. In a recent publication, Zhang et al. (1983) included reloading (as well as a Bauschinger effect) in their solution of the plane-strain mode I problem. More recently, but independently, Ponte Castañeda (1987b) advanced a new formulation of the problem in terms of a system of first order O.D.E.'s in the angular variations of the components of the stress and velocity fields, and included as well the effect of reloading in the solution of the antiplane strain, plane strain and plane stress (modes I and II) problems.

All these asymptotic solutions leave undetermined certain parameters in the expressions for the stress and deformation fields near the tip of the moving crack. In the perfectly-plastic case, the parameter in question is related to the size of the plastic zone ahead of the crack, but this parameter does not appear in the lowest order term of the asymptotic expansion of the fields as $r \to 0$. On the other hand, in the linear-hardening case, by analogy with the elastic problem, the amplitude of the lowest order term of the asymptotic expansion of the stress and deformation fields, as measured by the *plastic* stress intensity factor, is undetermined from the asymptotic analysis, and its determination introduces an important problem.

In this paper, we make use of the near-tip information available from the work of Ponte Castañeda (1987b) to complete the knowledge of the asymptotic fields of a steadily propagating crack in a linear-hardening material under small scale yielding conditions. This is accomplished by determining approximately the plastic stress intensity factor of these near-tip fields as a function of the hardening parameter. Other relevant information, such as the approximate size and shape of the active plastic zones, will result as by-products of our calculations.

Following an original idea by Budiansky (1986), we develop a simple, approximate technique based on a direct application of an appropriately chosen variational statement of compatibility. Thus we propose a trial function for the stress function of the problem, that makes use of the known asymptotic information in the near-tip and far-field limits, and depends on arbitrary parameters that measure the intensity of the near-tip fields and other global properties of the solution. Application of the variational statement then yields optimal choices for the values of these parameters, and hence determines the plastic stress intensity factor of the near-tip fields. The results obtained by this novel method will be compared to the finite element method results of Dean and Hutchinson (1980), Dean (1983), and Mataga (1986) for the linear-hardening material.

2 Antiplane Strain (Mode III)

2.1 The Plastic Stress Intensity Factor in Small Scale Yielding. Consider the steadily-propagating, semi-infinite crack depicted in Fig. 1. The Cartesian coordinate system $x_i (i = 1, 2, 3)$ convects with the crack tip, keeping its orientation fixed. The polar coordinates r, θ correspond to the inplane Cartesian coordinates $x_\alpha (\alpha = 1, 2)$. Under the small scale yielding assumption, the elastic singularity field is imposed in the remote limit so that the stress and velocity fields far away from the tip are given by

$$\tau(r,\theta) \sim K^{el}\bar{\tau}^\infty(\theta)(2\pi r)^{-1/2} \equiv \tau^\infty \quad \text{as } r\to\infty, |\theta| < \pi \qquad (2.1)$$
$$v(r,\theta) \sim -2(V/G)K^{el}\bar{v}^\infty(\theta)(2\pi r)^{-1/2} \equiv v^\infty$$

where τ^∞, v^∞ refer to the elastic fields, K^{el} is the *elastic* stress intensity factor, G is the modulus of elasticity in shear, V is the propagating speed of the crack, and $\bar{\tau}^\infty(\theta)$, $\bar{v}^\infty(\theta)$ are the well-known angular variations of the elastic fields in mode III, normalized such that $\bar{\tau}_2^\infty(0) = 1$ for consistency with the definition of K^{el}.

On the other hand, we require that in the near-tip limit

$$\tau(r,\theta) \sim K^{pl}\bar{\tau}^o(\theta)(2\pi r)^s \equiv \tau^o \quad \text{as } r\to 0 \qquad (2.2)$$
$$v(r,\theta) \sim K^{pl}(V/G)\bar{v}^o(\theta)(2\pi r)^s/s \equiv v^o$$

where τ^o, v^o refer to the near-tip solutions of Ponte Castañeda (1987b), K^{pl} defines the *plastic* stress intensity factor in small scale yielding, $s = s(\alpha)$ is the strength of the plastic singularity, and the angular variations of these near-tip fields, which are also functions of α, have been normalized such that $\bar{\tau}_2^o(0) = 1$.

For convenience, we make use of the dimensionless variables

$$\underline{r} = (\tau_o/K^{el})^2 r$$
$$\underline{\tau}_\alpha = \tau_\alpha/\tau_o \qquad (2.3)$$
$$\underline{v} = (G/\tau_o)(v/V)$$

where τ_o is the yield stress in shear.

In terms of these new variables the remote fields can be rewritten as

Downloaded 03 May 2010 to 171.66.16.27. Redistribution subject to ASME license or copyright; see http://www.asme.org/terms/Terms_Use.cfm

$$\underline{\tau}^{\infty}(r,\theta) = \bar{\tau}^{\infty}(\theta)(2\pi\underline{r})^{-1/2}$$
$$\underline{v}^{\infty}(r,\theta) = -2\,\bar{v}^{\infty}(\theta)(2\pi\underline{r})^{-1/2} \tag{2.4}$$

and the near-tip fields as

$$\underline{\tau}^{o}(r,\theta) = \kappa\,\bar{\tau}^{o}(\theta)(2\pi\underline{r})^{s}$$
$$\underline{v}^{o}(r,\theta) = \kappa\,\bar{v}^{o}(\theta)(2\pi\underline{r})^{s}/s \tag{2.5}$$

where κ is the dimensionless plastic stress intensity factor, and clearly depends only on α.

It follows from this nondimensionalization that the plastic stress intensity factor may be expressed as

$$K^{p1} \equiv \lim_{r\to 0}\,(2\pi\underline{r})^{-s}\tau_2(r,0) = \kappa(\alpha)\,(\tau_o)^{1+2s}\,(K^{e1})^{-2s} \tag{2.6}$$

and it now remains to determine the functional dependence of κ on α.

Note that, trivially, in the elastic limit we must have $K^{p1} = K^{e1}$, which implies that

$$\kappa(1) = 1$$

Alternatively, it is expected from the work of Chitaley and McClintock (1971) that in the perfectly-plastic limit $K^{p1} = \tau_o$, and therefore

$$\kappa(0) = 1$$

Note that, because the range of dominance of the near-tip asymptotic fields is expected to vanish as $\alpha \to 0$, this last statement should be interpreted with care (i.e., in some limiting sense).

2.2 The Variational Statement of the Problem. We wish to develop a simple, approximate method to determine the functional dependence of κ on α. In this connection we propose to make use of the following variational statement of compatibility:

Let A be the domain of the boundary value problem, with boundaries C_T and C_v, where the traction τ_n and the velocity v are prescribed, respectively.

If the stress field τ satisfies equilibrium

$$\nabla\cdot\tau = 0 \text{ in A} \tag{2.7a}$$

and the homogeneous boundary condition

$$\tau_n = \tau\cdot\mathbf{n} = 0 \text{ on } C_T \tag{2.7b}$$

and if the functional relation

$$\int_A \mathbf{G}\cdot\delta\tau\,dA = \int_{C_v} v^{*}\delta\tau_n\,ds \tag{2.7c}$$

*between the engineering strain rate **G**, and the velocity, prescribed on C_v, v^{*}, holds for arbitrary variations of the stress field $\delta\tau$, that satisfy conditions (2.7a) and (2.7b).*

*Then the strain-rate field **G** is compatible*

$$\mathbf{G} = \nabla v \tag{2.7d}$$

and the associated velocity field v satisfies the boundary condition

$$v = v^{*} \text{ on } C_v \tag{2.7e}$$

The constitutive relation to be used in conjunction with this statement is

$$\underline{\mathbf{G}} = \underline{\mathbf{T}} + \underline{\mathbf{G}}^{p1} \tag{2.8}$$

where $\underline{\mathbf{G}}$ is the dimensionless engineering strain-rate vector, $\underline{\mathbf{T}}$ is the dimensionless stress-rate vector, and

$$\underline{\mathbf{G}}^{p1} = \begin{cases} 0 & \text{in } A_e \\ (\alpha^{-1}-1)(\dot{\underline{\tau}}_e/\underline{\tau}_e)\underline{\tau} & \text{in } A_p \end{cases} \tag{2.9}$$

is the dimensionless plastic strain-rate vector, which depends on whether the material particle is in an *active* plastic zone A_p, or in a zone of current *elastic* behavior A_e. In this last equation, $\underline{\tau}_e$ is the magnitude of the stress vector, and ($\dot{}$) is the material derivative.

There are several good reasons for this particular variational statement. First, the choice of compatibility over equilibrium makes it easier to compute all the quantities involved in the variational statement, due to the specific nature of the constitutive relation. In fact, with the introduction of a stress function f, which ensures satisfaction of (2.7*a*) and (2.7*b*), we can easily compute all the quantities involved in the variational statement via simple differentiation

$$\underline{\tau} = \nabla \times (f\mathbf{e}_3)$$
$$\underline{\mathbf{T}} = -\dot{\underline{\tau}}_{,\underline{1}} \tag{2.10}$$

The analogous computations would necessarily have involved integrations as well as differentiations had a variational statement of equilibrium been selected. Second, the choice of a rate formulation is also most convenient, since it effectively ignores the plastic strains in the nonactive (wake) plastic zone. Finally, note that the choice of variations of stress rate, instead of variations of stress, in the variational statement would have led to unbounded integrals in the sequel.

The approximation in the method then consists in postulating the following *trial* function for f

$$f(\underline{r},\theta) = p(\underline{r})f^{o}(\underline{r},\theta) + q(\underline{r})f^{\infty}(\underline{r},\theta) \tag{2.11}$$

where

$f^{o}(\underline{r},\theta) = \kappa(\alpha)g^{o}(\theta)\underline{r}(2\pi\underline{r})^{s}$, $g^{o}(\theta) = -\bar{\tau}_{\theta}^{o}(\theta)/(1+s)$

is the stress function associated with the near-tip fields,

$f^{\infty}(\underline{r},\theta) = g^{\infty}(\theta)\underline{r}(2\pi\underline{r})^{-1/2}$, $g^{\infty}(\theta) = -2\cos(\theta/2)$

is the stress function associated with the remote fields, and where $p(\underline{r})$ and $q(\underline{r})$ are chosen so that the resulting stress and deformation fields conform with the given asymptotic conditions, i.e., equations (2.1) and (2.2). Hence, we must require

$$p(0) = 1 \quad p(\infty) = 0$$
$$q(0) = 0 \quad q(\infty) = 1$$

Also, since we must have that $f = f^{o} = f^{\infty}$ for $\alpha = 1$, we require that $p(\underline{r}) + q(\underline{r}) = 1$ for $\alpha = 1$. For simplicity, we select our trial functions $p(r)$ and $q(r)$ such that $p(\underline{r}) + q(\underline{r}) = 1$ for all values of α. Although two other possibilities were explored, it was found that

$$p(\underline{r}) = \gamma^2/(\gamma^2+\underline{r}^2) \quad \text{and} \quad q(\underline{r}) = \underline{r}^2/(\gamma^2+\underline{r}^2) \tag{2.12}$$

with γ arbitrary, gave the least numerical difficulties, and for that reason they were selected to be used in equation (2.11). In order to assess the accuracy of the proposed method, other choices for $p(r)$ and $q(r)$ should be explored in detail, and the results compared, but in this first study of the method, no such attempt will be made.

Having specified f, we use equations (2.10) to evaluate $\underline{\tau}$ and $\underline{\mathbf{T}}$

$$\underline{\tau}_1 = f_{,\underline{2}} = \sin\theta\, f_{,\underline{r}} + \underline{r}^{-1}\cos\theta\, f_{,\theta}$$
$$\underline{\tau}_2 = -f_{,\underline{1}} = -\cos\theta\, f_{,\underline{r}} + \underline{r}^{-1}\sin\theta\, f_{,\theta}$$
$$\underline{T}_1 = -f_{,\underline{21}} = -(1/2)\sin 2\theta\,(f_{,\underline{rr}} - \underline{r}^{-1}f_{,\underline{r}} - \underline{r}^{-2}f_{,\theta\theta}) - \cos 2\theta(\underline{r}^{-1}f_{,\underline{r}\theta} - \underline{r}^{-2}f_{,\theta})$$
$$\underline{T}_2 = f_{,\underline{11}} = \cos^2\theta\, f_{,\underline{rr}} + \sin^2\theta(\underline{r}^{-2}f_{,\theta\theta} + \underline{r}^{-1}f_{,\underline{r}}) - \sin 2\theta(\underline{r}^{-1}f_{,\underline{r}\theta} - \underline{r}^{-2}f_{,\theta})$$

In these expressions, the computation of the partial derivatives with respect to $\underline{r}$ is straightforward, but yields lengthy expressions which we will not include here, and the computation of the partials with respect to θ involves the following derivatives of $g^{o}(\theta)$

Downloaded 03 May 2010 to 171.66.16.27. Redistribution subject to ASME license or copyright; see http://www.asme.org/terms/Terms_Use.cfm

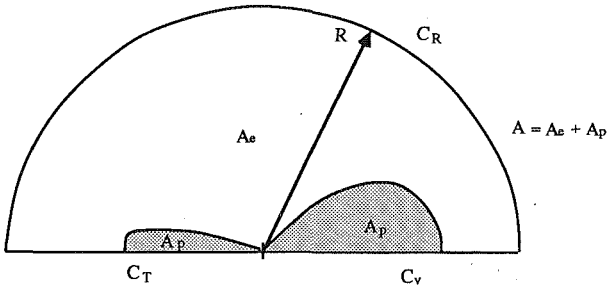


Fig. 2 *Domain for the variational statement of the steadily-propagating crack in SSY*

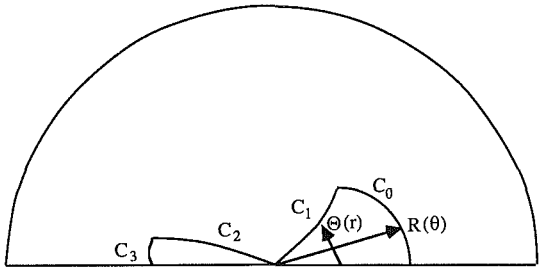


Fig. 3 **The elastic-plastic boundaries for the steadily-propagating crack in SSY**

$$(g^o)'(\theta) = \bar{\tau}_r^o(\theta) \quad (g^o)''(\theta) = (\bar{\tau}_r^o)'(\theta)$$

which are expressed in terms of quantities readily available from the numerical integration of system (2.5) in Ponte Castañeda (1987b).

The next step is to evaluate the variation of $\underline{\tau}$. Assuming that κ and γ are independent parameters, we have

$$\delta\underline{\tau} = (\partial\underline{\tau}/\partial\kappa)\delta\kappa + (\partial\underline{\tau}/\partial\gamma)\delta\gamma$$

Finally, we apply the variational statement to an appropriate domain A as shown in Fig. 2. A has been chosen for convenience to be a semicircle of large radius R, and is composed of two parts: the active plastic zones A_p and the zone of current elastic behavior A_e. Note that on the crack face C_T, $\tau_n = 0$ as required by equation (2.7*a*), and that on the line ahead of the crack C_v

$$v^* = 0 \Rightarrow \int_{C_v} v^* \delta\tau_n ds = 0$$

On the rest of the boundary C_R, we assume that R is large enough that we can take $v^* = v^\infty$. Then

$$v^* = O(r^{-1/2}) \text{ and } \delta\tau_n = O(r^{s-2}) \Rightarrow \int_{C_R} v^* \delta\tau_n ds \to 0 \text{ as } R \to \infty$$

Thus the variational statement reduces to

$$\int_A \underline{\mathbf{T}} \cdot (\partial\underline{\tau}/\partial\kappa) dA + (\alpha^{-1} - 1) \int_{A_p} (\dot{\underline{\tau}}_e/\underline{\tau}_e)\underline{\tau} \cdot (\partial\underline{\tau}/\partial\kappa) dA = 0$$

$$\int_A \underline{\mathbf{T}} \cdot (\partial\underline{\tau}/\partial\gamma) dA + (\alpha^{-1} - 1) \int_{A_p} (\dot{\underline{\tau}}_e/\underline{\tau}_e)\underline{\tau} \cdot (\partial\underline{\tau}/\partial\gamma) dA = 0 \tag{2.13}$$

where A is now the upper-half plane $x_2 \geq 0$, and A_p refers only to the active plastic zones. Note, therefore, that the plastic wake does not enter directly in the calculation of $\kappa(\alpha)$, and also, remarkably, that no integrations are needed beyond the quadrature of the explicit integrals in equations (2.13). Note further that, although the fields (and in fact also some of the integrands in (2.13)) are singular, and the domain of integration is unbounded, the integrals themselves are bounded.

Equations (2.13) form a system of two algebraic equations in κ and γ to be solved numerically using a secant method

Table 1 **The values of κ and γ as functions of α for antiplane strain**

α	κ	γ
0.9	1.030	2.895
0.8	1.044	1.880
0.7	1.054	1.524
0.6	1.058	1.318
0.5	1.055	1.163
0.4	1.044	1.006
0.3	1.005	0.685
0.2	0.976	0.513
0.1	0.943	0.509

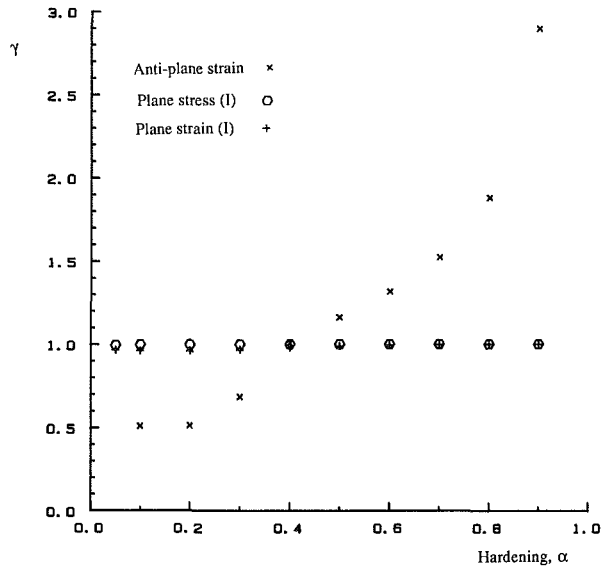


Fig. 4 **Plots of κ versus α for antiplane strain, plane strain (I) and plane stress (I)**

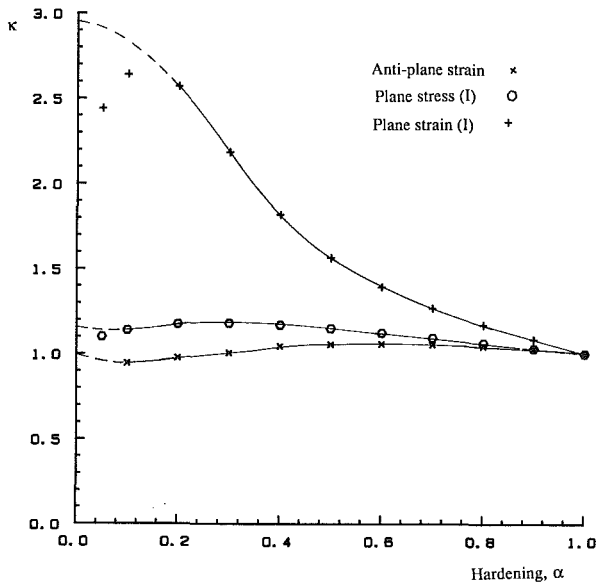


Fig. 5 **Plots of γ versus α for antiplane strain, plane strain (I) and plane stress (I)**

Downloaded 03 May 2010 to 171.66.16.27. Redistribution subject to ASME license or copyright; see http://www.asme.org/terms/Terms_Use.cfm

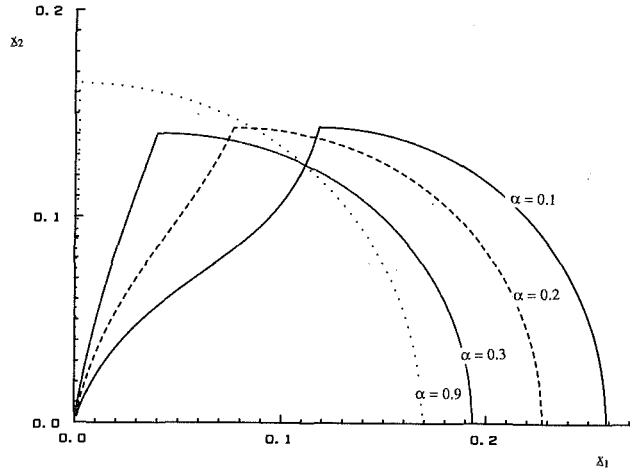


Fig. 6 Active plastic zones in antiplane strain

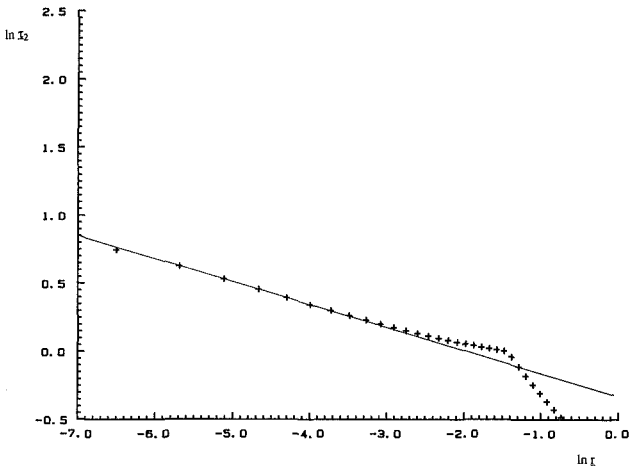


Fig. 7 F.E.M. results for the stress ahead of the crack ($\alpha = 0.1$)

Table 2 A comparison of the values of s and κ for antiplane strain

α	s	s^*	κ	κ^*
0.9	-0.483	-0.475	1.030	1.01
0.5	-0.394	-0.375	1.055	1.02
0.3	-0.325	-0.297	1.005	1.01
0.2	-0.276	-0.247	0.976	0.99
0.1	-0.207	-0.169	0.943	0.98

(*) F.E.M. results.

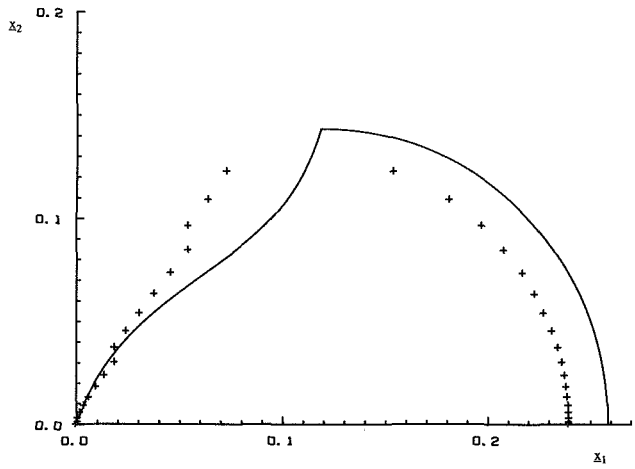


Fig. 8 Comparison of the F.E.M. active plastic zones in antiplane strain ($\alpha = 0.1$)

package available from I.M.S.L. The area integrals were evaluated as iterated integrals using successive Gaussian quadratures. The difficulty in the known singularity in r (as $r \to 0$) was treated by subtracting the singularity from the integrand and evaluating its contribution analytically. Alternatively, the difficulty in the known singularity in θ (as $\theta \to \pi$), was treated by a stretching technique.

For completeness sake, let us state the conditions that determine the elastic-plastic boundaries shown in Fig. 3. The plastic loading boundary C_0 is determined by the condition

$$\underline{\tau}_e^2 = \underline{\tau}_1^2 + \underline{\tau}_2^2 = 1$$

which is interpreted as an algebraic equation for the radial coordinate of the boundary $\underline{R}$ as a function of θ.

The elastic unloading boundary C_1 is determined by the condition

$$\underline{\tau}_e \dot{\underline{\tau}}_e = \underline{\tau}_1 \underline{T}_1 + \underline{\tau}_2 \underline{T}_2 = 0$$

which in turn is interpreted as an algebraic equation for the angular coordinate of the boundary Θ as a function of $\underline{r}$.

In antiplane strain, we will not consider values of the hardening parameter for which reloading takes place, and therefore we will not discuss reloading here, but it is clear that similar treatments would apply to the determination of the plastic reloading boundary C_2 and the secondary elastic unloading boundary C_3 (if necessary).

2.3 Results. The results of the numerical calculations are given in Table 1, and are depicted in Figs. 4 and 5. We observe that for mode III, $\kappa(\alpha)$ remains roughly constant, but γ varies dramatically, especially near $\alpha = 1$. As we have already remarked, $\kappa(1)$ is expected to be unity, but on the other hand, $\gamma(\alpha)$ is not determined by our choice of $p(\underline{r})$ and $q(\underline{r})$ as $\alpha \to 1$ (note that $p + q = 1$, independently of the value of γ), and hence its steep behavior near $\alpha = 1$ is not too disturbing. In the limit of small α, the behavior of κ seems to be consistent with $\kappa \to 1$, as expected, but our results are not conclusive since we do not trust our trial function for f for very small α. This is due to the fact that the limit as $\alpha \to 0$ of the near-tip fields is not uniform, and the range of dominance of these fields vanishes (see Ponte Castañeda, 1987b).

Figure 6 shows the active plastic zones corresponding to several values of α. Observe that the plastic zone is shifted forward as α decreases. Also note that there is a sharp kink at the intersection of the plastic loading and elastic unloading boundaries.

Next we will compare our results with the finite element method results for linear-hardening in mode III of Dean and Hutchinson (1980), as improved by Mataga (1986). Figure 7 is a logarithmic plot of his results for $\underline{\tau}_2$ in the line ahead of the crack versus $\underline{r}$, and corresponds to $\alpha = 0.1$. Similar plots were obtained for other values of α. Assuming that the power singularity solution holds close to the crack tip, we have that

$$\underline{\tau}_2(r,0) = \kappa^* \underline{r}^{s^*}$$

and therefore

$$ln\ \underline{\tau}_2(r,0) = ln\ \kappa^* + s^* ln \underline{r}$$

Thus fitting a straight line through those points in Fig. 7 that are close to the tip (but far from the elastic-plastic boundary,

Downloaded 03 May 2010 to 171.66.16.27. Redistribution subject to ASME license or copyright; see http://www.asme.org/terms/Terms_Use.cfm

which shows as a kink in the graph) allows us to compute values for s^* and κ^*. Table 2 shows the results for several values of α, and how they compare with our results for s and κ. It is found that s^* is not in good *quantitative* agreement with the theoretically correct s, particularly for the smaller values of α. Given this, we can only conclude that κ^* is in adequate *qualitative* agreement with κ.

Figure 8 compares the active plastic zone corresponding to the finite element method (crosses) with our plastic zone (solid line) for the particular value of $\alpha = 0.1$. Similar results were obtained for other values of α. In general, it is found that our plastic zones have the same general shape as the finite element plastic zones; however, it is not clear which plastic zones are more accurate. The finite element plastic zones probably suffer from inaccuracy due to the relative coarseness of the grid, particularly at the unloading boundary far away from the tip, where the results are very sensitive to the flat variation of τ_e. Alternatively, our results are probably not very good for the smaller values of α due to the expected decrease in the range of dominance of the near-tip fields.

3 Plane Strain (Mode I)

3.1 The Plastic Stress Intensity Factor in Small Scale Yielding. In plane strain the appropriate dimensionless variables are

$$\underline{r} = (\sigma_o/K^{el})^2 r$$
$$\underline{\sigma}_{\alpha\beta} = \sigma_{\alpha\beta}/\sigma_o \quad \underline{\sigma}_{33} = \sigma_{33}/\sigma_o \tag{3.1}$$
$$\underline{v}_\alpha = (E/\sigma_o)(v_\alpha/V)$$

where σ_o is the yield stress in tension.

Under small scale yielding conditions, the remote fields in dimensionless form are

$$\underline{\sigma}^\infty(r,\theta) = \underline{\sigma}^\infty(\theta)(2\pi\underline{r})^{-1/2} \qquad |\theta| < \pi \tag{3.2}$$
$$\underline{v}^\infty(r,\theta) = -2\,\tilde{v}^\infty(\theta)(2\pi\underline{r})^{-1/2}$$

where $\tilde{\sigma}^\infty(\theta)$ and $\tilde{v}^\infty(\theta)$ refer once again the well-known elastic angular variations, normalized such that $\tilde{\sigma}_{22}{}^\infty(0) = 1$.

The near-tip fields are

$$\underline{\sigma}^o(r,\theta) = \kappa\,\tilde{\sigma}^o(\theta)(2\pi\underline{r})^s$$
$$\underline{v}^o(r,\theta) = \kappa\,\tilde{v}^o(\theta)(2\pi\underline{r})^s/s \tag{3.3}$$

where now $s = s(\alpha, \nu)$, and the near-tip angular variations have also been normalised such that $\tilde{\sigma}_{22}{}^o(0) = 1$. It is clear from dimensional considerations that under small scale yielding conditions $\kappa = \kappa(\alpha, \nu)$, and therefore

$$K^{pl} = \lim_{r\to 0}(2\pi\underline{r})^{-s}\sigma_{22}(r,0) = \kappa(\alpha,\nu)(\sigma_o)^{1+2s}(K^{el})^{-2s} \tag{3.4}$$

Note that in the elastic limit we must have

$$\kappa(1,\nu) = 1$$

and that due to the high level of triaxiality in the line ahead of the propagating crack in the perfectly-plastic material (see Rice, 1980), we expect to have

$$\kappa(0,\nu) \cong 3$$

the exact value depending on the specific value of ν.

3.2 The Variational Statement of the Problem. In plane strain the appropriate variational statement of compatibility is:

If

$$\sigma_{\alpha\beta,\beta} = 0 \text{ in } A \tag{3.5a}$$
$$T_\alpha = \sigma_{\alpha\beta}n_\beta = 0 \text{ on } C_T \tag{3.5b}$$

and if

$$\int_A D_{\alpha\beta}\delta\sigma_{\alpha\beta}dA = \int_{C_v} v_q{}^*\delta T_\alpha ds \tag{3.5c}$$

for arbitrary $\delta\sigma_{\alpha\beta}$ *satisfying* (3.5*a*) *and* (3.5*b*).

Then

$$D_{\alpha\beta} = (1/2)(v_{q,\beta} + v_{\beta,\alpha}) \tag{3.5d}$$

and

$$\nu_\alpha = \nu_\alpha{}^* \text{ on } C_v \tag{3.5e}$$

where A, C_T, and C_v have the same meaning as before.

The constitutive relation in dimensionless form states

$$\underline{D}_{\alpha\beta} = (1+\nu)\underline{\Sigma}_{\alpha\beta} - \nu(\underline{\Sigma}_{\alpha\alpha} + \underline{\Sigma}_{33})\delta_{\alpha\beta} + \underline{D}_{\alpha\beta}{}^{pl} \tag{3.6}$$

where $\underline{\mathbf{D}}$ is the strain-rate tensor, $\underline{\Sigma}$ is the stress-rate tensor, and

$$\underline{D}^{pl}_{\alpha\beta} = \begin{cases} 0 & \text{in } A_e \\ (3/2)(\alpha^{-1}-1)(\underline{\dot{\sigma}}_e/\underline{\sigma}_e)\underline{S}_{\alpha\beta} & \text{in } A_p \end{cases} \tag{3.7}$$

refers to the plastic strain-rate tensor. Here

$$\underline{\sigma}_e{}^2 = \underline{\sigma}_{11}{}^2 + \underline{\sigma}_{22}{}^2 + \underline{\sigma}_{33}^2 + \underline{\sigma}_{12}{}^2 - \underline{\sigma}_{11}\underline{\sigma}_{22} - \underline{\sigma}_{22}\underline{\sigma}_{33} - \underline{\sigma}_{33}\underline{\sigma}_{11}$$

We can automatically satisfy (3.5*a*) by means of a stress function f such that

$$\underline{\sigma}_{11} = f_{,\underline{22}} \quad \underline{\sigma}_{22} = f_{,\underline{11}} \quad \underline{\sigma}_{12} = -f_{,\underline{12}} \tag{3.8}$$

In addition, we require $\underline{\sigma}_{33}$, which is determined by the plane-strain condition

$$\underline{D}_{33} = 0 = \begin{cases} \underline{\Sigma}_{33} - \nu\,\underline{\Sigma}_{\alpha\alpha} & \text{in } A_e \\ \underline{\Sigma}_{33} - \nu\,\underline{\Sigma}_{\alpha\alpha} + (3/2)(\alpha^{-1}-1)(\underline{\dot{\sigma}}_e/\underline{\sigma}_e)\underline{S}_{33} & \text{in } A_p \end{cases} \tag{3.9}$$

But this in general involves solving a complicated differential equation for $\underline{\sigma}_{33}$ in A_p, unless one is prepared to modify the variational statement. The difficulty is avoided by restricting our consideration to the case of $\nu = 1/2$, when

$$\underline{\sigma}_{33} = (1/2)\underline{\sigma}_{\alpha\alpha} \quad \text{in } A \tag{3.10}$$

The procedure for determining κ is then analogous to that of the mode III case. We take

$$f(\underline{r},\theta) = p(\underline{r})f^o(\underline{r},\theta) + q(\underline{r})f^\infty(\underline{r},\theta) \tag{3.11}$$

where now

$$f^o(\underline{r},\theta) = \kappa\,g^o(\theta)\underline{r}^2(2\pi\underline{r})^s,$$
$$g^o(\theta) = \tilde{\sigma}_{\theta\theta}{}^o(\theta)/[(1+s)(2+s)]$$
$$f^\infty(\underline{r},\theta) = g^\infty(\theta)\underline{r}^2(2\pi\underline{r})^{-1/2},$$
$$g^\infty(\theta) = (1/3)[3\cos(\theta/2) + \cos(3\theta/2)]$$

and where $p(\underline{r})$ and $q(\underline{r})$ are again given by equations (2.12).

Given f we use equations (3.8) to compute the stress components. We also compute the stress-rate components from

$$\underline{\Sigma}_{11} = -f_{,\underline{221}} \quad \underline{\Sigma}_{22} = -f_{,\underline{111}} \quad \underline{\Sigma}_{12} = f_{,\underline{112}} \quad \underline{\Sigma}_{33} = (1/2)\underline{\Sigma}_{\alpha\alpha}$$

In these calculations the following derivatives of $g^o(\theta)$ are needed

$$(g^o)'(\theta) = -\tilde{\sigma}_{r\theta}{}^o(\theta)/(1+s)$$
$$(g^o)''(\theta) = \tilde{\sigma}_{rr}{}^o(\theta) - (2+s)g^o(\theta)$$
$$(g^o)'''(\theta) = (\tilde{\sigma}_{rr}{}^o)'(\theta) - (2+s)(g^o)'(\theta)$$

all of which are expressed in terms of quantities readily available from the numerical integration of system (3.5) in Ponte Castañeda (1987b).

The variation of the stresses is obtained by assuming κ and γ to be independent

$$\delta\underline{\sigma}_{\alpha\beta} = (\partial\underline{\sigma}_{\alpha\beta}/\partial\kappa)\delta\kappa + (\partial\underline{\sigma}_{\alpha\beta}/\partial\gamma)\delta\gamma$$

Downloaded 03 May 2010 to 171.66.16.27. Redistribution subject to ASME license or copyright; see http://www.asme.org/terms/Terms_Use.cfm

Table 3 The values of κ and γ for plane strain mode I ($\nu = 1/2$)

α	κ	γ
0.9	1.085	1.001
0.8	1.170	1.001
0.7	1.268	0.999
0.6	1.392	0.995
0.5	1.565	0.989
0.4	1.817	0.980
0.3	2.184	0.968
0.2	2.568	0.960
0.1	2.640	0.960

and again it is found that if we take A to be the upper-half plane

$$\int_{C_v} v_\alpha^* \delta T_\alpha ds = 0$$

Thus the variational statement reduces to

$$\int_A [(1+\nu)\underline{\Sigma}_{\alpha\beta}\delta\underline{\sigma}_{\alpha\beta} - \nu(\underline{\Sigma}_{\alpha\alpha}+\underline{\Sigma}_{33})\delta\underline{\sigma}_{\alpha\alpha}]dA$$

$$+(\alpha^{-1}-1)\int_{A_p}(\underline{\dot{\tau}}_e/\underline{\tau}_e)[(3/2)\underline{\sigma}_{\alpha\beta}\delta\underline{\sigma}_{\alpha\beta} - (1/2)(\underline{\sigma}_{\alpha\alpha}+\underline{\sigma}_{33})\delta\underline{\sigma}_{\alpha\alpha}]dA = 0 \quad (3.12)$$

where A_p refers to the active plastic zones (both plastic loading and reloading.)

Again, for the case of $\nu = 1/2$, no integrations are needed beyond those explicitly shown in the variational statement, which provides a system of two nonlinear alebraic equations κ and γ to be solved for given α.

3.3 Results. The results of the numerical calculations for $\nu = 1/2$ are presented in Table 3, and are shown graphically in Figs. 4 and 5. It is observed that κ increases from unity as α decreases, whereas γ remains roughly constant for all α. However, it is found that even though the resulting values of κ for $\alpha = 0.05$ and 0.1 seem to be inconsistent with the rest of the values of κ, the general trend of κ as α approaches zero, outlined in the figure, is consistent with the perfectly-plastic result of $\kappa \cong 2.9476$ (Slepyan, 1974). The anomalous behavior of our small-α results for κ is a direct consequence of the deficiency in the values of s for small α (see Ponte Castañeda, 1987b).

The active plastic zones corresponding to several values of α are shown in Fig. 9, where the axis coordinates have been appropriately nondimensionalized. In spite of our comments in the previous paragraph, we have included in this figure the plastic zones corresponding to values of α equal to 0.05 and 0.1, for the purpose of explicitly showing some plastic reloading zones, which are an important feature of the plane-strain mode I problem. Another interesting feature is the fact that the extent of the plastic zones in the line ahead of the crack, r_p, is small, and in fact vanishes for $\alpha = 1$ and again for $\alpha \sim 0.1$. The fact that r_p vanishes for $\alpha = 1$ is intrinsic to the $\nu = 1/2$ case, but the fact that it vanishes again for $\alpha \sim 0.1$, depending on the specific value of ν, is more interesting, and its source can be traced to a change in sign of the quantity

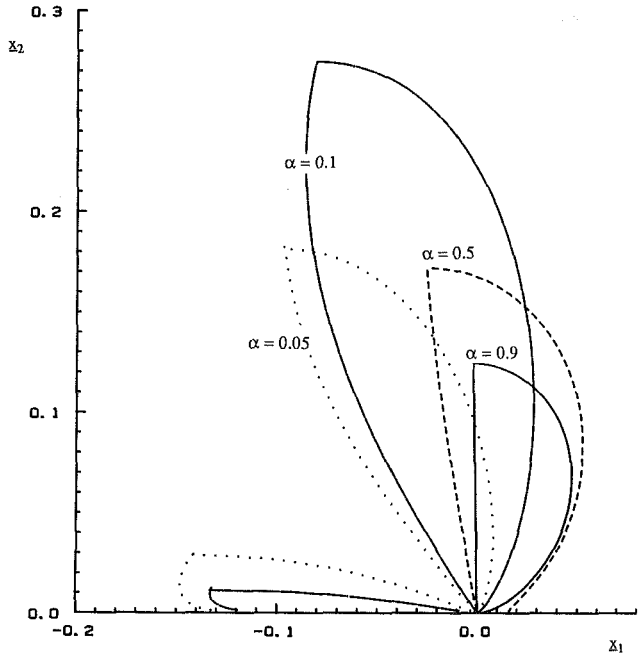


Fig. 9 Active plastic zones in plane-strain mode I

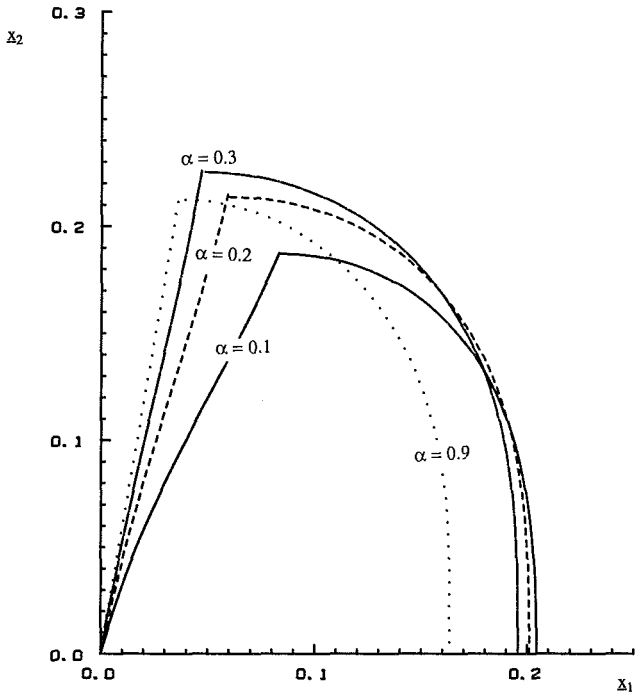


Fig. 10 Active plastic zones in plane-stress mode I

$\underline{\sigma}_{rr}^{\,o}(r, 0) - \underline{\sigma}_{\theta\theta}^{\,o}(r, 0)$, which forces $\underline{\sigma}_e^{\,o}(r, 0)$ to vanish when α takes on the critical value.

Unfortunately, no finite element results of the linear-hardening plane-strain mode I problem are available for comparison. Dean and Hutchinson (1980) only considered power hardening in mode I, and their results are quite different from ours.

4 Plane Stress (Mode I)

4.1 The Plastic Stress Intensity Factor. In plane stress the appropriate dimensionless variables are the same as in plane strain as given by equations (3.1) with the exception of $\underline{\sigma}_{33}$,

Downloaded 03 May 2010 to 171.66.16.27. Redistribution subject to ASME license or copyright; see http://www.asme.org/terms/Terms_Use.cfm

Table 4 The values of κ and γ for plane stress mode I ($\nu = 1/2$)

α	κ	γ
0.9	1.031	1.000
0.8	1.063	1.000
0.7	1.093	1.001
0.6	1.122	1.001
0.5	1.148	1.000
0.4	1.169	1.000
0.3	1.179	1.000
0.2	1.173	0.999
0.1	1.137	0.997

which is set equal to zero. The remote fields are given by equations (3.2), where $\tilde{\sigma}^{\infty}_{\alpha\beta}(\theta)$ and $\tilde{v}^{\infty}_{\alpha}(\theta)$ now correspond to the plane stress elastic angular variations. The near-tip fields have the same form as equations (3.3), but the strength of the singularity, and the angular variation of the fields are given in Section 4 of Ponte Castañeda (1987b). The plastic stress intensity factor then has the same general form as (3.4), where again $\kappa = \kappa(\alpha, \nu)$.

4.2 The Variational Statement of the Problem. The same development for plane strain applies for plane stress, provided that we set $\underline{\sigma}_{33}$ equal to zero, and we evaluate the pertinent quantities that go into the variational statement (3.12) using the appropriate near-tip and remote fields. Note that because $\underline{\sigma}_{33}$ is equal to zero, independently of the value of ν, the variational statement applies equally well for any value of ν. For definiteness, however, we will perform the computations here for $\nu = 1/2$ only.

Note that unlike s, which is known to be independent of ν, κ appears to be a function of ν as well as α. This is analogous to the corresponding stationary crack problem. Nevertheless, we expect κ to become independent of ν in the limit as α approaches zero, since it can be shown (Rice, 1982) that the stress field of the perfectly-plastic problem in plane stress is independent of ν.

4.3 Results. The results of the calculations corresponding to the value of $\nu = 1/2$ are presented in Table 4, and in Figs. 4 and 5. For plane stress, κ increases slightly from unity as α decreases, and γ remains roughly constant as α changes. Note that in the elastic limit κ approaches unity, but more interestingly, in the perfectly-plastic limit κ seems to be consistent with the result that one would expect from the solution of the perfectly-plastic problem with a centered-fan sector centered about the crack line (see Rice, 1982, and Dean, 1983), $\kappa = 2/\sqrt{3} \cong 1.1547$.

The active plastic zones obtained are shown in Fig. 10. They have a shape similar to the corresponding antiplane strain zones, but they are taller and skinnier, at least for the given range of α.

Dean (1983) produced the corresponding finite element method results for this problem. His results show again that the finite element method is not a very efficient method for predicting the strength of the plastic singularity for small values of α. However, we find that our plastic zones are similar in shape and size to his.

5 Concluding Remarks

This work has dealt with the problem of determining the plastic stress intensity factor associated with the near-tip stress and deformation fields of a two-dimensional crack propagating steadily and quasi-statically in a linear-hardening material under small scale yielding conditions. The form of these asymptotic fields, and the associated strength of the singularity had been given previously.

A new method to determine the plastic stress intensity factor is developed based on direct application of an appropriately chosen variational statement that incorporates known information about the near-tip and remote asymptotic fields into the formulation of the problem. The method has the advantage of simplicity, and that it is expected to predict most accurately (in relative terms) the physically important near-tip behavior, but it has the disadvantage that it depends exclusively on the availability of the near-tip fields. By comparison, conventional use of the finite element method is expected to give results which are inaccurate (again in relative terms) near the tip of the crack, but on the other hand, the finite element method can be applied to materials for which the near-tip asymptotic fields are not available.

In the application of our method to the linear-hardening material, difficulties were encountered in the small-α limit due to the fact that the range of dominance of the available near-tip asymptotic fields is expected to vanish in the limit as $\alpha \to 0$. Nonetheless, because the perfectly-plastic fields are fairly well understood, it was possible to make useful comparisons between the limits expected from the perfectly-plastic solutions, and our results for small α.

Finally, it should be pointed out that although the present work does not directly address the theoretical prediction of resistance curves, because it treats only the steady-state problem, it seems plausible that the method could be extended to accomplish this purpose.

Acknowledgments

This work was supported in part by the Office of Naval Research under Contract N00014-84-K-0510, and by the Division of Applied Sciences, Harvard University. Thanks are due to B. Budiansky for suggesting this project, and for providing valuable comments throughout its development, and to P. A. Mataga for insightful discussions.

References

Amazigo, J. C., and Hutchinson, J. W., 1977, "Crack-Tip Fields in Steady Crack Growth With Linear Strain-Hardening," *J. Mech. Phys. Solids*, Vol. 25, pp. 81–97.

Budiansky, B., 1986, Private Communication.

Chitaley, A. D., and McClintock, F. A., 1971, "Elastic-Plastic Mechanics of Steady Crack Growth Under Anti-Plane Shear," *J. Mech. Phys. Solids*, Vol. 19, pp. 147–163.

Dean, R. H., 1983, "Elastic-Plastic Crack Growth in Plane Stress," *Elastic-Plastic Fracture: Second Symposium, Volume I—Inelastic Crack Analysis*, ASTM STP 803, Philadelphia, pp. I-39–I-51.

Dean, R. H., and Hutchinson, J. W., 1980, "Quasi-Static Steady Crack Growth in Small-Scale Yielding," *Fracture Mechanics: Twelfth Conference*, ASTM STP 700, Philadelphia, pp. 383–405.

Drugan, W. J., Rice, J. R., and Sham, T. L., 1982, "Asymptotic Analysis of Growing Plane Strain Tensile Cracks in Elastic-Ideally Plastic Solids," *J. Mech. Phys. Solids*, Vol. 30, pp. 447–473.

Gao, Y.-C., 1980, "Elastic-Plastic Field at the Tip of a Crack Growing Steadily in Perfectly-Plastic Medium," in Chinese, *Acta Mechanica Sinica*, Vol. 1, pp. 48–56.

Mataga, P. A., 1986, unpublished work.

McClintock, F. A., 1958, "Ductile Fracture Instability in Shear," ASME Journal of Applied Mechanics, Vol. 25, pp. 582–588.

McClintock, F. A., and Irwin, G. R., 1965, "Plasticity Aspects of Fracture Mechanics," *Fracture Toughness Testing and its Applications*, ASTM STP 381, Philadelphia, pp. 84–113.

Downloaded 03 May 2010 to 171.66.16.27. Redistribution subject to ASME license or copyright; see http://www.asme.org/terms/Terms_Use.cfm

Ponte Castañeda, P., 1986, "Asymptotic Fields of a Perfectly-Plastic, Plane-Stress Mode II Growing Crack," ASME JOURNAL OF APPLIED MECHANICS, Vol. 53, pp. 831–833.

Ponte Castañeda, P., 1987a, "Asymptotic Analysis of a Mode I Crack Propagating Steadily in a Deformation Theory Material," ASME JOURNAL OF APPLIED MECHANICS, Vol. 54, pp. 79–86.

Ponte Castañeda, P., 1987b, "Asymptotic Fields in Steady Crack Growth With Linear Strain-Hardening," *J. Mech. Phys. Solids*, Vol. 35, pp. 227–268.

Rice, J. R., 1974, "Elastic-Plastic Models for Stable Crack Growth," *Mechanics and Mechanisms of Crack Growth*, May, M. J., ed., British Steel Corporation Physical Metallurgy Centre Publication, pp. 14–39.

Rice, J. R., and Sorensen, E. P., 1978, "Continuing Crack-Tip Deformation and Fracture for Plane-Strain Crack Growth in Elastic-Plastic Solids," *J. Mech. Phys. Solids*, Vol. 26, pp. 163–186.

Rice, J. R., Drugan, W. J., and Sham, T. L., 1980, "Elastic-Plastic Analysis of Growting Cracks," *Fracture Mechanics: Twelfth Conference*, ASTM-STP 700, Philadelphia, pp. 189–219.

Rice, J. R., 1982, "Elastic-Plastic Crack Growth," *Mechanics of Solids: The Rodney Hill 60th Anniversary Volume*, Hopkins, H. G., and Sewell, M. J., eds., Pergamon Press, Oxford, pp. 539–562.

Slepyan, L. I., 1973, "Deformation at the Edge of a Growing Crack," *Mekhanika Tverdogo Tela*, Vol. 8, pp. 139–148.

Slepyan, L. I., 1974, "Growing Crack During Plane Deformation of an Elastic-Plastic Body," *Mekhanika Tverdogo Tela*, Vol. 9, pp. 57–67.

Zhang, R., Zhang, X., and Hwang, K., 1983, "Near-Tip Fields for Plane Strain Mode I Steady Crack Growth in Linear-Hardening Material With Bauschinger Effect," *Proceedings of ICF International Symposium on Fracture Mechanics*, Hwang, K., Liu, C., and He, Q., eds., Science Press, Beijing.

Downloaded 03 May 2010 to 171.66.16.27. Redistribution subject to ASME license or copyright; see http://www.asme.org/terms/Terms_Use.cfm

J. W. Eischen[1]
Assoc. Mem. ASME

G. Herrmann
Professor,
Fellow ASME

Division of Applied Mechanics,
Stanford University,
Stanford, CA 94305

Energy Release Rates and Related Balance Laws in Linear Elastic Defect Mechanics

A simple and direct derivation of certain balance (or conservation) laws for linear dynamic elasticity is presented including nonhomogeneities, thermal effects, anisotropy, and body forces. Additionally, the connection between the balance laws and energy release rates for defect motions is established.

1 Introduction

Some time ago Knowles and Sternberg (1972) devoted an article to a systematic derivation via Noether's (1971) theorem of certain conservation (or balance) laws valid for linearized and finite elastostatics. This work was motivated primarily by the interest generated by Rice's (1968) J integral, and a quest for its theoretical underpinning. Knowles and Sternberg (1972) deduced that J was actually a vector component of a more general conservation law (J_k), and found two additional laws which were subsequently associated with the L_k and M integrals of defect mechanics by Budiansky and Rice (1973). Fletcher (1976) extended the invariant integrals presented by Knowles and Sternberg (1972) to linear elastodynamics, again relying on manipulations dictated by Noether's (1971) theorem.

It is the purpose of the present paper to extend the results of these earlier works to account for material nonhomogeneity, temperature gradients, anisotropy, and body force. Additionally, it will be shown that balance laws of the type described above can be deduced simply by subjecting the Lagrangian density to familiar operations from vector calculus such as gradient, curl, and divergence. A. G. Herrmann (1981, 1982a,b) introduced the notion of obtaining balance laws in this manner, but did not carry out the steps necessary to include the effects mentioned above. While derivations based on Noether's theorem are admittedly more satisfying from a theoretical standpoint, the attendant mathematical apparatus tends to obscure the relative simplicity of the end results. Therefore, alternative means of deriving balance laws for linear elasticity seems to be a credible objective.

The significance of balance laws would be quite restricted, were it not possible to relate them to energy release rates. These relations are derived here for the special case of a two-dimensional crack and culminate in the conclusion that total energy densities (Hamiltonian) lead directly to physically meaningful energy release rates, rather than Lagrangian densities.

2 Balance Laws

Consider a linear elastic solid occupying a closed, bounded, regular region Ω in three-dimensional space. The material within this region is acted upon by thermal, mechanical, and far-field (e.g., body force) loadings. The measure numbers of the displacement vector $\mathbf{u}$, at the point with position vector $\mathbf{x}$ are given by $u_i = u_i(x_j, t)$.[2] The components of the infinitesimal strain tensor are

$$\epsilon_{ij} = \frac{1}{2}(u_{i,j} + u_{j,i}) \tag{1}$$

In the presence of a temperature gradient, the strain tensor is decomposed into two parts: one associated with elastic strains (ϵ^E_{ij}) and another accounting for the free thermal expansion of the medium. Thus,

$$\epsilon_{ij} = \epsilon^E_{ij} + \alpha_{ij}(\mathbf{x})\Delta\Theta(\mathbf{x}) \tag{2}$$

where α_{ij} is a tensor storing the coefficients of thermal expansion, while $\Delta\Theta$ is the temperature change. Both of these quantities are assumed independent of time. According to Neumann's (1841) hypothesis, the stress is related to the elastic strain in the usual way, viz

$$\sigma_{ij} = c_{ijkl}(\mathbf{x})\epsilon^E_{ij} \tag{3}$$

where σ_{ij} are the components of the stress tensor and c_{ijkl} denotes components of the elasticity tensor. Attention is restricted to uncoupled thermoelasticity, consequently material properties are not dependent on the temperature change. Note that the material is nonhomogeneous in general, since the elasticity tensor and coefficients of thermal expansion depend on position. Furthermore, the material is not

[1] Currently Assistant Professor, Department of Mechanical and Aerospace Engineering, North Carolina State University, Raleigh, NC, 27695-7910.

Contributed by the Applied Mechanics Division for presentation at the 1987 Applied Mechanics, Biomechanics, and Fluids Engineering Conference, Cincinnati, OH, June 14–17, 1987, of the American Society of Mechanical Engineers.

Discussion of this paper should be addressed to the Editorial Department, ASME, United Engineering Center, 345 East 47th Street, New York, N.Y. 10017, and will be accepted until two months after final publication of the paper itself in the JOURNAL OF APPLIED MECHANICS. Manuscript received by ASME Applied Mechanics Division, June 10, 1986; final revision, November 14, 1986.

Paper No. 87-APM-33.

[2] The *summation convention* is used repeatedly in this paper. Summation over repeated subindices is implied. The range of the subindices is 1,2,3.

Copyright © 1987 by ASME
Downloaded 03 May 2010 to 171.66.16.27. Redistribution subject to ASME license or copyright; see http://www.asme.org/terms/Terms_Use.cfm

necessarily elastically or thermally isotropic. The equilibrium equations are

$$\sigma_{ij,\,j}+f_i=\rho\ddot{u}_i \tag{4}$$

where f_i are measure numbers of the body force density vector, and ρ the mass density. The superposed dots indicate time derivatives. The Lagrangian density L may be viewed as a function of the particle velocity, total strain tensor, and coordinates. Accordingly, it is defined by

$$L=L(\dot{\mathbf{u}},\boldsymbol{\epsilon},\mathbf{x})\equiv T-W$$

$$=\frac{1}{2}\,\rho(\mathbf{x})\dot{u}_p\dot{u}_p$$

$$-\frac{1}{2}\,c_{prst}(\mathbf{x})\,(\epsilon_{pr}-\alpha_{pr}(\mathbf{x})\Delta\Theta(\mathbf{x}))\epsilon_{st}-\alpha_{st}(\mathbf{x})\Delta\Theta(\mathbf{x})) \tag{5}$$

where T and W represent the kinetic and elastic strain energy densities, respectively. Given the particular form of equation (5), the usual variation of the Lagrangian will lead to the equations of motion, provided terms accounting for the work of the body forces and surface tractions are included.

The desired results are obtained next by simple vector and tensor calculus operations involving the Lagrangian.

Gradient. The first balance law is obtained by considering the gradient of the Lagrangian, i.e.,

$$\nabla L=L_{,k}=\frac{\partial L}{\partial\dot{u}_i}\frac{\partial\dot{u}_i}{\partial x_k}+\frac{\partial L}{\partial\epsilon_{ij}}\frac{\partial\epsilon_{ij}}{\partial x_k}+\left(\frac{\partial L}{\partial x_k}\right)_{\text{expl}}$$

$$=\frac{\partial L}{\partial\dot{u}_i}\frac{\partial\dot{u}_i}{\partial x_k}+\frac{\partial L}{\partial\epsilon^E_{ij}}\frac{\partial\epsilon_{ij}}{\partial x_k}+\left(\frac{\partial L}{\partial x_k}\right)_{\text{expl}}$$

$$=\rho\dot{u}_i\dot{u}_{i,k}-\sigma_{ij}u_{i,\,jk}+(L_{,k})_{\text{expl}} \tag{6}$$

The "explicit" derivation of the Lagrangian is calculated according to

$$\left(\frac{\partial L}{\partial x_k}\right)_{\text{expl}}=\frac{\partial}{\partial x_k}L(\dot{u}_i,\epsilon_{ij},x_i)\,\Big|_{\dot{u}_i=\text{const},\epsilon_{ij}=\text{const},x_i=\text{const for } i\neq k} \tag{7}$$

Specifically,

$$(L_{,k})_{\text{expl}}=\frac{1}{2}\,\rho_{,k}\dot{u}_p\dot{u}_p-\frac{1}{2}\,c_{prst,k}\epsilon^E_{pr}\epsilon^E_{st}$$
$$+\sigma_{pr}\alpha_{pr,k}\Delta\Theta+\sigma_{pr}\alpha_{pr}\Delta\Theta_{,k} \tag{8}$$

When the divergence of the stress tensor is introduced in equation (6), it follows that

$$L_{,\,j}\delta_{jk}+(\sigma_{ij}u_{i,k})_{,\,j}-\sigma_{ij,\,j}u_{i,k}-\rho\dot{u}_i\dot{u}_{i,k}=(L_{,k})_{\text{expl}} \tag{9}$$

The equilibrium equations are then substituted producing

$$(L\delta_{jk}+\sigma_{ij}u_{i,k})_{,\,j}-(\rho\ddot{u}_i-f_i)u_{i,k}-\rho\dot{u}_i\dot{u}_{i,k}=(L_{,k})_{\text{expl}} \tag{10}$$

Finally, it follows that

$$(L\delta_{jk}+\sigma_{ij}u_{i,k})_{,j}=\frac{\partial}{\partial t}(\rho\dot{u}_iu_{i,k})+(L_{,k})_{\text{expl}}-f_iu_{i,k} \tag{11}$$

This differential form represents a balance law valid for a linear, nonhomogeneous, anisotropic solid which is subjected to inertial, thermal, and body force loadings. If nonhomogeneity, thermal gradients, and body force loadings are absent, and the material is homogeneous, the resulting expression is in accord with equation (3.4) of the paper by Fletcher (1976). An integral form of equation (11) may be obtained upon application of the divergence theorem. If Ω is a regular bounded region enclosed by a surface Γ whose unit outward normal vector is $\mathbf{n}$, it follows that

$$\int_\Gamma(-Ln_k-\sigma_{ij}n_ju_{i,k}k)d\Gamma-\int_\Omega\left[-\frac{\partial}{\partial t}(\rho\dot{u}_iu_{i,k})\right.$$

$$\left.-(L_{,k})_{\text{expl}}+f_iu_{i,k}\right]d\Omega=0 \tag{12}$$

Curl. The second balance law is obtained by considering the curl of the "Lagrangian moment." That is,

$$\nabla\times(L\mathbf{x})=e_{kij}(Lx_j)_{,i}$$

$$=e_{kij}\left[\frac{\partial(Lx_j)}{\partial\dot{u}_m}\frac{\partial\dot{u}_m}{\partial x_i}+\frac{\partial(Lx_j)}{\partial\epsilon_{mn}}\frac{\partial\epsilon_{mn}}{\partial x_i}+\left(\frac{\partial(Lx_j)}{\partial x_i}\right)_{\text{expl}}\right]$$

$$=e_{kij}\left[\frac{\partial(Lx_j)}{\partial\dot{u}_m}\frac{\partial\dot{u}_m}{\partial x_i}+\frac{\partial(Lx_j)}{\partial\epsilon^E_{mn}}\frac{\partial\epsilon_{mn}}{\partial x_i}+\left(\frac{\partial(Lx_j)}{\partial x_i}\right)_{\text{expl}}\right]$$

$$=e_{kij}[\rho\dot{u}_m\dot{u}_{m,i}x_j-\sigma_{mn}u_{m,ni}x_j+(L_{,i})_{\text{expl}}x_j] \tag{13}$$

where $(L_{,i})_{\text{expl}}$ is the same as given in equation (8) provided that k is replaced by i. The alternator symbol is denoted by e_{kij}. If the divergence of the stress tensor is introduced, it follows that

$$e_{kij}[(Lx_j)_{,i}-\rho\dot{u}_m\dot{u}_{m,i}x_j+(\sigma_{mn}u_{m,i}x_j)_{,n}$$
$$-\sigma_{mn,n}u_{m,i}x_j-\sigma_{mn}u_{m,i}x_{j,n}]=e_{kij}(L_{,i})_{\text{expl}}x_j \tag{14}$$

When the equilibrium equations are substituted and the quantity $e_{kij}\sigma_{mi}u_{j,m}$ is added and subtracted to the left side of equation (14), it follows that

$$e_{kij}[(Lx_j)_{,i}+(\sigma_{mn}u_{m,i}x_j)_{,n}-\sigma_{mi}u_{j,m}]=$$
$$e_{kij}\left[\frac{\partial}{\partial t}(\rho\dot{u}_mu_{m,i}x_j)+(L_{,i})_{\text{expl}}x_j-f_mu_{m,i}x_j\right.$$
$$\left.-(\sigma_{mi}u_{j,m}-\sigma_{mj}u_{m,i})\right] \tag{15}$$

If the divergence of the stress tensor and the equilibrium equations are then substituted, the desired result is obtained as

$$(e_{kmj}Lx_j+e_{kij}\sigma_{mn}u_{n,i}x_j-e_{kij}\sigma_{mi}u_j)_{,m}=$$
$$e_{kij}\left[\frac{\partial}{\partial t}(\rho\dot{u}_mu_{m,i}x_j-\rho\dot{u}_iu_j)+(L_{,i})_{\text{expl}}x_j\right.$$
$$\left.+(f_iu_j-f_mu_{m,i}x_j)-(\sigma_{mi}u_{j,\text{m}}-\sigma_{mj}u_{m,i})\right] \tag{16}$$

Equation (16) represents another balance law. The first three quantities in parentheses on the right side account for material inertia, nonhomogeneity and thermal gradients, and body forces, respectively. The last quantity in parentheses vanishes when the material is isotropic, as shown in the Appendix. This equation is not in accord with Fletcher's (1976) equation (3.6) even if nonhomogeneity, thermal graidents, body force, and anisotropy are neglected. Equation (3.6) of Fletcher's paper is flawed, and should have a plus (+) sign preceding the term $e_{imj}x_ju_{l,m}\sigma_{lk}$, rather than a minus (−) sign. Equation (16) appears in integral form as

$$\int_\Gamma e_{kij}(-Lx_jn_i-\sigma_{mn}n_mu_{n,i}x_j+\sigma_{mi}n_mu_j)d\Gamma-$$

$$\int_\Omega e_{kij}\left[\frac{\partial}{\partial t}(-\rho\dot{u}_mu_{m,i}x_j+\rho\dot{u}_iu_j)-(L_{,i})_{\text{expl}}x_j-\right.$$
$$\left.(f_iu_j-f_mu_{m,i}x_j)+(\sigma_{mi}u_{j,m}-\sigma_{mj}u_{m,i})\right]d\Omega=0 \tag{17}$$

Divergence. A third balance law is obtained by considering the divergence of the "Lagrangian moment," i.e.,

$$\nabla\cdot(L\mathbf{x})=(Lx_k)_{,k}$$
$$=\frac{\partial(Lx_k)}{\partial\dot{u}_i}\frac{\partial\dot{u}_i}{\partial x_k}+\frac{\partial(Lx_k)}{\partial\epsilon_{ij}}\frac{\partial\epsilon_{ij}}{\partial x_k}+\left(\frac{\partial(Lx_k)}{\partial x_k}\right)_{\text{expl}}$$
$$=\frac{\partial(Lx_k)}{\partial\dot{u}_i}\frac{\partial\dot{u}_i}{\partial x_k}+\frac{\partial(Lx_k)}{\partial\epsilon^E_{ij}}\frac{\partial\epsilon_{ij}}{\partial x_k}+\left(\frac{\partial(Lx_k)}{\partial x_k}\right)_{\text{expl}}$$

Downloaded 03 May 2010 to 171.66.16.27. Redistribution subject to ASME license or copyright; see http://www.asme.org/terms/Terms_Use.cfm

$$= \rho \dot{u}_i \dot{u}_{i,k} x_k - \sigma_{ij} u_{i,jk} x_k + (L_{,k})_{\text{expl}} x_k$$

$$+ \frac{m}{2} \rho \dot{u}_i \dot{u}_i - \frac{m}{2} \sigma_{ij} d\epsilon^E_{i,j} \tag{18}$$

A parameter m has been introduced which is equal to 3 for three dimensions and 2 for two dimensions. This accounts for a term $x_{k,k}$ which arises from the operations indicated in equation (18). If the divergence of the stress tensor is introduced it follows that

$$(Lx_k)_{,k} + (\sigma_{ij} u_{i,k} x_k)_{,j} - \sigma_{ij,j} u_{i,k} x_k - \sigma_{ij} u_{i,k} x_{k,j}$$

$$= \rho \dot{u}_i \dot{u}_{i,k} x_k + (L_{,k})_{\text{expl}} x_k + \frac{m}{2} (\rho \dot{u}_i \dot{u}_i - \sigma_{ij} \epsilon^E_{ij}) \tag{19}$$

The equilibrium equations are then substituted resulting in

$$(Lx_j + \sigma_{ij} u_{i,k} x_k)_{,j} = \frac{\partial}{\partial t} (\rho \dot{u}_i u_{i,k} x_k) + \sigma_{ij} u_{i,j} + \frac{m}{2} (\rho \dot{u}_i \dot{u}_i - \sigma_{ij} \epsilon^E_{ij})$$

$$+ (L_{,k})_{\text{expl}} x_k - f_i u_{i,k} x_k \tag{20}$$

It proves convenient to write equation (20) as

$$(Lx_j + \sigma_{ij} u_{i,k} x_k)_{,j} = \frac{\partial}{\partial t} (\rho \dot{u}_i u_{i,k} x_k) + (-L + \rho \dot{u}_i \dot{u}_i) + (m-1)L$$

$$+ (L_{,k})_{\text{expl}} x_k - f_i u_{i,k} x_k + \sigma_{ij} \alpha_{ij} \Delta\Theta \tag{21}$$

The following two relationships are useful

$$L = \frac{1}{2} \left[\frac{\partial}{\partial t} (\rho \dot{u}_i u_i) - (\sigma_{ij} u_i)_{,j} \right] - \frac{1}{2} f_i u_i + \frac{1}{2} \sigma_{ij} \alpha_{ij} \Delta\Theta \tag{22}$$

$$-L + \rho \dot{u}_i \dot{u}_i = \frac{\partial}{\partial t} [-Lt + \rho t \dot{u}_i \dot{u}_i]$$

$$- t \left[(\sigma_{ij} \dot{u}_i)_{,j} + f_i \dot{u}_i - \frac{1}{2} \dot{\sigma}_{ij} \alpha_{ij} \Delta\Theta \right] \tag{23}$$

From this follows the desired result

$$\left[Lx_j + \sigma_{ij} \left(u_{i,k} x_k + t\dot{u}_i + \left(\frac{m-1}{2} \right) u_i \right) \right]_{,j} = \frac{\partial}{\partial t} \left[-Lt \right.$$

$$\left. + \rho \dot{u}_i \left(u_{i,k} x_k + t\dot{u}_i + \left(\frac{m-1}{2} \right) u_i \right) \right] + (L_{,k})_{\text{expl}} x_k$$

$$- f_i \left(u_{i,k} x_k + t\dot{u}_i + \left(\frac{m-1}{2} \right) u_i \right) + \frac{1}{2} t \dot{\sigma}_{ij} \alpha_{ij} \Delta\Theta$$

$$+ \left(\frac{m+1}{2} \right) \sigma_{ij} \alpha_{ij} \Delta\Theta \tag{24}$$

The term $\dot{\sigma}_{ij}$ may be written alternatively as

$$\dot{\sigma}_{ij} = c_{ijkl} \dot{u}_{k,l} \tag{25}$$

For $m = 3$, equation (24) is in accord with equation (3.5) of the paper by Fletcher (1976) if nonhomogeneity, thermal gradients, and body forces are neglected. Fletcher did not present results for the case $m = 2$. The integral form of equation (24) is

$$\int_\Gamma \left[-Lx_j n_j - \sigma_{ij} n_j \left(u_{i,k} x_k + t\dot{u}_i + \left(\frac{m-1}{2} \right) u_i \right) \right]_{,j} -$$

$$\int_\Omega \left[\frac{\partial}{\partial t} \left[Lt - \rho \dot{u}_i \left(u_{i,k} x_k + t\dot{u}_i + \left(\frac{m-1}{2} \right) u_i \right) \right] - (L_{,k})_{\text{expl}} x_k \right.$$

$$+ f_i \left(u_{i,k} x_k + t\dot{u}_i + \left(\frac{m-1}{2} \right) u_i \right) - \alpha_{ij} \Delta\Theta \left(\frac{1}{2} t c_{ijkl} \dot{u}_{k,l} \right.$$

$$\left. \left. + \left(\frac{m+1}{2} \right) \sigma_{ij} \right) \right] d\Omega = 0 \tag{26}$$

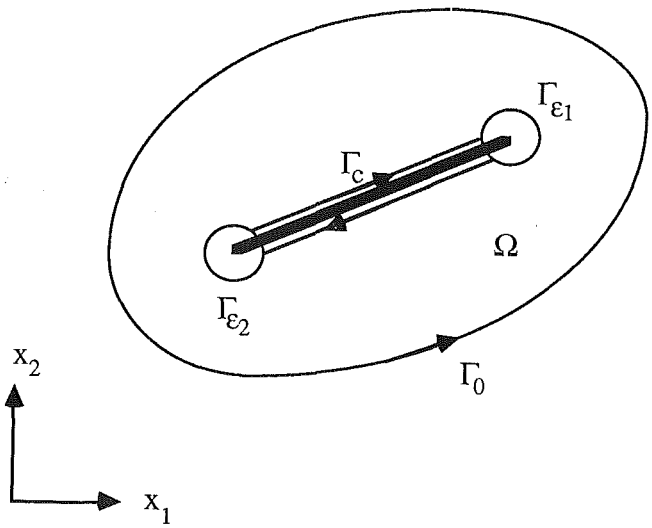


Fig. 1 Schematic of crack and definition of integration paths

3 Energy Release Rates

In this section expressions will be derived for the energy release rates associated with certain crack (defect) motions valid for two-dimensional fracture problems. An extension to three dimensions is straightforward. Figure 1 depicts a crack located in a two-dimensional elastic region. The energy released during three possible crack motions will be studied. These motions are: (*i*) rigid translation such that all points on the crack surfaces move with velocity $\mathbf{v} = v_k \mathbf{e}_k$, where v_k are constants; (*ii*) rigid rotation about the x_3 axis such that points on the crack surface move with velocity $\mathbf{v} = v_k \mathbf{e}_k = -e_{3kl} x_l \omega e_k$, where ω is a positive constant; (*iii*) self-similar expansion along the crack axis such that points on the crack surface move with velocity $\mathbf{v} = v_k \mathbf{e}_k = \alpha x_k \mathbf{e}_k$, where α is a positive constant.

The energy rate balance condition which must hold during any of these crack motions may be stated as follows (see Freund, 1972),

$$P + B = \dot{K} + \dot{U} + F \tag{27}$$

where

$$P = \lim_{\Gamma_\epsilon \to 0} \int_{\Gamma_0} \sigma_{ij} n_j \dot{u}_i d\Gamma \tag{28}$$

$$B = \lim_{\Gamma_\epsilon \to 0} \int_{\Omega(t)} f_i \dot{u}_i d\Omega \tag{29}$$

$$K = \lim_{\Gamma_\epsilon \to 0} \int_{\Omega(t)} \frac{1}{2} \rho \dot{u}_i \dot{u}_i d\Omega \tag{30}$$

$$U = \lim_{\Gamma_\epsilon \to 0} \int_{\Omega(t)} \frac{1}{2} \sigma_{ij} \epsilon^E_{ij} d\Omega \tag{31}$$

The quantities P, B, K, and U are the rate of work of the tractions on Γ_0, the rate of work of the body forces in Ω, the total kinetic energy and elastic strain energies in Ω, respectively. The quantity F is the energy absorption rate on both the crack surfaces and the crack tips measured as a change in energy per unit thickness per unit time. For brevity, the paths Γ_{ϵ_1} and Γ_{ϵ_2} are referred to collectively as Γ_ϵ. The paths Γ_ϵ and Γ_c move rigidly with the crack as it executes the motion described above. Therefore, the position of the paths Γ_ϵ and Γ_c is time-dependent, and the transport theorem must be used to evaluate $\dot{K}$ and $\dot{U}$. Consequently,

Downloaded 03 May 2010 to 171.66.16.27. Redistribution subject to ASME license or copyright; see http://www.asme.org/terms/Terms_Use.cfm

$$\dot{K}=\lim_{\Gamma_\epsilon\to 0}\left\{\int_\Omega \rho\ddot{u}_i\dot{u}_i d\Omega+\int_{\Gamma_\epsilon+\Gamma_c}\frac{1}{2}\rho\dot{u}_i\dot{u}_i v_k n_k d\Gamma\right\} \tag{32}$$

$$\dot{U}=\lim_{\Gamma_\epsilon\to 0}\left\{\int_\Omega \sigma_{ij}\dot{u}_{i,j}d\Omega+\int_{\Gamma_\epsilon+\Gamma_c}\frac{1}{2}\sigma_{ij}\epsilon^E_{ij}v_k n_k d\Gamma\right\} \tag{33}$$

After some manipulations it follows that,

$$F=\lim_{\Gamma_\epsilon\to 0}\int_{\Gamma_\epsilon+\Gamma_c}[(T+W)v_k n_k+\sigma_{ij}n_j\dot{u}_i]d\Gamma \tag{34}$$

Recall that T and W are the kinetic and elastic strain energy *densities*, respectively. This expression for the energy release rate will be split into two parts, one having to do with the energy absorbed at the crack tips and another accounting for energy absorbed along the crack surfaces.

$$F=F_{\text{tip}}+F_{\text{sur}} \tag{35}$$

where

$$F_{\text{tip}}=\lim_{\Gamma_\epsilon\to 0}[(T+W)v_k n_k+\sigma_{ij}n_j\dot{u}_i]d\Gamma \tag{36}$$

$$F_{\text{sur}}=\lim_{\Gamma_\epsilon\to 0}\int_{\Gamma_c}[(T+W)v_k n_k]d\Gamma \tag{37}$$

It can be shown that near the tip of an extending crack the field quantities obey the "transport assumption" (Ehrlacher, 1981)

$$\frac{\partial(\ )}{\partial t}=-v_k\frac{\partial(\ )}{\partial x_k} \tag{38}$$

Furthermore, observe that on Γ_c, $n_k^+ = n_k^-$ and $\sigma_{ij}n_j = 0$. After letting $T + W = E$ (kinetic + elastic strain energy density), it follows that

$$F_{\text{tip}}=\lim_{\Gamma_\epsilon\to 0}\int_{\Gamma_\epsilon}[Ev_k n_k-\sigma_{ij}n_j u_{i,k}v_k]d\Gamma \tag{39}$$

$$F_{\text{sur}}=\lim_{\Gamma_\epsilon\to 0}\int_{\Gamma_c}[E^+-E^-]v_k n_k^+ d\Gamma \tag{40}$$

The next step is to evaluate the expression for the crack tip energy release rate given above for the three crack motions discussed earlier.

Case (*i*). v_k = constant

$$\frac{F_{\text{tip}}}{v_k}=G_k^T=\lim_{\Gamma_\epsilon\to 0}\int_{\Gamma_\epsilon}[En_k-\sigma_{ij}n_j u_{i,k}]d\Gamma \tag{41}$$

The energy release rate measured as an energy change per unit translation per unit thickness is denoted G_k^T. This energy release rate can then be written in terms of line integrals around the remote paths Γ_0 and Γ_c, and a domain integral over Ω by applying the divergence theorem to equation (41). Introducing a symbol J_k (k = 1, 2), it follows that

$$J_k=G_k^T=\int_{\Gamma_0}[En_k-\sigma_{ij}n_j u_{i,k}]d\Gamma+\int_{\Gamma_c}[E^+-E^-]n_k^+ d\Gamma-$$

$$\int_\Omega[\rho\dot{u}_i\dot{u}_{i,k}-\rho\ddot{u}_i u_{i,k}+f_i u_{i,k}+(E_{,k})_{\text{expl}}]d\Omega \tag{42}$$

This expression may be thought of as an extension to the usual J integral found for crack problems. Equation (42) accounts for inertia, body force, nonhomogeneity, and thermal gradients. For completeness, the expression for $(E_{,k})_{\text{expl}}$ is

$$(E_{,k})_{\text{expl}}=\frac{1}{2}\rho_{,k}\dot{u}_p\dot{u}_p+\frac{1}{2}c_{prst,k}\epsilon^E_{pr}\epsilon^E_{st}$$
$$-\sigma_{pr}\alpha_{pr,k}\Delta\Theta-\sigma_{pr}\alpha_{pr}\Delta\Theta_{,k} \tag{43}$$

Case (*ii*). $v_k = -e_{3kl}x_l\omega$

$$\frac{F_{\text{tip}}}{\omega}=G^R=\lim_{\Gamma_\epsilon\to 0}\int_{\Gamma_\epsilon}e_{3ij}[-Ex_j n_i+\sigma_{mn}n_m u_{n,i}x_j]d\Gamma \tag{44}$$

The energy release rate measured as an energy change per unit angular rotation per unit thickness is denoted G^R. Again, this quantity can be expressed in terms of remote line integrals and a domain integral. Introducing the symbol L_3,

$$L_3=-G^R=\int_{\Gamma_0}e_{3ij}[Ex_j n_i-\sigma_{mn}n_m n_{n,i}x_j+\sigma_{mi}n_m u_j]d\Gamma+$$

$$\int_{\Gamma_c}e_{3ij}[E^+-E^-]x_j n_i^+ d\Gamma-$$

$$\int_\Omega e_{3ij}[\rho\dot{u}_m\dot{u}_{m,i}x_j-\rho\ddot{u}_m u_{m,i}x_j+\rho\ddot{u}_i u_j+(f_m u_{m,i}x_j-f_i u_j)+$$
$$(\sigma_{mi}u_{j,m}-\sigma_{mj}u_{m,i})+(E_{,i})_{\text{expl}}x_j]d\Omega \tag{45}$$

Case (*iii*). $v_k = \alpha x_k$

$$\frac{F_{\text{tip}}}{\alpha}=G^E=\lim_{\Gamma_\epsilon\to 0}\int_{\Gamma_\epsilon}[Ex_k n_k-\sigma_{ij}n_j u_{i,k}x_k]d\Gamma \tag{46}$$

The energy release rate measured as an energy change per unit thickness is denoted G^E. This quantity can be expressed in terms of remote line integrals and a domain integral. Introducing the symbol M,

$$M=G^E=\int_{\Gamma_0}[Ex_k n_k-\sigma_{ij}n_j u_{i,k}x_k]d\Gamma+\int_{\Gamma_c}[E^+-E^-]x_k n_k^+ d\Gamma-$$

$$\int_\Omega[(\rho\dot{u}_i\dot{u}_{i,k}x_k-\rho\ddot{u}_i u_{i,k}x_k+\rho\dot{u}_i\dot{u}_i)+f_i u_{i,k}x_k$$
$$-\sigma_{ij}\alpha_{ij}\Delta\Theta+(E_{,k})_{\text{expl}}x_k]d\Omega \tag{47}$$

A natural question to ask at this point is whether the balance laws derived earlier in Section 2 are connected in some way with the expressions for the energy release rates shown above. After all, Budiansky and Rice (1973) interpreted the integral forms of the conservation laws discovered by Knowles and Sternberg (1972) as energy release rates for the case of elastostatics in the absence of material nonhomogeneity, body forces, anisotropy, and temperature gradients. In the same way, it may be tempting to speculate that the balance laws given by equations (12), (17), and (26) lead to crack tip energy release rate expressions when the path Γ in those expressions is taken as Γ_ϵ and the domain Ω vanishes. If the path Γ is shrunk onto the crack tips, it is clear that the resulting expressions are not directly compatible with the relationships given by equations (41), (44), and (46). For example, equation (12) becomes

$$\int_{\Gamma_\epsilon}[-Ln_k-\sigma_{ij}n_j u_{i,k}]d\Gamma\neq G_k^T \tag{48}$$

One may question whether the domain integral in equation (12) indeed vanishes as $\Gamma\to\Gamma_\epsilon$. This is due to the inverse square root dependence on the distance from the crack tip and the particular angular variations about the crack tip exhibited by the stress and displacement gradient quantities in all fracture problems, independent of inertia, body force, thermal, nonhomogeneity, and anisotropy effects. This argument is made succinctly by Nakamura et al. (1985). The discrepancy between equation (48) and equation (41) is the appearance of the Lagrangian density in the expression derived from the balance law, rather than the quantity E which represents the sum of the kinetic and elastic strain energy densities.

It is instructive to note that if the operations ∇E, $\nabla\times(E\mathbf{x})$, and $\nabla\cdot(E\mathbf{x})$ had been considered, the resulting balance laws would have been in a form readily associated with energy release rates.

Downloaded 03 May 2010 to 171.66.16.27. Redistribution subject to ASME license or copyright; see http://www.asme.org/terms/Terms_Use.cfm

∇E:

$$\int_\Gamma [En_k - \sigma_{ij} n_j u_{i,k}] d\Gamma$$

$$- \int_\Omega [\rho \dot{u}_i \dot{u}_{i,k} - \rho \ddot{u}_i u_{i,k} + f_i u_{i,k} + (E_{,k})_{\text{expl}}] d\Omega = 0 \tag{49}$$

$\nabla \times (E\mathbf{x})$:

$$\int_\Gamma e_{3ij} [Ex_j n_i - \sigma_{mn} n_m u_{n,i} x_j + \sigma_{mi} n_m u_j] d\Gamma -$$

$$\int_\Omega e_{3ij} [\rho \dot{u}_m \dot{u}_{m,i} x_j - \rho \ddot{u}_m u_{m,i} x_j + \rho \ddot{u}_i u_j + (f_m u_{m,i} x_j - f_i u_j) +$$

$$(\sigma_{mi} u_{j,m} - \sigma_{mj} u_{m,i}) + (E_{,i})_{\text{expl}} x_j] d\Omega = 0 \tag{50}$$

$\nabla \cdot (E\mathbf{x})$:

$$\int_\Gamma [Ex_k n_k - \sigma_{ij} n_j u_{i,k} x_k] d\Gamma -$$

$$\int_\Omega [(\rho \dot{u}_i \dot{u}_{i,k} x_k - \rho \ddot{u}_i u_{i,k} x_k + \rho \dot{u}_i \dot{u}_i) + f_i u_{i,k} x_k$$

$$- \sigma_{ij} \alpha_{ij} \Delta\Theta + (E_{,k})_{\text{expl}} x_k] d\Omega = 0 \tag{51}$$

The expressions presented in equations (49)–(51) could have been derived in an alternate manner by eliminating L in favor of E in the balance laws shown earlier.

4 Conclusions

Three of the balance laws presented by Fletcher (1976) have been extended to account for material nonhomogeneity and anisotropy, body force, and thermal gradients. These new balance laws are derived in a systematic manner by subjecting the Lagrangian density to appropriate vector calculus operations. It is pointed out that these balance laws are not directly related to the energy release rates for defect motions. Rather, balance laws expressed in terms of the total (kinetic + elastic strain) energy density are shown to lead to energy release rate expressions.

Acknowledgments

Financial support from the Department of Energy under DOE Grant 12040 to Stanford University is gratefully acknowledged.

References

Budiansky, B., and Rice, J. R., 1973, "Conservation Laws and Energy Release Rates," ASME JOURNAL OF APPLIED MECHANICS, Vol. 40, pp. 201–203.

Ehrlacher, A., 1981, "Path Independent Integral for the Calculation of the Energy Release Rate in Elastodynamics," *Advances in Fracture Research—Fracture 81*, Vol. 5, pp. 2187–2194.

Eshelby, J. D., 1975, "The Elastic Energy Momentum Tensor," *Journal of Elasticity*, Vol. 5, Nos. 3–4, pp. 321–335.

Fletcher, D. C., 1976, "Conservation Laws in Linear Elastodynamics," *Archives for Rational Mechanics Analysis*, Vol. 60, pp. 330–353.

Freund, L. B., 1972, "Energy Flux Into the Tip of an Extending Crack in an Elastic Solid," *Journal of Elasticity*, Vol. 2, No. 4, pp. 341–349.

Herrmann, A. G., 1981, "On Conservation Laws of Continuum Mechanics," *International Journal of Solids and Structures*, Vol. 17, No. 1, pp. 1–8.

Herrmann, A. G., 1982a, "Material Momentum Tensor and Path-Independent Integrals of Fracture Mechanics," *International Journal of Solids and Structures*, Vol. 18, No. 4, pp. 319–326.

Herrmann, A. G., 1982b, "Characterization of Cracks and Other Defects in Elastic and Thermoelastic Solids," *Current Advances in Mechanical Design and Production*, Second Cairo University Conference MDP Conference, Cairo, Egypt.

Knowles, J. K., and Sternberg, E., 1972, "On a Class of Conservation Laws in Linearized and Finite Elastostatics," *Archives for Rational Mechanics Analysis*, Vol. 44, pp. 187–211.

Nakamura, T., Shih, C. F., and Freund, L. B., 1985, "Computational Methods Based on an Energy Integral in Dynamic Fracture," *International Journal of Fracture*, Vol. 27, pp. 229–243.

Neumann, F., 1841, *Alhandlungen der deutschen Akademie der Wissenschaften Berlin*, Part 2, pp. 1–254.

Noether, E., 1971, "Invariant Variational Problems," *Transport Theory and Statistical Physics*, Vol. 1, pp. 183–207.

Rice, J. R., 1968, "A Path Independent Integral and the Approximate Analysis of Strain Concentration by Notches and Cracks," ASME JOURNAL OF APPLIED MECHANICS, Vol. 35, pp. 379–386.

APPENDIX

Assertion: $e_{kij}[\sigma_{mi} u_{j,m} - \sigma_{mj} u_{m,i}] = b_k = 0$ for a linear elastic isotropic material.

Proof: The stress-strain law for a linear elastic isotropic material is

$$\sigma_{ij} = \lambda \delta_{ij} u_{k,k} + \mu (u_{i,j} + u_{j,i}) - (3\lambda + 2\mu) \alpha \Delta\Theta \delta_{ij}$$

where δ_{ij} is the Kronecker delta. After substituting this equation in the expression above, the following expression results

$$b_k = \mu e_{kij} (u_{i,m} u_{j,m} - u_{m,j} u_{m,i})$$

The next steps are to multiply both sides of this equation by e_{kst} and apply the identity $e_{kij} e_{kst} = \delta_{is}\delta_{jt} - \delta_{it}\delta_{js}$. It follows that

$$e_{kst} b_k = \mu (\delta_{i3}\delta_{jt} - \delta_{it}\delta_{js}) (u_{i,m} u_{j,m} - u_{m,j} u_{m,i})$$

Expanding this expression yields

$$b_k = 0$$

This completes the proof of the assertion above.

Downloaded 03 May 2010 to 171.66.16.27. Redistribution subject to ASME license or copyright; see http://www.asme.org/terms/Terms_Use.cfm

Subsurface Cracks Under Conditions of Slip, Stick, and Separation Caused by a Moving Compressive Load

S. D. Sheppard
Department of Mechanical Engineering,
Stanford University,
Stanford, CA 94305

J. R. Barber

M. Comninou
Department of Mechanical Engineering and
Applied Mechanics,
University of Michigan,
Ann Arbor, MI 48109

The Mode I and II stress intensity factors (K_I, K_{II}) *at the two tips of a subsurface crack subjected to a moving compressive load are studied. Coulomb friction along the crack faces results in a number of history dependent slip-stick configurations and nonsymmetric variation in* K_I *and* K_{II}. *The formulation used to study this variation involves a singular integral equation in two variables which must be solved numerically, and because of the history dependence, requires an incremental solution. Crack lengths and coefficients of friction that result in as many as three zones for any load location are considered in this paper, while a previous paper (Sheppard et al., in press) was limited to configurations involving two zones only.*

Introduction

The geometry shown in Fig. 1 depicts a subsurface crack that might lead to a spalling failure in a component experiencing rolling contact (e.g., roller and ball bearing, wheel and rail, cam and follower). P in this figure represents the load transferred from one component to another.

Experimental evidence (Ramanathan and Radhakriskhnan, 1977; Jahanmir and Suh, 1977) shows that the subsurface crack may grow parallel to the surface for some distance, after which a transverse crack forms, ultimately leading to detachment of a thin layer of material. Fatigue mechanisms are present in this growth. Additional evidence (Yoshimura et al., 1984) has shown that crack growth is greater from crack tip C (trailing crack tip) than from crack tip B (leading crack tip). This asymmetric behavior, (which may initially seem in conflict with the fully reversed shear stress predicted in Hertzian contact between elastic bodies) can be explained either by plastic deformation or by the presence of friction between the crack faces. The effect of crack face friction and the resulting history dependence are considered in this paper.

By assuming linear elastic fracture mechanics (LEFM), very small crack growth per load pass, and Coulomb crack face friction, Sheppard et al. (in press) studied the range of the Mode II stress intensity factors (ΔK_{II}) for cracks embedded in an elastic half-space, as shown in Fig. 1, subjected to a moving compressive surface load. Dimension a represents the crack depth, t the monotonically increasing load position, and B and

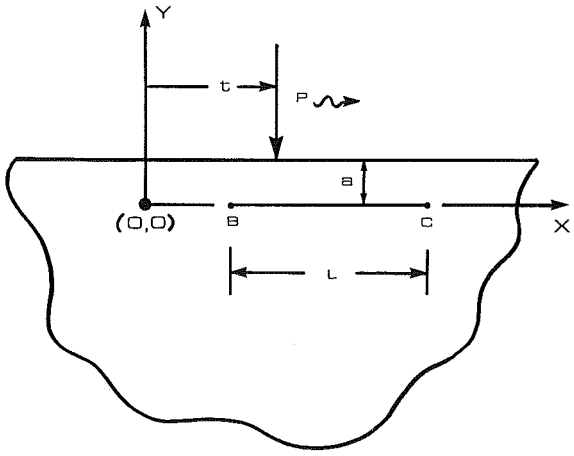


Fig. 1 Geometry of the problem

C the extent of the crack of length L. They found that as the load moves from left to right (slowly enough for inertia effects to be negligible), a number of stick-slip configurations develop, each of which is dependent on the previous load history, the crack length to depth ratio L/a, and the coefficient of crackface friction f. Because several of these configurations involve a growing stick zone, the problem had to be solved incrementally for reasons discussed in the work by Sheppard et al. (in press).

It was found that except for very short cracks (e.g., $f=0.10$, $L/a=0.10$), ΔK_{II} at C is greater than ΔK_{II} at B, which is consistent with the observed crack growth by Yoshimura et al. (1986). The investigation by Sheppard et al. (in press) was restricted to combinations of f and L/a that follow a pattern such that no configuration develops that consists of more than 2 zones. These combinations are referred to as "Short Cracks."

The present paper extends the formulation developed by

Contributed by the Applied Mechanics Division for presentation at the 1987 Applied Mechanics, Biomechanics, and Fluids Engineering Conference, Cincinnati, OH, June 14–17, 1987, of the American Society of Mechanical Engineers.
Discussion of this paper should be addressed to the Editorial Department, ASME, United Engineering Center, 345 East 47th Street, New York, N.Y. 10017, and will be accepted until two months after final publication of the paper itself in the JOURNAL OF APPLIED MECHANICS. Manuscript received by ASME Applied Mechanics Division, June 20, 1985; final revision, July 20, 1986.
Paper No. 87-APM-29.

Copyright © 1987 by ASME
Downloaded 03 May 2010 to 171.66.16.27. Redistribution subject to ASME license or copyright; see http://www.asme.org/terms/Terms_Use.cfm

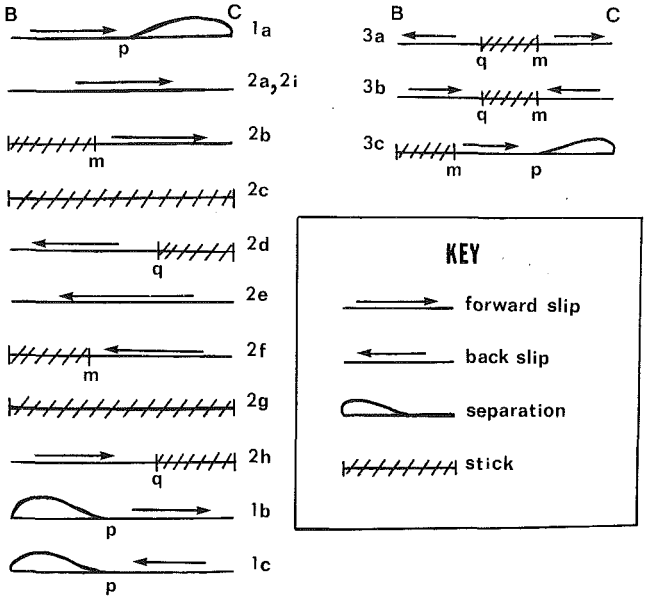


Fig. 2 Configurations investigated in the current work and in the work by Sheppard et al. (in press)

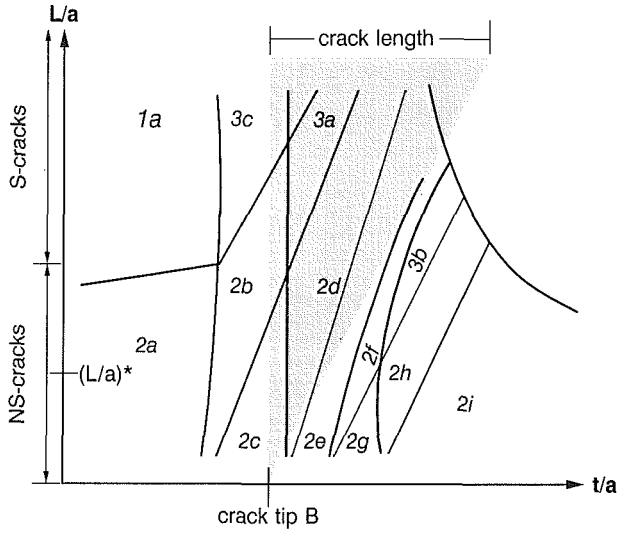


Fig. 3 Generic configuration map. Development of configurations with left to right load movement for a specific value of *L/a*.

Sheppard et al. (in press) to consider combinations that result in configurations where more than 2 zones and/or separation occur at some load location. The assumptions of LEFM, Coulomb crack face friction, and slow crack growth are retained, as is the geometry of Fig. 1. Of particular interest is the influence f and L/a on the range of stress intensity factors experienced at crack tips B and C.

Details of the analysis that are similar to those presented by Sheppard et al. (in press) are not repeated here.

The Semi-Inverse Method

One of four conditions can exist between the upper and lower crack faces, namely, forward slip, back slip, stick, or separation. Each condition is governed by two equalities and one or two inequalities. Furthermore, all portions of the crack are *not* necessarily under the same condition at a given load condition.

The pattern of configurations (i.e., the way in which different combinations of stick, slip and/or separation develop with load movement) is not known a priori. This necessitates that the solution be approached in a semi-inverse manner, i.e., a configuration for a particular load position is assumed and the resulting tractions are found using the governing equalities. The governing inequalities are then checked. If they are not violated, the assumed configuration is correct. If they are, the sense of the violation gives an indication of the true configuration for this load position, and the problem must be resolved with a new assumed configuration. In this manner, it is possible to determine what configurations develop with load movement, even though this is not known a priori.

The Configuration Map

As was mentioned previously, the investigation by Sheppard et al. (in press) was restricted to cracks of (L/a) such that only one and two zone configurations developed with load movement, as represented by configurations $(2a)$–$(2i)$ of Fig. 2. This particular situation develops only with cracks of (L/a) less than a critical value $(L/a)^*$, which is a function of the coefficient of friction f.

The transitions between configurations can be plotted as a function of load position and L/a, to give a configuration map, as shown in Fig. 3. This figure shows the development of configurations for a range of L/a ratios (vertical axis) with load movement (horizontal axis) for a particular coefficient of friction. It is read by selecting a specific level of L/a, then traversing the plot along a horizontal line at that level, noting that crossing a boundary line indicates a change in the configuration. At $L/a > (L/a)^*$, configurations involving 3-zones and/or separation develop in addition to those represented by $(2a)$–$(2i)$ presented by Sheppard et al. (in press). The results represented in this map must be interpreted from left to right because of the history dependent nature of the problem.

It is the objective of this current paper to explore crack patterns developed at $L/a > (L/a)^*$. The formulation of configurations $(2a)$–$(2i)$ is contained in the work by Sheppard et al. (in press), while that for additional configurations that develop at $L/a > (L/a)^*$ is presented below and in the work by Sheppard (1985). All of the configurations investigated by Sheppard et al. (in press) and in the present work are summarized in Fig. 2.

Formulation

The problem is formulated by using the solution for a compressive load on an unflawed half-plane, corrected by additional solutions which ensure that appropriate boundary conditions are met along the crack. The unflawed half-plane shear and normal tractions are given by the Flamant Solution, as was discussed by Sheppard et al. (in press).

One of the two corrective terms is represented by a distribution of edge dislocations of the glide type with density $B_x(x)$. This distribution depends on the position of the load, t, but the dependence is only indicated explicitly when needed for clarity. The shear and normal tractions associated with the glide dislocation distribution are given by the seconds terms in both equations (3) and (4) of the work by Sheppard et al. (in press), respectively, where K_s is replaced with K_{sg}, and K_n with K_{ng} in the current presentation. In the following development equations contained in the work by Sheppard et al. (in press) will be referred to by $\{xx\}$.

The second corrective term, which is only needed when separation is present, is represented by a distribution of edge dislocations of the climb type with density B_y along the separation zone. As with the B_x distribution, B_y depends on the position of the load, t, but the dependence is only indicated explicitly when needed for clarity. The shear and normal tractions associated with this climb dislocation distribution are (Schmueser et al., 1980):

$$S_c(x) = \frac{2\mu}{\pi(k+1)} \int_B^C B_y(\xi) K_{sc}(x,\xi) d\xi \qquad (1)$$

Downloaded 03 May 2010 to 171.66.16.27. Redistribution subject to ASME license or copyright; see http://www.asme.org/terms/Terms_Use.cfm

$$N_c(x)=\frac{2\mu}{\pi(k+1)}\int_B^C B_y(\xi)K_{nc}(x,\xi)d\xi \tag{2}$$

where

$$K_{sc}(x,\xi)=\frac{8a^3}{R^2}\left(3-\frac{16a^2}{R}\right) \tag{3}$$

$$K_{nc}(x,\xi)=\frac{1}{(x-\xi)}-\frac{(x-\xi)}{R}\left(-1+\frac{4a^3}{R}+\frac{64a^4}{R^2}\right) \tag{4}$$

and $R=4a^4+(\xi-x)^2$.

Combining the Flamant, glide, and climb terms for shear and normal tractions results in

$$S(x)=\frac{2Pa^2x_t}{\pi(a^2+x_t^2)^2}+\frac{2\mu}{\pi(k+1)}\int_B^C B_x(\xi)K_{sg}(x,\xi)d\xi$$

$$+\frac{2\mu}{\pi(k+1)}\int_B^C B_y(\xi)K_{sc}(x,\xi)d\xi \tag{5}$$

$$N(x)=\frac{-2Pa^3}{(a^2+x_t^2)^2}+\frac{2\mu}{\pi(k+1)}\int_B^C B_x(\xi)K_{ng}(x,\xi)d\xi$$

$$+\frac{2\mu}{\pi(k+1)}\int_B^C B_y(\xi)K_{nc}(x,\xi)d\xi \tag{6}$$

The Mode II stress intensity factors K_{II} at B and C are given in equations {5} and {6} and the horizontal shift $h(x)$ in {7} and {8}.

The Mode I stress intensity factors at B and C are

$$K_I(B)=-\lim_{x\to B}\left[\frac{2\mu}{\pi(k+1)}B_y(x)\sqrt{2\pi(x-B)}\right] \tag{7}$$

$$K_I(C)=\lim_{x\to C}\left[\frac{2\mu}{\pi(k+1)}B_y(x)\sqrt{2\pi(C-x)}\right] \tag{8}$$

We note that K_I is only nonzero if there is a separation zone adjacent to the crack tip. The vertical movement of the upper crack face relative to the lower face (i.e., gap) is

$$g(x)=v(x,0+)-v(x,0-) \tag{9}$$

and is related to $B_y(x)$ by

$$g(x)=-\int_B^x B_y(\xi)d\xi \tag{10}$$

To ensure uniqueness of displacements the integral of the dislocation distributions along the crack must be zero, i.e.,

$$\int_B^C B_y(\xi)d\xi=0 \tag{11}$$

The corresponding condition on B_x is equation {9}.

We assume that Coulomb friction exists between contacting crack faces, governed by the equations and inequalities shown below.

Forward slip:

$$S(x)=-fN(x);\quad g(x)=0 \tag{12a}$$

$$N(x)<0;\ \dot{h}(x)>0 \tag{12b}$$

Backslip:

$$S(x)=fN(x);\quad g(x)=0 \tag{13a}$$

$$N(x)<0;\ \dot{h}(x)<0 \tag{13b}$$

Stick:

$$\dot{h}(x)=0;\ g(x)=0 \tag{14a}$$

$$S(x)<-fN(x);\ N(x)<0 \tag{14b}$$

Separation:

$$S(x)=0;\ N(x)=0 \tag{15a}$$

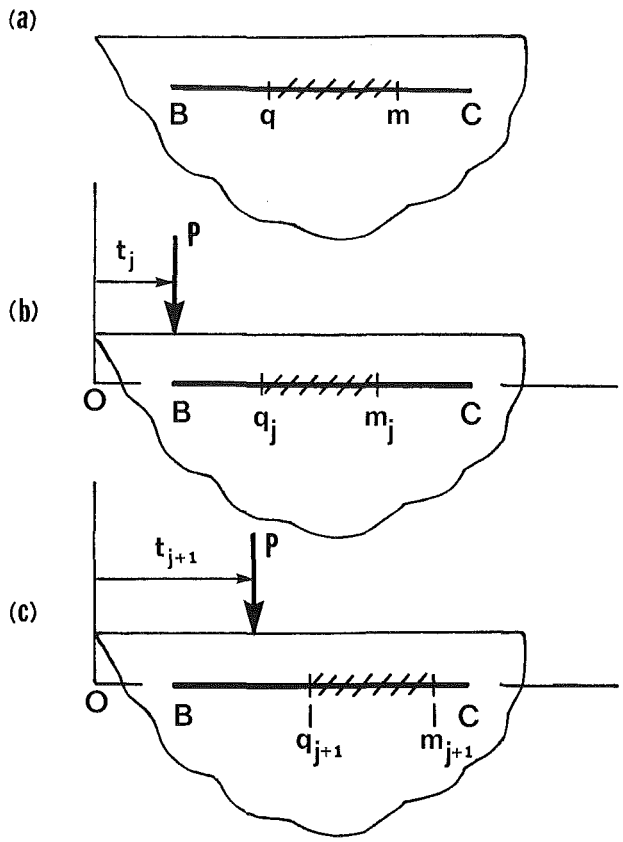


Fig. 4 3-zone configuration (3a): (a) general configuration; (b) configuration at $t=t_j$; (c) at $t=t_{j+1}$

$$g(x)>0 \tag{15b}$$

where $\dot{h}(x)=dh(x)/dt$.

For example, if a point R is a forward slip region, the expressions for N and S from equations (5) and (6) are substituted into the first equality of equation (12a) giving

$$\frac{2\pi}{\pi(k+1)}\int_B^C B_x(\xi)[K_{sg}(x,\xi)+fK_{ng}(x,\xi)]d\xi$$

$$+\frac{2\mu}{\pi(k+1)}\int_B^C B_y(\xi)[K_{sc}(x,\xi)+fK_{nc}(x,\xi)]d\xi \tag{16}$$

$$=\frac{2Pa^2(fa-x_t)}{(a^2+x_t^2)^2}\ \text{in}\ R$$

The second equality in equation (12a) requires

$$B_y(\xi)=0; \tag{17}$$

outside the separation zone.

(1a) Forward Slip with Separation. The configuration which involves a growing forward slip zone and separation is shown by (1a) in Fig. 2. It is described by equation (12) enforced over the range $B<x<C$, and the second equation of (15a) enforced over $p<x<C$ where $B<p<C$.

For some cracks a violation to the second inequality of (12b) is found just to the right of B before p has reached C. This indicates that stick begins at B. The configuration discussed in Section (3c) of stick, forward slip and separation then becomes appropriate. If p reaches C and no violation is found, a configuration of full forward slip develops, and Section 2(a) of the work by Sheppard et al. (in press) is appropriate.

(1b) Separation and Forward Slip. As the load moves to the right all combinations of f and L/a develop into a configuration of separation and forward slip, called (1b). This

Downloaded 03 May 2010 to 171.66.16.27. Redistribution subject to ASME license or copyright; see http://www.asme.org/terms/Terms_Use.cfm

configuration is basically the same as that presented in (1*a*) except that separation will extend over a region $B<x<p$, and forward slip over $p<x<C$. A Mode I stress intensity factor will develop at crack tip B, as given by equation (7), but was generally found to be small.

(1*c*) Separation and Backslip. For certain combinations of f and L/a, a configuration of separation and backslip develops after configuration (2*e*) of full backslip. The formulation for this separation-backslip configuration is identical to that of (1*b*) except that the direction of slip is reversed by substituting $-f$ for f in the relevant equations.

(3*a*) Backslip-Stick-Forward Slip. If a violation to the condition that $|S|<-fN$ occurs at B during configuration (2*b*) of growing stick and forward slip, the development of a backslip zone at B is indicated. When this occurs we must deal with configuration (3*a*), which is detailed in Fig. 4(*a*). A growing backslip zone exists in $B<x<q$ which observes condition (13), a shrinking forward slip zone exists in $m<x<C$, which observes condition (12), and a moving stick zone exists in $q<x<m$, which follows condition (14). The left zone is similar to the growing backslip zone of Section (2*d*) of the work by Sheppard et al. (in press) which did not require an incremental solution, while the right zone is similar to the growing stick zone as discussed in section (2*b*) of that same work, which did require an incremental solution. Using these ideas, the movement of q, the transition point between backslip and stick, and m, the transition point between stick and forward slip with load position, can be studied.

The shear and normal tractions at t are represented by equation (5) and (6), noting that the terms involving climb dislocations B_y are zero because there is no separation along the length of the crack. Substituting these into the first equality of (12*a*), used to describe the right zone, resuls in equation (16). Differentiating equation (16) with respect to load position, as was done in Section (2*b*) of the paper by Sheppard et al. (in press), results in an expression in which only the currently active dislocations are present:

$$\frac{2\mu}{\pi(k+1)}\int_m^C \dot{B}_x(\xi)[K_{sg}(x,\xi)+fK_{ng}(x,\xi)]d\xi$$
$$=\frac{-2\mu}{\pi(k+1)}\int_B^q \Delta\dot{B}_x(\xi)[K_{sg}(x,\xi)+fK_{ng}(x,\xi)]d\xi$$
$$+\frac{2Pa^2(4fax_t-3xt^2+a^2)}{\pi(a^2+x_t^2)^2};\quad m<x<C \tag{18}$$

The first term to the right of the equality sign represents the effect of the distribution of active dislocations in the left backslip zone on the differential problem, and, therefore, a coupling of the left and right zones. In the problem presented in Section (2*b*) of the paper by Sheppard et al. (in press) this term was zero as there was no backslip zone to account for.

Equation {23} is appropriate for partially enforcing uniqueness. Normalizing and discretizing equations (18) and (23) results in $(n+1)$ equations for finding the normalized values of $\dot{B}_x$ at specified integration points, and current load position t_{j+1}, if the transition point m_{j+1} between stick and forward slip, as shown in Fig. 4(*c*), is assumed known. The contribution from the coupling term (i.e., $\Delta\dot{B}_x$) is calculated from load position t_j, as will be discussed below.

We now turn our attention to the left slip zone where backslip is occurring. We start by writing equations (5) and (6), expressions for normal and shear tractions, in a modified form, where t_{j+1} and m_{j+1} refer to the current locations of load and stick-forward slip transition, and t_j and m_j refer to the previous locations of these points, as shown in Figs. 4(*b*) and 4(*c*).

$$S(x)=\left[\frac{2\mu}{\pi(k+1)}\int_B^q \Delta B_x(\xi)K_{sg}(x,\xi)d\xi+S_d(x)\right.$$
$$\left.+\frac{2\mu}{\pi(k+1)}\int_{t_j}^{t_{j+1}}\int_{m(z)}^C \dot{B}_x(\xi)K_{sg}(x,\xi)d\xi dz\right]$$
$$+\frac{2Pa^2x_t}{\pi(a^2+x_t^2)^2} \tag{19}$$

$$N(x)=\left[\frac{2\mu}{\pi(k+1)}\int_B^q \Delta B_x(\xi)K_{ng}(x,\xi)d\xi+N_d(x)\right.$$
$$\left.+\frac{2\mu}{\pi(k+1)}\int_{t_j}^{t_{j+1}}\int_{m(z)}^C \dot{B}_x(\xi)K_{ng}(x,\xi)d\xi dz\right]$$
$$-\frac{2Pa^3}{(a^2+x_t^2)^2} \tag{20}$$

where $x_t=x-t_{j+1}$. The bracketed term in each of these expressions represents the total effect of dislocations from the load location when stick just began at B, up to and including the present load location t_{j+1}, and is equivalent to the non-Flamant portions of equations (5) and (6). It is instructive to review what each of the parts of the bracketed terms in equations (19) and (20) represents. The first component represents the effect of the glide dislocations positioned in $B<\xi<q$, reflecting load movement from its position when backslip just begins at B up to t_{j+1}, the second component represents contributions from locked dislocations with load movement from the start of stick at B to t_j, and the final component reflects the effect from locked dislocations from local movement t_j to t_{j+1}. Substituting equations (19) and (20) into the first equality of equation (13*a*) and rearranging results in

$$\frac{2\mu}{\pi(k+1)}\int_B^q \Delta B_x(\xi)[K_{sg}(x,\xi)-fK_{ng}(x,\xi)]d\xi$$
$$=\frac{-2\mu}{\pi(k+1)}\int_{t_j}^{t_{j+1}}\int_{m(z)}^C \dot{B}_x(\xi)[K_{sg}(x,\xi)$$
$$-fK_{ng}(x,\xi)]d\xi-\frac{2Pa^2(fa+x_t)}{\pi(a^2+x_t^2)^2}+fN_d(x)-S_d(x);$$
$$B<x<q \tag{21}$$

Note that the range of equation (21) coincides with the limits of integration and that ΔB_x is bounded at q and unbounded at B. $\dot{B}_x$ is represented as in equation {24}. Uniqueness of the solution is enforced by

$$\int_B^q \Delta B_x(\xi)=0 \tag{22}$$

Normalizing equations (21) and (22), then discretizing, results in $(n+1)$ equations for finding the n values of $\Delta B_x(r)$ at specified integration points and the location of q_{j+1}, based on the value of t_{j+1} found from the solution of equations (18) and {23}, as was discussed above.

The change in the Mode II stress intensity factor at B is given by equation {43}, while that at C is given by {37}. Updates to "tracer" point stresses due to locked-in dislocations are made in the same manner as in Section (2*b*) of the work by Sheppard et al. (in press) (e.g., equation {35}).

As m moves towards C the value of forward slip dh/dt is continually monitored in the two slip zones. If it becomes positive adjacent to B the growth of a stick zone emanating from B is indicated and the problem will involve 4 zones. If the normal stress just to the right of B becomes positive, separation at this location is indicated. If separation or stick at B is not indicated, the $(j+2)$th step in the incremental solution is taken; namely finding t_{j+2} and q_{j+2} corresponding to m_{j+2}.

Before beginning calculations for this step, the left backslip

Downloaded 03 May 2010 to 171.66.16.27. Redistribution subject to ASME license or copyright; see http://www.asme.org/terms/Terms_Use.cfm

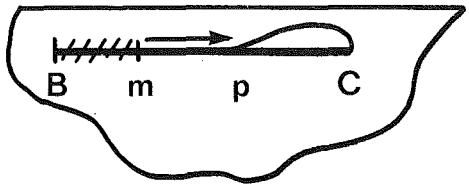


Fig. 5 3-zone configuration (3c) of stick-forward slip-separation

zone is viewed in an incremental manner at the $(j+1)$th step. This is done so that an accurate estimate can be made of first term to the right of the equality sign in equation (18) involving $\Delta\dot{B}_x(\xi)$, as was mentioned above. Equation (21) is differentiated with respect to t, and as $\Delta\dot{B}_x(\xi)$, $B<\xi<q_{j+1}$, is unbounded at both ends, provides $(n-1)$ equation is normalized, discretized form. A uniqueness requirement on $\Delta\dot{B}_x$ provides the nth equation necessary for finding $\Delta\dot{B}_x$. The accuracy of this estimate is based on the fact that load steps are small.

If a 4-zone configuration does not develop as m moves towards and finally reaches C, the problem once again becomes 2-zone in nature, following the growing backslip development of Section (2*d*) in the work by Sheppard et al. (in press).

(3*b*) Forward Slip-Stick-Backslip. In the event that configuration (3*b*) develops, as shown in Fig. 2, the formulation to be used is identical to that described in Section (3*a*) except for a change in the sign of f in appropriate equations.

(3*c*) Stick-Forward Slip-Separation. If the separation zone at end C does not disappear prior to an indication of stick at B, configuration (3*c*) develops, which is detailed in Fig. 5. Condition (12) describes the zone from $m<x<C$, while equation (15) describes $p<x<C$, and equation (14) describes $B<x<m$. This configuration differs from (1*a*) where separation was also present because the growing stick zone makes the configuration incremental in nature. The formulation used to investigate this configuration is similar to that of (2*b*), except that a distribution of climb dislocations must be included to account for the separation zone, and is detailed in the work by Sheppard (1985).

Results

Using the formulations described above and in the work by Sheppard et al. (in press), configuration maps for a number of realistic values of f were developed, an example of which is given in Fig. 6 for $f=0.5$. Note that as L/a approaches zero the results indicate that only one zone will be present at any load position.

The range of L/a ratios studied by Sheppard et al. (in press) (i.e., "Short Cracks") are indicated in this figure. "A" pattern cracks, which occur at slightly larger values of L/a than for "Short Cracks" experience a 3-zone configuration (3*b*) after the configuration of full backslip (2*e*), while "B" pattern cracks experience 3 zone configurations after full backslip (2*e*) as well as after full forward slip (2*a*). "C" pattern cracks are such that the separation zone to the left of crack tip C has not disappeared prior to the onset of stick at crack tip B (3*c*), but separation does disappear prior to an indication of backslip at B. Finally, "D" pattern cracks are such that separation has not disappeared prior to the indication of backslip at B.

It is interesting to note that for $f=0.5$ and $2.35<L/a<2.5$ configuration (1*c*) of separation and backslip develops after full backslip (2*e*). At a later load position a violation to the requirement that $(dh/dt<0)$ is found just to the left of C, indicating formation of a stick zone at this location. For $2.50<L/a<3.0$, separation develops at B during configuration (3*a*) of backslip, stick, and forward slip, and for $1.4<L/a<2.35$ during configuration (3*b*) of forward slip, stick and backslip, or (2*h*) of forward slip and stick.

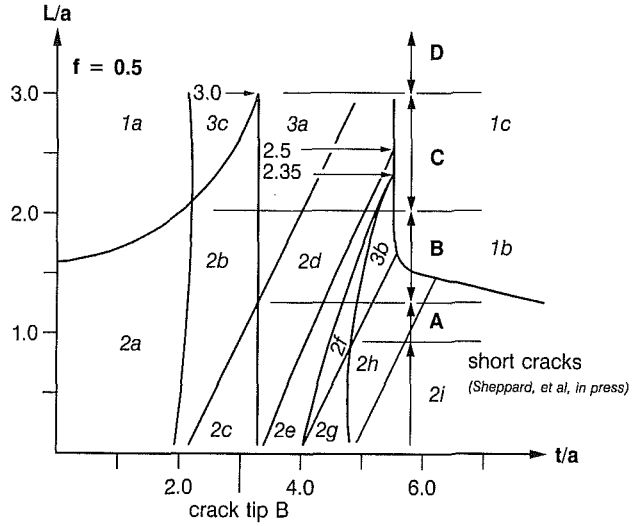


Fig. 6 Configuration map for $f=0.50$, showing configuration development for a variety of L/a values with load movement t/a

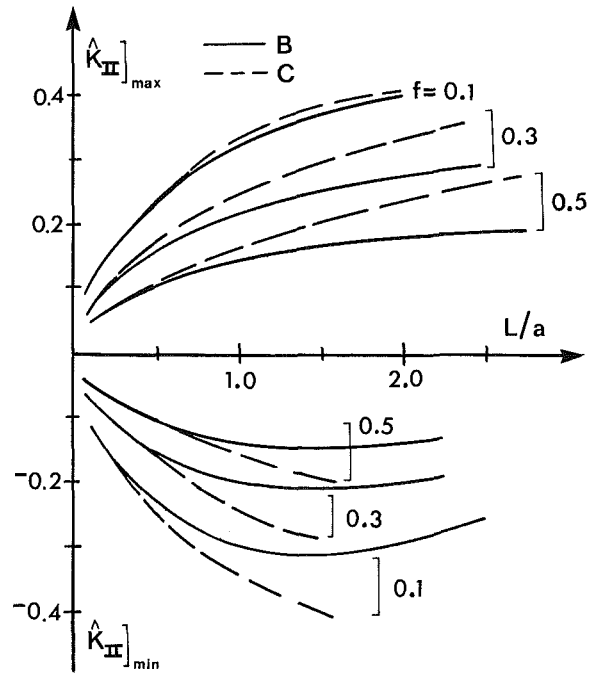


Fig. 7 Maximum and minimum values of Mode II stress intensity factors at B and C as functions of crack length L/a for various coefficients of friction

The maximum and minimum values of $\hat{K}_{II}=(\pi a^{1/2}/2P)K_{II}$ are shown in Fig. 7 as a function of crack length for various coefficients of friction. For a given L/a ratio, these values represent the maximum and minimum level of Mode II stress intensity experienced at the leading (end B) and trailing (end C) crack tips as the load moves over the crack. For all values of f considered, $\hat{K}_{IImin}(B)$ peaks at approximately $L/a=1.5$, then increases. $\hat{K}_{IImax}(C)$ appears to be leveling off in all cases. Increasing f serves to decrease all peak values.

The values of $\hat{K}_{Imax}(C)$ as a function of L/a are shown in Fig. 8 for a variety of f levels. This maximum occurs during configuration (1*a*), and similar values were found for $\hat{K}_{Imax}(B)$, which will of course occur sometime after separation has begun at B. Note how *small* these values are relative to the $\hat{K}_{II}$ values shown in Fig. 7.

Of particular importance for crack growth is the range of the stress intensity factors at the crack tips. Figure 9 shows this

Downloaded 03 May 2010 to 171.66.16.27. Redistribution subject to ASME license or copyright; see http://www.asme.org/terms/Terms_Use.cfm

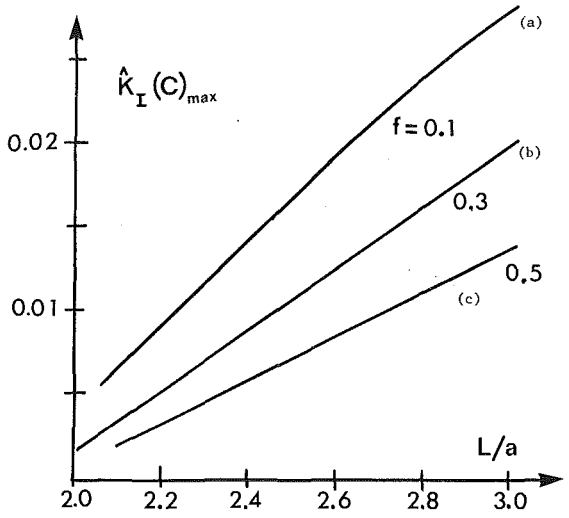


Fig. 8 Maximum values of Mode I stress intensity factors at *C* as a function of crack length *L/a* for various coefficients of friction

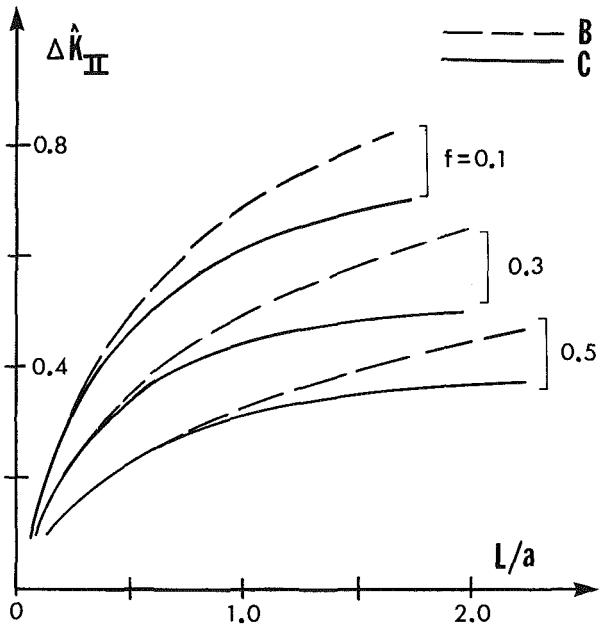


Fig. 9 The range ($\hat{K}_{IImax} - \hat{K}_{IImin}$) of Mode II stress intensity factors at *B* and *C* as functions of crack length *L/a* for various coefficients of friction

range for $\hat{K}_{II}$ as a function of L/a for various values of f. Except for very short cracks, this range is significantly greater at C than at B, indicating a tendency for cracks to grow from the trailing edge under repeated loading.

$\Delta\hat{K}_{II}$ values found in this study are compared with those presented by Hearle and Johnson (1984, 1985) in Fig. 10. At longer lengths, Hearle and Johnson's underestimation of $\Delta\hat{K}_{II}$ values is probably due to their use of an inexact model of the locked regions of the crack, and to a lesser degree due to their neglect of the influence of the free surface and crack face separation.

Conclusions

The method described allows for investigation of both Mode I (K_I) and Mode II (K_{II}) effects experienced by a subsurface crack as a load moves over the surface, as might represent fatigue in rolling contact. This method accurately reflects the history dependent nature of the problem caused by the presence of crack face friction.

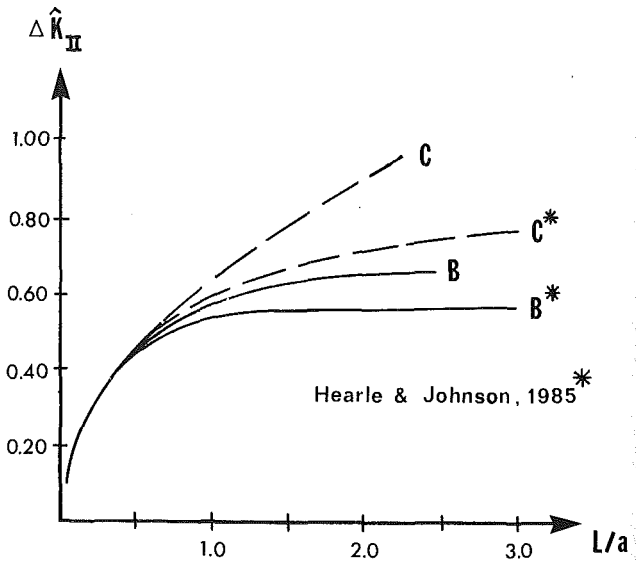


Fig. 10 Comparison of the maximum range of Mode II stress intensity factors ($\Delta\hat{K}_{II}$) with the approximate solution of Hearle and Johnson (1984, 1985): $f = 0.50$

It was found that a number of configuration patterns will result, depending upon the combination of L/a and f. However, these patterns are all such that the crack is left in a stress free state when the load is far away. The parallel nature of a number of the lines separating configurations, as shown in Fig. 6, leads us to anticipate that there is some limiting pattern which is experienced by all cracks beyond a certain length.

In all cases investigated, it was found that $\Delta K_{II}(C)$ is greater than or equal to $\Delta K_{II}(B)$, being equal only when L/a is small. This finding is consistent with the experimental evidence presented in by Yoshimura et al. (1984). As L/a increases, $\Delta K_{II}(B)$ and $\Delta K_{II}(C)$ appear to level off.

The Mode I stress intensity factors at both B and C are at least an order of magnitude smaller than K_{II}, and therefore most likely do not affect crack growth significantly. The presence of Mode I action must be included in the model however, in order to accurately describe interaction between the upper and lower crack faces. Increasing friction serves to decrease all stress intensity factors.

Acknowledgment

Support by the Office of Naval Research through the contract N00014-K-0287 during the course of this research is gratefully acknowledged.

References

Hearle, A. D., Johnson, K. L., 1985. "Mode II Stress Intensity Factors for a Crack Parallel to the Surface of an Elastic Half-Space Subjected to a Moving Point-Load," *J. Mech. Phys. Solids*, Vol. 33, No. 1, pp. 61-81.

Hearle, A. D., Johnson, K. L., "Mode II Stress Intensity Factors for a Crack Parallel to the Surface of an Elastic Half-Space Subjected to a Moving Point-Load," C-Mech/TR26, Cambridge University Engineering Department.

Jahanmir, S., Suh, N. P., 1977. "An Overview of the Delamination Theory of Wear," *Wear*, Vol. 45, pp. 1-16.

Ramanathan, V. M., Radhakrishnan, V. M., 1977. "Investigation of Rolling Contact Fatigue Damage in Case-Carburized Low Alloy Steel," *Wear*, Vol. 45, pp. 323-333.

Schmueser, D., Comninou, M., Dundurs, J., 1980. "Separation and Slip Between a Substrate Caused by a Tensile Load," *Int. J. Engng. Sci.*, Vol. 18, pp. 1149-1155.

Sheppard, S. D., 1985. "Subsurface Cracks in Rolling Contact," Ph.D. Thesis, University of Michigan, Mechanical Engineering.

Sheppard, S., Barber, J. R., Comninou, M., in press. "Short Subsurface Cracks Under Conditions of Slip and Stick Caused by a Moving Compressive Load," *J. of Appl. Mech.*

Yoshimura, H., Rubin, C. A., Hahn, G. T., 1984. "Cyclic Crack Growth Under Repeated Rolling Contact," *Wear*, Vol. 95, p. 29.

Downloaded 03 May 2010 to 171.66.16.27. Redistribution subject to ASME license or copyright; see http://www.asme.org/terms/Terms_Use.cfm

Energy Release Rates in a Fiber-Reinforced Strip

L. F. Mannion
Department of Mathematics
and Computer Science,
St. John's University,
Jamaica, NY 11439

This paper discusses Mode I fracture of a semi-infinite crack in a strip of fiber-reinforced material. The crack is opened by point forces applied to the crack faces. The problem is solved using two models for fiber reinforcement; these models are known as the inextensible and idealized theories and are both based on simplification of the equations of orthotropic elasticity. In the inextensible theory the problem is solved by conformal mapping while the idealized solution involves only stress resultants on free bodies. The energy release rates are calculated from the solution within each model and are then compared.

1 Introduction

Fiber-reinforced materials are anisotropic since the fibers define preferred directions. Stress analysis for such materials, especially in the presence of cracks, is more involved than that for corresponding isotropic problems. The fracture problem for a plane, unbounded anisotropic solid was discussed by Sih et al. (1965) and by Hoenig (1982). The difficulties increase for bounded regions since specific boundary conditions must be satisfied. It is therefore desirable to use models of fiber-reinforced materials which simplify the analysis and yet provide the main features of the elastic solution; this provides the motivation of the present work.

In this paper we examine a problem for a cracked strip of fiber-reinforced material using two models. These models are known as the inextensible and idealized theories of fiber-reinforced materials. They may be regarded as asymptotic approximations to orthotropic elasticity; the nature of this approximation is developed in Everstine and Pipkin (1973) and summarized in the review by Pipkin (1979). To motivate the equations on which the simpler models are based, the stress-strain equations of plane orthotropic elasticity are taken as a starting point.

The inextensible theory is derived in the following section while the idealized theory is given in Section 3; these sections also describe some unusual singularities which may occur in solutions within these models. The geometry of the strip is described in Section 4 and a point force loading problem is formulated. In Sections 5 and 6, respectively, the problem is solved in the inextensible and idealized theories; the former involves Laplace's equation while the latter requires only free body equilibrium.

The energy release rate in crack advance is a quantity of primary interest in fracture mechanics and the purpose of this paper is to show how it may be simply obtained with these models; the calculations are given in Section 7 and the expressions for the energy release rate from both models are compared. The results are discussed in Section 8.

2 The Inextensible Theory

In this section, the inextensible theory is developed as an approximation to orthotropic elasticity. This derivation is essentially that of Pipkin (1979); it is included here for completeness. The axes of a system of Cartesian coordinates x, y are chosen to coincide with the symmetry directions of the solid. In plane stress, the stress-strain equations may be written as

$$\begin{aligned} Eu_{,x} &= \sigma_{xx} - \nu\sigma_{yy}, \\ E'v_{,y} &= -\nu'\sigma_{xx} + \sigma_{yy}, \\ G(u_{,y} + v_{,x}) &= \sigma_{xy}. \end{aligned} \tag{1}$$

In equations (1), $\nu'/E' = \nu/E$, while u and v are the displacement components parallel to the x and y axes, respectively. (Here and in what follows, a comma followed by a subscript denotes a partial derivative.)

The equilibrium equations will be satisfied if the stresses are generated by an Airy stress function $U(x, y)$ as

$$\sigma_{xx} = U_{,yy} \quad , \quad \sigma_{yy} = U_{,xx} \quad , \quad \sigma_{xy} = -U_{,xy}. \tag{2}$$

The equation governing U is derived from the only nontrivial compatibility equation:

$$\epsilon_{xx,yy} + \epsilon_{yy,xx} - 2\epsilon_{xy,xy} = 0. \tag{3}$$

Using equations (1) and (2) in equation (3), we obtain

$$(E/E')U_{,xxxx} + (E/G - 2\nu)U_{,xxyy} - U_{,yyyy} = 0. \tag{4}$$

Equation (4) may be written in the factored form

$$[(1/\epsilon^2)\partial^2/\partial x^2 + \partial^2/\partial y^2](c^2\partial^2/\partial x^2 + \partial^2/\partial y^2)U = 0, \tag{5}$$

provided that

$$c^2/\epsilon^2 = E/E', \quad c^2 + 1/\epsilon^2 = E/G - 2\nu. \tag{6}$$

Contributed by the Applied Mechanics Division for presentation at the 1987 Applied Mechanics, Biomechanics, and Fluids Engineering Conference, Cincinnati, OH, June 14–17, 1987, of the American Society of Mechanical Engineers.
Discussion of this paper should be addressed to the Editorial Department, ASME, United Engineering Center, 345 East 47th Street, New York, N.Y. 10017, and will be accepted until two months after final publication of the paper itself in the JOURNAL OF APPLIED MECHANICS. Manuscript received by ASME Applied Mechanics Division, December 18, 1985; final revision, July 14, 1986.
Paper No. 87-APM-20.

Copyright © 1987 by ASME
Downloaded 03 May 2010 to 171.66.16.27. Redistribution subject to ASME license or copyright; see http://www.asme.org/terms/Terms_Use.cfm

From (6), $1/\epsilon^2$ and c^2 are the roots of the quadratic equation

$$(G/E)\lambda^2 - (1 - 2\nu G/E)\lambda + G/E' = 0. \tag{7}$$

It is at this point that the material is regarded as containing a set of straight fibers, parallel to the crack and continuously distributed. Therefore, in equations (1) the tensile modulus E in the fiber direction is assumed large in comparison with E', the modulus for tension across fibers; E is also assumed large compared with the shear modulus G. With these assumptions, the roots of equation (7) are approximately E/G and G/E'; therefore,

$$\epsilon^2 \approx G/E, \quad c^2 \approx G/E'. \tag{8}$$

Inextensible fibers are modeled by letting $\epsilon \to 0$ in the orthotropic equations. To aid in the passage to the limit, equations (1) are rewritten as

$$\begin{aligned} Gu_{,x} &= a\epsilon^2\sigma_{xx} - b\epsilon^2\sigma_{yy}, \\ Gv_{,y} &= -b\epsilon^2\sigma_{xx} + ac^2\sigma_{yy}, \\ G(u_{,y} + v_{,x}) &= \sigma_{xy}. \end{aligned} \tag{9}$$

The constants in equations (9) are related to those in equations (1) as follows:

$$a\epsilon^2 = G/E, \quad ac^2 = G/E', \quad b\epsilon^2 = G/E, \tag{10}$$

where

$$a = (1 - 2b\epsilon^2)/(1 + \epsilon^2 c^2). \tag{11}$$

Setting $\epsilon = 0$ in equations (9) and noting that $a = 1$ in equation (11), we obtain

$$u_{,x} = 0, \quad Gv_{,y} = c^2\sigma_{yy}. \tag{12}$$

Note that σ_{xx} is no longer given by a stress-strain equation since it is now a reaction to the inextensibility constraint. Equation $(12)_1$ shows that $u = u(y)$; then equation $(9)_3$ gives

$$\sigma_{xy} = G[u'(y) + v_{,x}(x,y)]. \tag{13}$$

Using equations $(12)_2$ and (13) in the equilibrium equation

$$\sigma_{xy,x} + \sigma_{yy,y} = 0 \tag{14}$$

gives the equation governing $v(x,y)$ as

$$v_{,xx} + (1/c^2)v_{,yy} = 0. \tag{15}$$

Boundary conditions are modified due to the kinematic constraints. Since $u = u(y)$, displacements cannot be specified independently at more than one point on a fiber, i.e., on any line $y =$ constant. The most unusual feature arises when a fiber forms part of the boundary, say at $y = 0$. Suppose that $u = 0$ throughout the body. Then, by equation (13),

$$\sigma_{xy}(x,0+) = Gv_{,x}(x,0+). \tag{16}$$

However, v may be determined from equation (15) with either displacement or normal traction boundary conditions, i.e., with only v or $v_{,y}$ prescribed on $y = 0$. In general, $v_{,x}$ as calculated from the solution of the boundary-value problem will not agree with the prescribed distribution of σ_{xy}. Hence there is a jump in the shear stress at $y = 0$. To balance this jump the fiber $y = 0$ carries a finite force. Fibers which carry finite forces are called singular fibers.

The occurrence of singular fibers is essentially a singular perturbation problem, controlled by the parameter ϵ. Through analysis of exact elastic solutions (Everstine and Pipkin, 1973; Pipkin, 1979), it is known that singular fibers correspond to thin layers of high stress in the corresponding elastic solution; in addition, the finite force predicts the level of the concentrated stress.

3 The Idealized Theory

The idealized theory is a more extreme simplification of the elastic theory. In this model, two orthogonal families of inextensible fibers are present, each parallel to a coordinate axis. While retaining equation $(12)_1$, there is the additional kinematic constraint that $v_{,y} = 0$, so that $v = v(x)$. This may be formally obtained from equation $(12)_2$ on letting $c \to 0$. The only stress now given by a constitutive equation is σ_{xy} in equation $(9)_3$; both σ_{xx} and σ_{yy} are reactions to constraints. The constraints $u_{,x} = v_{,y} = 0$ together describe an incompressible material with only one family of fibers and in plane strain. This interpretation shows the role of the parameter c in the inextensible theory as a measure of compressibility across fibers.

The remarks in Section 2 regarding boundary-value problems still apply, with the additional restriction that v cannot be specified at more than one point on any line $x =$ constant. A properly posed displacement problem can be solved using only the kinematic constraints, with all stresses calculated subsequently. Fibers through crack tips are usually singular as are fibers which meet the boundary at the point of application of a concentrated force. As in the inextensible theory, singular fibers in this model predict stress concentration layers in the elastic solution (Pipkin, 1979).

4 The Cracked Strip

An infinite strip of height $2h$ contains a semi-infinite crack along its center line. The origin of coordinates is placed at the crack tip and the crack occupies $y = 0, x < 0$. Equal and opposite point forces are applied to the crack faces at $(-a, 0+)$ and $(-a, 0-)$, while the edges at $y = \pm h$ are traction free. These conditions may be expressed as follows:

$$\sigma_{yy}(x,0\pm) = -F\delta(x+a), \quad x<0, \tag{17}$$

$$\sigma_{xy}(x,\pm h) = \sigma_{yy}(x,\pm h) = 0, \quad -\infty < x < \infty, \tag{18}$$

$$\sigma_{xy}(x,0\pm) = 0, \quad x<0. \tag{19}$$

Since the problem concerns the opening mode of fracture and the objective is to calculate the energy release rate, there is no loss of generality in taking $u = 0$ in the strip; in any case, this follows from fiber inextensibility with $u \to 0$ as $x \to \infty$. It is noted here that the distance from the crack tip to the point force introduces a characteristic length. Such problems are difficult to solve using integral transform and Weiner-Hopf methods. The isotropic version of the present problem is discussed by Fichter (1983) and by Foote and Buchwald (1985).

5 The Inextensible Solution

In this section the displacement $v(x,y)$ is found in the inextensible model. It is convenient to use coordinates (X, Y) where $X = x$ and $Y = cy$. The strip then occupies $-ch < Y < ch$. From equation (15) v is a harmonic function of X and Y, hence

$$v(x,y) = \mathrm{Re}[V(z)] \tag{20}$$

where V is an analytic function of the complex variable $z = X + iY$. The boundary conditions (17) and (18) may be written, on using equations $(12)_2$ and $(13)_1$, as

$$v_{,Y}(X,0\pm) = -(cF/G)\delta(X+a), \quad X<0, \tag{21}$$

$$v_{,X}(X,\pm ch) = v_{,Y}(X,\pm ch) = 0, \quad -\infty < X < \infty. \tag{22}$$

The conformal mapping

$$w = [1 - \exp(\pi z/ch)]^{1/2} \tag{23}$$

maps the cracked strip onto the upper half of the complex w plane, where $w = \xi + i\eta$. The crack surface is mapped onto $|\xi| < 1, \eta = 0$; the upper and lower edges of the strip correspond, respectively, to $\xi < -1, \eta = 0$, and $\xi > 1, \eta = 0$. The points of application of the forces correspond to $(\pm\xi_0, 0)$ where

$$\xi_0 = [1 - \exp(-\pi a/ch)]^{1/2}. \tag{24}$$

Downloaded 03 May 2010 to 171.66.16.27. Redistribution subject to ASME license or copyright; see http://www.asme.org/terms/Terms_Use.cfm

The conditions (21) and (22) become

$$v_{,\eta}(\xi,0)=(cF/G)[\delta(\xi-\xi_0)-\delta(\xi+\xi_0)]. \tag{25}$$

In equation (25),

$$v(\xi,\eta)=v(X(\xi,\eta),Y(\xi,\eta)) \tag{26}$$

and v satisfies

$$v_{,\xi\xi}+v_{,\eta\eta}=0, \quad -\infty<\xi<\infty,\eta>0. \tag{27}$$

The solution of equation (27), subject to equation (25), is

$$v(\xi,\eta)=\mathrm{Re}[\Phi(w)], \tag{28}$$

where

$$\Phi(w)=(cF/\pi G)ln[(w-\xi_0)/(w+\xi_0)]. \tag{29}$$

On comparing equations (20), (26), and (29), we have

$$V(z)=\Phi(w(z)). \tag{30}$$

Equation (29) may be solved for w. On using equation (23) and noting equation (30) we obtain $V(z)$ implicitly as

$$[1-\exp(\pi z/ch)]^{1/2}=-\xi_0\coth(\pi GV/2cF). \tag{31}$$

The asymptotic forms of σ_{yy} and $v(x,y)$ near the crack tip may be extracted from equation (31). Performing a Taylor expansion of the left-hand side around $z = 0$ and of the right-hand side around the corresponding value of V, $V(0) = icF/G$, we find on retaining lowest order terms that

$$V(z)\approx(iF/G)[c-2(cz/\pi h)^{1/2}/\xi_0], \quad \text{as } z\to 0. \tag{32}$$

Recalling that $z = x + icy$ and taking the real part, we find

$$v(x,y)\approx(2F/G\xi_0)(c/\pi h)^{1/2}R^{1/2}\sin(\theta/2), \quad R\to 0, \tag{33}$$

where

$$R^2=x^2+c^2y^2, \quad \theta=\arctan(cy/x). \tag{34}$$

In particular, we find that the shape of the crack face near the tip is, on letting $y = 0$ and $\theta = \pi$ in equation (33),

$$v(x,0)\approx(2F/G\xi_0)(c\,|x|/\pi h)^{1/2}, \quad x\to 0. \tag{35}$$

To find the stresses, equation (20) is used with equations $(12)_1$, (13) and the Cauchy-Riemann equations to obtain

$$GV'(z)=\sigma_{xx}-ic\sigma_{yy}. \tag{36}$$

Differentiating equation (32) and taking the imaginary part, we find

$$\sigma_{yy}\approx F(\pi chR)^{-1/2}\cos(\theta/2). \tag{37}$$

In particular, on the line ahead of the crack where $y = \theta = 0$,

$$\sigma_{yy}\approx F(\pi chx)^{-1/2} \quad \text{as } x\to 0+. \tag{38}$$

Also note that equation (36) gives the stresses at any point in the strip as follows. From equation (30),

$$dV/dz=(d\Phi/dw)(dw/dz). \tag{39}$$

Calculating $d\Phi/dw$ from equation (29), dw/dz from equation (23), and simplifying we obtain

$$\sigma_{xx}-ic\sigma_{yy}=$$

$$-(\xi_0F/h)[\exp(-\pi(z+a)/ch)-1]^{-1}\times[1-\exp(\pi z/ch)]. \tag{40}$$

6 The Idealized Solution

As in the previous section we take $u = 0$ in the strip so that

$$\sigma_{xy}=Gv'(x). \tag{41}$$

Take as a free body the part of the strip in $y > 0$ with $x_1 < x < x_2$, where $x_2 < 0$. The edge $y = h$ is traction free so force balance gives

$$\int_0^h[\sigma_{xy}(x_2,y)-\sigma_{xy}(x_1,y)]dy=\int_{x_1}^{x_2}\sigma_{yy}(x,0)dx. \tag{42}$$

Using equations (17) and (41), equation (42) reduces to

$$v'(x_2)-v'(x_1)=-(F/Gh)\int_{x_1}^{x_2}\delta(x+a)dx. \tag{43}$$

If $-a\notin[x_1,x_2]$ equation (43) gives $v'(x_1) = v'(x_2)$; in particular, if v is bounded as $x\to-\infty$ then

$$v'(x)=0, \quad x<-a. \tag{44}$$

Letting $x_1\to -a-$ and $x_2\to -a+$ in equation (43) we have

$$v'(-a+)-v'(-a-)=-F/Gh. \tag{45}$$

Using equation (44) in equation (45) and noting that $v(0) = 0$ by symmetry, we obtain

$$v(x)=\begin{cases}-Fx/Gh, & -a<x<0,\\ Fa/Gh, & x<-a.\end{cases} \tag{46}$$

In addition, $v(x) = 0$ for $x > 0$, by symmetry and inextensibility of fibers.

7 Energy Release Rates

In calculating the energy release rate $\mathcal{G}_1$ in the inextensible solution, we use the expression for Mode I fracture given by Rice (1968):

$$\mathcal{G}_1=\lim_{\epsilon\to 0}\epsilon^{-1}\int_0^{\epsilon}\sigma_{yy}(x,0)v(x-\epsilon,0)dx. \tag{47}$$

Using equations (35) and (38) for v and σ_{yy}, respectively, and evaluating the resulting integral, we find

$$\mathcal{G}_1=(F^2/Gh)[1-\exp(-\pi a/ch)]^{-1}. \tag{48}$$

In equation (48), equation (24) has been used to eliminate ξ_0.

The energy release rate in the idealized solution may be calculated directly as

$$\mathcal{G}_2=-\partial U/\partial a, \tag{49}$$

where U is the total potential energy of both beam arms and the point forces. In the sheared parts of the beam, the strain energy density is

$$W=\sigma_{xy}\epsilon_{xy}/2=F^2/2Gh^2 \tag{50}$$

from equations (41) and (46), so that $U = -aF^2/Gh$; then equation (49) gives

$$\mathcal{G}_2=F^2/Gh. \tag{51}$$

The accuracy of $\mathcal{G}_2$ as an estimate for $\mathcal{G}_1$ may be examined on using equations (48) and (50) to form the ratio

$$\mathcal{G}_1/\mathcal{G}_2=[1-\exp(-\pi a/ch)]^{-1}. \tag{52}$$

As $c\to 0$, equation (52) gives

$$\mathcal{G}_1/\mathcal{G}_2=1+\exp(-\pi a/ch). \tag{53}$$

8 Discussion

The inextensible and idealized theories may be regarded as models in their own right, although motivated by taking limits in the stress-strain equations of orthotropic elasticity. Each model highlights certain features of the elastic solution. For example, the idealized solution has singular fibers at $x = 0$ and $x = -a$; these indicate thin layers of high normal stress centered on $x = 0$ and $x = -a$ in the orthotropic solution. In addition, the effect on the energy release rate of compressibility across fibers is isolated in equation (48) for $\mathcal{G}_1$.

While it may be possible to solve the present problem within orthotropic elasticity, the resulting expressions for the stresses may be so complicated as to obscure the main features of the solution; this will be discussed in a future paper. Finally, equations (35) and (38) are essentially those of the corresponding

Downloaded 03 May 2010 to 171.66.16.27. Redistribution subject to ASME license or copyright; see http://www.asme.org/terms/Terms_Use.cfm

Mode III isotropic problem, apart from rescaling in the y direction. Therefore, with suitable rescaling and interpretation of boundary conditions, available antiplane shear isotropic solutions also provide solutions in the inextensible theory, at least in cases where the displacement parallel to the fiber direction vanishes.

References

Everstine, G. C., and Pipkin, A. C., 1973, "Boundary Layers in Fiber-Reinforced Materials," ASME JOURNAL OF APPLIED MECHANICS, Vol. 40, pp. 518–522.

Fichter, W. B., 1983, "The Stress Intensity Factor for the Double Cantilever Beam," *International Journal of Fracture*, Vol. 22, pp. 133–143.

Foote, R. M. L., and Buchwald, V. T., "An Exact Solution for the Stress Intensity Factor for a Double Cantilever Beam," *International Journal of Fracture*, Vol. 29, pp. 125–134.

Hoenig, A., 1982, "Near-Tip Behaviour of a Crack in a Plane Anisotropic Elastic Body," *Engineering Fracture Mechanics*, Vol. 16, pp. 393–403.

Pipkin, A. C., 1979, "Stress Analysis for Fiber-Reinforced Materials," *Advances in Applied Mechanics*, Vol. 19, Academic Press, New York, pp. 1–51.

Rice, J. R., 1968, "Mathematical Analysis in the Mechanics of Fracture," in *Fracture*, Vol. II, Academic Press, New York, pp. 191–311.

Sih, G. C., Paris, P. C., and Irwin, G. R., 1965, "On Cracks in Rectilinearly Anisotropic Bodies," *International Journal of Fracture Mechanics*, Vol. 1, pp. 189–203.

Downloaded 03 May 2010 to 171.66.16.27. Redistribution subject to ASME license or copyright; see http://www.asme.org/terms/Terms_Use.cfm

E. Kausel
Associate Professor of
Civil Engineering,
Massachusetts Institute of Technology,
Cambridge, MA 02139

S. H. Seale
Assistant Reseach Geophysicist,
Department of Geological Sciences,
University of California,
Santa Barbara, CA

Static Loads in Layered Halfspaces

A solution is presented for Mindlin's problem of point loads applied in the interior of a layered *elastic halfspace. The algorithm described differes from available numerical solutions for this problem in that the displacement functions found are expressed explicitly in the* spatial *domain. Thus, no numerical transformations are necessary. Furthermore, since the resulting equations can readily be subjected to mathematical manipulations (such as derivations or integrals), they could be used without difficulty as Green's functions in procedures in Elastomechanics such as the Boundary Integral Method.*

1 Introduction

The first fundamental solution of a Green's function for a point load acting in the interior of an unbounded, homogeneous, isotropic elastic space was provided by Sir William Thompson (Lord Kelvin) in 1848. The solution to the analagous, and perhaps more interesting, problem of a point load acting normally to the surface of halfspace presented greater difficulties because of the presence of the stress-free surface. It has been considered first by Clapeyron and Lamé in 1828, and was solved in 1878 by one of Saint Venant's best students, namley J. V. Boussinesq, using the method of potentials. The closely related problem concerning the contact of two elastic bodies was also independently solved, using potentials, by H. Hertz in 1881, a fact which is the more remarkable when one considers the Hertz's main line of work was electromagnetic theory. A year later, Cerruti (1882) presented the solution to the problem of a halfspace loaded on its surface with a tangential point load (i.e., a load with direction parallel to the surface), thus completing the set of formulas necessary for developing solutions to a host of other halfspace problems such as distributed surface loads and line loads. Examples are the solutions for ring loads given by Kermanidis (1975) and by Cruse et al. (1977).

The logical extension to the cases of vertical and horizontal point loads acting in the interior of an elastic halfspace remained unsolved for several decades, until Mindlin developed the necessary formulae in 1936 in the context of a doctoral dissertation. Mindlin's fomulae reduce to those of Boussinesq and Cerruti when the depth of the point load is taken as zero.

Closely related to Mindlin's formulae are the solutions that Rongved (1965), Dundurs and Hetényi (1965), and Plevako (1969) provided for the problem of a point load acting in the interior of two adhering halfspaces of differing material properties. Together with Bossinesq's, Cerruti's, Mindlin's, and Kelvin's formulae, they are the only closed-form solutions currently available to the problem of a point load acting within an infinite isotropic medium. Solutions for layered media, such as those presented by Burminster in 1945, or by Chan et al. in 1974, are based on Integral Transform techniques which must be evaluated numerically.

The finite element method is another numerical technique which has been applied to the problem of static loads in heterogeneous media of infinite extent. The difficulty of modeling the infinite dimension has been overcome in a number of ways. Most often, the boundary of the mesh is located "far enough" away from the load so that the stresses there are negligible (displacements may not be negligible, particularly for plane-strain, or two-dimensional solutions). Alternatively, special boundary conditions, normally referred to as "transmitting boundaries" or "infinite elements" may be provided at the periphery of the model to capture the elastic contribution of the missing field. An example is the exact solution (exact in the finite element sense) presented by Waas (1972) for the representation of a layered semi-infinite stratum from the local viewpoint of a plane vertical section, i.e., from the perspective of the boundary.

An explicit discrete solution for the problem of dynamic (or static) loads in layered strata, excluding halfspaces, was proposed in 1982 by Kausel and Peek. This approach entails a discretization of the medium in the direction of layering, and can be referred to as the Thin Layer Method. In essence, it is based on formulating stiffness matrices for the layered system in the so-called "wavenumber domain," i.e., in the Fourier or Hankel transform space that is the counterpart of the "spatial domain." The inverse transforms, which are required to find the displacements caused by loads placed at the interfaces, are then obtained in closed form. (That such an explicit inverse transform should be possible may not be obvious to the reader; its feasibility hinges on the special algebraic nature of the stiffness matrices for assemblies of discrete layers.) As a result, this technique avoids the difficulties inherent in direct numerical integrations over wavenumber, and provides the true dependence of the displacements on the horizontal coordinate. The reader is referred to related papers (Kausel, 1981; and Hull, 1984) for further details on this method.

This paper presents an extension to the Thin Layer Method that enables its use in the solution of Genreralized Mindlin's

Contributed by the Applied Mechanics Division for publication in the JOURNAL OF APPLIED MECHANICS.
Discussion on this paper should be addressed to the Editorial Department, ASME, United Engineering Center, 345 East 47th Street, New York, N.Y. 10017, and will be accepted until two months after final publication of the paper itself in the JOURNAL OF APPLIED MECHANICS. Manuscript received by ASME Applied Mechanics Division, May 16, 1986.

Copyright © 1987 by ASME
Downloaded 03 May 2010 to 171.66.16.27. Redistribution subject to ASME license or copyright; see http://www.asme.org/terms/Terms_Use.cfm

Problems: find the displacements occurring in an assembly of elastic layers resting on an elastic halfspace when the system is subjected to internal or external loads. To the best of the writers' knowledge, no comparable solution exists for these problems at the present time.

2 Theoretical Derivation

To avoid unnecessary duplication, the reader is referred to the original paper by Kausel and Peek (1982a) for definitions, notation, and the theoretical derivation corresponding to the stratum case. For the sake of conciseness, that paper will be referred to as K&P, and the equations therein as K&Pnn, with nn being the equation number. Since only the extension to the layered halfspace will be described herein, this paper is not self-contained.

In the stiffness matrix method, the relationship between loads and displacements in the frequency-wavenumber domain (identified by a superscript bar) is given by an expression of the form

$$\bar{\mathbf{P}} = \boldsymbol{K}\bar{\mathbf{U}} \tag{1}$$

with $\bar{\mathbf{P}}$, $\bar{\mathbf{U}}$ being the load and displacement vectors, and $\boldsymbol{K}$ being the stiffness matrix for the system of layers. This matrix is obtained by overlapping layer matrices $\boldsymbol{K}_j$ (i.e., $\boldsymbol{K} = \{\boldsymbol{K}_j\}$). For static problems, and when using the Thin Layer Method, the layer matrices are of the form:

$$\boldsymbol{K}_j = \mathbf{A}_j k^2 + \mathbf{B}_j k + \mathbf{G}_j \tag{2}$$

in which k = wavenumber; and $\mathbf{A}_j$, $\mathbf{B}_j$, $\mathbf{G}_j$ are layer matrices that depend only on the material properties of the layers; these are given in K&P.

If an elastic halfspace is added at the bottom of the layer assembly, it becomes necessary to overlap and add the contribution of the halfspace stiffness (Kausel and Roësset, 1981) to the appropriate location in the stiffness matrix, (i.e., in the last 3 × 3 submatrix of the stiffness matrix. Since the static halfspace stiffenss is algebraic in the wavenumber, the resulting global sitffness matrix is of the form

$$\boldsymbol{K} = \mathbf{A}k^2 + \mathbf{B}k + \mathbf{C} = \boldsymbol{K}(k) \tag{3}$$

In principle, for a vector of prescribed loadings $\bar{P}$, one may obtain the displacements $\bar{\mathbf{U}}$ for a given wavenumber k by inverting the global stiffness matrix $\boldsymbol{K}$, or solving by Gaussian elimination. Such a direct approach has the important disadvantage, however, that the inversion must be accomplished numerically for every wavenumber considered. A much more elegant and powerful alternative (K&P) is to carry out a spectral decomposition of the stiffness matrix in terms of the eigenvalues k_1 obtained from the quadratic eigenvalue problem

$$\boldsymbol{K}(k_l)\boldsymbol{\phi}_l = \mathbf{0} \tag{4}$$

since it is then possible to obtain an explicit representation of the flexibility matrix $\mathbf{F} = \boldsymbol{K}^{-1}$ in terms of the eigenvalues k_l and wavenumber k, as will be seen.

While the eigenvalue problem stated by equation (4) could be solved in one step for all the degrees of freedom involved, it is instead better to take advantage of the special structure of $\boldsymbol{K}$ and divide this problem into two smaller ones: an "antiplane," and an "in-plane" problem. For a system of N layers, including the halfspace, the solution of the antiplane problem yields $2N$ eigenvalues, whereas the solution of the in-plane problem yields $4N$ eigenvalues. In contrast to the case of stratum, in which only half of the eigenvalues were required for the spectral decomposition of the stiffness matrix, it will be found that all eigenvalues are required for the case of a layered halfspace. In the static case, the stiffness matrices are real, as the material properties do not include damping. Thus, the roots of the quadratic eigenvalue problem are either real, or appear as complex conjugate pairs. There are also three rigid-body modes (with zero eigenvalue), corresponding to each Cartesian direction. The contribution of these rigid-body modes to the flexibility of the layered profile will be shown to correspond to Boussinesq's flexibility, i.e., the halfspace flexibility.

3 Antiplane Case

From Kausel and Roësset (1981), the true antiplane stiffness of a halfspace with zero frequency and positive wavenumber is

$$K_r = kG_r \tag{5}$$

where G_r is the shear modulus of the halfspace ("rock"). By partitioning out the antiplane degrees of freedom from equation (4), we obtain the eigenvalue problem for the antiplane case of $N-1$ layers resting on a halfplane as

$$(\mathbf{A}_y k_j^2 + \mathbf{B}_y k_j + \mathbf{C}_y)\boldsymbol{\phi}_j = \mathbf{0} \tag{6}$$

where $\mathbf{A}_y$, $\mathbf{B}_y$, and $\mathbf{C}_y$ are symmetric matrices of dimension $N \times N$; $\mathbf{A}_y$, $\mathbf{C}_y$ are identical to those in K&P, except for the added degree-of-freedom at the base. While the overlying layers do not contribute to the $\mathbf{B}_y$ matrix, the halfspace contributes one term. Hence

$$\mathbf{B}_y = \text{diag}\,(0, 0, \ldots, G_r) \tag{7}$$

The $\mathbf{C}_y$ matrix by itself is singular, implying that the system admits a zero eigenvalue. Consider the case $k_1 = 0$. The eigenvalue problem reduces to

$$\mathbf{C}_y\boldsymbol{\phi}_1 = \mathbf{0} \tag{8}$$

By inspection of the structure of $\mathbf{C}_y$ (see K&P), one may select a vector of dimension N, satisfying equation (4), of the form

$$\boldsymbol{\phi}_1 = \mathbf{E} \equiv \{1, 1, \ldots, 1\}^T \tag{9}$$

in which every element is equal to one. This vector of equal displacements is the antiplane rigid-body mode of the layered soil system. In this mode, no forces are required to maintain a uniform displacement in the antiplane direction throughout the soil. The presence of the rigid-body mode is not a surprise since, for static problems, there are no constraints to prevent displacement of the system as a whole.

To obtain the remaining eigenvalues and eigenvectors, it is convenient to write the quadratic eigenvalue problem in the form of a linear eigenvalue problem of dimension $2N$ as

$$k_j \begin{bmatrix} \mathbf{0} & \mathbf{A}_y \\ \mathbf{A}_y & \mathbf{B}_y \end{bmatrix} \begin{bmatrix} k_j\boldsymbol{\phi}_j \\ \boldsymbol{\phi}_j \end{bmatrix} + \begin{bmatrix} -\mathbf{A}_y & \mathbf{0} \\ \mathbf{0} & \mathbf{C}_y \end{bmatrix} \begin{bmatrix} k_j\boldsymbol{\phi}_j \\ \boldsymbol{\phi}_j \end{bmatrix} = \begin{bmatrix} \mathbf{0} \\ \mathbf{0} \end{bmatrix} \tag{10}$$

Define the $2N \times 2N$ matrices $\tilde{\mathbf{A}}$, $\tilde{\mathbf{C}}$, $\mathbf{Z}$ and the $2N \times 1$ modal eigenvector $\mathbf{Z}_j$ as

$$\tilde{\mathbf{A}} = \begin{bmatrix} \mathbf{0} & \mathbf{A}_y \\ \mathbf{A}_y & \mathbf{B}_y \end{bmatrix} \quad \tilde{\mathbf{C}} = \begin{bmatrix} -\mathbf{A}_y & \mathbf{0} \\ \mathbf{0} & \mathbf{C}_y \end{bmatrix} \tag{11}$$

$$\mathbf{Z} = \begin{bmatrix} \boldsymbol{\Phi}\mathbf{K} \\ \boldsymbol{\Phi} \end{bmatrix} \quad \mathbf{Z}_j = \begin{bmatrix} \boldsymbol{\phi}_j k_j \\ \boldsymbol{\phi}_j \end{bmatrix}$$

in which $\boldsymbol{\Phi}$ is the $N \times 2N$ matrix of eigenvectors and $\mathbf{K}$ is the $2N \times 2N$ diagonal matrix of eigenvalues. Note that both $\mathbf{C}$ and $\tilde{\mathbf{C}}$ are singular. The linear eigenvalue problem can be then be written as

$$k_j\tilde{\mathbf{A}}\mathbf{Z}_j + \tilde{\mathbf{C}}\mathbf{Z}_j = \mathbf{0} \tag{12}$$

Notice that this eigenvalue problem is linear in k, and not in k^2, as was the case in K&P12. The reason is that, in the

Downloaded 03 May 2010 to 171.66.16.27. Redistribution subject to ASME license or copyright; see http://www.asme.org/terms/Terms_Use.cfm

present case, one must solve an eigenvalue problem of double dimension. Hence, twice the number of eigenvalues and eigenvectors are needed to form the inverse of K.

Since both $\mathbf{A}$ and $\mathbf{C}$ are symmetric, the eigenvectors must satisfy standard orthogonality conditions. For the first orthogonality condition choose the normalization

$$\mathbf{Z}^T\tilde{\mathbf{C}}\mathbf{Z} = -2\mathbf{K}^2 \tag{13}$$

This normalization is also satisfied by the rigid-body mode. On the other hand, the second orthogonality condition is obtained for the first one via the eigenvalue equation (12). The result is

$$\mathbf{Z}^T\tilde{\mathbf{A}}\mathbf{Z} = 2\tilde{\mathbf{K}} \tag{14}$$

where $\tilde{\mathbf{K}}$ is a modified spectral matrix which differs from $\mathbf{K}$ only in that the first element is not zero (the rigid-body mode has index $j = 1$);

$$\tilde{\mathbf{K}} = \text{diag}\left[\frac{1}{2}\, G_r, k_2, k_3, \ldots, k_{2N}\right] \tag{15}$$

Now consider the antiplane equilibrium equation (compare with K&P24 and notice the difference in the power of k)

$$(\tilde{\mathbf{A}}k + \tilde{\mathbf{C}})\tilde{\mathbf{U}} = \tilde{\mathbf{P}} \tag{16}$$

with

$$\tilde{\mathbf{U}} = \begin{bmatrix} k\tilde{\mathbf{U}} \\ \tilde{\mathbf{U}} \end{bmatrix} \quad \tilde{\mathbf{P}} = \begin{bmatrix} \mathbf{0} \\ \tilde{\mathbf{P}} \end{bmatrix} \tag{17}$$

Premultiplication by $\mathbf{Z}^T$ and introducing $\mathbf{Z}\mathbf{Z}^{-1} = \mathbf{I}$ yields

$$\mathbf{Z}^T(\tilde{\mathbf{A}}k + \tilde{\mathbf{C}})\mathbf{Z}\mathbf{Z}^{-1}\tilde{\mathbf{U}} = \mathbf{Z}^T\tilde{\mathbf{P}} \tag{18}$$

Applying the orthogonality conditions (17) and (18) gives

$$2(\tilde{\mathbf{K}}k - \mathbf{K}^2)\mathbf{Z}^{-1}\tilde{\mathbf{U}} = \mathbf{Z}^T\tilde{\mathbf{P}} \tag{19}$$

Then

$$\tilde{\mathbf{U}} = \frac{1}{2}\,\mathbf{Z}(k\mathbf{I} - \mathbf{K})^{-1}\tilde{\mathbf{K}}^{-1}\mathbf{Z}^T\tilde{\mathbf{P}} \tag{20}$$

or

$$\tilde{\mathbf{U}} = \frac{1}{2}\,\boldsymbol{\Phi}(k\mathbf{I} - \mathbf{K})^{-1}\tilde{\mathbf{K}}^{-1}\boldsymbol{\Phi}^T\tilde{\mathbf{P}}, \text{ with } \boldsymbol{\Phi} = \boldsymbol{\Phi}_y$$

Notice that $(k\mathbf{I} - \mathbf{K})^{-1} = \text{diag}\,\{1/(k - k_l)\}$. Defining the coefficient (once more, notice the difference with K&P35 concerning the power of k)

$$a_l = \frac{1}{2k_l(k - k_l)} \tag{21}$$

Then the elements of the antiplane flexibility are (compare wtih K&P34e)

$$f_{yy}^{mn} = \frac{1}{G_r k} + \sum_{l=2}^{2N} \phi_y^{ml}\phi_y^{nl}a_l^L \tag{22}$$

where the superscript L stands for "Love" (or antiplane) modes. The indices m, n refer to the interfaces at which the displacements are observed and the loads are applied, respectively. The term $1/G_r k$ is the contribution of the rigid-body mode to the flexibility matrix of the system; note that it is the inverse of the halfspace stiffness.

4 In-plane Case

The procedure followed here parallels that of the antiplane case. From Kausel and Roësset (1981), the stiffness of the halfspace with zero frequency and positive wavenumber is

$$\mathbf{K}_r = \frac{2kG_r}{(1 + \alpha_r^2)} \begin{bmatrix} 1 & -\alpha_r^2 \\ -\alpha_r^2 & 1 \end{bmatrix}, \quad k \geq 0 \tag{23}$$

where $\alpha_r = \sqrt{G_r/(\lambda_r + 2G_r)}$. The eigenvalue problem for the in-plane case is

$$(\mathbf{A}k_j^2 + \mathbf{B}k_j + \mathbf{C})\phi_j = \mathbf{0} \tag{24}$$

where $\mathbf{A}$, $\mathbf{B}$, and $\mathbf{C}$ are symmetric matrices of dimension $2N \times 2N$. The $\mathbf{B}$ matrix now receives contributions from both the halfspace and the stratum. Rearranging the degrees of freedom, the stiffness matrices are found to have the structures

$$\mathbf{A} = \begin{bmatrix} \mathbf{A}_x & \\ & \mathbf{A}_z \end{bmatrix} \quad \mathbf{B} = \begin{bmatrix} \mathbf{B}_x & \mathbf{B}_{xz} \\ \mathbf{B}_{xz}^T & \mathbf{B}_z \end{bmatrix} \quad \mathbf{C} = \begin{bmatrix} \mathbf{C}_x & \\ & \mathbf{C}_z \end{bmatrix} \tag{25}$$

where

$$\mathbf{B}_x = \mathbf{B}_z = \text{diag}\left[0, 0, \ldots, \frac{2G_r}{(1 + \alpha_r^2)}\right] \tag{26}$$

and $\mathbf{A}_x$, $\mathbf{A}_z$, $\mathbf{B}_{xz}$, $\mathbf{C}_x$, $\mathbf{C}_z$ are the same as in K&P (except for the added degrees-of-freedom at the base).

Using the same notation as in the antiplane case, and substituting in equation (10) the matrices $\mathbf{A}_y$, $\mathbf{B}_y$, $\mathbf{C}_y$ by the matrices $\mathbf{A}$, $\mathbf{B}$, $\mathbf{C}$ in equation (25), then the linear eigenvalue problem (12) and the associated orthogonality conditions (13), (14) remain unchanged, except that all matrices and vectors are now twice in size. As in the antiplane case, the $\mathbf{C}$ and $\tilde{\mathbf{C}}$ matrices are singular. In contrast to the antiplane problem, however, two distinct rigid-body modes are found in this case to satisfy the eigenvalue equation. These modes are

$$\boldsymbol{\phi}_1 = \begin{bmatrix} \mathbf{E} \\ \mathbf{E} \end{bmatrix} \quad \text{and} \quad \boldsymbol{\phi}_2 = \begin{bmatrix} \mathbf{E} \\ -\mathbf{E} \end{bmatrix} \tag{27}$$

with $\mathbf{E}$ given by equation (9), i.e., a column of ones. (The naive guesses $\boldsymbol{\phi}_1^T = \{\mathbf{E}^T\mathbf{0}\}$ and $\boldsymbol{\phi}_2^T = \{\mathbf{0}\,\mathbf{E}^T\}$ fail because they do not satisfy the orthogonality conditions.) The modified spectral matrix $\tilde{\mathbf{K}}$ is obtained by applying the second orthogonality condition (14) in combination with equations (25) and (26). The result is

$$\tilde{\mathbf{K}} = \text{diag}\left[\frac{2G_r(1 - \alpha_r^2)}{(1 + \alpha_r^2)}, 2G_r, k_3, \ldots, k_{4N}\right] \tag{28}$$

This matrix differs from the spectral matrix $\mathbf{K}$ only in the first two elements. Again, following the same procedure as for the antiplane case (equations (16) through (20)) one obtains the flexiblity matrix (compare with equation (22))

$$\mathbf{F} = \frac{1}{2}\,\boldsymbol{\Phi}(k\mathbf{I} - \mathbf{K})^{-1}\tilde{\mathbf{K}}^{-1}\boldsymbol{\Phi}^T, \text{ with } \boldsymbol{\Phi} = \begin{bmatrix} \boldsymbol{\Phi}_x \\ \boldsymbol{\Phi}_z \end{bmatrix} \tag{29}$$

The elements of this flexibility matrix are finally (compare with K&P34)

$$\begin{aligned}
f_{xx}^{mn} &= \frac{1}{2kG_r(1 - \alpha_r^2)} + \sum_{l=3}^{4N} \phi_x^{ml}\phi_x^{nl}a_l^R \\
f_{xz}^{mn} &= \frac{\alpha_r^2}{2kG_r(1 - \alpha_r^2)} + \sum_{l=3}^{4N} \phi_x^{ml}\phi_z^{nl}a_l^R \\
f_{zz}^{mn} &= \frac{1}{2kG_r(1 - \alpha_r^2)} + \sum_{l=3}^{4N} \phi_z^{ml}\phi_z^{nl}a_l^R \\
f_{zx}^{mn} &= \frac{\alpha_r^2}{2kG_r(1 - \alpha_r^2)} + \sum_{l=3}^{4N} \phi_z^{ml}\phi_x^{nl}a_l^R
\end{aligned} \tag{30}$$

where a_l^R is the coefficient defined in equation (21). The superscript ^{R} stands for "Rayleigh" (or in-plane) modes. As in the antiplane case, the contribution of the rigid body modes to the system flexibilities is the inverse of the halfspace stiffness (23).

Downloaded 03 May 2010 to 171.66.16.27. Redistribution subject to ASME license or copyright; see http://www.asme.org/terms/Terms_Use.cfm

Table 1 Integrals used to compute static displacements

$I_{1l}=\frac{1}{2k_l}\int_0^\infty \frac{kJ_0(k\rho)\,dk}{(k-k_l)}=$	$\frac{1}{2}\left[\frac{1}{\rho k_l}+\frac{\pi}{2}(\mathbf{H}_0(-\rho k_l)-Y_0(-\rho k_l))\right]$
$I_{2l}=\frac{1}{2k_2}\int_0^\infty \frac{kJ_1(k\rho)\,dk}{(k-k_l)}=$	$\frac{1}{2}\left[1-\frac{\pi}{2}(\mathbf{H}_1(-\rho k_l)-Y_1(-\rho k_l))\right]$
$I_{3l}=\frac{1}{2k_l}\int_0^\infty \frac{J_1(k\rho)\,dk}{(k-k_l)}=$	$\frac{1}{2k_l}\left[1-\frac{1}{\rho k_l}-\frac{\pi}{2}(\mathbf{H}_1(-\rho k_l)-Y_1(-\rho k_l))\right]$
Note: $I_{2l}=k_l I_{3l}+\frac{1}{2\rho k_l}\quad \frac{d}{d\rho}I_{3l}=I_{1l}-\frac{1}{\rho}I_{3l}$	In each case, $\lvert\arg(-k_l)\rvert<\pi$

$\mathbf{H}_\nu \rightarrow$ Struve Functions $Y_\nu \rightarrow$ Neumann Functions

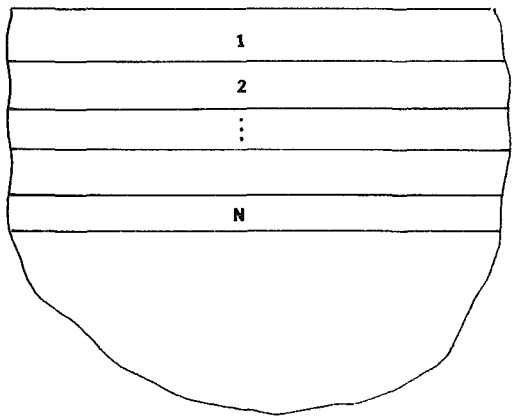


Fig. 1 Geometry of layered halfspace

5 Halfspace versus Stratum

Comparison of equations (22) and (30) with the corresponding equations for a stratum (K&P34) reveals similarities and differences. The principal changes introduced by the flexible halfspace are: (1) The leading terms contributed by the rigid body modes, which correspond to the Boussinesq-Cerruti flexibilities; (2) the upper bound on the summation (all modes are necessary); and (3) the definition of the coefficient a_1 (equation (21)), which is linear rather than quadratic in the wavenumber in the denominator. This leads in turn to different integral transforms (Table 1). These differences notwithstanding, it can be shown that both solutions agree when the stiffness of the halfspace is made appropriately large.

6 Eigenvalue Problems

The eigenvalue problems posed by equations (6) and (24) involve tridiagonal matrices, and are best solved by direct iteration. For the antiplane case, there are $2N$ eigenvalues, of which the first one is null (the rigid-body mode), and the second is real and negative. All other eigenvalues appear in complex conjugate pairs. By appropriate modifications, the iterations can be made to involve only real operations; moreover, the complex conjugate roots can be found simultaneously (see Seale, 1985). Of the $4N$ roots involved in the in-plane case, there are two null roots (rigid body modes), and two real, negative roots. All other roots also appear in complex conjugate pairs, which again can be found simultaneously by the scheme referred to above.

7 Displacements Due to Static Point Loads

To find the Green's function due to static point loads, one must first evaluate the Hankel transforms for these loads, i.e., they must be expresseed in the wavenumber domain (K&P2). Combining the transformed loads with the flexibilities given by equations (22) and (30), and performing an inverse Hankel transformation, one then obtains the desired displacements. The inverse transformations in this case involve the integrals listed in Table 1 (for further details, see K&P).

7.1 Horizontal Point Load. The Hankel transform for a horizontal point load is (compare with K&P39, with $q = 1/\pi R^2$, $R \rightarrow 0$)

$$\bar{\mathbf{P}}_1=\frac{1}{2\pi}\begin{bmatrix}1\\1\\0\end{bmatrix} \tag{31}$$

and the associated Green's functions are (with I_{2l}, I_{3l} given in Table 1)

$$u_\rho^{mn}=\frac{1}{2\pi}\left[\frac{1}{\rho G_r}+\sum_{l=3}^{4N}\phi_x^{ml}\phi_x^{nl}\frac{d}{d\rho}I_{3l}^R+\sum_{l=2}^{2N}\phi_y^{ml}\phi_y^{nl}\frac{1}{\rho}I_{3l}^L\right](\cos\theta)$$

$$u_\theta^{mn}=\frac{1}{2\pi}\left[\frac{1}{2\rho G_r(1-\alpha_r^2)}+\sum_{l=3}^{4N}\phi_x^{ml}\phi_x^{nl}\frac{1}{\rho}I_{3l}^R+\sum_{l=2}^{2N}\phi_y^{ml}\phi_y^{nl}\frac{d}{d\rho}I_{3l}^L\right](-\sin\theta) \tag{32}$$

$$u_z^{mn}=-\frac{1}{2\pi}\left[\frac{\alpha_r^2}{2\rho G_r(1-\alpha_r^2)}+\sum_{l=3}^{4N}\phi_z^{ml}\phi_x^{nl}I_{2l}^R\right](\cos\theta)$$

The terms before the summations are the Cerutti solutions for displacements on the surface of a halfspace due to a horizontal point load on the surface. Thus, the method of integral transforms considered herein is consistent in that the Cerutti solution is recovered when there are no layers resting on the halfspace. On the other hand, Mindlin's problem is obtained by taking $n \neq 1$, although the analogy with Mindlins formula is not evident in this case.

7.2 Vertical Point Load. The Hankel transform of a vertical point load is

Downloaded 03 May 2010 to 171.66.16.27. Redistribution subject to ASME license or copyright; see http://www.asme.org/terms/Terms_Use.cfm

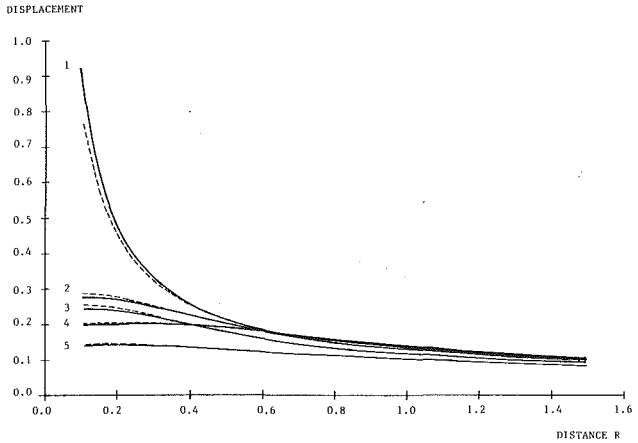


Fig. 2 Radial displacements due to radial point load at the surface: Exact versus semidiscrete solution (8 layers)

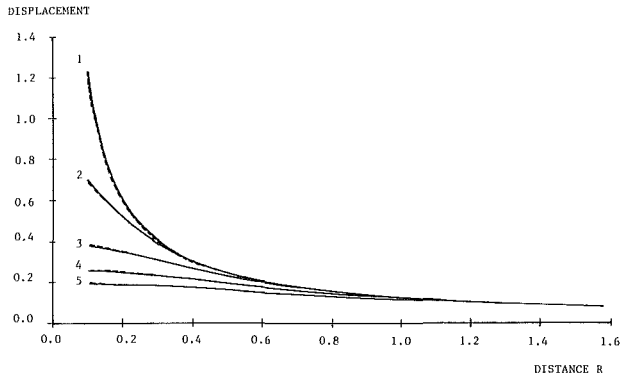


Fig. 3 Vertical displacements due to vertical point load at the surface: Exact versus semidiscrete solution (8 layers)

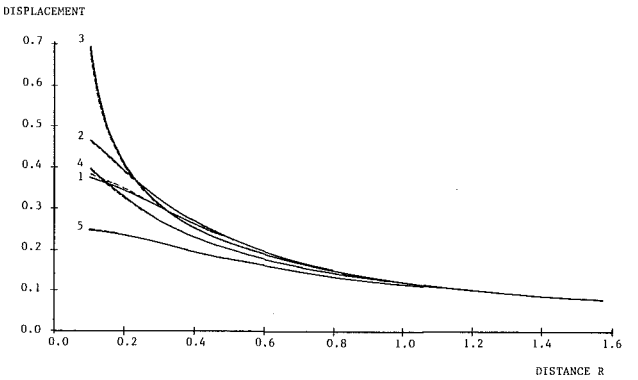


Fig. 4 Verticial displacements due to vertical buried point load (@ elevation 3): Exact versus semidiscrete solution (8 layers)

$$\tilde{\mathbf{P}}_0 = -\frac{1}{2\pi}\begin{bmatrix}0\\0\\1\end{bmatrix} \tag{33}$$

Following the same procedure as for the horizontal point load, one obtains the displacements

$$u_\rho^{mn} = \frac{1}{2\pi}\left[\frac{\alpha_r^2}{2\rho G_r(1-\alpha_r^2)} + \sum_{l=3}^{4N}\phi_x^{ml}\phi_z^{nl}I_{2l}^R\right]$$

$$u_\theta^{mn} = 0 \tag{34}$$

$$u_z^{mn} = \frac{1}{2\pi}\left[\frac{1}{2\rho G_r(1-\alpha_r^2)} + \sum_{l=3}^{4N}\phi_z^{ml}\phi_x^{nl}I_{1l}^R\right]$$

The terms before the summations are the Boussinesq solutions for the displacements on the surface of a halfspace due to a vertical point load on the surface. Again, the solution presented herein is consistent with the known solution for a halfspace.

8 Computational Procedure

An outstanding feature of the method described in this paper is its simplicity. The stiffness method has three steps:

(1) Assemble global stiffness matrices **A**, **B**, **C**.

(2) Extract eigenvalues and eigenvectors. The solution scheme is simple because of the tridiagonal nature of the matrices and the fact that the eigenvalues are either real or appear in complex conjugate pairs.

(3) Compute displacements from formula (32) and (34) and Table 1.

9 Examples

The accuracy of this scheme was tested by computing displacements in a homogeneous halfspace subjected to static point loads applied on or underneath the surface. The material properties are $\rho = \lambda = G = C_s = 1$. The overlying layer has depth $H = 1$ and is discretized into 8 sublayers. Elevations 1 through 5 correspond to depths $z = 0.0, 0.25, 0.5, 0.75$, and 1.0. Figures 2 through 4 show displacements versus distance ρ from the point of application of the load.

The solid lines are displacements computed with the approximation, the dashed lines are displacements computed with the analytical solutions of Mindlin, Cerutti, and Boussinesq. The plots all show displacements beginning at $\rho = 0.1$, since both the analytical solutions and the approximations have a $1/\rho$ singularity. Each pair of solid and dashed lines is labeled with the number of the elevation at which the displacements were computed.

Figure 2 shows displacements u_ρ at the five elevations due to a horizontal (or radial) unit point load applied at the surface. Agreement with the analytical solution is excellent everywhere. Figure 3 shows vertical displacements u_z due to a vertical point load at the surface. Again, agreement with the analytical solution is excellent everywhere. Figure 4 shows displacements u_z due to a buried vertical point load applied at elevation 3. Agreement with the analytical solution is once more excellent at all elevations.

Figures 2 through 4 are presented to demonstrate the accuracy of this method for a problem for which the analytical solution is known. Of course, the advantage of the proposed method is that it can be applied to solve for displacements when the analytical solution is not known, i.e., when the layers as well as the halfspace all have different material properties.

10 Conclusions

The method presented above for the calculation of displacements in layered solids is a significant improvement upon existing methods. The technique is efficient in that the stiffness matrices are relatively small, symmetric and banded, and accurate results are obtained even with a relatively coarse discretization. Since layering occurs in only the vertical direction and the stiffness of the halfspace is added directly to the system of equations, there is no need to apply artifical boundary conditions to the directions of infinite extent such as would be required for a finite element model of a halfspace.

The Green's functions obtained here have applications to several areas of engineering. In particular, they could be used in connection with the Boundary Element Method, which requires displacements due to point loads on the boundary of a solid. Stresses within the layers can be obtained by differen-

Downloaded 03 May 2010 to 171.66.16.27. Redistribution subject to ASME license or copyright; see http://www.asme.org/terms/Terms_Use.cfm

tiating the displacements (see also Kausel and Peek, 1982b). Point loads can be added to form double couple sources, while the integral of point loads applied over a surface area could be used to represent the pressure load of a footing on a layered soil. On the other hand, the proposed solution could also be applied to "practical" problems in geotechnical engineering, such as the calculation of equivalent material properties for a layered solid deposit, and so on.

Acknowledgment

The support of NSS Grant No. ECE-8600269 under the cognizance of Dr. Clifford J. Astill is gratefully acknowledged.

References

Boussinesq, J., 1878–1885, Citation No. 67 in *Love's Treatise on the Mathematical Theory of Elasticity*, 4th Ed., Dover Press, N.Y.

Burminster, D. M., 1945, "The General Theory of Stresses and Displacements in Layered Systems," *J. Appl. Phys.*, Vol. 16, No. 19, pp. 89–94, pp. 126–127, pp. 296–302.

Cerruti, V., 1882, Citation No. 68 in *Love's Treatise on the Mathematical Theory of Elasticity*, 4th Ed., Dover Press, N.Y.

Chan, K. S., Karasudhi, P., and Lee, S. L., 1974, "Force at a Point in the Interior of a Layered Elastic Half-Space," *International Journal of Solids and Structures*, Vol. 10, pp. 1179–1199.

Clapeyron, and Lamé, Citation in "Die Mechanik im 19. Jahrundert," by Mahreholtz, O., and Gaul, L., in *Zeitschrift der Universitat Hannover*, 1978, Heft 2, p. 37.

Cruse, T. A., Snow, D. A., and Wilson, R. B., 1977, "Numerical Solutions in Axisymmetric Elasticity," *Computers and Structures*, Vol. 7, pp. 445–551.

Dundurs, J., and Hetenyi, H., 1965, "Transmission of Force Between Two Semi-infinite Solids," ASME JOURNAL OF APPLIED MECHANICS, pp. 671–674.

Hertz, H., 1881, Citation No. 69 in *Love's Treatise on the Mathematical Theory of Elasticity*, 4th Ed., Dover Press, N.Y.

Hull, S. W., and Kausel, E., 1984, "Dynamic Loads in Layered Halfspaces," *Proceedings of the Fifth ASCE EMD Specialty Conference*, University of Wyoming, Laramie, WY, pp. 201–204.

Kausel, E., and Peek, R., 1982, "Dynamic Loads in the Interior of a Layered Stratum: an Explicity Solution," *Bull. Seism. Soc. Am.*, Vol. 72, No. 5, pp. 1459–1481. Note: See also the Errata in *Bull. Seism. Soc. Am.*, Vol. 74, pp. 1508, Aug. 1984.

Kausel, E., and Peek,, R., 1982, "Boundary Integral Method for Stratified Soils," Technical Report R82-50, Department of Civil Engineering, M.I.T., June.

Kausel, E.,, and Roesset, J. M., 1981, "Stiffness Matrices for Layered Soils," *Bull. Seism. Soc. Am.*, Vol. 71, No. 6, pp. 1743–1761.

Kermanidis, T., 1975, "A Numerical Solution for Axially Symmetrical Elasticity Problems," *Journal of Solids and Structures*, Vol. 11, pp. 493–500.

Mindlin, R. D., 1936, "Force at a Point in the Interior of a Semi-Infinite Solid," *J. Phys.*, Vol. 79, May, pp. 195–202.

Plevako, V. P., 1969, "A Point Force Inside a Pair of Cohering Halfspaces," *Osnovaniya Fundamenty i Mekhanika Gruntov*, No. 3, May, pp. 9–11.

Rongved, L., 1955, "Force Interior to One of Two Joined Semi-Infinite Solids," *Proceedings, Second Midwestern Conference on Solids Mechanics*, pp. 1–13.

Seale, S. B., 1985, "Dynamic Loads in Layered Halfspaces," Ph.D. thesis, Massachusetts Institute of Technology, Cambridge, MA.

Thompson, W., Lord Kelvin, 1848, "Note on the Integration of the Equations of Equilibrium of an Elastic Solid," *Cambridge and Dublin Math Journal*, Feb.

Waas, G., 1972, "Linear Two-Dimensional Analysis of Soil Dynamics Problems in Semi-Infinite Layered Media," Ph.D. thesis, University of California, Berkeley, CA.

Downloaded 03 May 2010 to 171.66.16.27. Redistribution subject to ASME license or copyright; see http://www.asme.org/terms/Terms_Use.cfm

An Approach to Calculating Random Vibration Integrals

P-T. D. Spanos
Professor,
Brown School of Engineering,
Rice University,
Houston, TX 77251
Mem. ASME

Integrals required for the determination of the response statistics of an arbitrary order linear and time-invariant dynamic system under stationary excitation are examined. These integrals are found as the solution of a set of linear algebraic equations. The application of the derived general formula is exemplified by considering as excitation models white noise, band-limited white noise, and other important stationary random processes. Besides random vibration applications, the derived formula has purely mathematical merit and can be used for the calculation of complicated integrals encountered in a variety of other technical fields.

Introduction

A class of integrals often encountered in random vibration calculations and other scientific fields is considered. These integrals can be related to the statistics of the stationary response of a stable, linear, and time-invariant dynamic system excited by a stationary random process. A pertinent formula is derived which includes as a special case the well-known James et al. (1965) integral of control engineering and random vibration applications which has also been derived by Spanos (1983) using an alternative approach; the latter approach is extended in the present paper. Note that the presented developments should be viewed in context with the Lyapunov equation of random vibration analysis (Lin, 1976) and the calculation of instantaneous correlation matrices of multi-degree-of-freedom systems under stationary random excitation (Yang and Iwan, 1972).

Examples of application of the derived general formula involving excitations with white, band-limited white noise, and other useful spectra, are discussed. Furthermore, it is pointed out that this formula also has purely mathematical merit irrespective of random vibration analysis interpretations.

Equations for Correlation Derivatives

The response of a linear system of order m to random excitation $w(t)$ is governed by the equation

$$[\lambda_m D^m + \lambda_{m-1} D^{m-1} + \lambda_{m-2} D^{m-2} + \ldots + \lambda_o] x(t) = w(t). \tag{1}$$

In this equation the symbol D denotes the operator of differentiation, and λ_k, $k = o, \ldots m$, are time-invariant constants.

Assume that $w(t)$ is stationary with power spectrum $S_w(\omega)$ and auto-correlation function

$$R_w(\tau) = < w(t) w(t-\tau) >, \tag{2}$$

where the symbol $< >$ denotes the operator of mathematical expectation. Assume that the values of λ_k are such that $x(t)$ becomes as $t \to \infty$, a stationary process with autocorrelation $R_x(\tau)$ and power spectrum $S_x(\omega)$. Clearly, $S_x(\omega)$ and $S_w(\omega)$ are related by the classical formula

$$S_x(\omega) = \frac{S_w(\omega)}{|\Lambda(s)|^2}. \tag{3}$$

The symbol $|.|$ represents the modulus of a complex number,

$$s = i\omega, \tag{4}$$

$$i = \sqrt{-1} \tag{5}$$

and

$$\Lambda(s) = \lambda_m s^m + \lambda_{m-1} s^{m-1} + \ldots + \lambda_o. \tag{6}$$

Further, consider the cross-correlation

$$R_{xw}(\tau) = < x(t) w(t-\tau) > \tag{7}$$

of $x(t)$ and $w(t-\tau)$. Then, relying on the formulas

$$< x(t) D^k x(t-\tau) > = (-1)^k D^k R_x(\tau) \tag{8}$$

and

$$< w(t-\tau) D^k x(t) > = D^k R_{xw}(\tau) \tag{9}$$

it can be proved that

$$[\lambda_m D^{\ell+m} + \lambda_{m-1} D^{\ell+m-1} + \ldots + \lambda_o D^{\ell}] R_{xw}(\tau) = D^{\ell} R_w(\tau), \ \ell = o, 1, \ldots \tag{10}$$

and

$$[\hat{\lambda}_m D^{n+m} + \hat{\lambda}_{m-1} D^{n+m-1} + \ldots + \hat{\lambda}_o D^{n}] R_x(\tau) = D^n R_{xw}(\tau), \ n = o, 1, \ldots \tag{11}$$

Contributed by the Applied Mechanics Division for presentation at the 1987 Applied Mechanics, Biomechanics, and Fluids Engineering Conference, Cincinnati, OH, June 14–17, 1987, of the American Society of Mechanical Engineers.
Discussion of this paper should be addressed to the Editorial Department, ASME, United Engineering Center, 345 East 47th Street, New York, N.Y. 10017, and will be accepted until two months after final publication of the paper itself in the JOURNAL OF APPLIED MECHANICS. Manuscript received by ASME Applied Mechanics Division, April 4, 1986; final revision, August 4, 1986.
Paper No. 87-APM-18.

Copyright © 1987 by ASME
Downloaded 03 May 2010 to 171.66.16.27. Redistribution subject to ASME license or copyright; see http://www.asme.org/terms/Terms_Use.cfm

where

$$\hat{\lambda}_k = (-1)^k \lambda_k, \; k = o, \ldots \tag{12}$$

Note that equations (10) and (11) are valid assuming that the orders ℓ and n of differentiation result in a meaningful, ordinary or generalized, functional interpretation of the derivatives of $R_w(\tau)$. Further, note that the stationary system response can be expressed in terms of the impulse response function $h(\tau)$

$$x(t) = \int_o^\infty h(u) w(t-u) du. \tag{13}$$

Multiplying equation (13) by $w(t-\tau)$ and ensemble averaging yields

$$R_{xw}(\tau) = \int_o^\infty h(u) R_w(\tau - u) du. \tag{14}$$

Thus, setting $\tau = o$,

$$R_{xw}(o) = \int_o^\infty h(u) R_w(u) du. \tag{15}$$

Further, differentiating equation (14) with respect to τ and setting $\tau = o$ yields

$$D^k R_{xw}(o) = \int_o^\infty R_w(u) D^k h(u) du, \; k = o, 1, \ldots \tag{16}$$

A Class of Integrals

Consider the integral

$$M_{2k} = \int_{-\infty}^\infty \frac{\omega^{2k} S_w(\omega)}{|\Lambda(s)|^2} d\omega. \tag{17}$$

Note that

$$R_x(\tau) = 2\int_o^\infty S_x(\omega) \cos(\omega\tau) d\omega. \tag{18}$$

Combining equations (3), (17), and (18) gives

$$M_{2k} = (-1)^k D^{2k} R_x(o). \tag{19}$$

Substituting equation (19) into equation (11) for $k = \ell = m-1, m-2, \ldots, o$ and taking into consideration equation (16) yields

$$\left.\begin{aligned} \lambda_{m-1} M_{2m-2} - \lambda_{m-3} M_{2m-4} + \lambda_{m-5} M_{2m-6} - \ldots\ldots = r_{m-1} \\ -\lambda_m M_{2m-2} + \lambda_{m-2} M_{2m-4} - \lambda_{m-4} M_{2m-6} + \ldots\ldots = r_{m-2} \\ 0 \quad . \quad . \quad \ldots = . \\ . \quad . \quad . \quad -\lambda_2 M_2 + \lambda_o M_o = r_o \end{aligned}\right\} \tag{20}$$

where

$$r_k = \int_o^\infty R_w(u) D^k h(u) du, \; k = o, 1, \ldots, m-1. \tag{21}$$

Thus, given the integrals $r_o, r_1 \ldots r_{m-1}$ the values of M_{2k} can be calculated by the solution of the system of equation (20). Specifically, in terms of determinants

$$M_{2k} = \frac{\det \Gamma_k}{\det \Gamma} =$$

$$\frac{\begin{vmatrix} \lambda_{m-1} & -\lambda_{m-3} & \lambda_{m-5} & -\lambda_{m-7} & \cdots & r_{m-1} & \cdot & \cdot & \cdot \\ -\lambda_m & \lambda_{m-2} & -\lambda_{m-4} & \lambda_{m-6} & \cdots & r_{m-2} & \cdot & \cdot & \cdot \\ 0 & -\lambda_{m-1} & \lambda_{m-3} & -\lambda_{m-5} & \cdots & r_{m-3} & \cdot & \cdot & \cdot \\ 0 & \lambda_m & -\lambda_{m-2} & \lambda_{m-4} & \cdots & r_{m-4} & \cdot & \cdot & \cdot \\ 0 & 0 & \cdot & \cdot & & \cdot & \cdot & \cdot & \cdot \\ 0 & 0 & & & \cdots & r_o & \cdot & -\lambda_2 & \lambda_o \end{vmatrix}}{\begin{vmatrix} \lambda_{m-1} & -\lambda_{m-3} & \lambda_{m-5} & -\lambda_{m-7} & \cdots & \cdot & \cdot & \cdot \\ -\lambda_m & \lambda_{m-2} & -\lambda_{m-4} & \lambda_{m-6} & \cdots & \cdot & \cdot & \cdot \\ 0 & -\lambda_{m-1} & \lambda_{m-3} & -\lambda_{m-5} & \cdots & \cdot & \cdot & \cdot \\ 0 & \lambda_m & -\lambda_{m-2} & \lambda_{m-4} & \cdots & \cdot & \cdot & \cdot \\ 0 & 0 & \lambda_{m-1} & \lambda_{m-3} & \cdots & \cdot & \cdot & \cdot \\ \cdot & \cdot & \cdot & \cdot & \cdots & \cdot & \cdot & \cdot \\ \cdot & \cdot & \cdot & \cdot & \cdots & \cdot & -\lambda_2 & \lambda_o \end{vmatrix}} \tag{22}$$

where

$$\Gamma = (\gamma_{m-1}, \gamma_{m-2}, \ldots, \gamma_o) \tag{23}$$

is the coefficient matrix of equation (20) with columns γ_{m-1}, $\gamma_{m-2}, \ldots, \gamma_o$ and Γ_k is the matrix obtained by replacing the $(m-k)^{th}$ column of Γ by the vector

$$\mathbf{r} = (r_{m-1}, \ldots, r_o)^T \tag{24}$$

with T denoting the operation of transposition.

Having determined M_{2k}, $k = o, \ldots, m-1$ any higher order moments can be determined recursively. Specifically, for $k > m-1$ equations (11) and (19) yield

$$\hat{\lambda}_m (-1)^{\frac{m+k}{2}} M_{m+k} + \hat{\lambda}_{m-1} (-1)^{\frac{m+k-1}{2}} M_{m+k-1} + \ldots + \hat{\lambda}_o (-1)^{\frac{k}{2}} M_k = D^k R_{xw}(o). \tag{25}$$

Note that the term $D^k R_{xw}(o)$ $k > m-1$ can be calculated recursively from equation (10) in terms of r_n, $n < k$. That is,

$$\lambda_m r_{\ell+m} = \lambda_m D^{\ell+m} R_{xw}(o) = D^\ell R_w(o) - \lambda_{m-1} r_{\ell+m-1} - \ldots - \lambda_o r_\ell, \; \ell = k+1-m = 1,2, \ldots \tag{26}$$

Note, as well, that any linear combination of M_{2k}, $k = o, 1, \ldots m-1$ can be determined by using equation (20). Consider the integral

$$I_m = \int_{-\infty}^\infty \frac{\Xi_m(\omega)}{|\Lambda(i\omega)|^2} S_w(\omega) d\omega \tag{27}$$

where

$$\Xi_m(\omega) = \xi_{m-1} \omega^{2m-2} + \xi_{m-2} \omega^{2m-4} + \ldots + \xi_o \tag{28}$$

and $\xi_o, \ldots, \xi_{m-1}$ are arbitrary constants. Clearly,

$$I_m = \xi_{m-1} M_{2m-2} + \xi_{m-2} M_{2m-4} + \ldots \xi_o M_o. \tag{29}$$

Further, combining equations (22) and (29) and taking into consideration the nullity of a determinant with two identical columns gives

Downloaded 03 May 2010 to 171.66.16.27. Redistribution subject to ASME license or copyright; see http://www.asme.org/terms/Terms_Use.cfm

$$I_m = \frac{\det \tilde{\Gamma}}{\det \Gamma} - 1 =$$

$$\begin{vmatrix}
\lambda_{m-1}+\xi_{m-1}r_{m-1} & -\lambda_{m-3}+\xi_{m-2}r_{m-1} & \lambda_{m-5}+\xi_{m-3}r_{m-1} & \cdots & \cdot & \cdot \\
-\lambda_m+\xi_{m-1}r_{m-2} & \lambda_{m-2}+\xi_{m-2}r_{m-2} & -\lambda_{m-4}+\xi_{m-2}r_{m-2} & \cdots & \cdot & \cdot \\
\xi_{m-1}r_{m-3} & -\lambda_{m-1}+\xi_{m-2}r_{m-3} & \lambda_{m-3}+\xi_{m-2}r_{m-3} & \cdots & \cdot & \cdot \\
\xi_{m-1}r_{m-4} & \lambda_m+\xi_{m-2}r_{m-4} & -\lambda_{m-2}+\xi_{m-2}r_{m-4} & \cdots & \cdot & \cdot \\
\xi_{m-1}r_{m-5} & \xi_{m-2}r_{m-4} & \lambda_{m-1}+\xi_{m-2}r_{m-5} & \cdots & \cdot & \cdot \\
\cdot & \cdot & \cdot & \cdots & \cdot & \cdot \\
\cdot & \cdot & \cdot & \cdots & \cdot & \cdot \\
\xi_{m-1}r_o & \xi_{m-2}r_o & \cdot & \cdots & -\lambda_2+\xi_1 r_o & \lambda_o+\xi_o r_o
\end{vmatrix}$$

$$-1+\frac{}{}$$

$$\begin{vmatrix}
\lambda_{m-1} & -\lambda_{m-3} & \lambda_{m-5} & \cdots & \cdot & \cdot \\
-\lambda_m & \lambda_{m-2} & -\lambda_{m-4} & \cdots & \cdot & \cdot \\
0 & -\lambda_{m-1} & \lambda_{m-3} & \cdots & \cdot & \cdot \\
0 & \lambda_m & -\lambda_{m-2} & \cdots & \cdot & \cdot \\
0 & 0 & \lambda_{m-1} & \cdots & \cdot & \cdot \\
\cdot & \cdot & \cdot & \cdots & \cdot & \cdot \\
\cdot & \cdot & \cdot & \cdots & \cdot & \cdot \\
\cdot & \cdot & \cdot & \cdots & -\lambda_2 & \lambda_o
\end{vmatrix} \tag{30}$$

That is, the matrix $\tilde{\Gamma}$ is defined by the equation

$$\tilde{\Gamma} = (\gamma_{m-1} + \xi_{m-1}\mathbf{r},\ \gamma_{m-2} + \xi_{m-2}\mathbf{r},\ \ldots,\ \gamma_o + \xi_o \mathbf{r}). \tag{31}$$

Impulse Response Determination

In calculating the instantaneous derivatives of the excitation-response cross-correlation which appear in equation (20), it is necessary to determine the impulse response function $h(\tau)$ of the system defined by equation (1). Assume that

$$\Lambda(s) = \alpha(s+s_1)^{m_1}(s+s_2)^{m_2} \ldots (s+s_n)^{m_n} \tag{32}$$

where α is a constant, $s_1, \ldots, s_n$ have positive real parts, and the integers $m_1, \ldots, m_n$ satisfy the equation

$$m_1 + m_2 + \ldots + m_n = m. \tag{33}$$

Then, the impulse response function $h(t)$ is given by the equation

$$h(t) = \sum_{k=1}^{n} \sum_{j=1}^{m_k} H_{kj} t^{m_k - j} e^{-s_k t} \tag{34}$$

where the constants H_{kj} are given by the equation (Korn and Korn, 1968)

$$H_{kj} = \frac{1}{(j-1)!(m_k - j)!} \frac{d^{j-1}}{ds^{j-1}} \left[\frac{(s+s_k)^{m_k}}{\Lambda(s)} \right]_{s=-s_k}. \tag{35}$$

Observe that if $\Lambda(s)$ has simple roots, that is

$$m_1 = m_2 = \ldots = m_n = 1,\ n = m \tag{36}$$

equation (35) yields the simpler formula

$$h(t) = \sum_{k=1}^{m} h_k e^{-s_k t}, \tag{37}$$

where

$$h_k = \left[1 / \frac{d\Lambda(s)}{ds} \right]_{s=-s_k}. \tag{38}$$

Thus, in either case, $\Lambda(s)$ with simple or multiple roots, the calculation of the components of the vector $\mathbf{r}$, equation (21), requires the computation of integrals with exponentially decaying integrands. This fact may simplify the computational effort required in applying equation (30) for a particular mathematical form of $S_w(\omega)$. This point will be demonstrated by some of the ensuing applications.

Applications

White Noise Excitation. Assume that $w(t)$ is a white noise process with

$$S_w(\omega) = 1,\ -\infty < \omega < \infty. \tag{39}$$

Then,

$$R_w(\tau) = 2\pi\delta(\tau) \tag{40}$$

where $\delta(\tau)$ is a two-sided delta function. Combining equations (16), (21) and (39) yields

$$r_k = D^k R_{xw}(o) = o,\ k = o, \ldots, m-2 \tag{41}$$

and

$$r_{m-1} = D^{m-1} R_{xw}(o) = \frac{\pi}{\lambda_m}. \tag{42}$$

Substituting equations (41) and (42) into equation (30) yields the classical integral given in Gradshteyn and Ryzhik (1965) and determined by two independent approaches in James et al. (1965) and Spanos (1983).

Observe that in this case the calculation of the integral I_m is accomplished without determining the roots of $\Lambda(s)$. Further, due to the uniformity of $S_w(\omega)$ over the entire frequency axis, equation (39), the moments M_{2k} for $k \geq m$ are infinite. That is, equation (25) is not applicable. These observations do not apply in the following case, involving random excitations, $w(t)$ with finite mean-square values.

Band-Limited White Noise Excitation. Assume that $w(t)$ is a band-limited white noise process with

$$S_w(\omega) = 1;\ o \leq \omega_1 \leq |\omega| \leq \omega_2 \tag{43}$$

and cut-off frequencies, ω_1, ω_2. Clearly, the auto-correlation of $w(t)$ is given by the equation

$$R_w(\tau) = \frac{2}{\tau}[\sin(\omega_2\tau) - \sin(\omega_1\tau)]. \tag{44}$$

Therefore, the determination of the components of the vector $\mathbf{r}$ for this case requires the calculation of integrals of the following form

$$I_\ell = \int_o^\infty \sin(\omega_c\tau)\tau^\ell e^{-s_k\tau} d\tau;\ \omega_c = \omega_1, \omega_2 \tag{45}$$

where

$$\ell = -1,\ o, 1, \ldots. \tag{46}$$

This integral is tabulated in Gradshteyn and Ryzhik (1965)

$$I_\ell = (-1)^\ell \frac{\partial^\ell}{\partial {s_k}^\ell} \left[\frac{s_k}{\omega_c^2 + s_k^2} \right],\ \ell \geq o \tag{47}$$

and

$$I_\ell = \tan^{-1}\left(\frac{\omega_c}{s_k}\right),\ \ell = -1. \tag{48}$$

Thus, for the case of band-limited noise the elements of the

Downloaded 03 May 2010 to 171.66.16.27. Redistribution subject to ASME license or copyright; see http://www.asme.org/terms/Terms_Use.cfm

vector $\mathbf{r}$ which appear in equation (20) can be determined in a closed form. In fact if $\Lambda(s)$ has only simple roots and if equation (37) applies, the components r_μ of $\mathbf{r}$ will be given by the expression

$$r_\mu = \sum_{k=1}^{m} h_k(-s_k)^\mu \tan^{-1}\left[\frac{s_k(\omega_2-\omega_1)}{s_k^2+\omega_1\omega_2}\right];\ \mu=0,\ \ldots \tag{49}$$

Obviously, setting $\omega_1 = o$, the case of clipped white noise is recovered. Further, upon determining the moments M_{2k}, $k=o,\ \ldots,\ m-1$ by using equation (22), any higher order moments can be determined by relying on equation (25). Note, that M_{2k} for $k \geq m$ are finite since $S_w(\omega)$ assumes zero values outside the intervals $0 \leq \omega_1 \leq |\omega| \leq \omega_2$.

Excitation with "Gaussian" Spectrum. Assume that $w(t)$ has power spectrum expressed as (Nigam, 1983)

$$S_w(\omega) = e^{-\omega^2},\ -\infty < \omega < \infty. \tag{50}$$

Then, its auto-correlation function will be given by the equation

$$R_w(\tau) = \sqrt{\pi} e^{-\frac{\tau^2}{4}}. \tag{51}$$

Substituting equation (50) into equation (27) yields a class of integrals which are often encountered in dealing with systems with random parameters (Aoki, 1967). Clearly, in calculating the integrals which appear in equation (21) it is required to determine the value of the integrals

$$\hat{I}_q = \int_o^\infty e^{-\frac{\tau^2}{4}-s_k\tau}\tau^q d\tau, \tag{52}$$

where

$$q = 0,\ 1,\ \ldots\ . \tag{53}$$

This integral is tabulated in Gradshteyn and Ryzhik (1965) for all values of q. Further, for the common case of simple roots s_k, that is $q = o$, it is found that

$$\hat{I}_o = \sqrt{\pi}\ \exp(s_k^2)[1-\Phi(s_k)], \tag{54}$$

where the symbol Φ denotes the error function. Thus, for the case of the "Gaussian" spectrum and simple s_k, the elements of the vector $\mathbf{r}$ will be given by the expression

$$r_\mu = \pi \sum_{k=1}^{m} h_k(-s_k)^\mu \exp(s_k^2)[1-\Phi(s_k)],\ \mu=o,\ 1,\ \ldots \tag{55}$$

Excitation with Oscillatory Spectrum. Assume that $w(t)$ has power spectrum given by the equation

$$S_w(\omega) = \frac{\tau_o}{2\pi}\left[\frac{\sin(\omega\tau_o/2)}{(\omega\tau_o/2)}\right]^2,\ -\infty < \omega < \infty \tag{56}$$

where τ_o is a positive constant. This spectral form relates to the useful class of stationary processes with auto-correlation function decaying from the peak value, at $\tau = o$, to zero at $|\tau| = \tau_o$. The auto-correlation function of $w(t)$ is nonzero only in the interval $[-\tau_o, \tau_o]$. It can be expressed as

$$R_w(\tau) = 1 - \frac{|\tau|}{\tau_o}. \tag{57}$$

Thus, in determining the integrals which appear in equation (21) it is necessary to calculate the values of the integrals

$$\bar{I}_q = \int_o^{\tau_o}\left(1-\frac{\tau}{\tau_o}\right)\tau^q e^{-s_k\tau} d\tau. \tag{58}$$

The value of this definite integral can be determined by relying on the identity (Gradshteyn and Ryzhik, 1965)

$$\int \tau^n e^{\alpha\tau} d\tau = e^{\alpha\tau}\left[\frac{\tau^n}{\alpha} + \sum_{k=1}^{n}(-1)^k \frac{n(n-1)\ldots(n-k+1)}{\alpha^{k+1}}\tau^{n-k}\right] \tag{59}$$

where n is a positive integer. Further, if the roots s_k are simple, equations (58) and (59) yield

$$\bar{I}_o = \frac{1}{s_k}\left(1+\frac{e^{-s_k\tau_o}-1}{s_k\tau_o}\right) \tag{60}$$

Thus, for the case of linearly decaying auto-correlation function and simple roots s_k, the elements of the vector $\mathbf{r}$ are given by the expression

$$r_\mu = -\sum_{k=1}^{m} h_k(-s_k)^{\mu-1}\left(1+\frac{e^{-s_k\tau_o}-1}{s_k\tau_o}\right),\ \mu=o,\ 1,\ \ldots \tag{61}$$

Some Numerical Results

For demonstration of the applicability of the preceding procedure, a numerical application will be given involving one of the complicated spectral forms examined. Specifically, consider the stochastic dynamics problem described by the equation of motion

$$\ddot{x} + \dot{x} + x = w(t), \tag{62}$$

where the power spectrum of $w(t)$ is given by equation (50). Evidently, the function $\Lambda(s)$ for this case is

$$\Lambda(s) = s^2 + s + 1 = (s+s_1)(s+s_2) \tag{63}$$

with

$$s_1 = \frac{1+i\sqrt{3}}{2}, \tag{64}$$

$$s_2 = \frac{1-i\sqrt{3}}{2} \tag{65}$$

and $m_1 = m_2 = 1$. (66)

Thus, using equations (54) and (55) and a table for the error function yields

$$r_o = \pi \sum_{k=1}^{2} \exp(s_k^2)[1-\Phi(s_k)]\frac{1}{1-2s_k} = 1.184 \tag{67}$$

and

$$r_1 = -\pi \sum_{k=1}^{2} s_k \exp(s_k^2)[1-\Phi(s_k)]\frac{1}{1-2s_k} = 0.679. \tag{68}$$

Further, relying on equation (26) one finds

$$r_2 = R_w(o) - r_o - r_1 = -0.091 \tag{69}$$

Then, equation (20) yields

$$M_2 = \int_{-\infty}^{\infty} \frac{\omega^2 e^{-\omega^2}}{\omega^4 + (\omega^2-1)^2}\, d\omega = r_1 = 0.679 \tag{70}$$

and

$$M_o = \int_{-\infty}^{\infty} \frac{e^{-\omega^2}}{\omega^4 + (\omega^2-1)^2}\, d\omega = M_2 + r_o = 1.863 \tag{71}$$

Next, combining equations (25), (69), and (70) yields

$$M_4 = \int_{-\infty}^{\infty} \frac{\omega^4 e^{-\omega^2}}{\omega^4 + (\omega^2-1)^2}\, d\omega = M_2 + r_2 = 0.588. \tag{72}$$

Note, that the values of M_o, M_2, and M_4 which are given by equations (70)–(72) have been verified by relying on a standard numerical quadrature algorithm. Further, observe that the recursive procedure used to determine M_4 can be followed to calculate higher order quantities M_{2k}, $k > 2$.

Concluding Remarks

Equation (30) has been derived by relying on the properties of the response auto-correlation, and of the response with ex-

Downloaded 03 May 2010 to 171.66.16.27. Redistribution subject to ASME license or copyright; see http://www.asme.org/terms/Terms_Use.cfm

citation cross-correlation of a dynamic system. This is a quite powerful formula. It yields as a special case the James et al. (1965) formula which is used extensively in random vibration and control calculations. Further, it provides an important generalization involving the response of a dynamic system to clipped white noise. Also, as it has been demonstrated by the case of the "Gaussian" power spectrum, it can lead to the calculation of complicated integrals which have their own mathematical merit and can be used in a variety of other technical fields. In fact, the developed formula is applicable as long as the elements of the vector **r** are available. Note that these elements involve integrals with exponentially decaying, in general, integrands. Therefore, in many cases, they can be determined analytically. Further, they lend themselves to routine numerical quadrature schemes.

It should be noted that within the scope of structural dynamics problems attention to systems of order higher than two is quite often necessary. For example, in many cases the spectra of loads induced by natural phenomena are modeled as the output of linear systems to white noise excitation. Thus, combining the mathematical representation of the load with the transfer function of the oscillatory system under consideration leads to a higher order abstract dynamic system. A similar situation arises when random vibration analysis of a cascade of structures, primary or secondary, is carried out (Singh, 1980).

Finally, attention is called to the work of Kako et al. (1986) which deals with the integration from zero to infinity of rational functions often encountered in random vibration analysis.

Acknowledgment

The financial support of this research by a PYI-84 grant from the National Science Foundation is gratefully acknowledged. Industrial matching funds to the PYI program provided by Brown and Root, Inc., Dow Chemical Co., Conoco Inc., N. L. Industries, Inc., and Tracor, Inc., are appreciated. Thanks are expressed to Professor L. Lutes for his constructive comments, and to J. Red-Horse for his computational assistance.

References

Aoki, M., 1967, *Optimization of Stochastic Systems*, Academic Press, New York.

Gradshteyn, I. S., and Ryzhik, I. M., 1965, *Tables of Integrals, Series and Products*, Academic Press, New York.

James, H. M., Nichols, N. B., and Philips, R. S., eds., 1965, *Theory of Servomechanisms*, Dover, New York.

Kato, T., Shinozuka, M., and Tsurui, A., 1986, "First Excursion Problems for Gaussian Vector Processes," in *Random Vibration—Status and Recent Developments*, Elishakoff, I., and Lyon, R. H., eds., Elsevier, New York.

Korn, A. G., and Korn, T. M., 1969, *Mathematical Handbook for Scientists and Engineers*, McGraw-Hill, New York.

Lin, Y. K., 1976, *Probabilistic Theory of Structural Dynamics*, R. E. Krieger, Huntington, New York.

Nigam, N. C., 1983, *Introduction to Random Vibrations*, The MIT Press, Cambridge, Mass.

Singh, M. P., 1980, Seismic Design Input for Secondary Systems, ASCE *Journal of the Structural Division*, Vol. 106, No. ST2, pp. 505–516.

Spanos, P-T. D., 1983, Spectral Moments Calculation of Linear System Output, ASME JOURNAL OF APPLIED MECHANICS, Vol. 50, pp. 901–903.

Yang, I-M, and Iwan, W. D., 1972, Calculation of Correlation Matrices for Linear Systems Subjected to Nonwhite Excitation, ASME JOURNAL OF APPLIED MECHANICS, pp. 559–562.

Downloaded 03 May 2010 to 171.66.16.27. Redistribution subject to ASME license or copyright; see http://www.asme.org/terms/Terms_Use.cfm

Exact Stationary-Response Solution for Second Order Nonlinear Systems Under Parametric and External White-Noise Excitations

Y. Yong
Research Associate.

Y. K. Lin
Charles E. Schmidt Professor and Director.

Center for Applied Stochastics Research,
Florida Atlantic University,
Boca Raton, FL 33431

Except for rare sporadic cases, exact stationary solutions for second order nonlinear systems under Gaussian white-noise excitations are known only for certain types of systems and only when the excitations are purely external (additive). Yet, in many engineering problems, random excitations may also be parametric (multiplicative). It is shown in this paper that the method of detailed balance developed by the physicists can be applied to obtain systematically the stationary solutions for a large class of nonlinear systems under either external random excitations or parametric random excitations, or both. Examples are given for those cases where solutions have been given previously in the literature as well as other cases where solutions are new. An unexpected result is revealed in one of the new solutions, namely, under suitable combination of the parametric and external excitations of Gaussian white noises, the response of a nonlinear system can be Gaussian.

Introduction

For many years, engineers and scientists in a great variety of disciplines have been interested in the common problems of system response to random excitations. Numerous publications on this general subject have appeared in the literature. The dynamic systems of concern may be linear or nonlinear, and the random excitations may be parametric (multiplicative) or external (additive). In the equations of motion, parametric excitations appear in the coefficients of the unknown, while external excitations appear as the inhomogeneous terms. The effects of the two types of excitations are very different, as noted by several authors. In particular, a parametric excitation causes the dynamic characteristics of a system to vary with time; thus, it can affect the stability of the system. At the present time, our knowledge of solutions for linear systems are reasonably complete when random excitations are purely external. When random parametric excitations are also involved, the known solutions are restricted only to some special cases.

For nonlinear systems, the use of approximate procedures is often necessary. The possibility for mathematically exact solutions does exist; however, it exists only when random excitations are independent at any two instants of time, and the system response, represented as a vector in a state space, is a Markov vector. In this case the probability density of the system response, conditional on the knowledge of the initial state (referred to usually as the transition probability density), satisfies a parabolic partial differential equation, called the Fokker-Planck equation, which can be derived from the equations of motion. Unfortunately, exact solution for the Fokker-Planck equation is known only for very special first order nonlinear systems [5]. For certain types of second order nonlinear systems, solutions have been obtained (e.g., [1-8], [11-13]) for the reduced Fokker-Planck equations, namely, Fokker-Planck equations without the time-derivative term. The unknown in a reduced Fokker-Planck equation is the unconditional probability density of the response vector when it reaches the state of statistical stationarity. Of course, a stationary response exists only if the excitations are stationary (namely, the excitations must be Gaussian white noises), and only after the system has been exposed to stationary excitations for a sufficiently long time.

Exact solutions given in the above references are restricted to external Gaussian white noise excitations. These solvable problems can be grouped in a general class as shown by Caughey and Ma [6]. Similar exact solutions for second order nonlinear systems under both external and parametric random excitations are practically nonexistent in the literature except,

Contributed by the Applied Mechanics Division for presentation at the 1987 Applied Mechanics, Biomechanics, and Fluids Engineering Conference, Cincinnati, OH, June 14-17, 1987, of the American Society of Mechanical Engineers.
Discussion of this paper should be addressed to the Editorial Department, ASME, United Engineering Center, 345 East 47th Street, New York, N.Y. 10017, and will be accepted until two months after final publication of the paper itself in the JOURNAL OF APPLIED MECHANICS. Manuscript received by ASME Applied Mechanics Division, June 10, 1986; final revision, November 4, 1986.
Paper No. 87-APM-30.

Copyright © 1987 by ASME
Downloaded 03 May 2010 to 171.66.16.27. Redistribution subject to ASME license or copyright; see http://www.asme.org/terms/Terms_Use.cfm

perhaps, for the one example given by Dimentberg [8]. However, since no explanation was given in [8] as to how the solution was obtained, a reasonable assumption is that it might have been discovered accidentally or through an inverse procedure. In any case, no generalization appears possible with only one known example.

In this paper, a general procedure is given for systematically solving the reduced Fokker-Planck equations based on the concept of detailed balance or microscopic reversibility [9, 15], which is applicable to nonlinear systems of any order and is not restricted to either type of random excitations. A brief review of the concept is first presented. Next, the procedure is applied to the same examples given in [4], [6], and [8]. Finally, some new solutions are obtained for nonlinear systems under both parametric and external random excitations. An unexpected result is revealed in one of the new solutions, namely, under a suitable combination of the parametric and external excitations of Gaussian white noises, the response of a nonlinear system can be Gaussian.

Principle of Detailed Balance

The concept of detailed balance was first applied by van Kampen in a paper [15] to master equations of which the Fokker-Planck equation is a special form. Graham and Haken [9] applied the concept to thermodynamic potentials which are not in the state of thermal equilibrium. In the following review of the basic concept, our presentation is similar to that of Graham and Haken.

Let the excitations on a dynamic system, linear or nonlinear, be Gaussian white noises, so that the response vector is Markovian. The components of the response vector may be classified as either odd or even variables, according to the transformation from x_i to $\tilde{x}_i$ upon the time reversal $t \to -t$. The even variables do not change their signs when time is reversed, whereas the odd variables do. Thus, we denote

$$\tilde{x}_i = \epsilon_i x_i \qquad \text{(no summation on } i\text{)} \tag{1}$$

where $\epsilon_i = \pm 1$ corresponding to even and odd variables, respectively. We define the state of detailed balance as

$$p_2(\mathbf{x},t;\mathbf{x}_o,t_o) = p_2(\tilde{\mathbf{x}}_o,t;\tilde{\mathbf{x}},t_o), \qquad t > t_o \tag{2}$$

where p_2 is the second order probability density of the Markov process. Alternatively, equation (2) may be written as

$$q(\mathbf{x},t|\mathbf{x}_o,t_o)p_1(\mathbf{x}_o,t_o) = q(\tilde{\mathbf{x}}_o,t|\tilde{\mathbf{x}},t_o)p_1(\tilde{\mathbf{x}},t_o) \tag{3}$$

where q is the transition probability density, and p_1 is the first order probability density. Since the excitations are Gaussian white noises, q depends only on $\tau = t - t_o$. Furthermore, after the Markov vector reaches statistical stationarity, equation (3) simplifies to

$$q(\mathbf{x},\tau|\mathbf{x}_o)p_s(\mathbf{x}_o) = q(\tilde{\mathbf{x}}_o,\tau|\tilde{\mathbf{x}})p_s(\tilde{\mathbf{x}}) \tag{4}$$

where the subscript for p_1 has been replaced by s to indicate statistical stationarity.

Equation (4) defines the state of detailed balance for a stationary Markov process, and it will be the basis for subsequent developments.

In passing, we note that since $q(\mathbf{x}, 0|\mathbf{x}_o) = \delta(\mathbf{x} - \mathbf{x}_o)$ and $q(\tilde{\mathbf{x}}_o, 0|\tilde{\mathbf{x}}) = \delta(\tilde{\mathbf{x}}_o - \tilde{\mathbf{x}})$, equation (4) implies

$$p_s(\tilde{\mathbf{x}}) = p_s(\mathbf{x}) \tag{5}$$

as can be shown by integrating equation (4) at $\tau = 0$ on both sides.

The transition probability density q satisfies the Fokker-Planck equation

$$\frac{\partial q(\mathbf{x},\tau|\mathbf{x}_o)}{\partial \tau} = -\frac{\partial}{\partial x_i}[A_i(\mathbf{x})q] + \frac{1}{2}\frac{\partial^2}{\partial x_i \partial x_j}[B_{ij}(\mathbf{x})q] \tag{6}$$

where

$$A_i(\mathbf{x}) = \lim_{\Delta t \to o} \frac{1}{\Delta t} E[X_i(t+\Delta t) - X_i(t) \,|\, \mathbf{X}(t) = \mathbf{x}] \tag{7}$$

$$B_{ij}(\mathbf{x}) = \lim_{\Delta t \to o} \frac{1}{\Delta t} E\{[X_i(t+\Delta t) - X_i(t)][X_j(t+\Delta t) - X_j(t)] \,|\, \mathbf{X}(t) = \mathbf{x}\} \tag{8}$$

Furthermore, if the stationary response exists, then q approaches p_s as τ tends to infinity. In other words, p_s satisfies the reduced Fokker-Planck equation

$$\frac{\partial}{\partial x_i}[A_i(\mathbf{x})p_s(\mathbf{x})] - \frac{1}{2}\frac{\partial^2}{\partial x_i \partial x_j}[B_{ij}(\mathbf{x})p_s(\mathbf{x})] = 0 \tag{9}$$

We now insert

$$q(\mathbf{x},\tau|\mathbf{x}_o) = \frac{p_s(\mathbf{x})}{p_s(\mathbf{x}_o)} q(\tilde{\mathbf{x}}_o,\tau|\tilde{\mathbf{x}}) \tag{10}$$

into equation (6) and obtain, upon using equation (9),

$$\frac{\partial q(\tilde{\mathbf{x}}_o,\tau|\tilde{\mathbf{x}})}{\partial \tau} + A_i(\mathbf{x})\frac{\partial}{\partial x_i} q(\tilde{\mathbf{x}}_o,\tau|\tilde{\mathbf{x}}) - \frac{1}{p_s(\mathbf{x})}\frac{\partial q(\tilde{\mathbf{x}}_o,\tau|\tilde{\mathbf{x}})}{\partial x_i}\frac{\partial [B_{ik}(\mathbf{x})p_s(\mathbf{x})]}{\partial x_k} - \frac{1}{2}B_{ik}(\mathbf{x})\frac{\partial^2 q(\tilde{\mathbf{x}}_o,\tau|\tilde{\mathbf{x}})}{\partial x_i \partial x_k} = 0 \tag{11}$$

The transition probability density q is also a solution of the Kolmogorov backward equation (e.g., [14]), from which we obtain

$$\frac{\partial q(\tilde{\mathbf{x}}_o,\tau|\tilde{\mathbf{x}})}{\partial \tau} = A_i(\tilde{\mathbf{x}})\frac{\partial}{\partial \tilde{x}_i} q(\tilde{\mathbf{x}}_o,\tau|\tilde{\mathbf{x}}) + \frac{1}{2}B_{ij}(\tilde{\mathbf{x}})\frac{\partial^2}{\partial \tilde{x}_i \partial \tilde{x}_j} q(\tilde{\mathbf{x}}_o,\tau|\tilde{\mathbf{x}}) \tag{12}$$

Equation (12) differs from the usual backward equation in that the backward time variable has been replaced by the forward time variable τ. Combination of equations (11) and (12) yields

$$\left\{\left[\frac{1}{p_s(\mathbf{x})}\frac{\partial [B_{ij}(\mathbf{x})p_s(\mathbf{x})]}{\partial x_j} - A_i(\mathbf{x}) - \epsilon_i A_i(\tilde{\mathbf{x}})\right] + \frac{1}{2}[B_{ij}(\mathbf{x}) - \epsilon_i\epsilon_j B_{ij}(\tilde{\mathbf{x}})]\frac{\partial}{\partial x_j}\right\}\frac{\partial}{\partial x_i} q(\tilde{\mathbf{x}}_o,\tau|\tilde{\mathbf{x}}) = 0 \tag{13}$$

Equations (13) holds for any τ, in particular for $\tau = 0$ when $q(\tilde{\mathbf{x}}_o,\tau|\tilde{\mathbf{x}})$ reduces to a product of delta functions. Then, if equation (13) is multiplied by an arbitrary, twice-differentiable function $F(\mathbf{x}_o)$ and integrated over $\mathbf{x}_o$, we obtain

$$\left[\frac{1}{p_s(\mathbf{x})}\frac{\partial B_{ij}(\mathbf{x})p_s(\mathbf{x})}{\partial x_j} - A_i(\mathbf{x}) - \epsilon_i A_i(\tilde{\mathbf{x}})\right]\frac{\partial}{\partial x_i} F(\tilde{\mathbf{x}}) + \frac{1}{2}[B_{ij}(\mathbf{x}) - \epsilon_i\epsilon_j B_{ij}(\tilde{\mathbf{x}})]\frac{\partial^2 F(\tilde{\mathbf{x}})}{\partial x_i \partial x_j} = 0 \tag{14}$$

Since $F(\tilde{\mathbf{x}})$ is arbitrary, the coefficients for each derivative of $F(\tilde{\mathbf{x}})$ must vanish, namely,

$$A_i(\mathbf{x})p_s(\mathbf{x}) + \epsilon_i A_i(\tilde{\mathbf{x}})p_s(\mathbf{x}) - \frac{\partial B_{ij}(\mathbf{x})p_s(\mathbf{x})}{\partial x_j} = 0 \tag{15}$$

$$B_{ij}(\mathbf{x}) - \epsilon_i\epsilon_j B_{ij}(\tilde{\mathbf{x}}) = 0 \tag{16}$$

Equations (15) and (16) are necessary conditions for detailed balance in the stationary state. It will be shown from the

Downloaded 03 May 2010 to 171.66.16.27. Redistribution subject to ASME license or copyright; see http://www.asme.org/terms/Terms_Use.cfm

following proof that the two equations combined are also sufficient conditions.

For a function S, having the form of

$$S(\mathbf{x},\mathbf{x}_o,\tau)=\frac{p_s(\mathbf{x})}{p_s(\mathbf{x}_o)}\,q(\tilde{\mathbf{x}}_o,\tau|\tilde{\mathbf{x}}) \tag{17}$$

it can be shown that

$$-\frac{\partial}{\partial x_i}[A_i(\mathbf{x})S]+\frac{1}{2}\frac{\partial^2}{\partial x_i\partial x_j}[B_{ij}(\mathbf{x})S]$$

$$=\frac{1}{p_s(\mathbf{x}_o)}\left\{-A_i(\mathbf{x})p_s(\mathbf{x})+\frac{\partial[B_{ij}(\mathbf{x})p_s(\mathbf{x})]}{\partial x_j}\right\}\frac{\partial q(\tilde{\mathbf{x}}_o,\tau|\tilde{\mathbf{x}})}{\partial x_i}$$

$$+\frac{1}{2}B_{ij}(\mathbf{x})\frac{p_s(\mathbf{x})}{p_s(\mathbf{x}_o)}\frac{\partial^2 q(\tilde{\mathbf{x}}_o,\tau|\tilde{\mathbf{x}})}{\partial x_i\partial x_j} \tag{18}$$

Imposing equations (15) and (16), the right-hand side of equation (18) becomes

$$\epsilon_i\frac{A_i(\tilde{\mathbf{x}})p_s(\mathbf{x})}{p_s(\mathbf{x}_o)}\cdot\frac{\partial q(\tilde{\mathbf{x}}_o,\tau|\tilde{\mathbf{x}})}{\partial x_i}$$

$$+\frac{1}{2}\epsilon_i\epsilon_j\frac{B_{ij}(\tilde{\mathbf{x}})p_s(\mathbf{x})}{p_s(\mathbf{x}_o)}\cdot\frac{\partial^2 q(\tilde{\mathbf{x}}_o,\tau|\tilde{\mathbf{x}})}{\partial x_i\partial x_j}$$

$$=\left[A_i(\tilde{\mathbf{x}})\frac{\partial q(\tilde{\mathbf{x}}_o,\tau|\tilde{\mathbf{x}})}{\partial\tilde{x}_i}+\frac{1}{2}B_{ij}(\tilde{\mathbf{x}})\frac{\partial^2 q(\tilde{\mathbf{x}}_o,\tau|\tilde{\mathbf{x}})}{\partial\tilde{x}_i\partial\tilde{x}_j}\right]\frac{p_s(\mathbf{x})}{p_s(\mathbf{x}_o)}$$

$$=\left[\frac{\partial}{\partial\tau}q(\tilde{\mathbf{x}}_o,\tau|\tilde{\mathbf{x}})\right]\frac{p_s(\mathbf{x})}{p_s(\mathbf{x}_o)}=\frac{\partial}{\partial\tau}S(\mathbf{x},\mathbf{x}_o,\tau) \tag{19}$$

Therefore, $S(\mathbf{x},\mathbf{x}_o,\tau)$ satisfies the Fokker-Planck equation. If S is normalized, namely, if

$$\int_{-\infty}^{\infty}S(\mathbf{x},\mathbf{x}_o,\tau)d\mathbf{x}=1 \tag{20}$$

then it must be uniquely

$$S(\mathbf{x},\mathbf{x}_o,\tau)=q(\mathbf{x},\tau|\mathbf{x}_o) \tag{21}$$

Combination of equations (17) and (21) leads to the definition of the state of detailed balance of a Markov process in the stationary state, equation (4). Thus, we have proved that satisfying equations (15) and (16) is sufficient for detailed balance.

Graham and Haken [9] have developed an alternative condition which is equivalent to equation (15) and is easier to use in obtaining solutions for reduced Fokker-Planck equations. This is achieved by separating each drift coefficient $A_i(\mathbf{x})$ into reversible and irreversible parts.

$$A_i(\mathbf{x})=A_i^I(\mathbf{x})+A_i^R(\mathbf{x}) \tag{22}$$

where

$$A_i^I(\mathbf{x})=\frac{1}{2}[A_i(\mathbf{x})+\epsilon_i A_i(\tilde{\mathbf{x}})] \tag{23}$$

$$A_i^R(\mathbf{x})=\frac{1}{2}[A_i(\mathbf{x})-\epsilon_i A_i(\tilde{\mathbf{x}})] \tag{24}$$

The adjectives "irreversible" and "reversible" refer to the fact that

$$A_i^I(\mathbf{x})=\epsilon_i A_i^I(\tilde{\mathbf{x}}) \tag{25}$$

$$A_i^R(\mathbf{x})=-\epsilon_i A_i^R(\tilde{\mathbf{x}}) \tag{26}$$

Now since $p_s(\mathbf{x})$ is nonnegative, it can always be expressed in the following form

$$p_s(\mathbf{x})=C\exp[-\phi(\mathbf{x})] \tag{27}$$

Substituting equations (22) and (27) into equation (15), we obtain

$$2A_i^I(\mathbf{x})-\frac{\partial B_{ij}(\mathbf{x})}{\partial x_j}+B_{ij}(\mathbf{x})\frac{\partial\phi(\mathbf{x})}{\partial x_j}=0 \tag{15'}$$

Equation (15′) is equivalent to equation (15). Function $\phi(\mathbf{x})$ must also satisfy

$$\frac{\partial A_i^R(\mathbf{x})}{\partial x_i}-A_i^R(\mathbf{x})\frac{\partial\phi(\mathbf{x})}{\partial x_i}=0 \tag{28}$$

which is obtained by substituting equations (22), (27), and (15′) into the reduced Fokker-Planck equation (9). Equation (15′) and (28) can be used conveniently to determine $\phi(\mathbf{x})$.

Applications

The application of the detailed balance principle will now be illustrated by several examples. Solutions to the first and second examples have been obtained before [4, 6]; the intent is to demonstrate the validity of the principle. Solutions to the remaining examples are new. Example 3 is a generalization of the one considered by Dimentberg [8].

Example 1. Consider the case of [4]

$$\ddot{X}+h(\Lambda)\dot{X}+f(X)=W(t) \tag{1-1}$$

where $W(t)$ is a Gaussian white noise with a spectral density K, $f(X)$ is the nonlinear spring force, $h(\Lambda)$ is an arbitrary function which must be positive when its argument becomes large, and Λ is the total potential

$$\Lambda=\frac{1}{2}\dot{X}^2+\int_0^X f(u)du \tag{1-2}$$

Let $X_1=X$ and $X_2=\dot{X}_1$. Equation (1-1) is equivalent to two Itô type stochastic differential equations [10]

$$dX_1=X_2dt \tag{1-3}$$

$$dX_2=[-h(\Lambda)X_2-f(X_1)]dt+\sqrt{2\pi K}\,dB(t) \tag{1-4}$$

where $B(t)$ is a unit Wiener process. The corresponding reduced Fokker-Planck equation is then

$$x_2\frac{\partial}{\partial x_1}p_s-\frac{\partial}{\partial x_2}\left\{[h(\lambda)x_2+f(x_1)]p_s\right\}-\pi K\frac{\partial^2}{\partial x_2^2}p_s=0 \tag{1-5}$$

where we have adopted the convention of using a lower case symbol to represent the state variable of a random quantity. For this example,

$A_1^I=0$, $A_1^R=x_2$, $A_2^I=-h(\lambda)x_2$, $A_2^R=-f(x_1)$,

$B_{11}=B_{12}=B_{21}=0$, $B_{22}=2\pi K$

Clearly, condition (16) is satisfied. Condition (15′) leads to

$$-2h(\lambda)x_2+2\pi K\frac{\partial\phi}{\partial x_2}=0 \tag{1-6}$$

with solution

$$\phi=\frac{1}{\pi K}\int_0^\lambda h(u)du+g_1(x_1) \tag{1-7}$$

In order that (28) can be satisfied also, function g_1 must be a constant, which may be taken as being zero without loss of generality. Thus,

$$p_s(x_1,x_2)=C_1\exp\left[-\frac{1}{\pi K}\int_0^\lambda h(u)du\right] \tag{1-8}$$

Example 2. Caughey and Ma [6] have generalized the case of example 1 to

$$\ddot{X}+\alpha\left[\Lambda_Y h(\Lambda)-\frac{\Lambda_{YY}}{\Lambda_Y}\right]\dot{X}+\frac{\Lambda_X}{\Lambda_Y}=W(t) \tag{2-1}$$

where Λ is now a more general energy integral corresponding to the following conservative oscillator

Downloaded 03 May 2010 to 171.66.16.27. Redistribution subject to ASME license or copyright; see http://www.asme.org/terms/Terms_Use.cfm

$$\ddot{X}+\frac{\Lambda_X}{\Lambda_Y}=0 \tag{2-2}$$

and where $Y = 1/2\,\dot{X}^2$ and each subscript X or Y denotes a partial differentiation. In this case,

$$A_1^I=0, A_1^R=x_2, A_2^I=-\alpha\left[\lambda_y h(\lambda)-\frac{\lambda_{yy}}{\lambda_y}\right]x_2$$

$$A_2^R=-\frac{\lambda_{x_1}}{\lambda_y}, B_{11}=B_{12}=B_{21}=0, B_{22}=2\pi K$$

Again, condition (16) is trivially satisfied, and condition (15′) leads to

$$-2\alpha\left[\lambda_y h(\lambda)-\frac{\lambda_{yy}}{\lambda_y}\right]x_2+2\pi K\frac{\partial\phi}{\partial x_2}=0 \tag{2-3}$$

with solution

$$\phi=\frac{\alpha}{\pi K}\left[\int_0^\lambda h(u)du-\ell n\,\lambda_y\right]+g_2(x_1) \tag{2-4}$$

In order for (28) to be satisfied also, it is necessary that

$$-x_2(\lambda_{x_1y}\lambda_y-\lambda_{yy}\lambda_{x_1})\lambda_y^{-2}-\frac{\alpha}{\pi K}x_2[h(\lambda)\lambda_{x_1}-\lambda_{x_1y}\lambda_y^{-1}]$$
$$-x_2 g_2'(x_1)+\frac{\alpha}{\pi K}\lambda_{x_1}\lambda_y^{-1}[\lambda_y h(\lambda)-\lambda_{yy}\lambda_y^{-1}]x_2=0 \tag{2-5}$$

which requires that $\alpha/\pi K = 1$ and $g_2(x_1)$ be a constant. Thus

$$p_s(x_1,x_2)=C_2\lambda_y\exp\left[-\int_0^\lambda h(u)du\right] \tag{2-6}$$

Example 3. We now consider the case of

$$\ddot{X}+[h(\Gamma)+\xi_2(t)]\dot{X}+\omega_o^2[1+\xi_1(t)]X=\xi_3(t) \tag{3-1}$$

where $\xi_j(t)$ are independent physical Gaussian white noises with spectral densities K_j, Γ is a linear potential defined as

$$\Gamma=\frac{1}{2}\dot{X}^2+\frac{1}{2}\omega_o^2X^2 \tag{3-2}$$

and $h(\Gamma)$ is subject to the same general restriction as in equation (1-1). Clearly, Γ is a special case of Λ given in equation (1-2) when $f(X)$ is linear.

Equation (3-1) governs a dynamic system under parametric excitations in the spring term as well as the damping term, in addition to the external excitation on the right-hand side. Each physical white noise $\xi_j(t)$ is considered to be the limit of a stationary Gaussian random process as the correlation time approaches to zero; it is different from the formal derivative of a Wiener process known as an ideal white noise. To convert equation (3-1) to the corresponding Itô equations, the well-known relations of Wong and Zakai [16] can be applied. Let $X_1 = X$ and $X_2 = \dot{X}$. The resulting Itô equations are

$$dX_1=X_2dt \tag{3-3}$$

$$dX_2=-\left\{[h(\Gamma)-\pi K_2]X_2+\omega_o^2X_1\right\}dt$$
$$+(2\pi)^{1/2}[\omega_o^4K_1X_1^2+K_2X_2^2+K_3]^{1/2}dB(t) \tag{3-4}$$

The reduced Fokker-Planck equation is given by

$$x_2\frac{\partial}{\partial x_1}p_s-\frac{\partial}{\partial x_2}\left\{[h(\gamma)x_2-\pi K_2x_2+\omega_o^2x_1]p_s\right\}$$
$$-\pi\frac{\partial^2}{\partial x_1\partial x_2}\left\{[\omega_o^4K_1x_1^2+K_2x_2^2+K_3]p_s\right\}=0 \tag{3-5}$$

By inspection, $A_1^I = 0$, $A_1^R = x_2$, $A_2^I = [-h(\gamma) + \pi K_2]x_2$, $A_2^R = -\omega_o^2 x_1$, $B_{11} = B_{12} = B_{21} = 0$, $B_{22} = 2\pi(\omega_o^4K_1x_1^2+K_2x_2^2+K_3)$.

The diffusion matrix B_{ij} satisfies condition (16). Imposing condition (15′), we obtain

$$2[-h(\gamma)+\pi K_2]x_2-4\pi K_2x_2+2\pi(\omega_o^4K_1x_1^2$$
$$+K_2x_2^2+K_3)\frac{\partial\phi}{\partial x_2}=0 \tag{3-6}$$

or

$$\frac{\partial\phi}{\partial x_2}=\frac{[h(\gamma)+\pi K_2]x_2}{\pi(\omega_o^4K_1x_1^2+K_2x_2^2+K_3)} \tag{3-7}$$

The integration of the right-hand side is greatly simplified if $K_2 = K_1\omega_o^2$, in which case

$$\phi=\int_0^\gamma\frac{h(u)+\pi K_2}{\pi(2K_2u+K_3)}du+g_3(x_1) \tag{3-8}$$

Imposing of equation (28) yields $g_3(x_1) =$ constant. Thus,

$$p_s(x_1,x_2)=C_3(2K_2\gamma+K_3)^{-1/2}\exp\left[-\frac{1}{\pi}\int_0^\gamma\frac{h(u)}{(2K_2u+K_3)}du\right] \tag{3-9}$$

It is of interest to note that if we restrict further to $h(\Gamma) = \beta\Gamma + \alpha$, we obtain

$$p_s(x_1,x_2)=C(2K_2\gamma+K_3)^{(\beta K_3/2\pi K_2^2-\alpha/\pi K_2-1)/2}\exp\left(-\frac{\beta\gamma}{2\pi K_2}\right) \tag{3-10}$$

Equation (3-10) is the same result obtained by Dimentberg [8] but in different notations.

Example 4. In the course of the present study we have discovered an unexpected result that under a suitable combination of parametric and external random excitations, the response of a nonlinear system under Gaussian excitations can be Gaussian. To illustrate, consider

$$\ddot{X}+(\alpha+\beta X^2)\dot{X}+\omega_0^2[1+\xi_1(t)]X=\xi_2(t) \tag{4-1}$$

where $\xi_j(t)$ are independent Gaussian physical white noises. With $X_1 = X$, $X_2 = \dot{X}$, it can be shown that $A_1^I = 0$, $A_1^R = x_2$, $A_2^I = -(\alpha + \beta x_1^2)x_2$, $A_2^R = -\omega_o^2x_1$, $B_{11} = B_{12} = B_{21} = 0$, $B_{22} = 2\pi(K_1x_1^2 + K_2)$. Again, condition (16) is satisfied trivially. Imposition of (15′) yields

$$\frac{\partial\phi}{\partial x_2}=\frac{(\alpha+\beta x_1^2)x_2}{\pi(K_1x_1^2+K_2)} \tag{4-2}$$

Thus,

$$\phi=\frac{(\alpha+\beta x_1^2)x_2^2}{2\pi(K_1x_1^2+K_2)}+g_4(x_1) \tag{4-3}$$

In the special combination $K_2/K_1 = \alpha/\beta$, we obtain

$$\phi=\frac{\beta}{2\pi K_1}x_2^2+g_4(x_1) \tag{4-4}$$

in which case, condition (28) provides

$$x_2g_4'(x_1)-\omega_o^2x_1\left(\frac{\beta}{\pi K_1}x_2\right)=0 \tag{4-5}$$

Without loss of generality, we may choose

$$g_4(x_1)=\frac{\beta\omega_o^2}{2\pi K_1}x_1^2 \tag{4-6}$$

Whence

$$p_s(x_1,x_2)=C_4\exp\left[-\frac{\beta}{2\pi K_1}(x_2^2+\omega_o^2x_1^2)\right] \tag{4-7}$$

Example 5. We now consider a multi-degree-of-freedom system

Downloaded 03 May 2010 to 171.66.16.27. Redistribution subject to ASME license or copyright; see http://www.asme.org/terms/Terms_Use.cfm

$$\ddot{Y}_i + h(\Gamma)\dot{Y}_i + \omega_i^2 Y_i + \sum_{j=1}^{n} \xi_{ij}(t)\dot{Y}_j + \sum_{j=1}^{n} \omega_j^2 \eta_{ij}(t) Y_j = \zeta_i(t) \tag{5-1}$$

where

$$\Gamma = \frac{1}{2}\sum_{j=1}^{n} (\dot{Y}_j^2 + \omega_j^2 Y_j^2) \tag{5-2}$$

and $\xi_{ij}(t)$, $\eta_{ij}(t)$ and $\zeta_i(t)$ are independent physical white noises. This dynamic system is a generalized version of (3-1). Let $X_{2i-1} = Y_i$ and $X_{2i} = \dot{Y}_i$. Equations (5-1) are replaced by

$$\begin{aligned} \dot{X}_{2i-1} &= X_{2i} \\ \dot{X}_{2i} &= h(\Gamma)X_{2i} - \omega_i^2 X_{2i-1} \\ &\quad - \sum_{j=1}^{n} [\xi_{ij}(t)X_{2j} + \omega_j^2 \eta_{ij}(t) X_{2j-1}] + \zeta_i(t) \end{aligned} \tag{5-3}$$

Under the restriction

$$\begin{aligned} E[\eta_{ij}(t)\eta_{ij}(t+\tau)] &= 2\pi K_{1j}\delta(\tau) \\ E[\xi_{ij}(t)\xi_{ij}(t+\tau)] &= 2\pi K_2 \delta(\tau) \\ E[\zeta_i(t)\zeta_i(t+\tau)] &= 2\pi K_3 \delta(\tau) \end{aligned} \tag{5-4}$$

we find $A^{\mathrm{I}}_{2i-1} = 0$, $A^{R}_{2i-1} = x_{2i}$, $A^{\mathrm{I}}_{2i} = [-h(\gamma) + \pi K_2]x_{2i}$, $A^{R}_{2i} = -\omega_i^2 x_{2i-1}$ and $B_{2i,2i} = 2\pi \Sigma_{j=1}^{n} (K_2 x_{2j}^2 + \omega_j^4 K_{1j} x_{2j-1}^2) + 2\pi K_3$. All other B elements are zero. Restricting further to $K_2 = K_{1j}\omega_j^2$, we obtain

$$\begin{aligned} B_{2i,2i} &= 2\pi K_2 \sum_{j=1}^{n} (x_{2j}^2 + \omega_j^2 x_{2j-1}^2) + 2\pi K_3 \\ &= 2\pi(2K_2\gamma + K_3) \end{aligned} \tag{5-5}$$

Imposing (15′),

$$\frac{\partial \phi}{\partial x_{2i}} = \frac{h(\gamma) + \pi K_2}{\pi(2K_2\gamma + K_3)} \tag{5-6}$$

or

$$\phi = \frac{1}{\pi}\int_0^{\gamma} \frac{h(u) + \pi K_2}{2K_2 u + K_3}\, du + g_5(x_1, x_3, \ldots, x_{2i-1}, x_{2i+1}, \ldots, x_{2n-1}) \tag{5-7}$$

Condition (28) dictates that

$$\sum_{j=1}^{n} \left(x_{2j} \frac{\partial \phi}{\partial x_{2j-1}} - \omega_j^2 x_{2j-1} \frac{\partial \phi}{\partial x_{2j}} \right) = 0 \tag{5-8}$$

Equation (5-8) can be satisfied only if g_5 is a constant, which can be taken as zero without loss of generality. Therefore,

$$p_s(x_1, \ldots, x_{2n}) = C_5(2K_2\gamma + K_3)^{-1/2} \exp\left[-\frac{1}{\pi}\int_0^{\gamma} \frac{h(u)}{2K_2 u + K_3}\, du \right] \tag{5-9}$$

Concluding Remarks

It is important to observe that a reduced Fokker-Planck equation, which possesses a stationary solution, may or may not satisfy the conditions for detailed balance. This has been demonstrated clearly in some of the examples where a rather restrictive relationship must be imposed on the spectral levels of various random excitations. However, if the conditions for detailed balance are satisfied, then they can be used to obtain the required stationary solution for the reduced Fokker-Planck equation.

Acknowledgment

The research reported in this paper was supported by the National Science Foundation under grant CEE-8405317. Opinions, findings, and conclusions expressed are those of the writers and do not necessarily reflect the views of NSF.

References

1 Andronov, A., Pontryagin, L., and Witt, A., 1933, "On the Statistical Investigation of Dynamical Systems," in Russian, *Zh. Eksperim, i Teor. Fiz.*, Vol. 3, pp. 165–180.

2 Ariaratnam, S. T., 1960, "Random Vibrations of Nonlinear Suspensions," *Journal of Mechanical Engineering Science*, Vol. 2, pp. 195–201.

3 Caughey, T. K., 1964, "On the Response of a class of Nonlinear Oscillators to Stochastic Excitation," *Proc. Colloq. Intern. du Centre National de la Recherche Scientifique*, No. 148, Marseille, Sept., pp. 393–402.

4 Caughey, T. K., 1971, "Nonlinear Theory of Random Vibrations," *Advances in Applied Mechanics*, Vol. 11, pp. 209–253.

5 Caughey, T. K., and Dienes, J. K., 1961, "Analysis of a Nonlinear First-Order System with a White Noise Input," *Journal of Applied Physics*, Vol. 23, pp. 2476–2479.

6 Caughey, T. K., and Ma, F., 1983, "The Exact Steady-state Solution of a Class of Nonlinear Stochastic Systems," *International Journal of Nonlinear Mechanics*, Vol. 17, No. 3, pp. 137–142.

7 Crandall, S. H., 1962, "Random Vibration of a Nonlinear System with a Set-up Spring," ASME JOURNAL OF APPLIED MECHANICS, Vol. 29, pp. 477–482.

8 Dimentberg, M. F., 1982, "An Exact Solution to a Certain Nonlinear Random Vibration Problem," *International Journal of Nonlinear Mechanics*, Vol. 17, pp. 231–236.

9 Graham, R., and Haken, H., 1971, "Generalized Thermo-dynamic potential for Markoff System in Detailed Balance and Far from Thermal Equilibrium," *Zeitschrift fur Physik*, Vol. 203, pp. 289–302.

10 Itô, K., 1951, "On Stochastic Differential Equations," *Memoirs of American Mathematical Society*, Vol. 4, pp. 51–89.

11 Klein, G. H., 1964, "Random Excitation of a Nonlinear System with Tangent Elasticity Characteristics," *The Journal of the Acoustical Society of America*, Vol. 36, pp. 2095–2105.

12 Kramers, H. A., 1940, "Brownian Motion in a Field of Force and Diffusion Model of Chemical Reactions," *Physica*, Vol. 7, pp. 284–304.

13 Lin, Y. K., 1967, *Probabilistic Theory of Structural Dynamics*, McGraw-Hill, New York, p. 266.

14 Stratonovich, R. L., 1963, *Topics in the Theory of Random Noise*, Vol. 1, Gordon and Beach, New York.

15 Van Kampen, N. G., 1957, "Derivation of the Phenomenological Equations from the Master Equation, II Even and Odd Variables," *Physica*, Vol. 23, pp. 816–829.

16 Wong, E., and Zakai, M., 1965, "On the Relation Between Ordinary and Stochastic Equations," *International Journal of Engineering Science*, Vol. 3, pp. 213–229.

Downloaded 03 May 2010 to 171.66.16.27. Redistribution subject to ASME license or copyright; see http://www.asme.org/terms/Terms_Use.cfm

K. H. Yae[1]
Graduate Research Assistant.

D. J. Inman
Professor.

Department of Mechanical
and Aerospace Engineering,
State University of New York at Buffalo,
Buffalo, NY 14260

Response Bounds for Linear Underdamped Systems

This paper examines simple bounds on the displacement response of linear oscillatory multiple degree of freeodm systems. Both the free and steady state forced responses are considered. The effect of mode coupling due to viscous damping is examined. The bounds are derived and stated in terms of the physical parameters of the structure and its inputs. Simple examples are given to illustrate the bounds and to compare the bounds developed here with previously published results.

1 Introduction

The analysis of the response of systems with a large number of degrees of freedom, such as a large flexible space structure, often requires too much computer time to be useful. In addition, vibration design requirements often result in bounds on final positions and displacements rather than complete specification of the response. Therefore, it is desired to obtain bounds on the response of a system, which are simple to calculate compared with calculating a detailed solution. The work presented here examines bounds on both the free and forced response (steady state) of damped linear dynamic systems and details how viscous damping affects the response bounds.

II Background

Bounds on the displacement response are derived in terms of physical parameters of the structure using integral inequalities. The main result is formulated in such a way that the effects of initial conditions, coupling, and driving force can be separated and examined individually. Bounds are derived for the free response, the forced response, normal mode systems and non-normal mode systems. Examples are given which clarify the effects of damped natural frequencies of the structure on the bounds.

In particular, this work examines the response bound on the Euclidean norm of the displacement vector for a linear underdamped dynamic system which is described by a vector differential equation:

$$M\ddot{\tilde{\mathbf{q}}}(t)+\tilde{C}\dot{\tilde{\mathbf{q}}}(t)+\tilde{K}\tilde{\mathbf{q}}(t)=\tilde{\mathbf{h}}(t)$$

where M, $\tilde{C}$, and $\tilde{K}$ are symmetric positive definite $n\times n$ mass, damping and stiffness matrices, respectively. The n-tuple vector $\tilde{\mathbf{q}}(t)$ represents the displacements of each of the n point masses in the system, the overdots represent total derivatives with respect to time t and $\tilde{\mathbf{h}}(t)$ represent a vector of the external forces acting on the system. This equation can be transformed into a more convenient form without loss of generality by making the substitution

$$\tilde{\mathbf{q}}(t)=M^{-1/2}\mathbf{q}(t)$$

and premultiplying by $M^{-1/2}$. Here $M^{-1/2}$ denotes the inverse of the square root of the positive definite matrix M.

The equations of motion then become

$$I\ddot{\mathbf{q}}(t)+C\dot{\mathbf{q}}(t)+K\mathbf{q}(t)=\mathbf{h}(t) \tag{1}$$

where $C = M^{-1/2}\tilde{C}M^{-1/2}$ and $K = M^{-1/2}\tilde{K}M^{-1/2}$ are still symmetric and positive definite and $\mathbf{h}(t) = M^{-1/2}\tilde{\mathbf{h}}(t)$. Note that $\mathbf{q}(t)$ still represents displacement and $\mathbf{h}(t)$ represents applied forces.

A response bound on the norm of the state vector of such systems has been investigated previously (Nicholson and Inman, 1983; Van Loan, 1977; Plaut and Infante, 1972; Hahn, 1963) by methods which require either the solution of a Liapunov matrix equation or the computation of the system eigenvalues and a condition number (Van Loan, 1977) which involves calculation of the (complex) system eigenvectors. Nicholson (1980) has provided a bound on the norm of a displacement vector (as opposed to the state vector) for the forced response in terms of eigenvalues of the damping and stiffness matrices.

In the spirit of Nicholson (1980), response bounds on the Euclidean norm of the displacement vector are found for both the free response and the forced response in terms of eigenvalues of the damping and stiffness matrices. A homogeneous normal mode system (Caughey and O'Kelley, 1965) is solved in the form of a Volterra equation (Burton, 1983). Then a nonnormal mode system is treated as a deviation from the normal mode system. After diagonalizing the stiffness matrix, the Euclidean norm of the nonzero off-diagonal elements of the damping matrix is used as a measure of "deviation distance" from the normal mode case.

Numerical examples are illustrated and compared with a previous method (Nicholson, 1980). Nicholson has obtained new bounds recently (Nicholson, 1982), however, they require more computational effort and hence these results were not

[1]Currently, Assistant Professor, Department of Mechanical Engineering, The University of Iowa, Iowa City, Iowa 52242.

Contributed by the Applied Mechanics Division for presentation at the 1987 Applied Mechanics, Biomechanics, and Fluids Engineering Conference, Cincinnati, OH, June 14-17, 1987, of the American Society of Mechanical Engineers.

Discussion of this paper should be addressed to the Editorial Department, ASME, United Engineering Center, 345 East 47th Street, New York, N.Y. 10017, and will be accepted until two months after final publication of the paper itself in the JOURNAL OF APPLIED MECHANICS. Manuscript received by ASME Applied Mechanics Division, September 20, 1985; final revision, March 4, 1986.

Paper No. 87-APM-34.

Copyright © 1987 by ASME
Downloaded 03 May 2010 to 171.66.16.27. Redistribution subject to ASME license or copyright; see http://www.asme.org/terms/Terms_Use.cfm

used in our comparison. The method used here needs approximately the same amount of numerical calculation as Nicholson's (1980), but provides a tighter bound for systems "close" to the normal mode case. Such systems arise in lightly damped structures such as commonly encountered in flexible space structures (Ashley, 1984). Also, this study examines the response bound of the free (transient) response for both normal and nonnormal mode systems. For the nonproportionally damped systems, the nonzero off-diagonal elements of the damping matrix (after diagonalizing the stiffness matrix) are used to estimate the bound instead of being neglected, as is the common practice.

III Derivation

In the development that follows we have chosen to change coordinates to a diagonal system and then consider the damping matrix as the sum of a diagonal matrix (the normal mode part) and an off-diagonal matrix.

Let us consider the orthogonal transformation $\mathbf{q}(t) = P\mathbf{x}(t)$, where P is an orthogonally similar transformation matrix such that

$$P^TKP = \Lambda_K = \text{diag}\{\lambda_i(K); i = 1,2, \ldots, n\}$$
$$P^TP = PP^T = I$$

Then equation (1) becomes

$$I\ddot{\mathbf{x}} + P^TCP\dot{\mathbf{x}} + \Lambda_K\mathbf{x} = \mathbf{f}(t) \tag{2}$$

where $\mathbf{f}(t) = P^T\mathbf{h}(t)$. Since P^TCP has nonzero off-diagonal elements in general (Caughey and O'Kelly, 1965), it can be expressed as the sum of a diagonal matrix, Λ_C, and an off-diagonal matrix, C_1, that is,

$$P^TCP = \Lambda_C + C_1$$

Equation (1) can now be written as

$$I\ddot{\mathbf{x}} + \Lambda_C\dot{\mathbf{x}} + \Lambda_K\mathbf{x} = -C_1\dot{\mathbf{x}} + \mathbf{f} \tag{3}$$

Next, consider the homogeneous normal mode system which is the left side of equation (3)

$$I\ddot{\mathbf{x}} + \Lambda_C\dot{\mathbf{x}} + \Lambda_K\mathbf{x} = 0 \tag{4}$$

It is assumed that $4\Lambda_K - \Lambda_C^2$ is positive definite, that is, the system (4) is underdamped (Inman and Andry, 1980). In addition, equation (4) is decoupled and can be treated as n single degree of freedom systems. If a trial solution $\mathbf{x}(t) = [\exp(At)]\mathbf{c}$ where $\mathbf{c}$ is a constant vector and $\exp(At)$ is the (diagonal) matrix exponential, is substituted into equation (4), then the homogeneous solution can be expressed as

$$\mathbf{x}(t) = \{\exp[(-\Lambda_C + i\Lambda_D)t/2]\}\mathbf{c}_1 + \{\exp[(-\Lambda_C - i\Lambda_D)t/2]\}\mathbf{c}_2 \tag{5}$$

where $i = \sqrt{-1}$ and $\Lambda_D = (4\Lambda_K - \Lambda_C^2)^{1/2}$. Note that the matrix A is $n \times n$, not $2n \times 2n$ as would be encountered in a state space approach.

The functions $\exp[(\Lambda_C \pm i\Lambda_D)t/2]$ can then be used as two integration factors to integrate equation (3). Integrating over the interval $[0, t]$ yields

$$\{\exp[(\Lambda_C + i\Lambda_D)t/2)]\}[\dot{\mathbf{x}} + (\Lambda_C - i\Lambda_D)\mathbf{x}/2] - [\dot{\mathbf{x}}_0 + (\Lambda_C - i\Lambda_D)\mathbf{x}_0/2] = \int_{[0,t]}\{\exp[(\Lambda_C + i\Lambda_D)s/2]\}[-C_1\dot{\mathbf{x}}(s) + \mathbf{f}(s)]ds \tag{6}$$

where $\dot{\mathbf{x}}_0 = \dot{\mathbf{x}}(0)$ and $\mathbf{x}_0 = \mathbf{x}(0)$ are given initial conditions. By using integration by parts, equation (6) becomes

$$\begin{aligned}\dot{\mathbf{x}}(t) + (\Lambda_C - i\Lambda_D)\mathbf{x}(t)/2 &= \{\exp[-(\Lambda_C + i\Lambda_D)t/2]\}[\dot{\mathbf{x}}_0 + (\Lambda_C - i\Lambda_D)\mathbf{x}_0/2 + C_1\mathbf{x}_0] \\ &- C_1\mathbf{x}(t) + [(\Lambda_C + i\Lambda_D)/2]\int_{[0,t]} \{\exp[(\Lambda_C - i\Lambda_D)(s-t)/2]\}C_1\mathbf{x}(s)ds \\ &+ \int_{[0,t]}\{\exp[(\Lambda_C + i\Lambda_D)(s-t)/2]\}\mathbf{f}(s)ds\end{aligned} \tag{7}$$

Integrating once more with the other integration factor yields

$$\begin{aligned}\mathbf{x}(t) &= \{\exp[-(\Lambda_C - i\Lambda_D)t/2]\}\mathbf{x}_0 \\ &+ \exp[-(\Lambda_C - i\Lambda_D)t/2]\int_{[0,t]} \exp[-i\Lambda_D\mu]d\mu[\dot{\mathbf{x}}_0 + (\Lambda_C - i\Lambda_D)\mathbf{x}_0 t/2 + C_1\mathbf{x}_0] \\ &- \int_{[0,t]}\{\exp[(\Lambda_C - i\Lambda_D)(\mu - t)/2]\}C_1\mathbf{x}(\mu)d\mu \\ &+ [(\Lambda_C + i\Lambda_D)/2]\int_{[0,t]}\{\exp[(\Lambda_C - i\Lambda_D)(\mu - t)/2]\}d\mu \\ &\cdot \int_{[0,\mu]}\{\exp[(\Lambda_C + i\Lambda_D)(s-\mu)/2]\}C_1\mathbf{x}(s)ds \\ &+ \int_{[0,t]}\{\exp[(\Lambda_C - i\Lambda_D)(\mu - t)/2]\}d\mu\int_{[0,\mu]} \{\exp[(\Lambda_C + i\Lambda_D)(s-\mu)/2]\}\mathbf{f}(s)ds\end{aligned} \tag{8}$$

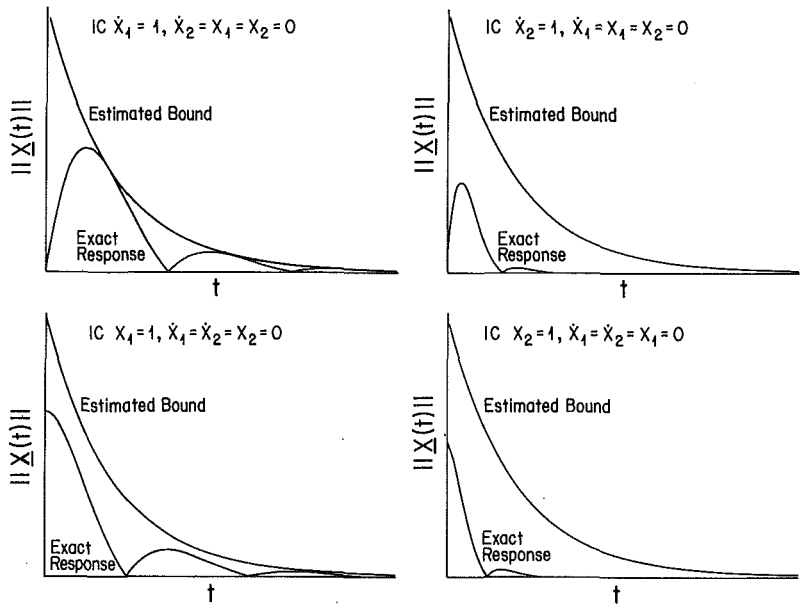


Fig. 1 Bounds on the various initial conditions

Downloaded 03 May 2010 to 171.66.16.27. Redistribution subject to ASME license or copyright; see http://www.asme.org/terms/Terms_Use.cfm

The following formula is presented by Burton (1983);

$$\int_{[0,t]}\{\exp[(\Lambda_C - i\Lambda_D)(\mu - t)/2]d\mu \cdot \int_{[0,\mu]}\{\exp[(\Lambda_C + i\Lambda_D)(s-\mu)/2]\}\mathbf{f}(s)ds = \int_{[0,t]}[\int_{[s,t]}\exp[(\Lambda_C - i\Lambda_D)(\mu - t)/2] \cdot \exp[(\Lambda_C + i\Lambda_D)(s-\mu)/2]d\mu]\mathbf{f}(s)ds = i\Lambda_D{}^{-1}\{\int_{[0,t]}\{\exp[(\Lambda_C - i\Lambda_D)(s-t)/2]\}\mathbf{f}(s)ds - \int_{[0,t]}\{\exp[(\Lambda_C - i\Lambda_D)(s-t)/2]\}\mathbf{f}(s)ds\}$$

Applying this last expression to equation (8) yields

$$\mathbf{x}(t) = \exp[-\Lambda_C t/2]\{\cos(\Lambda_D t/2)\mathbf{x}_0 + \sin(\Lambda_D t/2)[2\Lambda_D{}^{-1}(\dot{\mathbf{x}}_0 + (\Lambda_C/2 + C_1)\mathbf{x}_0)]\} + \int_{[0,t]}\exp[\Lambda_C(s-t)/2]\{\cos(\Lambda_D(s-t)/2) - \sin(\Lambda_D(s-t)/2)\Lambda_C\Lambda_D{}^{-1}\}C_1\mathbf{x}(s)ds + (-2\Lambda_D{}^{-1})\int_{[0,t]}\exp[\Lambda_C(s-t)/2]\sin[\Lambda_D(s-t)/2]\mathbf{f}(s)ds \quad (9)$$

The three terms in equation (9) can be identified as a response due to initial conditions, a perturbation due to nonzero off-diagonal elements of the damping matrix (i.e., the effect of nonproportional damping), and a response to the forcing function, respectively. Again, it is worth noting that $\mathbf{x}(t)$ in equation (9) is not a state vector ($2n$ elements) but rather the physical displacement vector (n elements). Thus, each term clearly indicates the effect it has on the displacement of each coordinate in the system.

IV Results

The above formulations lead to several new bounds on both the free and forced response of linear dynamic systems. One interesting and fruitful distinction between nonconservative systems is whether or not the damping couples the equations of motion, that is, whether or not the system possesses normal modes. Since this distinction has caused problems and controversies in the past, both normal mode and nonnormal mode systems are considered here separately.

IV.1 Normal Mode Systems. For the free response, equation (9) becomes

$$\mathbf{x}(t) = \exp(-\Lambda_C t/2)\{\cos(\Lambda_D t/2)\mathbf{x}_0 + \sin(\Lambda_D t/2)[2\Lambda_D{}^{-1}(\dot{\mathbf{x}}_0 + \Lambda_C\mathbf{x}_0/2)]\}$$

Taking the norm of both sides of this expression yields

$$\|\mathbf{x}(t)\| \le \alpha_0 \exp(-\lambda_{\min} t/2) \quad (10)$$

where $\alpha_0 = \|\mathbf{x}_0\| + \|2\Lambda_D{}^{-1}(\dot{\mathbf{x}}_0 + \Lambda_C\mathbf{x}_0/2)\|$ and $\lambda_{\min} = \min\{\lambda_i(\Lambda_C)\}$. The expression in equation (10) represents a simple bound on the free response in terms of the eigenvalues of the coefficient matrices and the initial conditions and does not depend on calculating the system eigenvalues or eigenvectors as the exact solution requires.

Next, consider the forced response and the bound that follows from equation (9). Let $\mathbf{f}(t) = \mathbf{f}_0\exp(i\omega t)$ and $\dot{\mathbf{x}}(0) = \mathbf{x}(0) = 0$. Then

$$\mathbf{x}(t) = (-2\Lambda_D{}^{-1})\int_{[0,t]}\exp[\Lambda_C(s-t)/2] \cdot \sin[\Lambda_D(s-t)/2]\mathbf{f}_0 e^{i\omega s}ds \quad (11)$$
$$= \{2\Lambda_D{}^{-1}\exp[-\Lambda_C t/2][-(\Lambda_C/2 + i\omega I) \cdot \sin(\Lambda_D t/2) - (\Lambda_D/2)\cos(\Lambda_D t/2)] + 1\} \cdot [(\Lambda_C/2 + i\omega I)^2 + (\Lambda_D/2)^2]^{-1}\mathbf{f}_0$$

By considering the steady state response only, equation (11) becomes

$$\mathbf{x}(t) = [(\Lambda_C/2 + i\omega I)^2 + (\Lambda_D/2)^2]^{-1}\mathbf{f}_0 \quad (12)$$

Taking the norm of both sides yields

$$\|\mathbf{x}(t)\| \le \|[(\Lambda_C/2) + i\omega I)^2 + (\Lambda_D/2)^2]^{-1}\| \cdot \|\mathbf{f}_0\| \quad (13)$$

Next, consider the matrix A defined by $A = (\Lambda_C/2 + i\omega I)^2 + (\Lambda_D/2)^2$; then $A = (\Lambda_K - \omega^2 I) + i\omega\Lambda_C$, since $\Lambda_D{}^2 = 4\Lambda_K - \Lambda_C{}^2$. Also, $\|A^{-1}\| = [\lambda_{\min}(A^H A)]^{-1/2}$. Since $A^H A$ is a diagonal matrix,

$$\lambda_{\min}(A^H A) = \lambda_{\min}(\Lambda_C{}^2\Lambda_D{}^2/4) = [\lambda_{\min}(\Lambda_C\Lambda_D)/2]^2 \text{ for all } \omega$$

Therefore,

$$\|\mathbf{x}(t)\|/\|\mathbf{f}_0\| \le 2/\lambda_{\min}(\Lambda_C\Lambda_D) \quad (14)$$

which again is a single bound on the steady state response requiring less computation than the actual steady state solution and depending on the input force and structural parameters only.

IV.2 Nonnormal Mode Systems. For the free response in the nonnormal mode case equation (9) becomes

$$\mathbf{x}(t) = \exp[-\Lambda_C t/2]\{\cos(\Lambda_D t/2) + \sin(\Lambda_D t/2)[2\Lambda_D{}^{-1}(\dot{\mathbf{x}}_0 + (\Lambda_C/2 + C_1)\mathbf{x}_0)]\} + \int_{[0,t]}\exp[\Lambda_C(s-t)/2]\{\cos(\Lambda_D(s-t)/2)\mathbf{x}_0 - \sin(\Lambda_D(s-t)/2)\Lambda_C\Lambda_D{}^{-1}\}C_1\mathbf{x}(s)ds$$

Using the well known theorem that $\|\int f(t)dt\| \le \int\|f(t)\|dt$, this expression yields

$$\|\mathbf{x}(t)\| \le \alpha\exp(-\mu_{\min} t/2) + \int_{[0,t]}\beta\|C_1\|\exp[\lambda_{\min}(s-t)/2]\|\mathbf{x}(s)\|ds \quad (15)$$

where $\alpha = \|\mathbf{x}_0\| + \|2\Lambda_D{}^{-1}[\dot{\mathbf{x}}_0 + (\Lambda_C/2 + C_1)\mathbf{x}_0]\|$ and $\beta = \|[I + (\Lambda_D{}^{-1}\Lambda_C)^2]^{1/2}\|$ equation (15) can be rewritten as

$$\|\mathbf{x}(t)\|\exp(\lambda_{\min} t/2) \le \alpha + \beta\|C_1\|\int_{[0,t]}\|\mathbf{x}(s)\|\exp(\lambda_{\min} s/2)ds \quad (15a)$$

Applying Gronwall's inequality (Burton, 1983) to (15*a*) yields

$$\|\mathbf{x}(t)\| \le \alpha\exp[(-\lambda_{\min}/2 + \beta\|C_1\|)t] \quad (16)$$

This last inequality yields the desired bound on the free response of a nonproportionally damped system.

Next, for the forced response consider the harmonic excitation given by $\mathbf{f}(t) = \mathbf{f}_0\exp(i\omega t)$. Assuming that the initial velocity and position are zero, equation (9) yields

$$\mathbf{x}(t) = \int_{[0,t]}\exp[\Lambda_C(s-t)/2]\{\cos(\Lambda_D(s-t)/2)\mathbf{x}_0 - \sin(\Lambda_D(s-t)/2)\Lambda_C\Lambda_D{}^{-1}\}C_1\mathbf{x}(s)ds + (-2\Lambda_D{}^{-1})\int_{[0,t]}\exp[\Lambda_D(s-t)/2] \cdot \sin[\Lambda_D(s-t)/2]\mathbf{f}_0 e^{i\omega s}ds$$

Since the second term is the same as equation (11), the same procedure outlined by equations (11)–(14) can be applied. Following these steps yields

$$\|\mathbf{x}(t)\| \le \beta\|C_1\|\int_{[0,t]}\exp[\lambda_{\min}(s-t)/2]\|\mathbf{x}(s)\|ds + 2\|\mathbf{f}_0\|/\lambda_{\min}(\Lambda_C\Lambda_D) \quad (17)$$

Again applying the Gronwall's inequality and taking a steady-state response yields

$$\|\mathbf{x}(t)\| \le [2\|\mathbf{f}_0\|/\lambda_{\min}(\Lambda_C\Lambda_D)]\exp[\beta\|C_1\|\int_{[0,t]}\exp[\lambda_{\min}(s-t)/2]ds] \quad (18)$$

Downloaded 03 May 2010 to 171.66.16.27. Redistribution subject to ASME license or copyright; see http://www.asme.org/terms/Terms_Use.cfm

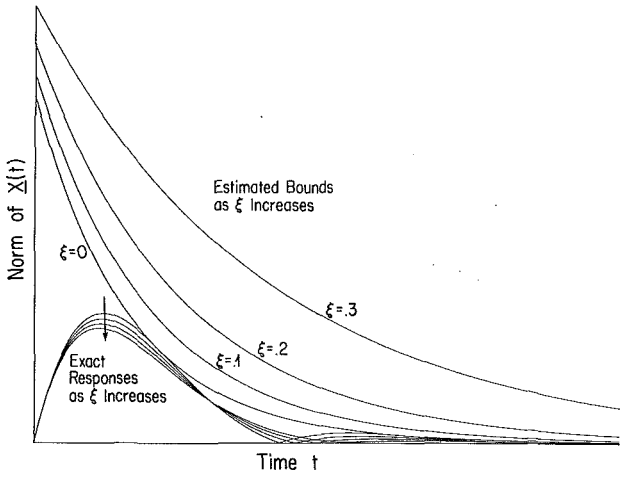


Fig. 2 Bounds on nonproportionally damped systems

Thus the desired bounds for the steady state response of the nonnormal mode case can be expressed as follows:

$$\|\mathbf{x}(t)\|/\|\mathbf{f}_0\| \leq [2/\lambda_{\min}(\Lambda_C \Lambda_D)] \exp[\beta \|C_1\|/\lambda_{\min}] \qquad (19)$$

The next section illustrates the use of these bounds with a few examples.

V Examples

The examples presented in this section are of low order for the convenience of presentation. They are included to illustrate the features of the bounds (i.e., strengths and weaknesses) and to provide a comparison between the theory presented here and theories developed by other authors. In addition, the bounds are compared to exact responses.

Example 1: Free Response. For the first set of examples consider the case defined by the homogeneous system

$$I\ddot{\mathbf{x}} + C\dot{\mathbf{x}} + K\mathbf{x} = 0$$

In the first case, shown in Fig. 1, K and C have the values ($n = 2$)

$$K = \begin{bmatrix} 5 & -1 \\ -1 & 1 \end{bmatrix} \text{ and } C = K/2 + I/2$$

Thus this system is proportionally damped. The estimated bounds are compared with exact responses for different sets of initial conditions. This example illustrates the effect of initial conditions on the bounds for a proportionally damped system.

In the second case, shown in Fig. 2, K and C have the values ($n = 4$)

$$K = \begin{bmatrix} 5 & -1.5 & 0. & 0. \\ -1.5 & 3 & -1.5 & 0. \\ 0. & -1.5 & 3 & -1.5 \\ 0. & 0. & -1.5 & 1.5 \end{bmatrix}$$

$$\text{and } C = K/2 + I/2 + \xi \begin{bmatrix} 1 & 0 & 0 & 0 \\ 0 & 0 & 0 & 0 \\ 0 & 0 & 0 & 0 \\ 0 & 0 & 0 & 1 \end{bmatrix}$$

where ξ introduces nonproportionality into the proportional system. Larger values of ξ correspond to strongly coupled systems and small values correspond to weakly coupled systems. Figure 2 points out that as ξ increases, the estimated bounds increase accordingly, but the exact responses do not change much.

Example 2: Forced Response. In this set of examples, the bounds for the forced response of a system are presented and compared with Nicholson's (1980) and the exact steady state response. The system is given by

$$I\ddot{\mathbf{x}} + C\dot{\mathbf{x}} + K\mathbf{x} = \mathbf{f}_0 \exp(i\omega t)$$

where $\mathbf{f}_0$ is a constant coefficient vector, $i = \sqrt{-1}$, and ω is a driving frequency. Note that the numerical response bounds of Nicholson (1980) are constructed by the authors based on the theory that Nicholson (1980) presented. Several different examples are presented to illustrate the effects of coupling as well as the size and spread of the natural frequencies of the system on the bound.

(*a*) Consider the example in Inman and Andry (1980) with a forcing function. The stiffness matrix is

$$K = \begin{bmatrix} 5 & -1 \\ -1 & 1 \end{bmatrix}$$

which has eigenvalues $\lambda(K) = 0.7639, 5.2361$. The damping matrix is

$$C = K/2 + I/2 + \xi \begin{bmatrix} 0 & 1 \\ 1 & 0 \end{bmatrix} = \begin{bmatrix} 3 & -0.5+\xi \\ -0.5+\xi & 1 \end{bmatrix}$$

and the value of $\mathbf{f}_0$ is given by $\mathbf{f}_0 = [1\ 0]^T$. Here again ξ introduces nonproportionality to the proportional system. This example has reasonably spaced and damped natural frequencies (see Table 1).

(*b*) Let us consider the example in Cronin (1976) for both light and heavy damping. The stiffness matrix is

$$K = \begin{bmatrix} 1.2 & -0.2 & 0. & 0. \\ -0.2 & 1.4 & -0.2 & 0. \\ 0. & -0.2 & 1.4 & -0.2 \\ 0. & 0. & -0.2 & 1.2 \end{bmatrix}$$

Table 1 Example 2(*a*)

	Response Bounds		
ξ	Exact	This paper	Nicholson (1980)
0.	1.30	1.50	1.30
-0.1	1.56	2.09	4.97
-0.2	1.62	3.05	5.41
-0.3	1.70	4.69	5.97
-0.4	1.78	8.60	6.69

Table 2 Example 2(*b*): light damping

	Response Bounds		
ξ	Exact	This paper	Nicholson (1980)
Ø.	50.0	50.25	50.00
Ø .005	44.4	55.51	45.91
Ø .01	40.0	59.68	44.25
Ø .015	36.4	62.75	43.48
Ø .02	33.4	64.94	43.05

Table 3 Example 2(*b*): heavy damping

	Response Bounds		
ξ	Exact	This Paper	Nicholson (1980)
0.	1.0	1.16	1.0
Ø.2	1.1	1.39	1.60
Ø.4	1.0	1.65	1.61
Ø.6	1.0	2.09	1.69
Ø.8	1.0	2.98	1.81

Table 4 Example 2(*c*)

	Response Bounds		
ξ	Exact	This paper	Nicholson (1980)
0.	4.30	4.30	4.30
Ø.1	4.23	5.33	22.7
Ø.2	4.22	6.57	21.7
Ø.3	4.22	8.54	21.0

Downloaded 03 May 2010 to 171.66.16.27. Redistribution subject to ASME license or copyright; see http://www.asme.org/terms/Terms_Use.cfm

and $\mathbf{f}_0 = [1\ 0\ 0\ 0]^T$. Note that in this case the eigenvalues of the stiffness matrix and hence the undamped natural frequencies are close to each other. In fact they are $\lambda(K) = 1.0$, 1.117, 1.4, 1.683. This simulates a problem often encountered in large space structures: low first natural frequency with closely spaced lower frequenies.

$$C = 0.02K + \xi \begin{bmatrix} 1 & 0 & 0 & 0 \\ 0 & 0 & 0 & 0 \\ 0 & 0 & 0 & 0 \\ 0 & 0 & 0 & 1 \end{bmatrix}$$

In the case with heavy damping (given in Table 3) the damping matrix is taken as:

$$C = K + \xi \begin{bmatrix} 1 & 0 & 0 & 0 \\ 0 & 0 & 0 & 0 \\ 0 & 0 & 0 & 0 \\ 0 & 0 & 0 & 1 \end{bmatrix}$$

As Tables 2 and 3 indicate, Nicholson's bounds (1980) are tighter in the lightly damped case. Our bounds are tighter up to a certain point in the more heavily damped case.

(*c*) This example is similar to (*b*) but the eigenvalues of K (or undamped natural frequencies) are widely spread with a low first natural frequency. The stiffness is given by

$$K = \begin{bmatrix} 5 & -1.5 & 0. & 0. \\ -1.5 & 3 & -1.5 & 0. \\ -1.5 & -1.5 & 3 & -1.5 \\ 0. & 0. & -1.5 & 1.5 \end{bmatrix}$$

which yields undamped natural frequencies $\lambda(K) = 0.237$, 1.920, 4.301, 6.042. The damping is taken to be

$$C = K/2 + I/2 + \xi \begin{bmatrix} 1 & 0 & 0 & 0 \\ 0 & 0 & 0 & 0 \\ 0 & 0 & 0 & 0 \\ 0 & 0 & 0 & 1 \end{bmatrix}$$

and again the force is applied to the first coordinate, i.e., $\mathbf{f}_0 = [1\ 0\ 0\ 0]^T$. Table 4 shows that our bounds are much tighter when the eigenvalues of K are widedy spread with moderate damping.

VI Discussion

The advantage of representing equation (1) in the form of Volterra equation is that the bound for free response in a normal mode system can be obtained without knowledge of any of the system eigenvectors. This is a great computational savings over other approaches involving the need to compute eigenvectors as well as over calculating the exact solution. In equation (16).

$$\alpha = \|\mathbf{x}_0\| + \|2\Lambda_D{}^{-1}(\dot{\mathbf{x}}_0 + \Lambda_C \mathbf{x}_0/2)\|$$

which in the original (physical) coordinates becomes

$$\alpha = \|\mathbf{q}_0\| + \|(4K - C^2)^{-1/2}(2\dot{\mathbf{q}}_0 + C\mathbf{q}_0)\|$$

Therefore, equation (16) can be written as

$$\|\mathbf{q}(t)\| \le [\|\mathbf{q}_0\| + \|(4K - C^2)^{-1/2}(2\dot{\mathbf{q}}_0 + C\mathbf{q}_0)\| \cdot \exp(-\lambda_{\min} t/2)$$

which is stated in terms of initial conditions and the system's physical parameters. Thus, besides presenting a useful method of calculating a response bound, the bound may be useful in design or control work where performance criteria are often specified in terms of maximum values of the displacement. This bound is illustrated in Fig. 1 (of Example 1).

As is pointed out by Fig. 2 (of Example 1), the larger the deviation from proportional damping the less accurate the bound presented here becomes. This is because Gronwall's inequality is applied on equations (15) and (17) to obtain the estimated bounds, a perturbational change in the damping matrix, which changes $\|C_1\|$ in equations (16) and (19), reuslts in a change of decay rate in equation (16) and an exponential increase of response bound in equation (19). Unfortuntely the corresponding change in the exact response is very small, compared with the estimated bounds. The trend of exact response can be either increasing or decreasing, but our bound in equation (19) is always increasing as a system goes farther away from the normal mode cases. This presents a limitation of the method presented here.

In Example 2 (Tables 1 through 4) we have compared our results with Nicholson's (1980), because the amount of calculation in both methods is comparable. Nicholson's bound jumps when the system goes from the normal mode to a nonnormal mode, but our bound is smoothly growing and smaller than Nicholson's up to a certain point. However, our conditions are more restrictive than Nicholson's such that: (*i*) all the system mode should be oscillatory; (*ii*) the system must stay "near" the normal mode case.

The bounds presented here may be of some use in design and control work as they represent a significant savings in computational time compared with computing detailed solutions and clearly point out the effects of various physical parameters on the bound of the displacement vector. This is the major advantage to working in physical coordinates rather than using state space methods.

Acknowledgement

This work was supported in part by NSF Grant No. MEA 8351807 and in part by AFOSR Grant No. AFOSR 820242 and AFOSR 850220.

References

Ashley, M., 1984, "On Passive Damping Mechanisms in Large Space Structures," *AIAA J. Spacecraft*, Vol. 21, No. 3, pp. 448-455.

Burton, T. A., 1983, "Structure of Solutions of Volterra Equations," *SIAM Review*, Vol. 25, No. 3, pp. 343-364.

Caughey, T. K., and O'Kelley, M. E. J., 1965, "Classical Normal Modes in Damped Linear Dynamic Systems," ASME JOURNAL OF APPLIED MECHANICS, Vol. 32, pp. 583-588.

Cronin, D. L., 1976, "Approximation for Determining Harmonically Excited Response of Nonclassically Damped Systems," ASME JOURNAL OF ENGINEERING FOR INDUSTRY, 98B, pp. 43-47.

Hahn, W., 1963, *Theory and Application of Liapunov's Direct Method*, Prentice-Hall, Englewood Cliffs, NJ, pp. 56-57.

Inman, D. J., and Andry, A. N., 1980, "Some Results on the Nature of Eignevalues of Discrete Damped Linear Systems," ASME JOURNAL OF APPLIED MECHANICS, Vol. 47, pp. 927-930.

Lancaster, P., 1969, *Matrix Analysis*, Academic Press, New York.

Muller, P. D., 1979, "Remarks on Vibrations of Damped Linear Systems," *Mech. Res. Comm.*, Vol. 6, pp. 7-15.

Nicholson, D. W., and Inman, D. J., 1983, "Stable Response of Damped Linear Systems," *The Shock and Vibration Digest*, Vol. 15, No. 11, pp. 19-25.

Nicholson, D. W., 1982, "Resonance Bounds for Asymptotically Stable Time-Invariant Linear Dynamic Systems," *IEEE Trans. Automat. Contr.*, Vol. AC-27, No. 3, pp. 704-706.

Nicholson, D. W., 1980, "Bounds on the Forced Response of Damped Linear Systems," *Mech. Res. Comm.*, Vol. 7, pp. 305-308.

Nicholson, D. W., 1978, "On the Forced Vibration of a Damped Linear System," *Mech. Res. Comm.*, Vol. 5, pp. 73-77.

Plaut, R. H., and Infante, E. F., 1972, "Bound on Motions of Some Lumped and Continuous Dynamic Systems," ASME JOURNAL OF APPLIED MECHANICS, Vol. 39, pp. 251-256.

Van Loan, C., 1977, "The Sensitivity of the Matrix Exponential," *SIAM Journal of Numerical Analysis*, Vol. 14, No. 6, 1977, pp. 971-981.

Downloaded 03 May 2010 to 171.66.16.27. Redistribution subject to ASME license or copyright; see http://www.asme.org/terms/Terms_Use.cfm

Kane's Equations With Undetermined Multipliers—Application to Constrained Multibody Systems

J. T. Wang[1]
Research Assistant,
Mem. ASME

R. L. Huston
Professor of Mechanics,
Mem. ASME

Department of Mechanical and Industrial Engineering,
University of Cincinnati,
Cincinnati, Ohio 45221-0072

A procedure for automated analysis of constrained multibody systems is presented. The procedure is based upon Kane's equations and the concept of undetermined multipliers. It is applicable with both free and controlled systems. As with Lagrange's equations, the multipliers are identified as scalar components of constraining forces and moments. The advantage of using Kane's equations is that they are ideally suited for development of algorithms for numerical analyses. Also, generalized speeds and quasi-coordinates are readily accommodated. A simple example illustrating the concepts is presented.

Introduction

During the past decade there has been a growing interest in multibody systems analysis—that is, in studying the dynamics of systems of connected (or loosely connected) bodies. The References document some of this research. Of particular interest recently, is the analysis of constrained multibody systems and systems with specified or restricted motion.

Many methods of analysis have been, and are being employed and developed. A leading and increasingly popular method is to use Kane's equations (or "Lagrange's form of d'Alembert's principle," or "the principle of virtual power") (Huston et al., 1978, 1979; Kane et al., 1961, 1980, 1983, 1985) to obtain the governing dynamical equations. For multibody systems, Kane's equations have been shown to possess the advantages of both Lagrange's equations and Newton-Euler methods but without the corresponding disadvantages. That is, with Kane's equations "non-working" constraint forces are automatically eliminated from the analysis without the introduction of scalar energy functions and their derivatives. Also, Kane's equations are ideally suited for accommodating generalized speeds and quasi-coordinates. The equations may be developed in forms which are easily converted into numerical algorithms (Huston et al., 1978, 1979).

There are occasions, however, when analysts may be interested in knowing the values of the eliminated constraint force components. One approach to determining these components is to introduce additional degrees of freedom and coordinates (for example, virtual displacements). This has the disadvantage of increasing the number of equations of the system. Also, the analyst must make conscious decisions about these degrees of freedom and their representation. Therefore, for numerical and theoretical reasons it is advantageous to have other methods for evaluating the constraint force components.

In this paper we present such a method. It is based upon a procedure long used with Lagrange's equations. In this sense the method herein adds another dimension to the use of Kane's equations.

The balance of the paper itself is divided into four parts with the following part providing some preliminary concepts useful in the analysis. The next part presents the details of the method. Examples are presented in the subsequent part and concluding remarks are given in the final part.

Preliminary Considerations

1 Coordinates, Degrees-of-Freedom, and Kinematics. Consider a multibody system S as depicted in Fig. 1. Let R be an inertial reference frame in which S moves. If S contains N bodies, it may have as many as $6N$ degrees-of-freedom. If the system is restrained such as by being constrained by joints, by having closed loops, or by having specified motion, it will have fewer degrees of freedom.

For the purpose of the analysis herein, consider first a multibody system S connected with joints which are all the same and such that no closed loops are formed. Let S have n degrees-of-freedom described by n generalized coordinates $x_\ell(\ell = 1, \ldots, n)$. For such a system, it has been shown that the angular velocities of the bodies and the velocities of the mass centers of the bodies, relative to R, may be written in the form (Huston et al., 1978, 1979):

[1] Currently at the General Motors Research Laboratories.

Contributed by the Applied Mechanics Division for presentation at the 1987 Applied Mechanics, Biomechanics, and Fluids Engineering Conference, Cincinnati, OH, June 14–17, 1987, of the American Society of Mechanical Engineers.

Discussion of this paper should be addressed to the Editorial Department, ASME, United Engineering Center, 345 East 47th Street, New York, N.Y. 10017, and will be accepted until two months after final publication of the paper itself in the JOURNAL OF APPLIED MECHANICS. Manuscript received by ASME Applied Mechanics Division, August 15, 1986; final revision, October 29, 1986.

Paper No. 87-APM-36.

Copyright © 1987 by ASME
Downloaded 03 May 2010 to 171.66.16.27. Redistribution subject to ASME license or copyright; see http://www.asme.org/terms/Terms_Use.cfm

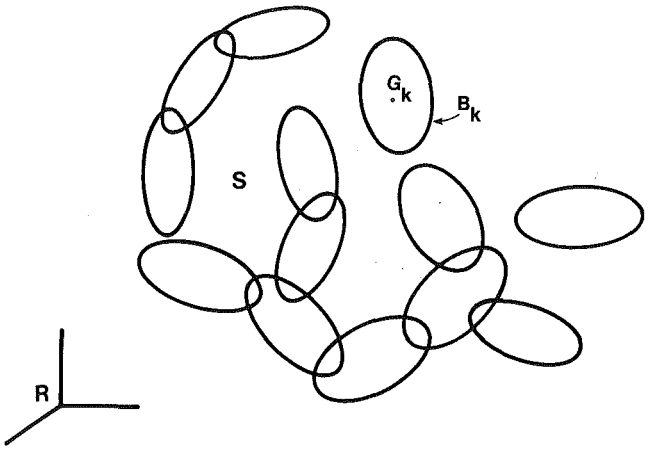


Fig. 1 A multibody system

$$\omega_k = \omega_{k\ell m} y_\ell \mathbf{n}_m \text{ and } \mathbf{v}_k = v_{k\ell m} y_\ell \mathbf{n}_m \tag{1}$$

where the subscript k refers to a typical body B_k and its mass center G_k. The $y_\ell (\ell = 1, \ldots, n)$ are *generalized speeds*, which are linear combinations of the generalized coordinate derivatives $\dot{x}_\ell$. The $\mathbf{n}_m$ $(m = 1,2,3)$ are unit vectors fixed in R. The coefficients $\omega_{k\ell m}$ and $v_{k\ell m}$ are scalar components of the "partial angular velocity" and "partial velocity" vectors of S as used by Kane and Levinson (1980, 1985). These coefficients are functions of the x_ℓ and time t, but not the y_ℓ. Finally, regarding notation, in equation (1) there is a sum for repeated indices over the range of the index.

The partial angular velocity and the partial velocity vectors may be defined as the derivatives $\partial\omega_k/\partial y_\ell$ and $\partial\mathbf{v}_k/\partial y_\ell$. Efficient algorithms have been written for the numerical evaluation of their components, and their derivatives (Huston et al., 1978, 1979).

By taking the time derivatives of ω_k and $\mathbf{v}_k$ we see from equation (1) that the angular acceleration of B_k and the acceleration of G_k, in R, may be written in the forms:

$$\alpha_k = (\dot{\omega}_{k\ell m} y_\ell + \omega_{k\ell m}\dot{y}_\ell)\mathbf{n}_m \text{ and } \mathbf{a}_k = (\dot{v}_{k\ell m} y_\ell + v_{k\ell m}\dot{y}_\ell)\mathbf{n}_m \tag{2}$$

2 Generalized Forces. Let S be subjected to a general force field. On a typical body B_k of S let this force field be represented by a single force $\mathbf{F}_k$ passing through G_k, together with a couple with torque $\mathbf{M}_k$. Then the *generalized active force* F_ℓ acting on the system corresponding to the generalized speed y_ℓ is defined as

$$F_\ell = \mathbf{F}_k \cdot (\partial\mathbf{v}_k/\partial y_\ell) + \mathbf{M}_k \cdot (\partial\omega_k/\partial y_\ell) = F_{km} v_{k\ell m} + M_{km}\omega_{k\ell m} \tag{3}$$

where F_{km} and M_{km} are the $\mathbf{n}_m$ components of $\mathbf{F}_k$ and $\mathbf{M}_k$. As before, there is a sum over repeated indices.

A feature of this definition is that constraining forces at the joints do not contribute to F_ℓ. Thus, these forces may be neglected in the evaluation of F_ℓ.

Similarly, let the inertia forces on S be represented on a typical body B_k by a single force $\mathbf{F}_k^*$ passing through G_k together with a couple with torque $\mathbf{M}_k^*$. Then the *generalized inertia force* acting on the system corresponding to the generalized speed y_ℓ is defined as:

$$F_\ell^* = \mathbf{F}_k^* \cdot (\partial\mathbf{v}_k/\partial y_\ell) + \mathbf{M}_k^* \cdot (\partial\omega_k/\partial y_\ell)$$
$$= F_{km}^* v_{k\ell m} + M_{km}^* \omega_{k\ell m} \tag{4}$$

where $\mathbf{F}_{km}^*$ and M_{km}^* are the $\mathbf{n}_m$ components of $\mathbf{F}_k^*$ and $\mathbf{M}_k^*$. $\mathbf{F}_k^*$ and $\mathbf{M}_k^*$ may be written in the forms (Kane and Levinson, 1985):

$$\mathbf{F}_k^* = -m_k \mathbf{a}_k \text{ and } \mathbf{M}_k^* = -\mathbf{I}_k \cdot \alpha_k - \omega_k X (\mathbf{I}_k \cdot \omega_k) \tag{5}$$

where m_k is the mass of B_k and $\mathbf{I}_k$ is the central inertia dyadic of B_k. (In this case, there is no sum on k).

3 Dynamics and Governing Equations. Kane's method as exposited by Kane et al., (1961, 1980, 1983, 1985) asserts that the equations of motion for S may be obtained by setting the sum of the generalized active and inertia forces equal to zero. That is,

$$F_\ell + F_\ell^* = 0 \quad (\ell = 1, \ldots, n) \tag{6}$$

By substituting from equations (1) to (5) these equations may be written in the explicit form

$$A_{\ell p}\dot{y}_p = f_\ell \tag{7}$$

where the $A_{\ell p}$ and f_ℓ are

$$A_{\ell p} = m_k v_{k\ell m} v_{kpm} + I_{ksm}\omega_{k\ell s}\omega_{kpm} \tag{8}$$

and

$$f_\ell = F_\ell - (m_k v_{k\ell m}\dot{v}_{kpm} y_p + I_{ksm}\omega_{k\ell s}\dot{\omega}_{kpm} y_p + e_{tsm} I_{ksr}\omega_{kpt}\omega_{kqr}\omega_{k\ell m} y_p y_q) \tag{9}$$

where e_{tsm} is the permutation symbol.

Observe the dominant role played by the $\omega_{k\ell m}$ and the $v_{k\ell m}$ and their derivatives.

Suppose now that additional constraints are placed on the system. For example, suppose the system has closed loops or specified motion of some of its points or bodies. Such constraints will lead to equations of the form:

$$B_{\ell p} y_p = g_\ell (\ell = 1, \ldots, m) \tag{10}$$

where $m < n$, and $B_{\ell p}$ and g_ℓ are functions of the x_ℓ and time t.

Equations (7) and (10) may be written in the matrix forms:

$$A\dot{y} = f \text{ and } By = g \tag{11}$$

where the matrices A and B and the arrays y, f, and g are defined by inspection of equations (7) and (10).

Two questions which arise are: (1) Since equations (7) and (10) are equivalent to a set of $m + n$ equations for n unknowns, what is the best way to reduce them to a consistent set of n equations? (2) What are the values of the constraining force and moment components associated with equations (10)? These questions are addressed in the following sections.

Analysis

1 Kane's Equations for Constrained Systems. One approach to reducing the governing equations is to solve equations (10) for m of the y_p in terms of the remaining $n-m$ y_p. Then by substituting into equations (1), "reduced" angular velocity and mass center velocities are obtained. This in turn leads to reduced partial angular velocity and partial velocity vectors, and to reduced generalized active and inertia forces. If these generalized forces are designated as K_ℓ and K_ℓ^*, $\ell = 1, \ldots, n-m$, then the dynamical equations are

$$K_\ell + K_\ell^* = 0 \text{ or } K + K^* = 0 \tag{12}$$

where K and K^* are column arrays of the generalized forces.

Equations (12) together with equations (10) then constitute a system of $n-m+m$, or n equations for the n y_p.

For large multibody systems the solution of equations (10) for m of the y_p may not always be practical or convenient. Also, in this procedure the constraining forces and moments are eliminated from the analysis. Although this elimination of forces and moments is often an advantage, it can also be a disadvantage if the values of the force and moment components are desired.

2 Constraint Forces and Moments. To develop an expanded analysis which exhibits the constraint force and moment components and, which retains the advantageous features of the foregoing analysis, let the constraining forces and moments associated with the constraint equations (10) be represented by a series of forces $\mathbf{F}_i'$ applied at points P_i, $i = 1, \ldots, N'$, together with a series of couples with moments $\mathbf{M}_j'$ applied to bodies $B_j, j = 1, \ldots, M'$. (Observe that the $\mathbf{F}_i'$ and

Downloaded 03 May 2010 to 171.66.16.27. Redistribution subject to ASME license or copyright; see http://www.asme.org/terms/Terms_Use.cfm

$\mathbf{M}'_i$ may each have as many as three constraining components. Hence, there may be as many as $3(N' + M')$ constraint equations. In the analysis which follows, m is taken as $3(N' + M')$. Similar procedures apply if m is less than $3(N' + M')$.)

Let the P_i and the B_j have specified motions given by $\mathbf{v}_{P_i}(t)$ and $\omega_j(t)$. (Some or all of these could be zero.) Let the scalar components of these vectors, relative to say $\mathbf{n}_m$, be collected into arrays ν and ω whose elements ν_i and ω_j may be identified with the g_ℓ of equations (10). That is,

$$\nu_i = g_i = b_{ip} y_p \quad (i = 1, \ldots, 3N') \tag{13}$$

and

$$\omega_j = g_h = b_{hp} y_p \quad (h = 3N' + j,\ j = 1, \ldots, 3M') \tag{14}$$

Next, let the components of $\mathbf{F}'_i$ and $\mathbf{M}'_j$ in the directions of the components of $\mathbf{v}_P$ and ω_j be designated as ϕ_i and μ_j. Then the "power" P produced by the constraining forces and moments is

$$P = \sum_{i=1}^{N'} \mathbf{F}'_i \cdot \mathbf{v}_P + \sum_{j=1}^{M'} \mathbf{M}'_j \cdot \omega_j = \sum_{i=1}^{3N'} \phi_i \nu_i + \sum_{j=1}^{3M'} \mu_j \omega_j \tag{15}$$

Let λ be an $m \times 1$ array whose elements are ϕ_i and μ_j. Then in view of equations (13), (14), and (15), P may be written as

$$P = \sum_{\ell=1}^{m} \lambda_\ell g_\ell = \lambda^T g = \lambda^T B y = \sum_{\ell=1}^{m} \sum_{p=1}^{n} \lambda_\ell b_{\ell p} y_p \tag{16}$$

where the λ_ℓ are the elements of λ and the superscript T designates the transpose. (In equations (15) and (16), the sums are written to show the ranges of the indices.)

Since neither the $\mathbf{F}'_i$ nor the $\mathbf{M}'_j$ are functions of the y_p, the generalized forces associated with these constraining forces and moments are

$$F'_p = \partial P / \partial y_p = \sum_{\ell=1}^{m} \lambda_\ell b_{\ell p} \tag{17}$$

This may be written in matrix form as

$$F' = B^T \lambda \tag{18}$$

where F' is the generalized *constraint* force array.

3 Kane's Equations with Undetermined Multipliers. Consider again the constrained multibody system S. Let the movement of S be described by all n y_p. In view of the foregoing analysis, let the generalized active forces be separated into two parts consisting of: (1) those developed from constraint forces and moments, and (2) those developed from applied forces and moments. Let these be designated by F'_p and $F_p (p = 1, \ldots, n)$ with the corresponding arrays being F' and F. Then Kane's equations are

$$F'_p + F_p + F^*_p = 0 \quad (p = 1, \ldots, n) \tag{19}$$

or simply

$$F' + F + F^* = 0 \tag{20}$$

Using equations (17) and (18), these may be expressed as

$$F_p + F^*_p + \lambda_\ell b_{\ell p} = 0 \text{ or } F + F^* + B^T \lambda = 0 \tag{21}$$

These expressions are called "Kane's equations with undetermined multipliers." Taken together with the constraint equations (10) they constitute a set of $n + m$ equations for the n y_p and the $m\lambda_\ell$.

4 Solution Procedures. Suppose an $nx(n-m)$ matrix C can be found such that

$$BC = 0 \text{ or } C^T B^T = 0 \tag{22}$$

Then by premultiplying the matrix form of equation (21) by C^T we obtain

$$C^T F + C^T F^* = 0 \tag{23}$$

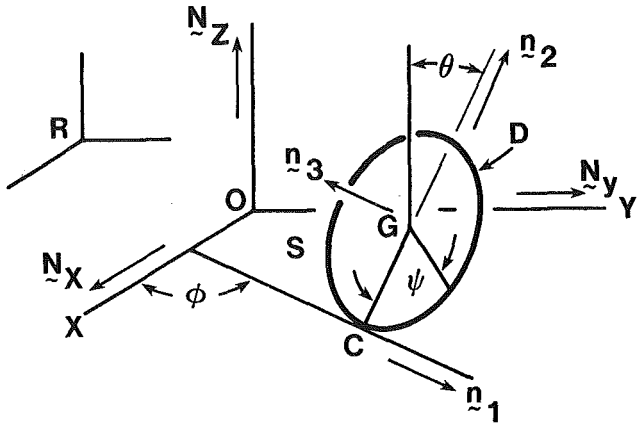


Fig. 2 A disk rolling on a moving surface

Equation (23) together with equations (10) then represent a set of $(n-m)+m$ equations for the n y_p. Once the y_p and the generalized coordinates are determined, the λ_ℓ may be determined by back substitution in equations (21).

The terms $C^T F$ and $C^T F^*$ may be seen to be equivalent to K and K^* of equations (12).

The matrix C, an "orthogonal complement" of B, may be found in several ways: One is by inspection. Another is by matrix manipulation as in Passerello and Huston (1973). These methods are useful for small systems. For large systems, we can form the $n \times n$ matrix $B^T B$ whose rank is less than or equal to m. Then $B^T B$ has at least $n-m$ zero eigenvalues. Let C be the matrix whose columns are the independent eigenvectors associated with these zero eigenvalues. Then

$$B^T BC = 0 \text{ or } C^T B^T BC = 0 \text{ or } (BC)^T (BC) = 0 \text{ or } BC = 0 \tag{24}$$

Hence, C is the desired orthogonal complement of B.

Examples

A A Rolling Coin. To illustrate these concepts first consider the classical problem of the rolling coin as depicted in Fig. 2. In this figure D is a sharp edged, uniform circular disk with radius r and mass m, which rolls on a moving surface S. The angles θ, ϕ, and ψ define the orientation of D as shown. G is the mass center of D and C is the contact point between D and S. 0 is origin of a rectangular coordinate system, XYZ, fixed in S. S translates in an inertia space R such that the movement of 0 in the X, Y, and Z directions is prescribed by the displacement functions $\xi(t)$, $\eta(t)$ and $\zeta(t)$. The system is thus "controlled" in the sense of Kirgetov (1967).

1 Kinematics. The angular velocity and the angular acceleration of D in R may be expressed as:

$$\omega = -\dot{\theta}\mathbf{n}_1 + \dot{\phi}c_\theta \mathbf{n}_2 + (\dot{\psi} + \dot{\phi}s_\theta)\mathbf{n}_3 \overset{D}{=} u_1 \mathbf{n}_1 + u_2 \mathbf{n}_2 + u_2 \mathbf{n}_3 \tag{25}$$

and

$$\alpha = (-\ddot{\theta} + \dot{\psi}\dot{\phi}c_\theta)\mathbf{n}_1 + (\ddot{\psi}\dot{\theta} + \ddot{\phi}c_\theta - \dot{\phi}\dot{\theta}s_\theta)\mathbf{n}_2 + (\ddot{\psi} + \ddot{\phi}s_\theta + \dot{\phi}\dot{\theta}c_\theta)\mathbf{n}_3 \tag{26}$$

$$= (\dot{u}_1 - u_2^2 s_\theta / c_\theta + u_2 u_3)\mathbf{n}_1 + (\dot{u}_2 + u_1 u_2 s_\theta / c_\theta - u_1 u_3)\mathbf{n}_2 + \dot{u}_3 \mathbf{n}_3$$

where s and c represent the sine and cosine and where the $\mathbf{n}_i (i = 1,2,3)$ are mutually perpendicular unit vectors as shown in Fig. 2.

The velocity and acceleration of G in R may be expressed as:

$$\mathbf{v}_G = (\dot{\xi} + \dot{x})\mathbf{N}_x + (\dot{\eta} + \dot{y})\mathbf{N}_y + (\dot{\zeta} + \dot{z})\mathbf{N}_z$$

$$= u_4 \mathbf{N}_x + u_5 \mathbf{N}_y + u_6 \mathbf{N}_z \tag{27}$$

and

Downloaded 03 May 2010 to 171.66.16.27. Redistribution subject to ASME license or copyright; see http://www.asme.org/terms/Terms_Use.cfm

$$\mathbf{a}_G = (\ddot{\xi}+\ddot{x})\mathbf{N}_x + (\ddot{\eta}+\ddot{y})\mathbf{N}_y + (\ddot{\zeta}+\ddot{z})\mathbf{N}_z$$
$$= \dot{u}_4\mathbf{N}_x + \dot{u}_5\mathbf{N}_y + \dot{u}_6\mathbf{N}_z \tag{28}$$

where x, y, and z are the X, Y, and Z coordinates of G, and where $\mathbf{N}_x$, $\mathbf{N}_y$, and $\mathbf{N}_z$ are parallel to the X, Y, and Z axes as shown in Fig. 2. From the figure, the unit vectors $\mathbf{n}_i (i = 1,2,3)$ may be related to $\mathbf{N}_x$, $\mathbf{N}_y$, and $\mathbf{N}_z$ by the expressions

$$\mathbf{n}_1 = c_\phi\mathbf{N}_x + s_\phi\mathbf{N}_y$$
$$\mathbf{n}_2 = -s_\theta s_\phi\mathbf{N}_x + s_\theta c_\phi\mathbf{N}_y + c_\theta\mathbf{N}_z \tag{29}$$
$$\mathbf{n}_3 = c_\theta s_\phi\mathbf{N}_x - c_\theta c_\phi\mathbf{N}_y + s_\theta\mathbf{N}_z$$

Since D rolls on S, the velocity of C in S is zero. Hence, the velocity of C in R is:

$$\mathbf{v}_c = \dot{\xi}\mathbf{N}_x + \dot{\eta}\mathbf{N}_y + \dot{\zeta}\mathbf{N}_z = (u_4 - \dot{x})\mathbf{N}_x + (u_5 - \dot{y})\mathbf{N}_y + (u_6 - \dot{z})\mathbf{N}_z \tag{30}$$

Finally, the $u_i (i = 1, \ldots, 6)$ defined in equations (25) and (27) are the *generalized speeds* of the system.

2 Constraint Equations. The velocities of G and C are related by the expression

$$\mathbf{v}_G = \mathbf{v}_C + \omega x (r\mathbf{n}_2) \tag{31}$$

By carrying out the indicated operations and by expressing the results in terms of $\mathbf{N}_x$, $\mathbf{N}_y$, $\mathbf{N}_z$, we obtain the equations:

$$-rc_\theta s_\phi u_1 + rc_\phi u_3 + u_4 = \dot{\xi}(t),\ rc_\theta c_\phi u_1 + rs_\phi u_3 + u_5 = \dot{\eta}(t)$$
$$-rs_\theta u_1 + u_6 = \dot{\zeta}(t) \tag{32}$$

These equations are nonholonomic constraint equations in the form of equations (10).

3 Partial Velocities and Partial Angular Velocities. From equations (25), (27), (30), and (31) the partial velocities of G and C with respect to the generalized speeds $u_i (i = 1, \ldots, 6)$ are

$$\mathbf{v}^G_{u_1} = \mathbf{v}^G_{u_2} = \mathbf{v}^G_{u_3} = 0,\ \mathbf{v}^G_{u_4} = \mathbf{N}_x,\ \mathbf{v}^G_{u_5} = \mathbf{N}_y,\ \mathbf{v}^G_{u_6} = \mathbf{N}_z \tag{33}$$

and

$$\mathbf{v}^C_{u_1} = -r\mathbf{n}_3,\ \mathbf{v}^C_{u_2} = 0,\ \mathbf{v}^C_{u_3} = r\mathbf{n}_1,\ \mathbf{v}^C_{u_4} = \mathbf{N}_x,\ \mathbf{v}_{u_5} = \mathbf{N}_y,\ \mathbf{v}^C_{u_6} = \mathbf{N}_z \tag{34}$$

where the subscript u_i indicates partial differentiation with respect to u_i. (Note that the partial velocities are determined by letting the system be temporarily unrestrained.)

Similarly, the partial angular velocities of D are

$$\omega_{u_1} = \mathbf{n}_1,\ \omega_{u_2} = \mathbf{n}_2,\ \omega_{u_3} = \mathbf{n}_3,\ \omega_{u_4} = \omega_{u_5} = \omega_{u_6} = 0 \tag{35}$$

4 Generalized Active Force Array. The only active forces are gravitational. These may be represented by the force: $-mg\mathbf{N}_z$ passing through G. The generalized active forces may then be evaluated from equations (3) and (33). These may be placed in an array F whose transpose F^T is

$$F^T = [0,\ 0,\ 0,\ 0,\ 0,\ -mg] \tag{36}$$

5 Generalized Constraint Force Array. Similarly, let the constraint forces at C be represented by the single force $\mathbf{C}$ given by

$$\mathbf{C} = C_x\mathbf{N}_x + C_y\mathbf{N}_y + C_z\mathbf{N}_z \tag{37}$$

Then from equations (3), (29), and (34) the generalized constraint force array is

$$F' = \begin{bmatrix} -rc_\theta s_\phi C_x + rc_\theta c_\phi C_y - rs_\theta C_z \\ 0 \\ rc_\phi C_x + rs_\phi C_y \\ C_x \\ C_y \\ C_z \end{bmatrix} \tag{38}$$

6 Use of Undetermined Multipliers. A feature of the foregoing procedure is that the results of equation (38) can be obtained directly from the constraint equations and without the use of vector multiplication (see equation (18)). Specifically, F' is simply

$$F' = B^T\lambda \tag{39}$$

where B is the array of coefficients of the generalized speeds in the constraint equations, and where λ is the array of undetermined multipliers, identified here with the constraint force components of C_x, C_y, and C_z. By inspection of equations (32) B is seen to be

$$B = \begin{bmatrix} -rc_\theta s_\phi & 0 & rc_\phi & 1 & 0 & 0 \\ rc_\theta c_\phi & 0 & rs_\phi & 0 & 1 & 0 \\ -rs_\theta & 0 & 0 & 0 & 0 & 1 \end{bmatrix} \tag{40}$$

A comparison of equations (38) and (40) demonstrates the validity of equation (39).

7 Generalized Inertia Force Array. Let the inertia force system acting on D be replaced by a force $\mathbf{F}^*$ passing through G together with a couple with torque $\mathbf{T}^*$, where $\mathbf{F}^*$ and $\mathbf{T}^*$ are:

$$\mathbf{F}^* = -m\mathbf{a}_G = -m(a_1\mathbf{n}_1 + a_2\mathbf{n}_2 + a_3\mathbf{n}_3) \tag{41}$$

and

$$\mathbf{T}^* = -\mathbf{I}\cdot\alpha - \omega x(\mathbf{I}\cdot\omega) = T_1\mathbf{n}_1 + T_2\mathbf{n}_2 + T_3\mathbf{n}_3 \tag{42}$$

where a_i and $T_i (i = 1,2,3)$ are the $\mathbf{n}_i$ components of $\mathbf{a}_G$ and $\mathbf{T}^*$, and where $\mathbf{I}$ is the central inertia dyadic of D. Then from equations (4), (33), and (35) the generalized inertia force array may be written as:

$$F^* = \begin{bmatrix} T_1 \\ T_2 \\ T_3 \\ -mc_\phi a_1 + ms_\theta s_\phi a_2 - mc_\theta s_\phi a_3 \\ -ms_\phi - ms_\theta c_\phi a_2 + mc_\theta c_\phi a_3 \\ -mc_\theta a_2 - ms_\theta a_3 \end{bmatrix} \tag{43}$$

8 Equations of Motion. From equations (20) the governing equations are

$$F + F' + F^* = 0 \tag{44}$$

Hence, using equations (36), (38), and (43), the equations of motion are

$$\begin{gathered} T_1 - rc_\theta s_\phi C_x + rc_\theta c_\phi C_y - rs_\phi C_z = 0 \\ T_2 = 0 \\ T_3 + rc_\phi C_x + rs_\phi C_y = 0 \\ -mc_\phi a_1 + ms_\theta s_\phi a_2 - mc_\theta s_\phi a_3 + C_x = 0 \\ -ms_\phi a_1 - ms_\theta c_\phi a_2 + mc_\theta c_\phi a_3 + C_y = 0 \\ -mc_\theta a_2 - ms_\theta a_3 - mg + C_z = 0 \end{gathered} \tag{45}$$

Downloaded 03 May 2010 to 171.66.16.27. Redistribution subject to ASME license or copyright; see http://www.asme.org/terms/Terms_Use.cfm

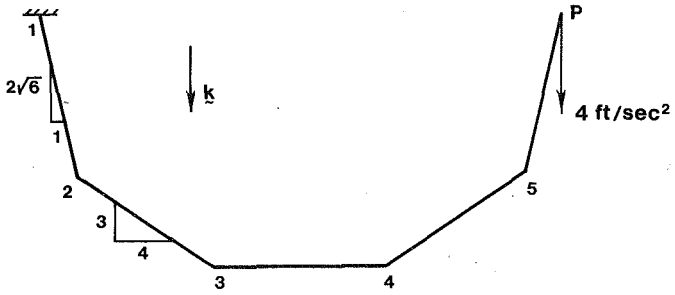


Fig. 3 An accelerated 5-link chain

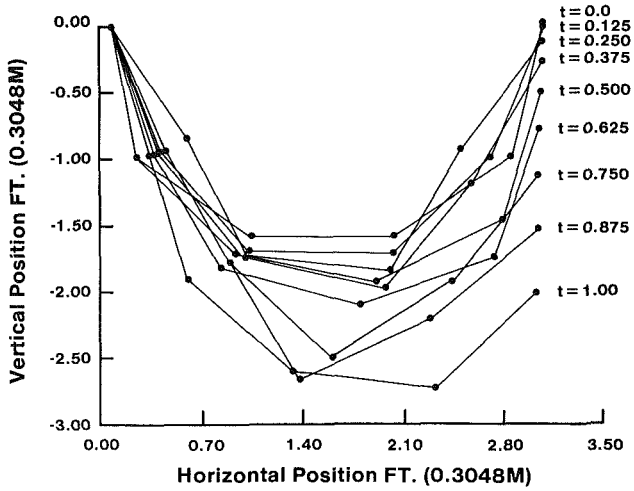


Fig. 4 System response

Equations (25), (27), (32), and (45) constitute fifteen equations for the fifteen variables θ, ϕ, ψ, x, y, z, C_x, C_y, C_z, and $u_i (i = 1, \ldots, 6)$. They are readily seen to be consistent with results found in the literature (Kane, 1968).

If the constraint forces are eliminated by solving the last three of equations (45) for C_x, C_y, and C_z and by substituting into the first three of equations (45), we obtain

$$T_1 - mra_3 - mgrs_\theta = 0$$
$$T_2 = 0 \tag{46}$$
$$T_3 + mra_1 = 0$$

These results could be obtained directly from equation (44), by multiplying by an orthogonal complement of the constraint matrix B of equation (40). In this case an orthogonal complement of B can be obtained by inspection by observing that B can be written in the partitioned form:

$$B = [\hat{B} \mid I] \tag{47}$$

where I is the 3×3 identity matrix and $\hat{B}$ is defined by comparison of the equations. Then the orthogonal complement is seen to be:

$$C = \left[\frac{I}{-\hat{B}}\right] \tag{48}$$

From equations (38), (40), and (48) we see that $C^T F'$ is zero. Hence, by multiplying equation (44) by C^T we obtain

$$C^T F + C^T F^* = 0 \tag{49}$$

This result produces the same equations as in equations (46).

B A Driven Chain. As a second example, consider the 5-link chain shown in Fig. 3. It consists of five identical 1 ft (0.3048 m), 32.2 lb (14.6 kg), pin-connected rods. The system is initially configured as shown in Fig. 3. The left end is fixed. The right end P, is given a downward acceleration of 4 ft/s^2 (1.219 m/s^2) as shown. Also, gravitational forces are applied in the downward (unit **k**) direction. The objective is to determine the system response and the interactive joint forces. An earlier version of this problem was considered by Kamman and Huston (1984). The response of the system is shown in Fig. 4. Figure 5 shows the magnitudes of the interactive constraint forces at the joints. These forces play the role of the multipliers in the analysis. The results were obtained using a computer program, called DYNOCOMBS, developed by Kamman and Huston (1985).

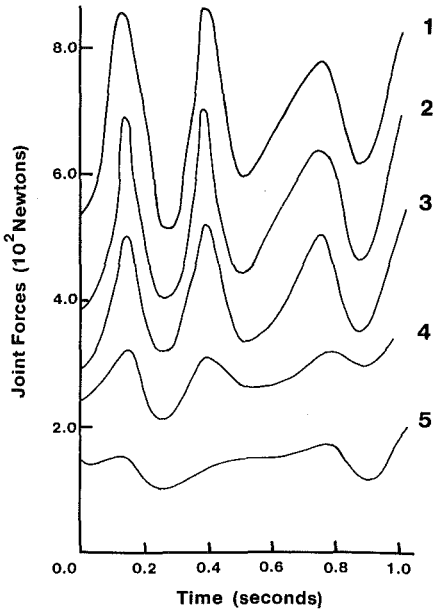


Fig. 5 Magnitude of interactive joint forces

Discussion

The method may be viewed as a generalization of the pseudo coordinate (or "fictitious coordinate") method found in the literature (Kane, 1968). Indeed, the analysis is developed with the system unrestrained. However, a difference is that the constraint forces and moments are formally introduced through a product of undetermined multipliers with coefficients of the constraint equations.

The concept is simple, but the implications extend beyond the task of finding constraint force and moment components. For example, when compared with Lagrange's equations with undetermined multipliers, the procedures are similar. However, with Kane's equations generalized speeds may be employed as the fundamental kinematical variables. Also, holonomic as well as simple nonholonomic constraints may be accommodated directly. Finally, the constraint force and moment components may be either evaluated or eliminated from the analysis. In the latter case the resulting equations are equivalent to the standard form of Kane's equations for constrained systems.

To illustrate these concepts consider Fig. 6 which depicts the generalized forces in the n-dimensional space of the generalized speeds. The force triangle is a representation of equation (20). In this context, the generalized forces K and K^*, used in Kane's equations for constrained systems, are seen to be projections of F and F^* onto the directions C^T, the orthogonal complement of the constraint array. In view of these features it is believed that the principal application of the method will be with automated analyses of large multibody systems. The method can accommodate various constraints applied simultaneously. The method can also be structured such that classes of constraints (for example, restrictions on relative

Downloaded 03 May 2010 to 171.66.16.27. Redistribution subject to ASME license or copyright; see http://www.asme.org/terms/Terms_Use.cfm

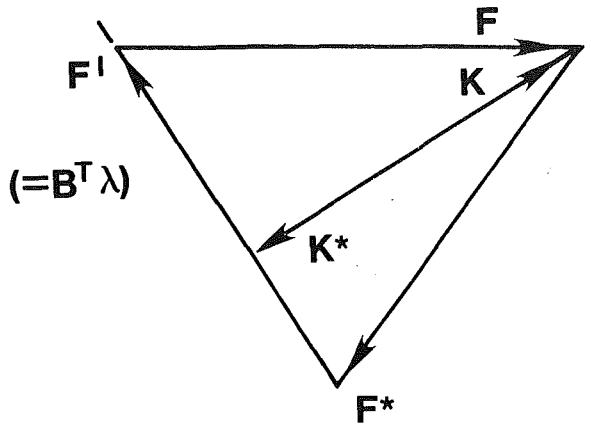


Fig. 6 A geometric interpretation of generalized force arrays

translation of the bodies at the joints) need not be considered. Finally, the method is expected to be useful for multibody systems simultaneously possessing a variety of joints (spherical, revolute, and prismatic) and with desired or specified motion of some of the bodies. Such systems are commonly encountered in robot and biodynamic modelling. The authors have successfully applied the method in determining interactive joint forces and moments (as in Example B) with general chain systems and biodynamic models. We believe that for large systems this is the most efficient method available for determining such forces and moments.

Acknowledgment

The research for this analysis was partially supported by the National Science Foundation under Grant MEP8313439 and is gratefully acknowledged. The authors also acknowledge the helpful suggestions of the reviewer.

References

Andrews, G. C., and Kesavan, H. K., 1977, "Simulation of Multibody Systems Using the Vector-Network Model," *Dynamics of Multibody Systems*, Magnus, K., ed., Springer, pp. 1–13.

Casey, J., and Lam, V. C., 1986, "A Tensor Method for the Kinematic Analysis of Systems of Rigid Bodies," *Mechanisms and Machine Theory*, Vol. 21, No. 1, pp. 87–97.

Conway, B. A., and Widham, J. W., 1985, "Equations of Motion for an N-Body Satellite with Moving Joints," *Journal of Guidance and Control*, Vol. 8, No. 4, pp. 537–539.

Haug, E. J., Wehage, R. A., and Barman, N. C., 1981, "Dynamic Analysis and Design of Constrained Mechanical Systems," *Journal of Mechanical Design*, Vol. 103, No. 3, pp. 560–570.

Hemami, H., 1982a, "A State Space Model for Interconnected Rigid Bodies," *IEEE Transactions on Automatic Control*, Vol. AC-27, No. 2, pp. 376–382.

Hemami, H., 1982b, "Some Aspects of Euler-Newton Equations of Motion," *Ingenieur-Archiv*, Vol. 52, pp. 167–176.

Hemami, H., and Weimer, F. C., 1981, "Modelling of Nonholonomic Dynamic Systems with Applications," ASME JOURNAL OF APPLIED MECHANICS, Vol. 48, pp. 177–182.

Hollerback, J. M., 1980, "A Recursive Lagrangian Formulation of Manipulator Dynamics and a Comparative Study of Dynamics of Formulation Complexity," *IEEE Transactions on Systems, Man and Cybernetics*, Vol. SMC-10, No. 11, pp. 730–736.

Huston, R. L., 1986, "Useful Procedures in Multibody Dynamics," *Dynamics of Multibody Systems*, IUTAM/IFT MM Symposium, Edine, Italy, Bianchi, G., Schiehlen, W., eds., Springer, pp. 69–77.

Huston, R. L., and Passerello, D. E., 1976, "Eliminating Singularities in Governing Equations of Mechanical Systems," *Mechanics Research Communications*, Vol. 3, pp. 361–365.

Huston, R. L., and Passerello, D. E., 1980, "Multibody Structural Dynamics Including Translation Between the Bodies," *Computers and Structures*, Vol. 11, pp. 713–720.

Huston, R. L., and Passerello, C. E., 1973, "On Lagrange's Form of d'Alembert's Principle," *The Matrix and Tensor Quarterly*, Vol. 23, pp. 109–112.

Huston, R. L., and Passerello, C. E., 1979, "On Multi-Rigid-Body System Dynamics," *Computers and Structures*, Vol. 10, pp. 439–446.

Huston, R. L., Passerello, C. E., and Harlow, M. W., 1978, "Dynamics of Multi-rigid-Body Systems," ASME JOURNAL OF APPLIED MECHANICS, Vol. 45, No. 4, pp. 889–894.

Jerkovsky, W., 1976, "The Tranformation Operator Approach to Multisystem Dynamics Part I: The General Approach," *The Matrix and Tensor Quarterly*, Vol. 27, No. 2, pp. 48–59.

Kamman, J. W., and Huston, R. L., 1984, "Dynamics of Constrained Multibody Systems," ASME JOURNAL OF APPLIED MECHANICS, Vol. 51, pp. 889–903.

Kamman, J. W., and Huston, R. L., 1985, "User's Manual for UCIN DYNOCOMBS," National Technical Information Service Report No. PB85-240075/AS.

Kane, T. R., 1968, *Dynamics*, Holt, Rinehart, and Winston, New York.

Kane, T. R., 1961, "Dynamics of Nonholonomic Systems," ASME JOURNAL OF APPLIED MECHANICS, Vol. 28, pp. 574–578.

Kane, T. R., and Levinson, D. A., 1985, *Dynamics: Theory and Applications*, McGraw-Hill, pp. 45–50.

Kane, T. R., and Levinson, D. A., 1980, "Formulation of Equations of Motion for Complex Spacecraft," *Journal of Guidance and Control*, Vol. 3, No. 2, pp. 99–112.

Kane, T. R., Likins, P. W., and Levinson, D. A., 1983, *Spacecraft Dynamics*, McGraw-Hill, New York.

Kirgetov, V. I., 1967, "The Motion of Controlled Mechanical Systems with Prescribed Constraints (Servo-constraints)," *Prikl. Mathem. Mekhan. (PMM)*, Vol. 31, pp. 433–446.

Lilov, L., and Chirikov, V. A., 1982, "On the Dynamics Equations of Systems of Interconnected Bodies," *PMM, Journal of Applied Mathematics and Mechanics*, Vol. 45, pp. 383–390.

Lilov, L., and Lorer, M., 1982, "Dynamic Analysis of Multi-Rigid-Body Systems Based on the Gauss Principle," *Zeitschrift fur Angwandte Mathematik and Mechanik*, Vol. 72, pp. 539–545.

Marshall, R. N., Jensen, R. K., and Wood, G. A., 1985, "A General Newtonian Simulation of an N-Segment Open Chain Model," *Journal of Biomechanics*, Vol. 18, No. 5, pp. 359–367.

Nikravesh, P. E., and Chung, I. S., 1981, "Application of Euler Parameters to the Dynamic Analysis of Three Dimensional Constrained Mechanical Systems," ASME Paper No. 81-DET-123.

Nikravesh, P. E., and Chung, I. S., 1982, "Application of Euler Parameters to the Dynamic Analysis of Three-Dimensional Constrained Mechanical Systems," *Journal of Mechanical Design*, Vol. 104, No. 4, pp. 785–791.

Nikravesh, P. E., Wehage, R. A., and Kwon, O. K., 1985, "Euler Parameters in Computational Kinematics and Dynamics," Parts 1 and 2, ASME *Journal of Mechanisms, Transmissions and Automation in Design*, Vol. 107, pp. 358–369.

Orin, D. E., McGhee, R. B., Vukobratovic, M., and Hartoch, G., 1979, "Kinematic and Kinetic Analysis of Open-Chain Linkages Utilizing Newton-Euler Methods," *Mathematical Biosciences*, Vol. 43, pp. 107–130.

Passerello, C. E., and Huston, R. L., 1973, "Another Look at Nonholonomic Systems," ASME JOURNAL OF APPLIED MECHANICS, Vol. 40, pp. 101–104.

Pennock, G. R., and Yang, A. T., 1983, "Dynamic Analysis of a Multi-Rigid-Body Open-Chain System," ASME *Journal of Mechanisms, Transmissions, and Automation in Design*, Vol. 105, pp. 28–38.

Roberson, R. E., 1984, "On the Practical Use of Euler-Rodrigues Parameters in Multibody System Dynamic Simulation," *Ingenieur-Archiv*, Vol. 54, pp. 114–123.

Roberson, R. E., 1985a, "On the Recursive Determination of Body Frames for Multibody Dynamic Simulation," ASME JOURNAL OF APPLIED MECHANICS, Vol. 52, No. 3, pp. 698–700.

Roberson, R. E., 1985b, "On the Ways to Use Normalized Euler Parameters as Kinematic State Variables in Dynamic Simulation," *Zeitschrift fur Angwandte Mathematik und Mechanik*, Vol. 65, No. 718, pp. 380–382.

Schwertassek, R., and Roberson, R. E., 1984, "A State-Space Dynamical Representation for Multibody Mechanical Systems Part I: Systems with Tree Configuration," *Acta Mechanic*, Vol. 50, pp. 141–161.

Silver, W. M., 1982, "On the Equivalence of Lagrangian and Newton Euler Dynamics for Manipulators," *The International Journal of Robotics Research*, Vol. 1, No. 2, pp. 60–70.

Singh, R. P., and Likins, P. W., 1985, "Singular Value Decomposition for Constrained Dynamical Systems," ASME JOURNAL OF APPLIED MECHANICS, Vol. 52, pp. 943–948.

Vukobratovic, M., 1978a, "Dynamics of Articulated Mechanisms and Synthesis of Artificial Motion," *Mechanisms and Machine Theory*, Vol. 13, pp. 1–18.

Vukobratovic, M., 1978b, "Computer Method for Dynamic Model Construction of Active Articulated Using Kinetostatic Approach," *Mechanisms and Machine Theory*, Vol. 13, pp. 19–39.

Wittenburg, J., 1977, *Dynamics of Systems of Rigid Bodies*, Teubner, Leitfaden der Angewandten Math. u. Mech. Bd. 33,

Downloaded 03 May 2010 to 171.66.16.27. Redistribution subject to ASME license or copyright; see http://www.asme.org/terms/Terms_Use.cfm

Response Bounds for Nonclassically Damped Mechanical Systems Under Transient Loads

D. W. Nicholson
Associate Professor,
Department of Mechanical Engineering,
Stevens Institute of Technology,
Hoboken, NJ 07030

Time-decaying upper bounds are derived for the response of damped linear mechanical systems under impulsive loads and under step loads. The bounds are expressed in terms of the extreme eigenvalues of the symmetric, positive definite constituent system matrices. The system is assumed to exhibit nonclassical damping by which we mean that classical normal modes do not occur: i.e., the modes are coupled (complex). The governing system equation is first reduced to a particular version of "state form" suited for application of the one-sided Lipschitz constant. A formal bound for general transient loads is then presented. This is specialized to the case of impulsive loads. For step loading, an overshoot measure is introduced which generalizes the corresponding notion for single degree-of-freedom systems. A bound is derived for the overshoot and for the settling time of the system. A simple example is given.

I Introduction

Response bounds for damped linear mechanical systems are the subject of several recent studies (Yae et al., 1986; Nicholson, 1983). They are potentially useful in design settings, in conjunction with active control of linear vibrations, and in providing supporting information for checking computations on large systems (Nicholson, 1983). Now for systems exhibiting classical normal modes (Caughey et al., 1960), bounds are readily obtained from the individual modes. But for nonclassically damped systems (wtih complex modes) they are far more difficult to derive.

In this paper, several new results for nonclassically damped systems are derived by using the one-sided Lipschitz constant for the matrix exponential function. The types of excitation considered include impulsive loading and step loading. For the latter case, an "overshoot" measure is introduced by extending a corresponding notion for single degree-of-freedom systems, and a bound is derived for it.

II System Equation

The system under study is governed by

$$\mathbf{M}\ddot{\mathbf{x}} + \mathbf{C}\dot{\mathbf{x}} + \mathbf{K}\mathbf{x} = \mathbf{f}(t) \qquad (1)$$

$$\dot{\mathbf{x}}(0) = \mathbf{0}, \quad \mathbf{x}(0) = \mathbf{0}.$$

Here $\mathbf{M}$, $\mathbf{C}$ and $\mathbf{K}$ are symmetric and positive definite n by n real matrices representing inertia, damping, and stiffness. The n by 1 vectors $\mathbf{x}$ and $\mathbf{f}$, respectively, denote the displacements and the applied loads. Without loss we assume that $\mathbf{M}$ is the identity matrix $\mathbf{I}$. Note that we do not make the conventional assumption of classical normal modes, so that we cannot transform equations (1) into n uncoupled equations representing single degree-of-freedom systems.

Equation (1) typically arises as a lumped-parameter idealization of vibrating systems. It also arises from finite element modeling of linear viscoelastic structures under dynamic loads.

Two cases are considered:

(*i*) Impulsive loading

$$\mathbf{f}(t) = \mathbf{f}_o u(t)$$

in which $u(t)$ is the unit impulse function (Dirac function).

(*ii*) Step loading

$$\mathbf{f}(t) = \mathbf{f}_o H(t)$$

for $H(t)$ the Heaviside function.

In addition we present formal results for general loadings (simply $\mathbf{f}(t)$).

III Mathematical Background

By way of mathematical background we note the following. Consider the matrix exponential function exp (**A**), where **A** is a real, n by n nonsingular matrix. The matrix norm induced by the Euclidean vector norm is denoted by $\|\exp(\mathbf{A})\|$. Now (Dekker et al., 1984) this norm is bounded above by

$$\|\exp(\mathbf{A})\| \leqq \exp(b_1(\mathbf{A}))$$

where $b_1(\mathbf{A})$ is the largest eigenvalue of $\mathbf{B} = \frac{1}{2}(\mathbf{A} + \mathbf{A}^T)$, in which $\mathbf{A}^T$ is the transpose of **A**. The quantity b_1 is called the

Contributed by the Applied Mechanics Division for presentation at the 1987 Applied Mechanics, Biomechanics, and Fluids Engineering Conference, Cincinnati, OH, June 14–17, 1987, of the American Society of Mechanical Engineers.
Discussion of this paper should be addressed to the Editorial Department, ASME, United Engineering Center, 345 East 47th Street, New York, N.Y. 10017, and will be accepted until two months after final publication of the paper itself in the JOURNAL OF APPLIED MECHANICS. Manuscript received by ASME Applied Mechanics Division, March 6, 1986; final revision, July 30, 1986.
Paper No. 87-APM-31.

Copyright © 1987 by ASME
Downloaded 03 May 2010 to 171.66.16.27. Redistribution subject to ASME license or copyright; see http://www.asme.org/terms/Terms_Use.cfm

one-sided Lipschitz constant for **A**. As a particularly convenient example of later interest, suppose that

$$\mathbf{A} = -\begin{bmatrix} \mathbf{P} & \mathbf{Q} \\ -\mathbf{Q}^T & \mathbf{R} \end{bmatrix} \tag{2}$$

where **P** and **R** are positive definite and symmetric. Then

$$b_1 = -\min(p_n, r_n)$$

for p_n and r_n the smallest eigenvalues of **P** and **R**.

An alternate bound for the matrix exponential function can be obtained in the form

$$\|\exp(\mathbf{A})\| \leqq k(\mathbf{T})\exp(a_1 t)$$

where

$$\mathbf{A} = \mathbf{T}^{-1}\mathbf{B}\mathbf{T} \quad \mathbf{B} = \operatorname{diag}(\lambda_j(\mathbf{A})).$$

Here a_j is the real part of the jth eigenvalue of **A**, and a_1 is the maximum of the a_j values. Also, $k(\mathbf{T})$ is the spectral condition number of **T**:

$$k(\mathbf{T}) = \|\mathbf{T}\|\|\mathbf{T}^{-1}\|$$

However, this bound does not hold much interest for us, for two reasons: (1) the quantities a_1 and $k(\mathbf{T})$ have no simple relation to the eigenvalues of the constituent system matrices and they are relatively difficult to compute (for example computing a_1 requires determining the complex eigenvalues of an asymmetric matrix); (2) the spectral condition number in many cases gives poor bounds. In this work, using the one-sided Lipschitz constant, bounds will be derived in terms of relatively easily computed quantities with a simple relation to the constituent system matrices.

IV Reduction to State Form

We now restate equations (1) in a version of "state form" consistent with equation (2). Consider the equation

$$\frac{d}{dt}\mathbf{X}\begin{Bmatrix} \dot{\mathbf{x}} \\ \mathbf{x} \end{Bmatrix} + \mathbf{A}\mathbf{X}\begin{Bmatrix} \dot{\mathbf{x}} \\ \mathbf{x} \end{Bmatrix} = \begin{Bmatrix} \mathbf{f} \\ 0 \end{Bmatrix} \tag{3}$$

and **X** and **A** are written as

$$\mathbf{X} = \begin{bmatrix} \mathbf{X}_{11} & \mathbf{X}_{12} \\ \mathbf{X}_{21} & \mathbf{X}_{22} \end{bmatrix} \qquad \mathbf{A} = \begin{bmatrix} \mathbf{A}_{11} & \mathbf{A}_{12} \\ \mathbf{A}_{21} & \mathbf{A}_{22} \end{bmatrix}.$$

Now equation (3) is equivalent to equations (1) if

$$\mathbf{A}_{11}(\mathbf{C}-\mathbf{A}_{11}) - \mathbf{A}_{21}\mathbf{A}_{12} = \mathbf{K} \quad \mathbf{A}_{21}(\mathbf{C}-\mathbf{A}_{11}) - \mathbf{A}_{22}\mathbf{A}_{21} = \mathbf{0}$$
$$\mathbf{X}_{11} = \mathbf{I} \quad \mathbf{X}_{21} = \mathbf{0} \quad \mathbf{X}_{12} = \mathbf{C}-\mathbf{A}_{11} \quad \mathbf{X}_{22} = -\mathbf{A}_{21}. \tag{4}$$

We now consider the choices of the blocks in **A** which (*i*) satisfy equations (4) and (*ii*) lead to the convenient form in equation (2), for which the Lipschitz constant is especially simple. Note that $\mathbf{A}_{11}$ and $\mathbf{A}_{22}$ must be symmetric and positive definite, and that $\mathbf{A}_{21}$ must equal $-\mathbf{A}_{12}^T$. Thus, for example, both $\mathbf{A}_{21}(\mathbf{C}-\mathbf{A}_{11})\mathbf{A}_{21}^{-1}$ and $\mathbf{A}_{11}(\mathbf{C}-\mathbf{A}_{11})$ must be symmetric and positive definite. The reader may easily verify that these conditions are satisfied by the following choices.

Let z be a positive constant such that $\mathbf{C}-z\mathbf{I}$ and $\mathbf{K}-z(\mathbf{C}-z\mathbf{I})$ are positive definite matrices. For this purpose it is sufficient if z satisfies

$$z \leqq \min[c_n, z^*]$$

where

$$z^* = \begin{cases} c_n, & \text{if } c_1^2 < 4k_n \\ [c_1 - (c_1^2 - 4k_n)^{1/2}]/2, & \text{otherwise} \end{cases}.$$

Here c_j and k_j are the eigenvalues of **C** and **K**, respectively. Now equation (3) is equivalent to (1) if

$$\mathbf{A}_{11} = \mathbf{C}-z\mathbf{I} \qquad \mathbf{A}_{12} = \mathbf{V}^{1/2}$$
$$\mathbf{A}_{21} = -\mathbf{V}^{1/2} \qquad \mathbf{A}_{22} = z\mathbf{I}$$
$$\mathbf{X}_{11} = \mathbf{I} \qquad \mathbf{X}_{12} = z\mathbf{I}$$
$$\mathbf{X}_{21} = \mathbf{0} \qquad \mathbf{X}_{22} = \mathbf{V}^{1/2}$$

where

$$\mathbf{V} = [\mathbf{K} - z(\mathbf{C} - z\mathbf{I})].$$

The relation of this modified state form to the Direct Method of Lyapunov is briefly discussed in the Appendix.

V Derivation of Bounds

(*i*) Formal General Bound. Now introducing **w** and **g** by means of

$$\mathbf{w} = \mathbf{X}\begin{Bmatrix} \dot{\mathbf{x}} \\ \mathbf{x} \end{Bmatrix} \qquad \mathbf{g} = \begin{Bmatrix} \mathbf{f} \\ \mathbf{0} \end{Bmatrix}$$

the system equation in state form leads to

$$\frac{d}{dt}[\exp(\mathbf{A}t)\mathbf{w}] = \exp(\mathbf{A}t)\mathbf{g}.$$

The general solution is of the form

$$\begin{Bmatrix} \dot{\mathbf{x}} \\ \mathbf{x} \end{Bmatrix} = \mathbf{X}^{-1}\int_0^t \exp(-\mathbf{A}(t-q))\mathbf{g}(q)\,dq. \tag{5}$$

We now state bounds applicable to equation (5). First note that

$$\|\exp(-\mathbf{A}t)\| \leqq \exp(-st)$$

where

$$s = \min[c_n - z, z].$$

Thus, in general,

$$|\mathbf{w}| \leqq \int_0^t \exp(-s(t-q))\,|\mathbf{g}(q)|\,dq.$$

(*ii*) Impulsive Loads. From the properties of the Dirac function $u(t)$,

$$\left|\begin{Bmatrix} \dot{\mathbf{x}} \\ \mathbf{x} \end{Bmatrix}\right| \leqq \|\mathbf{X}^{-1}\|\,|\mathbf{w}| \leqq \exp(-st)\,\|\mathbf{X}^{-1}\|\,|\mathbf{f}_0|.$$

(*iii*) Step Loads. For step loading the general solution is

$$\mathbf{w} = [\mathbf{I} - \exp(-\mathbf{A}t)]\mathbf{A}^{-1}\mathbf{g}_o.$$

Asymptotically, the solution approaches the steady state condition

$$\mathbf{w}_s = \mathbf{A}^{-1}\mathbf{g}_o$$

in which the subscript s implies the steady state values. In analogy with conventional notions applied to single degree-of-freedom systems, we introduce the generalized overshoot m_w by

$$m_w = |\mathbf{w} - \mathbf{w}_s| / |\mathbf{w}_s|.$$

Clearly,

$$m_w \leqq \exp(-at) \leqq 1.$$

Also

$$m_w \leqq m_{uw}$$

where

$$m_{uw} = \exp(-st)\,\|\mathbf{A}^{-1}\|\,|\mathbf{f}_o|.$$

However, our objective is to obtain bounds on **x** and $\dot{\mathbf{x}}$ rather than **w**. Furthermore, these bounds should be readily

Downloaded 03 May 2010 to 171.66.16.27. Redistribution subject to ASME license or copyright; see http://www.asme.org/terms/Terms_Use.cfm

computable, in contrast to the spectral condition number of **A** as previously discussed. But note that

$$\begin{Bmatrix} \dot{\mathbf{x}} \\ \mathbf{x} \end{Bmatrix} - \begin{Bmatrix} \dot{\mathbf{x}} \\ \mathbf{x} \end{Bmatrix}_s = \mathbf{X}^{-1}\exp(-\mathbf{A}t)\mathbf{X} \begin{Bmatrix} \dot{\mathbf{x}} \\ \mathbf{x} \end{Bmatrix}_s .$$

Thus, defining the new overshoot m_x by

$$m_x = \left| \begin{Bmatrix} \dot{\mathbf{x}} \\ \mathbf{x} \end{Bmatrix} - \begin{Bmatrix} \dot{\mathbf{x}} \\ \mathbf{x} \end{Bmatrix}_s \right| \Big/ \left| \begin{Bmatrix} \dot{\mathbf{x}} \\ \mathbf{x} \end{Bmatrix}_s \right|$$

it is immediate that $m \leqq m_x$ where

$$m_x = \|\mathbf{X}^{-1}\|\|\mathbf{X}\|\exp(-st). \tag{6.1}$$

We need to obtain simple estimates for $\|\mathbf{X}\|$ and $\|\mathbf{X}^{-1}\|$. But note that

$$\mathbf{X}^T\mathbf{X} = \begin{bmatrix} \mathbf{I} & z\mathbf{I} \\ z\mathbf{I} & z^2\mathbf{I}+\mathbf{V} \end{bmatrix} = \begin{bmatrix} \mathbf{I} & z\mathbf{I} \\ z\mathbf{I} & z^2\mathbf{I} \end{bmatrix} + \begin{bmatrix} \mathbf{0} & \mathbf{0} \\ \mathbf{0} & \mathbf{V} \end{bmatrix}.$$

Letting v_1 and v_n denote the maximum and minimum eigenvalues of the symmetric and positive definite matrix **V**, it follows that

$$\|\mathbf{X}\| = \|\mathbf{X}^T\mathbf{X}\|^{1/2} \leqq U_a$$

where

$$U_a = [1+z^2+v_1]^{1/2}. \tag{6.2}$$

Continuing, we note that

$$\mathbf{X}^{-1} = \begin{bmatrix} \mathbf{I} & -z\mathbf{V}^{-1/2} \\ \mathbf{0} & \mathbf{V}^{-1/2} \end{bmatrix} = \begin{bmatrix} \mathbf{I} & -z\mathbf{I} \\ \mathbf{0} & \mathbf{I} \end{bmatrix} \begin{bmatrix} \mathbf{I} & \mathbf{0} \\ \mathbf{0} & \mathbf{V}^{-1/2} \end{bmatrix}$$

Elementary matrix norm inequalities imply that

$$\|\mathbf{X}^{-1}\| \leqq U_b$$

where

$$U_b = [\tfrac{1}{2}\{2+z^2+(z^4+4z^2)^{1/2}\}]^{1/2}\max[1, v_n^{-1/2}]. \tag{6.3}$$

Using equations (6.1, 6.2, 6.3), the bound on the overshoot m is now

$$m \leqq m_x$$
$$m_x = U_a U_b \exp(-st). \tag{7}$$

Note that the quantities s, U_a, and U_b require evaluation only of the extreme eigenvalues of the positive definite symmetric matrices **C**, **K**, and **V**.

However, it may be shown that, if the system is underdamped (Inman et al., 1980) the overshoot m cannot exceed unity. Assuming this condition, we thus modify the bound to read as follows:

$$m_x = \min[1, U_a U_b \exp(-st)]. \tag{8}$$

Finally, we may use equation (7) to obtain an upper bound on the settling time of the system. In single degree-of-freedom systems under step input, the settling time t_s is the amount of time required for the amplitude of the oscillations of the output variable to decrease to a given fraction of the steady state value, say m_f. Referring to equation (7), it is evident that

$$t_s \leqq \log(U_a U_b / m_f)/s. \tag{9}$$

Example

To bring the foregoing results into focus and to estimate the "sharpness" of the bounds, we develop the following 2 by 2 example:

$$\begin{bmatrix} 1 & 0 \\ 0 & 1 \end{bmatrix} \begin{Bmatrix} \ddot{x}_1 \\ \ddot{x}_2 \end{Bmatrix} + \begin{bmatrix} 2\zeta\omega_1 & q \\ q & 2\zeta\omega_2 \end{bmatrix} \begin{Bmatrix} \dot{x}_1 \\ \dot{x}_2 \end{Bmatrix} + \begin{bmatrix} \omega_1^2 & 0 \\ 0 & \omega_2^2 \end{bmatrix} \begin{Bmatrix} x_1 \\ x_2 \end{Bmatrix} = \begin{Bmatrix} 1 \\ 1 \end{Bmatrix} H(t).$$

The particular values to be used are as follows:

$$\omega_1 = 1 \quad \omega_2 = 10 \quad \zeta = 0.2 \quad q = 0.01.$$

Owing to the presence of q, the system is nonclassically damped. In addition, the system is "stiff" in that there is a large spread in the eigenvalues of the stiffness and the damping matrices.

The steady state values are:

$$\begin{Bmatrix} \dot{x}_{1s} \\ \dot{x}_{2s} \\ x_{1s} \\ x_{2s} \end{Bmatrix} = \begin{Bmatrix} 0.00 \\ 0.00 \\ 1.00 \\ 0.01 \end{Bmatrix}$$

The true overshoot m is given as a function of time by

$$m(t) = \left| \begin{Bmatrix} \dot{x}_1 \\ \dot{x}_2 \\ x_1 \\ x_2 \end{Bmatrix} - \begin{Bmatrix} \dot{x}_{1s} \\ \dot{x}_{2s} \\ x_{1s} \\ x_{2s} \end{Bmatrix} \right| \Big/ \left| \begin{Bmatrix} \dot{x}_{1s} \\ \dot{x}_{2s} \\ x_{1s} \\ x_{2s} \end{Bmatrix} \right| .$$

A computer program has been written to calculate $m(t)$ using the Newmark method. The results of the computation are in column 2 of Table 1. The program was checked by comparing the computed values of $\dot{x}_1$, $\dot{x}_2$, x_1, and x_2 with the steady state values, and the computed values proved to be within 0.01 percent of the steady state values after transient terms appeared to have died out.

We now calculate the bounds m_w and m_x, for comparison with m. The eigenvalues of **C** and **K** are:

$$k_1 = 1 \quad k_2 = 100 \quad c_1 = 0.3999 \quad c_2 = 4.000.$$

The values of z and s are both 0.1999861, calculated as follows. The quantity z is first obtained using a simple computer code to compute

$$z = \min[c_2, z^*]$$

$$z^* = \begin{cases} c_2 & c_1^2 < 4k_2 \\ [c_1 - \{c_1^2 - 4k_2\}^{1/2}] & \text{otherwise.} \end{cases}$$

Then, the maximum value of s is obtained using

$$s = \begin{cases} c_2/2 & \text{if } z > c_2/2 \\ z & \text{otherwise} \end{cases}$$

and the value of z is reset using $z = s$. The eigenvalues of **V** are now found as

$$v_1 = 0.96 \quad v_2 = 99.24.$$

The quantities U_a and U_b and min [1, $U_a U_b \exp(-st)$] are then computed using the code.

Downloaded 03 May 2010 to 171.66.16.27. Redistribution subject to ASME license or copyright; see http://www.asme.org/terms/Terms_Use.cfm

Table 1 Comparison of overshoot with bounds

time	m	m_w	m_x
.0	1.00000	1.00000	1.00000
2.5	0.56711	0.61880	1.00000
5.0	0.38513	0.37534	1.00000
7.5	0.25516	0.22766	1.00000
10.0	0.14616	0.13809	1.00000
12.5	0.07815	0.08376	0.88973
15.0	0.04872	0.05080	0.53967
17.5	0.03366	0.03081	0.32733
20.0	0.02086	0.01869	0.19854
22.5	0.01132	0.01134	0.12043
25.0	0.00636	0.00688	0.07305
27.5	0.00430	0.00417	0.04431
30.0	0.00286	0.00253	0.02687
32.5	0.00166	0.00153	0.01630
35.0	0.00088	0.00093	0.00989
37.5	0.00054	0.00056	0.00600
40.0	0.00038	0.00034	0.00364
42.5	0.00023	0.00021	0.00221
45.0	0.00013	0.00013	0.00134
47.5	0.00007	0.00008	0.00081

Discussion

The objective of this investigation has been to derive time-decaying bounds on the response of damped linear systems to impulsive loads and to step loads. The system is nonclassically damped, with coupled (complex) modes. The system equation is stated in a particular version of "state form" which is well suited to the use of the one-sided Lipschitz constant. Formal bounds are derived for general transient loads. They are specialized to impulsive loads. For unit step loads, an "overshoot" measure is introduced by generalizing corresponding notions for single degree-of-freedom systems. A bound is obtained for it, which immediately leads to an upper bound on the settling time of the system. Finally, it should be noted that evaluation of the bounds merely requires the evaluation of the extreme eigenvalues of several symmetric positive definite matrices. A simple example is developed.

In Table 1 the true overshoot $m(t)$ is compared with the overshoot bounds $m_w(t)$ and $m_x(t)$ introduced in this investigation. The "weighted" quantity $m_w(t)$ is close to $m(t)$, but is slightly lower than it for relatively short times. The quantity $m_x(t)$ is about an order of magnitude greater than $m(t)$, reflecting the presence of the condition number of the matrix $\mathbf{X}$. Clearly, as expected, $m_x(t)$ is not very sharp. But it appears that the use of $m_w(t)$ provides a closer estimate of $m(t)$, at the risk of slightly underestimating the overshoot.

Of course, if classical normal modes are obtained, much better results can be readily obtained than those presented here. Furthermore, the present bounds do not reduce to classical normal mode relations when the condition normal modes are present. But, as previously stated, our concern is with the case of nonclassical damping, in which bounds may be of interest owing to the effort required to calculate the full system response.

References

Caughey, T. K., and O'Kelley, M. E. J., 1960, "Classical Normal Modes in Damped Linear Systems," ASME JOURNAL OF APPLIED MECHANICS, Vol. 25, No. 3, pp. 343-364.

Dekker, K., and Verwer, J. G., 1984, *Stability of Runge-Kutta Methods for Stiff Nonlinear Differential Equations*, Elsevier Science Publishers B.V., Amsterdam.

Inman, D. J., and Andry, A. N., 1980, "Some Results on the Nature of Eigenvalues of Discrete Damped Linear Systems," ASME JOURNAL OF APPLIED MECHANICS, Vol. 47, pp. 927-930.

Nicholson, D. W., and Inman, D. J., 1983, "Stable Response of Damped Linear Systems," *The Shock and Vibration Digest*, Vol. 15, No. 11, pp. 19-25.

Yae, K. H., and Inman, D. J., "Response Bounds for Linear Underdamped System," to appear in the ASME JOURNAL OF APPLIED MECHANICS.

APPENDIX

Lyapunov Function for the Current System

It is instructive to consider the relation between Lyapunov functions and the equation of state introduced in this study. Consider the Lyapunov function

$$L = \tfrac{1}{2}\{\dot{\mathbf{x}}^T\mathbf{x}^T\}^T\mathbf{X}^T\mathbf{X}\begin{Bmatrix}\dot{\mathbf{x}}\\ \mathbf{x}\end{Bmatrix}. \tag{10}$$

This function is clearly positive definite. Furthermore, using the current state equation with $\mathbf{f} = 0$,

$$\dot{L} = -\mathbf{w}^T\mathbf{A}\mathbf{w} \qquad \mathbf{w} = \mathbf{X}\begin{Bmatrix}\dot{\mathbf{x}}\\ \mathbf{x}\end{Bmatrix}.$$

But $\mathbf{w}$ is a real vector, from which we conclude that

$$\dot{L} = -\mathbf{w}^T\{\tfrac{1}{2}(\mathbf{A}+\mathbf{A}^T)\}\mathbf{w}.$$

It follows that $\dot{L}$ is negative definite, thus providing a simple proof of the asymptotic stability of the system.

Expanding the Lyapunov function in equation (10) furnishes

$$L = \tfrac{1}{2}\dot{\mathbf{x}}^T\dot{\mathbf{x}} + z\dot{\mathbf{x}}^T\mathbf{x} + \tfrac{1}{2}\mathbf{x}^T(2z^2\mathbf{I} + \mathbf{K} - z\mathbf{C})\mathbf{x}.$$

This appears to be similar to a Lyapunov function suggested by a reviewer.

Downloaded 03 May 2010 to 171.66.16.27. Redistribution subject to ASME license or copyright; see http://www.asme.org/terms/Terms_Use.cfm

Nonstationary Response Analysis of a Duffing Oscillator by the Wiener-Hermite Expansion Method

I. I. Orabi

G. Ahmadi

Department of Mechanical and Industrial Engineering, Clarkson University, Potsdam, NY 13676

The Wiener-Hermite functional series expansion method is used to analyze the nonstationary response of a Duffing oscillator under random excitations. The formal procedure for the derivation of the deterministic equations governing the Wiener-Hermite kernel functions is described. The first three terms in the series are retained. The nonstationary response of a damped Duffing oscillator subjected to a modulated white noise is studied. For several values of nonlinearity strength and different damping coefficients the nonstationary mean-square responses are obtained. The results are compared with those found by a single-term expansion and other methods. It is shown that mean-square responses obtained by the three-term expansion agree with the exact stationary variances and the simulation results.

Introduction

Study of the behavior of random nonlinear systems has attracted considerable attention due to its significance in response analysis of structures subjected to earthquakes, winds, and sea waves loadings. In the past two decades, several methods for response analysis of nonlinear random systems were developed. Extensive reviews of the subject were provided by Caughey (1970), Crandall and Zhu (1983), and Roberts (1984).

The method of equivalent linearization was used most extensively in structural mechanics for response analysis of nonlinear structures subjected to random excitations (Spanos, 1981; Roberts, 1981). Most of the earlier works were directed towards determining the stationary response statistics of randomly excited nonlinear systems (Lin, 1968; Iyengar and Dash, 1978; Ahmadi et al., 1978). Nonstationary or transient responses were studied more recently by Kaul and Penzien (1974), Iwan and Mason (1980), Wen (1980), Ahmadi (1980), Kimura and Sakata (1981), and Kimura et al. (1983). The method of equivalent linearization was basically developed for weakly nonlinear oscillators. However, for certain systems the method gave reasonable results even for large nonlinearities (Spanos, 1981; Iwan and Mason, 1980).

In practice, the method of equivalent linearization is restricted to Gaussian statistics. To improve the technique, Crandall (1980, 1985) introduced a non-Gaussian method. However, as pointed out by Crandall (1985), the realizability may be violated. That is, he found that the probability density function may become negative.

The objective of the present study is to develop a non-Gaussian and fully realizable method for nonstationary response analysis of nonlinear systems subjected to general random excitations. The technique is based on a functional series expansion method that was originally developed by Cameron and Martin (1947) and Wiener (1958). Meecham and Siegel (1964) and Meechan and Jeng (1968) referred to this technique as the Wiener-Hermite (W-H) expansion method and applied it to the closure problem of the Navier-Stokes equation for turbulent fluid motions. Recent works in this direction were reported by Lee et al. (1982). The method was also used in the analysis of strong electrostatic plasma turbulence by Ahmadi (1982). It was shown that the ground acceleration during an earthquake may be represented by the first term in the Wiener-Hermite series (Ahmadi, 1980). Preliminary results concerning the applicability of the method to nonlinear random vibrations were reported by Jahedi and Ahmadi (1983). Recently, Orabi and Ahmadi (1987) studied the response of the Duffing oscillator using only the first term of the Wiener-Hermite series. Although, the predictions were reasonably accurate, the results were essentially limited to Gaussian statistics. To capture the non-Gaussian statistics of the response, the higher order terms in the series must be included.

In the present work a randomly exicted Duffing oscillator is studied. The method of Wiener-Hermite expansion is employed for the response analysis. The first three terms in the series respresentation of the response are retained. The equations governing the dynamics of the deterministic kernel functions are derived. An approximate method for solving the resulting integrodifferential equations is developed. The transient mean-square responses of the Duffing oscillator are obtained and the results are compared with those found by other methods and the Monte-Carlo simulations. It is shown that

Contributed by the Applied Mechanics Division for presentation at the 1987 Applied Mechanics, Biomechanics, and Fluids Engineering Conference, Cincinnati, OH, June 14–17, 1987, of the American Society of Mechanical Engineers.

Discussion of this paper should be addressed to the Editorial Department, ASME, United Engineering Center, 345 East 47th Street, New York, N,Y. 10017, and will be accepted unitl two months after final publication of the paper itself in the JOURNAL OF APPLIED MECHANICS. Manuscript received by ASME Applied Mechanics Division, February 24, 1986; final revision, July 31, 1986.

Paper No. 87-APM-22.

Copyright © 1987 by ASME

Downloaded 03 May 2010 to 171.66.16.27. Redistribution subject to ASME license or copyright; see http://www.asme.org/terms/Terms_Use.cfm

the variances calculated using the three-term expansion are in good agreement with the simulation results and the exact stationary values.

Basic Formulation

The equation governing the dynamics of a Duffing oscillator subjected to a random force $f(t)$ is given by

$$\ddot{x}+2\xi\omega_o\dot{x}+\omega_o^2(x+\epsilon x^3)=f(t) \tag{1}$$

Here, x is the displacement, ω_o is the natural frequency of the corresponding linear system, ξ is the damping coefficient, and ϵ is a constant corresponding to the strength of nonlinearity.

To analyze the random response of equation (1), the W-H expansion method is used in the sequel. The elements of the Wiener-Hermite set, $H^{(i)}$, are zero-mean random functions (with the exception of $H^{(0)}$) and form a statistically orthogonal complete random base; i.e.,

$$\begin{aligned} &<H^{(i)}>=0 \quad \text{for} \quad i\neq 0, \\ &<H^{(i)}H^{(j)}>=0 \quad \text{for} \quad i\neq j. \end{aligned} \tag{2}$$

Here, an angular bracket stands for the expected value (ensemble average). Some properties of the Wiener – Hermite set are discussed in Appendix A.

The random force $f(t)$ and the response $x(t)$ are now expanded in terms of the Wiener – Hermite set.These are given by

$$\begin{aligned} f(t)=&\int_{-\infty}^{\infty}F^{(1)}(t,t_1)H^{(1)}(t_1)dt_1 \\ &+\int_{-\infty}^{\infty}\int_{-\infty}^{\infty}F^{(2)}(t,t_1,t_2)H^{(2)}(t_1,t_2)dt_1dt_2 \\ &+\int_{-\infty}^{\infty}\int_{-\infty}^{\infty}\int_{-\infty}^{\infty}F^{(3)}(t,t_1,t_2,t_3) \\ &H^{(3)}(t_1,t_2,t_3)dt_1dt_2dt_3+\ \ldots \end{aligned} \tag{3}$$

and

$$\begin{aligned} x(t)=&\int_{-\infty}^{\infty}X^{(1)}(t,t_1)H^{(1)}(t_1)dt_1 \\ &+\int_{-\infty}^{\infty}\int_{-\infty}^{\infty}X^{(2)}(t,t_1,t_2)H^{(2)}(t_1,t_2)dt_1dt_2 \\ &+\int_{-\infty}^{\infty}\int_{-\infty}^{\infty}\int_{-\infty}^{\infty}X^{(3)}(t,t_1,t_2,t_3) \\ &H^{(3)}(t_1,t_2,t_3)dt_1dt_2dt_3+\ \ldots \end{aligned} \tag{4}$$

where $F^{(i)}$ and $X^{(i)}$ are deterministic kernel functions.

The zeroth order term in a Wiener-Hermite series corresponds to the mean value. We have assumed that the mean of f and x is zero. Therefore, the zeroth order terms are omitted from the series expansions in equations (3) and (4). The first order term in the Wiener-Hermite series corresponds to the Gaussian part of the random process. The second and higher order terms correspond to the non-Gaussian part of the random function. Thus, if the response is not too far from a Gaussian process, considertion of the first few terms in the series expansion would be sufficient for an accurate representation of the random response function.

The Wiener-Hermite series given by equations (3) and (4) may be formally restated as

$$f=\sum_{i=1}^{\infty}F^{(i)}H^{(i)}, \quad x=\sum_{i=1}^{\infty}X^{(i)}H^{(i)}, \tag{5}$$

where the kernal functtions $F^{(i)}$ are known for a given random excitation. Multiplying equation (1) by an element of the Wiener-Hermite set $H^{(j)}$, using equations (5) and (2) and taking ensemble average the result becomes (Orabi and Ahmadi, 1987)

$$\begin{aligned} &\ddot{X}^{(j)}+2\xi\omega_o\dot{X}^{(j)}+\omega_o^2X^{(j)} \\ &+\epsilon\omega_o^2<H^{(j)}\left(\sum_{i=1}^{\infty}X^{(i)}H^{(i)}\right)^3>=F^{(j)}. \end{aligned} \tag{6}$$

Equation (6) is a deterministic equation for the unknown kernel function $X^{(j)}$. The nonlinearity leads to coupling between the equations governing the dynamics of various order kernels. The equations governing the dynamics of the first three kernel functions are:

$$\begin{aligned} &\ddot{X}^{(1)}(t,t_1)+2\xi\omega_o\dot{X}^{(1)}(t,t_1)+\omega_o^2X^{(1)}(t,t_1) \\ &+3\epsilon\omega_o^2X^{(1)}(t,t_1)\int_{-\infty}^{\infty}[X^{(1)}(t,t_2)]^2dt_2 \\ &+18\epsilon\omega_o^2\int_{-\infty}^{\infty}\int_{-\infty}^{\infty}X^{(1)}(t,t_2)X^{(1)}(t,t_3) \\ &X^{(3)}(t,t_1,t_2,t_3)dt_2dt_3=F^{(1)}(t,t_1), \end{aligned} \tag{7}$$

$$\begin{aligned} &\ddot{X}^{(2)}(t,t_1,t_2)+2\xi\omega_o\dot{X}^{(2)}(t,t_1,t_2)+\omega_o^2X^{(2)}(t,t_1,t_2) \\ &+6\epsilon\omega_o^2X^{(1)}(t,t_1)\int_{-\infty}^{\infty}X^{(1)}(t,t_3)X^{(2)}(t,t_2,t_3)dt_3 \\ &+6\epsilon\omega_o^2X^{(1)}(t,t_2)\int_{-\infty}^{\infty}X^{(1)}(t,t_3)X^{(2)}(t,t_1,t_3)dt_3 \\ &+6\epsilon\omega_o^2X^{(2)}(t,t_1,t_2)\int_{-\infty}^{\infty}[X^{(1)}(t,t_3)]^2dt_3 \\ &=F^{(2)}(t,t_1,t_2), \end{aligned} \tag{8}$$

and

$$\begin{aligned} &\ddot{X}^{(3)}(t,t_1,t_2,t_3)+2\xi\omega_o\dot{X}^{(3)}(t,t_1,t_2,t_3) \\ &+\omega_o^2X^{(3)}(t,t_1,t_2,t_3) \\ &+\epsilon\omega_o^2\Big\{X^{(1)}(t,t_1)X^{(1)}(t,t_2)X^{(1)}(t,t_3) \\ &+3X^{(3)}(t,t_1,t_2,t_3)\int_{-\infty}^{\infty}[X^{(1)}(t,t_4)]^2dt_4 \\ &+6\int_{-\infty}^{\infty}X^{(1)}(t,t_1)X^{(1)}(t,t_4)X^{(3)}(t,t_2,t_3,t_4)dt_4 \\ &+6\int_{-\infty}^{\infty}X^{(1)}(t,t_2)X^{(1)}(t,t_4)X^{(3)}(t,t_1,t_3,t_4)dt_4 \\ &+6\int_{-\infty}^{\infty}X^{(1)}(t,t_3)X^{(1)}(t,t_4)X^{(3)}(t,t_1,t_2,t_4)dt_4\Big\} \\ &=F^{(3)}(t,t_1,t_2,t_3) \end{aligned} \tag{9}$$

Here, the terms involving second or higher order of $X^{(2)}$ and $X^{(3)}$ are neglected.

Equations (7)–(9) are three coupled integrodifferential equations for determining the three unknowns $X^{(1)}$, $X^{(2)}$, and $X^{(3)}$. Once the deterministic kernel functions are found, equation (4) provides an explicit series expansion for the random response of the structure. From this series and the known properties of the Wiener-Hermite set, various statistics of the response can be generated. For instance, the variance of x is given by

$$\sigma_x^2(t)=<X^2(t)>=\int_{-\infty}^{\infty}[X^{(1)}(t,t_1)]^2dt_1$$

Downloaded 03 May 2010 to 171.66.16.27. Redistribution subject to ASME license or copyright; see http://www.asme.org/terms/Terms_Use.cfm

$$+2\int_{-\infty}^{\infty}\int_{-\infty}^{\infty}[X^{(2)}(t,t_1,t_2)]^2dt_1dt_2$$

$$+6\int_{-\infty}^{+\infty}\int_{-\infty}^{+\infty}\int_{-\infty}^{+\infty}[X^{(3)}(t,t_1,t_2,t_3)]^2dt_1dt_2dt_3+\ldots \quad (10)$$

Other statistical moments of the response could be obtained by algebraic manipulations in a similar fashion.

Response to Gaussian White Noise Excitations

When the excitation $f(t)$ is a Gaussian process, the expansion of $f(t)$ in terms of the Wiener-Hermite series contains only a single term, i.e.,

$$f(t)=\int_{-\infty}^{\infty}F(t,t_1)H^{(1)}(t_1)dt_1, \quad (11)$$

where, $F(t,t_1)$ is a specific kernel function and $H^{(1)}(t_1) = n(t_1)$, is a unit-spectrum white noise process (see also Appendix A). That is, $F^{(1)}(t,t_1) = F(t, t_1)$ and all other kernels in equation (3) vanish indentically. Particular choices of the kernel function, $F(t,t_1)$ lead to various Gaussian excitations. For instance, choosing

$$F(t,t_1)=(2\pi S_o)^{1/2}e(t_1)\delta(t-t_1), \quad (12)$$

equation (11) reduces to

$$f(t)=(2\pi S_o)^{1/2}e(t)n(t). \quad (13)$$

The excitation given by equation (13) is a shaped white noise process with a constant power spectrum S_o. Here, $e(t)$ is a deterministic envelope function.

In the sequel, the response of the Duffing oscillator to a shaped white noise excitation is analyzed. It is assumed that

$$e(t)=u(t)=\begin{cases}1 & t\geq 0,\\ 0 & t<0,\end{cases} \quad (14)$$

where $u(t)$ is a unit step function. When the motion starts from rest, the appropriate initial conditions are

$$X^{(1)}(0,t_1)=X^{(2)}(0,t_1,t_2)=X^{(3)}(0,t_1,t_2,t_3)=0, \quad (15)$$

$$\dot{X}^{(1)}(0,t_1)=\dot{X}^{(2)}(0,t_1,t_2)=\dot{X}^{(3)}(0,t_1,t_2,t_3)=0. \quad (16)$$

Furthermore, the kernel functions $X^{(i)}(t,t_1,t_2\ldots)$ are identically zero for negative t's and when t_1, t_2, . . . are greater than t.

For Gaussian excitations, $F^{(2)} = F^{(3)} = 0$. Equation (8) then becomes a homogeneous linear equation for $X^{(2)}$ subjected to initial conditions (15) and (16). Jahedi and Ahmadi (1983) showed that

$$X^{(2)}\equiv 0 \quad (17)$$

is an exact solution. Furthermore, it is assumed that the response is close to a Gaussian random process so that $|X^{(3)}| << |X^{(1)}|$. Equations (7) and (9) may now be restated as

$$\ddot{X}^{(1)}(t,t_1)+2\xi\omega_o\dot{X}^{(1)}(t,t_1)+\omega_e^2(t)X^{(1)}(t,t_1)=F(t,t_1), \quad (18)$$

and

$$\ddot{X}^{(3)}(t,t_1,t_2,t_3)+2\xi\omega_o\dot{X}^{(3)}(t,t_1,t_2,t_3)+\omega_e(t)X^{(3)}(t,t_1,t_2,t_3)$$
$$=-\epsilon\omega_o^2\{X^{(1)}(t,t_1)X^{(1)}(t,t_2)X^{(1)}(t,t_3)$$
$$+6\int_o^t X^{(1)}(t,t_1)X^{(1)}(t,t_4)X^{(3)}(t,t_2,t_3,t_4)dt_4$$
$$+6\int_o^t X^{(1)}(t,t_2)X^{(1)}(t,t_4)X^{(3)}(t,t_1,t_3,t_4)dt_4$$
$$+6\int_o^t X^{(1)}(t,t_3)X^{(1)}(t,t_4)X^{(3)}(t,t_1,t_2,t_4)dt_4\}. \quad (19)$$

Here,

$$\omega_e^2(t)=\omega_o^2(1+3\epsilon\sigma_1^2(t)), \quad (20)$$

where

$$\sigma_1^2(t)=\int_o^t[X^{(1)}(t,t_1)]^2dt_1. \quad (21)$$

It is observed that equation (18) is now decoupled from (19) and can be solved independently for $X^{(1)}$. The results may then be used in (19) which is an equation for determining $X^{(3)}$.

In the earlier work by Orabi and Ahmadi (1986), a single-term Wiener-Hermite series was used for response analysis. That is, $X^{(3)}$ was neglected. For a slowly varying $\omega_e(t)$, the formal solution to equation (18) was expressed as

$$X^{(1)}(t,\tau)=\begin{cases}(2\pi S_o)^{1/2}e(\tau)\dfrac{\exp\{-\xi\omega_o(t-\tau)\}}{[\omega_A(t)\omega_A(\tau)]^{1/2}}\sin\left(\displaystyle\int_\tau^t\omega_A(\theta)d\theta\right), & 0\leq\tau\leq t,\\ 0 & \text{otherwise,}\end{cases} \quad (22)$$

where

$$\omega_A^2(t)=\omega_e^2(t)-\xi^2\omega_o^2. \quad (23)$$

An iterative method was employed by Orabi and Ahmadi (1987) and $X^{(1)}$ was determined. The results were then used to evaluate the statistical properties of the response. It was shown that the mean-square responses calculated by the single-term Wiener-Hermite expansion agree well with those obtained by the method of equivalent linearization of Iwan and Mason (1980). However, both methods underestimate the simulation results and the exact variances of the stationary limit. To improve the accuracy, the contribution of the third term in the series must be included.

Equation (19) is a rather formidable integrodifferential equation governing the dynamics of $X^{(3)}$. Its complexity originates from the integral terms on the right-hand side of the equation. To simplify the governing equation we propose to replace the integral terms by their equivalent algebraic terms. That is we assume

$$\int_o^t X^{(3)}(t,t_2,t_3,t_4)X^{(1)}(t,t_4)dt_4=\alpha(t)X^{(1)}(t,t_2)X^{(1)}(t,t_3). \quad (24)$$

Here, $\alpha(t)$ is an unknown function of time. Minimizing the square error in replacing the integral by an algebraic expression in equation (24), we find

$$\alpha(t)=\frac{1}{\sigma_1^4(t)}\int_o^t dt_2\int_o^t dt_3\int_o^t dt_4X^{(3)}(t,t_2,t_3,t_4)$$
$$X^{(1)}(t,t_2)X^{(1)}(t,t_3)X^{(1)}(t,t_4). \quad (25)$$

Numerical calculations show that α is small and a slowly varying function of time. Using equation (24), equation (19) may be restated as

$$\ddot{X}^{(3)}(t,t_1,t_2,t_3)+2\xi\omega_o\dot{X}^{(3)}(t,t_1,t_2,t_3)+\omega_e^2(t)X^{(3)}(t,t_1,t_2,t_3)$$
$$=-\epsilon\omega_o^2X^{(1)}(t,t_1)X^{(1)}(t,t_2)X^{(1)}(t,t_3)[1+18\alpha(t)]. \quad (26)$$

The approximate solution to equation (26) is given as

$$X^{(3)}(t,t_1,t_2,t_3)=-\epsilon\omega_o^2\int_o^t[1+18\alpha(\tau)]h(t,\tau)$$
$$X^{(1)}(\tau,t_1)X^{(1)}(\tau,t_2)X^{(1)}(\tau,t_3)u(\tau-t_1)u(\tau-t_2)u(\tau-t_3)d\tau, \quad (27)$$

where

Downloaded 03 May 2010 to 171.66.16.27. Redistribution subject to ASME license or copyright; see http://www.asme.org/terms/Terms_Use.cfm

$$h(t,\tau)=\frac{e^{-\xi\omega_o(t-\tau)}}{[\omega_A(t)\omega_A(\tau)]^{1/2}}\sin\left(\int_\tau^t \omega_A(\theta)d\theta\right)u(t-\tau), \tag{28}$$

is the approximate impulse response for equation (26).

Using equation (27) in equation (25), to the first order in α, the result is

$$\alpha(t)=-\frac{\epsilon\omega_o^2}{\sigma_1^4(t)}\int_o^t d\tau h(t,\tau)R_1^3(t,\tau), \tag{29}$$

where

$$R_1(t,\tau)=\int_o^{\mathrm{Min}(t,\tau)} X^{(1)}(t,t_1)X^{(1)}(\tau,t_1)dt_1, \tag{30}$$

is the autocorrelation of the response when a single term Wiener-Hermite expansion is used. $R_1(t,\tau)$ is assumed to be sharply peaked around $\tau=t$.

The mean-square response as given by equation (10) now becomes

$$\sigma_x^2(t)=\sigma_1^2(t)+\sigma_3^2(t), \tag{31}$$

where σ_1^2 is given by equation (21) and

$$\sigma_3^2(t)=6\int_o^t\int_o^t\int_o^t [X^{(3)}(t,t_1,t_2,t_3)]^2dt_1dt_2dt_3. \tag{32}$$

Using equations (27) and (32), assuming that α is slowly varying, the result may be restated as

$$\sigma_3^2(t)=6\epsilon^2\omega_o^4(1+18\alpha(t))^2\int_o^t d\tau_1$$

$$\int_o^t d\tau_2 h(t,\tau_1)h(t,\tau_2)[R_1(\tau_1,\tau_2)]^3 \tag{33}$$

Equation (33) is a convenient form for evaluating the contribution of the third term in the Weiner-Hermite series to the mean-square response.

Numerical Solutions and Results

Equations (22) and (27) are two equations for determining the kernel functions $X^{(1)}$ and $X^{(3)}$. The iterative technique as developed by Orabi and Ahmadi (1987) may be used for solving equation (22). When $X^{(1)}$ is known, equation (27) gives the kernel function $X^{(3)}$. The Wiener-Hermite series given by equation (4) then provides an explicit expression for the random response. From this series, various statistics of the response may be evaluated. In particular, the mean-square response is given by equation (31).

For $S_o = 1/2\pi$ cm^2/s^3, $\omega_o = 1$ rad/s, and several values of ϵ and ξ, the transient mean-square responses of the Duffing oscillator as given by equation (31) are evaluated and the results are plotted in Fig. 1–9. The method of time dependent

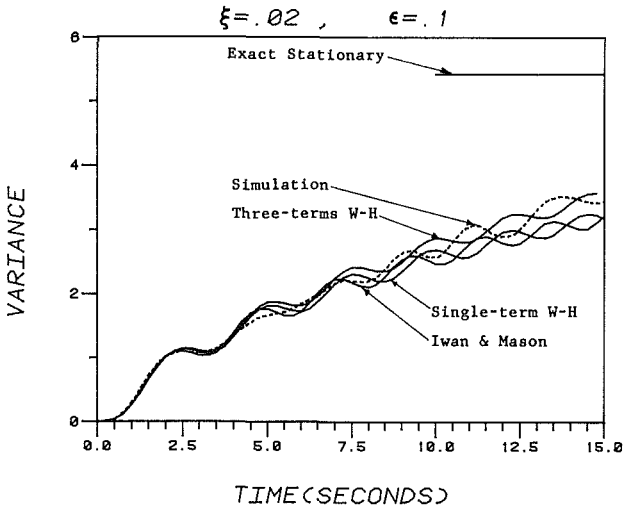


Fig. 1 Mean-square displacement response of a Duffing oscillator subjected to a white excitation with a unit step envelope function

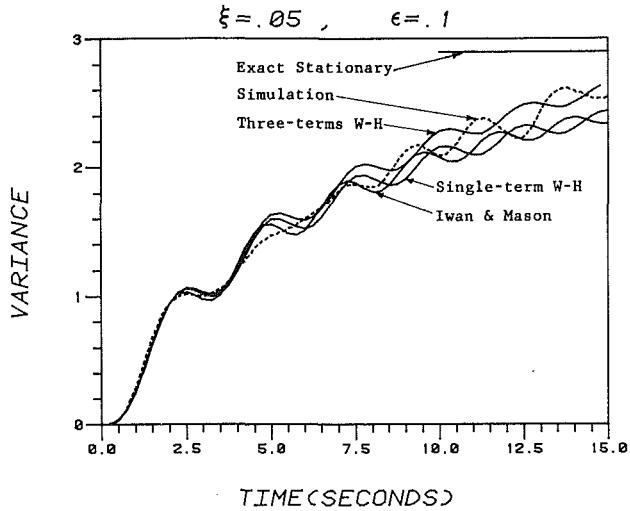


Fig. 2 Mean-square displacement response of a Duffing oscillator subjected to a white excitation with a unit step envelope function

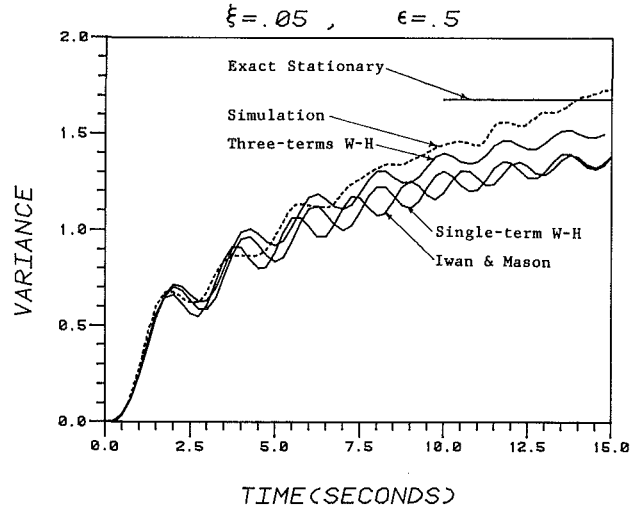


Fig. 3 Mean-square displacement response of a Duffing oscillator subjected to a white excitation with a unit step envelope function

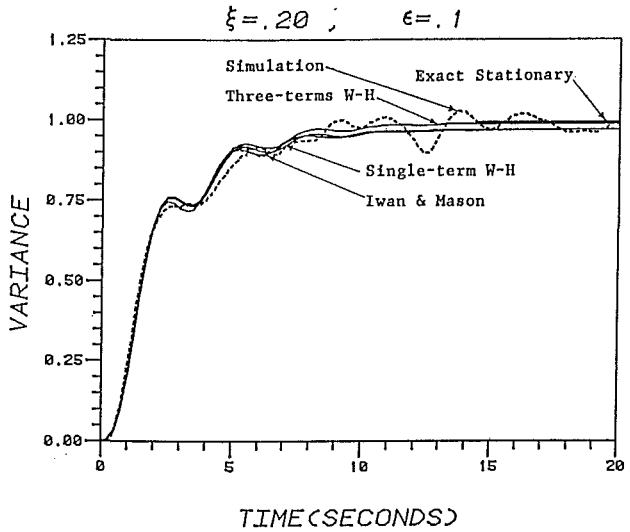


Fig. 4 Mean-square displacement response of a Duffing oscillator subjected to a white excitation with a unit step envelope function

Downloaded 03 May 2010 to 171.66.16.27. Redistribution subject to ASME license or copyright; see http://www.asme.org/terms/Terms_Use.cfm

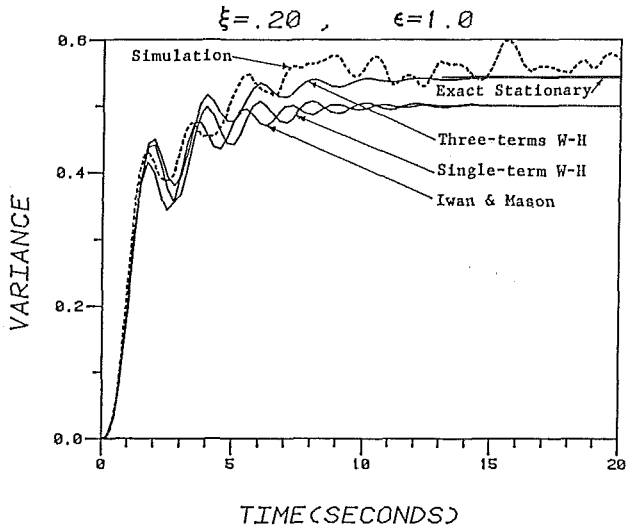


Fig. 5 Mean-square displacement response of a Duffing oscillator subjected to a white excitation with a unit step envelope function

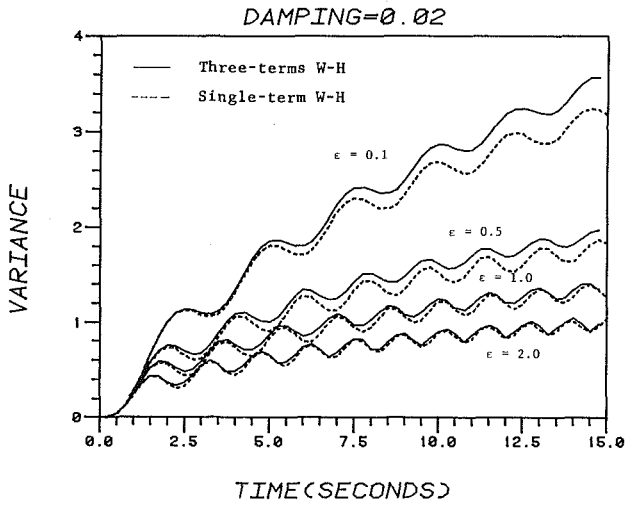


Fig. 6 Mean-square displacement response of a Duffing oscillator for different ϵ

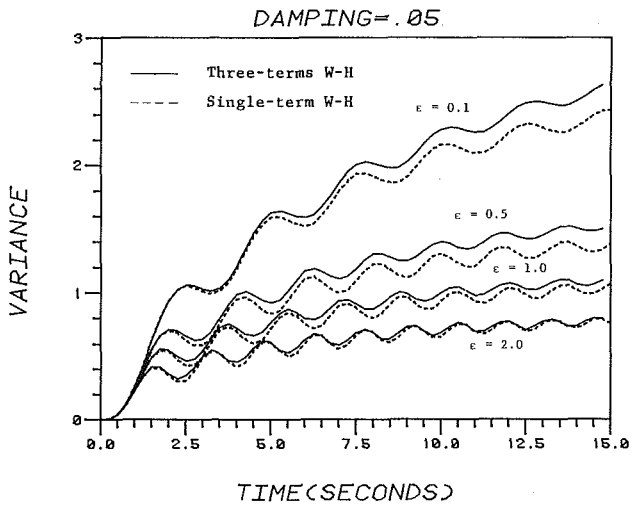


Fig. 7 Mean-square displacement responses of a Duffing oscillator for different ϵ

linearization as developed by Iwan and Mason (1980) and Wen (1980) is employed and the mean-square responses are also calculated. These results, together with the predictions of the

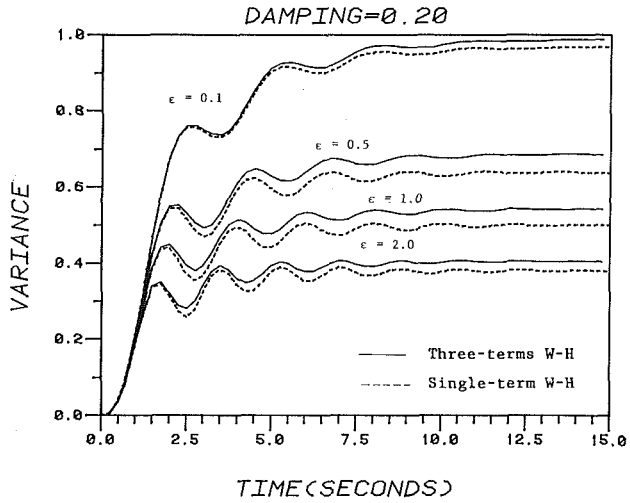


Fig. 8 Mean-square displacement response of a Duffing oscillator for different ϵ

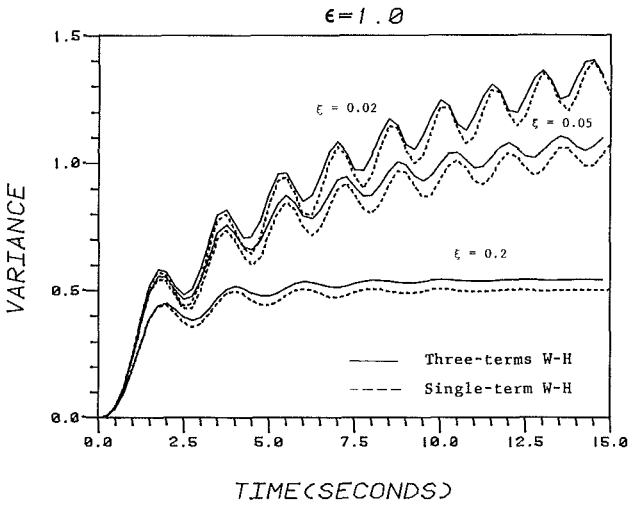


Fig. 9 Mean-square displacement responses of a Duffing oscillator for different damping coefficients

single term W-H expansions used by Orabi and Ahmadi (1987) are shown in Figs. 5. 1–5. Furthermore, the exact stationary variances as obtained by solving the Fokker-Planck equation (Lin, 1967; Ahmadi et al., 1978) are plotted in these figures. Since no exact solution for the transient mean-square response is available, a Monte-Carlo type simulation is performed. Ensembles of one thousand samples are used and the resulting mean-square responses are shown by dotted lines in the figures.

An examination of Figs. 1–5 reveals that the linearization method used by Iwan and Mason (1980) and Wen (1980) and the single-term expansion used by Orabi and Ahmadi (1987) always underestimate the exact stationary variances and the simulation results. The mean-square responses as predicted by the present three-term W-H expansion method appear to agree very well with the simulation data in all the cases studied. Figures 4 and 5 show that the present method (unlike the other techniques) also leads to the exact variances in the stationary limit for both small and large values of ϵ.

Figures 6–8 show the effect of nonlinearity strength on the mean-square responses for damping coefficients of 0.02, 0.05, and 0.20, respectively. It is observed that the mean-square responses decrease as ϵ increases.

For $\epsilon = 1$, the mean-square responses of the Duffing oscillator for several damping coefficients are shown in Fig. 9.

Downloaded 03 May 2010 to 171.66.16.27. Redistribution subject to ASME license or copyright; see http://www.asme.org/terms/Terms_Use.cfm

It is clear from that figure that the response variances decrease rapidly as ξ increases.

To clarify the significance of the third term of the W-H series, the mean-square responses as obtained by a single term expansion are shown in Figs. 6–9 by dotted lines. It is observed that the variances predicted by the single term expansion of equation (32) are always lower than those obtained by the three-term expansion method. The differences are larger for larger values of ϵ.

Figures 1–9 imply that the methods used by Iwan and Mason (1980) and Orabi and Ahmadi (1987) underestimate, to various degrees, the mean-square responses of the Duffing oscillator. The reason, we believe, is that these techniques are all based on Gaussian statistics. The non-Gaussian part of the response is lost in these analysis. Here, by considering the third term in the W-H series expansion, the non-Gaussian statistics of the random response is in part captured. The differences observed between the predictions of the single-term expansion used by Orabi and Ahmadi (1987) and the present method in Figs. 1–9 are precisely the contributions of the non-Guassian parts of the random response. It is clearly observed that as the strength of nonlinearity increases, the response departs further away from a Gaussian process.

Conclusions

The Wiener-Hermite series expansion method is used and the transient mean-square responses of a Duffing oscillator are analyzed. The predicted mean-square responses are in excellent agreement with those obtained by the Monte-Carlo simulation. At the stationary limit, the method leads to variances which are also identical to those obtained from the solution of the Fokker-Planck equation.

Based on the presented results it is concluded that the Wiener-Hermite expansion method provides a systematic tool for response analysis of nonlinear structures subjected to random excitations. When only the first term in the series is retained, the method becomes similar to the Gaussian statistical linearization of Iwan and Mason (1980) and Wen (1980). By including the higher order terms in the series, the technique provides information on the non-Gaussian statistics of the random response.

One important advantage of the Wiener-Hermite expansion method over the other non-Gaussian approximation should be emphasized. The Wiener-Hermite method provides a series representation of the random response. This not only facilitates the calculations of various response statistics, but it ensures the realizability of the solution. That is, since the response, for any order of approximation, is represented by an explicit series, the corresponding probability density function is always nonnegative.

The functional equations governing the dynamics of the kernel function are solved by an iteration method. The developed scheme appears to be quite accurate. The needed computer time to carry out the analysis is also quite reasonable.

Although, Gaussian white noise excitations were used in the present examples the method is, in principle, capable of handling nonlinear structures with nonwhite, non-Gaussian excitations.

Note that in the present method of solution, it is assumed that the response is not too far from a Gaussian process. Furthermore, the equivalent natural frequency $\omega_e(t)$ and the function $\alpha(t)$ as defined by equation (25) are smoothly varying functions of time. The presented results justify these assumptions. That is, the contributions of the third term provide corrections to those of the first term of the W-H series. ω_e is also a reasonably smooth function of time and the numerically evaluated values for $\alpha(t)$ (not shown in the figures) show that it remains almost a constant. Thus, the technique of solution leads to reasonably accurate results for the response of the Duffing oscillator.

The W-H expansion method is expected to be applicable to systems with any kind of nonlinearities. However, accuracy of the technique of solution used in this work cannot be assessed a priori. Currently the application of the W-H expansion method to the response analysis of hysteretically nonlinear systems is under study and the results will be reported in the near future.

Acknowledgments

The authors would like to thank Mrs. R. Wilson for typing the manuscript.

References

Ahmadi, G., 1982, "Wiener-Hermite Closure Method in Strong Plasma Turbulence," *Bull. Am. Phys. Soc.*, Vol. 27, pp. 1203–1205.

Ahmadi, G., 1980, "A Note on the Wiener-Hermite Representation of the Earthquake Ground Acceleration," *Mech. Research Comm.,*, Vol. 7, pp. 129–137.

Ahmadi, G., 1980, "Mean-Square Response of Nonlinear Plates," *J. Sound Vib.*, Vol. 71, pp. 9–15.

Ahmadi, G., Tadjbakhsh, I., Farshad, M., 1978, "On the Response of Nonlinear Plates to Random Loads," *Acustica*, Vol. 40, pp. 316–322.

Cameron, R. H., and Martin, W. T., 1947, "The Orthogonal Development of Nonlinear Functional in Series of Fourier-Hermite Functionals," *J. Ann. Math.*, Vol. 48, pp. 385–392.

Caughey, T. K., 1971, "Nonlinear Theory of Random Vibrations," in *Advances in Applied Mechanics*, Vol. 11, Academic Press, New York, pp. 209–253.

Crandall, S. H., 1980, "Non-Gaussian Closure for Random Vibration of Nonlinear Oscillators," *Int. J. Nonlinear Mech.*, Vol. 15, pp. 303–313.

Crandall, S. H., 1985, "Non-Gaussian Closure Techniques for Stationary Random Vibration," *Int. J. NonLinear Mech.*, Vol. 20, pp. 1–8.

Crandall, S. H., and Zhu, W. Q., 1983, "Random Vibration: A Survey of Recent Developments," ASME JOURNAL OF APPLIED MECHANICS, Vol. 50, pp. 953–962.

Iwan, W. D., and Mason, A. B., Jr., 1980, "Equivalent Linearization for Systems Subjected to Nonstationary Random Excitation," *Int. J. Nonlin. Mech.*, Vol. 15, pp. 71–82.

Iyengar, R. N., and Dash, D. K., 1978, "Study of the Random Vibration of Nonlinear System by the Gaussian Closure Technique," ASME JOURNAL OF APPLIED MECHANICS, Vol. 45, pp. 393–394.

Jahedi, A., and Ahmadi, G., 1983, "Application of Wiener-Hermite Expansion to Nonstationary Random Vibration of a Duffing Oscillator," ASME JOURNAL OF APPLIED MECHANICS, Vol. 50, pp. 436–442.

Kaul, M. K., and Penzien, J., 1974, "Stochastic Seismic Analysis of Yielding Offshore Towers," *J. Engng. Mech. Div .*, ASCE, Vol. 100, pp. 1025–1038.

Kimura, K., and Sakata, M., 1981, "Non-Stationary Response of a Non-Symmetric Nonlinear System Subjected to a Wide Class of Random Excitation," *J. Sound Vib.*, Vol. 76, pp. 261–272.

Kimura, K., Yagasaki, and Sakata, M., 1983, "Nonstationary Responses of a System with Bilinear Hysteresis Subjected to Nonwhite Random Excitation," *J. Sound Vib.*, Vol. 91, pp. 181–194.

Lee, C. P., Meecham, W. C., and Hogge, H. D., 1982, "Application of the Wiener-Hermite Expansion to Turbulence of Moderate Reynolds Numbers," *Phys. Fluids*, Vol. 25, pp. 1322–1327.

Lin, Y. K., 1967, *Probabilistic Theory of Structure Dynamics*, McGraw-Hill, N.Y.

Meecham, W. C., and Siegel, A., 1964, "Wiener-Hermite Expansion in Model Turbulence at Large Reynolds Numbers," *Phys. Fluids*, Vol. 7, pp. 1178–1190.

Meecham, W. C., and Jeng, D. T., 1968, "Use of Wiener-Hermite Expansion for Nearly Normal Turbulence," *J. Fluid Mech.*, Vol. 32, pp. 225–249.

Orabi, I. I., and Ahmadi, G., 1987, "A Functional Series Expansion Method for Response Analysis of Nonlinear Systems Subjected to Random Excitations," *Int. J. of Nonlinear Mech.*, to appear.

Roberts, J. B., 1981, "Response of Nonlinear Mechanical Systems to Random Excitation, Part 2, Equivalent Linearization and Other Methods," *Shock and Vib. Dig.*, Vol. 13, pp. 15–29.

Roberts, J. B., 1984, "Techniques For Nonlinear Random Vibration Problems," *Shock Vib. Dig.*, Vol. 16, pp. 3–14.

Spanos, P. T. D., 1981, "Stochastic Linearization in Structural Dynamics," *Appl. Mech. Rev.*, Vol. 34, pp. 1–8.

Wen, Y. K., 1980, "Equivalent Linearization for Hysteretic Systems Under Random Excitation," ASME JOURNAL OF APPLIED MECHANICS, Vol. 47, pp. 150–154.

Wiener, N., 1958, *Nonlinear Problem in Random Theory*, Wiley, NY.

Downloaded 03 May 2010 to 171.66.16.27. Redistribution subject to ASME license or copyright; see http://www.asme.org/terms/Terms_Use.cfm

APPENDIX A

The first few terms of the Wiener-Hermite series are given by

$$H^{(0)} = 1,$$

$$H^{(1)}(t) = n(t),$$

$$H^{(2)}(t_1,t_2) = n(t_1)n(t_2) - \delta(t_1 - t_2),$$

$$H^{(3)}(t_1,t_2,t_3) = n(t_1)n(t_2)n(t_3) - n(t_1)\delta(t_2 - t_3) - n(t_2)\delta(t_3 - t_1) - n(t_3)\delta(t_1 - t_2). \quad (A\text{-}1)$$

Here $n(t)$ is a white noise process with the following statistical properties

$$< n(t) > = 0,$$

$$< n(t_1)n(t_2) > = \delta(t_1 - t_2), \quad (A\text{-}2)$$

and δ ( ) is the Dirac delta function.

The elements of the Wiener-Hermite base satisfy the following statistical norms:

$$< H^{(0)}H^{(0)} > = 1,$$

$$< H^{(1)}(t_1)H^{(1)}(t_2) > = \delta(t_1 - t_2),$$

$$< H^{(2)}(t_1,t_2)H^{(2)}(t_3,t_4) > = \delta(t_1 - t_3)\delta(t_2 - t_4) + \delta(t_1 - t_4)\delta(t_2 - t_3). \quad (A\text{-}3)$$

Downloaded 03 May 2010 to 171.66.16.27. Redistribution subject to ASME license or copyright; see http://www.asme.org/terms/Terms_Use.cfm

S. P. Girrens
Staff Member,
Los Alamos National Laboratory,
Los Alamos, NM 87545
Assoc. Mem. ASME

F. W. Smith
Professor of Mechanical Engineering and
Associate Dean for Research and Graduate Studies,
Colorado State University,
Fort Collins, CO 80523
Fellow ASME

Constituent Diffusion in a Deformable Thermoelastic Solid

Solid mixtures containing initially uniform dilute concentrations of impurity elements may, upon the application of mechanical and thermal loading, develop regions of high impurity concentration that could result in local degradation of material properties. To address these degradation processes, a fully coupled thermomechanical-diffusion theory has been developed to describe the mass transport of mobile constituents driven by gradients in concentration, strain dilatation and temperature in a solid deformable parent material. A finite element code has been assembled to solve plane transient thermomechanical-diffusion problems. The theory presented and the resulting code have been successfully used to model internal hydrogen redistribution in β-phase Ti alloys induced by elastic strain gradients during bending.

I Introduction

Hydrogen embrittlement and stress-corrosion cracking are two examples of degradation processes resulting from the redistribution of dilute concentrations of impurity elements within a solid material. The mass transport of a solute species through a solid deformable parent material is fundamental to these degradation processes. Material scientists have traditionally used continuum diffusion equations, formulated as functions of concentration, stress and temperature gradients, to model the diffusion of mobile constituents in solids. This analysis procedure neglects the coupled effects between the diffusing constituents and the mechanical and thermal response of the solid mixture. One reason for the omission of coupling terms in theoretical developments of mass diffusion in solids is the resulting complexity of governing equations if all coupling effects are retained. Recently, enormous advances have been made in the computational aspects of continuum mechanics resulting in accepted numerical procedures for solving systems of partial differential equations. These considerations indicate that a significant contribution towards analyzing material degradation problems can be made with the development of a coupled thermomechanical-diffusion theory, based on the principles of modern continuum mechanics, consistent with phenomenological descriptions published in the material science literature.

An early attempt at deriving the fundamental relations and governing equations for the process of coupled thermal diffusion in solids was presented by Podstrigach and Pavlina (1965) and Podstrigach and Shevchuk (1969). Podstrigach considered as a thermodynamic system a deformed solid representing a two-component solid solution, and accepting a Gibb's relation to define the mixture equilibrium state, posed a variational equation to describe the governing equations and equations of state. Departing from the free energy functional developed by Podstrigach, Nowacki (1971, 1974, 1976) posed constitutive equations relating stress, entropy and concentration to strain, temperature, and chemical potential. Nowacki also developed phenomenological expressions for the heat and mass fluxes considering only thermal and diffusive cross effects, but dropped all nonlinear coupling terms when substituting the flux expressions into the diffusion and energy balance laws.

In the absence of thermal effects, the classical nonequilibrium thermodynamics considers the gradient of the chemical potential as the fundamental driving force in developing phenomenological equations for the mass flux (Shewman, 1963; Cahn, 1968). Mechanical effects are coupled into expressions for the mass flux by utilizing relations for the chemical potential that are functions of the solid mixture stress (Waisman et al., 1973; Pardee and Paton, 1980). This analysis method results in diffusion equations that are coupled to stress but neglects the coupling of concentration variation on the mechanical response.

The continuum theory of mixtures as set forth by Truesdell (1984) and refined by Bowen (1976), considers each constituent as a continuous medium capable of exchanging momentum and energy and supporting a stress within the mixture. Aifantis and Gerberich (1977a, 1977b) used the Bowen approach to propose a theory for gaseous diffusion in stressed thermoelastic solids. However, the thermomechanical model for the solid was assumed to be independent of the presence of the gas.

In the present work, a coupled thermomechanical-diffusion theory is proposed to model the motion of dilute mobile constituents in a deforming solid. The mixture of mobile constituents and deformable solid is considered a single body satisfying balance laws for mass, momentum, energy, and entropy

Contributed by the Applied Mechanics Division for presentation at the 1987 Applied Mechanics, Biomechanics, and Fluids Engineering Conference, Cincinnati, OH, June 14–17, 1987, of the American Society of Mechanical Engineers.
Discussion of this paper should be addressed to the Editorial Department, ASME, United Engineering Center, 345 East 47th Street, New York, N.Y. 10017, and will be accepted until two months after final publication of the paper itself in the JOURNAL OF APPLIED MECHANICS. Manuscript received by ASME Applied Mechanics Division, May 16, 1986; final revision, September 16, 1986.
Paper No. 87-APM-16.

Copyright © 1987 by ASME
Downloaded 03 May 2010 to 171.66.16.27. Redistribution subject to ASME license or copyright; see http://www.asme.org/terms/Terms_Use.cfm

growth for the mixture as a whole and a mass balance for each constituent. The theory includes coupling effects between concentration, strain, and temperature. The coupling coefficients arising from the constitutive development are found to be consistent with constants familiar in the material science literature. The coupled theory is used to analyze data from published experiments on the internal diffusion of hydrogen caused by strain gradients in β-phase Ti alloys.

II Balance Laws and Continuum Mixture Thermodynamics

To begin, we will consider a mixture consisting of a solid deformable parent and N mobile constituents. Let x_k (X_K, t) denote the position at time t in the spatial reference frame of a mixture particle which was initially located at X_K in the material reference frame. The balance laws for the mixture and mass balance for each constituent are expressed in the following. The balance of mass is given by

$$\dot{\rho} + \rho \text{ div } \dot{x}_i = 0, \tag{1}$$

where ρ is the mixture density and $\dot{x}_i$ the mixture velocity. The balance of linear momentum neglecting inertia is expressed by

$$\text{div } \sigma_{ij} + \rho f_i = 0, \tag{2}$$

with σ_{ij} the mixture stress tensor and f_i the body force vector. The balance of energy is given by

$$\rho\dot{\eta} = \text{div}(\sigma_{ij}\dot{x}_i - g_i) + \rho r + \rho\dot{x}_i f_i, \tag{3}$$

where η is the mixture specific internal energy, g_i the total mixture heat flux, and r the internal heat generation. The balance of mass for each constituent is written

$$\dot{c}_\alpha = -\text{ div } j_{\alpha i} + m_\alpha, \tag{4}$$

where c_α is the mass concentration of constituent α, $j_{\alpha i}$ is the specific mass flux of constituent α, and m_α is the specific mass supply rate to constituent α. All variables are taken to be functions of the material coordinates, X_K, and time, t. In equations (1) through (4), it is assumed that couple stresses are not present. The abbreviations grad and div denote the spatial gradient and spatial divergence, respectively, and the superimposed dot denotes the material time derivative.

Upon substituting equation (2) into equation (3), the energy equation may be written

$$\rho\dot{\eta} = -\text{ div } g_i + \sigma_{ij}L_{ij} + \rho r \tag{5}$$

where the velocity gradient of the mixture has been defined as

$$L_{ij} = \text{grad } \dot{x}_i. \tag{6}$$

Following the formulation of Gurtin and Vargas (1971), the total mixture heat flux g_i may be defined $g_i = q_i + h_i$ where q_i is the heat flux due to thermal diffusion and h_i is the energy flux due to mass diffusion. Using this definition allows (5) to be rewritten as

$$\rho\dot{\eta} = -\text{div}(q_i + h_i) + \sigma_{ij}D_{ij} + \rho r \tag{7}$$

where D_{ij} is the symmetric part of the velocity gradient and is known as the rate of deformation tensor.

In the present development, the mixture is assumed dilute in mobile constituents. As a result of this assumption, one may argue that $\rho_\alpha \ll \rho_p$, where ρ_α is the density of constituent α and ρ_p is the solid parent material density, and approximate the mixture density by

$$\rho = \rho_p + \sum_{\alpha=1}^{N} \rho_\alpha \simeq \rho_p. \tag{8}$$

The subscript p will refer the variable to the deformable parent material. Another argument resulting from the dilute mobile constituent assumption is that the rate of deformation tensor for the mixture may be approximated by

$$D_{ij} \simeq D_{pij} \tag{9}$$

in which the terms associated with the deformation rate of the mobile constituents have been neglected. It may also be argued that the partial stresses of the constituents are negligible in comparison to the stresses in the parent material. Utilizing these approximations, equations (1), (2), and (7) reduce to

$$\rho_o/\rho = \sqrt{III_C}, \tag{10}$$

$$\sigma_{pji,\,j} + \rho f_i = 0, \text{ and} \tag{11}$$

$$\rho\dot{\eta} = -q_{i,i} - h_{i,i} + \sigma_{ij}D_{pji} + \rho r, \tag{12}$$

respectively, where ρ_o is the mixture density in the initial undeformed condition and III_C is the third invariant of the Green deformation tensor for the parent material with C defined by

$$C = C_{IJ} = x_{k,I}x_{k,J} = F_{kI}F_{kJ}. \tag{13}$$

The thermodynamic theory for the mixture includes the following assumptions:

(*i*) All constituents and the parent material have the same temperature at a given location and time.

(*ii*) The mixture internal energy and specific entropy are state functions determined by the independent parameters θ (the nonnegative mixture temperature), F_{pkK} (the parent deformation gradient given by $F_{pkK} = x_{pk,K}$), and c_α (the mobile constituent concentrations).

(*iii*) A mixture specific free energy, ψ, exists and is defined by

$$\psi = \eta - \theta s \tag{14}$$

where s is the mixture specific entropy.

(*iv*) The second axiom of thermodynamics, governing entropy growth and restricting the form of the constitutive relations for the mixture, is postulated to be the local form of the Clausius-Duhem inequality

$$\rho\dot{s} + \text{div}(q_i/\theta) - \rho r/\theta \geq 0. \tag{15}$$

In view of equations (12) and (14), the inequality (15) can also be written

$$\rho(\dot{\psi} + \dot{\theta}s) + q_i\theta_{,i}/\theta + h_{i,i} - \sigma_{pij}D_{pji} \leq 0. \tag{16}$$

A thermodynamic process for the mixture is completely described if the following nine functions of the parent material coordinates, X_{pi}, and time, t, are known: (1) the spatial position vector, x_{pi}, of the parent body; (2) the parent stress tensor, σ_{pij}; (3) the constituent concentrations, c_α; (4) the constituent chemical potentials, μ_α; (5) the thermal heat flux vector, q_i; (6) the constituent mass flux vectors, $j_{\alpha i}$; (7) the specific mixture entropy, s; (8) the local mixture temperature, θ; and (9) the mixture specific free energy, ψ. It is sufficient to prescribe only these nine functions since the parent body density, ρ_p, the body force vector, f_i, and heat generation, r, are taken to be given.

Motivated by Gurtin and Vargas (1971), the energy flux due to mass diffusion is defined by

$$h_i = \rho\mu_\alpha j_{\alpha i}. \tag{17}$$

The constituent chemical potentials, μ_α, account for free energy changes in the mixture caused by mass diffusion. It should be noted that it is not necessary to formulate the diffusive energy flux, h_i, in terms of products of the constituent chemical potentials and mass fluxes. The formulation could also have been presented in terms of a functional description for the diffusive energy flux directly rather than the constituent chemical potentials. In this work, the chemical potential substitution is used to provide consistency with formulations found in the material science literature.

The restrictions placed on the thermodynamic process are that the set of functions satisfy the conservation equations (4),

Downloaded 03 May 2010 to 171.66.16.27. Redistribution subject to ASME license or copyright; see http://www.asme.org/terms/Terms_Use.cfm

(11), and (12), satisfy the local Clausius-Duhem inequality (16), and obey the constitutive axioms of causality, equipresence, and objectivity.

III Constitutive Structure for Linear Elastic Mixture

For a homogeneous elastic solid containing N constituents, a total of $15 + 5N$ unknowns, $(\sigma_{pij}, q_i, \psi, s, \theta, x_{pi}, \mu_\alpha, c_\alpha, j_{\alpha i})$, result and must satisfy the $4 + N$ basic field equations. In order to determine the unknown functions subject to a given set of boundary conditions, $11 + 4N$ additional equations must be specified. The required set of $11 + 4N$ relations are known as the constitutive equations and characterize the material response.

Following the axioms of causality and equipresence, the $11 + 4N$ constitutive equations for the mixture are assumed in this development to be given by a smooth function f such that

$$(\sigma_{pij}, s, \psi, \mu_\alpha, q_i j_{\alpha i}) = f(\theta, \theta_{,I}, c_\alpha, c_{\alpha,I}, F_{piI}, F_{piI,I}). \tag{18}$$

The constitutive equations, (18), satisfy the axiom of material objectivity if they are written as

$$\begin{aligned} s &= \bar{s}(\theta, \theta_{,I}, c_\alpha, c_{\alpha,I}, C_{IJ}, C_{IJ,I}) \\ \psi &= \bar{\psi}(\theta, \theta_{,I}, c_\alpha, c_{\alpha,I}, C_{IJ}, C_{IJ,I}) \\ \mu_\alpha &= \bar{\mu}_\alpha(\theta, \theta_{,I}, c_\alpha, c_{\alpha,I}, C_{IJ}, C_{IJ,I}) \\ q_i &= F_{piI}\bar{q}_i(\theta, \theta_{,I}, c_\alpha, c_{\alpha,I}, C_{IJ}, C_{IJ,I}) \\ j_{\alpha i} &= F_{piI}\bar{j}_{\alpha i}(\theta, \theta_{,I}, c_\alpha, c_{\alpha,I}, C_{IJ}, C_{IJ,I}) \\ \sigma_{ij} &= F_{piI}\bar{\sigma}_{pij}(\theta, \theta_{,I}, c_\alpha, c_{\alpha,I}, C_{IJ}, C_{IJ,I})F_{pIi} \end{aligned} \tag{19}$$

In equation (19), C_{IJ} is the Green deformation tensor for the parent material.

Following Girrens (1986), the condition that all possible processes must satisfy the second law restrictions imposed by equation (16) on the constitutive equations results in

$$\begin{aligned} \psi &= \hat{\psi}(\theta, c_\alpha, E_{IJ}) \\ s &= -\frac{\partial \psi}{\partial \theta} \\ \mu_\alpha &= \frac{\partial \psi}{\partial c_\alpha} \\ \sigma_{pij} &= \rho F_{piI}\frac{\partial \psi}{\partial E_{IJ}}F_{pIi} \\ q_i &= F_{piI}\hat{q}_i(\theta_{,I}, c_{\alpha,I}, E_{IJ,I}) \\ j_{\alpha i} &= F_{piI}\hat{j}_{\alpha i}(\theta_{,I}, c_{\alpha,I}, E_{IJ,I}) \end{aligned} \tag{20}$$

where E_{IJ} is the Lagrangian strain measure for the parent material defined by $2E_{IJ} = C_{IJ} - \delta_{IJ}$ and δ_{IJ} is the unit matrix. After the conditions of equations (20) are introduced, the Clausius-Duhem inequality and the local form of the energy equation reduce to

$$\rho j_{\alpha k}\mu_{\alpha,k} + q_k\theta_{,k}/\theta \le 0, \text{ and} \tag{21}$$

$$\rho\theta\dot{s} + q_{k,k} + \rho j_{\alpha k}\mu_{\alpha,k} - \rho r = 0, \tag{22}$$

respectively.

At this stage in the development of the constitutive theory, θ and c_α are redefined to be the increments above a reference value for temperature and concentration, respectively. Restricting the theory to conditions of infinitesimal strain, ϵ_{kl} is substituted for the Lagrangian strain measure and when approximated in terms of parent displacements in spatial coordinates, u_k, is written

$$\epsilon_{kl} = \frac{1}{2}(u_{k,l} + u_{l,k}). \tag{23}$$

The free energy potential, $\Phi = \rho\,\psi\,(\theta, c_\alpha, \epsilon_{ij})$, is expanded in a power series in terms of the independent variables ignoring all terms higher than the second order. The free energy potential for a linear isotropic elastic mixture is assumed to have the form

$$\Phi = G\epsilon_{ij}\epsilon_{ij} + \frac{\lambda}{2}\epsilon_{ii}\epsilon_{jj} - \beta_\theta\theta\,\epsilon_{ii} - \beta_{c\alpha}c_\alpha\epsilon_{ii} - \frac{\rho d}{2T_o}\theta^2 + \frac{\rho}{2}\zeta\,c_\alpha^2 + \rho\omega c_\alpha\theta \tag{24}$$

with G and λ denoting Lame constants, $\beta_\theta = 3\kappa\alpha_\theta$, $\beta_{c\alpha} = 3\kappa\alpha_c$, where $\kappa = \lambda + (2/3)G$ is the bulk modulus, and α_θ and α_c are the coefficients of linear thermal and diffusive expansion. The coefficients d, T_o, ζ, and ω are the specific heat at constant strain and concentration, the reference mixture temperature, the material constant relating concentration to chemical potential, and the material constant relating concentration to entropy, respectively. Applying the second law restrictions (20_2), (20_3), and (20_4) to (24) results in the following constitutive equations for the parent material stress, the mixture entropy and the constituent chemical potential

$$\sigma_{pij} = 2G\epsilon_{ij} + (\lambda\, e - \beta_\theta\theta - \beta_{c\alpha}c_\alpha)\delta_{ij}, \tag{25}$$

$$s = \frac{\beta_\theta}{\rho}e + \frac{d}{T_o}\theta - \omega c_\alpha, \text{ and} \tag{26}$$

$$\mu_\alpha = -\frac{\beta_{c\alpha}}{\rho}e + \zeta\,c_\alpha + \omega\,\theta, \tag{27}$$

respectively. For convenience e has been substituted for the strain dilatation term ϵ_{ii}. The simplest possible linear forms of the constitutive expressions for the heat and mass fluxes are

$$q_i = -(K\theta_{,i} + B\,c_{\alpha,i} - N\,e_{,i}) \tag{28}$$

$$j_{\alpha i} = -(D\,c_{\alpha,i} + A\,\theta_{,i} - Me_{,i}). \tag{29}$$

The coefficients K, D, B, and A are identified in order as the thermal conductivity, the diffusion coefficient, the Soret coefficient, and the Dufour coefficient. The variables N and M relate the strain dilatation gradient with the heat flux and constituent mass flux, respectively.

IV Determination of Constitutive Constants from the Classical Thermodynamics Literature

The conservation equations (4), (11), and (22), along with the constitutive equations (25)–(29), represent a new coupled theory describing constituent diffusion in a deformable thermoelastic solid. The constitutive theory development resulted in equations containing material dependent coefficients that couple the effects of concentration, strain, and temperature in a thermomechanical-diffusion process. Methods for determining numerical values for the identifiable constants, G, λ, β_θ, d, K, D, B, and A, are readily available in the literature. However, the remaining coupling coefficients, $\beta_{c\alpha}$, M, N, ζ, and ω, are not standard and require further discussion. In the following section, procedures are developed for calculating numerical values for the coefficients $\beta_{c\alpha}$, M, ζ, and ω. Expressions are derived by comparing the constitutive equations developed in the present study with relations from classical diffusion theories. Utilizing these expressions, values for the coupling coefficients may be estimated from familiar material constants and experimental results. The equations developed here are used in a later section to compute the coupling coefficients for comparison with numerical analysis results of a coupled diffusion experiment.

According to developments based upon the classical nonequilibrium thermodynamics, the fundamental driving force for isothermal diffusion is a gradient in the chemical potential as expressed by

Downloaded 03 May 2010 to 171.66.16.27. Redistribution subject to ASME license or copyright; see http://www.asme.org/terms/Terms_Use.cfm

$$j_i = \Gamma \text{ grad } \mu \tag{30}$$

(Shewman, 1963; Cahn, 1968; Waisman et al., 1973). The coefficient Γ is called the mobility and is generally defined as

$$\Gamma = \frac{Dc}{RT} \tag{31}$$

where R is the universal gas constant, T is the absolute temperature, D is the diffusion coefficient, and c the mobile constituent concentration. Considering only one mobile constituent in a deformable solid, equation (27) is substituted into (30) resulting in the following expression

$$j_i = \frac{Dc}{RT}\frac{\beta_c}{\rho} e_{,i} - \frac{Dc}{RT}\zeta c_{,i}. \tag{32}$$

A relationship between the partial molar volume, $\bar{V}$, and the coefficient coupling stress and concentration, β_c, is obtained by the following exercise. Consider an isothermal mixture of material that is allowed to expand freely during the addition of uniformly distributed constituent. The dilatation, obtained by contracting equation (25), becomes

$$e = \frac{\beta_c}{\kappa} c. \tag{33}$$

By definition, $e \equiv \Delta V/V_o$ where ΔV is the material volume change and V_o is the constituent free material volume. Also by definition, $\Delta V \equiv \bar{V}N$ where N is the moles of constituent. Substituting the expressions for e and ΔV into equation (33) results in the relation

$$\beta_c = \kappa \bar{V}\rho/a \tag{34}$$

where a is the constituent atomic weight and ρ the mixture density. Using equation (34) a numerical value for β_c can be obtained from published data for $\bar{V}$. Equation (34) is in agreement with an expression derived by Pardee and Paton (1980) for the constituent induced strain dilatation. Substituting equation (34) for β_c into equation (32) and equating the coefficients multiplying the gradient terms in equation (32) with those in equation (29) gives the following relations

$$M = \frac{D\kappa\bar{V}}{RTa} c, \text{ and} \tag{35}$$

$$\zeta = \frac{RT}{c}. \tag{36}$$

The coupling coefficients, ζ and ω, are material constants resulting from the coupled theory development relating concentration to constituent chemical potential and mixture entropy, respectively. Having obtained an analytic expression for ζ, equation (36), a relationship can also be determined for the coupling constant ω. Consider as a thermodynamic system a mixture, consisting of one mobile constituent within an elastically deformed solid, and assume no internal heat generation and that the surface of the mixture body is adiabatic and impermeable to mass flow. Applying the energy equation (22) to the system indicates that the deformation process is isentropic. Accepting $s = 0$ for a relative datum, equation (26) becomes

$$0 = \frac{\beta_\theta}{\rho} e + \frac{d}{T_o}\theta - \omega c. \tag{37}$$

Recall that θ and c are the local increments in temperature and concentration, respectively. Since the deformation process is performed isothermally, $\theta = 0$, solving equation (37) for ω results in

$$\omega = \frac{\beta_\theta}{\rho}\frac{e}{c}. \tag{38}$$

The coupling coefficients β_c, M, ζ, and ω can be approximated using equations (34), (35), (36), and (38), respectively, in terms of known material constants and measurable temperature, concentration, and strain conditions. Approximate values for the coupling coefficients obtained using these expressions will be compared to numerical results from finite element simulations of a coupled diffusion experiment in the following section of this paper.

V Comparison of Theory with Experiment

The reduced governing equations describing coupled thermomechanical-diffusion of a single constituent in an isotropic elastic solid are obtained by combining the conservation laws and constitutive relations. An equilibrium equation is obtained by substituting equations (23) and (25) into (11). A diffusion equation results from substituting equation (29) into equation (4). A nonlinear energy equation is obtained upon substitution of equations (26)–(29) into equation (22). Hence the equilibrium, diffusion, and energy equations are, respectively,

$$[G(u_{i,j} + u_{j,i}) + (\lambda e - \beta_\theta\theta - \beta_c c)\delta_{ij}]_{,j} + \rho f_i = 0 \tag{39}$$

$$c_{,t} = Dc_{,ii} + A\theta_{,ii} - Me_{,ii} \tag{40}$$

$$\rho d\theta_{,t} + T_o\beta_\theta e_{,t} - \rho\omega T_o c_{,t} = K\theta_{,ii} + Bc_{,ii} - Ne_{,ii} + M\beta_c(e_{,i})^2 + D\zeta(c_{,i})^2\rho + A\omega(\theta_{,i})^2\rho - (M\zeta\rho + D\beta_c)e_{,i}c_{,i} + \rho r + (D\omega\rho + A\zeta\rho)\theta_{,i}c_{,i} - (M\omega\rho + A\beta_c)\theta_{,i}e_{,i} \tag{41}$$

where the specific mass supply rate has been set to zero.

Finite element equations were formulated from the reduced governing equations (39)–(41) and incorporated into a code for numerical solution. The finite element code is presently capable of analyzing plane transient thermomechanical-diffusion problems by solving for the parent material displacements, strain dilatation, constituent concentration, and mixture temperature. Details of the finite element formulation and a comparison of numerical results with closed-form analytical solutions for one-dimensional problems are presented in Girrens (1986).

The coupled theory and resulting finite element code were used to analyze published experimental data on the strain induced internal diffusion of hydrogen in three β-phase titanium alloys. Adler and Schulte (1978, 1981) and Adler et al. (1980) measured the change in hydrogen concentration as a function of strain in β-Ti beam specimens subjected to four-point bending. Linear strain gradients, resulting from the applied loading, induced steady-state linear concentration redistributions in the beam specimens. Data were also presented on the transient stress-assisted hydrogen diffusion by measuring the time-dependent concentration change following a reversal of the stress gradient.

The finite element code was applied to simulate the bending experiments using the initial concentrations, diffusion coefficients, and mechanical properties reported directly in the experimental publications. The β_c coefficient, computed for each alloy with equation (34), ranged from $4.0 - 6.2 \times 10^5$ MPa depending upon the Young's modulus of the material. The calculations for β_c used the value of $\bar{V}_H = 1.6 \times 10^{-6}$ m^3/mol reported by Waisman et al. (1973) for hydrogen in β-phase Ti. Assuming isothermal conditions and impermeable specimen boundaries, the steady-state bending experiment condition was numerically modeled with various assumed values for M until the computed concentrations matched the measured hydrogen concentration levels. Once the coefficient M was established from simulation of the steady-state experiment, the transient stress reversal problem was modeled numerically. Figures 1–3 illustrate the excellent agreement obtained between experimentally measured transient stress-induced concentration variations and the concentration changes resulting from strain gradients predicted by the cou-

Downloaded 03 May 2010 to 171.66.16.27. Redistribution subject to ASME license or copyright; see http://www.asme.org/terms/Terms_Use.cfm

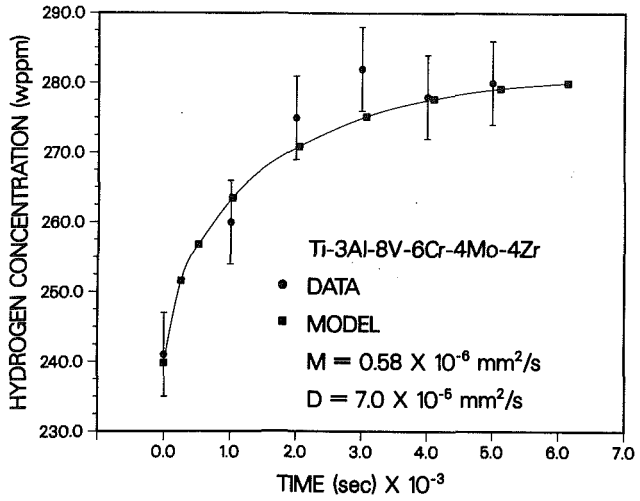


Fig. 1 Comparison of predicted and measured transient hydrogen concentration change in β-phase Ti-3Al-8V-6Cr-4Mo-4Zr accompanying an elastic stress reversal

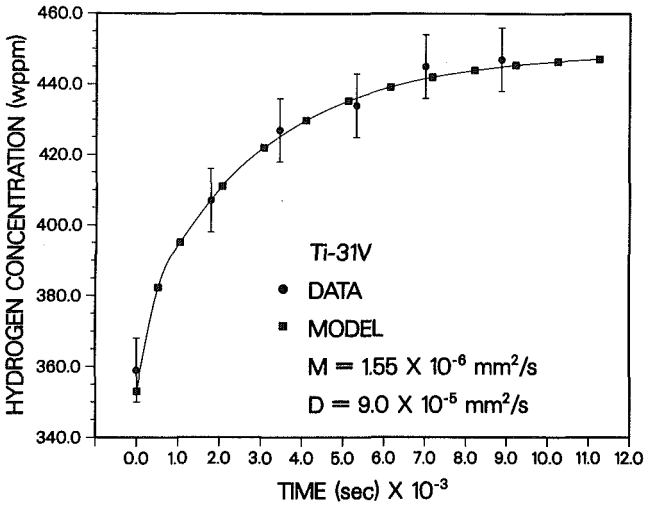


Fig. 3 Comparison of predicted and measured transient hydrogen concentration change in β-phase Ti-31V accompanying an elastic stress reversal

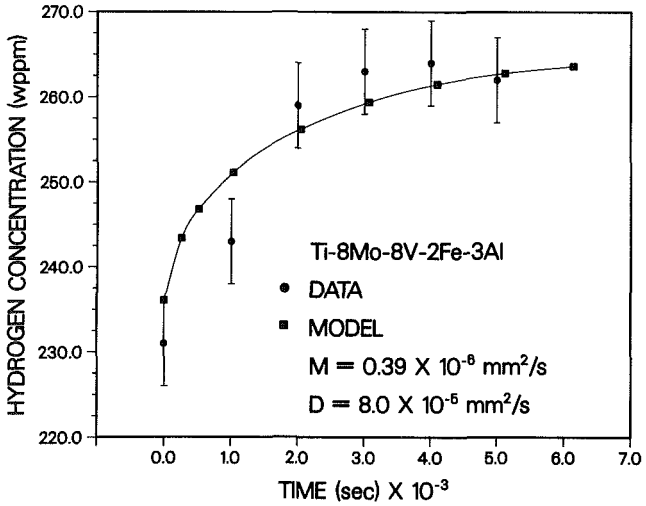


Fig. 2 Comparison of predicted and measured transient hydrogen concentration change in β-phase Ti-8Mo-8V-2Fe-3Al accompanying an elastic stress reversal

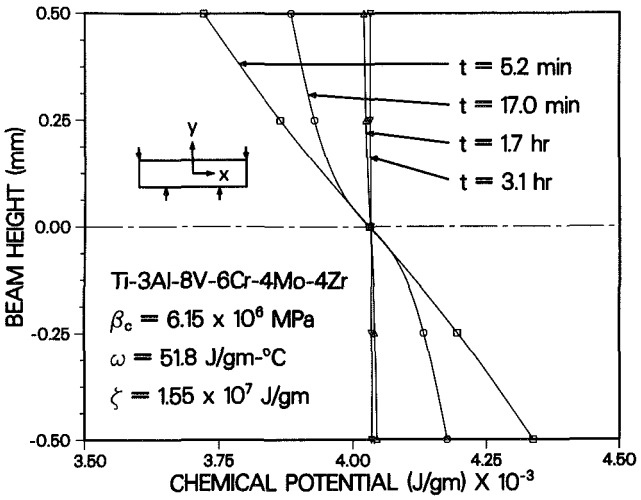


Fig. 4 Computed transient chemical potential profiles for hydrogen diffusion in a Ti-3A1-8V-6Cr-4Mo-4Zr beam specimen accompanying an elastic strain gradient

Table 1 Computed piezodiffusive coefficients, M, for hydrogen in β-phase Titanium alloys

ALLOY	M(m^2/s)
Ti-3Al-8V-6Cr-4Mo-4Zr	0.58×10^{-12}
Ti-8Mo-8V-2Fe-3Al	0.39×10^{-12}
Ti-31V	1.55×10^{-12}

Table 2 Comparison of computed coupling coefficients for hydrogen diffusion in Titanium alloy Ti-8Al-8V-6Cr-4Mo-4Zr

COMPUTED USING	COEFFICIENT		
	M(m^2/s)	ζ(J/kg)	ω(J/kg − °K)
Code	0.58×10^{-12}	1.55×10^{10}	5.18×10^{4}
Equation	(35)	(36)	(38)
Result	0.96×10^{-12}	0.94×10^{10}	5.50×10^{4}

pled thermomechanical diffusion theory. The coupling between strain dilatation and mass flux implied by the piezodiffusive coefficient, M, is required if the coupled theory is to predict the experimental data. The piezodiffusive coupling constants given in Table 1 were determined for each of the three Ti alloys using the procedure described earlier. It was found that the concentration variation in the stressed material had very little effect on the mechanical response. Strains calculated including the β_c coupling constant produced a 0.8 percent difference when compared to strain results computed with β_c set to zero.

In addition to providing sufficient information for the determination of the piezodiffusive coefficient, the data from the bending experiments can also be used to obtain quantitative values for the coupling constants ζ and ω. The chemical potential of constituent α, μ_α, accounts for free energy changes in the mixture caused by the diffusion of constituent α into or out of the mixture. For no mass crossing the system boundary, and considering only one constituent, μ is constant throughout the system at equilibrium. Since the bending experiments were performed isothermally and at equilibrium, μ is a constant, differentiating equation (27) over the beam thickness results in

$$\zeta=\frac{\beta_c}{\rho}\frac{\Delta e}{\Delta c}. \tag{42}$$

Concentration and dilatation results computed by simulating the bending experiment for titanium alloy Ti-8Al-8V-6Cr-4Mo-4Zr with the code were substituted into equations (38) and (42) to obtain values for ω and ζ, respectively. Substituting published values for the material constants and temperature, strain, and concentration data reported in the bending experiment publications, approximate values for M,

Downloaded 03 May 2010 to 171.66.16.27. Redistribution subject to ASME license or copyright; see http://www.asme.org/terms/Terms_Use.cfm

ζ, and ω were also calculated using the analytic expressions (35), (36), and (38). Table 2 compares the values obtained from the finite element analysis to results computed using the approximate expressions derived earlier. The close agreement between the code and the analytically determined coupling coefficients indicates that the thermomechanical-diffusion theory presented in this work is consistent with formulations published in the material science literature.

Figure 4 is a plot of the computed transient chemical potential distribution through the beam specimen from the initial load application until a steady-state concentration profile is reached. As shown in Fig. 4, at equilibrium (internal diffusion complete), the local chemical potential returns to a constant value since the net mass flow into the beam during deformation is zero. A nonlinear energy equation, resulting from the inclusion of the coupling coefficients M, ζ, and ω, must be solved in order to obtain the chemical potential results. The curves in Fig. 4 are also in agreement with the classical thermodynamic statement that the fundamental driving force for diffusion is a gradient in the chemical potential.

VI Summary and Conclusions

An applied coupled thermomechanical-diffusion theory has been developed to model the thermal and mechanically assisted mass transport of mobile constituents through a deformable elastic solid. The mixture of mobile constituents and deformable solid was considered a continuum. Constitutive relations were developed for the solid stress, mixture entropy, mixture heat flux, constituent chemical potential, and constituent mass flux. The theory was incorporated into a finite element code to produce a usable tool for numerical modeling of coupled diffusion processes. Excellent agreement was obtained between the numerical simulation and experimental results for both the steady-state and transient internal hydrogen redistribution in β-phase Ti alloys induced by elastic strain gradients during bending. A value for the piezodiffusive coefficient, M, which couples the strain dilatation in the solid to the constituent mass flux, was determined for three titanium alloys as a result of modeling the hydrogen diffusion experiments. Values for the coupling coefficients, ζ and ω, which relate concentration to chemical potential and concentration to entropy, respectively, were also computed from the finite element simulations. Expressions were developed for obtaining approximate values for the new coupling coefficients M, ζ, and ω in terms of familiar material constants and measurable temperature, concentration, and strain conditions. Estimates obtained utilizing these expressions were found to be in good agreement with results from numerical simulations of the bending experiments. The combination of excellent accuracy in modeling the diffusion experiments and good agreement between numerically and analytically computed coupling coefficients indicates that the coupled theory developed is consistent with experimental observations and theoretical formulations found in the material science literature.

VII Acknowledgment

This work was performed under the Institutional Supporting Research and Development program at the Los Alamos National Laboratory.

References

Adler, P. N., and Schulte, R. L., 1978, "Stress-Induced Hydrogen Migration in β-Phase Titanium," *Scripta Metallurgica*, Vol. 12, pp. 669–672.

Adler, P. N., Schulte, R. L., Schneid, E. J., Kamykowski, E. A., and Kuehne, F. J., 1980, "Stress Induced Hydrogen Redistribution in Commercial Titanium Alloys," *Metallurgical Transactions A*, Vol. 11A, pp. 1617–1623.

Adler, P. N., and Schulte, R. L., 1981, "Stress-Induced Hydrogen Concentration Changes in Titanium," Grumman Aerospace Corporation Report AD-A098100, Bethpage, NY.

Aifantis, E. C., and Gerberich, W. W., 1977a, "Gaseous Diffusion in a Stressed-Thermoelastic Solid. Part I: The Thermomechanical Formulation," *Acta Mechanica*, Vol. 28, pp. 1–24.

Aifantis, E. C., and Gerberich, W. W., 1977b, "Gaseous Diffusion in a Stressed-Thermoelastic Solid. Part II: Thermodynamic Structure and Transport Theory," *Acta Mechanica*, Vol. 28, pp. 25–47.

Bowen, R. M., 1976, "Theory of Mixtures," *Continuum Physics*, Vol. 3, Eringen, A. C., ed., Academic Press, New York, pp. 1–127.

Cahn, J. W., 1968, "Spinodal Decomposition," *Transactions of the Metallurgical Society of AIME*, Vol. 242, pp. 166–180.

Girrens, S. P., 1986, "Coupled Thermomechanical-Diffusion of Mobile Constituents in a Deformable Solid," Ph.D. Dissertation, Colorado State University, Fort Collins, CO.

Gurtin, M. E., and Vargas, A. S., 1971, "On the Classical Theory of Reacting Fluid Mixtures," *Archive for Rational Mechanics and Analysis*, Vol. 43, pp. 179–197.

Nowacki, W., 1971, "Certain Problems of Thermodiffusion in Solids," *Archives of Mechanics*, Vol. 23, No. 6, pp. 731–755.

Nowacki, W., 1974, "Dynamic Problems of Thermodiffusion in Elastic Solids," *Proceedings of Vibration Problems*, Vol. 15, No. 2, pp. 105–128.

Nowacki, W., 1976, "Dynamic Problems of Diffusion in Solids," *Engineering Fracture Mechanics*, Vol. 8, pp. 261–266.

Pardee, W. J., and Paton, N. E., 1980, "Model of Sustained Load Cracking by Hydride Growth in Ti Alloys," *Metallurgical Transactions A*, Vol. 11A, pp. 1391–1400.

Podstrigach, J. C., and Pavlina, V. S., 1965, "Fundamental Equations of Thermodiffusion in Isotropic Deformable Solids," *Prikladnaia Mekhanika*, Vol. 1, No. 3, pp. 101–106.

Podstrigach, J. C., and Shevchuk, P. R., 1969, "Variational Form of the Equations of the Theory of Thermodiffusion Processes in a Deformable Solid," *Prikladnaia Matematika I Mekhanika*, Vol. 33, No. 4, pp. 774–776.

Shewman, P. G., 1963, *Diffusion in Solids*, McGraw-Hill, New York.

Truesdell, C., 1984, *Rational Thermodynamics*, Second Edition, Springer-Verlag, New York, pp. 219–352.

Waisman, J. L., Sines, G., and Robinson, L. B., 1973, "Diffusion of Hydrogen in Titanium Alloys Due to Composition, Temperature, and Stress Gradients," *Metallurgical Transactions*, Vol. 4, pp. 291–302.

Downloaded 03 May 2010 to 171.66.16.27. Redistribution subject to ASME license or copyright; see http://www.asme.org/terms/Terms_Use.cfm

W. L. Chow
Professor of Mechanical Engineering, Mem. ASME

Alice A. L. Ting
Research Assistant.

P. H. Tsai
Research Assistant.

Department of Mechanical and Industrial Engineering,
University of Illinois at Urbana-Champaign,
Urbana, IL 61801

Discharge From a Vessel Through an Axisymmetric Control Valve

The problem of an incompressible flow discharge through an axisymmetric control valve has been examined through the method of hodograph transformation. The boundary value problem in the hodograph plane has an unusual feature in that part of the boundary is overlapped. Certain manipulations have been applied to produce the realistic free streamline configuration. The rate of discharge is obtained for various locations of the valve. This investigation provides the evidence that the method of hodograph transformation coupled with numerical computation is indeed effective in dealing with problems of this kind.

Introduction

Discharge from a vessel is of considerable interest in its practical applications. Whether the medium is a liquid or a gas, and the discharge is controlled or uncontrolled, they all have immediate application to practical flow situations. Early theoretical studies focused on the incompressible inviscid flows. Conformal transformations (e.g., Milne-Thompson, 1950) can be readily employed to solve these two-dimensional problems. In fact, it has been extended by Von Mises (1917) to solve problems with nonsymmetric flow configurations. The inviscid analysis is adequate since, in practice, the viscous effects are very small. Since this subject usually involves simple flow geometry, it later became a typical example for testing mathematical techniques of studying two-dimensional potential flow with free boundaries. For practical applications, the flow is usually of an axisymmetric configuration. Theoretical studies were directed exclusively toward uncontrolled nozzle discharge. Perhaps due to the more complicated geometry no analysis has been carried out to examine the valve-controlled flows.

The present effort examines the discharge of a fluid from a vessel through a control valve. The method of analysis is based on the hodograph transformation coupled with numerical computation. Viscous effects are completely ignored since they have, at the most, a small modifying influence to the flow.

Hodograph transformation is an effective mathematical technique for converting a nonlinear gas dynamic problem to a linear problem in the hodograph plane. By taking speed V and flow direction θ of the fluid as independent variables, the potential and the stream functions, as well as the physical coordinates x and y are all functions of the hodograph variable V, θ. Although this seems to be an indirect approach to the physical problem, with the advent of high speed computers the disadvantage of this method has been greatly reduced if not completely eliminated.

Indeed, the senior author of this paper recognized the merit of this technique and applied it to many problems whose solutions are strongly influenced by gravitation (e.g., Chow and Han, 1979, Han and Chow, 1981, Chan et al., 1985). Later, this analysis was also applied to examine the vector-thrust capability of two-dimensional asymmetric nozzles (Wu and Chow, 1985). The detailed treatment to the flow through a control valve is presented in the following sections.

Analytical Consideration

The problem under consideration is depicted in Fig. 1. The fluid is restricted to be incompressible and the reservoir is large enough that the approaching flow velocity is vanishingly small. Certainly, the present study can be extended to consider the compressible flow discharge, vessels with finite approaching flow velocity, valves with more complicated geometry, including valves with valve stems, and also reservoir

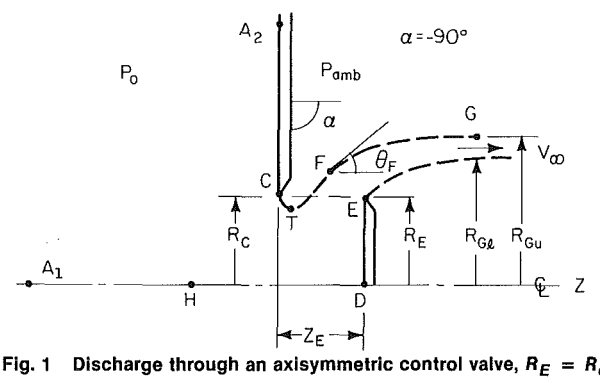


Fig. 1 Discharge through an axisymmetric control valve, $R_E = R_C$

Contributed by the Applied Mechanics Division for presentation at the 1987 Applied Mechanics, Biomechanics, and Fluids Engineering Conference, Cincinnati, OH, June 14–17, 1987, of the American Society of Mechanical Engineers.

Discussion of this paper should be addressed to the Editorial Department, ASME, United Engineering Center, 345 East 47th Street, New York, N.Y. 10017, and will be accepted until two months after final publication of the paper itself in the JOURNAL OF APPLIED MECHANICS. Manuscript received by ASME Applied Mechanics Division, April 16, 1986; final revision, August 27, 1986.

Paper No. 87-APM-23.

Copyright © 1987 by ASME
Downloaded 03 May 2010 to 171.66.16.27. Redistribution subject to ASME license or copyright; see http://www.asme.org/terms/Terms_Use.cfm

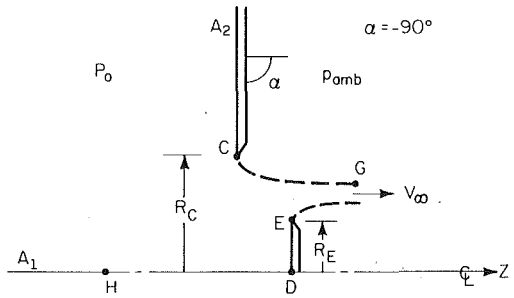


Fig. 2 Discharge from a reservoir with $R_E < R_c$

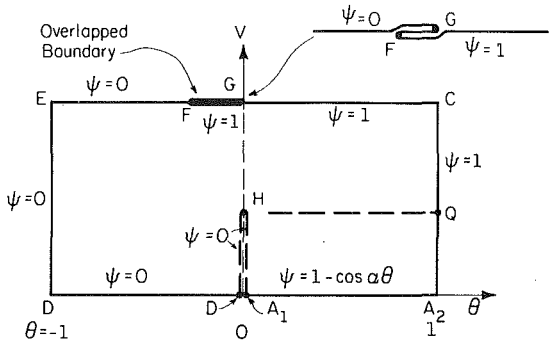


Fig. 3 The hodograph with overlapping boundary ($\theta_F < 0$)

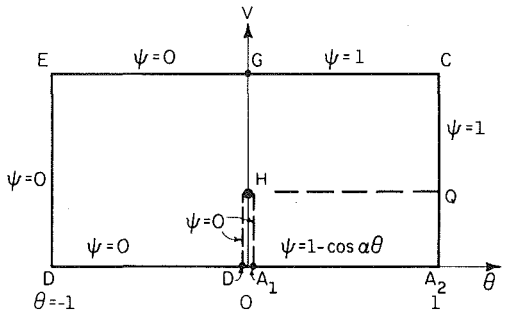


Fig. 4 The hodograph without overlapping boundary ($\theta_F = 0$)

walls with different angles (i.e., $\alpha \neq -90$ deg). It is understood that the free jet boundaries, *CFG* and *EG*, whose configurations are to be determined as part of the solution are lines of constant velocity according to Bernoulli's principle.

As one will see later, in order to promote a thorough understanding of the problem, it is necessary to examine a more general one where the valve radius R_E is smaller than the opening radius R_c, and the accompanied free jet flow pattern is depicted in Fig. 2. The top free jet streamline turns smoothly toward the horizontal downstream direction after it leaves the solid wall. On the other hand, for the case shown in Fig. 1, the top free jet streamline must turn around (diverted by the valve) and into a state of maximum positive angle (identified by point *F*) before it settles down toward the asymptotic state *G* at the far downstream position. Since the asymptotic state for axisymmetric flow must occur at a position where all streamlines are horizontal, it is nature to expect that both free steamlines follow the configuration as depicted in Fig. 1. This behavior presents an unusual mathematical feature of the problem in the hodograph plane. Figure 3 shows such a hodograph where the coordinates are already normalized by α and V_∞, respectively. Three portions of the free streamlines provide an overlapping boundary between points *F* and *G* in the hodograph plane. With the unknown volumetric rate of discharge ψ_o as the normalizing factor for the stream function, they assume zero and unity stream function values, respectively. It should be stressed that inasmuch as the free streamline is a line of constant velocity and the asymptotic state must assume a horizontal flow direction, the overlapping boundary is a special feature of the axisymmetric incompressible flow. The authors are unaware of any other problem with overlapping boundary of this nature and are at a loss in an attempt to deal with this situation rigorously. For the case presented in Fig. 2 whose hodograph is shown in Fig. 4, the overalapping boundary no longer exists. It is interesting to note that in both cases, the center streamline accelerates initially to a state *H* and decelerates subsequently until the stagnation state *D* is reached. This fact imposes the condition of $\psi = 0$ along the vertical line A_1H and *HD* in the hodograph plane. Although A_1H and *HD* are essentially the same segments along the vertical line *AG* in the hodograph, they do correspond to separate segments along the axis of symmetry in the physical plane. It is now clear that values of the stream function are completely specified along the boundary of the hodograph domain. For the overlapping boundary, it seems to be reasonable that the condition of $\psi = 1$ should be imposed since it is the stream function of the bounding streamline immediately adjacent to the hodograph domain. Thus, they provide a well posed boundary value problem in the hodograph plane. The velocity at the point *H*, V_H, and the angle at the point *F*, θ_F, are important parameters of the problem.

Governing Equations. In parallel with the hodograph transformation for the two-dimensional flow, Fenain et al. (1974), obtained the corresponding equations for the axisymmetric problem. In order to make a self-contained presentation for the present investigation, the derivation is briefly outlined below:

From the conventional definitions of

$$\phi_z = u = V\cos\theta,\ \phi_r = v = V\sin\theta^1$$

$$\psi_r = ru,\ \psi_z = -rv$$

for the axisymmetric potential flow, one has

$$d\phi = V\cos\theta\, dz + V\sin\theta\, dr \tag{1a}$$

$$d\psi = -r\,V\sin\theta\, dz + r\,V\cos\theta\, dr. \tag{1b}$$

Upon treating $d\phi$ and $d\psi$ as functions of V and θ, so that

$$d\phi = \phi_V dV + \phi_\theta d\theta$$

$$d\psi = \psi_V dV + \psi_\theta d\theta,$$

one may solve dz and dr from equation (1) and obtain

$$dz = \left(\frac{\cos\theta}{V}\phi_V - \frac{\sin\theta}{rV}\psi_V\right)dV + \left(\frac{\cos\theta}{V}\phi_\theta - \frac{\sin\theta}{rV}\psi_\theta\right)d\theta \tag{2a}$$

$$dr = \left(\frac{\sin\theta}{V}\phi_V + \frac{\cos\theta}{rV}\psi_V\right)dV + \left(\frac{\sin\theta}{V}\phi_\theta + \frac{\cos\theta}{rV}\psi_\theta\right)d\theta. \tag{2b}$$

Equation (2) implies that

$$z_V = \frac{\cos\theta}{V}\phi_V - \frac{\sin\theta}{rV}\psi_V,$$

$$z_\theta = \frac{\cos\theta}{V}\phi_\theta - \frac{\sin\theta}{rV}\psi_\theta \tag{3a}$$

[1] Here subscripts denote differentiation.

Downloaded 03 May 2010 to 171.66.16.27. Redistribution subject to ASME license or copyright; see http://www.asme.org/terms/Terms_Use.cfm

$$r_V=\frac{\sin\theta}{V}\phi_V+\frac{\cos\theta}{r\,V}\psi_V,$$

$$r_\theta=\frac{\sin\theta}{V}\theta_\theta+\frac{\cos\theta}{r\,V}\psi_\theta. \tag{3b}$$

Since $z_{V\theta}=z_{\theta V}$, and $r_{V\theta}=r_{\theta V}$, equations (3a) and (3b) may be cross differentiated to yield

$$\phi_\theta=\frac{V\psi_V}{r} \tag{4a}$$

$$\phi_V=\frac{1}{r\,V}\left[-\psi_\theta+\frac{V}{2y}(y_\theta\psi_V-y_V\psi_\theta)\right] \tag{4b}$$

with $y=r^2/2$. Equation (3b) can be written now as

$$y_\theta=\sin\theta\,\psi_V+\frac{\cos\theta}{V}\psi_\theta \tag{5a}$$

$$y_V=\frac{1}{V}\left[\psi_V\cos\theta-\frac{\sin\theta}{V}\psi_\theta+\frac{S}{V}\right] \tag{5b}$$

with

$$S=\frac{V(y_\theta\psi_V-y_V\psi_\theta)\sin\theta}{2y}. \tag{5c}$$

Equation (3a) can also be written as

$$rz_\theta=\cos\theta\,\psi_V-\frac{\sin\theta}{V}\psi_\theta \tag{6a}$$

and

$$rz_V=\frac{1}{V}\left(-\frac{\cos\theta}{V}\psi_\theta-\sin\theta\,\psi_V+\frac{S}{V}\cot\theta\right). \tag{6b}$$

Since $y_{\theta V}=y_{V\theta}$, cross differentiations of equations (5a) and (5b) yield

$$V^2\psi_{VV}+V\psi_V+\psi_{\theta\theta}=\frac{1}{\sin\theta}\frac{\partial S}{\partial\theta} \tag{7}$$

where S can also be written as

$$S=\frac{(V^2\psi_V{}^2+\psi_\theta{}^2)\sin^2\theta}{2\,y\,V+\sin\theta\,\psi_\theta} \tag{8}$$

on account of equations (5a) and (5b). It is recognized that the right-hand side term of equation (7) is the only difference between the governing equations of a two-dimensional and an axisymmetric flow.

So far, all these equations are expressed in dimensional quantities. It will be extremely convenient to normalize V, θ, z, r, ψ by V_∞, α, R_c and ψ_o, respectively, ψ_o being the unknown volumetric rate of discharge per radian from the vessel. After normalization, equations (5) through (8) are changed, respectively, into

$$V^2\psi_{VV}+V\psi_V+\psi_{\theta\theta}/\alpha^2=\frac{1}{\alpha\sin(\alpha\,\theta)}\frac{\partial S}{\partial\theta} \tag{9}$$

$$S=\frac{(V^2\psi_V{}^2+\psi_\theta{}^2/\alpha^2)\sin^2(\alpha\,\theta)}{2\,y\,V\left(\frac{R_c{}^2V_\infty}{\psi_o}\right)+\frac{\sin(\alpha\,\theta)}{\alpha}\psi_\theta} \tag{10}$$

$$y_\theta=\frac{\psi_o}{R_c{}^2V_\infty}\left(\alpha\sin(\alpha\,\theta)\psi_V+\frac{\cos(\alpha\,\theta)}{V}\psi_\theta\right) \tag{11a}$$

$$y_V=\frac{\psi_o}{R_c{}^2V_\infty}\left[\frac{\psi_V\cos(\alpha\,\theta)}{V}-\frac{\sin(\alpha\,\theta)}{\alpha\,V^2}\psi_\theta+\frac{S}{V^2}\right] \tag{11b}$$

$$r\,z_\theta=\frac{\psi_o}{R_c{}^2V_\infty}\left(\alpha\cos(\alpha\,\theta)\psi_V-\frac{\sin(\alpha\,\theta)}{V}\psi_\theta\right) \tag{12a}$$

$$r\,z_v=\frac{\psi_o}{R_c{}^2V_\infty}\left(-\frac{\cos(\alpha\,\theta)}{\alpha\,V^2}\psi_\theta-\frac{\sin(\alpha\,\theta)}{V}\psi_V+\frac{S\cot(\alpha\,\theta)}{V^2}\right) \tag{12b}$$

where all variables are dimensionless. $\psi_o/R_c{}^2\,V_\infty$ becomes an important parameter. If one defines a discharge coefficient C_d from

$$C_d=\frac{\psi_o}{\frac{R_c{}^2V_\infty}{2}} \tag{13}$$

$\psi_o/R_c^2\,V_\infty$ is precisely one-half of the unknown discharge coefficient.

Numerical Solution. With the boundary values completely specified for the hodograph domain as shown in Figs. 3 or 4, solutions for equation (9) is established through numerical computations for selected parametric values of V_H and θ_F. It should be noted that discontinuities of ψ along the boundaries of the hodograph domain are inherent to the method of hodograph transformation. It was our experience that no special treatment of these singularities, such as that outlined by Fenain et al. (1974), is necessary. Equation (9) is, in fact, nonlinear. It may be solved through iterations by assuming initially the function S vanishing everywhere throughout the domain. After the ψ values are established through numerical computations, the derivatives ψ_θ and ψ_V may be formed through differentiations and the y values may be obtained through integration of equations (11a) and (11b). The function S can now be established throughout the hodograph domain. These processes are repeated until the function S does not change more than a small margin for every grid point. The solution is thus established. The values of z_E and R_E may be found by performing additional integration of equation (12). Free streamlines may also be traced. These numerical procedures are briefly described in a step-by-step fashion as follows:

(1) For a typical grid (i, j), where i and j are the indices of θ and V coordinates, respectively, the central finite difference form of equation (8) may be written as

$$\left(V_j^2-\frac{V_j\Delta V}{2}\right)\psi_{i,j-1}-\left(2\,V_j^2+\frac{2\,\Delta V^2}{\alpha^2\,\Delta\theta^2}\right)\psi_{i,j}+\left(V_j^2+\frac{V_j\,\Delta V}{2}\right)\psi_{i,j+1}$$

$$=-\frac{(\Delta V)^2}{\alpha^2(\Delta\theta)^2}(\psi_{i+1,j}+\psi_{i-1,j})-RS(\Delta V)^2 \tag{14}$$

where RS stands for $1/(\alpha\sin\theta)\,\partial S/\partial\theta$.

With $RS=0$ initially, ψ values at any point in the hodograph plane may be computed through the Gauss-Seidal point-by-point relaxation procedure or the successive line over relaxation scheme. An over relaxation factor may be used. Computation of the ψ function is carried out until the change of ψ is less than an arbitrarily small number for every grid point (e.g., 10^{-6}). The ψ function is now converged.

(2) The derivatives ψ_θ and ψ_V may be formed afterwards through

$$\psi_{\theta(i,j)}=(\psi_{i+1,j}-\psi_{i-1,j})/2\,\Delta\theta \tag{15}$$

Downloaded 03 May 2010 to 171.66.16.27. Redistribution subject to ASME license or copyright; see http://www.asme.org/terms/Terms_Use.cfm

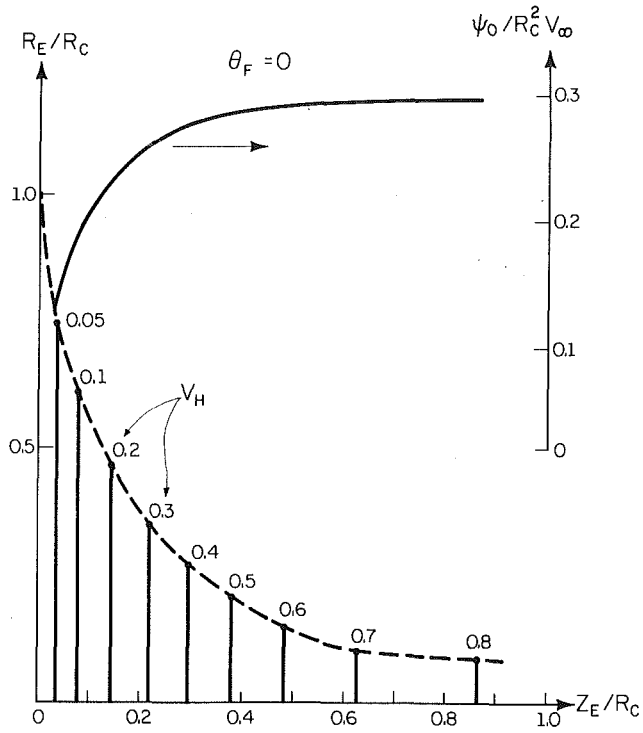


Fig. 5 Results for $\theta_F = 0$

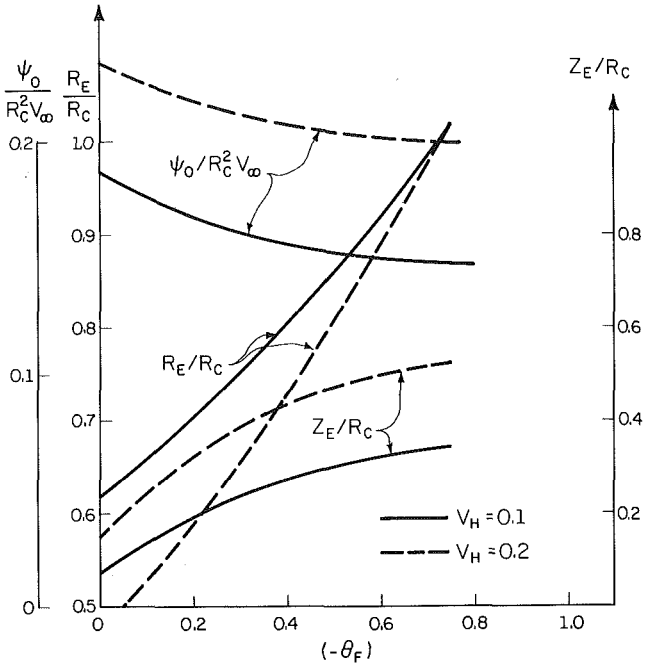


Fig. 6 Typical results for $\theta_F < 0$

$$\psi_{V(i,j)} = (\psi_{i,j+1} - \psi_{i,j-1})/2\,\Delta\,V. \tag{16}$$

For points on the boundary, one-sided difference form is employed for ψ_θ or ψ_V. Typical expressions of this nature may be given by

$$\psi_{\theta(1,j)} = (-3\,\psi_{1,j} + 4\,\psi_{2,j} - \psi_{3,j})/2\,\Delta\,\theta \tag{17}$$

and

$$\psi_{V(i,m)} = (3\,\psi_{i,m} - 4\,\psi_{i,m-1} + \psi_{i,m-2})/2\,\Delta\,V. \tag{18}$$

(3) One now integrates equation (11*a*) from H to Q in the hodograph plane with the initial condition of $y_H = 0$. Subsequently, equation (11*b*) is integrated from Q toward C. In all these integrations, the factor $\psi_o/R_c^2\ V_\infty$ is needed and its value is established through iterations by imposing the end condition of $y_c = 1/2$. Also within each step of the integration of equation (11*b*), S and thus y values are needed for the evaluation of the integrand and local iterations are employed to establish their values. These iterative processes have been found to be rapidly convergent.

(4) With the established factor $\psi_o/R_c^2\ V_\infty$, function y may be established for all grid points by integrating equation (11*a*). S function may be also be established accordingly.

(5) With the S function established, the factor $1/(\alpha \sin \alpha\theta)$ $\partial S/\partial\theta$ may be formed through numerical differentiation. For all points of $\theta = 0$ but with $V > V_H$, this factor should be evaluated instead by

$$\frac{1}{\alpha \sin}\frac{\partial S}{\partial \theta}\bigg|_{\theta\to 0} = \frac{V^2\psi_V{}^2 + \psi_\theta{}^2/\alpha^2}{y\,V\left(\dfrac{R_c{}^2 V_\infty}{\psi_o}\right)}. \tag{19}$$

(6) With the revised RS factor, procedures 1 through 5 may be repeated until the change in S function for each grid point is less than a small margin. Since the second-order central-difference formula has been adopted for expressions of derivatives, the small margin should be of the order of $(\Delta V)^2$ or $(\Delta\theta)^2$. Margins smaller than this may yield nonsensible computations.

Results of Computation

A 41 × 21 uniform grid was employed for these computations (i.e., $\Delta\,V = \Delta\,\theta = 0.05$). One may expect that for some values of V_H and θ_F, S function corresponding to the solution may be quite large and it must be brought to the final solution slowly and smoothly. This anticipation suggests that under relaxation factors must be used. This was indeed the case.

Figure 5 shows the results for $\theta_F = 0$ but with a wide range of V_H values. The corresponding axial locations Z_E and the valve radius R_E are presented in the lower portion of the graph. The corresponding values of $\psi_o/R_c{}^2\ V_\infty$ are also reported. The under relaxation factor for S functions varied from 0.5 for $0.1 \le V_H \le 0.4$, 0.25 for $0.5 \le V_H \le 0.8$. Iteration of S function would lead to divergence if 0.5 were used for the case of $V_H = 0.5$. However, an under relaxation factor of 0.05 was needed for the case of $V_H = 0.05$. A good check of accuracy of computations came from the fact that tracing the free streamines CG and EG after convergence would establish the radii R_{Gu}, R_{Gl} at the asymptotic state G. The difference $y_{Gu} - y_{Gl}$ should be equivalent to $\psi_o/R_c{}^2\ V_\infty$. These two values have been found to be agreeable within a fraction of one percent for all cases presented here including $V_H = 0.05$.

Figure 6 shows the results for different negative θ_F values for both cases of $V_H = 0.1$ and $V_H = 0.2$. As expected, larger negative θ_F values correspond to valves with larger radius R_E, however, located at a somewhat greater distance from the opening. The flow rate is also correspondingly reduced. Under-relaxation factors even smaller than the corresponding cases of $\theta_F = 0$ were needed to obtain these results. The solution for a valve with $R_E = 1$ at each constant V_H value can be obtained from interpolation. These interpolated results for different V_H values are presented in Fig. 7. It must be mentioned that considerable difficulty has been encountered for the case of $V_H = 0.05$. The results presented for this case were obtained after an additional transformation was introduced into the analysis. This transformation will be discussed in the next section. It is also interesting to note from interpolations of these results that the condition of $R_E = 1$ invariably occurred in the vicinity of $\theta_F = -0.72$. In tracing the free streamlines after the solution has been obtained for specific

Downloaded 03 May 2010 to 171.66.16.27. Redistribution subject to ASME license or copyright; see http://www.asme.org/terms/Terms_Use.cfm

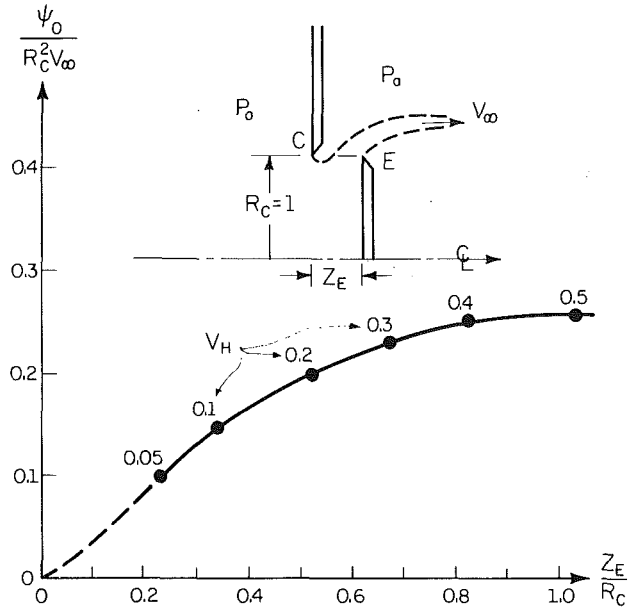


Fig. 7 Discharge characteristics of a valve

values of V_H and θ_F, the top free streamline ($\psi = 1$) can be easily established from C to T and T to F by integrating equations (11*a*) and (12*a*); T being the point of vanishing streamline angle below point C as indicated in Fig. 1. However, for the portion from F to G, if unity ψ value were used to evaluate ψ_V, needed in equations (11*a*) and (12*a*), retracing of the segment FT in the physical plane would have occurred since the only difference between tracing of the two parts in the hodograph plane was the direction of tracing. Similarly if $\psi = 0$ were employed for the lower free streamline between states F and G, a large change in ψ_V would occur in the vicinity of the point F which, in turn, would produce a more drastic change in the shape of the lower streamline. Both parts of these streamlines would not be realistic. It was then decided that a common average value of 0.5 was used for both streamlines within the range from F to G. Two sets of results so obtained are presented in Figs. 8(*a*) and 8(*b*). They depict, a more realistic picture of the flow, although confirmation of the accuracy of numerical computations from the asymptotic width of the jet as mentioned for cases of $\theta_F = 0$ can no longer rely upon the results obtained from such a manipulation.

Discussion

Referring to the set of results for $\theta_F = 0$ presented in Fig. 5, one may observe that for a valve situated at a specific axial loation, but having a radius larger than that indicated in the figure, it would offer more blockage to the jet flow, resulting in a negative θ_F value and in a corresponding reduction of the rate of discharge. On the other hand, for a valve with a radius smaller than that indicated in the figure, this condition may be treated as a result of upstream movement of a valve of this smaller size originally located at a certain downstream position on this curve. This upstream movement would reduce the rate of discharge in comparison with that at the original position, again yielding a negative θ_F value after the adjustment of the flow. This line of reasoning leads to the conclusion that θ_F shall always be negative although it may be very small and close to zero.

Furthermore, it seems that a limiting case can be expected for $\theta_F = 0$, i.e., a valve of vanishingly small size situated at a far downstream location. This case may be comparable with the case without a control valve, even when the present analysis always involves a stagnation process on the center streamline toward the state D and a subsequent acceleration to

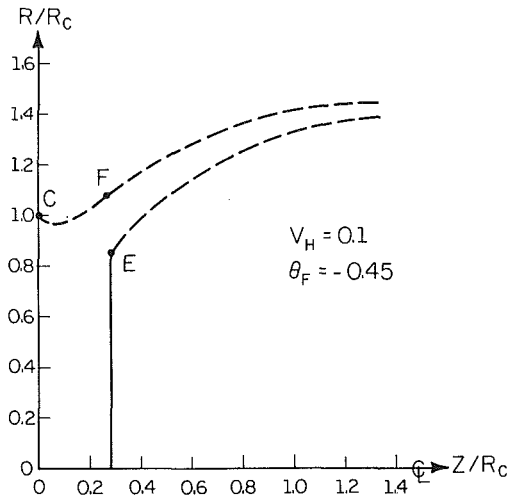


Fig. 8(*a*) Free streamline configurations for $V_H = 0.1$, $\theta_F = -0.45$

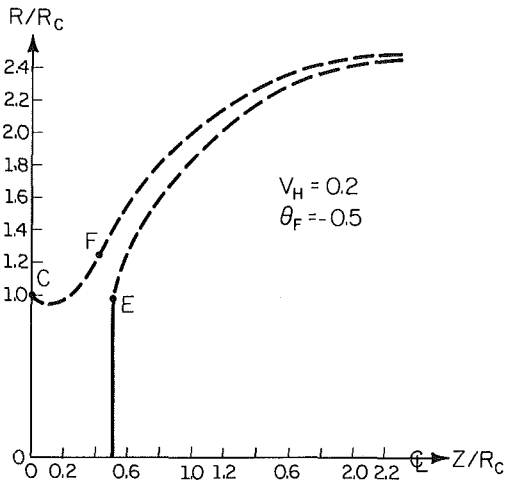


Fig. 8(*b*) Free streamline configurations for $V_H = 0.2$, $\theta_F = 0.5$

the state E. The discharge coefficients of the two cases are not much different. Incidentally, the flow discharge through an orifice from a reservoir (without a control valve) has been examined by Fenain et al. (1974), but the results have not been reported for cases of incompressible flow with different reservoir wall angles. The present computer program can easily be modified to produce these results. By imposing $\psi = 0$ throughout the vertical line A_1G in Fig. 3, restriction of the computations to only the right half of the rectangle produced the results presented in Fig. 9 where the contracting coefficients for different wall angles are plotted. No underrelaxation factor was needed (i.e., unity relaxation factor has been employed) for all angles of $|\alpha| \leq 120$ deg. It was indeed surprising to find that under relaxation factors of 0.2 and 0.1 were needed to obtain convergent results for $|\alpha| = 130$ deg and 140 deg, respectively. The corresponding well known results for two-dimensional flow are also plotted in the same figure for comparison purposes. The discharge coefficients for the axisymmetric case are, of course, the square of the contracting coefficient.

For values of $R_E = 1$, according to Fig. 6, it seems that the maximum rate of discharge has almost been reached at $z_E/R_c = 0.8$. This discharge coefficient is slightly below the corresponding value of discharge without a control valve. This seems to be reasonable since θ_F must assume a finite negative value for the discharge through a control valve.

Since the resolution of V_H in the 41 × 21 grid is limited, it was originally planned that a transformation in V coordinate

Downloaded 03 May 2010 to 171.66.16.27. Redistribution subject to ASME license or copyright; see http://www.asme.org/terms/Terms_Use.cfm

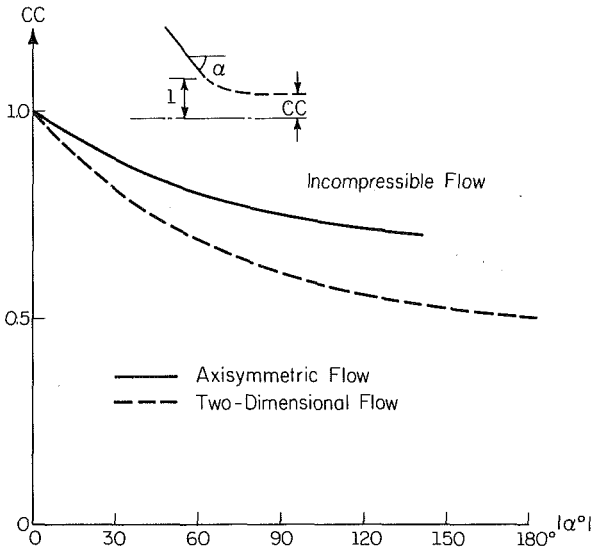


Fig. 9 Contracting coefficients of discharge through an orifice

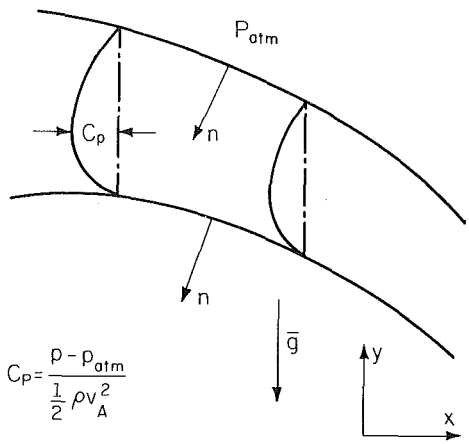


Fig. 10 Jet configuration and the pressure distribution across a free falling jet

be implemented so that any V_H value can be transformed to be coincident with a fixed grid point in the transformed coordinate. A transformation given by

$$w = \frac{v + Av^2}{1 + A} \tag{20}$$

was introduced. It is obvious that $w = 0$ at $v = 0$ and $w = 1$ at $v = 1$. The constant A is determined from the condition that $w = 0.1$ for any small V_H values. Such a transformation did promote faster convergence for $V_H > 0.1$ and also reproduced the results obtained without transformation. It has also produced the results for $V_H = 0.05$ although the free streamline tracings did not produce the correct configuration. The ψ variations became much more pronounced near the $w = 1$ grids due to this transformation.

Although no experimental data are available to verify the obtained discharge characteristics, the authors are confident that the performance of the valve obtained by the present investigation should not be far off from the actual flow situation. Certainly any experimental verification in the laboratory would provide an invaluable support for this present investigation.

It should now be mentioned that in the presence of gravity, the free streamlines can possess downward curved trajectories, even though the inside fluid has a higher-than-ambient pressure level. Taking the free falling jet from a sharp crested weir as an example (Han and Chow, 1981), the pressure distribution across the jet and the jet configuration are shown in Fig. 10. By examining the equation of motion normal to the streamline given as

$$\frac{V_s^2}{R} = -\frac{1}{\rho}\frac{\partial p}{\partial n} - g\frac{\partial y}{\partial n} \tag{21}$$

one notes that for the lower streamline, both $\partial p/\partial n$ and $\partial y/\partial n$ are less than zero, and the effect of curvature is balanced by the pressure and gravitational forces. For the top streamline, $\partial p/\partial n$ is now positive. Both the effect of curvature and the pressure force are balanced by the gravitational force. This consideration supports the conclusion that the jet configuration is curved downward even though the pressure of the fluid within the jet is higher than the ambient pressure. This is also the reason why the top free jet boundary assumes the shape given by that shown in Fig. 1 and reproduced in Fig. 8 from computations. However, one should realize that the gravitational effects cannot be considered in the present problem, since it would change itself into a three-dimensional case. Thus the manipulation of taking the average value of the stream function on the overlapping boundary was merely trying to reproduce a realistic jet boundary compatible with the only geometry which the jet can assume. Although it seems to be arbitrary, this manipulation can also be interpreted by the fact that the middle streamline ($\psi = 0.5$) is following such a trajectory. It may also be noted that taking the average of the two streamlines is possible only when the two are overlapping in the hodograph plane.

It may be further added that the present analysis has been extended to compressible flow regime. For supercritical pressure ratios, the sonic line and the free jet pattern have been successfully established. Under these conditions the phenomenon of overlapping boundary has been completely eliminated.

Conclusion

It may be concluded from this investigation that the hodograph transformation is indeed an effective method to deal with many problems of this type. Although, iteration of the solution must be carried out to match a given flow geometry, computations by modern computers can be so effectively executed that the disadvantage of the indirectness of the method has been entirely suppressed if not eliminated.

References

Chan, P., Han, T., and Chow, W. L., 1985, "Gravitational Flow from a Horizontal Duct," ASME JOURNAL OF APPLIED MECHANICS, Vol. 52, No. 1, pp. 167–171.

Chow, W. L., and Han, T., 1979, "Inviscid Solution for the Problem of Free Overall," ASME JOURNAL OF APPLIED MECHANICS, Vol. 46, No. 1, pp. 1–5.

Fenain, M., Dutouquet, L., and Solignac, J. L., 1974, "Calcul des Performances d'une Tu Yere Propulsive Convergente," *Proc. of the 9th Congress of the International Council of the Aeronautical Sciences*, Haifa, Vol. 2, pp. 691–705.

Han, T. Y., and Chow, W. L., 1981, "The Study of Sluice Gate and Sharp-Crested Weir Through Hodograph Transformation," ASME JOURNAL OF APPLIED MECHANICS, Vol. 48, pp. 229–238.

Milne-Thompson, L. M., 1950, *Theoretical Hydrodynamics*, 2nd Ed., McMillan, NY, p. 285.

Mises, R. V., 1917, "Berechnung von Ausfluss und Veherfallzahlen," *Zeitschrift des Vereines Deutshen Ingenieure*, Vol. 61, No. 22, pp. 469–474.

Wu, C., and Chow, W. L., 1985, "Study of an Asymmetric Flap Nozzle as a Vector-Thrust Device," *AIAA J. of Propulsive and Power*, Vol. 1, No. 4, pp. 286–291.

Downloaded 03 May 2010 to 171.66.16.27. Redistribution subject to ASME license or copyright; see http://www.asme.org/terms/Terms_Use.cfm

Journal of Applied Mechanics

Brief Notes

A Brief Note is a short paper that presents a specific solution of technical interest in mechanics but which does not necessarily contain new general methods or results. A Brief Note should not exceed 1500 words *or equivalent* (a typical one-column figure or table is equivalent to 250 words; a one line equation to 30 words). Brief Notes will be subject to the usual review procedures prior to publication. After approval such Notes will be published as soon as possible. The Notes should be submitted to the Technical Editor of the JOURNAL OF APPLIED MECHANICS. Discussions on the Brief Notes should be addressed to the Editorial Department, ASME, United Engineering Center, 345 East 47th Street, New York, N. Y. 10017, or to the Technical Editor of the JOURNAL OF APPLIED MECHANICS. Discussions on Brief Notes appearing in this issue will be accepted until two months after publication. Readers who need more time to prepare a Discussion should request an extension of the deadline from the Editorial Department.

The Strain-Energy Density of Compressible, Rubber-Like Axishells[1]

J. G. Simmonds[2]

A recent method for deriving, by descent from three dimensions, strain-energy densities in a first-approximation, large-strain theory of incompressible, elastically isotropic shells of revolution undergoing torsionless, axisymmetric deformation (axishells) is adapted to axishells made of compressible material. Application is made to the Blatz-Ko strain-energy densities for a polyurethane ("continuum") rubber and a foam rubber.

Introduction

In finite elasticity, incompressibility is a convenient mathematical assumption which is a good approximation in some rubbers but not all, as Blatz and Ko (1962) have observed. Moreover, spongy elastic materials such as foam rubber are obviously quite compressible. The aim herein is to show how to derive an approximate two-dimensional strain energy per unit undeformed area, V, for a circular plate of constant undeformed thickness h undergoing torsionless, axisymmetric deformation by descent from an isotropic three-dimensional strain energy per unit undeformed volume, W. I have the audacity to use "axishell" in the title because the first-approximation strain-energy density in a homogeneous shell, in which the undeformed reference surface is the midsurface, can be replaced by that for a plate to within a relative error of $O(hb + h^2k^2)$, where b is a measure of the curvature of the undeformed midsurface and k is a measure of the bending strains (Simmonds, 1985).

In a shell made of compressible material, we may, as does Koiter (1960) in the small-strain theory of elastic shells, assume a state of plane stress, i.e., we may assume that the derivative of W with respect to the transverse normal (Lagrangian) strain is zero. If this relation can be solved for the component of the Green's deformation tensor $\mathbf{G}$ associated with the direction of the axis of symmetry, then we are at a point where all the analysis developed by Simmonds (1986) for an incompressible plate applies.

An an example, V is computed for two special Blatz-Ko (1962) materials. In the limit as a "Poisson ratio" $\nu \to \frac{1}{2}$ for the continuum rubber, we recover the neo-Hookean strain-energy density for a plate derived by Simmonds (1986). To avoid unnecessary repetition, I will assume that the reader has Simmonds (1986) at hand.

Analysis

Let $d\bar{\mathbf{x}}$ denote the deformed image of a differential line element $d\mathbf{x}$. Then the Green deformation tensor is defined implicitly by $d\bar{\mathbf{x}}\cdot d\bar{\mathbf{x}} = d\mathbf{x}\cdot\mathbf{G}\cdot d\mathbf{x}$. The standard isotropic strain invariants (see, for example, Green and Adkins, 1970) are given in terms of $\mathbf{G}$ by $I_1 = \mathrm{tr}\mathbf{G}$, $I_2 = \frac{1}{2}(\mathrm{tr}\mathbf{G})^2 - \frac{1}{2}\mathrm{tr}\mathbf{G}^2$, and $I_3 = \det\mathbf{G}$, where tr denotes trace.

If a body undergoes axisymmetric deformation, then in a standard set of circular cylindrical coordinates (r, θ, z), the physical components of $\mathbf{G}$ are related to the physical components of the Lagrange strain tensor by

$$\begin{bmatrix} G_r & 0 & 2\Gamma \\ 0 & G_\theta & 0 \\ 2\Gamma & 0 & G_z \end{bmatrix} \equiv \begin{bmatrix} 1+2\Gamma_r & 0 & 2\Gamma \\ 0 & 1+2\Gamma_\theta & 0 \\ 2\Gamma & 0 & 1+2\Gamma_z \end{bmatrix}. \quad (1)$$

Furthermore,

$$I_1 = G_r + G_\theta + G_z \quad (2)$$

$$I_2 = G_rG_\theta + G_\theta G_z + G_zG_r - 4\Gamma^2 \quad (3)$$

$$I_3 = G_rG_\theta G_z - 4G_\theta\Gamma^2 \quad (4)$$

and the plane stress condition, because $G_z = 1 + 2\Gamma_z$, can be taken the form

$$\partial W/\partial G_z = 0. \quad (5)$$

If $W = W(I_1, I_2, I_3)$, then, by equations (1)–(4) and the chain rule, equation (5) implies that

$$W_1 + (G_r + G_\theta)W_2 + G_rG_\theta W_3 = 0, \quad (6)$$

where

$$W_i = \partial W/\partial I_i = \hat{W}_i(G_r, G_\theta, G_z, \Gamma^2). \quad (7)$$

Suppose that equation (6) has a solution of the form

$$G_z = \hat{G}_z(G_r, G_\theta, \Gamma^2). \quad (8)$$

Substituting this into equations (2)–(4) and the resulting expressions into $W \equiv Cw(I_1, I_2, I_3)$, where C is a convenient constant having the same dimensions as W, we have

$$w = \hat{w}(G_r, G_\theta, \hat{G}_z(G_r, G_\theta, \Gamma^2), \Gamma^2). \quad (9)$$

In a first-approximation shell theory, the effects of transverse shearing strains are ignored. To estimate the errors so incurred, assume that $\hat{w}$ is a differentiable function of Γ^2 for all

[1]This research was supported by the National Science Foundation under grant MSM-8412334.

[2]Department of Applied Mathematics, University of Virginia, Charlottesville, VA 22901.

Manuscript received by ASME Applied Mechanics Division, July 18, 1986.

Copyright © 1987 by ASME
Downloaded 03 May 2010 to 171.66.16.27. Redistribution subject to ASME license or copyright; see http://www.asme.org/terms/Terms_Use.cfm

values of G_r and G_θ of interest. Then using the mean value theorem and equations (2)–(5), we have

$$w = \hat{w}(G_r, G_\theta, \hat{G}_z(G_r, G_\theta, 0), 0) + (\partial \hat{w}/\partial \Gamma^2)_* \Gamma^2 \equiv \mathfrak{W}(G_r, G_\theta) - 4(w_2 + G_\theta w_3)_* \Gamma^2, \tag{10}$$

where the asterisk (*) indicates that a function is to be evaluated at $(G_r, G_\theta, \Gamma_*^2)$ with Γ_* some value between 0 and Γ. This expression is of the same form as the right side of equation (14) of Simmonds (1986). *Without invoking incompressibility*, that paper goes from equation (14) to equation (35), recopied here as

$$v \equiv \overset{0}{\mathfrak{W}} + \tfrac{1}{2}[(\overset{0}{\mathfrak{W}}_{(1,0)} + 2\lambda_r^2 \overset{0}{\mathfrak{W}}_{(2,0)})k_r^{*2} + 4\overset{0}{\mathfrak{W}}_{(1,1)}\lambda_r\lambda_\theta k_r^* k_\theta^* + (\overset{0}{\mathfrak{W}}_{(0,1)} + 2\lambda_\theta^2 \overset{0}{\mathfrak{W}}_{(0,2)})k_\theta^{*2}]\int q_0^2 \epsilon^2. \tag{11}$$

In this equation, $v \equiv V/Ch$; $\lambda_r = \sqrt{\overset{0}{G}_r}$ and $\lambda_\theta = \sqrt{\overset{0}{G}_\theta}$ are midsurface radial and hoop stretches; k_r^* and k_θ^* are dimensionless bending strains; q_0 is a function of the dimensionless variables $r^* \equiv r/L$ and $z^* \equiv 2z/h$, where L is any length characteristic of the deformation pattern; $\int$ is short for $\int_{-1}^{1} dz^*$; and $\epsilon = \tfrac{1}{2}(h/L)$. Furthermore, the following notation has been used: if $f = f(X, Y)$, $X = X(x, y, \epsilon)$, and $Y = Y(x, y, \epsilon)$, then

$$\overset{0}{f} \equiv f \text{ at } \epsilon = 0 \text{ and } f_{(m,n)} \equiv \frac{\partial^{m+n} f}{\partial X^m Y^n}. \tag{12}$$

Finally, we note that if the deformed reference surface $\bar{\mathcal{S}}$ has the vector parametric representation $\bar{\xi}(r, \theta)$, then q_0 is a first approximation to the component of $\bar{\mathbf{x}} - \bar{\xi}$ along the unit normal to $\bar{\mathcal{S}}$. In Simmonds (1986), q_0 is determined by the dynamic consistency condition $\int q_0 = 0$ and the incompressibility condition in the limit as $\epsilon \to 0$. Here, this latter condition is replaced by equation (8) in the limit as $\epsilon \to 0$ which, in view of equations (25)–(28) of Simmonds (1986), takes the form

$$\partial q_0/\partial z^* = \sqrt{\hat{G}_z(\lambda_r^2, \lambda_\theta^2, 0)}. \tag{13}$$

The solution of this equation satisfying the dynamic consistency condition is

$$q_0 = z^* \sqrt{\hat{G}_z(\lambda_r^2, \lambda_\theta^2, 0)}. \tag{14}$$

Examples: Two Blatz-Ko Materials

(*a*) *Polyurethane Rubber.* On the basis of their experiments on these rubbers, Blatz and Ko (1962) remark ". . . that [continuum] rubber is not nearly as incompressible as the linear theory would indicate" and propose the strain-energy density

$$W = \tfrac{1}{2}\mu\left(I_1 + \frac{1-2\nu}{\nu} I_3^{-\nu/(1-2\nu)} - \frac{1+\nu}{\nu}\right). \tag{15}$$

As the strains grow small, μ may be identified with the shear modulus $\tfrac{1}{2}E/(1+\nu)$, where E is Young's modulus, and ν with Poisson's ratio. Note that equation (15) approaches a neo-Hookean material as $\nu \to \tfrac{1}{2}$.

In view of equations (2)–(4), equation (6) takes the form

$$1 - G_r G_\theta (G_r G_\theta G_z - 4G_\theta \Gamma^2)^{-(1-\nu)/(1-2\nu)} = 0 \tag{16}$$

and hence from equations (2), (4), (10), and (15), with $C = E$,

$$\mathfrak{W} = \frac{1}{4(1+\nu)}\left[G_r + G_\theta + \frac{1-\nu}{\nu}(G_r G_\theta)^{-\nu/(1-\nu)} - \frac{1+\nu}{\nu}\right]. \tag{17}$$

(Another obvious choice for C is μ). Furthermore,

$$q_0 = z^*(\lambda_r \lambda_\theta)^{-\nu/(1-\nu)}. \tag{18}$$

Thus, equation (11) takes the form

$$v = \frac{1}{4(1+\nu)}\left\{\left[\lambda_r^2 + \lambda_\theta^2 + \frac{1-\nu}{\nu}(\lambda_r\lambda_\theta)^{-2\nu/(1-\nu)} - \frac{1+\nu}{\nu}\right] + \frac{h^2}{12(\lambda_r\lambda_\theta)^{2(1+\nu)/(1-\nu)}}\left[\left(\frac{1+\nu}{1-\nu} + \lambda_r^{2(1-\nu)}\lambda_\theta^{2\nu/(1-\nu)}\right)\lambda_\theta^2 k_r^2 + \frac{4\nu}{1-\nu}\lambda_r\lambda_\theta k_r k_\theta + \left(\frac{1+\nu}{1-\nu} + \lambda_r^{2\nu/(1-\nu)}\lambda_\theta^{2/(1-\nu)}\right)\lambda_r^2 k_\theta^2\right]\right\}, \tag{19}$$

where k_r and k_θ are dimensional bending strains. As $\nu \to \tfrac{1}{2}$, this expression approaches equation (45) of Simmonds (1986), providing we replace his erroneous factor of 1/8 by 1/6.

(*b*) *Foam Rubber.* For a polyurethane foam, 47 percent of whose volume consists of voids of about 40 microns in diameter, Blatz and Ko (1962) recommend, on the basis of experiments, the strain energy density

$$W = \tfrac{1}{2}\mu(I_2/I_3 + 2\sqrt{I_3} - 5). \tag{20}$$

Again, with $C = E$, it flows from equations (2)–(6) that

$$\mathfrak{W} = \frac{1}{4(1+\nu)}\left[3(G_r G_\theta)^{1/3} + \frac{1}{G_r} + \frac{1}{G_\theta} - 5\right] \tag{21}$$

while equation (14) reduces to

$$q_0 = z^*(\lambda_r\lambda_\theta)^{-1/3}. \tag{22}$$

Hence from equation (11),

$$v = \frac{1}{4(1+\nu)}\left\{[3(\lambda_r\lambda_\theta)^{2/3} + \lambda_r^{-2} + \lambda_\theta^{-2} - 5] + \frac{h^2}{12(\lambda_r\lambda_\theta)^2}\left[\left(3\lambda_r^{-8/3} - \frac{1}{3}\lambda_\theta^{2/3}\right)k_r^2 + \frac{4}{3}\lambda_r\lambda_\theta k_r k_\theta + \left(3\lambda_\theta^{-8/3} - \frac{1}{3}\lambda_r^{2/3}\right)k_\theta^2\right]\right\}. \tag{23}$$

Setting $\lambda_r^2 = 1 + 2\gamma_r$ and $\lambda_\theta^2 = 1 + 2\gamma_\theta$ and expanding the above expression in powers of the strains, one verifies that the leading terms are quadratic in the extensional and bending strains and agree with those of an elastically isotropic plate with Poisson's ratio $\nu = 1/4$.

References

Blatz, P. J., and Ko, W. L., 1962, "Application of Finite Elastic Theory to the Deformation of Rubbery Materials," *Trans. Soc. Rheology*, Vol. 6, pp. 233–251.

Koiter, W. T., 1960, "A Consistent First Approximation in the General Theory of Elastic Shells," The Theory of Thin Elastic Shells, Proc. Symp. Delft, 1959, Koiter, W. T., ed., North-Holland, pp. 12–33.

Simmonds, J., 1985, "The Strain Energy Density of Rubber-Like Shells," *Int. J. Solids Structures*, Vol. 21, pp. 67–77.

Simmonds, J. G., 1986, "The Strain-Energy Density of Rubber-Like Shells of Revolution Undergoing Torsionless, Axisymmetric Deformation (Axishells)," ASME Journal of Applied Mechanics, Vol. 53, pp. 593–596.

An Approximation for Deep Crack-Front Perturbation

L. R. F. Rose[3]

Introduction

Rice (1985) has recently derived an integral representation for the first-order variation δK in the stress intensity factor K

[3]Senior Research Scientist, Aeronautical Research Laboratories, Melbourne, 3001, Australia.

Manuscript received by ASME Applied Mechanics Division, July 8, 1986; final revision September 29, 1986.

Downloaded 03 May 2010 to 171.66.16.27. Redistribution subject to ASME license or copyright; see http://www.asme.org/terms/Terms_Use.cfm

values of G_r and G_θ of interest. Then using the mean value theorem and equations (2)–(5), we have

$$w = \hat{w}(G_r, G_\theta, \hat{G}_z(G_r, G_\theta, 0), 0) + (\partial \hat{w}/\partial \Gamma^2)_* \Gamma^2 \equiv \mathcal{W}(G_r, G_\theta) - 4(w_2 + G_\theta w_3)_* \Gamma^2, \tag{10}$$

where the asterisk $(*)$ indicates that a function is to be evaluated at $(G_r, G_\theta, \Gamma_*^2)$ with Γ_* some value between 0 and Γ. This expression is of the same form as the right side of equation (14) of Simmonds (1986). *Without invoking incompressibility*, that paper goes from equation (14) to equation (35), recopied here as

$$v \equiv \overset{0}{\mathcal{W}} + \tfrac{1}{2}[(\overset{0}{\mathcal{W}}_{(1,0)} + 2\lambda_r^2 \overset{0}{\mathcal{W}}_{(2,0)})k_r^{*2} + 4\overset{0}{\mathcal{W}}_{(1,1)}\lambda_r\lambda_\theta k_r^* k_\theta^* + (\overset{0}{\mathcal{W}}_{(0,1)} + 2\lambda_\theta^2 \overset{0}{\mathcal{W}}_{(0,2)})k_\theta^{*2}]\int q_0^2 \epsilon^2. \tag{11}$$

In this equation, $v \equiv V/Ch$; $\lambda_r = \sqrt{\overset{0}{G}_r}$ and $\lambda_\theta = \sqrt{\overset{0}{G}_\theta}$ are midsurface radial and hoop stretches; k_r^* and k_θ^* are dimensionless bending strains; q_0 is a function of the dimensionless variables $r^* \equiv r/L$ and $z^* \equiv 2z/h$, where L is any length characteristic of the deformation pattern; $\int$ is short for $\int_{-1}^{1} dz^*$; and $\epsilon = \tfrac{1}{2}(h/L)$. Furthermore, the following notation has been used: if $f = f(X, Y)$, $X = X(x, y, \epsilon)$, and $Y = Y(x, y, \epsilon)$, then

$$\overset{0}{f} \equiv f \text{ at } \epsilon = 0 \text{ and } f_{(m,n)} \equiv \frac{\partial^{m+n} f}{\partial X^m Y^n}. \tag{12}$$

Finally, we note that if the deformed reference surface $\bar{\mathcal{S}}$ has the vector parametric representation $\bar{\xi}(r, \theta)$, then q_0 is a first approximation to the component of $\bar{\mathbf{x}} - \bar{\xi}$ along the unit normal to $\bar{\mathcal{S}}$. In Simmonds (1986), q_0 is determined by the dynamic consistency condition $\int q_0 = 0$ and the incompressibility condition in the limit as $\epsilon \to 0$. Here, this latter condition is replaced by equation (8) in the limit as $\epsilon \to 0$ which, in view of equations (25)–(28) of Simmonds (1986), takes the form

$$\partial q_0/\partial z^* = \sqrt{\hat{G}_z(\lambda_r^2, \lambda_\theta^2, 0)}. \tag{13}$$

The solution of this equation satisfying the dynamic consistency condition is

$$q_0 = z^* \sqrt{\hat{G}_z(\lambda_r^2, \lambda_\theta^2, 0)}. \tag{14}$$

Examples: Two Blatz-Ko Materials

(*a*) *Polyurethane Rubber.* On the basis of their experiments on these rubbers, Blatz and Ko (1962) remark ". . . that [continuum] rubber is not nearly as incompressible as the linear theory would indicate" and propose the strain-energy density

$$W = \tfrac{1}{2}\mu\left(I_1 + \frac{1-2\nu}{\nu} I_3^{-\nu/(1-2\nu)} - \frac{1+\nu}{\nu}\right). \tag{15}$$

As the strains grow small, μ may be identified with the shear modulus $\tfrac{1}{2}E/(1+\nu)$, where E is Young's modulus, and ν with Poisson's ratio. Note that equation (15) approaches a neo-Hookean material as $\nu \to \tfrac{1}{2}$.

In view of equations (2)–(4), equation (6) takes the form

$$1 - G_r G_\theta (G_r G_\theta G_z - 4G_\theta \Gamma^2)^{-(1-\nu)/(1-2\nu)} = 0 \tag{16}$$

and hence from equations (2), (4), (10), and (15), with $C = E$,

$$\mathcal{W} = \frac{1}{4(1+\nu)}\left[G_r + G_\theta + \frac{1-\nu}{\nu}(G_r G_\theta)^{-\nu/(1-\nu)} - \frac{1+\nu}{\nu}\right]. \tag{17}$$

(Another obvious choice for C is μ). Furthermore,

$$q_0 = z^*(\lambda_r \lambda_\theta)^{-\nu/(1-\nu)}. \tag{18}$$

Thus, equation (11) takes the form

$$v = \frac{1}{4(1+\nu)}\left\{\left[\lambda_r^2 + \lambda_\theta^2 + \frac{1-\nu}{\nu}(\lambda_r\lambda_\theta)^{-2\nu/(1-\nu)} - \frac{1+\nu}{\nu}\right] + \frac{h^2}{12(\lambda_r\lambda_\theta)^{2(1+\nu)/(1-\nu)}}\left[\left(\frac{1+\nu}{1-\nu} + \lambda_r^{2(1-\nu)}\lambda_\theta^{2\nu/(1-\nu)}\right)\lambda_\theta^2 k_r^2 + \frac{4\nu}{1-\nu}\lambda_r\lambda_\theta k_r k_\theta + \left(\frac{1+\nu}{1-\nu} + \lambda_r^{2\nu/(1-\nu)}\lambda_\theta^{2/(1-\nu)}\right)\lambda_r^2 k_\theta^2\right]\right\}, \tag{19}$$

where k_r and k_θ are dimensional bending strains. As $\nu \to \tfrac{1}{2}$, this expression approaches equation (45) of Simmonds (1986), providing we replace his erroneous factor of 1/8 by 1/6.

(*b*) *Foam Rubber.* For a polyurethane foam, 47 percent of whose volume consists of voids of about 40 microns in diameter, Blatz and Ko (1962) recommend, on the basis of experiments, the strain energy density

$$W = \tfrac{1}{2}\mu(I_2/I_3 + 2\sqrt{I_3} - 5). \tag{20}$$

Again, with $C = E$, it flows from equations (2)–(6) that

$$\mathcal{W} = \frac{1}{4(1+\nu)}\left[3(G_r G_\theta)^{1/3} + \frac{1}{G_r} + \frac{1}{G_\theta} - 5\right] \tag{21}$$

while equation (14) reduces to

$$q_0 = z^*(\lambda_r\lambda_\theta)^{-1/3}. \tag{22}$$

Hence from equation (11),

$$v = \frac{1}{4(1+\nu)}\left\{[3(\lambda_r\lambda_\theta)^{2/3} + \lambda_r^{-2} + \lambda_\theta^{-2} - 5] + \frac{h^2}{12(\lambda_r\lambda_\theta)^2}\left[\left(3\lambda_r^{-8/3} - \frac{1}{3}\lambda_\theta^{2/3}\right)k_r^2 + \frac{4}{3}\lambda_r\lambda_\theta k_r k_\theta + \left(3\lambda_\theta^{-8/3} - \frac{1}{3}\lambda_r^{2/3}\right)k_\theta^2\right]\right\}. \tag{23}$$

Setting $\lambda_r^2 = 1 + 2\gamma_r$ and $\lambda_\theta^2 = 1 + 2\gamma_\theta$ and expanding the above expression in powers of the strains, one verifies that the leading terms are quadratic in the extensional and bending strains and agree with those of an elastically isotropic plate with Poisson's ratio $\nu = 1/4$.

References

Blatz, P. J., and Ko, W. L., 1962, "Application of Finite Elastic Theory to the Deformation of Rubbery Materials," *Trans. Soc. Rheology*, Vol. 6, pp. 233–251.

Koiter, W. T., 1960, "A Consistent First Approximation in the General Theory of Elastic Shells," The Theory of Thin Elastic Shells, Proc. Symp. Delft, 1959, Koiter, W. T., ed., North-Holland, pp. 12–33.

Simmonds, J., 1985, "The Strain Energy Density of Rubber-Like Shells," *Int. J. Solids Structures*, Vol. 21, pp. 67–77.

Simmonds, J. G., 1986, "The Strain-Energy Density of Rubber-Like Shells of Revolution Undergoing Torsionless, Axisymmetric Deformation (Axishells)," ASME Journal of Applied Mechanics, Vol. 53, pp. 593–596.

An Approximation for Deep Crack-Front Perturbation

L. R. F. Rose[3]

Introduction

Rice (1985) has recently derived an integral representation for the first-order variation δK in the stress intensity factor K

[3]Senior Research Scientist, Aeronautical Research Laboratories, Melbourne, 3001, Australia.

Manuscript received by ASME Applied Mechanics Division, July 8, 1986; final revision September 29, 1986.

Copyright © 1987 by ASME

Downloaded 03 May 2010 to 171.66.16.27. Redistribution subject to ASME license or copyright; see http://www.asme.org/terms/Terms_Use.cfm

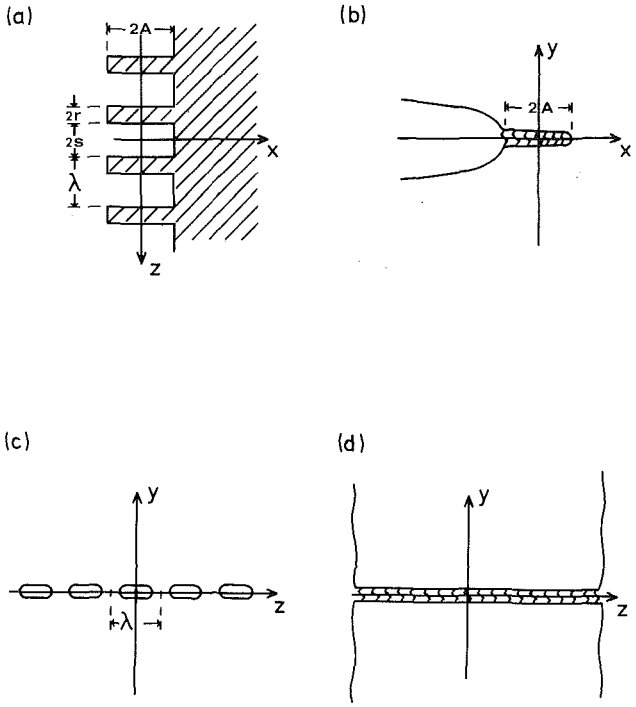


Fig. 1 *(a)* **Shape of crack-front perturbation considered; *(b)* equivalent reinforced crack tip; (c) periodic crack array in a slice taken along $x=0$; *(d)* equivalent springs**

due to a small-amplitude perturbation for an initially straight crack front. For a sinusoidal perturbation of amplitude A and wavelength λ, δK was shown to contain a contribution of order A/λ, which had not been obtained in a previous study by Meade and Keer (1984). This note presents a physically-based approximation for deep perturbations ($A>>\lambda$).

Analysis

Consider a planar semi-infinite crack with an initially straight crack front coinciding with the z axis, the crack lying along the half-plane $x<0$, $y=0$. Let the stress distribution for $x^2+y^2\to\infty$ reduce to the standard Mode I crack field of linear elasticity, specified by a nominal stress intensity factor K^N which will be assumed to remain fixed (so that $dK^N/da_o=0$ in equations (31), (33) of Rice, 1985). Consider now a periodic crack-front perturbation of the form shown in Fig. 1(*a*), having in mind especially the limit $A>>\lambda$. It seems reasonable to suggest that this configuration can be approximated by regarding the crack to extend to $x=A$, but with a uniform distribution of springs acting between the crack faces over the segment $|x|<A$, as indicated in the cross section in Fig. 1(*b*). To obtain the appropriate spring-constant, consider a thin slice taken along $x=0$, as shown in Fig. 1(*c*), with a view to modelling the periodic array of cracks along $y=0$ by springs, as indicated in Fig. 1(*d*). For fixed crack length $2s$ and spacing λ in Fig. 1(*c*), the corresponding springs in Fig. 1(*d*) transmit a stress σ_{yy} proportional to the crack-face displacement u_y as follows

$$\sigma_{yy}=E'ku_y,\ y\to 0+, \tag{1}$$

where $E'=E/(1-\nu^2)$ denotes the reduced Young's modulus for plane strain ($\epsilon_{xx}=0$). The spring constant k can be estimated by equating the interaction energy due to the presence of cracks in Fig. 1(*c*) with that due to the springs in Fig. 1(*d*), assuming a uniform applied stress. This gives

$$k\lambda=(\pi/2)/\log[\sec(\pi s/\lambda)]. \tag{2}$$

Using the correspondence between Fig. 1(*c*) and Fig. 1(*d*), one can associate a stress intensity factor K_L with a given spring-stretch $u_y(y\to 0+)$ in Fig. 1(*d*) as follows,

$$K_L=E'ku_y(y\to 0+)\{\lambda\tan(\pi s/\lambda)\}^{1/2} \tag{3}$$

This stress intensity factor is relevant to *lateral* crack growth for the configuration in Fig. 1(*a*), i.e., for increasing s with A fixed (Rose, 1987b).

The stress analysis for the sprung-crack configuration in Fig. 1(*b*) can be formulated as an integral equation for the dislocation density. The case where the spring constant k is assumed to be independent of x has been studied by Rose (1987a,b). Explicit results were obtained for the stress intensity factor K at the crack tip $x=A$ and for the crack opening at the trailing end of the sprung zone $u_y(x=-A,\ y\to 0+)$, in terms of the nominal (far-field) stress intensity factor K^N.

Discussion

The essential point of this note is to propose that the effect of deep crack-front perturbations can be approximated analytically, by using a straight crack front but with a boundary condition which differs from the usual stress-free boundary-condition across cracks. This approximation which is similar in spirit to the slender-body approximation for load-transfer to fibers (Russel and Acrivos, 1972), cannot provide a detailed prescription for the K-variation along the crack front in Fig. 1(*a*). However, the average stress intensity factor for the segments parallel to the x axis in Fig. 1(*a*) can be estimated from equation (3), and the crack opening at $x=-A$ in Fig. 1(*b*) can similarly be expected to provide an estimate for the average K over the trailing portions of the crack front lying on $x=-A$ in Fig. 1(*a*). It is also reasonable to suggest that the stress intensity factor K for the straight-fronted crack in Fig. 1(*b*) gives an estimate of $\bar{K}$, the average K along the leading portion of the crack front lying on $x=A$ in Fig. 1(*a*), in the sense that the energy release rate for advancing that leading portion, with s, λ fixed, can be equated to the energy release rate through the crack tip in Fig. 1(*b*), i.e.,

$$\bar{K}/K^N=(\lambda/2s)^{1/2}K/K^N, \tag{4}$$

$$=(\lambda/2s)^{1/2}F_1(2kA). \tag{5}$$

The important feature of this estimate is that the presence of springs in Fig. 1(*b*) introduces a characteristic length k^{-1} and the behavior for $kA>>1$ is different from that for $kA<<1$. In particular, for $kA>>1$, the variation $\delta\bar{K}$ (defined as $\bar{K}-K^N$) is obtained from equation (5) and Rose (1987a,b) as

$$\delta\bar{K}/K^N=-1+(\lambda/2s)^{1/2}(4\pi kA)^{-1/2},\ kA>>1, \tag{6}$$

i.e., $\delta\bar{K}/K^N$ is of order unity, unlike the result for shallow perturbations where $\delta K/K^N$ is of order A/λ (Rice, 1985). The approximation presented above is intuitively plausible only for $A>>\lambda$, but is reassuring to note that it provides the right order-of-magnitude estimate for $\delta\bar{K}$ in the limit $A<<\lambda$.

Acknowledgment

The writer is grateful to Professor J. R. Rice for his constructive comments on an earlier version of the present work.

References

Meade, K. P., and Keer, L. M., 1984, "Stress-Intensity Factors for a Semi-Infinite Crack with a Wavy Front," *Journal of Elasticity*, Vol. 14, pp. 79–92.

Rice, J. R., 1985, "First-Order Variation in Elastic Fields Due to Variation in Location of a Planar Crack Front," ASME JOURNAL OF APPLIED MECHANICS, Vol. 52, pp. 571–579.

Rose, L. R. F., 1987a, "Crack Reinforcement by Distributed Springs," *Journal of the Mechanics and Physics of Solids*, in press.

Rose, L. R. F., 1987b, "Toughening due to Crack-Front Interaction with a Second-Phase Dispersion," *Mechanics of Materials*, in press.

Russel, W. B., and Acrivos, A., 1972, "On the Effective Moduli of Composite Materials: Slender Rigid Inclusions at Dilute Concentrations," *Journal of Applied Mathematics and Physics (ZAMP)*, Vol. 23, pp. 434–463.

Downloaded 03 May 2010 to 171.66.16.27. Redistribution subject to ASME license or copyright; see http://www.asme.org/terms/Terms_Use.cfm

On the Mechanical Properties of Electro-Rheological Fluids

N. G. Stevens,[4] J. L. Sproston,[4] and R. Stanway[4]

1 Introduction

Electro-rheological (ER) fluids are formed by contaminating a base liquid with semiconducting particles. The application of an electrical field of sufficient intensity causes the particles to form chains which bridge the electrodes. By varying the electrical field, the resistance to flow of the ER fluid can be controlled and this phenomenon has a number of possible engineering applications. The application of ER fluids in torque transmission was suggested by Winslow (1947) and other uses, notably in vibrations engineering (Eige and Fraser, 1961) have been reported since then. However, it is only recently that engineers have recognized the wider possibilities of using ER fluids as an interface between various mechanical systems and the electronic circuits which provide control (Stangroom, 1983).

In previous articles (Sproston et al., 1983; Stevens et al., 1984, 1985) the authors have demonstrated that the construction and operation of ER devices is relatively straightforward although some control problems remain to be solved. Contributions at recent seminars (Institution of Mechanical Engineers, 1985) have shown that the engineering industry has been quick to grasp the possibilities of ER fluids and it appears that, behind closed doors, considerable developments are in progress. Unfortunately, the ease with which such developments can proceed does tend to obscure the fact that the basic mechanism through which ER fluids operate is still not properly understood. Such understanding is essential, of course, not only for academic satisfaction, but also to optimise the fluids chosen for use in engineering devices.

In addition to the continuing development of ER devices, current work at the University of Liverpool is aimed towards the derivation of mathematical models of ER fluids. Some of this work has been directed towards specific objectives, for example, the determination of a combined viscous plus Coulomb friction model to characterize the nonlinear behaviour of ER fluids in vibration (Stanway et al., 1985). At a more fundamental level, experiments are being developed to determine the static properties of ER fluids subjected to a range of combined electrical and mechanical stresses.

In what follows here, the authors describe one possible approach for obtaining the static properties of ER fluids in shear using equipment designed for the tensile testing of solids. The aim of the investigation is to determine the extent to which the shear properties of ER fluids can be controlled through the application of an external electrical field and to establish the influence of critical dimensions (electrode area and spacing, etc.) on the performance.

The tests are performed using only simple ER fluids and as such the maximum shear stress levels are lower than those which might be achieved using more recent products. Nevertheless, the authors believe that the characteristics of the ER fluids are accurately reflected and it was felt that a representative selection of results would be of interest to potential users of ER fluids as well as to those currently engaged in the development of mathematical models to describe their behavior.

[4]Department of Mechanical Engineering, P.O. Box 147, The University of Liverpool, Liverpool, England L69 3BX.

Manuscript received by ASME Applied Mechanics Division, March 4, 1986; final revision, July 14, 1986.

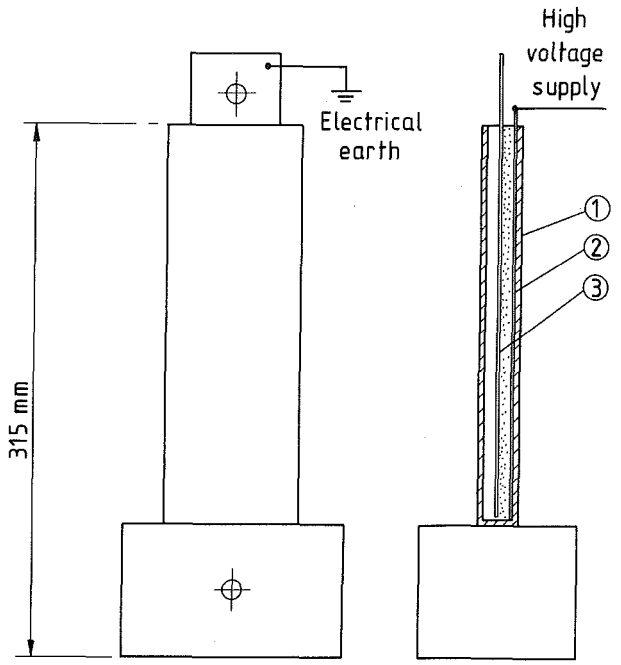


Fig. 1 Jig for shear testing of electro-rheological fluids (numbers are referred to in the text)

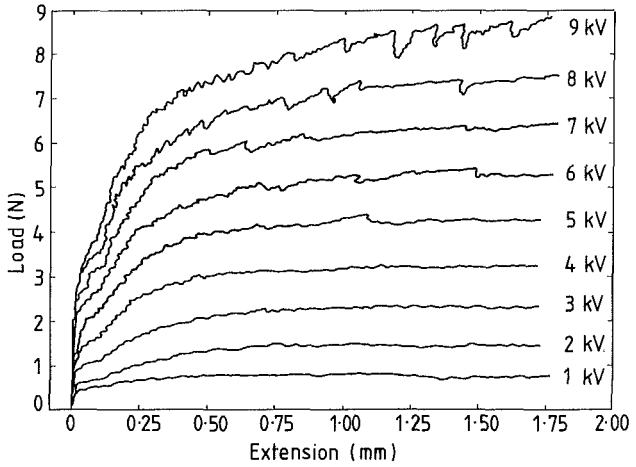


Fig. 2 Typical load versus extension characteristics for 100 cSt fluid, electrode separation of 6 mm and electrode area of 100 cm^2

2 Experimental Arrangement

2.1 Mechanical Apparatus. Under normal circumstances, it would not be appropriate to apply to fluids techniques which are designed to evaluate the static properties of solids. This is because the relatively high molecular spacings and low intermolecular forces associated with conventional fluids implies that fluids can sustain only negligibly small tensile and shear forces: thus the resolution available from a machine intended for testing solids would not be sufficient to produce meaningful results. In ER fluids, however, the application of an electric field of increasing intensity (e.g., from 0 to 3 kV/mm) results in the transition from a fluid to a solid state. Consequently, it is feasible to treat an ER fluid as though it were a solid.

A commercially-available tensile testing facility was used for the experiments. This machine provided a direct readout of stress/strain relationships for applied loads within the range from 0.05 N to 20 kN. The strain rate was variable from 0.5 to 7.5 mm/min and a control system ensured that the chosen rate was independent of the applied stress. To accom-

Copyright © 1987 by ASME
Downloaded 03 May 2010 to 171.66.16.27. Redistribution subject to ASME license or copyright; see http://www.asme.org/terms/Terms_Use.cfm

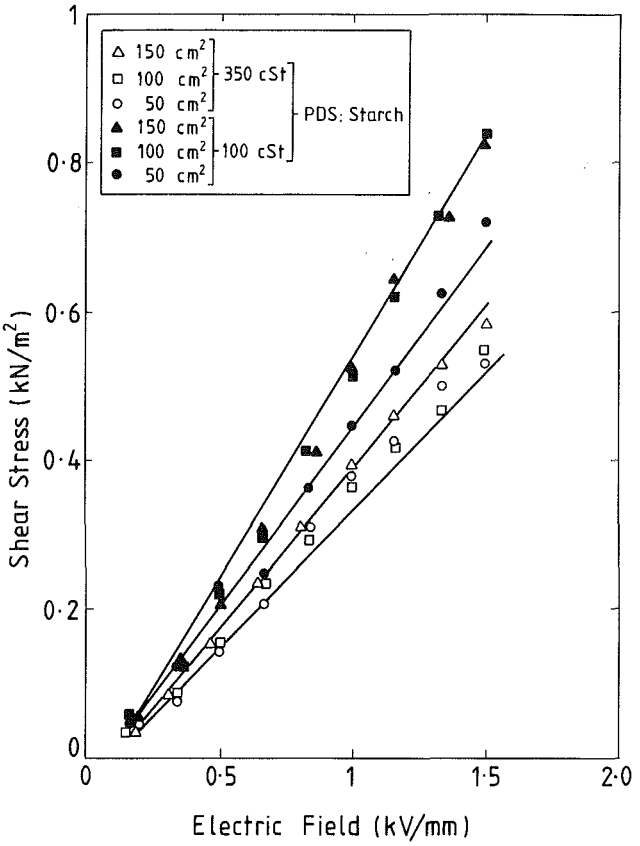


Fig. 3 Maximum sustainable shear stress versus electric field strength for both fluids, and for various active areas

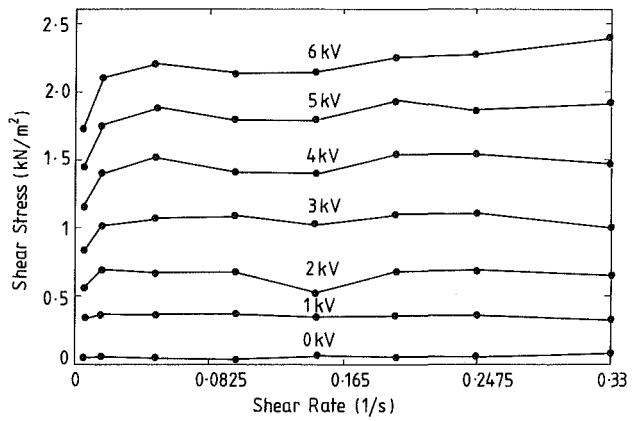


Fig. 4 Shear stress versus shear rate for 100 cSt fluid, active electrode area of 100 cm^2 and electrode gap of 3 mm

modate ER fluids (rather than solid test specimens) a series of jigs was designed and constructed: a typical jig is shown in Fig. 1. Referring to Fig. 1, the outer casing (1) is fabricated from insulating material. The inside faces of the casing are lined with thin copper sheets (2) which form the stationary, positive electrode. Bearings were machined from low-friction material (PTFE) to allow the negative electrode – a brass plate (3) – to slide freely inside the casing.

The ER fluid was contained in the gap between the two electrodes. In the tests described here, two jigs were used: one with a maximum effective electrode area of $A = 125$ cm^2, the other with a maximum area of $A = 250$ cm^2.

2.2 Electrical Arrangements. The electric field which excited the ER fluid was derived from a commercial high-voltage d-c generator which was capable of providing a potential difference of up to 30 kV between the electrodes. The applied voltage was measured by an analogue voltmeter while the current flowing through the ER fluid was measured by a digital ammeter. The electrical power supply was provided with an automatic circuit-breaker which interrupted the supply (in the experiments described here) when the field strength exceeded 5 kV/mm.

2.3 Electro-Rheological Fluids. The ER fluids used in the present experiments were identical to those used by the authors in previous studies of engineering applications (Stevens et al., 1984). The base liquid was polydimethylsiloxane (PDS) fluid contaminated in a 1:1 mass ratio by particles of soluble aliphatic starch whose size was in the range 5–50 μm. Two grades of PDS fluid were used – one with a viscosity of 100 cSt and the other with a viscosity of 350 cSt.

3 Experimental Work

3.1 Test Procedure. After carefully degreasing and then drying the electrodes, the jig (Fig. 1) was mounted on the tensile testing facility. The translating, negative electrode (3) was attached to the moving cross-head of the machine, while the casing (1) was attached to the fixed cross-head. To compensate for the weight of the moving electrode, the apparatus was adjusted initially so that the load-cell gave a zero reading. The reading of the internal extensometer (which indicates the position of the translating electrode) was also set to zero.

For a constant strain rate of 1 mm/min and for applied voltages in the range 0–10 kV, the translating electrode was dragged a total distance of $d = 2$ mm relative to the stationary electrode. During each test, the load/extension characteristic was recorded. A further series of tests was conducted with up to $d = 10$ mm of relative motion between the electrodes. The whole series of tests described above was then repeated using constant strain rates with values of up to 60 mm/min.

3.2 Typical Results. Figure 2 shows a typical set of load/extension characteristics at a number of discrete applied voltages from 1 to 9 kV. These results were obtained using a 100 cSt fluid, $d = 6$ mm and $A = 100$ cm^2. Again for $d = 6$ mm, the *maximum* shear stresses for both fluids and for three active electrode areas are shown plotted in Fig. 3. All the results shown in Figs. 2 and 3 were obtained using a constant strain rate of 1 mm/min.

A typical series of results showing the influence of shear rate on shear stress is presented in Fig. 4. These results were obtained using a 100 cSt fluid with $A = 100$ cm^2.

Throughout the entire series of tests the ambient temperatures remained within ± 1.5 percent of 19°C. The electrical excitation was not applied for a long enough time to cause any significant temperature rises in the ER fluid.

3.3 Discussion of Results. The load extension characteristics in Fig. 2 show that the ER fluid rapidly reaches a yield point and beyond this point the strain increases without any appreciable change in the applied load. The limiting shear load is determined by the applied potential. If the applied electric field strength is increased beyond the levels shown on Fig. 2, then electrical breakdown will eventually occur and this obviously places a limit on the maximum load which a given fluid can sustain. A further limitation is imposed by the ratchetting which was observed at higher field strengths. This ratchetting (which was more pronounced in the 100 cSt fluid) suggests that, beyond the yield point, a cycle involving brittle fracture followed by reformation is being established. Further work is required to explain this phenomenon which may be a feature of the particular ER fluids and test apparatus used in the investigations.

If the maximum shear stress is plotted against the electric field strength, Fig. 3, then the influence of the various active

Downloaded 03 May 2010 to 171.66.16.27. Redistribution subject to ASME license or copyright; see http://www.asme.org/terms/Terms_Use.cfm

areas increases with the electric field strength. The shear stress is generally a linear function of the electric field but the influence of the base fluid is evident: the base fluid with the lower viscosity (100 cSt) produces larger sustainable stresses.

In all the shear tests it was found that, apart from minor deviations at shear rates below 0.01/s, the shear stress was *not* dependent upon shear rate. This point is illustrated by the results in Fig. 4 which show that for a given electric field strength the shear stress is essentially constant up to a shear rate of 0.33/s. It transpires that it is indeed legitimate to treat the ER fluid as though it were a solid, provided that the electric field is strong enough to cause solidification.

4 Concluding Remarks

It is now well established that ER fluids are potentially valuable in a number of engineering applications. However, there is a noticeable absence of published data on the static and dynamic properties of these fluids and this will inevitably hinder the design and optimisation of devices which exploit the effect.

To complement a theoretical study to develop mathematical models, the authors have also embarked upon an experimental investigation. The tests described in this paper have been performed using commercially-available tensile testing apparatus and have shown that chemically simple ER fluids are capable of sustaining significant static shear loads and will produce consistent and repeatable results.

The maximum shear stress which the ER fluid can sustain is readily controlled through the applied electric field and is essentially a linear function of the field strength. Furthermore, the results show that the shear stress is essentially independent of the shear rate.

While the trends described above can be discerned from the results obtained so far, there remains considerable scope for the development of material testing techniques for use with ER fluids. Tests involving larger inter-electrode gaps give quite different results and indicate that further work is required to eliminate the effects of the test geometry. With larger gaps it is obviously more difficult to obtain uniform electrical and stress fields in the ER fluid. One simple improvement which can be made to future experimental apparatus is to introduce a control circuit which maintains a uniform electrical field irrespective of the relative positions of the electrodes. Work to develop such a circuit is currently underway.

Acknowledgments

The authors wish to acknowledge financial support of this work by the Ford Motor Company (U.K.).

References

Eige, J. J., and Fraser, E. C., 1961, "Feasibility Study of Vibration and Shock Exciter Using Electric Field Modulation of Hydraulic Power," WADD Technical Report No. 61-185, U.S.A.F. Stanford Research Institute, A.D. 268094.

Institution of Mechanical Engineers, 1984, Discussion Meeting on *Electroviscous Fluids and Their Applications*, London, and Institution of Electrical Engineers, 1985, Colloquium on *Electrically Active Fluids*, London, U.K.

Sproston, J. L., Stevens, N. G., and Page, I. M., 1983, "An Investigation of Torque Transmission Using Electrically-Stressed Dielectric Fluids," *Proceedings of "Electrostatics '83,"* University of Oxford, U.K., pp. 53–58.

Stangroom, J. E., 1983, "Electro-Rheological Fluids," *Physics in Technology*, Vol. 14, pp. 290–296.

Stanway, R., Sproston, J. L., and Stevens, N. G., 1985, "Nonlinear Identification of an Electro-Rheological Vibration Damper," *Proc. 7th IFAC Symposium on Identification and System Parameter Estimation*, York, U.K., pp. 195–200.

Stevens, N. G., Sproston, J. L., and Stanway, R., 1984, "Experimental Evaluation of a Simple Electroviscous Damper," *Journal of Electrostatics*, Vol. 15, pp. 275–283.

Stevens, N. G., Sproston, J. L., and Stanway, R., 1985, "The Influence of Pulsed D.C. Input Signals on Electro-Rheological Fluids," *Journal of Electrostatics*, Vol. 17, pp. 181–191.

Winslow, W. M., 1947, "Method and Means for Translating Electrical Impulses in Mechanical Force," US Patent Specification No. 2,417,850.

A Path-Independent Integral for Plates

K. B. Broberg[5]

Introduction

The J-integral is a very useful tool in fracture mechanics. It is formulated for plane cases and has, therefore, mostly been used to describe the stress intensity of cracks situated in plates subjected to in-plane loading. However, it is well known that such cases are mixed: plane strain is approached in the plate interior near the crack edge, plane stress far away. Therefore, an integral which preserves path-independence for plates would be advantageous. Indeed, such an integral exists.

The Path-Independent P-Integral

The path-independent $P(late)$-integral for in-plane loading is

$$P=\int_\Gamma [W_{av}dx_2-(n_j\sigma_{ji}\partial u_i/\partial x_1)_{av}ds] \quad (i=1,2,3;\ j=1,2) \tag{1}$$

where index av indicates the average over the plate thickness, Γ is a path in the midplane of the plate, W the strain energy per unit of volume, n_j a unit normal of Γ, u_i the displacement, x_j Cartesian coordinates with x_3 in the thickness direction, and s the arc-length along Γ. The stress σ_{ji} $(i, j=1,2,3)$ is defined as $\partial W/\partial u_{i,j}$ where $u_{i,j}=\partial u_i/\partial x_j$. With this definition the equilibrium equations take the form

$$\sigma_{ji,j}=0 \quad (i, j=1,2,3) \tag{2}$$

The path-independence can be proved by first considering the expression

$$P_1=\frac{1}{h}\int_S (Wn_1-n_j\sigma_{ji}\partial u_i/\partial x_1)dS \quad (i, j=1,2,3) \tag{3}$$

where S is the total surface of a plate bounded by the planes $x_3=\pm h/2$ and a cylindrical surface S_Γ parallel to the x_3 direction and cutting the plane $x_3=0$ along a closed path Γ entirely inside the plate. n_j is the outwards unit normal of S. By applying Green's theorem the surface integral can be transformed to a volume integral:

$$P_1=\frac{1}{h}\int_V [\partial W/\partial x_1-\partial(\sigma_{ji}\partial u_i/\partial x_1)/\partial x_j]dV \tag{4}$$

where V is the volume inside S. The equilibrium equations (2) together with the fact that W is a function of $u_{i,j}$ imply that

$$P_1=\frac{1}{h}\int_V (\partial W/\partial u_{i,j}\cdot\partial u_{i,j}/\partial x_1-\sigma_{ji}\partial^2 u_i/\partial x_j\partial x_1)dV \tag{5}$$

Thus $P_1=0$ because $\sigma_{ji}=\partial W/\partial u_{i,j}$.

The intersection between S_Γ and the plate surfaces encloses a surface A_+ on $x_3=h/2$ and A_- on $x_3=-h/2$. Then equation (3) can be written

$$P_1=\int_\Gamma [W_{av}n_1-(n_j\sigma_{ji}\partial u_i/\partial x_1)_{av}]ds$$

$$-\frac{1}{h}\int_{A_++A_-} n_3\sigma_{3i}\partial u_i/\partial x_1 dS \tag{6}$$

where $j\neq 3$, index av denotes the average over the plate thickness and s is the arc length along Γ, increasing in the direction for which n_i points to the right, seen from the positive x_3 side.

[5]Lund Institute of Technology, S-221 00 Lund, Sweden.

Manuscript received by ASME Applied Mechanics Division, September 10, 1986.

Downloaded 03 May 2010 to 171.66.16.27. Redistribution subject to ASME license or copyright; see http://www.asme.org/terms/Terms_Use.cfm

areas increases with the electric field strength. The shear stress is generally a linear function of the electric field but the influence of the base fluid is evident: the base fluid with the lower viscosity (100 cSt) produces larger sustainable stresses.

In all the shear tests it was found that, apart from minor deviations at shear rates below 0.01/s, the shear stress was *not* dependent upon shear rate. This point is illustrated by the results in Fig. 4 which show that for a given electric field strength the shear stress is essentially constant up to a shear rate of 0.33/s. It transpires that it is indeed legitimate to treat the ER fluid as though it were a solid, provided that the electric field is strong enough to cause solidification.

4 Concluding Remarks

It is now well established that ER fluids are potentially valuable in a number of engineering applications. However, there is a noticeable absence of published data on the static and dynamic properties of these fluids and this will inevitably hinder the design and optimisation of devices which exploit the effect.

To complement a theoretical study to develop mathematical models, the authors have also embarked upon an experimental investigation. The tests described in this paper have been performed using commercially-available tensile testing apparatus and have shown that chemically simple ER fluids are capable of sustaining significant static shear loads and will produce consistent and repeatable results.

The maximum shear stress which the ER fluid can sustain is readily controlled through the applied electric field and is essentially a linear function of the field strength. Furthermore, the results show that the shear stress is essentially independent of the shear rate.

While the trends described above can be discerned from the results obtained so far, there remains considerable scope for the development of material testing techniques for use with ER fluids. Tests involving larger inter-electrode gaps give quite different results and indicate that further work is required to eliminate the effects of the test geometry. With larger gaps it is obviously more difficult to obtain uniform electrical and stress fields in the ER fluid. One simple improvement which can be made to future experimental apparatus is to introduce a control circuit which maintains a uniform electrical field irrespective of the relative positions of the electrodes. Work to develop such a circuit is currently underway.

Acknowledgments

The authors wish to acknowledge financial support of this work by the Ford Motor Company (U.K.).

References

Eige, J. J., and Fraser, E. C., 1961, "Feasibility Study of Vibration and Shock Exciter Using Electric Field Modulation of Hydraulic Power," WADD Technical Report No. 61-185, U.S.A.F. Stanford Research Institute, A.D. 268094.

Institution of Mechanical Engineers, 1984, Discussion Meeting on *Electroviscous Fluids and Their Applications*, London, and Institution of Electrical Engineers, 1985, Colloquium on *Electrically Active Fluids*, London, U.K.

Sproston, J. L., Stevens, N. G., and Page, I. M., 1983, "An Investigation of Torque Transmission Using Electrically-Stressed Dielectric Fluids," *Proceedings of "Electrostatics '83,"* University of Oxford, U.K., pp. 53–58.

Stangroom, J. E., 1983, "Electro-Rheological Fluids," *Physics in Technology*, Vol. 14, pp. 290–296.

Stanway, R., Sproston, J. L., and Stevens, N. G., 1985, "Nonlinear Identification of an Electro-Rheological Vibration Damper," *Proc. 7th IFAC Symposium on Identification and System Parameter Estimation*, York, U.K., pp. 195–200.

Stevens, N. G., Sproston, J. L., and Stanway, R., 1984, "Experimental Evaluation of a Simple Electroviscous Damper," *Journal of Electrostatics*, Vol. 15, pp. 275–283.

Stevens, N. G., Sproston, J. L., and Stanway, R., 1985, "The Influence of Pulsed D.C. Input Signals on Electro-Rheological Fluids," *Journal of Electrostatics*, Vol. 17, pp. 181–191.

Winslow, W. M., 1947, "Method and Means for Translating Electrical Impulses in Mechanical Force," US Patent Specification No. 2,417,850.

A Path-Independent Integral for Plates

K. B. Broberg[5]

Introduction

The J-integral is a very useful tool in fracture mechanics. It is formulated for plane cases and has, therefore, mostly been used to describe the stress intensity of cracks situated in plates subjected to in-plane loading. However, it is well known that such cases are mixed: plane strain is approached in the plate interior near the crack edge, plane stress far away. Therefore, an integral which preserves path-independence for plates would be advantageous. Indeed, such an integral exists.

The Path-Independent P-Integral

The path-independent $P(late)$-integral for in-plane loading is

$$P=\int_\Gamma [W_{av}dx_2-(n_j\sigma_{ji}\partial u_i/\partial x_1)_{av}ds] \quad (i=1,2,3;\ j=1,2) \tag{1}$$

where index av indicates the average over the plate thickness, Γ is a path in the midplane of the plate, W the strain energy per unit of volume, n_j a unit normal of Γ, u_i the displacement, x_j Cartesian coordinates with x_3 in the thickness direction, and s the arc-length along Γ. The stress σ_{ji} $(i, j=1,2,3)$ is defined as $\partial W/\partial u_{i,j}$ where $u_{i,j}=\partial u_i/\partial x_j$. With this definition the equilibrium equations take the form

$$\sigma_{ji,j}=0 \quad (i, j=1,2,3) \tag{2}$$

The path-independence can be proved by first considering the expression

$$P_1=\frac{1}{h}\int_S (Wn_1-n_j\sigma_{ji}\partial u_i/\partial x_1)dS \quad (i, j=1,2,3) \tag{3}$$

where S is the total surface of a plate bounded by the planes $x_3=\pm h/2$ and a cylindrical surface S_Γ parallel to the x_3 direction and cutting the plane $x_3=0$ along a closed path Γ entirely inside the plate. n_j is the outwards unit normal of S. By applying Green's theorem the surface integral can be transformed to a volume integral:

$$P_1=\frac{1}{h}\int_V [\partial W/\partial x_1-\partial(\sigma_{ji}\partial u_i/\partial x_1)/\partial x_j]dV \tag{4}$$

where V is the volume inside S. The equilibrium equations (2) together with the fact that W is a function of $u_{i,j}$ imply that

$$P_1=\frac{1}{h}\int_V (\partial W/\partial u_{i,j}\cdot\partial u_{i,j}/\partial x_1-\sigma_{ji}\partial^2 u_i/\partial x_j\partial x_1)dV \tag{5}$$

Thus $P_1=0$ because $\sigma_{ji}=\partial W/\partial u_{i,j}$.

The intersection between S_Γ and the plate surfaces encloses a surface A_+ on $x_3=h/2$ and A_- on $x_3=-h/2$. Then equation (3) can be written

$$P_1=\int_\Gamma [W_{av}n_1-(n_j\sigma_{ji}\partial u_i/\partial x_1)_{av}]ds$$

$$-\frac{1}{h}\int_{A_++A_-} n_3\sigma_{3i}\partial u_i/\partial x_1 dS \tag{6}$$

where $j\neq 3$, index av denotes the average over the plate thickness and s is the arc length along Γ, increasing in the direction for which n_i points to the right, seen from the positive x_3 side.

[5]Lund Institute of Technology, S-221 00 Lund, Sweden.

Manuscript received by ASME Applied Mechanics Division, September 10, 1986.

Copyright © 1987 by ASME
Downloaded 03 May 2010 to 171.66.16.27. Redistribution subject to ASME license or copyright; see http://www.asme.org/terms/Terms_Use.cfm

In the case of in-plane loading $\sigma_{3i} = 0$ on A_+ and A_-. Then the second integral of equation (6) vanishes, i.e.,

$$P_1 = \int_\Gamma [W_{av} n_1 - (n_j \sigma_{ji} \partial u_i / \partial x_1)_{av}] ds = 0 \quad (i = 1,2,3;\ j = 1,2) \tag{7}$$

Since the integral coincides with the P-integral for a closed path, the proof of the path-independence of P is completed.

In plane stress $\sigma_{j3} = 0$ and in-plane strain $\partial u_3 / \partial x_1 = 0$. Thus in both cases equation (7) yields

$$P = J = \int_\Gamma [W dx_2 - n_j \sigma_{ji} \partial u_i / \partial x_1 ds] = 0 \quad (i, j = 1,2) \tag{8}$$

where J is the J-integral. Index av could be dropped because both terms in the integrand are independent of x_3.

Application to Crack Problems

In the case of a plate subjected to in-plane loading and containing a crack

$$-a \le x_1 \le a, \quad x_2 = 0 \tag{9}$$

through the whole plate thickness, the P-integral is path-independent for paths starting from one crack surface and ending on the other one, since both dx_2 and $n_j \sigma_{ji}$ vanish on the crack surfaces. (Expression (9) may represent either an edge crack or an internal crack.)

Assume that the plate thickness $h \ll a$ and that also $h \ll b$, where b is the smallest ligament from the crack edge. Then plane stress conditions are approximated at a path Γ_r far from the crack edge. Towards the edge (except at $x_3 = \pm h/2$) plane strain is approached, even though the relation $\partial u_3 / \partial x_1 = 0$ does not hold. However, it appears that $\partial u_3 / \partial x_1$ is nonsingular (Yang and Freund, 1985) and, therefore, its contribution to P vanishes when Γ is shrunk to zero. Hence P equals J for a path Γ_n very close to the crack edge.

Since the P-integral is path-independent over the whole plate, one obtains

$$P = J_{\Gamma = \Gamma_r} = J_{\Gamma = \Gamma_n} \tag{10}$$

Plane stress conditions dominate in the plate as a whole, whereas plane strain conditions are confined to a very small part. In fact it appears that plane stress dominates outside the distance $0.5h$ from the crack edge (cf Yang and Freund, 1985; Rosakis and Ravi-Chandar, 1986). Therefore, the conditions $h \ll a$ and $h \ll b$ are too restrictive and could safely be exchanged by $h \le a$ and $h \le b$. Under these restrictions the stress-strain state far away from the crack edge would come very close to the one calculated under the assumption of plane stress throughout.

As an example, regard a central crack in a large plate, subjected to a remote tensile stress σ_∞ normal to the crack. Assumption of plane stress throughout leads to

$$J = \pi \sigma_\infty^2 a / E \tag{11}$$

where E is the modulus of elasticity. Hence

$$J_{\Gamma = \Gamma_n} = J_{\Gamma = \Gamma_r} \approx \pi \sigma_\infty^2 a / E \tag{12}$$

Since the near-tip value of J is a plane strain value, the plane stress intensity factor is

$$K_I \approx \sigma_\infty (\pi a)^{1/2} (1 - \nu^2)^{-1/2} \tag{13}$$

The $\approx$ sign should be interpreted so that K_I comes much closer to the expression (13) than to $\sigma_\infty (\pi a)^{1/2}$.

Conclusions

The path-independent P-integral provides a somewhat more adequate tool for analysis of cracks in plates than the J-integral. It is closely related to the J-integral and the two coincide in cases of plane stress or plane strain. Therefore, the P integral can be used to connect plane stress and plane strain regions in analysis of crack problems. Since it holds even for nonlinear elasticity and large strains (with the definition of stress used) it should be applicable also to elastic-plastic cases as long as proportional loading is approximated. This, however, cannot be relied upon for the vicinity of the crack edge. Even fairly small amounts of plastic flow can, therefore, cause considerable deviations from plane strain conditions along the crack edge, especially towards its ends.

References

Rosakis, A. J., and Ravi-Chandar, K., 1986, "On Crack-Tip Stress State: An Experimental Evaluation of Three-Dimensional Effects," *Int. J. Solids and Structures*, Vol. 13, pp. 121–134.

Yang, W., and Freund, L. B., 1985, "Transverse Shear Effects for Through-Cracks in an Elastic Plate," *Int. J. Solids and Structures*, Vol. 21, pp. 977–994.

A Simple Analysis for the Blowup Phenomenon of Inelastic Members in Compression

P. Vielsack[6]

Iceplates, flat concrete constructions, or laminated rock can break into pieces. The elastic bending deformations of such a multibody system can often be neglected with respect to rigid body displacements and local effects in the vicinity of the joints. As an example we consider a symmetrical, one-dimensional problem of two homogenous blocks with length ℓ and weight G, lying on a horizontal surface and compressed by end-forces $H > 0$. Let ℓ be much bigger than the height of the blocks but smaller than what results from the ultimate bending strength of a single block, which is simply supported and loaded by its own weight. The system in Fig. 1 can be generated by cracks or a plastic hinge in the middle of one block of length 2ℓ. Adding more members to the free ends would not change the problem in principle.

Two modes of failure are easy to imagine. Raising the compression, the system can always remain in the straight, trivial equilibrium state until the ultimate compressive strength of the material over the whole cross section is reached. The corresponding ultimate force $H = N_U$ is easily calculated. More interesting is a stability problem called unilateral buckling or blowup phenomenon. Neglecting elastic deflections, the corresponding nontrivial state is an isosceles triangle with angles φ between the horizontal plane and the inclined members. Different from the statical treatment of conservative elastica (Vielsack, 1981; Kerr and Shade, 1984), a dynamic approach is needed because of energy dissipation. For this purpose we must define a mechanical law for the internal applied moments M acting as dry frictional-type resistances on both sides of the joint. Microscopic stress distributions, which arise from local plastic deformations and increasing numbers of cracks during motion, can be modelled macroscopically using the assumption

$$M = M_o - 2d\varphi, \quad \varphi \gtrless 0, \quad \dot{\varphi} \gtrless 0. \tag{1}$$

Equation (1) gives the representation of a generally incremental law for the ranges $\varphi \gtrless 0$ of the generalized coordinate and $\dot{\varphi} \gtrless 0$ of the angular velocity, respectively. A unidirectional velocity $\dot{\varphi} > 0$ leads to the collapse of the system. A sufficient condition for nontrivial equilibrium states $\varphi > 0$ is the reversal

[6]Professor Dr. Ing. P. Vielsack, Institut für Mechanik, Universität Karlsruhe, 7500 Karlsruhe, Postfach 6980, Federal Republic of Germany.

Manuscript received by ASME Applied Mechanics Division, May 16, 1986; final revision, November 12, 1986.

Downloaded 03 May 2010 to 171.66.16.27. Redistribution subject to ASME license or copyright; see http://www.asme.org/terms/Terms_Use.cfm

In the case of in-plane loading $\sigma_{3j} = 0$ on A_+ and A_-. Then the second integral of equation (6) vanishes, i.e.,

$$P_1 = \int_\Gamma [W_{av} n_1 - (n_j \sigma_{ji} \partial u_i / \partial x_1)_{av}] ds = 0 \quad (i = 1,2,3;\ j = 1,2) \tag{7}$$

Since the integral coincides with the P-integral for a closed path, the proof of the path-independence of P is completed.

In plane stress $\sigma_{j3} = 0$ and in-plane strain $\partial u_3 / \partial x_1 = 0$. Thus in both cases equation (7) yields

$$P = J = \int_\Gamma [W dx_2 - n_j \sigma_{ji} \partial u_i / \partial x_1 ds] = 0 \quad (i, j = 1,2) \tag{8}$$

where J is the J-integral. Index av could be dropped because both terms in the integrand are independent of x_3.

Application to Crack Problems

In the case of a plate subjected to in-plane loading and containing a crack

$$-a \le x_1 \le a, \quad x_2 = 0 \tag{9}$$

through the whole plate thickness, the P-integral is path-independent for paths starting from one crack surface and ending on the other one, since both dx_2 and $n_j \sigma_{ji}$ vanish on the crack surfaces. (Expression (9) may represent either an edge crack or an internal crack.)

Assume that the plate thickness $h \ll a$ and that also $h \ll b$, where b is the smallest ligament from the crack edge. Then plane stress conditions are approximated at a path Γ_r far from the crack edge. Towards the edge (except at $x_3 = \pm h/2$) plane strain is approached, even though the relation $\partial u_3 / \partial x_1 = 0$ does not hold. However, it appears that $\partial u_3 / \partial x_1$ is nonsingular (Yang and Freund, 1985) and, therefore, its contribution to P vanishes when Γ is shrunk to zero. Hence P equals J for a path Γ_n very close to the crack edge.

Since the P-integral is path-independent over the whole plate, one obtains

$$P = J_{\Gamma = \Gamma_r} = J_{\Gamma = \Gamma_n} \tag{10}$$

Plane stress conditions dominate in the plate as a whole, whereas plane strain conditions are confined to a very small part. In fact it appears that plane stress dominates outside the distance $0.5h$ from the crack edge (cf Yang and Freund, 1985; Rosakis and Ravi-Chandar, 1986). Therefore, the conditions $h \ll a$ and $h \ll b$ are too restrictive and could safely be exchanged by $h \le a$ and $h \le b$. Under these restrictions the stress-strain state far away from the crack edge would come very close to the one calculated under the assumption of plane stress throughout.

As an example, regard a central crack in a large plate, subjected to a remote tensile stress σ_∞ normal to the crack. Assumption of plane stress throughout leads to

$$J = \pi \sigma_\infty^2 a / E \tag{11}$$

where E is the modulus of elasticity. Hence

$$J_{\Gamma = \Gamma_n} = J_{\Gamma = \Gamma_r} \approx \pi \sigma_\infty^2 a / E \tag{12}$$

Since the near-tip value of J is a plane strain value, the plane stress intensity factor is

$$K_I \approx \sigma_\infty (\pi a)^{1/2} (1 - \nu^2)^{-1/2} \tag{13}$$

The $\approx$ sign should be interpreted so that K_I comes much closer to the expression (13) than to $\sigma_\infty (\pi a)^{1/2}$.

Conclusions

The path-independent P-integral provides a somewhat more adequate tool for analysis of cracks in plates than the J-integral. It is closely related to the J-integral and the two coincide in cases of plane stress or plane strain. Therefore, the P integral can be used to connect plane stress and plane strain regions in analysis of crack problems. Since it holds even for nonlinear elasticity and large strains (with the definition of stress used) it should be applicable also to elastic-plastic cases as long as proportional loading is approximated. This, however, cannot be relied upon for the vicinity of the crack edge. Even fairly small amounts of plastic flow can, therefore, cause considerable deviations from plane strain conditions along the crack edge, especially towards its ends.

References

Rosakis, A. J., and Ravi-Chandar, K., 1986, "On Crack-Tip Stress State: An Experimental Evaluation of Three-Dimensional Effects," *Int. J. Solids and Structures*, Vol. 13, pp. 121–134.

Yang, W., and Freund, L. B., 1985, "Transverse Shear Effects for Through-Cracks in an Elastic Plate," *Int. J. Solids and Structures*, Vol. 21, pp. 977–994.

A Simple Analysis for the Blowup Phenomenon of Inelastic Members in Compression

P. Vielsack[6]

Iceplates, flat concrete constructions, or laminated rock can break into pieces. The elastic bending deformations of such a multibody system can often be neglected with respect to rigid body displacements and local effects in the vicinity of the joints. As an example we consider a symmetrical, one-dimensional problem of two homogenous blocks with length ℓ and weight G, lying on a horizontal surface and compressed by end-forces $H > 0$. Let ℓ be much bigger than the height of the blocks but smaller than what results from the ultimate bending strength of a single block, which is simply supported and loaded by its own weight. The system in Fig. 1 can be generated by cracks or a plastic hinge in the middle of one block of length 2ℓ. Adding more members to the free ends would not change the problem in principle.

Two modes of failure are easy to imagine. Raising the compression, the system can always remain in the straight, trivial equilibrium state until the ultimate compressive strength of the material over the whole cross section is reached. The corresponding ultimate force $H = N_U$ is easily calculated. More interesting is a stability problem called unilateral buckling or blowup phenomenon. Neglecting elastic deflections, the corresponding nontrivial state is an isosceles triangle with angles φ between the horizontal plane and the inclined members. Different from the statical treatment of conservative elastica (Vielsack, 1981; Kerr and Shade, 1984), a dynamic approach is needed because of energy dissipation. For this purpose we must define a mechanical law for the internal applied moments M acting as dry frictional-type resistances on both sides of the joint. Microscopic stress distributions, which arise from local plastic deformations and increasing numbers of cracks during motion, can be modelled macroscopically using the assumption

$$M = M_o - 2d\varphi, \quad \varphi \gtrless 0, \quad \dot{\varphi} \gtrless 0. \tag{1}$$

Equation (1) gives the representation of a generally incremental law for the ranges $\varphi \gtrless 0$ of the generalized coordinate and $\dot{\varphi} \gtrless 0$ of the angular velocity, respectively. A unidirectional velocity $\dot{\varphi} > 0$ leads to the collapse of the system. A sufficient condition for nontrivial equilibrium states $\varphi > 0$ is the reversal

[6]Professor Dr. Ing. P. Vielsack, Institut für Mechanik, Universität Karlsruhe, 7500 Karlsruhe, Postfach 6980, Federal Republic of Germany.

Manuscript received by ASME Applied Mechanics Division, May 16, 1986; final revision, November 12, 1986.

Copyright © 1987 by ASME
Downloaded 03 May 2010 to 171.66.16.27. Redistribution subject to ASME license or copyright; see http://www.asme.org/terms/Terms_Use.cfm

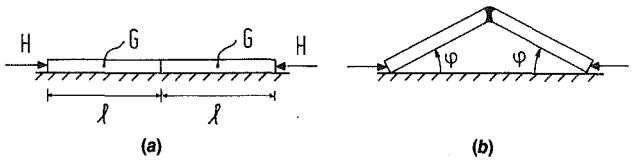


Fig. 1 Two blocks in compression: (a) straight configuration; (b) blowup mechanism

of velocity indicated by $\dot{\varphi}=0$. In the case of ideal plastic material, M_o is the fully plastic moment of a plastic hinge in the joint. In the case of brittle material, M_o defines a threshold value of the interaction between bending and compressive strength before softening begins. The parameter d describes softening in the vicinity of the joint while increasing the relative rotation 2φ of both blocks. Generally, M_o and d depend on the state of compression. Therefore, equation (1) must be considered as a first order Taylor expansion, valid only in a certain range of the compressive force, especially about the ultimate force N_U.

We can expect that blowup occurs at a very small angle φ. Therefore, we restrict the considerations to a geometrically linear treatment of the problem. Moreover, geometrical imperfections, as for example an initial angle, are not taken into account. Then $H(\varphi)$, generally depending on the horizontal displacement during motion, can be equalled by its maximum value $H(0)=N$ in the straight configuration. Denoting the kinetic energy by T we obtain the quadratic approximation for energy and work of one block

$$T-T_o+\frac{G\ell}{2}\varphi-\frac{N\ell}{2}\varphi^2=-\int_o^{\varphi}M(\alpha)\,|d\alpha|. \tag{2}$$

In this representation T_o is the initial kinetic energy subjected to the system in the straight configuration by a sudden impact. According to the theory of dynamic stability, this corresponds to a special type of disturbance, namely a perturbation of the angular velocity $\dot{\varphi}$ at the beginning of the motion. Inserting equation (1) into equation (2) leads to the first integral for the motion equation

$$T-\frac{(N\ell+2d)}{2}(\varphi-\varphi_L)^2=T_o-\frac{(G\ell+2M_o)^2}{8(N\ell+2d)};$$
$$\varphi\gtrless 0;\quad \dot{\varphi}\gtrless 0 \tag{3}$$

with the abbreviation

$$\varphi_L=\frac{G\ell+2M_o}{2(N\ell+2d)}. \tag{4}$$

The sufficient condition for the existence of a nontrivial equilibrium state $0<\varphi<\varphi_L$ is $\dot{\varphi}=0$ or equivalently $T=0$. This implies

$$T_o<\frac{(G\ell+2M_o)^2}{8(N\ell+2d)}. \tag{5}$$

Because of the inelastic material behavior (1) all deformations are irreversible. Arriving at $\dot{\varphi}=0$ the two blocks are inclined by a final angle $\varphi\neq 0$. The range of these new equilibrium positions $0\lessgtr\varphi<\varphi_L$ is given by the limit value (4). The final equilibrium state $\varphi<\varphi_L$ differs from the initial state $\varphi=0$. This situation implies the definition of practical stability as shown by Vielsack (1986). The system is practically stable as long as the inequality (5) holds, that means, as long as unavoidable disturbances applied to the trivial state are sufficiently small. If (5) is violated, blowup occurs, indicated by a unidirectional motion $\varphi>0$ and $\dot{\varphi}>0$. This corresponds to instability by divergence.

The stability criterion (5) allows the discussion of the blowup phenomenon in principle. Provided the initial disturbance is kept fixed, the danger of instability is reduced by increasing G and M_o and raised by increasing N and d, respectively. The influence of the inelastic material behavior can be seen from the consideration of two ideal rigid blocks having no rotational constraints in the joint. In this case we have to set $M_o=0$ and $d=0$, and stability depends on the ratio $\ell G^2/N$. Comparing this result with (5), softening has the same effect as increasing the compressive force, whereas plastification has a similar stabilizing influence as gravity. Depending on the suitable choice of parameters, the right-hand side of the inequality (5) can be arbitrarily small. Then blowup is possible at arbitrarily small disturbances even for $N<N_U$. Summarising the results, the blowup phenomenon of inelastic members is totally different from ordinary stability problems in structural mechanics because no buckling force exists and, moreover, no safe lower bound for critical values of the force as for elastica (Vielsack, 1981) can be given. The condition (5) only describes the sensitivity of the system to unavoidable disturbances.

References

Kerr, A. D., and Shade, P. J., 1984, "Analysis of Concrete Pavement Blowups," *Acta Mechanica*, Vol. 52, pp. 201–224.

Vielsack, P., 1981, "Einseitiges Knicken eines Schweren Stabes," *Zeitschrift für Angewandte Mathematik und Mechanik*, Vol. 61, pp. 55–58.

Vielsack, P., 1986, "Praktische Stabilität und Kollaps eines Stabes mit Trockener Reibung in den Lagern," *Ingenieurarchiv*, Vol. 56, pp. 229–240.

Sudden Loading of an Orthotropic Plate Containing a Central Crack

M. K. Kassir[7,9] and J. Xu[8,9]

The purpose of this note is to determine the elastodynamic response of an orthotropic plate containing a central crack deformed by the application of dynamic loading. The material of the plate is assumed to possess three mutually perpendicular axes of elastic symmetry, two of which lie in the plane of the plate and the third is in the normal direction. The faces of the crack coincide with one of the planes of orthotropy of the material. Such material can be used to model some of the structural plate elements in current use. Examples include, laminated plates, corrugated sheets, decks of bridges and ships, composite materials, and others.

Several studies are available which treat the effect of orthotropy on elastic waves in solids (see, for example, the works of Freedman and Keer 1973; Achenbach and Bazant, 1975; Vinson and Chow, 1975; Kassir and Tse, 1983; and others). The response of a plane strain orthotropic medium containing a central crack deformed by the application of sudden stresses to its surfaces has been obtained by Kassir and Bandyopadhayay (1983). The dynamic stress-intensity factors, $k_1(t)$ and $k_2(t)$, were computed and compared with the corresponding isotropic values to reveal the influence of material orthotropy on the magnitude of the overshoot in the stress-intensity factors and the time interval required to reach the peak value.

In this note, a similar integral transform solution is used to reduce the corresponding plate bending problem to the solution of a Fredholm integral equation of the second kind. The

[7]Professor, Member ASME.

[8]Graduate Student.

[9]Department of Civil Engineering, City College of City University of New York, New York, NY 10031.

Manuscript received by ASME Applied Mechanics Division, November 4, 1985; final revision, October 3, 1986.

Downloaded 03 May 2010 to 171.66.16.27. Redistribution subject to ASME license or copyright; see http://www.asme.org/terms/Terms_Use.cfm

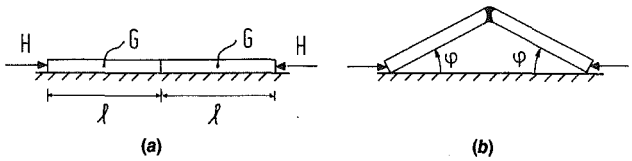


Fig. 1 Two blocks in compression: (a) straight configuration; (b) blowup mechanism

of velocity indicated by $\dot{\varphi}=0$. In the case of ideal plastic material, M_o is the fully plastic moment of a plastic hinge in the joint. In the case of brittle material, M_o defines a threshold value of the interaction between bending and compressive strength before softening begins. The parameter d describes softening in the vicinity of the joint while increasing the relative rotation 2φ of both blocks. Generally, M_o and d depend on the state of compression. Therefore, equation (1) must be considered as a first order Taylor expansion, valid only in a certain range of the compressive force, especially about the ultimate force N_U.

We can expect that blowup occurs at a very small angle φ. Therefore, we restrict the considerations to a geometrically linear treatment of the problem. Moreover, geometrical imperfections, as for example an initial angle, are not taken into account. Then $H(\varphi)$, generally depending on the horizontal displacement during motion, can be equalled by its maximum value $H(0)=N$ in the straight configuration. Denoting the kinetic energy by T we obtain the quadratic approximation for energy and work of one block

$$T-T_o+\frac{G\ell}{2}\varphi-\frac{N\ell}{2}\varphi^2=-\int_o^{\varphi}M(\alpha)\,|d\alpha|. \tag{2}$$

In this representation T_o is the initial kinetic energy subjected to the system in the straight configuration by a sudden impact. According to the theory of dynamic stability, this corresponds to a special type of disturbance, namely a perturbation of the angular velocity $\dot{\varphi}$ at the beginning of the motion. Inserting equation (1) into equation (2) leads to the first integral for the motion equation

$$T-\frac{(N\ell+2d)}{2}(\varphi-\varphi_L)^2=T_o-\frac{(G\ell+2M_o)^2}{8(N\ell+2d)};$$
$$\varphi\gtrless 0;\quad \dot{\varphi}\gtrless 0 \tag{3}$$

with the abbreviation

$$\varphi_L=\frac{G\ell+2M_o}{2(N\ell+2d)}. \tag{4}$$

The sufficient condition for the existence of a nontrivial equilibrium state $0<\varphi<\varphi_L$ is $\dot{\varphi}=0$ or equivalently $T=0$. This implies

$$T_o<\frac{(G\ell+2M_o)^2}{8(N\ell+2d)}. \tag{5}$$

Because of the inelastic material behavior (1) all deformations are irreversible. Arriving at $\dot{\varphi}=0$ the two blocks are inclined by a final angle $\varphi\neq 0$. The range of these new equilibrium positions $0\lessgtr\varphi<\varphi_L$ is given by the limit value (4). The final equilibrium state $\varphi<\varphi_L$ differs from the initial state $\varphi=0$. This situation implies the definition of practical stability as shown by Vielsack (1986). The system is practically stable as long as the inequality (5) holds, that means, as long as unavoidable disturbances applied to the trivial state are sufficiently small. If (5) is violated, blowup occurs, indicated by a unidirectional motion $\varphi>0$ and $\dot{\varphi}>0$. This corresponds to instability by divergence.

The stability criterion (5) allows the discussion of the blowup phenomenon in principle. Provided the initial disturbance is kept fixed, the danger of instability is reduced by increasing G and M_o and raised by increasing N and d, respectively. The influence of the inelastic material behavior can be seen from the consideration of two ideal rigid blocks having no rotational constraints in the joint. In this case we have to set $M_o=0$ and $d=0$, and stability depends on the ratio $\ell G^2/N$. Comparing this result with (5), softening has the same effect as increasing the compressive force, whereas plastification has a similar stabilizing influence as gravity. Depending on the suitable choice of parameters, the right-hand side of the inequality (5) can be arbitrarily small. Then blowup is possible at arbitrarily small disturbances even for $N<N_U$. Summarising the results, the blowup phenomenon of inelastic members is totally different from ordinary stability problems in structural mechanics because no buckling force exists and, moreover, no safe lower bound for critical values of the force as for elastica (Vielsack, 1981) can be given. The condition (5) only describes the sensitivity of the system to unavoidable disturbances.

References

Kerr, A. D., and Shade, P. J., 1984, "Analysis of Concrete Pavement Blowups," *Acta Mechanica*, Vol. 52, pp. 201–224.

Vielsack, P., 1981, "Einseitiges Knicken eines Schweren Stabes," *Zeitschrift für Angewandte Mathematik und Mechanik*, Vol. 61, pp. 55–58.

Vielsack, P., 1986, "Praktische Stabilität und Kollaps eines Stabes mit Trockener Reibung in den Lagern," *Ingenieurarchiv*, Vol. 56, pp. 229–240.

Sudden Loading of an Orthotropic Plate Containing a Central Crack

M. K. Kassir[7,9] and J. Xu[8,9]

The purpose of this note is to determine the elastodynamic response of an orthotropic plate containing a central crack deformed by the application of dynamic loading. The material of the plate is assumed to possess three mutually perpendicular axes of elastic symmetry, two of which lie in the plane of the plate and the third is in the normal direction. The faces of the crack coincide with one of the planes of orthotropy of the material. Such material can be used to model some of the structural plate elements in current use. Examples include, laminated plates, corrugated sheets, decks of bridges and ships, composite materials, and others.

Several studies are available which treat the effect of orthotropy on elastic waves in solids (see, for example, the works of Freedman and Keer 1973; Achenbach and Bazant, 1975; Vinson and Chow, 1975; Kassir and Tse, 1983; and others). The response of a plane strain orthotropic medium containing a central crack deformed by the application of sudden stresses to its surfaces has been obtained by Kassir and Bandyopadhayay (1983). The dynamic stress-intensity factors, $k_1(t)$ and $k_2(t)$, were computed and compared with the corresponding isotropic values to reveal the influence of material orthotropy on the magnitude of the overshoot in the stress-intensity factors and the time interval required to reach the peak value.

In this note, a similar integral transform solution is used to reduce the corresponding plate bending problem to the solution of a Fredholm integral equation of the second kind. The

[7]Professor, Member ASME.

[8]Graduate Student.

[9]Department of Civil Engineering, City College of City University of New York, New York, NY 10031.

Manuscript received by ASME Applied Mechanics Division, November 4, 1985; final revision, October 3, 1986.

Copyright © 1987 by ASME
Downloaded 03 May 2010 to 171.66.16.27. Redistribution subject to ASME license or copyright; see http://www.asme.org/terms/Terms_Use.cfm

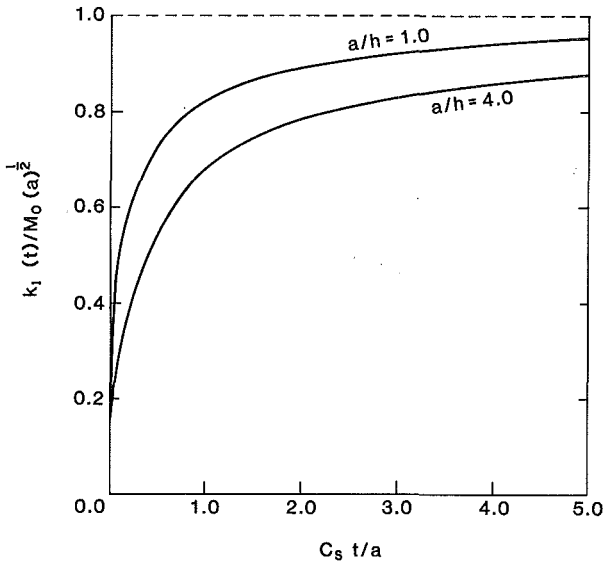


Fig. 1 Variation of moment-intensity factor with time (Boron/Epoxy composite)

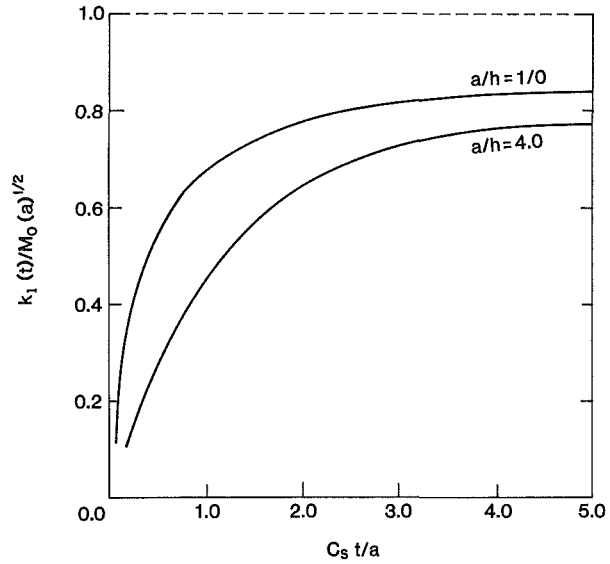


Fig. 2 Normalized moment-intensity factor versus normalized time (Graphite/fiber composite—50 percent)

classical theory of plate deflection is used to find the influence of impact loading on the cracked element. As is well known, this theory is governed by a fourth order differential equation and is associated with Kirchhoff boundary conditions. In contrast to previous studies, the dynamic moment-intensity factor is less than the statical value. This response is similar to that obtained for the isotropic plate (Chen and Sih, 1977) and may be attributed to the approximate nature of the plate theory employed. Reducing plate thickness results in smaller values of the moment-intensity factors for small intervals in time.

Basic Equations and Method of Solution

Consider a thin, orthotropic, infinite plate of thickness (h) containing a central crack of length ($2a$). It is assumed that (h) is less than (a). In terms of a system of Cartesian coordinates with its origin located at the center of the middle surface of the plate, the faces of the crack are described by $|x| \le a$, $y = 0$, $|z| \le h/2$, and those of the plate by the planes $z = \mp h/2$. Let E_x, E_y, ν_{xy}, ν_{yx}, and G_{xy} ($E_x\ \nu_{yx} = E_y\ \nu_{xy}$) designate the elastic constants in the xy plane and G_{xz} and G_{yz} the transverse shearing modulii. The faces of the crack are subjected to dynamic bending moments in which the time required to apply the moment from the start to its maximum value is very short. The applied loading and the resulting deformations are obviously symmetric with respect to the crack plane.

By neglecting the effects of transverse shear deformation and rotatory inertia on the flexural motion of the plate, it is readily shown that the equation of motion of the plate reduces to:

$$D_x \frac{\partial^4 w}{\partial x^4} + 2B \frac{\partial^4 w}{\partial x^2 \partial y^2} + D_y \frac{\partial^4 w}{\partial y^4} + h\rho \frac{\partial^2 w}{\partial t^2} = 0, \qquad (1)$$

in which, $w(x,y,t)$, represents the deflection of the middle surface of the plate, ρ is the mass density of the material, t is the time variable and D_x, D_y, D_{xy}, and B denote the flexural rigidities of the plate defined by the relations:

$$\left.\begin{aligned} &D_x = E_x h^3/12(1-\nu_{xy}\nu_{yx}),\ D_y = (E_y/E_x)D_x \\ &D_{xy} = G_{xy}h^3/12,\ B = \nu_{yx}D_x + 2D_{xy} \end{aligned}\right\}, \qquad (2)$$

The Kirchhoff's shears per unit length (V_x, V_y) and the bending and twisting moments per unit length (M_x, M_y, M_{xy}) are obtained from the expression of the deflection. In particular,

$$V_y = -\frac{\partial}{\partial y}\left[D_y \frac{\partial^2 w}{\partial y^2} + (B+2D_{xy})\frac{\partial^2 w}{\partial x^2}\right], \qquad (3)$$

$$M_y = -D_y\left(\frac{\partial^2 w}{\partial y^2} + \nu_{xy}\frac{\partial^2 w}{\partial x^2}\right), \qquad (4)$$

Because of the symmetry of the problem under discussion, it is sufficient to consider the region $y \ge 0$, and to determine the deflection, $w(x,y,t)$, by solving equation (1) subject to the following conditions on $y = 0$.

$$V_y = 0, \quad \text{all } x, \qquad (5a)$$

$$M_y = -M_o H(t), \quad |x| \le a, \qquad (5b)$$

$$w = 0, \quad |x| > a, \qquad (5c)$$

In equation (5b), the constant, M_o, denotes the magnitude of the applied bending moment and, $H(t)$, stands for the Heaviside step function. In addition to conditions (5), the deflection must vanish at remote distances from the crack region. Assuming zero initial conditions for the plate deflection, the time variable can be removed from equations (1)–(5) by the application of the usual Laplace transform. In subsequent work, the Laplace transform of $w(x,y,t)$ is denoted by $\hat{w}(x,y;p)$, and similarly for other quantities. In the transformed plane, an integral solution of $\hat{w}$ which satisfies the symmetry condition implied in equation (5a) and vanishes at large distances from the origin is

$$\hat{w}(x,y;p) = \int_o^\infty A(s,p)\left[e^{-\gamma_1 y} - \beta(s,p)e^{-\gamma_2 y}\right]\cos(sx)\,ds, \qquad (6)$$

where γ_1 and γ_2 are complex conjugate quantities with positive real parts. They are given by the relations:

$$\gamma_{\frac{1}{2}}(s,p) = (B/D_y)^{1/2}\left[s^2 \pm i\sqrt{\rho h p^2 D_y/B^2 - \left(1 - \frac{D_x D_y}{B^2}\right)s^4}\right]^{\frac{1}{2}}, \qquad (7)$$

In equation (6), $A(s,p)$ is an arbitrary transform parameter to be determined from the remaining boundary conditions and, $\beta(s,p)$, designates the abbreviation

$$\beta(s,p) = \frac{\gamma_1}{\gamma_2}\left[\frac{s^2(B+2D_{xy}) - \gamma_1^2 D_y}{s^2(B+2D_{xy}) - \gamma_2^2 D_y}\right], \qquad (8)$$

Following a procedure outlined in Kassir and Ban-

Downloaded 03 May 2010 to 171.66.16.27. Redistribution subject to ASME license or copyright; see http://www.asme.org/terms/Terms_Use.cfm

dyopadhayay (1983), it may be shown that the moment-intensity factor in the transformed plane is given by

$$\hat{k}_1(p) = M_o(a)^{1/2}\,\frac{\Phi(1,p)}{p}, \tag{9}$$

where the auxiliary function, $\Phi(r,p)$, is governed by the Fredholm integral equation

$$\Phi(r;p) + \int_o^1 \Phi(y;p)L(ar,ay;p)dy = r^{1/2}, \tag{10}$$

and the kernel, $L(ar,ay;p)$, stands for the expression

$$L(ar,ay;p) = (ry)^{1/2}\int_o^\infty u\left[F\left(\frac{u}{a};p\right) - 1\right]J_o(ur)J_o(yu)du, \tag{11}$$

Here, J_o, denotes the usual Bessel function of the first kind of order zero and, $F(s,p)$, designates the abbreviation

$$\left.\begin{aligned} F(s,p) &= \frac{\gamma_1\gamma_2 s^2 B_1 + \gamma_1^2\gamma_1^2 + \nu_{xy}s^2(s^2B_1 - \gamma_1^2 - \gamma_1\gamma_2 - \gamma_2^2)}{s\gamma_1\gamma_2(\gamma_1+\gamma_2)} \\ B_1 &= 2\nu_{xy} + 4\,D_{xy}/D_y \end{aligned}\right\}, \tag{12}$$

Since γ_1 and γ_2 are complex conjugates, the function, $F(s,p)$, is real. Moreover, it can be readily shown that $F(s,p) \sim 1 + 0(s^{-2})$ for large s and, accordingly, equation (10) may be solved numerically by a method outlined in Krylov and Kantrorovich (1957) to yield the values of $\Phi(r,p)$. Finally, the time-dependence of the moment-intensity factor can be recovered in inverting the Laplace transform indicated in equation (9). This can be done by a method similar to the one employed by Miller and Guy (1966).

Numerical Results and Discussion

In order to illustrate the application of the solution, two plate elements with distinct orthotropic properties are considered. The first is made of boron-epoxy composite with the following elastic constants: $E_x = 55.16 \times 10^9$ N/m^2 (8×10^6 psi), $E_y = 170.65 \times 10^9$ N/m^2 (24.75×10^6 psi), $G_{xy} = 4.83 \times 10^9$ N/m^2 (0.7×10^6 psi) and $\nu_{xy} = 0.036$. The second material is a graphite-fiber composite (50 percent) with $E_x = 173.75 \times 10^9$ N/m^2 (25.2×10^6 psi), $E_y = 6.89 \times 10^9$ N/m^2 (1.0×10^6 psi), $G_{xy} = 3.79 \times 10^9$ N/m^2 (0.55×10^6 psi), and $\nu_{xy} = 0.28$. For each element, the values of $\Phi(1,p)$ are computed from equation (10) for crack length/plate thickness ratios $(a/h) = 1, 4$. The results are then used in conjunction with the Laplace inversion indicated in equation (9) to obtain the variation of the moment-intensity factor, $k_1(t)$, with time. The plots of $k_1(t)/M_o(a)^{1/2}$ versus $C_s t/a$, where $C_s^2 = G_{xy}/\rho$, are displayed graphically in Figs. (1) and (2). In both cases, $k_1(t)$ starts from zero and increases with time and approaches the corresponding statical value for large time. Because of the nature of the loading, one would expect, at short times, an overshoot in the moment-intensity factor near the crack tip. Indeed, the analysis employed here has predicted such overshoots in several similar problems (Kassir and Bandyopadhayay, 1983). However, in the present case, the analysis does not seem to predict a peak. This may be due to the approximate nature of the Kirchhoff plate equations used in formulating the problem. Similar results have been reported by Chen and Sih (1977) for the isotropic solid. Figures (1) and (2) indicate that by decreasing the ratio a/h results in an increase in the magnitude of the moment-intensity factor. This conclusion, however, can only be made for the materials considered.

References

Achenbach, J. D., and Bazant, Z. P., 1975, "Elastodynamic Near-Tip Stress and Displacement Fields for Rapidly Propagating Cracks in Orthotropic Materials," ASME JOURNAL OF APPLIED MECHANICS, Vol. 42, pp. 183–189.

Chen, E. P., and Sih, G. C., 1977, *Elastodynamic Crack Problems*, Noordhoff International Publishing, Leyden, The Netherlands.

Freedman, J. M., and Keer, L. M., 1973, "Vibratory Motion of a Body on an Orthotropic Half-Plane," ASME JOURNAL OF APPLIED MECHANICS, Vol. 40, pp. 221–229.

Kassir, M. K., and Bandyopadhayay, K. K., 1983, "Impact Response of a Cracked Orthotropic Medium," ASME JOURNAL OF APPLIED MECHANICS, Vol. 50, pp. 630–636.

Kassir, M. K., and Tse, S., 1983, "Moving Griffith Crack in an Orthotropic Material," *International Journal of Engineering Science*, Vol. 21, pp. 315–325.

Krylov, V. I., and Kantorovich, L. V., 1957, *Approximate Methods of Higher Analysis*, Interscience Publishers, New York, pp. 97–161.

Miller, M. K., and Guy, W. T., 1966, "Numerical Inversion of the Laplace Transform by Use of Jacobi Polynomials," *SIAM Journal of Numerical Analysis*, Vol. 3, pp. 624–635.

Vinson, J. R., and Chow, T. W., 1975, *Composite and Their Use in Structures*, Wiley, New York.

The Effect of Pore Fluid Flow on Extrusion

E. P. Fahrenthold[10] and J. B. Cheatham, Jr.[11]

1 Introduction

The collapse of well casing in hydrocarbon reservoirs has in some cases been preceded by fluidization or extrusion of rock through casing perforations. Analysis of this problem requires consideration of the effect of pore fluid flow on extrusion.

Much work in the field of deformable porous media focuses upon the coupling of fluid and solid motion (Bowen, 1982), and the role of solid matrix compaction in the maintenance of pore pressure. At first glance, the process of extrusion of a porous medium would seem to be dominated by similar compaction phenomena. However, recent study of the casing collapse process suggests that such may not be the case. Pattillo and Smith (1985) studied the effect of formation flow on casing integrity using the finite element method. These authors indicated that in the vicinity of a perforation, considerable solid material experiences shear failure and limited post-yield dilatation, modeled by the theory of perfect plasticity. Although this failure mode was not characteristic of the rock formation as a whole, these results suggest that an extrusion model aimed at describing deformation in the proximity of a perforation may adopt the assumptions of incompressibility, Tresca yield, and perfect plasticity employed in some previous extrusion studies (Prager, 1959; Ford, 1977). This allows uncoupling of the solution of the fluid and solid deformation problems, and the use of a complex potential to describe the pore pressure distribution. The analysis which follows employs this approach.

2 Plastic Deformation of a Porous Material

Consider a porous solid experiencing plastic deformation and subjected to a nonuniform pore pressure distribution. If the solid is rigid-perfectly plastic and incompressible, obeys a Tresca yield condition, and is in a state plane strain, the governing equations for the deformation are as follows.

[10]Assistant Professor, Department of Mechanical Engineering, University of Texas, Austin, TX 78712.

[11]Professor, Department of Mechanical Engineering and Materials Science, Rice University, Houston TX 77251.

Manuscript received by ASME Applied Mechanics Division, March 7, 1986; final revision, December 2, 1986.

Downloaded 03 May 2010 to 171.66.16.27. Redistribution subject to ASME license or copyright; see http://www.asme.org/terms/Terms_Use.cfm

dyopadhayay (1983), it may be shown that the moment-intensity factor in the transformed plane is given by

$$\hat{k}_1(p) = M_o(a)^{1/2}\,\frac{\Phi(1,p)}{p}, \tag{9}$$

where the auxiliary function, $\Phi(r,p)$, is governed by the Fredholm integral equation

$$\Phi(r;p) + \int_o^1 \Phi(y;p)L(ar,ay;p)dy = r^{1/2}, \tag{10}$$

and the kernel, $L(ar,ay;p)$, stands for the expression

$$L(ar,ay;p) = (ry)^{1/2}\int_o^\infty u\left[F\left(\frac{u}{a};p\right) - 1\right]J_o(ur)J_o(yu)du, \tag{11}$$

Here, J_o, denotes the usual Bessel function of the first kind of order zero and, $F(s,p)$, designates the abbreviation

$$\left.\begin{aligned} F(s,p) &= \frac{\gamma_1\gamma_2 s^2 B_1 + \gamma_1^2\gamma_1^2 + \nu_{xy}s^2(s^2B_1 - \gamma_1^2 - \gamma_1\gamma_2 - \gamma_2^2)}{s\gamma_1\gamma_2(\gamma_1+\gamma_2)} \\ B_1 &= 2\nu_{xy} + 4\,D_{xy}/D_y \end{aligned}\right\}, \tag{12}$$

Since γ_1 and γ_2 are complex conjugates, the function, $F(s,p)$, is real. Moreover, it can be readily shown that $F(s,p) \sim 1 + 0(s^{-2})$ for large s and, accordingly, equation (10) may be solved numerically by a method outlined in Krylov and Kantrorovich (1957) to yield the values of $\Phi(r,p)$. Finally, the time-dependence of the moment-intensity factor can be recovered in inverting the Laplace transform indicated in equation (9). This can be done by a method similar to the one employed by Miller and Guy (1966).

Numerical Results and Discussion

In order to illustrate the application of the solution, two plate elements with distinct orthotropic properties are considered. The first is made of boron-epoxy composite with the following elastic constants: $E_x = 55.16 \times 10^9$ N/m^2 (8×10^6 psi), $E_y = 170.65 \times 10^9$ N/m^2 (24.75×10^6 psi), $G_{xy} = 4.83 \times 10^9$ N/m^2 (0.7×10^6 psi) and $\nu_{xy} = 0.036$. The second material is a graphite-fiber composite (50 percent) with $E_x = 173.75 \times 10^9$ N/m^2 (25.2×10^6 psi), $E_y = 6.89 \times 10^9$ N/m^2 (1.0×10^6 psi), $G_{xy} = 3.79 \times 10^9$ N/m^2 (0.55×10^6 psi), and $\nu_{xy} = 0.28$. For each element, the values of $\Phi(1,p)$ are computed from equation (10) for crack length/plate thickness ratios $(a/h) = 1, 4$. The results are then used in conjunction with the Laplace inversion indicated in equation (9) to obtain the variation of the moment-intensity factor, $k_1(t)$, with time. The plots of $k_1(t)/M_o(a)^{1/2}$ versus $C_s t/a$, where $C_s^2 = G_{xy}/\rho$, are displayed graphically in Figs. (1) and (2). In both cases, $k_1(t)$ starts from zero and increases with time and approaches the corresponding statical value for large time. Because of the nature of the loading, one would expect, at short times, an overshoot in the moment-intensity factor near the crack tip. Indeed, the analysis employed here has predicted such overshoots in several similar problems (Kassir and Bandyopadhayay, 1983). However, in the present case, the analysis does not seem to predict a peak. This may be due to the approximate nature of the Kirchhoff plate equations used in formulating the problem. Similar results have been reported by Chen and Sih (1977) for the isotropic solid. Figures (1) and (2) indicate that by decreasing the ratio a/h results in an increase in the magnitude of the moment-intensity factor. This conclusion, however, can only be made for the materials considered.

References

Achenbach, J. D., and Bazant, Z. P., 1975, "Elastodynamic Near-Tip Stress and Displacement Fields for Rapidly Propagating Cracks in Orthotropic Materials," ASME JOURNAL OF APPLIED MECHANICS, Vol. 42, pp. 183–189.

Chen, E. P., and Sih, G. C., 1977, *Elastodynamic Crack Problems*, Noordhoff International Publishing, Leyden, The Netherlands.

Freedman, J. M., and Keer, L. M., 1973, "Vibratory Motion of a Body on an Orthotropic Half-Plane," ASME JOURNAL OF APPLIED MECHANICS, Vol. 40, pp. 221–229.

Kassir, M. K., and Bandyopadhayay, K. K., 1983, "Impact Response of a Cracked Orthotropic Medium," ASME JOURNAL OF APPLIED MECHANICS, Vol. 50, pp. 630–636.

Kassir, M. K., and Tse, S., 1983, "Moving Griffith Crack in an Orthotropic Material," *International Journal of Engineering Science*, Vol. 21, pp. 315–325.

Krylov, V. I., and Kantorovich, L. V., 1957, *Approximate Methods of Higher Analysis*, Interscience Publishers, New York, pp. 97–161.

Miller, M. K., and Guy, W. T., 1966, "Numerical Inversion of the Laplace Transform by Use of Jacobi Polynomials," *SIAM Journal of Numerical Analysis*, Vol. 3, pp. 624–635.

Vinson, J. R., and Chow, T. W., 1975, *Composite and Their Use in Structures*, Wiley, New York.

The Effect of Pore Fluid Flow on Extrusion

E. P. Fahrenthold[10] and J. B. Cheatham, Jr.[11]

1 Introduction

The collapse of well casing in hydrocarbon reservoirs has in some cases been preceded by fluidization or extrusion of rock through casing perforations. Analysis of this problem requires consideration of the effect of pore fluid flow on extrusion.

Much work in the field of deformable porous media focuses upon the coupling of fluid and solid motion (Bowen, 1982), and the role of solid matrix compaction in the maintenance of pore pressure. At first glance, the process of extrusion of a porous medium would seem to be dominated by similar compaction phenomena. However, recent study of the casing collapse process suggests that such may not be the case. Pattillo and Smith (1985) studied the effect of formation flow on casing integrity using the finite element method. These authors indicated that in the vicinity of a perforation, considerable solid material experiences shear failure and limited post-yield dilatation, modeled by the theory of perfect plasticity. Although this failure mode was not characteristic of the rock formation as a whole, these results suggest that an extrusion model aimed at describing deformation in the proximity of a perforation may adopt the assumptions of incompressibility, Tresca yield, and perfect plasticity employed in some previous extrusion studies (Prager, 1959; Ford, 1977). This allows uncoupling of the solution of the fluid and solid deformation problems, and the use of a complex potential to describe the pore pressure distribution. The analysis which follows employs this approach.

2 Plastic Deformation of a Porous Material

Consider a porous solid experiencing plastic deformation and subjected to a nonuniform pore pressure distribution. If the solid is rigid-perfectly plastic and incompressible, obeys a Tresca yield condition, and is in a state plane strain, the governing equations for the deformation are as follows.

[10]Assistant Professor, Department of Mechanical Engineering, University of Texas, Austin, TX 78712.

[11]Professor, Department of Mechanical Engineering and Materials Science, Rice University, Houston TX 77251.

Manuscript received by ASME Applied Mechanics Division, March 7, 1986; final revision, December 2, 1986.

Copyright © 1987 by ASME

Downloaded 03 May 2010 to 171.66.16.27. Redistribution subject to ASME license or copyright; see http://www.asme.org/terms/Terms_Use.cfm

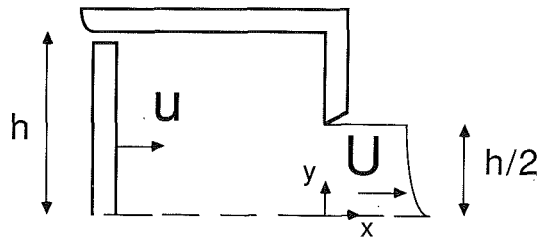


Fig. 1 Plane strain extrusion

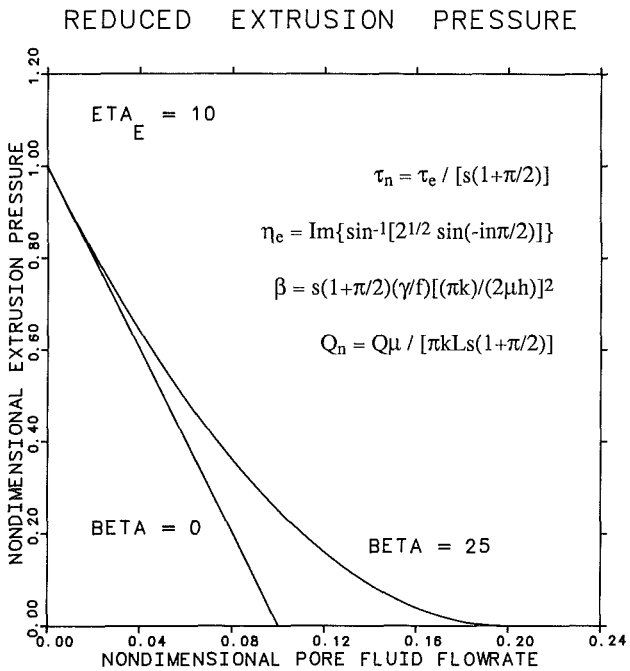


Fig. 2 Variation of the required mechanical extrusion pressure with pore fluid flow rate

The yield condition may be written in terms of the effective stress (σ_{ij})

$$\sigma_{ij} = \tau_{ij} - \delta_{ij}P \tag{1}$$

where τ_{ij} is the total stress, P is the pore pressure, δ_{ij} is the Kronecker delta, and compression is taken as positive. The yield condition is

$$(1/4)(\sigma_{xx} - \sigma_{yy})^2 + \sigma_{xy}{}^2 = s^2. \tag{2a}$$

where s is the yield strength in pure shear and the deformation is in the xy plane.

The equilibrium equations are, in terms of the total stress,

$$\frac{\partial \tau_{xx}}{\partial x} + \frac{\partial \tau_{xy}}{\partial y} = 0 \tag{3a}$$

$$\frac{\partial \tau_{yy}}{\partial y} + \frac{\partial \tau_{xy}}{\partial x} + 0. \tag{3b}$$

The Levy-Mises flow rule written in terms of the deviatoric effective stress (σ'_{ij}) is (Ford, 1977)

$$\dot{e}_{ij} = \dot{\lambda}\sigma'_{ij} \tag{4a}$$

where the $\dot{e}_{ij}$ are the strain rates for the porous solid, $\dot{\lambda}$ is a scalar proportionality function, and

$$\sigma'_{ij} = \sigma_{ij} - (1/3)\delta_{ij}\sigma_{\alpha\alpha}. \tag{4b}$$

The repeated index α indicates a sum over $\alpha = x, y, z$.

Since the deviatoric effective and deviatoric total stresses are equal, the yield condition and flow rule written in terms of the effective stress reduce to the conventional forms despite the introduction of a nonuniform pore pressure. Thus the total stress distribution in the mixture may be found from a method of characteristics solution, and the effects of pore fluid flow may be estimated using an appropriate potential flow solution.

3 Extrusion of a Porous Material

Consider the extrusion of a wide billet of solid material through a smooth die, with the extruded sheet having half the thickness of the original billet (see Fig. 1). The half-thickness of the billet is h, while the piston and extruded sheet velocities are u and U, respectively. The horizontal stress applied to the die is given by Ford (1977) as

$$\tau_{xx} = 2s\left(1 + \frac{\pi}{2}\right). \tag{5}$$

If the extruded billet is porous, and subjected to steady flow of an incompressible fluid from the direction of the permeable piston towards the die opening, the pore pressure distribution is determined by standard methods (Churchill, Brown, and Verhey, 1974) and has the form

$$P = \frac{Q\mu}{\pi kL} Im\left\{\sin^{-1}\left[\sqrt{2}\sin\left(\frac{\pi}{2h}(y - ix)\right)\right]\right\} \tag{6}$$

where Q is the fluid volumetric flowrate, L is the billet width, μ is the fluid viscosity, k is the billet permeability, Im denotes the imaginary part of a complex number, and $i = \sqrt{-1}$.

The application of mass and momentum balance laws to a deformable control volume bounded by the piston and the die exit gives the resulting force per unit width on the upper half of the piston as

$$F = hs\left(1 + \frac{\pi}{2}\right) + \rho u^2 h + \gamma f(u + v)^2 h \tag{7}$$

where v is the average fluid velocity relative to the solid at the piston, γ is the fluid density, ρ is the bulk solid density, f is the porosity, and $Q = 2Lfhv$.

In the case of a porous material, the extrusion pressure is composed of mechanical and pore fluid components

$$\frac{F}{h} = \tau_e + P_e. \tag{8}$$

The pore pressure P_e is calculated approximately from equation (6) with

$$y = 0;\ x = -nh \tag{9a,b}$$

where n is determined by the billet length in the x direction.

The nondimensional mechanical pressure (τ_n) required to initiate extrusion ($u \to 0$) is shown in Fig. 2 as a function of the nondimensional flow rate (Q_n) and the parameter β for a billet length corresponding to $\eta_e = 10$. The mechanical load required to initiate extrusion is reduced, to a variable extent determined by the material properties of the solid and the fluid.

4 References

Bowen, R. M., 1982, "Compressible Porous Media Models by Use of Theory of Mixtures," *International Journal of Engineering Science*, Vol. 20, No. 6, pp. 697–735.

Churchill, R. V., Brown, J. W, and Verhey, R. F., 1974, *Complex Variables and Applications*, McGraw-Hill, New York, pp. 195–238.

Ford, Sir Hugh, 1977, *Advanced Mechanics of Materials*, Wiley, New York.

Pattillo, P. D., and Smith, M. B., 1985, "The Effect of Formation Flow on the Integrity of Perforated Casing," *Society of Petroleum Engineers Journal*, pp. 637–646.

Prager, W., 1959, *An Introduction to Plasticity*, Addison-Wesley Publishing Co., Reading, Mass.

Downloaded 03 May 2010 to 171.66.16.27. Redistribution subject to ASME license or copyright; see http://www.asme.org/terms/Terms_Use.cfm

Surface Waves Perturbed by Rotation

T. Wren[12,14] and J. S. Burdess[13,14]

1 Introduction

A two-dimensional surface wave propagating over an isotropic half space, perturbed by rotation about an axis normal to the sagittal plane, is investigated using a singular perturbation method. Current interest in this problem stems from the possibility of detecting and measuring rotation through its effects on travelling surface waves. It was proposed by Lao (1980) that this mechanism could be used in the design of a robust inertial rate sensor.

2 Analysis

It will be assumed that the wave motion is described by displacement components, U and V, in the directions OX and OY of a right-handed Cartesian coordinate system. All quantities are assumed to be independent of the Z direction, and the half space, given by $x \leq 0$, is taken to rotate with constant angular velocity, Ω, about the axis OZ.

For convenience, the equations of motion and the surface boundary conditions will be expressed in terms of the dimensionless variables: $X = x/L_c$, $Y = y/L_c$, and $T = t/T_c$, where L_c and T_c are, respectively, a characteristic length and time, later chosen to be the wavelength and period of the surface wave. Similarly, unless it is otherwise stated, all other quantities appearing within this note are implicitly dimensionless.

If the rotation of the half space is represented by the dimensionless parameter $\epsilon = 2\Omega T_c$, and the characteristic time T_c is chosen to ensure that $\epsilon \ll 1$, then the equations of motion (Achenbach, 1980) can be written to first order in ϵ, as

$$C_T^2 \nabla^2 \mathbf{u} + (C_L^2 - C_T^2) \nabla(\nabla \cdot \mathbf{u}) - \epsilon \hat{z} \times \frac{\partial \mathbf{u}}{\partial T} = \frac{\partial^2 \mathbf{u}}{\partial t^2} \tag{1}$$

where

$$\nabla = \hat{i}\frac{\partial}{\partial X} + \hat{j}\frac{\partial}{\partial Y}, \quad \mathbf{u} = \hat{i}U + \hat{j}V, \quad C_L = \frac{\sqrt{\lambda + 2\mu}}{\rho}\frac{T_c}{L_c}$$

$$\text{and } C_T = \frac{\sqrt{\mu}}{\rho}\frac{T_c}{L_c}.$$

Here, C_T and C_L are the dimensionless speeds of propagation of the transverse and longitudinal bulk waves, λ and μ are the Lame constants, and ρ is the density of the material.

The stress free boundary conditions at the surface of the half space are given by

$$\frac{\partial U}{\partial X} + \frac{\partial V}{\partial Y} + \frac{2C_T^2}{(C_L^2 - 2C_T^2)}\frac{\partial U}{\partial X} = 0, \tag{2}$$

and

$$\frac{\partial U}{\partial Y} + \frac{\partial V}{\partial X} = 0. \tag{3}$$

These equations can be further simplified, if the displacement components, U and V, are replaced by the derivatives of both a scalar potential, Φ, and a vector potential, $\Psi\hat{z}$, using the relations

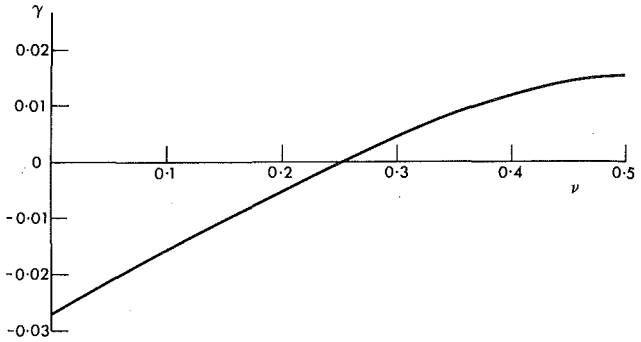


Fig. 1 γ as a function of Poisson's ratio

$$U = \frac{\partial \Phi}{\partial X} + \frac{\partial \Psi}{\partial Y}, \tag{4}$$

and

$$V = \frac{\partial \Phi}{\partial Y} - \frac{\partial \Psi}{\partial X}, \tag{5}$$

in which case a sufficient condition for the solution of equations (1) is that the potential displacements satisfy the following coupled wave equations,

$$C_L^2 \nabla^2 \phi - \frac{\partial^2 \Phi}{\partial T^2} - \epsilon \frac{\partial \Psi}{\partial T} = 0, \tag{6}$$

and

$$C_t^2 \nabla^2 \Psi - \frac{\partial^2 \Psi}{\partial T^2} + \epsilon \frac{\partial \Phi}{\partial T} = 0, \tag{7}$$

together with the transformed boundary conditions,

$$\frac{\partial^2 \Phi}{\partial X^2} + s\frac{\partial^2 \Psi}{\partial X \partial Y} + r\frac{\partial^2 \Phi}{\partial Y^2} = 0 \tag{8}$$

and

$$2\frac{\partial^2 \Phi}{\partial X \partial Y} + \frac{\partial^2 \Psi}{\partial Y^2} - \frac{\partial^2 \Psi}{\partial X^2} = 0 \tag{9}$$

at $X = 0$, where $s = 2C_T^2/C_L^2$ and $r = 1 - s$.

It is now assumed the solutions to the surface wave problem with rotation can be expressed in terms of the parameter ϵ, by a series of the form

$$\Phi(X,Y) = \phi_0(X,Y) + \epsilon\phi_1(X,Y) + 0(\epsilon^2) \tag{10}$$

and

$$\Psi(X,Y) = \psi_0(X,Y) + \epsilon\psi_1(X,Y) + 0(\epsilon^2) \tag{11}$$

Using regular perturbation methods, hereafter, to determine the functions ϕ_i and ψ_i would result in series solutions which were only valid when both X and Y were less than $0(1/\epsilon^2)$. To obtain solutions valid for all X and Y, it is necessary to use the method of multiple variable expansions, (Kevorkian and Cole, 1981). Using this approach all terms in the series solutions above are made to be dependent upon the parameter ϵ, through the change of variables

$$\begin{aligned} X^+ &= X\{1 + 0(\epsilon^2)\}, \\ Y^+ &= Y\{1 + 0(\epsilon^2)\}, \\ X^- &= X\epsilon, \\ Y^- &= Y\epsilon, \end{aligned} \tag{12}$$

and hence

$$\frac{\partial}{\partial X} = \frac{\partial}{\partial X^+} + \epsilon\frac{\partial}{\partial X^-} + 0(\epsilon^2),$$

$$\frac{\partial}{\partial Y} = \frac{\partial}{\partial Y^+} + \epsilon\frac{\partial}{\partial Y^-} + 0(\epsilon^2).$$

[12] Research Associate.
[13] Lecturer.
[14] Department of Mechanical Engineering, University of Newcastle upon Tyne, Newcastle upon Tyne, England NE1 7RU.

Manuscript received by ASME Applied Mechanics Division, December 10, 1985; final revision, September 8, 1986.

Copyright © 1987 by ASME
Downloaded 03 May 2010 to 171.66.16.27. Redistribution subject to ASME license or copyright; see http://www.asme.org/terms/Terms_Use.cfm

Rewriting each of the foregoing equations, using equations (12), and thereafter substituting the series solutions (10) and (11) into equations (6), (7), (8), and (9), yields equations of motion and boundary conditions associated with each power of ϵ.

The zeroth order equations of motion, associated with powers of ϵ^0, are found to be

$$C_L^2 \nabla_+^2 \phi_0 - \frac{\partial^2}{\partial T^2} \phi_0 = 0, \tag{13}$$

and

$$C_T^2 \nabla_+^2 \psi_0 - \frac{\partial^2}{\partial T^2} \psi_0 = 0, \tag{14}$$

where

$$\nabla_+^2 = \frac{\partial^2}{\partial X^{+2}} + \frac{\partial^2}{\partial Y^{+2}}$$

Likewise, the zeroth order boundary conditions are given by

$$\frac{\partial^2 \phi_0}{\partial X^{+2}} + s \frac{\partial^2 \psi_0}{\partial X^+ \partial Y^+} + r \frac{\partial^2 \phi_0}{\partial Y^{+2}} = 0, \tag{15}$$

and

$$2 \frac{\partial^2 \phi_0}{\partial X^+ \partial Y^+} + \frac{\partial^2 \psi_0}{\partial Y^{+2}} - \frac{\partial^2 \psi_0}{\partial X^{+2}} = 0, \tag{16}$$

at

$$X^+ = X^- = 0.$$

Surface wave solutions of the form:

$$\phi_0 = \alpha_0 A_0(X^-, Y^-) e^{b_1 X^+} e^{i(kY^+ - \omega T)} \tag{17}$$

and

$$\psi_0 = \beta_0 B_0(X^-, Y^-) e^{b_2 X^+} e^{i(kY^+ - \omega T)}, \tag{18}$$

will satisfy equations (13) and (14) provided the decay constants b_1 and b_2 are related to the wave vector, k, through the following relations

$$b_1^2 = k^2(1 - C^2/C_L^2), \tag{19}$$

and

$$b_2^2 = k^2(1 - C^2/C_T^2), \tag{20}$$

where $c = \omega/k$.

Solving the boundary conditions, (15) and (16), for all Y, requires that $A_0(0, Y^-) = B_0(0, Y^-)$, and thereafter, gives the familiar equation determining the phase velocity of the unperturbed surface wave,

$$(2 - C^2/C_T^2)^2 - 4(1 - C^2/C_L^2)^{1/2}(1 - C^2/C_T^2)^{1/2} = 0, \tag{21}$$

together with the relation: $\beta_0 = 2i\alpha_0(1 - C^2/C_L^2)^{1/2}/(2 - C^2/C_T^2) = i\alpha_0\theta$, say.

To determine the remaining unknowns A_0 and B_0, it is necessary to consider the first order equations of motion, which are found to be

$$C_L^2 \nabla_+^2 \phi_1 - \frac{\partial^2}{\partial T^2} \phi_1 = \frac{\partial}{\partial T} \psi_0 - 2C_L^2 \left\{ \frac{\partial^2 \phi_0}{\partial X^+ \partial X^-} + \frac{\partial^2 \phi_0}{\partial Y^+ \partial Y^-} \right\}, \tag{22}$$

and

$$C_T^2 \nabla_+^2 \psi_1 - \frac{\partial^2}{\partial T^2} \psi_1 = -\frac{\partial}{\partial T} \phi_0 - 2C_T^2 \left\{ \frac{\partial^2 \psi_0}{\partial X^+ \partial X^-} + \frac{\partial^2 \psi_0}{\partial Y^+ \partial Y^-} \right\}. \tag{23}$$

The terms contained in each of the brackets given above can be shown, by using equations (17) to (20), to be solutions of the homogeneous equations corresponding to equations (22) and (23). Therefore, if retained, these terms would lead to particular solutions involving factors of X^+ and Y^+, and hence to series solutions unbounded at infinity. Solutions valid for all X^+ and Y^+ can be obtained if the bracketed terms are set to zero; this can be achieved if the functions A_0 and B_0 are chosen so that

$$\left(b_1 \frac{\partial}{\partial X^-} + ik \frac{\partial}{\partial Y^-} \right) A_0(X^-, Y^-) = 0, \tag{24}$$

and

$$\left(b_2 \frac{\partial}{\partial X^-} + ik \frac{\partial}{\partial Y^-} \right) B_0(X^-, Y^-) = 0. \tag{25}$$

By separating variables and imposing the restrictions that $A_0(0, Y^-) = B_0(0, Y^-)$, the appropriate solutions to equations (24) and (25) are found to be

$$A_0(X^-, Y^-) = e^{\gamma(kX^- + i b_1 Y^-)}, \tag{26}$$

and

$$B_0(X^-, Y^-) = e^{\gamma\left(k \frac{b_1}{b_2} X^- + i b_1 Y^-\right)}, \tag{27}$$

where γ is a scaled separation constant yet to be determined. The solutions to the first order equations of motion, having set the bracketed terms to zero, are then given by,

$$\phi_1 = \left\{ \alpha_1 A_1(X^-, Y^-) e^{b_1 X^+} + \Lambda_1 \alpha_0 e^{\gamma\left(\frac{b_1}{b_2} kX^- + i b_1 Y^-\right)} e^{b_2 X^+} \right\} \times e^{i(kY^+ - \omega T)}, \tag{28}$$

and

$$\psi_1 = \left\{ \beta_1 B_1(X^-, Y^-) e^{b_2 X^+} + i\Lambda_2 \alpha_0 e^{\gamma(kX^- + i b_1 Y^-)} e^{b X^+} \right\} \times e^{i(kY^+ - \omega T)}, \tag{29}$$

where

$$\Lambda_1 = \frac{kC\theta}{(b_2^2 - b_1^2) C_L^2}, \text{ and } \Lambda_2 = \frac{-kC}{(b_2^2 - b_1^2) C_T^2}.$$

The first order boundary conditions are the final equations to be solved, and are given by,

$$\frac{2\partial^2 \phi_0}{\partial X^+ \partial X^-} + 2r \frac{\partial^2 \phi_0}{\partial Y^+ \partial Y^-} + \frac{\partial^2 \phi_1}{\partial X^{+2}} + r \frac{\partial^2 \phi_1}{\partial Y^{+2}} + s \frac{\partial^2 \psi_0}{\partial Y^+ \partial X^-} + s \frac{\partial^2 \psi_0}{\partial Y^- \partial X^+} + s \frac{\partial^2 \psi_1}{\partial X^+ \partial Y^+} = 0, \tag{30}$$

and

$$\frac{\partial^2 \phi_0}{\partial Y^+ \partial X^-} + \frac{\partial^2 \phi_0}{\partial Y^- \partial X^+} + \frac{\partial^2 \phi_1}{\partial Y^+ \partial X^+} + \frac{\partial^2 \psi_0}{\partial Y^+ \partial X^-} + \frac{1}{2} \frac{\partial^2 \psi_1}{\partial Y^{+2}} - \frac{\partial^2 \psi_0}{\partial X^+ \partial X^-} - \frac{1}{2} \frac{\partial^2 \psi_1}{\partial X^{+2}} = 0, \tag{31}$$

at $X^+ = X^- = 0$. These conditions can be satisfied by expressions (17), (18), (28), and (29), for all Y, only if $A_1(0, Y^-) = B_1(0, Y^-)$, whereupon they can be written in the form,

$$\begin{pmatrix} b_1^2 - rk^2 & ikb_2 s \\ 2ikb_1 & -(k^2 + b_2^2) \end{pmatrix} \begin{pmatrix} \alpha_1 \\ \beta_1 \end{pmatrix} = \begin{pmatrix} \gamma\eta_1 + \eta_3 \\ \gamma\eta_2 i + \eta_4 i \end{pmatrix}, \tag{32}$$

where

Downloaded 03 May 2010 to 171.66.16.27. Redistribution subject to ASME license or copyright; see http://www.asme.org/terms/Terms_Use.cfm

$$\eta_1 = 2rb_1k + \frac{sb_1}{b_2}k^2\theta + sb_1b_2\theta - 2kb_1$$

$$\eta_2 = 4kb_1\theta - 2k^2 - 2b_1^2,$$

$$\eta_3 = \Lambda_1(rk^2 - b_2^2) + \Lambda_2 sb_1k. \tag{33}$$

and

$$\eta_4 = \Lambda_2(k^2 + b_1^2) - 2b_2k\Lambda_1.$$

The system has solutions only if the ranks of the coefficient and augmented matrices are equal. The coefficient matrix can be seen to have rank one through comparison with equation (21). For this to be also true of the augmented matrix, requires that

$$\gamma = \frac{(k^2 + b_2^2)\eta_3 - kb_2s\eta_4}{kb_2s\eta_2 - (k^2 + b_2^2)\eta_1} \tag{34}$$

which then fully determines expressions (17) and (18).

It is now possible to derive the displacement components from the potentials, (17) and (18), through use of equations (4) and (5). These can be rewritten in terms of X and Y, by using equations (12), to give

$$u \simeq \alpha_0\left[(b_1 + \Delta b_1)e^{(b_1+\Delta b_1)X} - \theta(k + \Delta k)e^{(b_2+\Delta b_2)X}\right] \times e^{i(k+\Delta k)Y - \omega T}, \tag{35}$$

and

$$v \simeq \alpha_0 i\left[(k + \Delta k)e^{(b_1+\Delta b_1)X} - \theta(b_2 + \Delta b_2)e^{(b_2+\Delta b_2)X}\right] \times e^{i(k+\Delta k)Y - \omega T} \tag{36}$$

By choosing T_C to be the period of the surface wave, and L_C to be the wavelength, the dimensions are restored to all variables, in which case,

$$\Delta b_1 = 4\pi\gamma k\left(\frac{\Omega}{\omega}\right),$$

$$\Delta b_2 = 4\pi\gamma kb_1/b_2\left(\frac{\Omega}{\omega}\right),$$

$$\Delta k = 4\pi\gamma b_1\left(\frac{\Omega}{\omega}\right) \tag{37}$$

where b_1, b_2, and k are now given in m^{-1}, and Ω and ω are given in rads/s. The difference between the phase velocities of the perturbed and unperturbed surface waves is then obtained as

$$\Delta C = \frac{\omega}{k + \Delta k} - \frac{\omega}{k} \simeq -\frac{C\Delta k}{k} \tag{38}$$

The previous analysis applies to a forward travelling surface wave. To obtain the corresponding expressions for a backward travelling wave, ω is simply replaced by $-\omega$ throughout; in which case the difference in the phase velocities of two counterpropagating waves is shown to be $2\Delta C$.

Equations (35), (36), and (37) show explicitly how the peak amplitudes, decay constants, and phase velocity are changed by rotation. These changes are essentially determined by the dimensionless quantity γ, the magnitude and sign of which depends only upon the Poisson's ratio of the material, as is shown in Fig. 1.

The changes Δb_1, Δb_2, Δk, and Δc, for a given rate of turn, can be obtained from Fig. 1 simply by scaling the ordinate by the appropriate factors appearing in equations (37) and (38), in which case the results show good agreement with those given by Lao (1980).

3 Concluding Remarks

The problem of a surface wave perturbed by rotation has been successfully solved using singular perturbation methods and the effects of rotation discussed. Explicit results have been derived and it is shown that two counterpropagating waves travel at different velocities. Numerical results determined from the perturbation analysis are in good agreement with previously derived results, showing the usefulness of singular perturbation methods when applied to nonstandard wave problems.

References

Achenbach, J. D., 1980, *Wave Propagation in Elastic Solids*, North Holland, pp. 65–66.

Kevorkian, J., and Cole, J. D., 1981, *Perturbation Methods in Applied Mathematics*, Springer Verlag, pp. 465–468.

Lao, B. Y., 1980, *Gyroscopic Effect in Surface Acoustic Waves*, 1980, Ultrasonics Symposium Proceedings, IEEE Cat. No. 80 CH 1602 2, Institute of Electrical and Electronic Engineers, New York, pp. 687.

A Differential Effective Medium Theory With a Composite Sphere Embedding

Y. Benveniste[15]

Introduction

The concept of incremental homogenization originally proposed by Bruggeman (1952) has been recently elaborated and generalized by Norris et al. (1985) in the context of the transport properties of two-phase composites, and by Norris (1985) in the context of the mechanical properties. The generalization proposed in these works assumes a third phase which acts as a "backbone." The other two phases are progressively added to the backbone material such that each addition takes place in an effectively homogeneous medium. This is in contrast to the original formulation of Bruggeman (1952), in which one phase is taken as the backbone and only the second phase is added at every stage of the homogenization process.

We do not intend to review in this short note previous work on the differential scheme. The method has been comprehensively reviewed by Norris et al. (1985) and Norris (1985), where an extensive list of references can also be found on this subject. In these last two works, both constituents are added at every stage of the homogenization process in the form of separate particles. For composites made of a matrix phase containing particulate inclusions on the other hand, an imbedding in the form of a particle surrounded by a matrix shell appears to be a plausible alternative. We consider this alternative in this note, limiting ourselves for simplicity to spherical particles only. Although the presented treatment is valid for transport properties in general, we will use here the terminology of heat conduction. The resulting differential equation for the effective conductivity is integrated for a specific class of the homogenization process, leading to a closed form expression for this quantity. The classical differential approximation of Bruggeman (1952), and the Hashin-Shtrikman composite-spheres assemblage (Hashin and Shtrikman, 1962) are obtained as special cases of the homogenization scheme presented in this paper.

[15]Department of Solid Mechanics, Materials and Structures, Faculty of Engineering, Tel-Aviv University, Ramat-Aviv 69978, Israel.

Manuscript received by ASME Applied Mechanics Division, October 1, 1986; final revision, January 10, 1987.

Downloaded 03 May 2010 to 171.66.16.27. Redistribution subject to ASME license or copyright; see http://www.asme.org/terms/Terms_Use.cfm

$$\eta_1 = 2rb_1k + \frac{sb_1}{b_2}k^2\theta + sb_1b_2\theta - 2kb_1$$

$$\eta_2 = 4kb_1\theta - 2k^2 - 2b_1^2,$$

$$\eta_3 = \Lambda_1(rk^2 - b_2^2) + \Lambda_2 sb_1k. \tag{33}$$

and

$$\eta_4 = \Lambda_2(k^2 + b_1^2) - 2b_2k\Lambda_1.$$

The system has solutions only if the ranks of the coefficient and augmented matrices are equal. The coefficient matrix can be seen to have rank one through comparison with equation (21). For this to be also true of the augmented matrix, requires that

$$\gamma = \frac{(k^2 + b_2^2)\eta_3 - kb_2s\eta_4}{kb_2s\eta_2 - (k^2 + b_2^2)\eta_1} \tag{34}$$

which then fully determines expressions (17) and (18).

It is now possible to derive the displacement components from the potentials, (17) and (18), through use of equations (4) and (5). These can be rewritten in terms of X and Y, by using equations (12), to give

$$u \simeq \alpha_0\left[(b_1 + \Delta b_1)e^{(b_1+\Delta b_1)X} - \theta(k + \Delta k)e^{(b_2+\Delta b_2)X}\right] \times e^{i(k+\Delta k)Y - \omega T}, \tag{35}$$

and

$$v \simeq \alpha_0 i\left[(k + \Delta k)e^{(b_1+\Delta b_1)X} - \theta(b_2 + \Delta b_2)e^{(b_2+\Delta b_2)X}\right] \times e^{i(k+\Delta k)Y - \omega T} \tag{36}$$

By choosing T_C to be the period of the surface wave, and L_C to be the wavelength, the dimensions are restored to all variables, in which case,

$$\Delta b_1 = 4\pi\gamma k\left(\frac{\Omega}{\omega}\right),$$

$$\Delta b_2 = 4\pi\gamma kb_1/b_2\left(\frac{\Omega}{\omega}\right),$$

$$\Delta k = 4\pi\gamma b_1\left(\frac{\Omega}{\omega}\right) \tag{37}$$

where b_1, b_2, and k are now given in m^{-1}, and Ω and ω are given in rads/s. The difference between the phase velocities of the perturbed and unperturbed surface waves is then obtained as

$$\Delta C = \frac{\omega}{k + \Delta k} - \frac{\omega}{k} \simeq -\frac{C\Delta k}{k} \tag{38}$$

The previous analysis applies to a forward travelling surface wave. To obtain the corresponding expressions for a backward travelling wave, ω is simply replaced by $-\omega$ throughout; in which case the difference in the phase velocities of two counterpropagating waves is shown to be $2\Delta C$.

Equations (35), (36), and (37) show explicitly how the peak amplitudes, decay constants, and phase velocity are changed by rotation. These changes are essentially determined by the dimensionless quantity γ, the magnitude and sign of which depends only upon the Poisson's ratio of the material, as is shown in Fig. 1.

The changes Δb_1, Δb_2, Δk, and Δc, for a given rate of turn, can be obtained from Fig. 1 simply by scaling the ordinate by the appropriate factors appearing in equations (37) and (38), in which case the results show good agreement with those given by Lao (1980).

3 Concluding Remarks

The problem of a surface wave perturbed by rotation has been successfully solved using singular perturbation methods and the effects of rotation discussed. Explicit results have been derived and it is shown that two counterpropagating waves travel at different velocities. Numerical results determined from the perturbation analysis are in good agreement with previously derived results, showing the usefulness of singular perturbation methods when applied to nonstandard wave problems.

References

Achenbach, J. D., 1980, *Wave Propagation in Elastic Solids*, North Holland, pp. 65–66.

Kevorkian, J., and Cole, J. D., 1981, *Perturbation Methods in Applied Mathematics*, Springer Verlag, pp. 465–468.

Lao, B. Y., 1980, *Gyroscopic Effect in Surface Acoustic Waves*, 1980, Ultrasonics Symposium Proceedings, IEEE Cat. No. 80 CH 1602 2, Institute of Electrical and Electronic Engineers, New York, pp. 687.

A Differential Effective Medium Theory With a Composite Sphere Embedding

Y. Benveniste[15]

Introduction

The concept of incremental homogenization originally proposed by Bruggeman (1952) has been recently elaborated and generalized by Norris et al. (1985) in the context of the transport properties of two-phase composites, and by Norris (1985) in the context of the mechanical properties. The generalization proposed in these works assumes a third phase which acts as a "backbone." The other two phases are progressively added to the backbone material such that each addition takes place in an effectively homogeneous medium. This is in contrast to the original formulation of Bruggeman (1952), in which one phase is taken as the backbone and only the second phase is added at every stage of the homogenization process.

We do not intend to review in this short note previous work on the differential scheme. The method has been comprehensively reviewed by Norris et al. (1985) and Norris (1985), where an extensive list of references can also be found on this subject. In these last two works, both constituents are added at every stage of the homogenization process in the form of separate particles. For composites made of a matrix phase containing particulate inclusions on the other hand, an imbedding in the form of a particle surrounded by a matrix shell appears to be a plausible alternative. We consider this alternative in this note, limiting ourselves for simplicity to spherical particles only. Although the presented treatment is valid for transport properties in general, we will use here the terminology of heat conduction. The resulting differential equation for the effective conductivity is integrated for a specific class of the homogenization process, leading to a closed form expression for this quantity. The classical differential approximation of Bruggeman (1952), and the Hashin-Shtrikman composite-spheres assemblage (Hashin and Shtrikman, 1962) are obtained as special cases of the homogenization scheme presented in this paper.

[15]Department of Solid Mechanics, Materials and Structures, Faculty of Engineering, Tel-Aviv University, Ramat-Aviv 69978, Israel.

Manuscript received by ASME Applied Mechanics Division, October 1, 1986; final revision, January 10, 1987.

Copyright © 1987 by ASME
Downloaded 03 May 2010 to 171.66.16.27. Redistribution subject to ASME license or copyright; see http://www.asme.org/terms/Terms_Use.cfm

Analysis

The incremental homogenization process as described in Norris et al. (1985) starts with a volume V_o of a backbone material which will be denoted here by the index $\alpha=0$. A small volume of V_o is taken out, and replaced by an equal volume containing grains of materials ($\alpha=1$, 2) that constitute the two-phase composite. The resulting solid is assumed to be homogeneous and the same procedure is repeated stage after stage.

Let ϕ_0, ϕ_1, ϕ_2 define the volume fractions of the three constituents at any stage of the construction, so that $\phi_0+\phi_1+\phi_2=1$. In order to arrive to a composite containing only the phases $\alpha=1$ and $\alpha=2$, one possibility is to continue the homogenization process until the volume fraction of the backbone material vanishes. Another alternative is to start with either of the phases, say the matrix ($\alpha=1$), as the backbone material. It should be noted however that the framework presented by Norris et al. (1985) can also be used to model the conductivity of a three-phase composite with the backbone material ($\alpha=0$) being the matrix, and the components $\alpha=1,2$ denoting the inclusion phases.

The incremental homogenization presented in Norris et al. (1985) is done in the form of addition of separate particles of each phase. The present note proposes an incremental embedding in the form of a composite sphere containing a particle core surrounded by a matrix shell. As is well known, this idea of composite sphere embedding has already been used in the literature in the context of self-consistent approximations (see Hashin, 1968, for example), and is specially suitable for composites containing a matrix phase. The coated sphere concept has also been useful in self-similar modeling of rocks (Sen et al., 1981). Its use in the framework of a differential scheme, however, is new and contributes to the versatility of the differential homogenization method.

The homogenization process can be described by a certain path in the (ϕ_1, ϕ_2) plane or alternatively in the (v_1, v_2) plane where v_1 and v_2 denote the volumes of the used up materials during the construction scheme. The following relations between the variables v_1, v_2 and ϕ_1, ϕ_2 derived in Norris et al. (1985), remain to be valid in the present version of the theory

$$V_o\dot{\phi}_1=(1-\phi_1)\dot{v}_1-\phi_1\dot{v}_2, \quad V_o\dot{\phi}_2=(1-\phi_2)\dot{v}_2-\phi_2\dot{v}_1, \tag{1}$$

$$\dot{v}_1/V_o=[(1-\phi_2)\dot{\phi}_1+\phi_1\dot{\phi}_2]/(1-\phi),$$
$$\dot{v}_2/V_o=[(1-\phi_1)\dot{\phi}_2+\phi_2\dot{\phi}_1]/(1-\phi), \tag{2}$$

where the dot denotes differentiation with respect to the time t and $\phi=\phi_1+\phi_2$.

Let us now proceed to the description of the differential equation which governs the evolution of the effective conductivity during the homogenization process. The intensity H_i and heat flux q_i are defined by

$$H_i=(\partial\Phi/\partial x_i), \quad q_i=k_{ij}H_j, \tag{3}$$

where Φ denotes the temperature field, x_i represents the coordinate system, and k_{ij} is the symmetric conductivity tensor. We limit ourselves here to isotropic constituents with conductivity k_α ($\alpha=1,2$) and to effectively isotropic composites, so that the effective conductivity is described by $k^*_{ij}=\delta_{ij}k^*$, where δ_{ij} is the Kronecker delta.

The governing differential equation for k^* obtained in Norris et al. (1985) is given by

$$\dot{k}^*(t)=-(G_1\dot{\phi}_1+G_2\dot{\phi}_2)-(G_1\phi_1+G_2\phi_2)[\dot{\phi}/(1-\phi)], \tag{4}$$

with G_α being defined as

$$G_\alpha(k^*)=(k^*-k_\alpha)g_\alpha, \quad g_\alpha=\bar{H}_i^{(\alpha)}/H_i^o, \quad \alpha=1,2, \tag{5}$$

where H_i^o are constant intensity components defined through homogeneous boundary conditions on the temperature field $\Phi(S)=-H_i^o x_i$, with S denoting the surface of the composite, and $\bar{H}_i^{(\alpha)}$ are the average intensity field in each phase resulting under these boundary conditions.

The differential equation (4) continues to be valid for the present case in which a composite sphere is embedded at every stage of the homogenization process. The functions g_α are now related to the average intensity in the matrix shell ($\alpha=1$) and particle core ($\alpha=2$). They can be determined by solving the auxiliary problem of a composite sphere embedded in a homogeneous medium of conductivity k^*, the whole geometry being subjected to homogeneous boundary conditions on the temperature field. Let a and ρ denote, respectively, the inside and outside radius of the composite sphere and assume continuity of the temperature field and normal component of the heat flux at $r=a$, and $r=\rho$. The solution for the temperature field of this problem can be found in Hashin (1968). The average intensity fields in the particle core and matrix shell can be readily computed, yielding:

$$g_1=[3(\lambda+2)(k^*/k_1)]/[A+(k^*/k_1)B],$$
$$g_2=[9(k^*/k_1)]/[A+(k^*/k_1)B], \tag{6}$$

where $\lambda=k_2/k_1$ and,

$$A=(\lambda+2)+2c'(\lambda-1), \quad B=2(\lambda+2)+2c'(1-\lambda) \tag{7}$$

with c' being given by $c'=a^3/\rho^3$.

The differential equation (4) can easily be integrated along straight line segments in the (ϕ_1, ϕ_2) plane. Consider here such a homogenization scheme described by a line, starting at (0, 0) with the initial condition $k^*(0)=k_o$, where k_o denotes conductivity of the backbone material, and ending at $(\tilde{\phi}_1, \tilde{\phi}_2)$. Equations (1) and (2) imply that this process is described by a line with the same slope in both (ϕ_1, ϕ_2), (v_1, v_2) planes, that is,

$$\phi_2=C\phi_1, \quad v_2=Cv_1, \quad C=\tilde{\phi}_2/\tilde{\phi}_1. \tag{8}$$

Furthermore, if c' as appearing in equations (7) denotes the volume fraction of the embedded sphere, it follows that

$$c'=\Delta v_2/(\Delta v_1+\Delta v_2)=C/(1+C). \tag{9}$$

The differential equation (4) can now be integrated, yielding

$$\int_{k_o}^{k^*}\frac{d\eta}{(1-c')G_1(\eta)-c'G_2(\eta)}=ln(1-\tilde{\phi})=ln\tilde{\phi}_o, \tag{10}$$

where in the integrand, the integration parameter η has replaced k^*; $\tilde{\phi}=\tilde{\phi}_1+\tilde{\phi}_2$, and $\tilde{\phi}_o$ denotes the volume fraction of the backbone material at the end of the integration process. Using equations (5), (6), and (7) and integrating we obtain after some manipulation the following solution for k^*

$$(k^*/k_o)^{-1/3}[-A+(B/2)(k^*/k_1)]/$$
$$[-A+(B/2)(k_o/k_1)]=\tilde{\phi}_o. \tag{11}$$

Consider now the situation in which the backbone material is totally replaced, that is, $\tilde{\phi}_o\to 0$. Under this condition, since $\tilde{\phi}_1+\tilde{\phi}_2=1$, using equations (8) we get $\tilde{\phi}_1(1+C)=1$, where now $\tilde{\phi}_1=\nu_1$, $\tilde{\phi}_2=\nu_2$, with ν_1 and ν_2 denoting the actual volume fractions of the phases $\alpha=1$ and $\alpha=2$. Solving for C as $C=(1/\nu_1)-1$ and substituting in equation (9), it is seen that $\tilde{\phi}_o\to 0$ implies $c'=\nu_2$. Using these relations in equation (11) yields for k^*,

$$(k^*/k_1)=[(\lambda+2)+2\nu_2(\lambda-1)]/$$
$$[(\lambda+2)+\nu_2(1-\lambda)], \quad \tilde{\phi}_o\to 0, \tag{12}$$

which, interestingly enough, is exactly the composite sphere assemblage result of Hashin and Shtrikman (1962), leading thus to another realization of this geometry. It should be noted here that equation (12) could also have been obtained by substituting the expression for g_2 in equations (6) to the differential equation of Bruggeman which is itself the special case

Downloaded 03 May 2010 to 171.66.16.27. Redistribution subject to ASME license or copyright; see http://www.asme.org/terms/Terms_Use.cfm

of equation (4) with $\phi_1 = \tilde{\phi}_1 = 0$. Bruggeman's result was, on the other hand, obtained by employing the solution of a particle in an infinite effective medium, that is $g_2 = 3k^*/(2k^* + k_2)$.

Consider now the case in which the backbone material is identified with one of the phases, say the matrix. Letting $\tilde{\phi}_2 = \nu_2$, $\tilde{\phi}_o + \tilde{\phi}_1 = \nu_1$, and using the last of equations (8) together with equation (9), provides $c' = \nu_2/(1 - \tilde{\phi}_o)$, which means that the arbitrariness in the choice of $\tilde{\phi}_o$ mentioned in Norris et al. (1985) can now be interpreted as an arbitrariness in c'. Demanding the physical conditions $0 \leqq c' \leqq 1$, $0 \leqq \tilde{\phi}_o \leqq 1$, implies that in fact we need to have: $\nu_2 \leqq c' \leqq 1$ and $0 \leqq \tilde{\phi}_o \leqq 1 - \nu_2$. Under $k_o = k_1$, equation (11), therefore, becomes

$$(k^*/k_1)^{-1/3}[-A + (B/2)(k^*/k_1)]/[3c'(1-\lambda)] = (c' - \nu_2)/c'. \quad (13)$$

This equation is a cubic equation for k^* which can readily be proved to possess only one positive real root. For $c' = \nu_2$, equation (12) is recovered, and for $c' = 1$ Bruggeman's result is obtained.

The use of a composite sphere embedding in the framework of a differential scheme was presented in this note as a natural way of modeling the effective properties of composites consisting of a matrix and particulate inclusion phases. The conductivity context and the case of spherical particles were chosen for the sake of brevity and clarity in the presentation. Consideration of spheroidal particles representing short fibers, or the analysis of the mechanical properties of particulate media, although being more elaborate, can in principle be dealt with in the framework of the procedure presented in this note. For example, computation of the effective shear modulus of a composite containing spherical inclusions along the same lines should yield a new prediction for a situation in which a composite sphere assemblage result does not exist. Concerning short-fiber composites, following the solution of the auxiliary problem which can be found in Hatta and Taya (1986), it is possible to obtain the relevant versions of equation (11) and its limiting result (12). Another application of the differential scheme, in which the composite sphere appears to be the most proper embedding form, is composites exhibiting a thermal contact resistance at constituent interfaces (see Benveniste and Miloh, 1986). Finally, it should be mentioned that although the treatment in this note was limited to two-phase media, the presented framework can readily be used for the prediction of the effective conductivity of three-phase coated filler composites. Such composites have been recently discussed by Hatta and Taya (1986) and have been reported to possess desirable properties, especially in the electric conductivity context.

References

Benveniste, Y., and Miloh, T., 1986, "The Effective Conductivity of Composites with Imperfect Thermal Contact at Constituent Interfaces," *Int. J. Engng. Sci.*, Vol. 24, pp. 1537–1552.

Bruggeman, D. A. G., 1952, "Berechnung Verschiedener Physikalischer Konstanten von Heterogenen Substanzen," *Annal en der Physik*, Vol. 23, pp. 779–784.

Hashin, Z., 1968, "Assessment of the Self-Consistent Scheme Approximation: Conductivity of Particulate Composites," *J. of Composite Materials*, Vol. 2, pp. 284–300.

Hashin, Z., and Shtrikman, 1962, "Variational Approach to the Theory of the Effective Magnetic Permeability of Multiphase Materials," *J. Appl. Phys.*, Vol. 33, pp. 3125–3131.

Hatta, H., and Taya, M., 1986, "Thermal Conductivity of Coated Filler Composites," *J. of Applied Physics*, Vol. 59, pp. 1851–1860.

Norris, A. N., 1985, "A Differential Scheme for the Effective Moduli of Composites," *Mechanics of Materials*, Vol. 4, pp. 1–16.

Norris, A. N., Callegari, A. J., and Sheng, P., 1985, "A Generalized Differential Effective Medium Theory," *Journal of the Mechanics and Physics of Solids*, Vol. 33, pp. 525–543.

Sen, P. N., Scala, C., and Cohen, M. H., 1981, "A Self-Similar Model for Sedimentary Rocks with Application to the Dielectric Constant of Fused Glass Beads," *Geophysics*, Vol. 46, pp. 781–795.

Transient Waves in a Beam Excited by Sinusoidal Edge Shear Force

W. L. Hallauer, Jr.[16]

Introduction

The problem considered in this Note was motivated by dynamic response observed during the author's (1987) experimental study of structural waves in a plane grid of thin-walled beams. The excitation used to produce flexural waves in the grid was out-of-plane force applied at a point on the grid's boundary and varying with time as a suddenly applied sinusoid, $u(t)\sin\Omega t$, where $u(t)$ is the unit step at time $t = 0$ and Ω is radian frequency. This excitation was intended to expedite measurement of group and phase velocities in the dispersive grid, just as a similar type of excitation can in a beam. Bozich (1971) showed that suddenly applied sinusoidal displacement on the edge of a semi-infinite beam produces a displacement "wavefront" traveling at the group velocity into the beam's interior; the wavefront is preceded by low level, high frequency precursor waves and followed by higher level synchronous waves, i.e., waves having the frequency of the sinusoidal excitation and traveling at the phase velocity.

The author (1987) observed experimentally that displacement response of the plane grid to suddenly applied sinusoidal point-force excitation included a dominant nonoscillatory component which increased monotonically for some time after the start of excitation, appearing almost to be a secular component. The observed behavior was duplicated numerically with a finite element model of the grid and a modal finite series solution. But the series solution cannot be interpreted physically and is useful only for numerical evaluation. Therefore, it was desirable to seek a physically clearer solution for a qualitatively similar but mathematically simpler problem, a single beam under the same type of excitation.

Accordingly, the purposes of this Note are: to outline the solution for transient response of a semi-infinite Euler-Bernoulli beam to suddenly applied sinusoidal edge shear force excitation; to show that there is a secular component of displacement response, and that it increases as the square root of time; and to illustrate the physical character of the response, including both secular and oscillatory components.

Timoshenko beam theory or a more precise theory is required if flexural wavelengths are on the order of the beam's thickness or less and frequencies are correspondingly high. However, Euler-Bernoulli beam theory is quite satisfactory for the beams in the author's (1987) experiment. The grid was composed of beams only 3.2 mm (1/8 in.) thick, and excitation with frequencies of 240 Hz or lower was applied. The measurable oscillatory component of response consisted of waves with lengths at least two orders of magnitude greater than the beam thickness. Moreover, a suddenly applied sinusoidal excitation of frequency Ω, despite being impulsive, does not excite response at substantially higher frequencies; the Fourier transform of this function peaks sharply at Ω but decays steeply with increasing frequency above Ω.

Few exact closed-form solutions for transient forced response of Euler-Bernoulli beams have been published previously. Jones' (1954) solutions for applied unit step shear force on infinite and semi-infinite beams were probably the first. The most relevant predecessor of the solution presented herein is Bozich's (1971) solution discussed above, which was based on Steele's (1967) work.

[16]Professor, Department of Aerospace and Ocean Engineering, Virginia Polytechnic Institute and State University, Blacksburg, VA 24061.

Manuscript received by ASME Applied Mechanics Division, January 5, 1987.

Downloaded 03 May 2010 to 171.66.16.27. Redistribution subject to ASME license or copyright; see http://www.asme.org/terms/Terms_Use.cfm

of equation (4) with $\phi_1 = \tilde{\phi}_1 = 0$. Bruggeman's result was, on the other hand, obtained by employing the solution of a particle in an infinite effective medium, that is $g_2 = 3k^*/(2k^* + k_2)$.

Consider now the case in which the backbone material is identified with one of the phases, say the matrix. Letting $\tilde{\phi}_2 = \nu_2$, $\tilde{\phi}_o + \tilde{\phi}_1 = \nu_1$, and using the last of equations (8) together with equation (9), provides $c' = \nu_2/(1 - \tilde{\phi}_o)$, which means that the arbitrariness in the choice of $\tilde{\phi}_o$ mentioned in Norris et al. (1985) can now be interpreted as an arbitrariness in c'. Demanding the physical conditions $0 \leqq c' \leqq 1$, $0 \leqq \tilde{\phi}_o \leqq 1$, implies that in fact we need to have: $\nu_2 \leqq c' \leqq 1$ and $0 \leqq \tilde{\phi}_o \leqq 1 - \nu_2$. Under $k_o = k_1$, equation (11), therefore, becomes

$$(k^*/k_1)^{-1/3}[-A + (B/2)(k^*/k_1)]/[3c'(1-\lambda)] = (c' - \nu_2)/c'. \quad (13)$$

This equation is a cubic equation for k^* which can readily be proved to possess only one positive real root. For $c' = \nu_2$, equation (12) is recovered, and for $c' = 1$ Bruggeman's result is obtained.

The use of a composite sphere embedding in the framework of a differential scheme was presented in this note as a natural way of modeling the effective properties of composites consisting of a matrix and particulate inclusion phases. The conductivity context and the case of spherical particles were chosen for the sake of brevity and clarity in the presentation. Consideration of spheroidal particles representing short fibers, or the analysis of the mechanical properties of particulate media, although being more elaborate, can in principle be dealt with in the framework of the procedure presented in this note. For example, computation of the effective shear modulus of a composite containing spherical inclusions along the same lines should yield a new prediction for a situation in which a composite sphere assemblage result does not exist. Concerning short-fiber composites, following the solution of the auxiliary problem which can be found in Hatta and Taya (1986), it is possible to obtain the relevant versions of equation (11) and its limiting result (12). Another application of the differential scheme, in which the composite sphere appears to be the most proper embedding form, is composites exhibiting a thermal contact resistance at constituent interfaces (see Benveniste and Miloh, 1986). Finally, it should be mentioned that although the treatment in this note was limited to two-phase media, the presented framework can readily be used for the prediction of the effective conductivity of three-phase coated filler composites. Such composites have been recently discussed by Hatta and Taya (1986) and have been reported to possess desirable properties, especially in the electric conductivity context.

References

Benveniste, Y., and Miloh, T., 1986, "The Effective Conductivity of Composites with Imperfect Thermal Contact at Constituent Interfaces," *Int. J. Engng. Sci.*, Vol. 24, pp. 1537–1552.

Bruggeman, D. A. G., 1952, "Berechnung Verschiedener Physikalischer Konstanten von Heterogenen Substanzen," *Annal en der Physik*, Vol. 23, pp. 779–784.

Hashin, Z., 1968, "Assessment of the Self-Consistent Scheme Approximation: Conductivity of Particulate Composites," *J. of Composite Materials*, Vol. 2, pp. 284–300.

Hashin, Z., and Shtrikman, 1962, "Variational Approach to the Theory of the Effective Magnetic Permeability of Multiphase Materials," *J. Appl. Phys.*, Vol. 33, pp. 3125–3131.

Hatta, H., and Taya, M., 1986, "Thermal Conductivity of Coated Filler Composites," *J. of Applied Physics*, Vol. 59, pp. 1851–1860.

Norris, A. N., 1985, "A Differential Scheme for the Effective Moduli of Composites," *Mechanics of Materials*, Vol. 4, pp. 1–16.

Norris, A. N., Callegari, A. J., and Sheng, P., 1985, "A Generalized Differential Effective Medium Theory," *Journal of the Mechanics and Physics of Solids*, Vol. 33, pp. 525–543.

Sen, P. N., Scala, C., and Cohen, M. H., 1981, "A Self-Similar Model for Sedimentary Rocks with Application to the Dielectric Constant of Fused Glass Beads," *Geophysics*, Vol. 46, pp. 781–795.

Transient Waves in a Beam Excited by Sinusoidal Edge Shear Force

W. L. Hallauer, Jr.[16]

Introduction

The problem considered in this Note was motivated by dynamic response observed during the author's (1987) experimental study of structural waves in a plane grid of thin-walled beams. The excitation used to produce flexural waves in the grid was out-of-plane force applied at a point on the grid's boundary and varying with time as a suddenly applied sinusoid, $u(t)\sin\Omega t$, where $u(t)$ is the unit step at time $t = 0$ and Ω is radian frequency. This excitation was intended to expedite measurement of group and phase velocities in the dispersive grid, just as a similar type of excitation can in a beam. Bozich (1971) showed that suddenly applied sinusoidal displacement on the edge of a semi-infinite beam produces a displacement "wavefront" traveling at the group velocity into the beam's interior; the wavefront is preceded by low level, high frequency precursor waves and followed by higher level synchronous waves, i.e., waves having the frequency of the sinusoidal excitation and traveling at the phase velocity.

The author (1987) observed experimentally that displacement response of the plane grid to suddenly applied sinusoidal point-force excitation included a dominant nonoscillatory component which increased monotonically for some time after the start of excitation, appearing almost to be a secular component. The observed behavior was duplicated numerically with a finite element model of the grid and a modal finite series solution. But the series solution cannot be interpreted physically and is useful only for numerical evaluation. Therefore, it was desirable to seek a physically clearer solution for a qualitatively similar but mathematically simpler problem, a single beam under the same type of excitation.

Accordingly, the purposes of this Note are: to outline the solution for transient response of a semi-infinite Euler-Bernoulli beam to suddenly applied sinusoidal edge shear force excitation; to show that there is a secular component of displacement response, and that it increases as the square root of time; and to illustrate the physical character of the response, including both secular and oscillatory components.

Timoshenko beam theory or a more precise theory is required if flexural wavelengths are on the order of the beam's thickness or less and frequencies are correspondingly high. However, Euler-Bernoulli beam theory is quite satisfactory for the beams in the author's (1987) experiment. The grid was composed of beams only 3.2 mm (1/8 in.) thick, and excitation with frequencies of 240 Hz or lower was applied. The measurable oscillatory component of response consisted of waves with lengths at least two orders of magnitude greater than the beam thickness. Moreover, a suddenly applied sinusoidal excitation of frequency Ω, despite being impulsive, does not excite response at substantially higher frequencies; the Fourier transform of this function peaks sharply at Ω but decays steeply with increasing frequency above Ω.

Few exact closed-form solutions for transient forced response of Euler-Bernoulli beams have been published previously. Jones' (1954) solutions for applied unit step shear force on infinite and semi-infinite beams were probably the first. The most relevant predecessor of the solution presented herein is Bozich's (1971) solution discussed above, which was based on Steele's (1967) work.

[16]Professor, Department of Aerospace and Ocean Engineering, Virginia Polytechnic Institute and State University, Blacksburg, VA 24061.

Manuscript received by ASME Applied Mechanics Division, January 5, 1987.

Copyright © 1987 by ASME
Downloaded 03 May 2010 to 171.66.16.27. Redistribution subject to ASME license or copyright; see http://www.asme.org/terms/Terms_Use.cfm

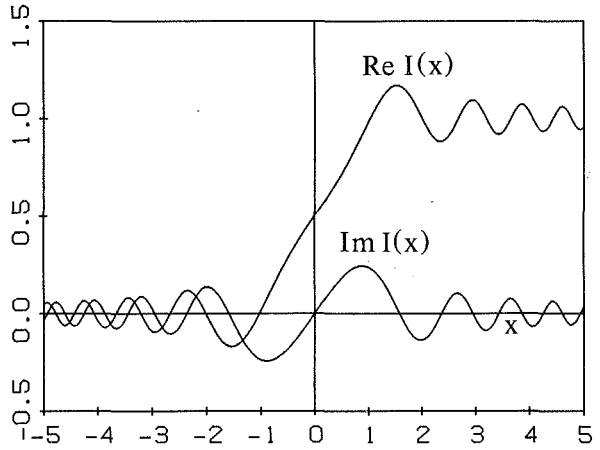


Fig. 1 Auxiliary error function *I(x)*

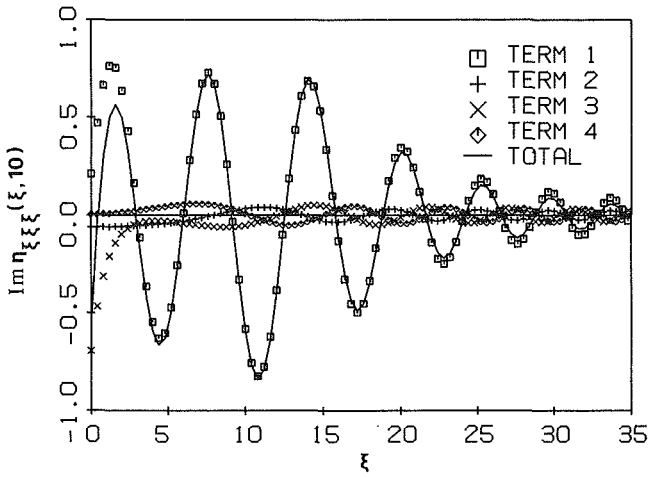


Fig. 2 Dimensionless shear force at $\tau = 10$

Analysis and Discussion

Consider a uniform Euler-Bernoulli beam with bending stiffness EI and mass per unit length ρA. The beam is semi-infinite, with spatial coordinate $x \geqq 0$. The dependent variable is transverse displacement $v(x, t)$ for time $t \geqq 0$. The only excitation is concentrated sinusoidal shear force $S_0 \sin \Omega t$ on the beam's boundary $x = 0$, beginning at $t = 0$. Bending moment is zero on the boundary. The entire beam is stationary prior to $t = 0$.

Dimensionless variables appropriate to this problem are $\tau = \Omega t$, $\xi = (\Omega/C)x$, and $\eta(\xi, \tau) = (EI/S_0)(\Omega/C)^3 v(x, t)$, where phase velocity $C = (EI\Omega^2/\rho A)^{1/4}$. It is convenient in the solution procedure to use the complex exponential $e^{i\tau}$ as the excitation, and then to take the imaginary part of the solution as the response to the actual excitation, $\sin\tau$. Accordingly, the partial differential equation of motion, boundary conditions, and initial conditions are

$$\eta_{\xi\xi\xi\xi} + \eta_{\tau\tau} = 0 \text{ for } \xi \geqq 0, \tau \geqq 0 \tag{1a}$$

$$\eta_{\xi\xi\xi} = e^{i\tau} \text{ and } \eta_{\xi\xi} = 0 \text{ for } \xi = 0, \tau \geqq 0 \tag{1b}$$

$$\eta = 0 \text{ and } \eta_\tau = 0 \text{ for } \xi \geqq 0, \tau = 0 \tag{1c}$$

The form of (1) is suitable for Laplace transformation with the definition

$$\bar{\eta}(\xi; s) = \int_{\tau=0}^{\infty} e^{-s\tau} \eta(\xi, \tau) d\tau, \ \mathrm{Re}(s) > 0 \tag{2}$$

Transforming equation (1*a*) and accounting for (1*c*) gives

$$\bar{\eta}'''' + s^2 \bar{\eta} = 0 \tag{3a}$$

Transforming (1*b*) gives

$$\bar{\eta}'''(0; s) = 1/(s - i) \text{ and } \bar{\eta}''(0; s) = 0 \tag{3b}$$

The solution of (3) that decays toward zero as $\xi \to \infty$ is

$$\bar{\eta}(\xi; s) = (1/\sqrt{2})[\exp(-e^{i\pi/4}\xi\sqrt{s}) + \exp(-e^{-i\pi/4}\xi\sqrt{s})]/[s^{3/2}(s - i)] \tag{4}$$

The inverse Laplace transform of equation (4) can be determined by use of Campbell and Foster's (1948) book, an extensive collection of transform pairs. Indeed, this book includes transform pairs that can be used to solve the Euler-Bernoulli beam equation (1*a*) in closed form for various combinations of boundary conditions and various forms of boundary excitation, the conditions (1*b*) being just one of many solvable cases.

From equation (4), the type of transform to be inverted is

$$\bar{f}_1(s) = e^{-a\sqrt{s}}/[s^{3/2}(s + b^2)] \tag{5}$$

where a and b are constants. The inverse of $\bar{f}_1(s)$ is not given by Campbell and Foster, but the inverse of $\bar{f}_2(s) = s\bar{f}_1(s)$ is. Hence, one can determine the inverse of $\bar{f}_1(s)$ from the identity $f_1(\tau) = \int_0^\tau f_2(\zeta) d\zeta$. A lengthy integration gives

$$f_1(\tau) = [2\sqrt{(\tau/\pi)} e^{-a^2/4\tau} - a\, erfc(a/2\sqrt{\tau})]/b^2 - ie^{-b^2\tau}[e^{iab} erfc(a/2\sqrt{\tau} + ib\sqrt{\tau}) - e^{-iab} erfc(a/2\sqrt{\tau} - ib\sqrt{\tau})]/2b^3 \tag{6}$$

where $erfc(z)$ is the complementary error function (Gautschi, 1966).

Now, use of the transform pair (5) and (6) gives the inverse of (4). After some algebraic manipulation, one finds

$$\eta(\xi, \tau) = i\sqrt{(8\tau/\pi)}\cos(\xi^2/4\tau) - i4\xi\, \mathrm{Re}[\alpha I(-\xi/2\sqrt{\tau})] - \alpha e^{i(\tau-\xi)} I(\sqrt{\tau} - \xi/2\sqrt{\tau}) + \alpha e^{i(\tau+\xi)} I(-\sqrt{\tau} - \xi/2\sqrt{\tau}) - \alpha e^{(i\tau-\xi)} I(\sqrt{\tau} + i\xi/2\sqrt{\tau}) + \alpha e^{(i\tau+\xi)} I(-\sqrt{\tau} + i\xi/2\sqrt{\tau}) \tag{7}$$

where $\alpha = 1/2\,(1 + i)$ and $I(z) = 1/2\, erfc(e^{-i3\pi/4} z)$. The auxiliary error function $I(z)$ is especially appropriate for transient waves in Euler-Bernoulli beams. Steele (1967, 1971) described $I(z)$ and used it for moving load problems. Figure 1, from Steele's papers, illustrates the function for real argument.

The first term of equation (7) is unbounded at any ξ as $\tau \to \infty$. The unbounded character of motion is particularly simple at the point of excitation. Evaluating equation (7) at $\xi = 0$ with the use of error function identities (Gautschi, 1966), and then taking the imaginary part, which corresponds to $\sin\tau$ excitation, one finds

$$Im\eta(0, \tau) = \sqrt{(8\tau/\pi)} + \sqrt{2}\sin(\tau - 3\pi/4) + 4Im[\alpha e^{i\tau} I(-\sqrt{\tau})] \tag{8}$$

The third term of equation (8) is significant for only a short time, becoming negligible after just one cycle of excitation, $\tau > 2\pi$. The type of motion described by equation (8) was observed in the author's (1987) plane grid experiment.

For comparison with equation (7), the steady-state bounded wave solution of (1*a*) and (1*b*), without regard to (1*c*), is

$$\eta^{ss}(\xi, \tau) = -\alpha e^{i(\tau-\xi)} - \alpha e^{(i\tau-\xi)} \tag{9}$$

Referring to Fig. 1, one sees that equation (9) is the limit for $\tau \to \infty$ and $\xi << 2\tau$ of the last four terms of equation (7). But the first two terms of equation (7) are absent from equation (9), so equation (9) is not a limit solution of the complete initial-boundary-value problem (1).

In equation (7), the products of exponentials and error

Downloaded 03 May 2010 to 171.66.16.27. Redistribution subject to ASME license or copyright; see http://www.asme.org/terms/Terms_Use.cfm

functions represent oscillatory motion, including traveling waves. However, the character of the oscillations is illustrated most clearly by the dimensionless shear force, $\eta_{\xi\xi\xi}$. One could determine $\eta_{\xi\xi\xi}$ by differentiating equation (7), but it is easier to differentiate the transform (4) and then to obtain the inverse transform directly from Campbell and Foster (1948),

$$\eta_{\xi\xi\xi}(\xi,\tau) = -i\alpha e^{i(\tau-\xi)} I(\sqrt{\tau}-\xi/2\sqrt{\tau}) - i\alpha e^{i(\tau+\xi)} I(-\sqrt{\tau}-\xi/2\sqrt{\tau}) + \alpha e^{(i\tau+\xi)} I(-\sqrt{\tau}+i\xi/2\sqrt{\tau}) + \alpha e^{(i\tau+\xi)} I(-\sqrt{\tau}+i\xi/2\sqrt{\tau}) \quad (10)$$

The imaginary parts of equation (10) and each of its individual terms are plotted in Fig. 2 for $\tau = 10$. Fortran subroutine MERRCZ of the IMSL Library (1984) was used for evaluation of the error function. Shear force is bounded, unlike displacement, and the steady-state shear force wave solution, $\eta^{ss}_{\xi\xi\xi}$ from equation (9), does equal the limit of equation (10) for $\tau \to \infty$ and $\xi << 2\tau$.

Shear force solution (10) is very similar to the displacement solution determined by Bozich (1971) for response to a suddenly applied sinusoidal edge displacement. Bozich described several interesting characteristics of the solution. As Fig. 2 illustrates, the first term of equation (10) is quite dominant everywhere except near $\xi = 0$. Each of the functions in the first term represents rightward traveling waves. The exponential represents synchronous waves oscillating at the excitation frequency and traveling at the phase velocity. The error function represents a modulating envelope traveling at the group velocity, which is twice the phase velocity. The group velocity wavefront is defined as the point $\xi = 2\tau$, where $I(0) = 0.5$. This wavefront is preceded by low level, high frequency precursor waves and followed by higher level synchronous waves.

Acknowledgments

This work was sponsored by AFOSR Contract F49620-85-C-0024, Dr. A. K. Amos, Structural Mechanics Program Manager. Mr. D. J. Trivedi programmed the calculations and plotting.

References

Anonymous, 1984, *User's Manual, IMSL Library*, ed. 9.2, Vol. 3, International Mathematical and Statistical Libraries Inc., Houston, Ch. M.

Bozich, W. F., 1971, "Wave Propagation in Simple Nonhomogeneous Systems with a Transition Point," Ph.D. Dissertation, Department of Aeronautics and Astronautics, Stanford University, pp. 6-16.

Campbell, G. A., and Foster, R. M., 1948, *Fourier Integrals for Practical Applications*, D. Van Nostrand Company Inc., New York, pp. 92-94.

Gautschi, W., 1966, "Error Function and Fresnel Integrals," *Handbook of Mathematical Functions*, Abramowitz, M., and Stegun, I. A., eds., National Bureau of Standards, Applied Mathematics Series 55, pp. 295-329.

Hallauer, W. L., Jr., and Trivedi, D. J., 1987, "An Experimental Study of Transient Waves in a Plane Grid Structure," AIAA Paper 87-0943-CP, AIAA Dynamics Specialists Conference, Monterey, CA.

Jones, R. P. N., 1954, "The Wave Method for Solving Flexural Vibration Problems," ASME JOURNAL OF APPLIED MECHANICS, Vol. 21, No. 1, pp. 75-80.

Steele, C. R., 1967, "The Finite Beam With a Moving Load," ASME JOURNAL OF APPLIED MECHANICS, Vol. 34, No. 1, pp. 111-118.

Steele, C. R., 1971, "Beams and Shells With Moving Loads," *International Journal of Solids and Structures*, Vol. 7, pp. 1171-1198.

Interface Stress Singularities at a Notch Tip in Antiplane Shear

D. Durban[17,18] and E. Ore[18]

[17]Currently at Cambridge University, Department of Engineering, Trumpington Street, Cambridge, England CB2 1PZ (on sabbatical leave here until September 1987).

[18]Department of Aeronautical Engineering, Technion – Israel Institute of Technology, Haifa 32000, Israel.

Manuscript received by ASME Applied Mechanics Division, June 23, 1986; final revision, November 11, 1986.

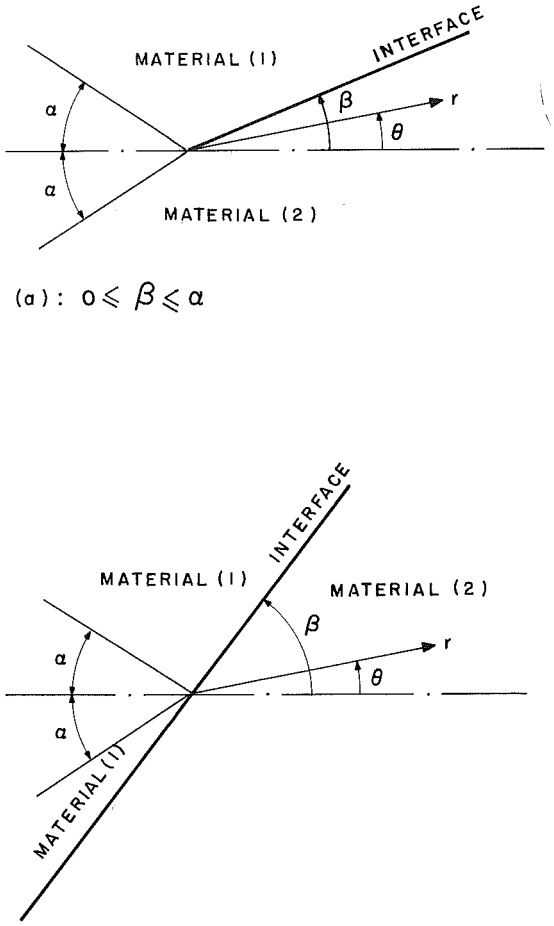


Fig. 1 Notation for the notch-tip field. The notch angle is 2α and the angle of inclination is β. In case (a) $0 \le \beta \le \alpha$ and in case (b) $\alpha \le \beta \le \pi - \alpha$.

We consider the local singular plastic field near the tip of a notch whose sharp edge touches the interface between two different materials. The deformation pattern is assumed to be in a state of antiplane shear, and the uniaxial stress-strain curve is represented by the linear-hardening characteristic

$$\epsilon_P^{(i)} = \left(\frac{1}{E_T^{(i)}} - \frac{1}{E^{(i)}}\right)(\sigma_e^{(i)} - Y^{(i)}) \quad i = 1,2 \quad (1)$$

where ϵ_P is the total effective plastic strain, σ_e is the effective stress, Y is the yield stress, E and E_T are the elastic and tangent moduli, respectively, and the index $i = 1, 2$ refers to materials 1 and 2.

With 2α denoting the notch angle and β being the angle of inclination, there are just two possible geometries as shown in Fig. 1. Thus, for $0 \le \beta \le \alpha$ we need to consider continuity conditions at the interface $\theta = \beta$, while for $\alpha \le \beta \le \pi - \alpha$ it is necessary to comply with continuity requirements at $\theta = \beta$ and at $\theta = \beta - \pi$.

Interfacial cracks in elastic bimaterials have received considerable attention in the literature. A list of references can be found in Atkinson's (1979) review. It is well known that oscillatory terms arise, in problems of this kind, over certain domains of the governing parameters.

Here, we show that the stresses admit *simple singularities* of the form r^{s-1}, where $0 < s < 1$, over the *entire range* of notch tip geometry and material constants.

The analysis is based on the usual small strain deformation

Downloaded 03 May 2010 to 171.66.16.27. Redistribution subject to ASME license or copyright; see http://www.asme.org/terms/Terms_Use.cfm

functions represent oscillatory motion, including traveling waves. However, the character of the oscillations is illustrated most clearly by the dimensionless shear force, $\eta_{\xi\xi\xi}$. One could determine $\eta_{\xi\xi\xi}$ by differentiating equation (7), but it is easier to differentiate the transform (4) and then to obtain the inverse transform directly from Campbell and Foster (1948),

$$\eta_{\xi\xi\xi}(\xi,\tau) = -i\alpha e^{i(\tau-\xi)} I(\sqrt{\tau}-\xi/2\sqrt{\tau}) - i\alpha e^{i(\tau+\xi)} I(-\sqrt{\tau}-\xi/2\sqrt{\tau}) + \alpha e^{(i\tau-\xi)} I(\sqrt{\tau}+i\xi/2\sqrt{\tau}) + \alpha e^{(i\tau+\xi)} I(-\sqrt{\tau}+i\xi/2\sqrt{\tau}) \quad (10)$$

The imaginary parts of equation (10) and each of its individual terms are plotted in Fig. 2 for $\tau = 10$. Fortran subroutine MERRCZ of the IMSL Library (1984) was used for evaluation of the error function. Shear force is bounded, unlike displacement, and the steady-state shear force wave solution, $\eta^{ss}_{\xi\xi\xi}$ from equation (9), does equal the limit of equation (10) for $\tau \to \infty$ and $\xi << 2\tau$.

Shear force solution (10) is very similar to the displacement solution determined by Bozich (1971) for response to a suddenly applied sinusoidal edge displacement. Bozich described several interesting characteristics of the solution. As Fig. 2 illustrates, the first term of equation (10) is quite dominant everywhere except near $\xi = 0$. Each of the functions in the first term represents rightward traveling waves. The exponential represents synchronous waves oscillating at the excitation frequency and traveling at the phase velocity. The error function represents a modulating envelope traveling at the group velocity, which is twice the phase velocity. The group velocity wavefront is defined as the point $\xi = 2\tau$, where $I(0) = 0.5$. This wavefront is preceded by low level, high frequency precursor waves and followed by higher level synchronous waves.

Acknowledgments

This work was sponsored by AFOSR Contract F49620-85-C-0024, Dr. A. K. Amos, Structural Mechanics Program Manager. Mr. D. J. Trivedi programmed the calculations and plotting.

References

Anonymous, 1984, *User's Manual, IMSL Library*, ed. 9.2, Vol. 3, International Mathematical and Statistical Libraries Inc., Houston, Ch. M.

Bozich, W. F., 1971, "Wave Propagation in Simple Nonhomogeneous Systems with a Transition Point," Ph.D. Dissertation, Department of Aeronautics and Astronautics, Stanford University, pp. 6-16.

Campbell, G. A., and Foster, R. M., 1948, *Fourier Integrals for Practical Applications*, D. Van Nostrand Company Inc., New York, pp. 92-94.

Gautschi, W., 1966, "Error Function and Fresnel Integrals," *Handbook of Mathematical Functions*, Abramowitz, M., and Stegun, I. A., eds., National Bureau of Standards, Applied Mathematics Series 55, pp. 295-329.

Hallauer, W. L., Jr., and Trivedi, D. J., 1987, "An Experimental Study of Transient Waves in a Plane Grid Structure," AIAA Paper 87-0943-CP, AIAA Dynamics Specialists Conference, Monterey, CA.

Jones, R. P. N., 1954, "The Wave Method for Solving Flexural Vibration Problems," ASME JOURNAL OF APPLIED MECHANICS, Vol. 21, No. 1, pp. 75-80.

Steele, C. R., 1967, "The Finite Beam With a Moving Load," ASME JOURNAL OF APPLIED MECHANICS, Vol. 34, No. 1, pp. 111-118.

Steele, C. R., 1971, "Beams and Shells With Moving Loads," *International Journal of Solids and Structures*, Vol. 7, pp. 1171-1198.

Interface Stress Singularities at a Notch Tip in Antiplane Shear

D. Durban[17,18] and E. Ore[18]

[17]Currently at Cambridge University, Department of Engineering, Trumpington Street, Cambridge, England CB2 1PZ (on sabbatical leave here until September 1987).

[18]Department of Aeronautical Engineering, Technion – Israel Institute of Technology, Haifa 32000, Israel.

Manuscript received by ASME Applied Mechanics Division, June 23, 1986; final revision, November 11, 1986.

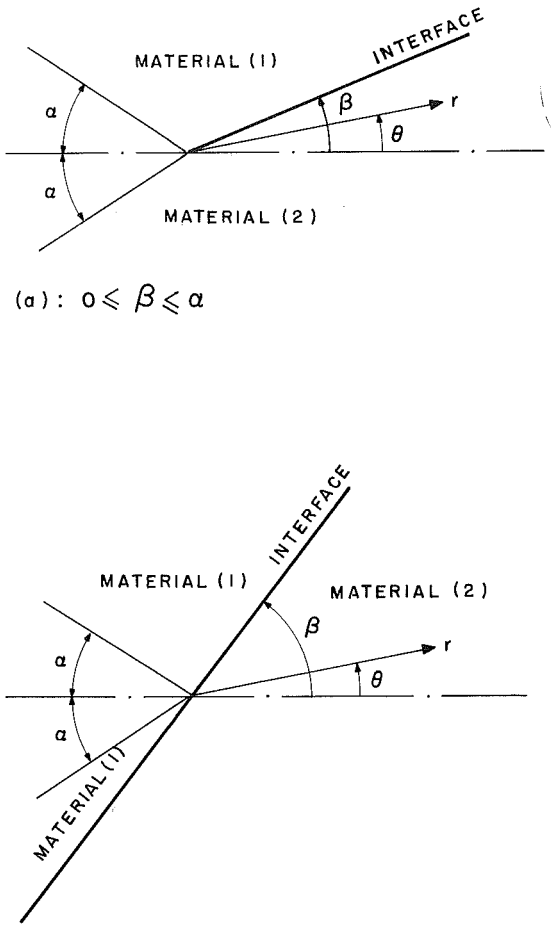


Fig. 1 Notation for the notch-tip field. The notch angle is 2α and the angle of inclination is β. In case (a) $0 \le \beta \le \alpha$ and in case (b) $\alpha \le \beta \le \pi - \alpha$.

We consider the local singular plastic field near the tip of a notch whose sharp edge touches the interface between two different materials. The deformation pattern is assumed to be in a state of antiplane shear, and the uniaxial stress-strain curve is represented by the linear-hardening characteristic

$$\epsilon_P^{(i)} = \left(\frac{1}{E_T^{(i)}} - \frac{1}{E^{(i)}}\right)(\sigma_e^{(i)} - Y^{(i)}) \quad i = 1,2 \quad (1)$$

where ϵ_P is the total effective plastic strain, σ_e is the effective stress, Y is the yield stress, E and E_T are the elastic and tangent moduli, respectively, and the index $i = 1, 2$ refers to materials 1 and 2.

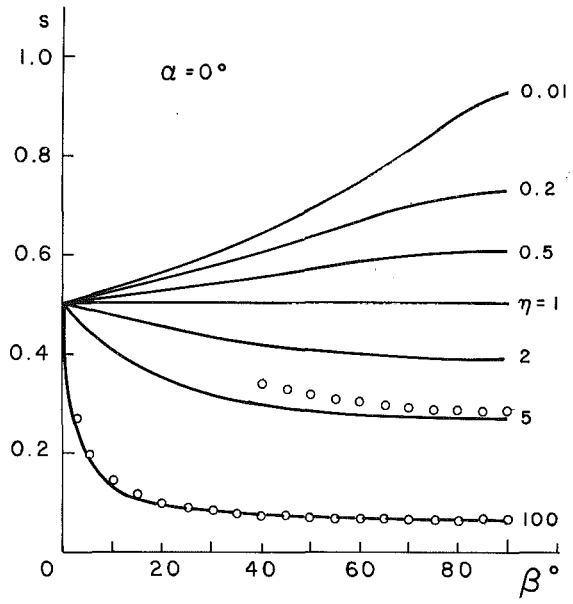
With 2α denoting the notch angle and β being the angle of inclination, there are just two possible geometries as shown in Fig. 1. Thus, for $0 \le \beta \le \alpha$ we need to consider continuity conditions at the interface $\theta = \beta$, while for $\alpha \le \beta \le \pi - \alpha$ it is necessary to comply with continuity requirements at $\theta = \beta$ and at $\theta = \beta - \pi$.

Interfacial cracks in elastic bimaterials have received considerable attention in the literature. A list of references can be found in Atkinson's (1979) review. It is well known that oscillatory terms arise, in problems of this kind, over certain domains of the governing parameters.

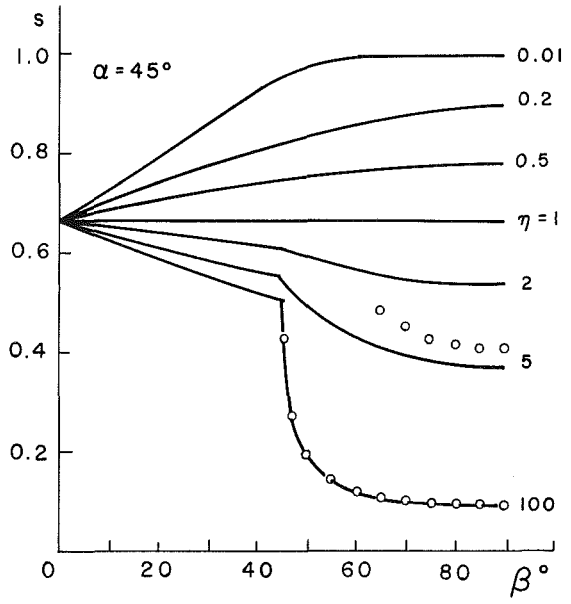
Here, we show that the stresses admit *simple singularities* of the form r^{s-1}, where $0 < s < 1$, over the *entire range* of notch tip geometry and material constants.

The analysis is based on the usual small strain deformation

Copyright © 1987 by ASME
Downloaded 03 May 2010 to 171.66.16.27. Redistribution subject to ASME license or copyright; see http://www.asme.org/terms/Terms_Use.cfm



(a)



(b)

Fig. 2 Dependence of the eigenvalue s on the angle of inclination β for different values of the material parameter β. Case (a) is for a crack with $\alpha = 0$ deg. Case (b) is for a 90 deg notch. The level of the stress singularity is 1 – s. The circles show values from the asymptotic expansion (17).

theory of plasticity. The only nonvanishing displacement $w = w(r, \theta)$ is in the out-of-plane direction (z) and the shear strains are simply

$$2\gamma_{rz} = w_{,r} \quad 2\gamma_{\theta z} = r^{-1} w_{,\theta} \tag{2}$$

The constitutive relations can be written as

$$w_{,r} = g r^{-1} F_{,\theta} \quad w_{,\theta} = -grF_{,r} \tag{3}$$

where F is the stress function, so that $\tau_{rz} = r^{-1}F_{,\theta}$ and $\tau_{\theta z} = -F_{,r}$, and

$$g = \frac{1}{G} + 3\frac{\epsilon_P}{\sigma_e} \tag{4}$$

with G standing for the elastic shear modulus. Note that the effective stress is given by $\sigma_e = \sqrt{3}\,|\nabla F|$.

Relations (3) may now be conjoined to form the compatibility equation

$$\nabla \cdot (g \nabla F) = 0 \tag{5}$$

where ∇ is the plane gradient operator.

The partial differential equation (5), along with proper boundary conditions, governs the antiplane shear deformations for arbitrary hardening characteristics. Notch-tip singularities for pure power hardening single phase materials have been obtained from (5) by Rice (1967) and, more recently, by Atkinson and Champion (1984), Bassani (1984), and Ore (1984).

With the bilinear response function (1) we find that in the singular field near the tip, where σ_e becomes very large, the compliance g from equation (4) is essentially a constant, viz

$$g \sim g_\infty = \frac{1}{G} + 3\left(\frac{1}{E_T} - \frac{1}{E}\right) = \frac{3}{E_T} - \frac{1-2\nu}{E} \tag{6}$$

This constant will assume different values for each material but equation (5) is reduced, asymptotically, to the harmonic

$$\nabla^2 F = 0 \tag{7}$$

independent of material parameters.

Now we assume that the near tip field is described by a separation of variable solution $F = r^s \phi(\theta)$ with $0 < s < 1$. Substituting that solution in equation (7) we find

$$\phi = A\sin s\theta + B\cos s\theta \tag{8}$$

with the associated stress components

$$\tau_{rz} = s r^{s-1}(A\cos s\theta - B\sin s\theta) \tag{9}$$

$$\tau_{\theta z} = -s r^{s-1}(A\sin s\theta + B\cos s\theta) \tag{10}$$

and displacement, from equation (3) with $g \sim g_\infty$,

$$w = g_\infty r^s (A\cos s\theta - B\sin s\theta) \tag{11}$$

The integration constants A, B are different for each region but parameter s (the eigenvalue) is expected to have the same value over the entire near-tip singular field.

For the case $0 \le \beta \le \alpha$ we have the stress-free conditions ($\tau_{\theta z} = 0$) at the boundaries $\theta = \pm(\pi - \alpha)$, and two continuity conditions (of w and $\tau_{\theta z}$) at the interface $\theta = \beta$. These four requirements lead to four linear homogeneous equations with the integration constants as unknowns. The existence of a nontrivial solution requires that the determinant of that system should vanish. That requirement takes the form of the transcendental equation

$$\tan s(\beta - \alpha + \pi) - \eta \tan s(\beta + \alpha - \pi) = 0 \tag{12}$$

where

$$\eta = \frac{g_\infty^{(2)}}{g_\infty^{(1)}} = \left(\frac{E_T^{(1)}}{E_T^{(2)}}\right) \frac{3 - (1-2\nu^{(2)})\dfrac{E_T^{(2)}}{E^{(2)}}}{3 - (1-2\nu^{(1)})\dfrac{E_T^{(1)}}{E^{(1)}}} \tag{13}$$

Similarly, for $\alpha \le \beta \le \pi - \alpha$, we have two stress-free conditions along with four continuity requirements at the two interfaces ($\theta = \beta$ and $\theta = \beta - \pi$). The determinant associated with the resulting system of equations is now of the sixth order, and the requirement for a nontrivial solution becomes

$$\tan s\pi + \eta[\tan s(\beta - \alpha) - \tan s(\beta + \alpha - \pi)] + \eta^2 (\tan s\pi)[\tan s(\beta - \alpha)][\tan s(\beta + \alpha - \pi)] = 0 \tag{14}$$

Of course, equations (12) and (14) coincide when $\alpha = \beta$.

Figure 2 shows the dependence of the eigenvalue s on the inclination angle β, with different values of η, and for the

Downloaded 03 May 2010 to 171.66.16.27. Redistribution subject to ASME license or copyright; see http://www.asme.org/terms/Terms_Use.cfm

representative cases of a crack ($\alpha = 0$ deg) and a 90 deg notch ($\alpha = 45$ deg). If $E >> E_T$, for both materials, then η gives simply the ratio between the tangent moduli. That relation holds also for the case of incompressible phases. For a single phase material $\eta = 1$ with the standard result $s = (1/2)$ $\pi/(\pi - \alpha)$. It may be concluded from Fig. 2 that for $\eta < 1$ the level of stress singularity decreases as β increases so that the worst situation would be at zero inclination. For $\eta > 1$, by contrast, the singularity level increases with β leading to the strongest singularity when the notch is perpendicular to the interface.

The harmonic (7), as well as the subsequent analysis, are valid also for linear-elastic materials where $E \equiv E_T$. In that case η will be exactly the ratio of the respective shear moduli $G^{(1)}/G^{(2)}$. It is worth mentioning, however, that for plastic materials the value of parameter η can become very large (or very small) when one of the phases is nearly perfectly-plastic.

Finally we note that the transcendental equations (12) and (14) can be further reduced for certain geometries. Thus, for the perpendicular crack, with $\alpha = 0$ deg and $\beta = 90$ deg, we find from equation (14)

$$\tan\frac{s\pi}{2} = \eta^{-1/2} \tag{15}$$

a result already observed by Atkinson (1975). When η becomes very large we get $s \sim (2/\pi)\eta^{-1/2}$ which compares well with the numerical results of Fig. 2(*a*), for $\eta = 5$ and $\eta = 100$.

As a second example consider the 90 deg notch perpendicular to the interface. Here $\alpha = 45$ deg, $\beta = 90$ deg, and a direct trigonometric manipulation of equation (14) gives

$$\tan\frac{s\pi}{4} = (2\eta + 1)^{-1/2} \tag{16}$$

For large values of η we have from equation (16) $s \sim (4/\pi)(2\eta)^{-1/2}$, again in agreement with the results shown in Fig. 2(*b*) for high values of η.

When η becomes very small we get from equation (15) $s \sim 1 - (2/\pi)\eta^{1/2}$, and from equation (16) $s \sim 1 - (2/\pi)\eta$. These asymptotic results should be helpful when one material is nearly perfectly plastic.

A more general asymptotic expression can be obtained from equation (14) when η is large and, consequently, s becomes smaller as β increases. A straightforward expansion of equation (14) gives

$$s \sim \left(\frac{\pi - 2\alpha}{\pi(\beta - \alpha)(\pi - \alpha - \beta)}\right)^{1/2} \eta^{-1/2}, \quad \alpha < \beta < \pi - \alpha \tag{17}$$

That expression agrees with the asymptotic solutions of equations (15)–(16) mentioned above. The validity of (17) can be assessed from comparison with the exact results shown in Fig. 2.

References

Atkinson, C., 1975, "On the Stress Intensity Factors Associated with Cracks Interacting with an Interface Between two Elastic Media," *International Journal of Engineering Science*, Vol. 13, pp. 489–504.

Atkinson, C., 1979, "Stress Singularities and Fracture Mechanics," *Applied Mechanics Reviews*, Vol. 32, pp. 123–135.

Atkinson, C., and Champion, C. R., 1984, "Some Boundary Value Problems for the Equation $\nabla\cdot(|\nabla\phi|^N\nabla\phi) = 0$," *The Quarterly Journal of Mechanics and Applied Mathematics*, Vol. 37, pp. 401–419.

Bassani, J. L., 1984, "Notch Tip Stresses in a Creeping Solid," ASME JOURNAL OF APPLIED MECHANICS, Vol. 51, pp. 475–480.

Ore, E., 1984, "The Plastic Zone Near a Notch Tip Subjected to Anti-Plane Shear," M.Sc. Research Thesis, Technion, Haifa.

Rice, J. R., 1967, "Stresses Due to a Sharp Notch in a Work-Hardening Elastic-Plastic Material Loaded by Longitudinal Shear," ASME JOURNAL OF APPLIED MECHANICS, Vol. 34, pp. 287–298.

On the Singular Nature of Linearization of Certain Constrained Theories of Shells

M. B. Rubin[19]

Introduction

By way of background, we recall that the general nonlinear theory of a Cosserat surface (Naghdi, 1972) with a single director includes both the effects of transverse normal strain and transverse shear deformation. Constrained theories which exclude both of these effects (Naghdi, 1972, Sec. 10), and which exclude only transverse shear deformation (Birickoglu and Kalnins, 1971; Naghdi, 1982) have been considered. However, a constrained theory which excludes transverse normal strain but includes transverse shear deformation does not appear to have been developed previously. Therefore, one of the objectives of this note is to develop such a constrained theory.

Of course, the main motivation for developing a constrained theory is to exploit certain simplifying features exhibited by a specific shell by developing appropriate constraints which reduce the number of independent kinematic quantities to be determined. In this regard, we note that the constrained theory presented here could be used to model the core of a sandwich shell composed of a soft rubber core with thin metal skins, because during bending of the shell the dominant effect of the core is to transmit shear to the skins.

Another objective of this note is to show that linearization of certain nonlinear constrained theories of shells is singular in the sense that the required number of boundary conditions and constitutive equations is less for the linear theory than for the nonlinear theory. This singular nature arises in connection with the theory presented here and with a constrained theory which requires the director to have constant length (Green and Naghdi, 1974).

After summarizing some basic equations of the theory of a Cosserat surface (Naghdi, 1972), which models a shell-like body, we outline the development of a constrained theory which excludes transverse normal strain. Then, it is shown that linearization of this theory is singular in nature.

Basic Equations

Details of the theory of a Cosserat surface may be found in Naghdi (1972) and Green and Naghdi (1979). Here, we use the notation in Naghdi (1982) and recall that in the present configuration material points on the Cosserat surface are located by the position vector $\mathbf{r}$, and that the director $\mathbf{d}$ is identified with a material fiber through the thickness of the shell. Both $\mathbf{r}$ and $\mathbf{d}$ are functions of the convected coordinates[20] θ^α and time t, and $\mathbf{a}_\alpha = \mathbf{r}_{,\alpha}$ and $\mathbf{a}_3$ are the tangent vectors to the shell surface and unit normal vector, respectively, where a comma denotes partial differentiation with respect to θ^α.

Following the discussions in Naghdi (1972, 1982), and confining attention to the purely mechanical theory we note that the boundary integral appearing in the energy equation takes the form

$$\int_{\partial P} (\mathbf{n}\cdot\mathbf{v} + \mathbf{m}\cdot\mathbf{w})ds = \int_{\partial P} (n^i v_i + m^i w_i)ds \tag{1}$$

[19]Faculty of Mechanical Engineering, Technion, Israel Institute of Technology, Haifa 32000, Israel.

[20]Throughout the text Greek letters take the range (1, 2), Latin letters take the range (1, 2, 3), and the usual summation convention over repeated indices is used.

Manuscript received by ASME Applied Mechanics Division, December 4, 1984; final revision, December 15, 1985.

Downloaded 03 May 2010 to 171.66.16.27. Redistribution subject to ASME license or copyright; see http://www.asme.org/terms/Terms_Use.cfm

representative cases of a crack ($\alpha = 0$ deg) and a 90 deg notch ($\alpha = 45$ deg). If $E >> E_T$, for both materials, then η gives simply the ratio between the tangent moduli. That relation holds also for the case of incompressible phases. For a single phase material $\eta = 1$ with the standard result $s = (1/2)$ $\pi/(\pi - \alpha)$. It may be concluded from Fig. 2 that for $\eta < 1$ the level of stress singularity decreases as β increases so that the worst situation would be at zero inclination. For $\eta > 1$, by contrast, the singularity level increases with β leading to the strongest singularity when the notch is perpendicular to the interface.

The harmonic (7), as well as the subsequent analysis, are valid also for linear-elastic materials where $E \equiv E_T$. In that case η will be exactly the ratio of the respective shear moduli $G^{(1)}/G^{(2)}$. It is worth mentioning, however, that for plastic materials the value of parameter η can become very large (or very small) when one of the phases is nearly perfectly-plastic.

Finally we note that the transcendental equations (12) and (14) can be further reduced for certain geometries. Thus, for the perpendicular crack, with $\alpha = 0$ deg and $\beta = 90$ deg, we find from equation (14)

$$\tan\frac{s\pi}{2} = \eta^{-1/2} \tag{15}$$

a result already observed by Atkinson (1975). When η becomes very large we get $s \sim (2/\pi)\eta^{-1/2}$ which compares well with the numerical results of Fig. 2(*a*), for $\eta = 5$ and $\eta = 100$.

As a second example consider the 90 deg notch perpendicular to the interface. Here $\alpha = 45$ deg, $\beta = 90$ deg, and a direct trigonometric manipulation of equation (14) gives

$$\tan\frac{s\pi}{4} = (2\eta + 1)^{-1/2} \tag{16}$$

For large values of η we have from equation (16) $s \sim (4/\pi)(2\eta)^{-1/2}$, again in agreement with the results shown in Fig. 2(*b*) for high values of η.

When η becomes very small we get from equation (15) $s \sim 1 - (2/\pi)\eta^{1/2}$, and from equation (16) $s \sim 1 - (2/\pi)\eta$. These asymptotic results should be helpful when one material is nearly perfectly plastic.

A more general asymptotic expression can be obtained from equation (14) when η is large and, consequently, s becomes smaller as β increases. A straightforward expansion of equation (14) gives

$$s \sim \left(\frac{\pi - 2\alpha}{\pi(\beta - \alpha)(\pi - \alpha - \beta)}\right)^{1/2} \eta^{-1/2}, \quad \alpha < \beta < \pi - \alpha \tag{17}$$

That expression agrees with the asymptotic solutions of equations (15)–(16) mentioned above. The validity of (17) can be assessed from comparison with the exact results shown in Fig. 2.

References

Atkinson, C., 1975, "On the Stress Intensity Factors Associated with Cracks Interacting with an Interface Between two Elastic Media," *International Journal of Engineering Science*, Vol. 13, pp. 489–504.

Atkinson, C., 1979, "Stress Singularities and Fracture Mechanics," *Applied Mechanics Reviews*, Vol. 32, pp. 123–135.

Atkinson, C., and Champion, C. R., 1984, "Some Boundary Value Problems for the Equation $\nabla\cdot(|\nabla\phi|^N\nabla\phi) = 0$," *The Quarterly Journal of Mechanics and Applied Mathematics*, Vol. 37, pp. 401–419.

Bassani, J. L., 1984, "Notch Tip Stresses in a Creeping Solid," ASME JOURNAL OF APPLIED MECHANICS, Vol. 51, pp. 475–480.

Ore, E., 1984, "The Plastic Zone Near a Notch Tip Subjected to Anti-Plane Shear," M.Sc. Research Thesis, Technion, Haifa.

Rice, J. R., 1967, "Stresses Due to a Sharp Notch in a Work-Hardening Elastic-Plastic Material Loaded by Longitudinal Shear," ASME JOURNAL OF APPLIED MECHANICS, Vol. 34, pp. 287–298.

On the Singular Nature of Linearization of Certain Constrained Theories of Shells

M. B. Rubin[19]

Introduction

By way of background, we recall that the general nonlinear theory of a Cosserat surface (Naghdi, 1972) with a single director includes both the effects of transverse normal strain and transverse shear deformation. Constrained theories which exclude both of these effects (Naghdi, 1972, Sec. 10), and which exclude only transverse shear deformation (Birickoglu and Kalnins, 1971; Naghdi, 1982) have been considered. However, a constrained theory which excludes transverse normal strain but includes transverse shear deformation does not appear to have been developed previously. Therefore, one of the objectives of this note is to develop such a constrained theory.

Of course, the main motivation for developing a constrained theory is to exploit certain simplifying features exhibited by a specific shell by developing appropriate constraints which reduce the number of independent kinematic quantities to be determined. In this regard, we note that the constrained theory presented here could be used to model the core of a sandwich shell composed of a soft rubber core with thin metal skins, because during bending of the shell the dominant effect of the core is to transmit shear to the skins.

Another objective of this note is to show that linearization of certain nonlinear constrained theories of shells is singular in the sense that the required number of boundary conditions and constitutive equations is less for the linear theory than for the nonlinear theory. This singular nature arises in connection with the theory presented here and with a constrained theory which requires the director to have constant length (Green and Naghdi, 1974).

After summarizing some basic equations of the theory of a Cosserat surface (Naghdi, 1972), which models a shell-like body, we outline the development of a constrained theory which excludes transverse normal strain. Then, it is shown that linearization of this theory is singular in nature.

Basic Equations

Details of the theory of a Cosserat surface may be found in Naghdi (1972) and Green and Naghdi (1979). Here, we use the notation in Naghdi (1982) and recall that in the present configuration material points on the Cosserat surface are located by the position vector $\mathbf{r}$, and that the director $\mathbf{d}$ is identified with a material fiber through the thickness of the shell. Both $\mathbf{r}$ and $\mathbf{d}$ are functions of the convected coordinates[20] θ^α and time t, and $\mathbf{a}_\alpha = \mathbf{r}_{,\alpha}$ and $\mathbf{a}_3$ are the tangent vectors to the shell surface and unit normal vector, respectively, where a comma denotes partial differentiation with respect to θ^α.

Following the discussions in Naghdi (1972, 1982), and confining attention to the purely mechanical theory we note that the boundary integral appearing in the energy equation takes the form

$$\int_{\partial P} (\mathbf{n}\cdot\mathbf{v} + \mathbf{m}\cdot\mathbf{w})ds = \int_{\partial P} (n^i v_i + m^i w_i)ds \tag{1}$$

[19]Faculty of Mechanical Engineering, Technion, Israel Institute of Technology, Haifa 32000, Israel.

[20]Throughout the text Greek letters take the range (1, 2), Latin letters take the range (1, 2, 3), and the usual summation convention over repeated indices is used.

Manuscript received by ASME Applied Mechanics Division, December 4, 1984; final revision, December 15, 1985.

Copyright © 1987 by ASME
Downloaded 03 May 2010 to 171.66.16.27. Redistribution subject to ASME license or copyright; see http://www.asme.org/terms/Terms_Use.cfm

where ds is the arc length on the boundary ∂P, $\mathbf{n} = n^i\mathbf{a}_i = N^{i\alpha}\nu_\alpha\mathbf{a}_i$ is the contact force, $\mathbf{m} = m^i\mathbf{a}_i = M^{i\alpha}\nu_\alpha\mathbf{a}_i$ is the contact moment, $\boldsymbol{\nu} = \nu_\alpha\mathbf{a}^\alpha$ is the unit outward normal to ∂P, $\mathbf{v} = \dot{\mathbf{r}} = v_i\mathbf{a}^i$ is the velocity, $\mathbf{w} = \dot{\mathbf{d}} = w_i\mathbf{a}^i$ is the director velocity, a superposed dot denotes time differentiation holding θ^α fixed, and all tensor quantities are referred to the base vectors $\mathbf{a}_i$ or their reciprocal vectors $\mathbf{a}^i$. Recalling (Naghdi, 1972, Sec. 15) that the gradient of an arbitrary function $F = F(\theta^\alpha, t)$ may be expressed in terms of its normal and tangential derivatives $\partial F/\partial\nu$ and $\partial F/\partial s$, respectively, we may integrate equation (1) by parts, assume continuity on ∂P, and rewrite it in the form

$$\int_{\partial P}\left[P^i(v_i) + m^\sigma\left(\dot{d}_\sigma - \nu_\sigma d^\beta\frac{\partial v_\beta}{\partial\nu} - \nu_\sigma d_3\frac{\partial v_3}{\partial\nu}\right) + m^3\left(\dot{d}_3 + d^\beta\nu_\beta\frac{\partial v_3}{\partial\nu}\right)\right]ds \tag{2}$$

where P^i are given by

$$P^\sigma = [n^\sigma + m^\beta(d^\lambda\Gamma^\sigma_{\lambda\beta} - d_3 b^\sigma_\beta) + m^3 d^\beta b^\sigma_\beta] + \frac{\partial}{\partial s}[m^\beta d^\sigma\lambda_\beta], \tag{3a}$$

$$P^3 = (n^3 + m^\beta d^\sigma b_{\alpha\beta}) + \frac{\partial}{\partial s}[(m^\beta d_3 - m^3 d^\beta)\lambda_\beta]. \tag{3b}$$

In the above, $b_{\alpha\beta}$ is the curvature tensor of the surface, $\Gamma^\sigma_{\lambda\beta}$ is the Christoffel symbol and $\boldsymbol{\lambda} = \lambda_\alpha\mathbf{a}^\alpha$ is the unit tangent vector to ∂P.

Furthermore, we recall (Naghdi, 1972) the mechanical power expression

$$P = \hat{N}^{\alpha\beta}\dot{e}_{\alpha\beta} + k^i\dot{\gamma}_i + M^{i\alpha}\dot{\kappa}_{i\alpha}, \tag{4}$$

where $\hat{N}^{\alpha\beta}$, k^i, $M^{i\alpha}$ require constitutive equations and $e_{\alpha\beta}$, γ_i, $\kappa_{i\alpha}$ are strain measures. Finally, in the reference configuration, $\mathbf{r} = \mathbf{R}(\theta^\alpha)$ and we identify the director with the direction of the material fiber normal to the surface and take

$$\mathbf{D} = \mathbf{A}_3, \tag{5}$$

where $\mathbf{D}$ and $\mathbf{A}_3$ are the reference values of $\mathbf{d}$ and $\mathbf{a}_3$, respectively.

Nonlinear Theory

Here, we briefly describe a nonlinear constrained theory of shells which excludes transverse normal strain but includes transverse shear deformation. For this theory, the director $\mathbf{d}$, which is associated with a material fiber, is constrained to have a constant normal component so that

$$d_3 = \mathbf{d}\cdot\mathbf{a}_3 = \mathbf{D}\cdot\mathbf{A}_3 = 1, \quad (\gamma_3 = 0, \dot{\gamma}_3 = 0). \tag{6a,b}$$

Using well established procedures (Green et al. 1970; Green and Naghdi, 1976, 1977), it follows that k^3 in equation (4) separates into two additive parts: one part denoted by $\hat{k}^3$ is determined by a constitutive equation; and the other part $\bar{k}^3$ is workless and is determined by the $\mathbf{a}^3$ component of director momentum. In view of equations (6), d_3 and $\dot{d}_3$ are replaced by one and zero, respectively, in (2) and it may be observed that the constraint (6) does not reduce the required number of boundary conditions for the nonlinear theory. Specifically, six boundary conditions must be specified by an appropriate combination of kinetic quantities (P^i, m^i) and their dual kinematic quantities in the parentheses in (2). Further, using equations (4) and (6b) it is apparent that the required number of constitutive equations is reduced by one ($\hat{k}^3$ may be absorbed into $\bar{k}^3$) for this constrained theory. Specifically, eleven ($\hat{N}^{\alpha\beta}$ is symmetric) constitutive equations must be provided for ($\hat{N}^{\alpha\beta}$, k^α, $M^{i\alpha}$). Once these equations are supplied the kinematic quantities ($\mathbf{r}$, d_α) may be determined by the remaining equations of motion and appropriate initial conditions.

Linear Theory

For the linear theory it is assumed that the displacements $\mathbf{u} = \mathbf{r} - \mathbf{R}$, $\boldsymbol{\delta} = \mathbf{d} - \mathbf{D}$, and the kinetic quantities $\mathbf{n}$, $\mathbf{k}$, $\mathbf{m}$ are small enough that quadratic terms in these quantities may be neglected. With the help of equations (6) it follows that the rate of work integral (2) reduces considerably to

$$\int_{\partial P}\left[P^i v_i + m^\sigma\left(\dot{d}_\sigma - \nu_\sigma\frac{\partial v_3}{\partial\nu}\right)\right]ds, \tag{7}$$

where

$$P^\sigma = n^\sigma - m^\beta B^\sigma_\beta, \quad P^3 = n^3 + \frac{\partial}{\partial s}(m^\beta\lambda_\beta), \tag{8a,b}$$

and where B^σ_β is the reference value of the curvature tensor b^σ_β. Most importantly, we note that the number of boundary conditions associated with (7) is only five as compared with six for the nonlinear theory. This reduction arises because the kinematic term multiplying m^3 in (2) is of second order in the linear theory.

A corresponding reduction in the number of kinetic quantities requiring a constitutive equation can be observed by noting that for the linear theory

$$\kappa_{3\alpha} = B^\sigma_\alpha\gamma_\sigma, \tag{9}$$

so the mechanical power P in equation (4) reduces to

$$P = \hat{N}^{\alpha\beta}\dot{e}_{\alpha\beta} + V^\alpha\dot{\gamma}_\alpha + M^{\alpha\beta}\dot{\kappa}_{\alpha\beta}, \tag{10a}$$

$$V^\alpha = k^\alpha + B^\alpha_\sigma M^{3\sigma}. \tag{10b}$$

Furthermore, it can be shown that the equations of motion depend on $M^{3\alpha}$ only through the quantity V^α so that, without loss in generality, we may take $M^{3\alpha} = 0$ ($m^3 = 0$). It follows that only nine constitutive equations must be provided for ($\hat{N}^{\alpha\beta}$, V^α, $M^{\alpha\beta}$) as compared with eleven for the nonlinear theory.

When attention is confined to the linear theory of an isotropic plate, $B_{\alpha\beta}$ vanishes, extensional and bending modes uncouple, and the bending equations can be shown to be equivalent to those of Reissner (1945) and Green and Naghdi (1967).

Conclusions

A nonlinear constrained theory of shells is developed which excludes transverse normal strain but includes transverse shear deformation. Linearization of this theory is shown to be singular in the sense that the required number of boundary conditions and constitutive equations for the linear theory is reduced as compared with the required numbers for the nonlinear theory. This same singular nature is exhibited by the theory which constrains the director to have constant length (Green and Naghdi, 1974). In contrast, linearization of the constrained theory which excludes both transverse normal strain and transverse shear deformation (Naghdi, 1972, Sec. 10, 15) and of that which excludes transverse shear deformation but includes transverse normal strain (Naghdi, 1982) is not singular in this sense.

Acknowledgment

This research was supported by the US Air Force Office of Scientific Research under Contract F49620-84-K-0001 with SRI International, Menlo Park, California.

References

Birickoglu, V., and Kalnins, A., 1971, "Large Elastic Deformations of Shells with the Inclusion of Transverse Normal Strain," *International Journal Solids Structures*, Vol. 7, pp. 431–444.

Green, A. E., and Naghdi, P. M., 1967, "The Linear Theory of an Elastic Cosserat Plate," *Proc. Camb. Phil. Soc.*, Vol. 63, pp. 537–550.

Green, A. E., and Naghdi, P. M., 1974, "On the Derivation of Shell Theories by Direct Approach," ASME JOURNAL OF APPLIED MECHANICS, Vol. 41, No. 1, pp. 173–176.

Downloaded 03 May 2010 to 171.66.16.27. Redistribution subject to ASME license or copyright; see http://www.asme.org/terms/Terms_Use.cfm

Green, A. E., and Naghdi, P. M., 1976, "Directed Fluid Sheets," *Proceedings of the Royal Society of London*, Vol. A347, pp. 447–473.

Green, A. E., and Naghdi, P. M., 1977, "A Note on Thermodynamics of Constrained Materials," ASME JOURNAL OF APPLIED MECHANICS, Vol. 44, No. 4, pp. 787–788.

Green, A. E., and Naghdi, P. M., 1979, "On Thermal Effects in the Theory of Shells," *Proceedings of the Royal Society of London*, Vol. A365, pp. 161–190, Vol. A367, p. 572.

Green, A. E., Naghdi, P. M., and Trapp, J. A., 1970, "Thermodynamics of a Continuum with Internal Constraints," *International Journal Engineering Science*, Vol. 8, pp. 891–908.

Naghdi, P. M., 1972, "The Theory of Shells and Plates," in *S. Flügge's Handbuch der Physik*, Vol. VIa/2, Truesdell, C., eds., Springer Verlag, Berlin, pp. 425–640.

Naghdi, P. M., 1982, "Finite Deformation of Elastic Rods and Shells," *Proceedings IUTAM Symposium on "Finite Elasticity,"* Bethlehem, PA, 1980, Carlson, D. E., and Shield, R. T., eds., Martinus Nijhoff Publishers, the Hague, pp. 47–103.

Reissner, E., 1945, "The Effect of Transverse Shear Deformation on Bending of Elastic Plates," ASME JOURNAL OF APPLIED MECHANICS, Vol. 12, pp. 69–77.

The Shrink Fit with Nonlinearly Hardening Elastic-Plastic Hub

Udo Gamer[21]

Based on Tresca's yield criterion and the associated flow rule, stresses and displacement in a rotating shrink fit consisting of an elastic disk and a partially plasticized annulus are calculated for an arbitrary nonlinear hardening law. It is shown that the elastic-plastic border radius and the stresses in the elastic region of the hub do not depend on the hardening law.

1 Introduction

It is well known that, based on Tresca's yield criterion, the stresses in the elastic region of the partially plasticized hub of a shrink fit agree with the one occurring in the unrestrictedly elastic hub, provided that the interference is identical. This observation holds for perfectly plastic behavior as well as for material with linear hardening, and it does not matter whether the shrink fit is at rest or is spinning (Gamer and Lance, 1982; Gamer, 1986).

As yet, a physical interpretation of this phenomenon is lacking. A new derivation of the displacement in the hub yields the explanation. It is found that the hardening law does not have an influence on the elastic-plastic border radius nor on the stresses in the elastic region of the hub (Gamer, 1987). Furthermore, the new derivation opens up the possibility of the mathematical treatment of the shrink fit for arbitrarily nonlinear hardening of the hub material without much numerical effort.

As usual, it is assumed that the shrink fit consists of a circular disk and an annulus, both of which are under plane stress condition (Fig. 1).

2 The Displacement

First, the plastic part of the hub adjacent to the interface is considered. From the elastic solution, one knows that Tresca's yield criterion adopts the form

$$\sigma_\theta - \sigma_r = \sigma_Y, \tag{2.1}$$

where the yield stress, σ_Y, grows with the equivalent plastic strain, ϵ_E^p, in some manner. The dependence need not be specified yet since no use of the yield condition is made at this early stage. However, the form of the yield condition governs the flow rule, and this is the starting point of the derivation. The flow rule associated to the yield condition (2.1) reads

$$d\epsilon_r^p / d\epsilon_\theta^p = -1, \quad d\epsilon_z^p = 0. \tag{2.2}$$

With the increments of the plastic strains in radial and circumferential direction being equal but of opposite sign, the sum of radial and circumferential strain follows Hooke's law,

$$E\left(\frac{du}{dr} + \frac{u}{r}\right) = (1-\nu)(\sigma_r + \sigma_\theta). \tag{2.3}$$

From this equation, σ_θ is eliminated with the help of the equation of motion,

$$\frac{d\sigma_r}{dr} + \frac{\sigma_r - \sigma_\theta}{r} = -\rho\omega^2 r. \tag{2.4}$$

By rearrangement

$$E\frac{d}{dr}(ru) = (1-\nu)\frac{d}{dr}\left(r^2\sigma_r + \frac{1}{4}\rho\omega^2 r^4\right) \tag{2.5}$$

and, after integration,

$$Eu = (1-\nu)\left(r\sigma_r + \frac{1}{4}\rho\omega^2 r^3\right) + \frac{C}{r}. \tag{2.6}$$

Reexamining once more the steps of the derivation of equation (2.6), one sees that it is valid for an arbitrary hardening law, provided that plastic deformation be governed by the flow rule (2.2). However, equation (2.6) holds also for elastic behavior. Thus, since displacement and radial stress have to be continuous at the elastic-plastic border, equation (2.6) gives the displacement in the entire hub and, with $C=0$, also the displacement in the shaft.

The kinematical condition

$$u^H - u^S = i \tag{2.7}$$

for the interface radius, $r=a$, yields

$$C = Eai. \tag{2.8}$$

The superscripts H and S refer to hub and shaft, respectively, and i denotes the interference. Therewith, the displacement and the stresses in the elastic region of the hub are already established, as is shown in the following section.

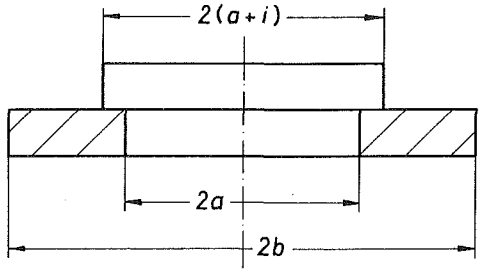


Fig. 1 Shrink fit before assemblage

3 The Elastic Region of the Hub

The displacement and the radial stress in a rotating elastic disk read (e.g., Timoshenko and Goodier, 1970)

$$Eu = (1+\nu)\frac{A}{r} + (1-\nu)Br - \frac{1}{8}(1-\nu^2)\rho\omega^2 r^3, \tag{3.1}$$

$$\sigma_r = -\frac{A}{r^2} + B - \frac{1}{8}(3+\nu)\rho\omega^2 r^2, \tag{3.2}$$

respectively. Eliminating B from the displacement, one obtains by comparison with equation (2.6)

$$A = \frac{1}{2}C = \frac{1}{2}Eai. \tag{3.3}$$

[21] Institut für Mechanik, Technische Universität Wien, Karlsplatz 13, A-1040 Wien, Austria.

Manuscript received by ASME Applied Mechanics Division, June 27, 1986; final revision, November 3, 1986.

Downloaded 03 May 2010 to 171.66.16.27. Redistribution subject to ASME license or copyright; see http://www.asme.org/terms/Terms_Use.cfm

Green, A. E., and Naghdi, P. M., 1976, "Directed Fluid Sheets," *Proceedings of the Royal Society of London*, Vol. A347, pp. 447–473.

Green, A. E., and Naghdi, P. M., 1977, "A Note on Thermodynamics of Constrained Materials," ASME JOURNAL OF APPLIED MECHANICS, Vol. 44, No. 4, pp. 787–788.

Green, A. E., and Naghdi, P. M., 1979, "On Thermal Effects in the Theory of Shells," *Proceedings of the Royal Society of London*, Vol. A365, pp. 161–190, Vol. A367, p. 572.

Green, A. E., Naghdi, P. M., and Trapp, J. A., 1970, "Thermodynamics of a Continuum with Internal Constraints," *International Journal Engineering Science*, Vol. 8, pp. 891–908.

Naghdi, P. M., 1972, "The Theory of Shells and Plates," in *S. Flügge's Handbuch der Physik*, Vol. VIa/2, Truesdell, C., eds., Springer Verlag, Berlin, pp. 425–640.

Naghdi, P. M., 1982, "Finite Deformation of Elastic Rods and Shells," *Proceedings IUTAM Symposium on "Finite Elasticity,"* Bethlehem, PA, 1980, Carlson, D. E., and Shield, R. T., eds., Martinus Nijhoff Publishers, the Hague, pp. 47–103.

Reissner, E., 1945, "The Effect of Transverse Shear Deformation on Bending of Elastic Plates," ASME JOURNAL OF APPLIED MECHANICS, Vol. 12, pp. 69–77.

The Shrink Fit with Nonlinearly Hardening Elastic-Plastic Hub

Udo Gamer[21]

Based on Tresca's yield criterion and the associated flow rule, stresses and displacement in a rotating shrink fit consisting of an elastic disk and a partially plasticized annulus are calculated for an arbitrary nonlinear hardening law. It is shown that the elastic-plastic border radius and the stresses in the elastic region of the hub do not depend on the hardening law.

1 Introduction

It is well known that, based on Tresca's yield criterion, the stresses in the elastic region of the partially plasticized hub of a shrink fit agree with the one occurring in the unrestrictedly elastic hub, provided that the interference is identical. This observation holds for perfectly plastic behavior as well as for material with linear hardening, and it does not matter whether the shrink fit is at rest or is spinning (Gamer and Lance, 1982; Gamer, 1986).

As yet, a physical interpretation of this phenomenon is lacking. A new derivation of the displacement in the hub yields the explanation. It is found that the hardening law does not have an influence on the elastic-plastic border radius nor on the stresses in the elastic region of the hub (Gamer, 1987). Furthermore, the new derivation opens up the possibility of the mathematical treatment of the shrink fit for arbitrarily nonlinear hardening of the hub material without much numerical effort.

As usual, it is assumed that the shrink fit consists of a circular disk and an annulus, both of which are under plane stress condition (Fig. 1).

2 The Displacement

First, the plastic part of the hub adjacent to the interface is considered. From the elastic solution, one knows that Tresca's yield criterion adopts the form

$$\sigma_\theta - \sigma_r = \sigma_Y, \tag{2.1}$$

where the yield stress, σ_Y, grows with the equivalent plastic strain, ϵ_E^p, in some manner. The dependence need not be specified yet since no use of the yield condition is made at this early stage. However, the form of the yield condition governs the flow rule, and this is the starting point of the derivation. The flow rule associated to the yield condition (2.1) reads

$$d\epsilon_r^p / d\epsilon_\theta^p = -1, \quad d\epsilon_z^p = 0. \tag{2.2}$$

With the increments of the plastic strains in radial and circumferential direction being equal but of opposite sign, the sum of radial and circumferential strain follows Hooke's law,

$$E\left(\frac{du}{dr} + \frac{u}{r}\right) = (1-\nu)(\sigma_r + \sigma_\theta). \tag{2.3}$$

From this equation, σ_θ is eliminated with the help of the equation of motion,

$$\frac{d\sigma_r}{dr} + \frac{\sigma_r - \sigma_\theta}{r} = -\rho\omega^2 r. \tag{2.4}$$

By rearrangement

$$E\frac{d}{dr}(ru) = (1-\nu)\frac{d}{dr}\left(r^2\sigma_r + \frac{1}{4}\rho\omega^2 r^4\right) \tag{2.5}$$

and, after integration,

$$Eu = (1-\nu)\left(r\sigma_r + \frac{1}{4}\rho\omega^2 r^3\right) + \frac{C}{r}. \tag{2.6}$$

Reexamining once more the steps of the derivation of equation (2.6), one sees that it is valid for an arbitrary hardening law, provided that plastic deformation be governed by the flow rule (2.2). However, equation (2.6) holds also for elastic behavior. Thus, since displacement and radial stress have to be continuous at the elastic-plastic border, equation (2.6) gives the displacement in the entire hub and, with $C=0$, also the displacement in the shaft.

The kinematical condition

$$u^H - u^S = i \tag{2.7}$$

for the interface radius, $r=a$, yields

$$C = Eai. \tag{2.8}$$

The superscripts H and S refer to hub and shaft, respectively, and i denotes the interference. Therewith, the displacement and the stresses in the elastic region of the hub are already established, as is shown in the following section.

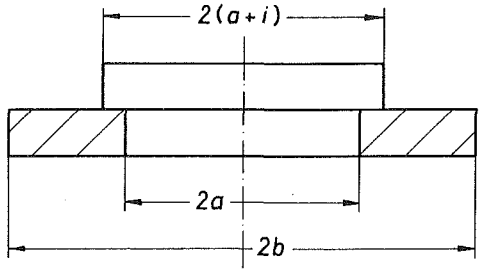


Fig. 1 Shrink fit before assemblage

3 The Elastic Region of the Hub

The displacement and the radial stress in a rotating elastic disk read (e.g., Timoshenko and Goodier, 1970)

$$Eu = (1+\nu)\frac{A}{r} + (1-\nu)Br - \frac{1}{8}(1-\nu^2)\rho\omega^2 r^3, \tag{3.1}$$

$$\sigma_r = -\frac{A}{r^2} + B - \frac{1}{8}(3+\nu)\rho\omega^2 r^2, \tag{3.2}$$

respectively. Eliminating B from the displacement, one obtains by comparison with equation (2.6)

$$A = \frac{1}{2}C = \frac{1}{2}Eai. \tag{3.3}$$

[21] Institut für Mechanik, Technische Universität Wien, Karlsplatz 13, A-1040 Wien, Austria.

Manuscript received by ASME Applied Mechanics Division, June 27, 1986; final revision, November 3, 1986.

Copyright © 1987 by ASME
Downloaded 03 May 2010 to 171.66.16.27. Redistribution subject to ASME license or copyright; see http://www.asme.org/terms/Terms_Use.cfm

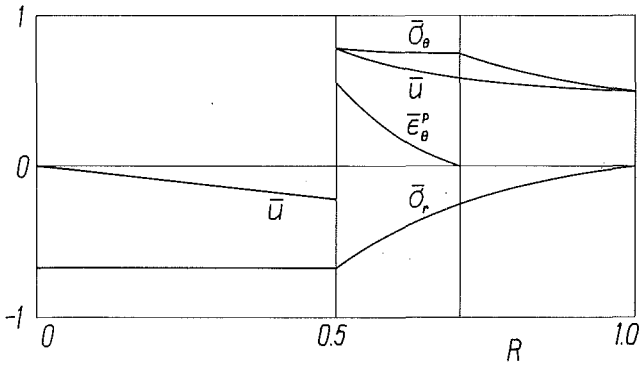


Fig. 2 Stresses, displacement, and plastic strain in shaft and hub as functions of radius

Now, the condition of vanishing radial stress at the free edge $r=b$ of the hub together with equation (3.3) yields

$$B^H=\frac{1}{2}E\frac{ai}{b^2}+\frac{1}{8}(3+\nu)\rho\omega^2b^2. \tag{3.4}$$

These results complete the explanation of the insensitivity of the elastic region of the hub to the occurrence of plastic flow around the interface.

4 The Elastic-Plastic Border

At the elastic-plastic border, the plastic strain has to vanish. The plastic strain in the circumferential direction is the difference of the total strain, given as $E\epsilon_\theta r$ by equation (2.6), and the elastic strain, which is determined with the help of Hooke's law and the stresses σ_r and $\sigma_\theta=\sigma_Y+\sigma_r$. It reads

$$E\epsilon^p_\theta=-\sigma_Y+\frac{1}{4}(1-\nu)\rho\omega^2r^2+E\frac{ai}{r^2}. \tag{4.1}$$

At the elastic-plastic border, $r=z$, the yield stress, σ_Y, equals the initial yield limit, σ_o. From equation (4.1) one obtains

$$z^2=2\frac{\sigma_o-\sqrt{\sigma_o^2-(1-\nu)\rho\omega^2Eai}}{(1-\nu)\rho\omega^2} \tag{4.2}$$

and for shrink fits at rest

$$z=\sqrt{\frac{Eai}{\sigma_o}}. \tag{4.3}$$

The elastic-plastic border radius proves independent of the hardening law, too.

Closely related to the shrink fit problem is the problem of a circular disk subjected to a temperature field which depends only on radius and time, if plastic flow starts near the edge under the yield condition (2.1). The displacement in the total disk is governed by a relation analogous to equation (2.6), and again, the outer elastic region is not influenced by the occurrence of plastic flow nor by the hardening law (Gamer and Mack).

5 The Plastic Region of the Hub

The yield stress, σ_Y, occurring in the plastic strain, is a monotonously growing generally nonlinear function of the equivalent plastic strain,

$$\sigma_Y=\sigma_Y(\epsilon^p_E). \tag{5.1}$$

For vanishing plastic strain, the yield stress equals the initial yield limit, σ_o. From the consideration of the increment of plastic work together with the yield condition (2.1) and the associated flow rule (2.2) there follows that the equivalent plastic strain equals the circumferential plastic strain. After having replaced the argument of the function (5.1) with the plastic strain (4.1), one can determine the dependence of the yield stress on the radius numerically.

The yield stress, which equals the difference of circumferential and radial stress according to the yield condition (2.1), is inserted into the equation of motion (2.4), and integration gives

$$\sigma_r=\int\frac{\sigma_Y}{r}dr-\frac{1}{2}\rho\omega^2r^2+D. \tag{5.2}$$

Thus, for an arbitrary hardening law, the numerical effort amounts merely to the calculation of the function $\sigma_Y=\sigma_Y(r)$ and the calculation of an indefinite integral.

The integration constants D and B^S are determined with the help of the condition of continuity of radial stress at the elastic-plastic border, $r=z$, and at the interface of shaft and hub, $r=a$, respectively. One finds

$$D=-\int_a^z\frac{\sigma_Y}{x}dx-\frac{1}{2}Eai\left(\frac{1}{z^2}-\frac{1}{b^2}\right)+$$

$$+\frac{1}{8}\rho\omega^2[(3+\nu)b^2+(1-\nu)z^2], \tag{5.3}$$

$$B^S=D-\frac{1}{8}(1-\nu)\rho\omega^2a^2. \tag{5.4}$$

These results complete the determination of stress and displacement in hub and shaft.

6 An Example

A specific hardening law is assumed in the form

$$\sigma_Y=\sigma_o(1+\eta\epsilon^p_E)^k, \tag{6.1}$$

where η and k are material constants. Inserting the circumferential plastic strain (4.1), one obtains

$$\frac{E}{\eta}\left(\frac{\sigma_Y}{\sigma_o}\right)^{\frac{1}{k}}+\sigma_Y=\frac{E}{\eta}+\frac{1}{4}(1-\nu)\rho\omega^2r^2+\frac{Eai}{r^2}. \tag{6.2}$$

Now, k is chosen 1/2, and the further calculation is restricted to a shrink fit at rest. Equation (6.2) gives

$$\bar{\sigma}_Y=-\frac{H}{2}+\sqrt{\frac{H\bar{I}}{R^2}+K} \tag{6.3}$$

with the material parameter $H:=\sigma_o\eta/E$, the nondimensional interference, $\bar{I}:=Eai/(\sigma_ob^2)$, the nondimensional stress, $\bar{\sigma}_{ij}:=\sigma_{ij}/\sigma_o$, the nondimensional radius, $R:=r/b$, and the abbreviation $K:=1+H^2/4$. For the shrink fit at rest, the radial stress in the plastic zone reads

$$\bar{\sigma}_r=-\int_R^{\sqrt{\bar{I}}}\frac{\bar{\sigma}_Y}{X}dX-\frac{1}{2}(1-\bar{I}), \tag{6.4}$$

where use was made of equations (5.3) and (4.3). The integration can be performed, and the result is

$$\bar{\sigma}_r=-\frac{H}{4}\log\frac{R^2}{\bar{I}}+\sqrt{K}\log\frac{R\sqrt{K}+\sqrt{H\bar{I}+KR^2}}{\left(\sqrt{K}+1+\frac{H}{2}\right)\sqrt{\bar{I}}}-$$

$$-\frac{1}{R}\sqrt{H\bar{I}+KR^2}+1+\frac{H}{2}-\frac{1}{2}(1-\bar{I}). \tag{6.5}$$

Figure 2 shows the distribution of stresses, $\bar{\sigma}_{ij}:=\sigma_{ij}/\sigma_o$, displacement, $\bar{u}:=Eu/(\sigma_ob)$, and plastic strain, $\bar{\epsilon}^p_\theta:=E\epsilon^p_\theta/\sigma_o$, in shaft and hub for $\nu=1/3$, $k=1/2$, $H=2$, $a/b=1/2$ and $\bar{I}=1/2$. Except for the sign, radial and circumferential plastic strains are equal. The agreement of circumferential stress and displacement at the interface, $R=0.5$, is incidental.

Downloaded 03 May 2010 to 171.66.16.27. Redistribution subject to ASME license or copyright; see http://www.asme.org/terms/Terms_Use.cfm

References

Gamer, U., and Lance, R. H., 1982, "Elastisch-Plastische Spannungen im Schrumpfsitz," *Forsch. Ing.-Wes.*, Vol. 48, No. 6, pp. 192-198.

Gamer, U., 1986, "The Rotating Elastic-Plastic Shrink Fit with Hardening," *Acta Mechanica*, Vol. 61, No. 1, pp. 15-27.

Gamer, U., 1987, "Die Teilplastizierte Nabe eines Preβverbandes," *ZAMM*, Vol. 67, No. 1, pp. 65-66.

Gamer, U., and Mack, W., "Zur Elastisch-Plastischen Deformation Drehsymmetrisch Erhitzter Kreisscheiben," *ZAMP*, in print.

Timoshenko, S. P., and Goodier, J. N., 1970, *Theory of Elasticity*, McGraw-Hill, New York.

Forced Flexural Motions of Plates

P. B. Beaudan[22] and H. Reismann[23]

1 Introduction

The steady state dynamic response and induced stresses in a plate strip subjected to transverse loads of constant intensity which move parallel to the edges of the plate are dependent not only upon the magnitude and spatial distribution of the loads, but also strongly upon their speed of propagation. We shall consider a plate which is unbounded in the direction of propagation of the pressure load, and present a solution within the framework of the classical theory of thin, elastic plates. The special case of a line load suddenly accelerating or decelerating through a critical speed is analyzed.

2 Problem Formulation and Solution

We assume that the load intensity consists of three distinct superposed quantities: Directly applied transverse forces of intensity p; translational inertia forces of intensity $-m\,\partial^2 w/\partial t^2$, where m is the mass per unit area of the plate; and viscous damping forces of intensity $-2\epsilon\,\partial w/\partial t$, where 2ϵ is the damping coefficient. The classical equation of motion is then

$$\nabla^4 w + \frac{\partial^2 w}{\partial t^2} + 2\epsilon \frac{\partial w}{\partial t} = p \tag{1.1}$$

with admissible boundary conditions along the infinite edges

$$w(x,0,t) = w(x,\pi,t) = 0,$$

$$M_{yy}(x,0,t) = M_{yy}(x,\pi,t) = 0 \tag{1.2}$$

$$\lim_{x\to\infty} w(x,y,t) = \lim_{x\to-\infty} w(x,y,t) = 0 \tag{1.3}$$

The load is assumed to be arbitrarily distributed and characterized by a Fourier sine series. A product solution which satisfies the boundary conditions and results in a harmonic decomposition of equation (1.1) is given by

$$p(x,y,t) = \sum_{n=1}^{n=\infty} p_n(x,t)\,\sin ny,$$

$$w(x,y,t) = \sum_{n=1}^{n=\infty} w_n(x,t)\,\sin ny \tag{2}$$

Upon substitution of equations (2) into equation (1.1), we obtain the $y-$ independent partial differential equation

$$\frac{\partial^4 w_n}{\partial x^4} + 2n^2 \frac{\partial^2 w_n}{\partial x^2} + n^4 w_n + \frac{\partial^2 w_n}{\partial t^2} + 2\epsilon \frac{\partial w_n}{\partial t} = p_n \tag{3}$$

Transforming the deformation function in the fixed reference frame (x, y) and the load distribution in a system attached to its traveling front as

$$w_n(x,t) = \int_0^\infty (F(\alpha,t)\cos\alpha x + G(\alpha,t)\sin\alpha x)\,d\alpha,$$

$$p_n(x,t) = \int_0^\infty (A(\alpha)\cos\alpha\xi + B(\alpha)\sin\alpha\xi)\,d\alpha \tag{4}$$

where $\xi = x - \phi(t)$, and $\phi(t) = \int_0^t v(\tau)d\tau + \phi_0$, we obtain from equation (3)

$$\frac{\partial^2 F}{\partial t^2} + 2\epsilon \frac{\partial F}{\partial t} + (\alpha^2 + n^2)^2 F = A\cos\alpha\phi - B\sin\alpha\phi \tag{5.1}$$

$$\frac{\partial^2 G}{\partial t^2} + 2\epsilon \frac{\partial G}{\partial t} + (\alpha^2 + n^2)^2 G = A\sin\alpha\phi + B\cos\alpha\phi \tag{5.2}$$

which are two linearly independent, nonhomogeneous, differential equations, that can be solved by classical methods.

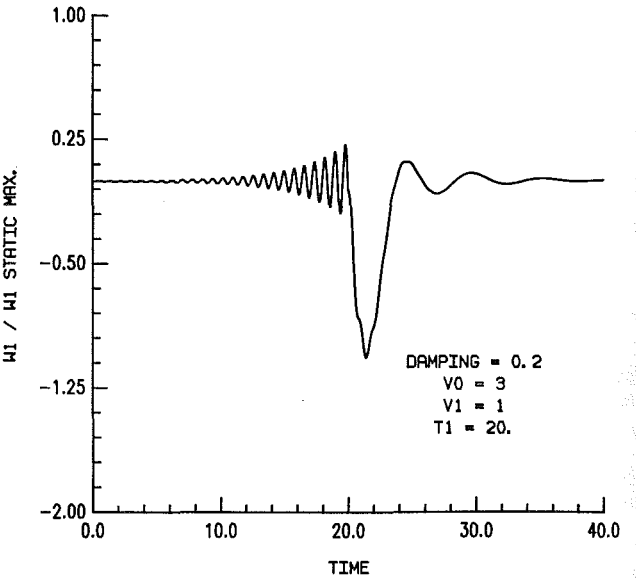


Fig. 1 Line load decelerating through the lowest critical velocity. First component of the step response.

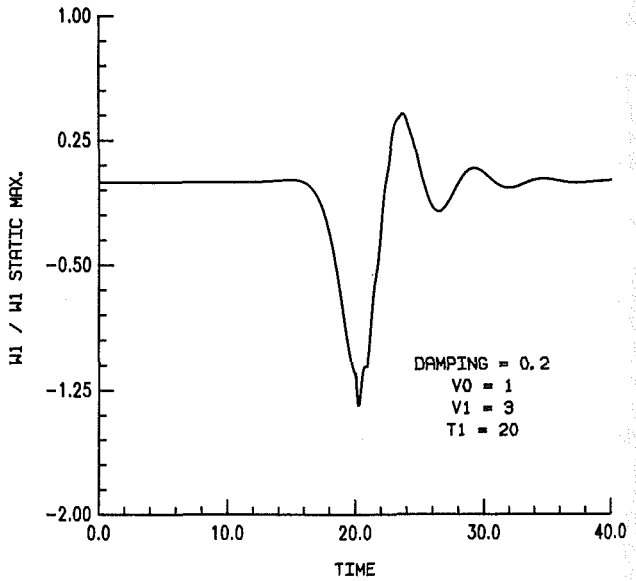


Fig. 2 Line load accelerating through the lowest critical velocity. First component of the step response.

[22]Graduate Student, State University of New York, Department of Mechanical and Aerospace Engineering, Buffalo, NY 14260.

[23]Professor, State University of New York, Department of Mechanical and Aerospace Engineering, Buffalo, NY 14260.

Manuscript received by ASME Applied Mechanics Division May 21, 1986; final revision, November 24, 1986.

Downloaded 03 May 2010 to 171.66.16.27. Redistribution subject to ASME license or copyright; see http://www.asme.org/terms/Terms_Use.cfm

References

Gamer, U., and Lance, R. H., 1982, "Elastisch-Plastische Spannungen im Schrumpfsitz," *Forsch. Ing.-Wes.*, Vol. 48, No. 6, pp. 192-198.

Gamer, U., 1986, "The Rotating Elastic-Plastic Shrink Fit with Hardening," *Acta Mechanica*, Vol. 61, No. 1, pp. 15-27.

Gamer, U., 1987, "Die Teilplastizierte Nabe eines Preβverbandes," *ZAMM*, Vol. 67, No. 1, pp. 65-66.

Gamer, U., and Mack, W., "Zur Elastisch-Plastischen Deformation Drehsymmetrisch Erhitzter Kreisscheiben," *ZAMP*, in print.

Timoshenko, S. P., and Goodier, J. N., 1970, *Theory of Elasticity*, McGraw-Hill, New York.

Forced Flexural Motions of Plates

P. B. Beaudan[22] and H. Reismann[23]

1 Introduction

The steady state dynamic response and induced stresses in a plate strip subjected to transverse loads of constant intensity which move parallel to the edges of the plate are dependent not only upon the magnitude and spatial distribution of the loads, but also strongly upon their speed of propagation. We shall consider a plate which is unbounded in the direction of propagation of the pressure load, and present a solution within the framework of the classical theory of thin, elastic plates. The special case of a line load suddenly accelerating or decelerating through a critical speed is analyzed.

2 Problem Formulation and Solution

We assume that the load intensity consists of three distinct superposed quantities: Directly applied transverse forces of intensity p; translational inertia forces of intensity $-m\,\partial^2 w/\partial t^2$, where m is the mass per unit area of the plate; and viscous damping forces of intensity $-2\epsilon\,\partial w/\partial t$, where 2ϵ is the damping coefficient. The classical equation of motion is then

$$\nabla^4 w + \frac{\partial^2 w}{\partial t^2} + 2\epsilon \frac{\partial w}{\partial t} = p \tag{1.1}$$

with admissible boundary conditions along the infinite edges

$$w(x,0,t) = w(x,\pi,t) = 0,$$

$$M_{yy}(x,0,t) = M_{yy}(x,\pi,t) = 0 \tag{1.2}$$

$$\lim_{x\to\infty} w(x,y,t) = \lim_{x\to-\infty} w(x,y,t) = 0 \tag{1.3}$$

The load is assumed to be arbitrarily distributed and characterized by a Fourier sine series. A product solution which satisfies the boundary conditions and results in a harmonic decomposition of equation (1.1) is given by

$$p(x,y,t) = \sum_{n=1}^{n=\infty} p_n(x,t)\,\sin ny,$$

$$w(x,y,t) = \sum_{n=1}^{n=\infty} w_n(x,t)\,\sin ny \tag{2}$$

Upon substitution of equations (2) into equation (1.1), we obtain the $y-$ independent partial differential equation

$$\frac{\partial^4 w_n}{\partial x^4} + 2n^2 \frac{\partial^2 w_n}{\partial x^2} + n^4 w_n + \frac{\partial^2 w_n}{\partial t^2} + 2\epsilon \frac{\partial w_n}{\partial t} = p_n \tag{3}$$

Transforming the deformation function in the fixed reference frame (x, y) and the load distribution in a system attached to its traveling front as

$$w_n(x,t) = \int_0^\infty (F(\alpha,t)\cos\alpha x + G(\alpha,t)\sin\alpha x)\,d\alpha,$$

$$p_n(x,t) = \int_0^\infty (A(\alpha)\cos\alpha\xi + B(\alpha)\sin\alpha\xi)\,d\alpha \tag{4}$$

where $\xi = x - \phi(t)$, and $\phi(t) = \int_0^t v(\tau)d\tau + \phi_0$, we obtain from equation (3)

$$\frac{\partial^2 F}{\partial t^2} + 2\epsilon \frac{\partial F}{\partial t} + (\alpha^2 + n^2)^2 F = A\cos\alpha\phi - B\sin\alpha\phi \tag{5.1}$$

$$\frac{\partial^2 G}{\partial t^2} + 2\epsilon \frac{\partial G}{\partial t} + (\alpha^2 + n^2)^2 G = A\sin\alpha\phi + B\cos\alpha\phi \tag{5.2}$$

which are two linearly independent, nonhomogeneous, differential equations, that can be solved by classical methods.

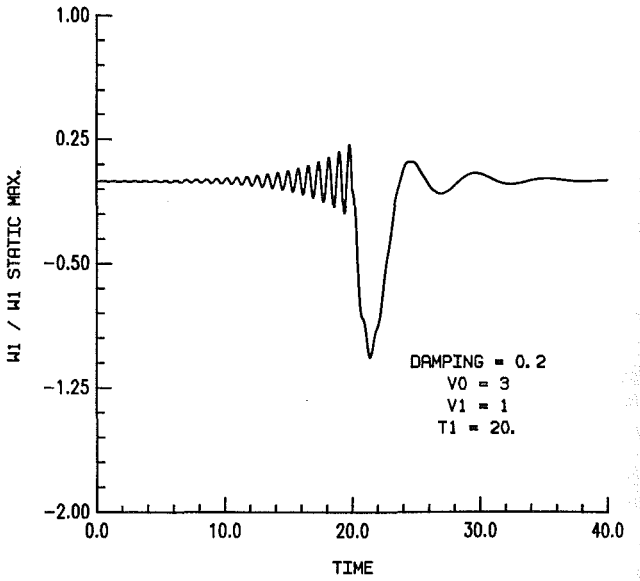


Fig. 1 Line load decelerating through the lowest critical velocity. First component of the step response.

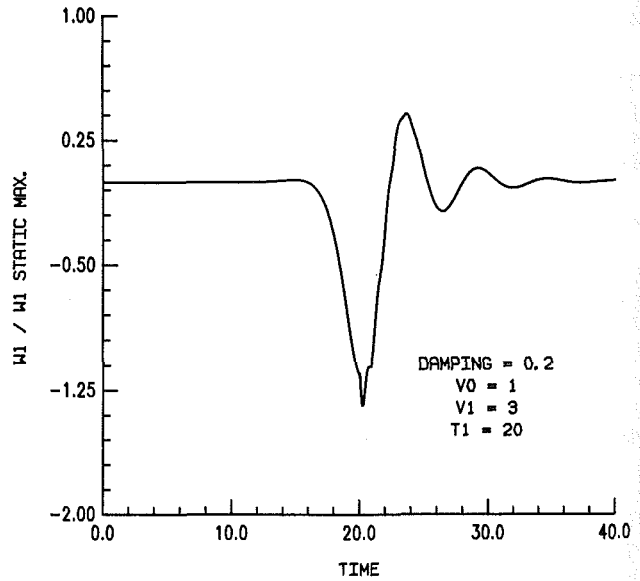


Fig. 2 Line load accelerating through the lowest critical velocity. First component of the step response.

[22]Graduate Student, State University of New York, Department of Mechanical and Aerospace Engineering, Buffalo, NY 14260.

[23]Professor, State University of New York, Department of Mechanical and Aerospace Engineering, Buffalo, NY 14260.

Manuscript received by ASME Applied Mechanics Division May 21, 1986; final revision, November 24, 1986.

Copyright © 1987 by ASME
Downloaded 03 May 2010 to 171.66.16.27. Redistribution subject to ASME license or copyright; see http://www.asme.org/terms/Terms_Use.cfm

Table 1 Dimensionless quantities

Dimensionless quantity	To convert to dimensional quantities multiply by	Physical interpretation
x	$\frac{\ell}{\pi}$	fixed Cartesian coordinate
y	$\frac{\ell}{\pi}$	fixed Cartesian coordinate
w	ℓ	plate vertical deflection
t	$\frac{\sqrt{m}}{\sqrt{D}}\left(\frac{\ell}{\pi}\right)^2$	time
p	$\frac{\pi^4}{\ell^3}D$	pressure load intensity
ϕ	$\frac{\ell}{\pi}$	distance traveled by p at time t
ℓ	1	width of plate strip

Defining

$$[w_n(x,t)]_{t=0} = \int_0^\infty (F_o\cos\alpha x + G_o\sin\alpha x)\,d\alpha,$$

$$\left[\frac{\partial w_n(x,t)}{\partial t}\right]_{t=0} = \int_0^\infty (\dot{F}_o\cos\alpha x + \dot{G}_o\sin\alpha x)\,d\alpha \tag{6}$$

the solution may be characterized as

$$w_n(x,t) = e^{-\epsilon t}\int_0^\infty \frac{(\epsilon F_o + \dot{F}_o)\cos\alpha x + (\epsilon G_o + \dot{G}_o)\sin\alpha x}{\sqrt{(\alpha^2+n^2)^2-\epsilon^2}}$$
$$\sin\sqrt{(\alpha^2+n^2)^2-\epsilon^2}\,t\;d\alpha + e^{-\epsilon t}\int_0^\infty [F_o\cos\alpha x$$
$$+ G_o\sin\alpha x]\cos\sqrt{(\alpha^2+n^2)^2-\epsilon^2}\,t\;d\alpha$$
$$+\int_0^\infty \frac{1}{\sqrt{(\alpha^2+n^2)^2-\epsilon^2}}\int_0^t e^{-\epsilon(t-\tau)}[A(\alpha)\cos\alpha(x$$
$$-\phi(\tau)) + B(\alpha)\sin\alpha(x-\phi(\tau))]$$
$$\sin\sqrt{(\alpha^2+n^2)^2-\epsilon^2}\,(t-\tau)d\tau\;d\alpha \tag{7}$$

3 Solution in Terms of Influence Functions

Substituting the integral definitions of the Fourier transform coefficients into the general result, it may be readily established that an equivalent form of equation (7) is

$$w_n(x,t) = \frac{e^{-\epsilon t}}{2\pi}\int_{-\infty}^{+\infty} w_n(\bar{x},0)\int_{-\infty}^{+\infty}\left[\frac{\epsilon\sin P(\alpha)t}{P(\alpha)}\right.$$
$$\left.+\cos P(\alpha)t\right]d\alpha d\bar{x} + \frac{e^{-\epsilon t}}{2\pi}\int_{-\infty}^{+\infty} w_n(\bar{x},0)$$
$$\int_{-\infty}^{+\infty}\frac{\cos\alpha(x-\bar{x})\sin P(\alpha)t}{P(\alpha)}\,d\alpha d\bar{x}$$
$$+\frac{1}{2\pi}\int_{-\infty}^{+\infty} P_n(\bar{\xi})\int_{-\infty}^{+\infty}\frac{1}{P(\alpha)}\int_0^t e^{-\epsilon(t-\tau)}\cos\alpha(\xi$$
$$-\bar{\xi})\sin P(\alpha)(t-\tau)d\tau d\alpha d\bar{\xi} \tag{8}$$

where $P(\alpha) = \sqrt{(\alpha^2+n^2)^2-\epsilon^2}$. This form of the solution identifies the contributions of the initial deformation, local rate of deformation, and of the pressure distribution to the global dynamic response of the plate strip. With reference to equation (8), we define, in particular, the influence function of the load distribution as

$$w_n(x,t;\bar{x},\bar{t}) = \frac{1}{2\pi}\int_{-\infty}^{+\infty}\frac{1}{P(\alpha)}\int_0^t e^{-\epsilon(t-\tau)}\cos\alpha\left(x-\bar{x}\right.$$
$$\left.-\int_\tau^{\bar{t}} v(\xi)d\xi\right)\sin P(\alpha)(t-\tau)d\tau d\alpha \tag{9}$$

Equation (9) expresses the influence of the deformation at $\bar{x}$ at time $\bar{t}$ upon the deformation at x at time t. Defining $\phi_o = \bar{x} + \int_0^t v(\eta)d\eta$, we conclude that the steady state deformation induced by a line load is $w_n(x,t)/p_n = w_n(x,t;\bar{x};\bar{t})$ so that the spatial distribution of the pressure load may be abstracted from the problem by analyzing an idealized line pressure distribution.

4 Step Change in Velocity Through a Critical Speed

An analysis of the influence function of the pressure distribution (Beaudan, 1986) revealed the existence of critical values of the velocity as $v_{cr} = 2n$. We consequently consider the following problem: At time $t = 0$ all initial conditions are arbitrary. At that instant, the load starts accelerating in some arbitrary fashion to a constant velocity v_o, such that there exists a nonzero integer n_o for which $2n_o \le v_o \le 2n_o + 1$. Once the steady state response of the plate has been attained, the velocity abruptly changes at $t = t_1$ to a velocity $2n_o - 1 \le v_1 \le 2n_o$, and thereafter remains at that constant value. In the case of a line load accelerating thorugh a critical velocity, the physical situation will be defined identically with $v_o \le v_1$. We analyze the response due to $w_{n_o}(x, t)$ at x_{cr} where the velocity abruptly changes, and denote $n = n_o$ and $x = x_{cr}$.

In the first time interval $0 \le t \le t_1$, we may write

$$\int_0^t e^{-\epsilon(t-\tau)}\cos\alpha(x-\phi(\tau))\sin\sqrt{(\alpha^2+n^2)^2-\epsilon^2}\,(t-\tau)d\tau$$
$$= \int_0^t e^{-\epsilon(t-\tau)}\cos\alpha\left(x-\phi_o\right.$$
$$\left.-\int_0^\tau v_o(\xi)d\xi\right)\sin\sqrt{(\alpha^2+n^2)^2-\epsilon^2}\,(t-\tau)d\tau \tag{10.1}$$

and for $t_1 \le t$

$$\int_0^t e^{-\epsilon(t-\tau)}\cos\alpha(x-\phi(\tau))\sin\sqrt{(\alpha^2+n^2)^2-\epsilon^2}\,(t-\tau)d\tau$$
$$= \int_0^t e^{-\epsilon(t-\tau)}\cos\alpha\left(x-\phi_o\right.$$

Downloaded 03 May 2010 to 171.66.16.27. Redistribution subject to ASME license or copyright; see http://www.asme.org/terms/Terms_Use.cfm

$$-\int_0^{\tau} v_o(\xi)d\xi\Big)\sin\sqrt{(\alpha^2+n^2)^2-\epsilon^2}\,(t-\tau)d\tau$$

$$-\int_0^{t-t_1} e^{-\epsilon(t-t_1-\tau)}\cos\alpha\Big(x-\phi_o$$

$$-\int_0^{t_1+\tau} v_o(\xi)d\xi\Big)\sin\sqrt{(\alpha^2+n^2)^2-\epsilon^2}\,(t-t_1-\tau)d\tau$$

$$+\int_0^{t-t_1} e^{-\epsilon(t-t_1-\tau)}\cos\alpha\Big(x-\phi_o-\int_0^{t_1} v_o(\xi)d\xi$$

$$-\int_0^{t_1+\tau} v_1(\xi)d\xi\Big)\sin\sqrt{(\alpha^2+n^2)^2-\epsilon^2}\,(t-t_1-\tau)d\tau \qquad (10.2)$$

The first two integrals in equation (10.2) will merely contribute a transient response, so that the steady state is uniquely defined by $v_1(t)$. The parameter ϕ_0 being arbitrary is set equal to zero. The transients for $t \geq t_1$ associated with a step change in velocity between two constant values are derived from equation (7) as

$$tr_n(x,t)=\frac{p_n e^{-\epsilon(t-t_1)}}{\pi}\int_0^{\infty}\frac{((\alpha^2+n^2)^2-\alpha^2v_o^2)\cos\sqrt{(\alpha^2+n^2)^2-\epsilon^2}\,(t-t_1)}{((\alpha^2+n^2)^2-\alpha^2v_o^2)^2+4\epsilon^2\alpha^2v_o^2}\,d\alpha$$

$$+\frac{p_n\epsilon e^{-\epsilon(t-t_1)}}{\pi}\int_0^{\infty}\frac{((\alpha^2+n^2)^2+\alpha^2v_o^2)\sin\sqrt{(\alpha^2+n^2)^2-\epsilon^2}\,(t-t_1)}{(((\alpha^2+n^2-\alpha^2v_o^2)^2+4\epsilon^2\alpha^2v_o^2)\sqrt{(\alpha^2+n^2)^2-\epsilon^2}}\,d\alpha$$

$$-\frac{p_n e^{-\epsilon(t-t_1)}}{\pi}\int_0^{\infty}\frac{((\alpha^2+n^2)^2-\alpha^2v_1^2)\cos\sqrt{(\alpha^2+n^2)^2-\epsilon^2}\,(t-t_1)}{((\alpha^2+n^2)^2-\alpha^2v_1^2)^2+4\epsilon^2\alpha^2v_1^2}\,d\alpha$$

$$-\frac{p_n\epsilon e^{-\epsilon(t-t_1)}}{\pi}\int_0^{\infty}\frac{((\alpha^2+n^2)^2+\alpha^2v_1^2)\sin\sqrt{(\alpha^2+n^2)^2-\epsilon^2}\,(t-t_1)}{(((\alpha^2+n^2)^2-\alpha^2v_1^2)^2+4\epsilon^2\alpha^2v_1^2)\sqrt{(\alpha^2+n^2)^2-\epsilon^2}}\,d\alpha$$

(11)

As the damping parameter ϵ and the difference v_1-2n or v_o-2n diminish, the poles of integrand functions tend to the real axis, so that the deformation components oscillate between correspondingly larger extremal amplitudes. The transients being antisymmetric in v_o and v_1 vanish as $v_o \to v_1$, reducing the solution to that of a constant speed line load. The steady states for both acceleration and deceleration are found by transforming the constant speed load solution with the use of equation (10) (Beaudan, 1986).

In the case of a suddenly decelerating line load, an oscillation of small period and exponentially increasing amplitude characterizes the motion at x in the neighborhood of $t \leq t_1$. As the velocity abruptly assumes a subcritical value at $t = t_1$, the forcing phenomenon suddenly attempts to induce at x a response in which the presence of the load is felt merely in a small neighborhood surrounding its point of application (Beaudan, 1986; Reismann, 1963). The wave of large period and amplitude, created by the supercritical regime and standing behind x at $t = t_1$ is thus heavily attenuated by the external damping as it propagates over x, as shown in Fig. 1. Its period is almost twice its value in the case where the load propagates constantly at supercritical speed, and its maximum amplitude is smaller than it is in both cases of constant super and subcritical velocities.

In the case of an accelerating line load, the presence of the load is felt merely in a small neighborhood of x for times $t \leq t_1$. At $t = t_1$, a signal which tends to heavily damp oscillations is propagating toward x, but due to the step change to a supercritical speed, a wave of large amplitude is generated at that time behind the load. The global response is shown in Fig. 2, where the attenuation of the wave for $t \geq t_1$ is caused principally by the increasing distance with time between x and the load. The maximum deflection in this case is larger than that which would be induced by a constant supercritical or subcritical regime.

5 References

Beaudan, P. B., 1986, "Dynamic Response of an Elastic Plate Strip to a Pressure Load Moving with Time Dependent Velocity," Master's thesis, State University of New York at Buffalo.

Kokhmanyuk, S. S., and Filippov, A. P., 1967, "Dynamic Effects on a Beam Due to a Load Moving at Variable Speed," in Russian, *Stroitelnaya Mekhanika i Raschet Sooruzhenii*, Vol. 9.

Kolesnik, I. A., and Yarovoi, V. E., 1966, "Vibration of Combined Systems Under the Action of a Load Moving at Variable Speed," in Russian, *Prikladnaya Mekhanika*, Vol. 2.

Reismann, H., 1963, "Response of Elastic Structures to Moving Loads," Technical Report, Martin Company, Denver, Colorado.

Reismann, H., 1963, "Dynamic Response of an Elastic Plate Strip to a Moving Line Load," *AIAA Journal*, Vol. 1, No. 2, pp. 354–360.

Downloaded 03 May 2010 to 171.66.16.27. Redistribution subject to ASME license or copyright; see http://www.asme.org/terms/Terms_Use.cfm

Journal of Applied Mechanics

Discussion

Stresses in Bi-Metal Thermostats[1]

A. G. Razaqpur.[2] The author presents an interesting solution to the problem of stresses in bi-metal thermostats. The writer is not, however, convinced that the stresses reported satisfy basic equilibrium requirements.

Considering Fig. 5, first let us examine the shear stresses τ_{xy}. The author has shown these stresses to be maximum at $x=\ell$ while in reality they must be zero at this location. This is so because the section at $x=\ell$ is a free boundary without prescribed tractions and, therefore, τ_{yx} equals to zero. It follows, therefore, that the conjugate shear τ_{xy} is also zero.

Next consider the peeling stresses σ_y. The author has shown these stresses as tensile (+) along the interface of the two strips. However, to satisfy equilibrium in the y direction, the resultant of these stresses must be zero because there are no applied forces or other stress resultants in this direction. These stresses are in reality selfequilibrating so they change sign from tension to compression within the length $x=0$ to $x=\ell$.

Finally, because the slope of the normal stress diagram is proportional to the shear stress at any section, the normal stress distribution shown does not seem totally correct, i.e., at the free boundary the slope should be equal to zero rather than the steep slope shown by the author. This leads me to conclude that the author's solution, despite its mathematical appeal, is no more accurate than the simple solution of this problem presented in elementary strength of material books.

Author's Closure

The author would like to emphasize that his study has been performed using Timoshenko type of theory, i.e., by applying elementary methods of Structural Mechanics, rather than methods of Mathematical Physics (The Ribière solution for a long-and-narrow strip was utilized in the analysis, with some simplifications, only for the purpose of obtaining a formula for the compliance sufficient). Therefore, the obtained results retain all the "shortcomings" of the Timoshenko approach, including the fact that some boundary conditions are not satisfied. Of course, this was obvious to the author, to the reviewers, and, to all appearances, to the overwhelming majority of the readers.

At the same time the suggested analytical model also possesses the main merit of the Timoshenko approach—its simplicity. Because of this the obtained formulas are easy-to-use and clearly indicate the role of various factors affecting the stresses. The basic step forward, made in my analysis, has to do with the utilization of the concept of the interfacial compliance. This concept enables one to evaluate the interfacial stresses responsible for the adhesive and cohesive strength of the attachment material. This is important, for instance, in the case of thermostat-like bi-material assemblies, which are used in electronic packages.

The equilibrium conditions are evidently fulfilled, so that the discusser's statement that the peeling stresses in my analysis do not satisfy the equilibrium conditions is incorrect. Moreover, these stresses were determined on the basis of the equilibrium condition (24), where, however, the stresses directed upward and distributed over small portions of the strips near the edges were substituted, for the sake of simplicity, by concentrated forces N_o, applied at the edges (Fig. 4). As follows from the formulas (14), (27), and (28), these forces equilibrate the distributed peeling stresses directed downwards (it is the author's belief that such a simplification results in a reasonable overestimation of the actual stresses). In Fig. 5 only the distributed stresses are shown.

Finally, I would like to make two comments concerning the discusser's conclusion:

1. My analysis has nothing to do with any attempt to obtain a more accurate solution to any problem. On the contrary, the author hopes that he succeeded in obtaining some useful results within the framework of an elementary, and hence "inaccurate," Timoshenko approach.
2. As far as I know, the thermostat problem, where bending is essential, is usually not included into strength-of-material books. These examine only the simplest case of tensile and compressive thermal stresses. Therefore, I would certainly appreciate if the discusser indicates the "elementary strength of material books," in which he found "the simple solution to this problem."

Mechanics of Fatigue Damage and Degradation in Random Short-Fiber Composites: Part II – Analysis of Anisotropic Property Degradation[3]

S. Nemat-Nasser.[4] In this second part of an interesting two-part contribution, Wang et al. (1986) shows that the self-consistent method used in conjunction with their experimentally established distribution density of microcracks in a fiber-reinforced composite produces results for the overall elastic moduli, in good accord with experimental observations. Although they assume elliptical cracks, to which Eshelby's

[1] By E. Suhir and published in the September, 1986, issue of the ASME JOURNAL OF APPLIED MECHANICS, Vol. 53, pp. 657-660.

[2] Assistant Professor, Department of Civil Engineering, Carleton University, Ottawa, Ontario, Canada K1S 5B6.

[3] By S. S. Wang, E. S.-M. Chim, and H. Suemasu and published in the June 1986 issue of the ASME JOURNAL OF APPLIED MECHANICS, Vol. 53, pp. 347-353.

[4] Professor of Applied Mechanics and Engineering Sciences, University of California, San Diego, La Jolla, CA 92093.

Copyright © 1987 by ASME
Downloaded 03 May 2010 to 171.66.16.27. Redistribution subject to ASME license or copyright; see http://www.asme.org/terms/Terms_Use.cfm

Journal of Applied Mechanics

Book Reviews

Introduction to Continuum Damage Mechanics, by L. M. Kachanov. Martinus Nijhoff Publishers, The Netherlands, 1986. 135 pages. Price: $39.50.

REVIEWED BY D. KRAJCINOVIC[1]

Every book is, almost by definition, a personal statement; it is a view of a subject colored by the opinions of the author. This is especially true of monographs dealing with the newly developing branches of engineering theories characterized by many competing and even contrasting models. A fundamental dilemma facing each author is whether to attempt to present a wide spectrum of ideas and models consistent with the underlying theoretical framework, or to follow a narrow path associated with a single train of thought.

In the case of the reviewed book the author was at the same time the progenitor of the entire field. As expected he selected the latter alternative following his original ideas and applying them over an impressive spectrum of different problems. While an approach is, under the circumstances, just as valid as any other, this reviewer, nevertheless, would have preferred a more ecumenical view. Naturally, a 128-page-long monograph can hardly spare the room for vacillation and agonizing over the shortcomings of a particular model. And, in fact, this reviewer is glad to state that the book is expertly written with a sense of elegance and a clear hierarchy of priorities. In other words, what is written is written well. However, much has been left out, to be added, hopefully, in the following volumes on this topic.

After an all too brief introduction the author embarks on the problems related to "creep and fracture under uniaxial stress." A series of one-dimensional problems, amenable to a closed-form solution, offers a suitable medium to emphasize the utility and versatility of the continuum damage mechanics (CDM). The author, at his very best, derives a series of useful time to rupture estimates for a rod in tension, beam in bending, rotating shaft, etc. Every one of these estimates should be a delight for designers.

The subsequent Chapter dealing with multiaxial conditions is somewhat lean in size. It is as if the author finds little pleasure and less willingness to deal with complex systems of equations, which are unavoidable in the case of three-dimensional problems and nonproportional loadings.

The last three Chapters, "Crack Growth under Creep Conditions," "Damage Models for Ductile Fracture," and "Fatigue Damage," represent further attempts to extend the utility of the scalar representation of damage to the problems of propagation of macrocracks interacting with microcracks around its tip.

In summary, this rather short but well written monograph represents a useful introduction into the CDM. Restricting his discussion to purely phenomenological models, the author was able to retain a remarkable simplicity over a wide range of problems. A restricted list of references is, perhaps, a logical consequence of the adopted strategy but is, nevertheless, not entirely helpful for a reader interested in other views of CDM.

Photoelasticity, Proceedings of the International Symposium on Photoelasticity, Tokyo, 1986, Edited by M. Nishida and K. Kawata. Springer-Verlag, Tokyo, 1986. 292 pages. Price: $51.60.

REVIEWED BY A. S. KOBAYASHI[2]

Despite the editor's broad definition of photoelasticity, photomechanics would have been a more appropriate title for this conference proceedings of the thirty five papers which were presented at the International Symposium on Photoelasticity in Tokyo, 1986. Most papers, which included moire, interferometry, holography, caustics, and speckles as "branches of photoelasticity," are review or application-oriented articles. Three papers reported on new developments and one paper dealt with the hybrid experimental-numerical procedure. Eighteen Japanese papers were matched by seventeen foreign papers from eleven countries.

The two survey papers by E. Moench and M. Nishida offered different perspectives where the former reviewed the historical developments in photoelasticity, primarily in Germany, while the latter provided an upbeat report on the recent Japanese developments in this field. Moench's lament on a loss of the chair in photoelasticity in 1984 demonstrates the need for developing new techniques and applications if photomechanics is to survive the onslaught of computational methods in solid mechanics. For the benefit of those who are searching for specific subject matters, brief descriptions of each paper are provided in the following.

S. Miki determined the time variation in birefringence of mixed polyester under creep in the temperature range of $-100°C$ to $130°C$. S. Sugimori et al. presented a simplified photoviscoelastic theory for measuring the residual stress developed through rapid cooling of thermosetting resin plates. P. R. Dietz reported on silver chloride as a possible photoplastic material without investigating the unloading response. Seven of the twenty figures were missing from the text in this paper.

D. Post reviewed the advances which he made in moire interferometry and Y. Morimoto et al. report on a digital image processing procedure which effectively reduces the line den-

[1]Professor, Department of Civil Engineering, Mechanics and Metallurgy, University of Illinois at Chicago, Chicago, IL 60680.

[2]Professor, Department of Mechanical Engineering, Univeristy of Washington, Seattle, WA 98195. Fellow ASME.

Copyright © 1987 by ASME
Downloaded 03 May 2010 to 171.66.16.27. Redistribution subject to ASME license or copyright; see http://www.asme.org/terms/Terms_Use.cfm

sities of the crowded fringes in moire interferometry. This procedure could be useful in post-processing moire fringes. Schumann provided the basic equations for the heterodyne method, sandwich method, and the two rigidly linked reference source method for generating holographic interferometry associated wtih the virtual deformation of an opaque body. I. Yamaguchi reported on his laser-speckle strain gage which is based on an optoelectronic method to detect speckle displacement with a strain sensitivity of 3 mV/microstrain over a gage length of 1 mm and a time resolution of at least 1 kHz.

K. Kawata et al. and S. Hashimoto et al. discussed dynamic stress concentration factors and dynamic states of stress, respectively, which were obtained by dynamic photoelasticity. J. W. Dally reported on his findings on dynamic fracture mechanics using dynamic photoelasticity. H. Shimada et al. described a preliminary photoelastic-schliern system for visualizing pulsed ultrasound waves.

J. F. Kalthoff reviewed his work on elasto-dynamic fracture mechanics and K. Shimizu et al. demonstrated a trivial use of combined photoelastic and caustic analysis. K. Takahashi modeled craze growth in polymethyl methacrylate sheets with caustics associated with a two-stage Dugdale model which was initiated by a critical equivalent stress intensity factor. The paper by H. P. Rossmanith reviewed his work in dynamic photoelasticity and caustics involving stress wave interaction with cracks and contact problems. P. C. Theocaris' work on pseudocaustics for evaluating the order of singularity is interesting but its experimental accuracy requires improvement.

L. S. Srinath presented, without experimental success, Raman scattering for measuring the crack-tip stress field. A procedure for stress separation was proposed by superimposing the photoelastic patterns of two identical slices, one with a known live load and the other from a frozen stress three-dimensional model. R. Shintani et al. demonstrated the utility of micro-photoelasticity in stretched and bend 200 to 400 micrometer diameter monofilaments. M. Nishida et al. reported on an epoxy resin with less model deformation at stress freezing temperature. G. Matsui et al. used the reflection moire method in a membrane analogy of a wooden column under torsion. S. Sakai et al. developed a simplified optical procedure for accurately locating the isoclinics and J. T. Pindera reviewed his work on isodyne and strain gradient photoelasticity.

G. Matsui et al. used two-dimensional photoelasticity with elasticity theory to determine the local constraints in beam-column joints and K. Uchino et al. reported on a three-dimensional photoelasticity analysis of rotating jet engine components. M. W. Hyer and V. J. Parks discussed the use of photo-orthotropic-elasticity for analyzing birefringent composite plates. The latter also used three-dimensional photoelasticity to study bonded joints. Other practical examples include J. Javor's use of photoelastic coating for in-situ testing of bridges.

Both H. K. Aben and M. Kuramoto reviewed their previous work on integrated photoelasticity and scattered light photoelasticity applied to axisymmetric problems. C. E. Taylor extolled the merits of coherent optics in experimental mechanics and Y. Mitsui et al. used boundary element method in conjunction with two-dimensional photoelasticity to separate the stresses. The paper by A. Lagarde presents a nondestructive procedure for three-dimensional photoelasticity analysis which is an attractive alternative to scattered light photoelasticity. The final paper by T. P. Broadbent et al. reports on the use of a practical micropolariscope.

This proceedings could be a useful reference book for those involved in photomechanics. The many review papers in this proceeding also provide the neophytes with a quick introduction to the states of science in their respective fields.

Engineering Rheology, by R. I. Tanner. Oxford University Press, New York, 1986. 451 pages. Price: $79.00.

REVIEWED BY R. S. RIVLIN[3]

Professor Tanner has written an interesting book which expresses a strong personality. It will be read with attention by many rheologists and engineers concerned with the application of nonlinear continuum mechanics to problems of technological importance, which involve the flow of viscoelastic fluids. The book is unusually well-written; one rarely has to read a sentence twice to understand its meaning.

In the first chapter Professor Tanner gives an excellent review of the wide variety of behavior exhibited by non-Newtonian fluids. This is followed by an account of the more basic equations of nonlinear continuum mechanics, which has the merit of succinctness, if not of depth or completeness.

Much of the first half of the book is taken up with a discussion of the various constitutive equations which have been proposed for the flow of viscoelastic fluids and their suitability for the description of particular simple types of flow—viscometric, elongational, one-step and two-step shear flows, and so on. The measurements are based on their alleged ability to model experimental results and culminate in the table on pages 222 and 223 in which the author indulges a professorial tendency to award grades. However, the experimental results are often too limited to lead to a definitive evaluation, and many would be led to quite different conclusions from those reached by Professor Tanner.

In his assessments, Professor Tanner democratically treats constitutive equations of a general character, developed from fundamental, substantially self-evident assumptions, on the same basis as special cases of equations that are more-or-less whimsically proposed. Curiously, in some cases he dismisses the general equation, while attaching great value to the special case.

The second half of the book is mainly concerned with a number of problems of technological concern. This is by far the most interesting part of the book. In it the effect of non-Newtonian behavior of the fluid on lubrication, calendaring, fiber spinning, and extrusion are discussed. Typically, the predictions for a Newtonian fluid are compared with experimental results for non-Newtonian fluids and attempts are made to close the gap by including in the constitutive model for the fluid some non-Newtonian character, usually in an *ad hoc* manner.

This part of the book can be enthusiastically recommended to graduate students who wish to embark on research in one or other of the areas covered. They will readily identify important unsolved problems to which they can devote their efforts.

Finite Difference Methods in Dynamics of Continuous Media, by J. L. Davis. Macmillan Publishing Co., New York, 1986. 236 pages. Price: $45.00.

REVIEWED BY G. RAVICHANDRAN[4]

This book is concerned with the development of finite difference methods for solving transient problems in mechanics. It also places due emphasis on analytical methods in dealing

[3]Center for the Application of Mathematics, Lehigh University, Bethlehem, PA 18015.

[4]Graduate Aeronautical Laboratories, California Institute of Technology, Pasadena, CA 91125.

Copyright © 1987 by ASME
Downloaded 03 May 2010 to 171.66.16.27. Redistribution subject to ASME license or copyright; see http://www.asme.org/terms/Terms_Use.cfm

with partial differential equations. The governing equations are developed in the context of a physical model and both analytical and numerical methods to solve the problem are explained.

The first two chapters serve as introductory material for the subject treated in the book. In Chapter 1 the different difference approximations for derivatives are introduced. The important concepts in finite difference methods, such as error analysis and stability are treated well. Efforts have been made to distinguish between implicit and explicit methods in solving problems. In Chapter 2 the author discusses methods of solution for the first order partial differential equations. The method of characteristics is introduced and the applications of difference methods are reviewed.

Chapter 3 forms a major part of the book, gives a thorough treatment to the development of second order hyperbolic partial differential equations and various analytical methods for solving them. The concepts of domains of influence and dependence are explained well. The author has also dealt with conservation laws and propagation of discontinuities in the context of the wave equation. The latter part of this chapter contains several examples dealing with the application of difference methods in solving both linear and nonlinear wave propagation problems. In Chapter 4 parabolic equations have received only a cursory treatment in comparison to the hyperbolic system in the previous chapter. In the context of heat conduction both implicit and explicit difference methods for solving the problems are illustrated. Stability analysis has been carried out for the difference schemes discussed in Chapters 3 and 4. Chapter 5 deals with analytical treatment of the governing equations in fluid dynamics. Though the subject has been dealt with in some detail, it does not contain any description of difference methods for dealing with shocks or other fluid dynamics problems. The exercises at the end of the chapters places emphasis on analytical methods.

The inclusion of a list of references for further study would have been useful to motivated readers to further their knowledge in this field. A nice feature of this book is that it gives a good blend of analytical and numerical methods for solving problems. This book could serve as an introductory text to students in engineering sciences and as a guide to practicing engineers to acquaint them with difference methods for solving transient problems.

Numerical Methods in Engineering and Science, by G. de Vahl Davis. Allen and Unwin, Inc., Winchester, MA, 1986. 286 pages. Price: cloth/$34.95; paper/$19.95.

REVIEWED BY P. D. RICHARDSON[5]

Professor de Vahl Davis has published extensively on convective transport using computational methods. In this book, based on roughly twenty-five years' experience in research and teaching, he presents numerical methods for students of engineering and science in an introductory course. His approach is to teach the *application* of numerical methods to the solution of equations (algebraic, transcendental, and differential) which are encountered frequently. The methods are taught as tools, and theoretical foundations for the methods are not covered rigorously (but references are given).

The teaching of the methods as *tools* shows itself in two ways in particular. The book is full of useful hints on tricks to use and traps to avoid. And Professor de Vahl Davis repeatedly asks the reader to become convinced on various points by *trying* various techniques. He gives emphasis to the point that students will understand numerical methods only once they have used them. The range of understanding here includes not only the principles by which algorithms lead to solution of equations, but also the convergence and stability of the methods and the predictability of the relation of order of error to step size. He encourages efficient style in programming and expects it to develop through self-critical practice.

The eight chapters consist of an introduction, solution of single equations, simultaneous equations (with the switch from direct to iterative methods being discussed in terms of numbers of arithmetic operations involved, and with special treatment of tridiagonal and pentadiagonal systems), interpolation, differentiation and integration, ordinary differential equations (with fine discussion of primitive methods, predictor-corrector, and Runga-Kutta-Merson approaches), partial differential equations (a chapter each for elliptic and parabolic equations) and finally an introduction to integral methods for solution of boundary value problems (weighted residuals, finite elements and boundary elements). de Vahl Davis includes a few useful aids from previous generations of numerical analysts, such as Bickley's difference tables for their pedagogical value (which evoked personal memories from my student days of seeing Professor Bickley's remarkable performance of writing out such tables on a large blackboard when he was alread blind), and Richardson's extrapolation (still a tool for computational economy in some circumstances).

Many of the problems can be worked out by students using small programmable pocket calculators. Some problems require use of a desk-top computer or terminal. The book contains some flowcharts and several Fortran listings (stripped of I/O details that usually vary from place to place). The book can be used in a course of 40-45 lecture hours; the author recommends spreading this over an academic year if possible, to give students time to assimilate ideas and to gain practice through the many exercises given. Upper level engineering undergraduates would be obvious targets for such a course. Because of the breath of useful information given here, the book is likely to be very useful also to professionals who use numerical methods occasionally.

[5] Professor of Engineering and Physiology, Brown University, Providence, RI 02912. Fellow ASME.

Downloaded 03 May 2010 to 171.66.16.27. Redistribution subject to ASME license or copyright; see http://www.asme.org/terms/Terms_Use.cfm

with partial differential equations. The governing equations are developed in the context of a physical model and both analytical and numerical methods to solve the problem are explained.

The first two chapters serve as introductory material for the subject treated in the book. In Chapter 1 the different difference approximations for derivatives are introduced. The important concepts in finite difference methods, such as error analysis and stability are treated well. Efforts have been made to distinguish between implicit and explicit methods in solving problems. In Chapter 2 the author discusses methods of solution for the first order partial differential equations. The method of characteristics is introduced and the applications of difference methods are reviewed.

Chapter 3 forms a major part of the book, gives a thorough treatment to the development of second order hyperbolic partial differential equations and various analytical methods for solving them. The concepts of domains of influence and dependence are explained well. The author has also dealt with conservation laws and propagation of discontinuities in the context of the wave equation. The latter part of this chapter contains several examples dealing with the application of difference methods in solving both linear and nonlinear wave propagation problems. In Chapter 4 parabolic equations have received only a cursory treatment in comparison to the hyperbolic system in the previous chapter. In the context of heat conduction both implicit and explicit difference methods for solving the problems are illustrated. Stability analysis has been carried out for the difference schemes discussed in Chapters 3 and 4. Chapter 5 deals with analytical treatment of the governing equations in fluid dynamics. Though the subject has been dealt with in some detail, it does not contain any description of difference methods for dealing with shocks or other fluid dynamics problems. The exercises at the end of the chapters places emphasis on analytical methods.

The inclusion of a list of references for further study would have been useful to motivated readers to further their knowledge in this field. A nice feature of this book is that it gives a good blend of analytical and numerical methods for solving problems. This book could serve as an introductory text to students in engineering sciences and as a guide to practicing engineers to acquaint them with difference methods for solving transient problems.

Numerical Methods in Engineering and Science, by G. de Vahl Davis. Allen and Unwin, Inc., Winchester, MA, 1986. 286 pages. Price: cloth/$34.95; paper/$19.95.

REVIEWED BY P. D. RICHARDSON[5]

Professor de Vahl Davis has published extensively on convective transport using computational methods. In this book, based on roughly twenty-five years' experience in research and teaching, he presents numerical methods for students of engineering and science in an introductory course. His approach is to teach the *application* of numerical methods to the solution of equations (algebraic, transcendental, and differential) which are encountered frequently. The methods are taught as tools, and theoretical foundations for the methods are not covered rigorously (but references are given).

The teaching of the methods as *tools* shows itself in two ways in particular. The book is full of useful hints on tricks to use and traps to avoid. And Professor de Vahl Davis repeatedly asks the reader to become convinced on various points by *trying* various techniques. He gives emphasis to the point that students will understand numerical methods only once they have used them. The range of understanding here includes not only the principles by which algorithms lead to solution of equations, but also the convergence and stability of the methods and the predictability of the relation of order of error to step size. He encourages efficient style in programming and expects it to develop through self-critical practice.

The eight chapters consist of an introduction, solution of single equations, simultaneous equations (with the switch from direct to iterative methods being discussed in terms of numbers of arithmetic operations involved, and with special treatment of tridiagonal and pentadiagonal systems), interpolation, differentiation and integration, ordinary differential equations (with fine discussion of primitive methods, predictor-corrector, and Runga-Kutta-Merson approaches), partial differential equations (a chapter each for elliptic and parabolic equations) and finally an introduction to integral methods for solution of boundary value problems (weighted residuals, finite elements and boundary elements). de Vahl Davis includes a few useful aids from previous generations of numerical analysts, such as Bickley's difference tables for their pedagogical value (which evoked personal memories from my student days of seeing Professor Bickley's remarkable performance of writing out such tables on a large blackboard when he was alread blind), and Richardson's extrapolation (still a tool for computational economy in some circumstances).

Many of the problems can be worked out by students using small programmable pocket calculators. Some problems require use of a desk-top computer or terminal. The book contains some flowcharts and several Fortran listings (stripped of I/O details that usually vary from place to place). The book can be used in a course of 40-45 lecture hours; the author recommends spreading this over an academic year if possible, to give students time to assimilate ideas and to gain practice through the many exercises given. Upper level engineering undergraduates would be obvious targets for such a course. Because of the breath of useful information given here, the book is likely to be very useful also to professionals who use numerical methods occasionally.

[5] Professor of Engineering and Physiology, Brown University, Providence, RI 02912. Fellow ASME.

Copyright © 1987 by ASME
Downloaded 03 May 2010 to 171.66.16.27. Redistribution subject to ASME license or copyright; see http://www.asme.org/terms/Terms_Use.cfm